AD-760 684

OPTIMIZATION OF FOWARD FOIL LIFT CONTROL FOR AG(EH) HYDROFOIL CRAFT. VOLUME I: HYDRODYNAMICS

Howard R. Wright, Jr.

Grumman Aerospace Corporation

Prepared for:

Naval Ship Research and Development Center

December 1972

DISTRIBUTED BY:

NTIS

National Technical Information Service
U. S. DEPARTMENT OF COMMERCE
5285 Port Royal Road, Springfield Va. 22151

AD 760684

Interim Report

optimization of forward foil lift control for ag(eh) hydrofoil craft

volume I
hydrodynamics



THIS RESEARCH WAS SPONSORED BY THE
SYSTEMS DEVELOPMENT OFFICE
OF THE NAVAL SHIP RESEARCH AND DEVELOPMENT CENTER
UNDER THE NAVAL SHIP SYSTEM COMMAND
SUBPROJECT S 46 06, TASK 01709
CONTRACT N00014-71-C-0160

REPRODUCTION IN WHOLE OR IN PART IS PERMITTED FOR ANY PURPOSE OF THE
UNITED STATES GOVERNMENT.

[illegible] T A
[illegible] se;
[illegible]

GRUMMAN

GRUMMAN AEROSPACE CORPORATION

REPORT NO. HCG-72-19(I)

Interim Report

optimization of forward foil lift control for ag(eh) hydrofoil craft

volume I hydrodynamics

BY

H. RAYMOND WRIGHT, JR.

DECEMBER 1972

APPROVED BY:

R. J. JOHNSTON, MARINE

APPROVED BY:

W. R. MURPHY, AERODYNAMICS

ACKNOWLEDGMENT

This report is in partial fulfillment of the objectives set forth in Contract No. N00014-71-C-0160 sponsored by the Naval Ship Research and Development Center.

The cooperation and assistance in this program of Dr. E. K. Bender of Bolt, Beranek and Newman, Inc., and of Mr. William C. O'Neill and Mr. Alan C. Conolly of the Naval Ship Research and Development Center is acknowledged with gratitude.

UNCLASSIFIED
Security Classification

DOCUMENT CONTROL DATA - R & D

(Security classification of title, body of abstract and indexing annotation must be entered when the overall report is classified)

1. ORIGINATING ACTIVITY (Corporate author)
Grumman Aerospace Corporation
South Oyster Bay Road
Bethpage, New York 11714

2a. REPORT SECURITY CLASSIFICATION
Unclassified

2b. GROUP

3. REPORT TITLE
Interim Report on Optimization of Forward Foil Lift Control for AG(EH) Hydro Craft - Volume I: Hydrodynamics

4. DESCRIPTIVE NOTES (Type of report and inclusive dates)
Interim Report March 1971 - October 1972

5. AUTHOR(S) (First name, middle initial, last name)
Howard R. Wright, Jr.

6. REPORT DATE	7a. TOTAL NO. OF PAGES	7b. NO. OF REFS
December 1972	Open	33

8a. CONTRACT OR GRANT NO	9a. ORIGINATOR'S REPORT NUMBER(S)
N00014-71-C-0160	
b. PROJECT NO.	HCG-72-19(I)
S 46 06	9b. OTHER REPORT NO(S) (Any other numbers that may be assigned this report)
Task 01709	

10. DISTRIBUTION STATEMENT

11. SUPPLEMENTARY NOTES

12. SPONSORING MILITARY ACTIVITY
Systems Development Office, Naval Ship Research and Development Center, Department of the Navy, Washington, D. C. 20034

13. ABSTRACT

(U) This volume presents the foil and craft characteristics required by the Grumman Specific Linear Optimal Control Program for hydrofoil craft (SLOCOP). The characteristics are presented in generalized form, compared with certain experimental measurements, and evaluated for the AG(EH).

The prediction confidence level is deficient in three significant areas:

1. Hinge moment, particularly for flaps
2. Unsteady loading, particularly for orbital motion
3. Flap cavitation boundaries

SLOCOP trending studies are underway to establish the sensitivity of the autopilot design to the unsteady loading representation employed. These studies are intended to identify those unsteady loading responses for which further experimental effort is required for confident autopilot design.

DD FORM 1 NOV 68 1473 (PAGE 1)
S/N 0102-014-6600

UNCLASSIFIED
Security Classification

14. KEY WORDS	LINK A		LINK B		LINK C	
	ROLE	WT	ROLE	WT	ROLE	WT
Hydrofoil						
Unsteady Loads						
Cavitation Effects						
Wave Loads						
AG(EH) (Foil loads)						

VOLUME I

ERRATA

1. Page 3, $C_{H_{C_{L_\delta}}}$ should be defined dC_H/dC_{L_δ}

2. Page 1-2, in last line of Table 1-1, Ref. 2 should be Ref. 1-4

3. Page 3-2, in tenth line, (MCC'/C) should be (MAC'/MAC)

4. Page 5-15, in second line, Figures 5-24 and 5-25 should be Figures 5-26 and 5-27

6. Page A-1, in Eq. (A3), $\frac{1-4\frac{\lambda}{c}}{A} + \frac{1-\lambda}{1+\lambda}$ should be $\frac{1-4\frac{\lambda}{c}}{A} \times \frac{1-\lambda}{1+\lambda}$

CONTENTS

NOTE: References are found at the end of each section.

Section		Page
	ABSTRACT	iii
	INTRODUCTION	1
	CONCLUSIONS	2
	SYMBOLS	3
	DISCUSSION	1-1
1.	REFERENCE CRAFT CONFIGURATION	1-1
2.	NOMENCLATURE	2-1
3.	GENERAL FOIL LIFT, PITCHING MOMENT, AND FLAP HINGE MOMENT	3-1
4.	TRIM CHARACTERISTICS	4-1
	4.1 Lift Curve Slope	4-1
	4.2 Residual Lift	4-4
	4.3 Foil Pitching Moment Slope	4-6
	4.4 Residual Foil Pitching Moment	4-10
	4.5 Comparison with Prototype Data	4-14
	4.6 Flap Hinge Moment	4-21
	4.7 Foil Pitching Moment Due to Flap	4-23
5.	UNSTEADY LOAD CHARACTERISTICS	5-1
	5.1 Jones' Foil Motion and Gust Functions	5-2
	5.2 Heave Lift	5-4
	5.3 Heave Moment	5-6
	5.4 Pitch Lift	5-9
	5.5 Pitch Moment	5-10
	5.6 Flap Lift	5-13
	5.7 Flap Moment	5-14

Preceding page blank

CONTENTS (Continued)

Section		Page
	5.8 Flap Motion Foil Hinge Moment	5-15
	5.9 Foil Heave Flap Hinge Moment	5-16
	5.10 Foil Pitch Flap Hinge Moment	5-18
	5.11 Orbital Motion Lift	5-18
	5.12 Orbital Motion Foil Moment	5-25
	5.13 Orbital Motion Flap Hinge Moment	5-32
	5.14 Summary	5-32
6.	CAVITATION CHARACTERISTICS	6-1
	6.1 Incidence Lift Cavitation	6-1
	6.2 Flap Lift Cavitation	6-5
	6.3 Flap Operation Modes	6-11
	6.4 Orbital Motion Effect	6-12
Appendix A	Body Lift Aerodynamic Center	A-1
Appendix B	AG(EH) Forward Foil Data Crossplots	B-1
Appendix C	Evaluation of Flap Hinge Moment Derivatives	C-1
Appendix D	Analysis of Hystad Model Cavitation Characteristics	D-1
Appendix E*	Analysis of AG(EH) Towing Tank Data	E-i

* A separate table of contents is included for Appendix E, which consists of 123 pages.

ILLUSTRATIONS

Figure		Page
1-1	Craft Geometry	1-4
1-2	Fwd. Foil Geometry	1-5
1-3	Aft Foil Geometry	1-6
2-1	Nomenclature	2-2
4-1	Pitch Lift Curve Slope	4-37
4-2	Incidence Lift Curve Slope	4-38
4-3	Fwd. Foil Zero Lift Angle	4-39
4-4	Aft Foil Zero Lift Angle	4-40
4-5	Fwd. Foil Aerodynamic Center, Incidence Lift Hinge Moment	4-41
4-6	Fwd. Foil Aerodynamic Center, Pitch Lift Hinge Moment	4-42
4-7	Aft Foil Aerodynamic Center	4-43
4-8	Aft Foil Residual Hinge Moment	4-44
4-9	Fwd. Foil Residual Hinge Moment	4-45
4-10	Prototype Foil Angles	4-46
4-11	Prototype Fwd. Foil Hinge Moment	4-47
4-12	Prototype Aft Foil Hinge Moment	4-48
4-13	Prototype Fwd. Foil Lift and Hinge Moment	4-49
4-14	Prototype Aft Foil Lift and Hinge Moment	4-50
4-15	Flap Hinge Moment Derivative C_{h_α}	4-51
4-16	Flap Hinge Moment Derivative C_{h_δ}	4-52
5-1	Jones' Foil Motion Function	5-44
5-2	Jones' Gust Function	5-45
5-3	Pattison's Steady State Lift Curve Slope, 2-D	5-46
5-4	Heave Lift Attenuation, 2-D, d/c = .995	5-47
5-5	Heave Lift Phase, 2-D, d/c = .995	5-48
5-6	Heave Moment Amplitude, 2-D, d/c = .405	5-49
5-7	Heave Moment Phase, 2-D, d/c = .405	5-50

ILLUSTRATIONS (Continued)

Figure		Page
5-8	Pitch Lift Attenuation, H/MGC = .32	5-51
5-9	Pitch Lift Phase, H/MGC = .32	5-52
5-10	Pitch Lift Attenuation, H/MGC = .062	5-53
5-11	Pitch Lift Phase, H/MGC = .062	5-54
5-12	Pitch Lift Attenuation, H/c = 1/4	5-55
5-13	Pitch Lift Phase, H/c = 1/4	5-56
5-14	Pitch Moment Slope, H/MGC = .32	5-57
5-15	Pitch Moment Phase, H/MGC = .32	5-58
5-16	Pitch Moment Slope, H/MGC = .062	5-59
5-17	Pitch Moment Phase, H/MGC - .062	5-60
5-18	Pitch Moment Amplitude, 2-D, H/c = 1/4	5-61
5-19	Pitch Moment Phase, 2-D, H/ - 1/4	5-62
5-20	Flap Lift Attenuation	5-63
5-21	Flap Lift Phase	5-64
5-22	Flap Hinge Moment Derivative C_{h_α}	5-65
5-23	Flap Hinge Moment Derivative C_{h_δ}	5-66
5-24	Flap Moment Attenuation, 2-D, .25c Flap	5-67
5-25	Flap Moment Phase, 2-D, .25c Flap	5-68
5-26	Flap Moment Attenuation, AG(EH) Fwd. Foil	5-69
5-27	Flap Moment Phase, AG(EH) Fwd. Foil	5-70
5-28	Flap Foil Hinge Moment Attenuation	5-71
5-29	Flap Foil Hinge Moment Phase	5-72
5-30	Heave Flap Hinge Moment Amplitude	5-73
5-31	Heave Flap Hinge Moment Phase	5-74
5-32	Heave Flap Hinge Moment Analysis	5-75
5-33	Pitch Flap Hinge Moment Amplitude	5-76
5-34	Pitch Flap Hinge Moment Phase	5-77

ILLUSTRATIONS (Continued)

Figure		Page
5-35	Orbital Motion, Steele's Data, Attenuation	5-78
5-36	Orbital Motion, Steele's Data, Phase	5-79
5-37	Orbital Motion, Steele's Data, Attenuation	5-80
5-38	Orbital Motion, Steele's Data, Phase	5-81
5-39	Orbital Motion, O'Neill's Data, Attenuation	5-82
5-40	Orbital Motion, O'Neill's Data, Phase	5-83
5-41	Orbital Motion Foil Pitching Moment Amplitude	5-84
5-42	Orbital Motion Foil Pitching Moment Phase	5-85
5-43	Orbital Motion Foil Pitching Moment	5-86
5-44	Orbital Motion Flap Hinge Moment Attenuation	5-87
5-45	Orbital Motion Flap Hinge Moment Phase	5-88
6-1	Spanwise Lift Distribution	6-18
6-2	Pressure Coefficient Distribution	6-19
6-3	Foil Cavitation Buckets	6-20
6-4	Cavitation Lift Effect	6-21
6-5	Cavitation Drag Effect	6-22
6-6	Cavitation Effect Boundaries	6-23
6-7	Flap Basic Load Distribution	6-24
6-8	Flap Cavitation Bucket, Fixed Foil Incidence	6-25
6-9	Optimum Flap Cavitation Bucket	6-26
6-10	Effect of $C\ell_{ref}$ On Cavitation Bucket	6-27
6-11	Flapped Cavitation Bucket in Seas, $C\ell_{ref} = .167$	6-28
6-12	Flapped Cavitation Bucket in Seas, $C\ell_{ref} = .202$	6-29
6-13	Flap Deflection vs. Speed	6-30

TABLES

Table		Page
1-1	Gross Lift Curve Slopes - Fwd.	1-2
1-2	Gross Lift Curve Slopes - Aft	1-3
3-1	Values of T	3-5
4-1	AG(EH) Foil Lift Characteristics	4-28
4-2	AG(EH) Foil Moment Slopes	4-30
4-3	AG(EH) Foil Moments	4-32
4-4	Numerical Evaluation for Trim Parameters	4-33
4-5	Numerical Evaluation for Trim Equations	4-34
4-6	Flap Hinge Moment - Fwd. Only	4-36
5-1	Unsteady Load Response Terminology	5-35
5-2	Unsteady Load Response Predictions	5-38
5-3	Unsteady Load Data Reviewed	5-39
5-4	Unsteady Load Comparisons	5-40
5-5	Unsteady Load Confidence Levels	5-42
6-1	Cavitation Parameters	6-16

INTRODUCTION

The work under this contract essentially consisted of adapting the existing Grumman Specific Linear Optimal Control Program to the hydrofoil case and of illustrating the utility of that adaptation by application to the AG(EH) hydrofoil craft. The computer program itself, the adaptations required, and the application to the AG(EH) are all discussed in Volume II of this report. This volume is limited to consideration of the foil and craft hydrodynamic characteristics required by the Specific Linear Optimal Control Program.

The hydrodynamic study was heavily influenced by O'Neill's demonstration in Reference 5-9 that unsteady loading effects can be significant to hydrofoil craft of larger sizes. Much of this volume is devoted to evaluation of the magnitude and confidence level for unsteady loading effects. Another major area of consideration was the limitation imposed by cavitation on the linear range for foil and flap lift.

The hydrodynamic and control studies were of comparable magnitude and proceeded concurrently. Consequently, the hydrodynamic characteristics employed in the control study were preliminary estimates and are not consistent with the hydrodynamic conclusions. Similarly, the hydrodynamic characteristics are carried in full detail because the control optimization program was not available for the evaluation of reductions in form for those characteristics.

Because Volumes I and II of this report concern distinct disciplinary fields, no attempt has been made to employ a common nomenclature for the two volumes.

CONCLUSIONS

NOTE: All conclusions conerning the flap are reserved for Appendix E.

Steady-State Loadings

- Theory, towing tank measurements, and prototype measurements for the AG(EH) forward foil hinge moment are contradictory. The experimental measurements are inconclusive with respect to the aerodynamic center and residual hinge moment individually and reflect doubt upon the confidence level for foil hinge moment generally. Further model testing with symmetric and cambered sections on identical, simpler planforms would be desirable.

Unsteady Loading

- For foil motions, the unsteady loading responses of this report are basically classic aerodynamic responses though some of Theodorsen's "T" coefficients have been replaced by practical values, Jones' 3-dimensional foil motion function has been employed in place of Theodorsen's function, and the 3-dimensional hydrodynamic lift curve slope has been employed. The experimental data examined for this report do not require any more detailed accountability for the free surface

- The confidence level for lift and foil hinge moment response to foil motion is generally adequate, subject to SLOCOP studies of the sensitivity of the autopilot design to these responses, though experimental evidence is inadequate. The principal limitation upon the prediction of the foil moment response is the prediction of the steady-state foil moment.

- The celerity of gravity waves presents a significant distinction between the aerodynamic and hydrodynamic orbital motion (gust) cases. Correlation of theory and experiment is poor/fair for lift and inadequate for foil hinge moment. SLOCOP studies under way are intended to establish the accuracy requirement in this area.

Cavitation Characteristics

- Optimum cavitation characteristics for the AG(EH) forward foil with a 20% chord flap result when the incidence is fixed at an angle producing a lift coefficient of .167 (1185 psf foil loading at 50 knots). Varying the foil incidence with speed to trim the flap at 1g is disadvantageous for cavitation

- Conclusions concerning flap effectiveness and cavitation effect boundaries are reserved for Appendix E.

SYMBOLS

NOTES:

1. All units in ft./#/sec./rad. unless otherwise noted.
2. Parenthesis distinguish force or moment source from slope; e.g., $(C_L)_i$ is C_L due to incidence.
3. Primes indicate exposed foil, or phase referenced to orbital angle at half chord, or characteristic measured in plane perpendicular to quarter-chord line.
4. Refer to Table 5-1 for summary of unsteady load symbols.
5. For dual signs ($\pm$, $\mp$); upper sign refers to upper surface, lower sign to lower surface.
6. In general, unsteady characteristics are distinguished from steady-state characteristics by symbol identifying the unsteady motion; e.g., C_{L_h} is C_L response to heave motion; Δ_h is normalized response, C_{L_h}/C_L. C_L is a scalar, C_{L_h} is a vector.

A	Aspect ratio
a.c.	Aerodynamic center
B	Buoyancy
b	Span
c	Chord. May be MAC, MAC', MGC, etc.
C_B	Buoyancy coefficient, B/qS
C_D	Drag coefficient, D/qS
c_f	Flap chord
C_H	Incidence hinge moment coefficient, H/qSc
C_h	Flap hinge moment coefficient, $h/qS_f c_f$
$C_{H_{C_L}}$	$dC_H/dC_L = \frac{H}{C}$ - a.c.
$C_{H_{C_{L_\delta}}}$	dC_H/dC_{L_α}
C_{H_i}	dC_H/di

C_{H_α}	$dC_H/d\alpha$
$\underline{C_{h_\alpha}}$	3-D $dC_h/d\alpha$
C_{h_α}	2-D or 3-D $dC_h/d\alpha$
$\underline{C_{h_\delta}}$	3-D $dC_h/d\delta$
C_{h_δ}	2-D or 3-D $dC_h/d\delta$
C(K)	Jones' 3-D foil motion function. 2-D form is virtually identical with Theodorsen's function. See Eq. (3.4)
C_L	Lift coefficient, L/qS
ΔC_L	O'Neill's C_{L_i}
c_ℓ	Section lift coefficient
c_{ℓ_a}	Additional (type) lift contribution of flap
c_{ℓ_b}	Basic (type) lift contribution of flap
c_{ℓ_F}	Total lift contribution of flap, $c_{\ell_a} + c_{\ell_b}$
C_{L_i}	Incidence lift curve slope, dC_L/di,
c_{ℓ_i}	Design lift coefficient (camber)
$c_{\ell_{i_{eff.}}}$	Effective design lift coefficient, $c_{\ell_\alpha = 0}$
c_{ℓ_x}	Total lift less flap lift
$C_{L_{ref}}$	Zero flap C_L
C_{L_T}	Pattison's C_{L_h}
c_{ℓ_α}	Section lift curve slope
C_{L_α}	Foil lift curve slope
C_{L_δ}	Flap lift curve slope
$(c_\ell/C_L)_F$	Max. or min. c_ℓ/C_L on foil for flap lift
$(c_\ell/C_L)_i$	Max. or min. c_ℓ/C_L on foil for incidence lift
$(c_\ell/C_L)_\alpha$	Max. or min. c_ℓ/C_L on foil for pitch lift

$C_{M_{a.c.}}$	Moment coefficient about a.c., $C_{M_{C_{L=0}}}$, for design lift coeff.
$C_{M_{a.c._{eff.}}}$	Actual $C_{M_{ac}}$, see Eq. (4.4.1)
$C_{M_{ac_F}}$	$C_{M_{a.c.}}$ due to flap
C_{M_B}	Moment coefficient about C.G. due to buoyancy, $M_B/qS\ell$
C_{M_T}	Pattison's C_{H_h}
C_{M_α}	Moment coefficient about C.G. due to craft pitch, $M/qS\ell$ (not slope)
$C_{M_{\alpha_{a.c.}}}$	Moment coefficient slope about a.c. in orbital motion
$C_{M_{0L}}$	Moment coefficient about C.G. due to residual lift
$C_{M_{0M}}$	Moment coefficient about C.G. due to residual moment
C_w	Wave celerity, $\sqrt{\lambda g/2\pi}$
D	Pod diameter
d	Depth
$d\alpha/d\delta$	Flap effectiveness
F_n	Froude number, $V/\sqrt{gd}$
G	Normalized lift response to orbital motion, $C_{L_{\alpha_w}}/C_{L_\alpha} = C_{L_w}/C_L$, or centroid for flap basic load distribution referenced to c/4 and expressed as fraction of chord
G(k)	Jones' gust response function which is C_{L_w}/C_L referenced in in phase to orbital angle at L.E.. Virtually identical with Sears' function except that Sears' function is referenced to orbital angle at mid-chord. See Eq. (3.5). Note that Jones' function is 3-D and Sears' function is 2-D.
g	Acceleration of gravity
H	Distance between L.E. and incidence hinge, or normalized incidence hinge moment response, $C_{H_{\alpha_v}}/C_{H_\alpha}$
h	Distance between L.E. and flap hinge, or heave, + up, or occasinally depth

$(-\dot{h}/v)$	Angle of attack due to heave motion
ht	Wave height, crest to trough
I	Normalized incidence moment response, $C_{H_{i_U}} / C_{H_i}$
i	Incidence angle, + nose up, or imaginary part of
J(k)	Bessel function
k	$C_{\ell_\alpha} / 2\pi$, or section area/tc, or normalized inverse wavelength, $\pi / \frac{\lambda}{c}$
k'	$k(1 + C_w/V) = \omega c/2V$
$K_{W(B)}$, $K_{B(W)}$ $k_{W(B)}$, $k_{B(W)}$	Wing/body interaction factors from Chart 1, Reference 4-1
L	Lift, + up
ℓ	Foil base, distance between fwd and aft foil hinges
L_M	Steele's L_w
l_n	Distance between pod L.E. and pod a.c. (c.p.)
l_s	Distance between pod L.E. and shoulder (max. dia.)
M	Moment, + nose up
MAC	Mean aerodynamic chord
MAC'	Mean aerodynamic chord for exposed foil
MBC	Mean buoyant chord
M_f	Moment due to flap deflection, + nose up
MGC	Mean geometric chord
M_H	Moment about incidence hinge, + nose up
M_h	Moment about flap hinge, + nose up
P	Local pressure
P_A	Atmospheric pressure, 2116 psf
P_{cav}	$P_0 - P_V = P_A + \rho gd - P_V$
P_0	Ambient pressure, $P_A + \rho gd$
P_V	Vapor pressure, 72 psf

q	Dynamic pressure, $\frac{1}{2} \rho V^2$
S	Area, or distance, or total foil area
$\sqrt{S}$	Pressure coefficient, $1 + (P_0 - P)/q$
S'	Exposed area
S_N	Nose cross-section area, $\pi D^2/4$
T	Theodorsen's coefficients. See Table 3-1
t	Thickness
V	Speed, + for craft fwd
V_K	Speed, knots
V_e	Velocity of encounter, $V + C_w$
V_S	Volume of pod nose
v/V	Local velocity increment due to thickness
$\Delta v/V$	Local velocity increment due to camber
$\Delta v_a/V$	Local velocity increment due to angle of attack for unit $(c_\ell - c_{\ell_i})_{eff}$
$(\Delta v/V)_F$	Local velocity increment due to flap basic loading for unit δ, $= \frac{1}{4}$ of Allen's $P_{b_\delta}/C_{n_{b_\delta}}$
W	Weight
w_g	Orbital velocity, $\frac{ht.}{2} \sqrt{2\pi g/\lambda}\ e^{-2\pi d/\lambda}$
W/S	Foil loading
$(W/S)_{ref}$	Foil loading for zero flap
$\overline{x}B(W)$	Distance from exposed foil root chord L.E. to body lift c.p. (a.c.)
α	Angle of attack in general, θ, i, $(-\dot{h}/V)$, w_g/V. + nose up
δ	Flap deflection, + nose up
ζ	A flap basic (type) load parameter, $C_{H_\delta}/G\, c_{\ell_\alpha} \frac{d\alpha}{d\delta}$
η	Span station, or normalized flap moment response, $C_{h_{\alpha_U}}/C_{h_\alpha}$
θ	Pitch angle, + nose up
Λ	Sweep angle, quarter-chord unless otherwise specified, or normalized lift response, $C_{L_{\alpha_U}}/C_{L_\alpha}$

λ	Taper ratio or wavelength
λ_h	Normalized flap moment response to heave motion, $C_{h_h} \Big/ \left(-\frac{\dot{h}}{V}\right) \Big/ C_{h_\alpha}$
ξ_i	$(c_\ell / C_L)_i / (c_\ell / C_L)_F - 1$, a cavitation parameter
ξ_α	$(c_\ell / C_L)_\alpha / (c_\ell / C_L)_F - 1$, a cavitation parameter
ρ	Density, 1.9905 slugs/ft.^{3} (# sec.^{2}/ft.^{4})
σ	Cavitation number $(P_0 - P_V)/q$
ϕ_{MT}	Pattison's phase for C_{H_h}
ψ	A cavitation parameter, $\frac{v}{V} \pm \frac{\Delta v}{V} \mp C_{\ell_{i_{eff}}} \frac{\Delta v_a}{V}$
ω	Reduced frequency, $2\pi V_e/\lambda = \frac{2V}{c} k'$, or a cavitation parameter $\zeta\left[\frac{\Delta v_a}{V} - \left(\frac{\Delta v}{V}\right)_F\right]$

SUBSCRIPTS

a	About Theodorsen's point a where $a = 2\frac{H}{C} - 1$
B	Body, or due to buoyancy
C	Circulatory component
c/4	Referenced to quarter-chord
$c_\ell = 0$	For $c_\ell = 0$
F	For foil motion, or for flap motion
f	Flap
foil	of or for the foil
H	For foil hinge moment
h	For flap hinge moment, or for unsteady heave
i	Due to steady or unsteady incidence
i_H	For incidence, due to heave
L.E.	Leading edge
max	Maximum

NC	Non-circulatory (inertial) component
O	Orbital motion, or residual (value for $\alpha = i = \delta = 0$)
0L	At zero lift
P	For unsteady pitch
r	Root
t	Tip
trim	Steady-state
U	For unsteady foil motion generally, represents P and/or h
w	For orbital motion
δ	Due to flap angle
θ	For unsteady pitch
1	Fwd
2	Aft
∞	At infinite depth (aerodynamic)

1. REFERENCE CRAFT CONFIGURATION

The AG(EH) ("Plainview") has been employed as the model throughout this report to illustrate the generalized hydrodynamic relationship. A craft weight of 320 tons with a 90/10 distribution is assumed throughout this volume of the report. The foil position references are the foil incidence hinge lines and the craft geometry is shown on Figure 1-1. Figures 1-2 and 1-3 present the foil geometries.

The net foil lift and moment characteristics of this report are derived by the methods of Reference 1-1. Reference 1-1 refers to the gross lift and moment characteristics of the complete foil, neglecting the pod, and of the "exposed foil", which is a hypothetical foil consisting of the two exposed panels of the actual configuration joined together at their root chords. The gross lift curve slopes for the complete and exposed foils for the AG(EH) forward and aft configurations are derived in Tables 1-1 and 1-2 by the methods of Reference 1-2. The complete foil and exposed foil mean aerodynamic chords and aerodynamic centers, also derived from Reference 1-2, are shown on Figures 1-2 and 1-3.

1.1 REFERENCES

1-1 Pitts, Nielsen, and Kaattare, "Lift and Center of Pressure of Wing-Body-Tail Combinations at Subsonic, Transonic, and Supersonic Speeds", NACA Report 1307, 1959.

1-2 DeYoung and Harper, "Theoretical Symmetric Span Loading at Subsonic Speeds for Wings Having Arbitrary Plan Form", NACA Report 921, 1948.

1-3 Lindsey, Stevenson, and Daley, "Aerodynamic Characteristics of 24 NACA 16 - Series Airfoils at Mach Numbers Between 0.3 and 0.8," NACA TN 1546, September 1948.

1-4 Richter and Palmer, "AG(EH) Hydrofoil Reserach Ship Hydrodynamic Report of Model Test Program," Grumman Aerospace Corp. Report M23.77, 8/21/62, Rev. 1/15/63.

TABLE 1-1 GROSS LIFT CURVE SLOPES-FWD

CHARACTERISTIC	REFERENCE	COMPLETE FOIL	EXPOSED FOIL
Aspect Ratio, A		3	2.805
Taper ratio, λ		.3	.329
c/4 sweep, Λ, deg.		35.2	35.2
Section		16 - (.353) 08	16 - (.353) 08
Section $k = c_{\ell_\alpha}/2\pi$	NOTE 1.	.9	.9
A/k		3.34	3.12
$C^o_{L_\alpha}/k$	Fig. 4, Ref. 1-2	.0556	.0540
Lift curve slope C_{L_α}		2.87	2.79
Ref. 2 C_{L_α} Prediction		3.01	2.92

NOTES:

1. From an unpublished compilation of measured characteristics of Reference 1-3. Section lift curve slope was measured at Reynolds number of $.85 \times 10^6$ and Mach number of .3. Slope is function of section thickness ratio only and this table is valid for model and prototype.

2. Predictions of this report differ from those of Reference 1-4 in use of .9k rather than 1.0k and in interpolation in various charts employed.

TABLE 1-2 GROSS LIFT CURVE SLOPES - AFT

CHARACTERISTIC	REFERENCE	COMPLETE FOIL	EXPOSED FOIL
Aspect Ratio, A		3	2.75
Taper Ratio, λ		.3	.339
c/4 sweep, Λ, deg.		35.2	35.2
Section		16 - (.353) 08	16 - (.353) 08
Section $k = c_{\ell_\alpha} / 2\pi$	Note 1	.9	.9
A/k		3.34	3.055
$C_{L_\alpha}^{o}$ /k	Fig. 4, Ref. 1-2	.0556	.0535
Lift curve slope C_{L_α}		2.87	2.76
Ref. 2 C_{L_α} Prediction		3.01	2.92

See notes on Table 1-1.

NOTES: 1. ALL DIMENSIONS IN FT.

2. * ARE FROM BUSHIPS FOIL CONTRACT GUIDANCE PLAN AG(EN) 800 2068282, SHEET 1, UNDATED

3. CG LOCATED FOR 90/10 DISTRIBUTION.

4. 320 TON WEIGHT ASSUMED.

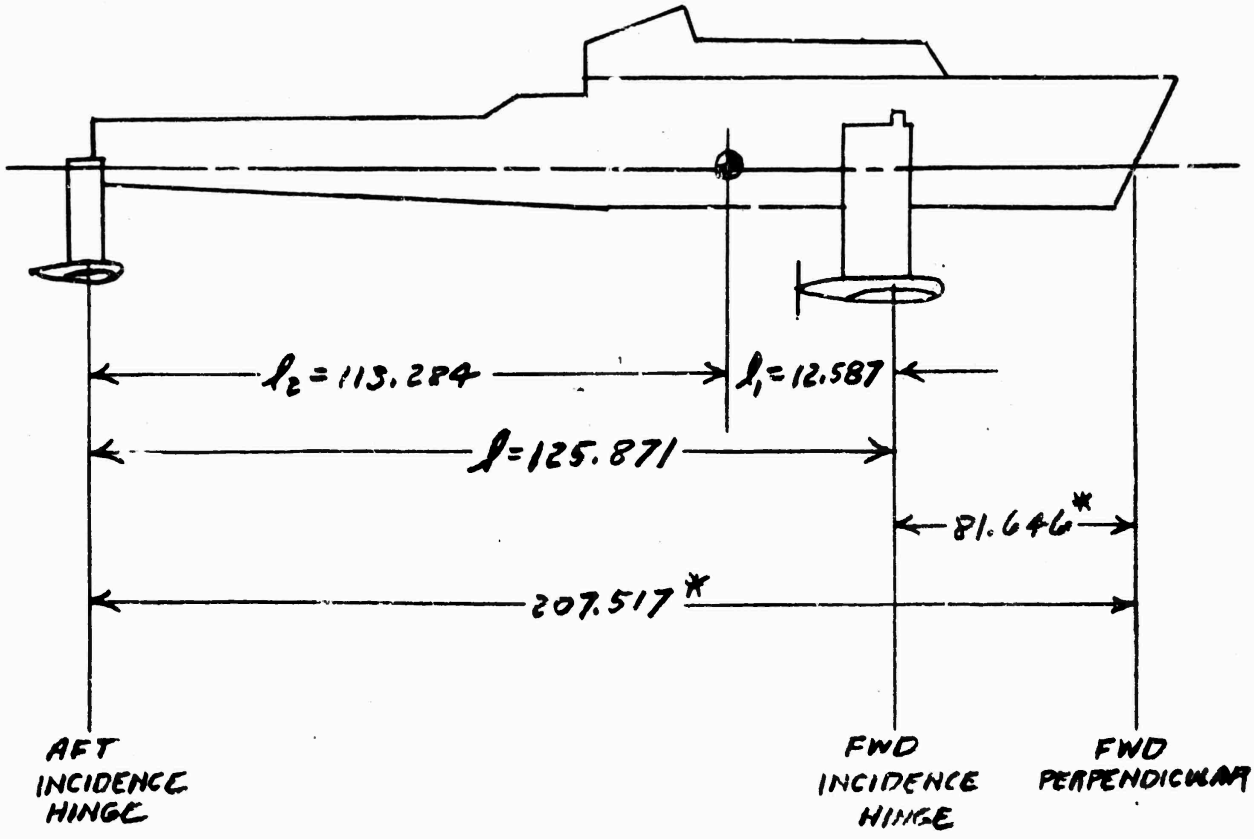
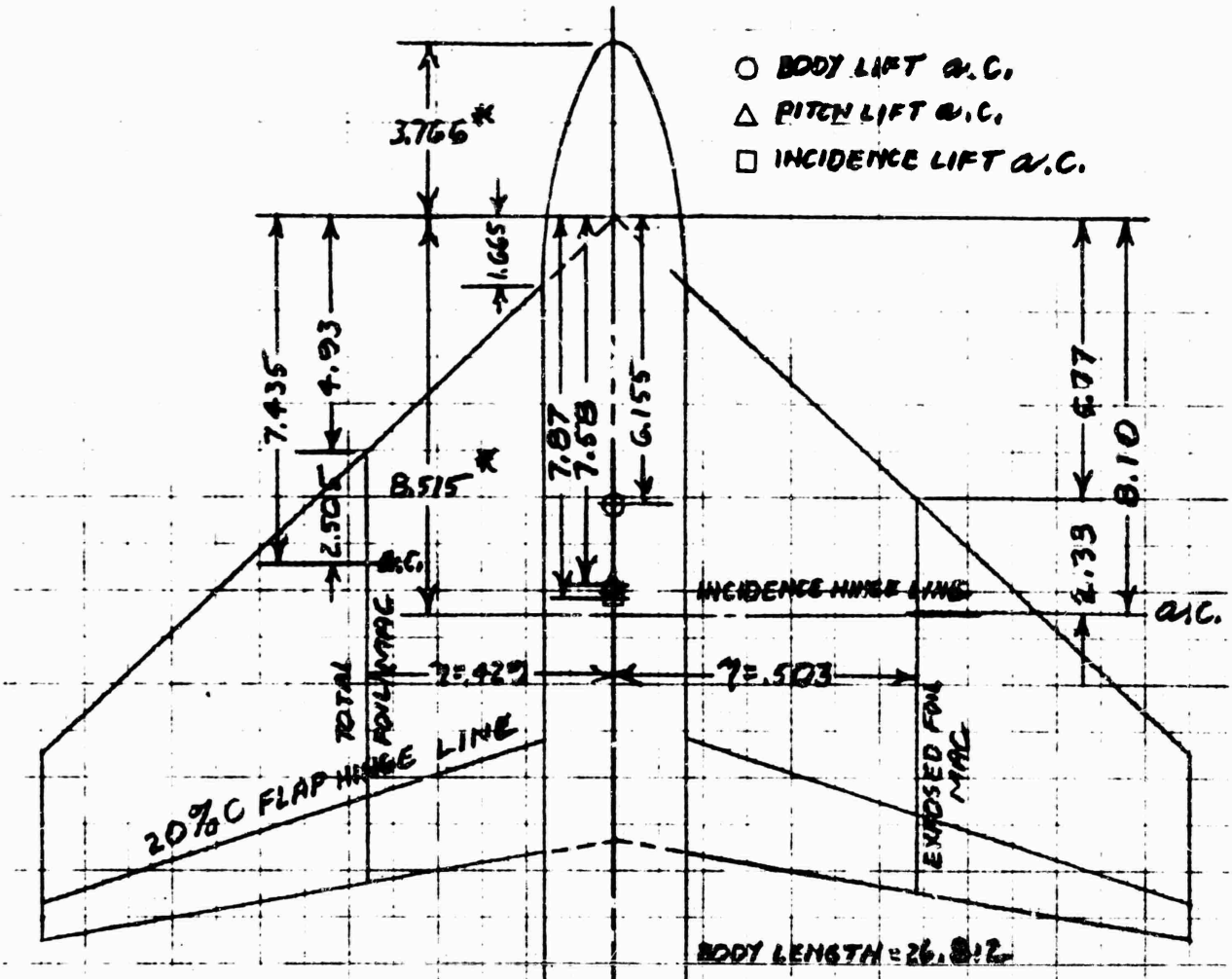


Figure 1-1. Craft Geometry

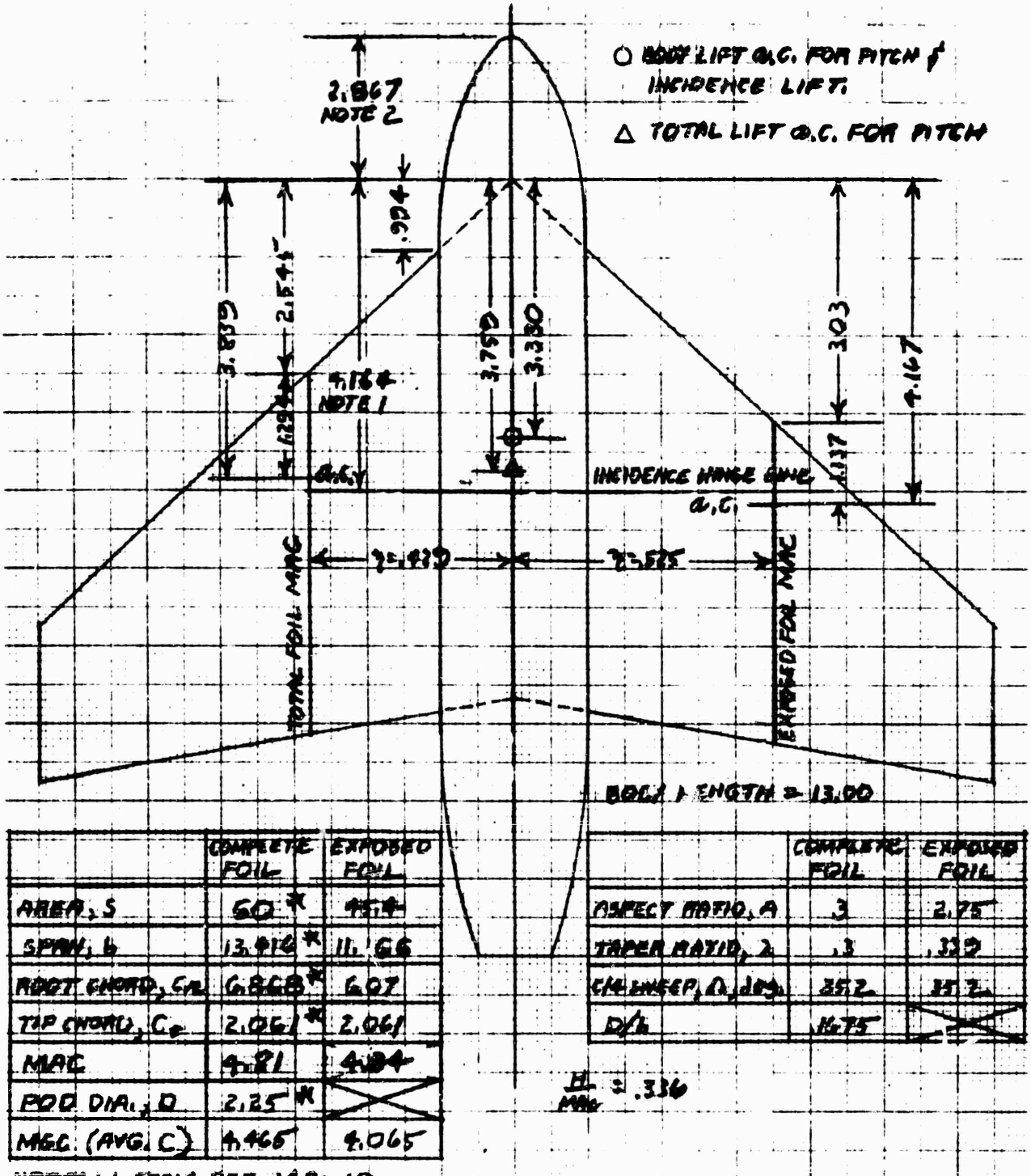


	COMPLETE FOIL	EXPOSED FOIL
AREA, S	225*	182.8
SPAN, b	26*	22.67
ROOT CHORD, C_R	13.314*	12.12
TIP CHORD, C_T	3.994*	3.994
MAC	9.33	8.64
POD DIA., D	3.333*	
MGC (AVG. C)	8.65	8.057

	COMPLETE FOIL	EXPOSED FOIL
ASPECT RATIO, A	3	2.805
TAPER RATIO, λ	.3	.329
C/4 SWEEP, $\Lambda_{c/4}$, deg	35.2	35.2
D/b	.1283	
$\frac{H}{MAC}$ = .385		

NOTES: 1. MODEL SECTIONS ARE 16-(.353)08 NORMAL TO QUARTER CHORD.
2. PROTOTYPE SECTION IS 16-(.390)08 NORMAL TO QUARTER CHORD.
3. SECTIONS ARE ASSUMED DEFINED STREAMWISE THROUGHOUT THIS REPORT.
4. ALL DIMENSIONS IN FT.
5. * ARE FROM BUSHIPS FOIL CONTRACT GUIDANCE PLAN AG(EH)-DD 2068282, SHEET 1, UNDATED.

Figure 1-2. Forward Foil Geometry



	COMPLETE FOIL	EXPOSED FOIL
AREA, S	60 *	45.4
SPAN, b	13.916 *	11.66
ROOT CHORD, C_R	6.868 *	6.07
TIP CHORD, C_t	2.061 *	2.061
MAC	4.81	4.34
BOD DIA., D	2.25 *	
MGC (AVG. C)	4.466	4.065

	COMPLETE FOIL	EXPOSED FOIL
ASPECT RATIO, A	3	2.75
TAPER RATIO, λ	.3	.339
C/4 SWEEP, $\Lambda_{c/4}$, deg.	35.2	35.2
D/b	.1675	

$\frac{H_L}{MAC} = .336$

NOTES: 1. FROM REF. 14 Pg. 19.
2. DERIVED FROM BOEING FOIL CONTRACT GUIDANCE PLAN AG(EN) POD 2068 232, SHEET 1, UNDATED.
3. * ARE FROM CONTRACT GUIDANCE PLAN APPROVAL.
4. MODEL SECTION IS NACA -(.343)08 NORMAL TO QUARTER-CHORD. PROTOTYPE SECTION IS BELIEVED TO BE THE SAME BUT WITHOUT AUTHORITY.
5. SECTION IS ASSUMED DEFINED STREAMWISE THROUGHOUT THIS REPORT.
6. ALL DIMENSIONS IN FT.

Figure 1-3. Aft Foil Geometry

2. NOMENCLATURE

The principal items of nomenclature employed in this volume are illustrated on Figure 2-1; all symbols are defined in the list of symbols.

The sign sense of this volume differs from Theodorsen for lift and heave which are both taken as positive up in this volume. Note that the half-chord is never employed in this volume and that the symbol "b" is employed for foil span.

In discussions concerning the total craft configuration, subscripts are employed to distinguish forward and aft characteristics; e.g.,

C_{L_1} = fwd lift coefficient

C_{L_2} = aft lift coefficient

C_L = craft lift coefficient = $\frac{S_1}{S} C_{L_1} + \frac{S_2}{S} C_{L_2}$

In discussions of a single foil, the foil location is not identified by subscript.

Exponential representation for vectors is avoided in this volume, vectors being presented as complex numbers and phase shifts symbolized by $\angle \pm \phi$. All angles are in radians unless symbolized ϕ^{o}.

The lift curve slope for incidence motions on the side of a fixed pod differs from that for a foil rigidly attached to the pod. The two cases are distinguished verbally here as "pitch lift" and "incidence lift" and are distinguished symbolically as C_{L_α} and C_{L_i}. In seas "incidence lift control" systems (including flap lift control systems) respond to craft and orbital motions on the pitch lift curve slope, it is only incidence motions (including flap motions) which produce lift at the incidence lift curve slope rate.

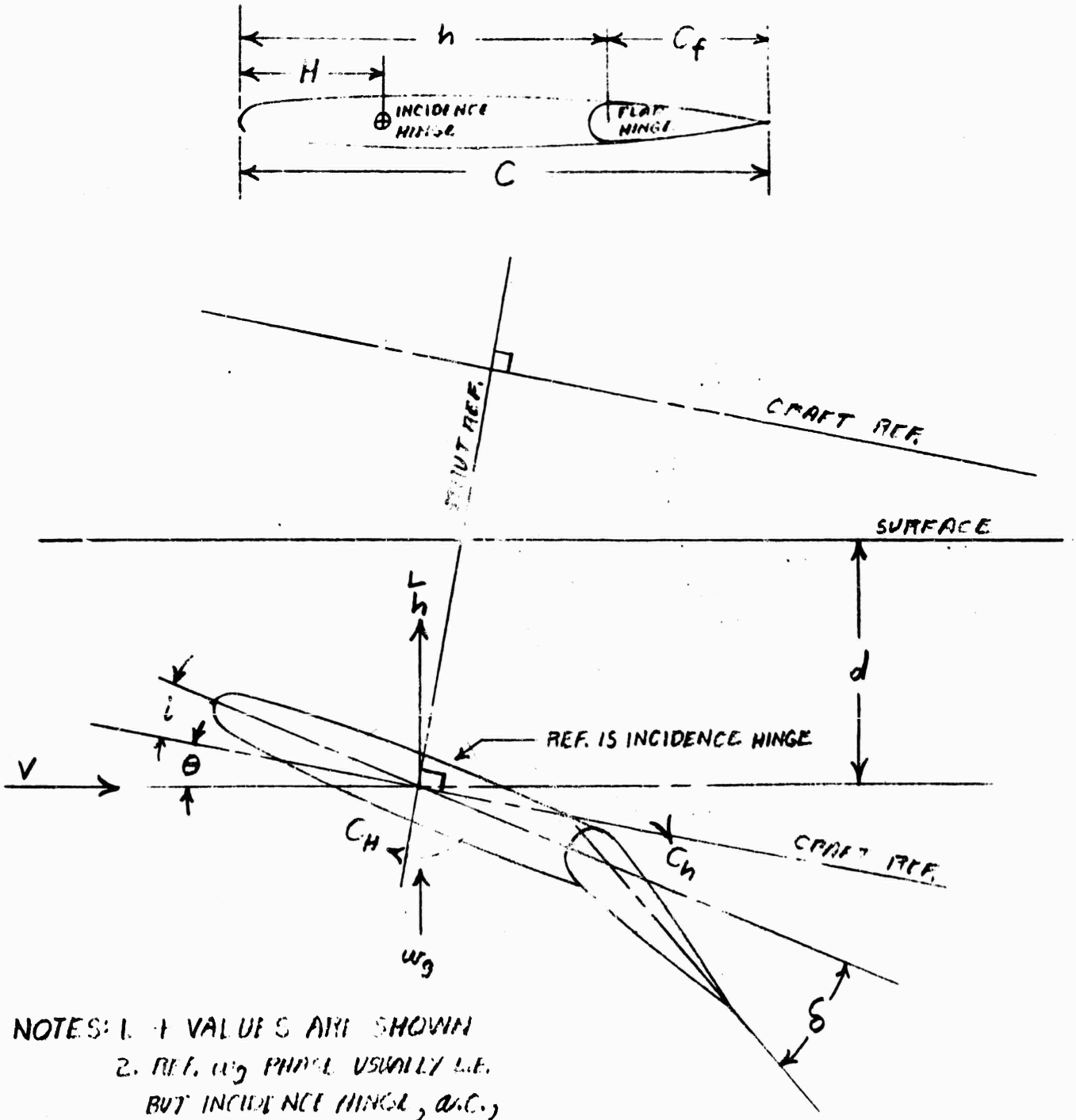


Figure 2-1. Nomenclature

3. GENERAL FOIL LIFT, PITCHING MOMENT, AND FLAP HINGE MOMENT

The instantaneous foil lift, incidence hinge moment, and flap hinge moment are the sum of foil motion and orbital velocity induced components superimposed on a steady-state or trim value.

Theodorsen presents the foil motion components for the two dimensional foil in Reference 3-1. Theodorsen's equations are accommodated to the three dimensional foil in this report by the following modifications:

- Theodorsen's function, C(k), is employed in Jones' three dimensional form of Reference 3-2
- Theodorsen's lift curve and flap hinge moment slopes (which are 2-dimensional, thin airfoil theory) are replaced by a practical, 3-dimensional estimate. The estimates of Reference 3-3 are employed in this report
- Theodorsen's flap effectiveness, T_{10}/π (which is 2-dimensional, thin airfoil theory), is identified as $d\alpha/d\delta$ for evaluation by practical methods
- Inertial terms which are functions of incidence or flap motion are reduced by the ratio of exposed to total foil area
- Jones' gust function, G(k), is added to account for orbital motion
- A trim, steady-state value is added.

The result of these modifications to Theodorsen's Eqs. (XVIII) - (XX) of Reference 3-1 may be written:

$$C_L = \frac{L}{qS} = \frac{2\pi}{c} k'^2 h + \pi k' \left[2\left(\frac{H}{c} - \frac{1}{2}\right) k' + i \right] \left(\theta + \frac{S'}{S} i \right)$$

$$+ \pi \frac{S'}{S} k' \left[\frac{T_1}{\pi} k' - i \frac{T_4}{\pi} \right] \delta + \left\{ -i \frac{2}{c} k' h + \left[1 + i\, 2\left(\frac{3}{4} - \frac{H}{c}\right) k' \right] \left(\theta + \frac{C_{L_i}}{C_{L_\alpha}} i \right) + \frac{C_{L_i}}{C_{L_\alpha}} \right.$$

$$\times \left. \left[\frac{d\alpha}{d\delta} + i \frac{1}{2} \frac{T_{11}}{\pi} k' \right] \delta \right\} C_{L_\alpha} C(k) + C_{L_\alpha} \frac{w_g}{V} G(k) \left[2 \frac{H}{c} k + C_{L_{trim}} \right.$$

$$= C_{L_{NC_F}} + C_{L_{C_F}} + C_{L_w} + C_{L_{trim}} \qquad (3.1)$$

where the reference phase is the orbital angle at the incidence hinge.

$$C_H = \frac{M_H}{q\,S\,MAC} = \frac{2\pi}{c}\,\frac{S'}{S}\,\frac{MAC'}{MAC}\left(\frac{H}{c} - \frac{1}{2}\right)k'^2\,h$$

$$+ 2\pi\,\frac{S'}{S}\,\frac{MAC'}{MAC}\,k'\left\{\left[\frac{1}{32} + \left(\frac{H}{c} - \frac{1}{2}\right)^2\right]k' - i\,\frac{1}{2}\left(\frac{3}{4} - \frac{H}{c}\right)\right\}\theta$$

$$- \frac{\pi}{2}\,\frac{S'}{S}\,\frac{MAC'}{MAC}\left\{\frac{T_4}{\pi} + \frac{d\alpha}{d\delta} + \left[\frac{T_7}{\pi} + 2\left(\frac{h}{c} - \frac{H}{c}\right)\frac{T_1}{\pi}\right]k'^2\right.$$

$$\left. + i\left[\frac{T_1}{\pi} - \frac{T_8}{\pi} - 2\left(\frac{h}{c} - \frac{H}{c}\right)\frac{T_4}{\pi} + \frac{1}{2}\,\frac{T_{11}}{\pi}\right]k'\right\}\delta$$

$$+ \left(\frac{H}{c} - \frac{1}{4}\right)C_{L_{C_F}} + \left(\frac{H}{c} - \frac{1}{4}\right)C_{L_w} + .1\,C_{L_w}\underline{\left|\pm\frac{\pi}{2}\right.} + C_{H_{trim}}$$

$$= C_{H_{NC_F}} + C_{H_{C_F}} + C_{H_0} + C_{H_{trim}} \qquad (3.2)$$

where two important observations are in order:

- Eq. (3.2) yields the hinge moment presented to the incidence control system; in the craft equations of motion (S'/S) X (MGC'/C) factor becomes unit in the non-circulatory heave and pitch terms
- The orbital motion term is doubtful.

The reference phase is the orbital angle at the hinge

$$C_h = \frac{M_h}{q\,S_f\,c_f} = \frac{b}{b'}\left(\frac{c}{c_f}\right)^2\frac{M_h}{q\,Sc} = \frac{\pi}{c}\left(\frac{c}{c_f}\right)^2\frac{T_1}{\pi}\,k'^2\,h$$

$$+ \pi\left(\frac{c}{c_f}\right)^2 k'\left\{\frac{T_{13}}{\pi}\,k' + i\,\frac{1}{2}\left[\frac{2}{\pi}\left(T_9 - \frac{a}{2}\,T_4\right) + \frac{1}{2}\,\frac{T_4}{\pi} + \frac{T_1}{\pi}\right]\right\}\theta$$

$$+ \left\{C_{h_\delta} - \frac{d\alpha}{d\delta}\,C_{h_\alpha} - \frac{1}{2}\left(\frac{c}{c_f}\right)^2\frac{T_3}{\pi}\,k'^2 + i\,\frac{\pi}{4}\left(\frac{c}{c_f}\right)^2\frac{T_4}{\pi} - \frac{T_{11}}{\pi}\,k'\right\}\delta$$

$$+ C_{h_\alpha} \left\{ -i\frac{2}{c} k' h + \left[1 + i\,2\left(\frac{3}{4} - \frac{H}{c}\right)k' \right]\theta + \left[\frac{d\alpha}{d\delta} + i\frac{1}{2}\frac{T_{11}}{\pi} k' \right] \delta \right\} C(k)$$

$$+ C_{h_\alpha} \frac{w_g}{V} G(k) \underline{\left| 2\frac{H}{c} k - \frac{1}{2} k \right.} + C_{h_{trim}} = C_{h_{NC_F}} + C_{h_{C_F}} + C_{h_w} + C_{h_{trim}} \qquad (3.3)$$

where the orbital motion term is doubtful and the reference phase is the orbital angle at the incidence hinge.

Theodorsen's "T" coefficients are tabulated in Table 3-1 for certain flap chords.

Jones' foil motion function as given by Eq. (39) and by the inverse wavelength transform of Eq. (30) of Reference 3-2 may be written

$$C(k)_{A=\infty} = 1 - \frac{i\,.165\,k}{.045 + i\,k} - \frac{i\,.335\,k}{.3 + i\,k}$$

$$C(k)_{A=6} = 1 - \frac{i\,.361\,k}{.381 + i\,k}$$

$$C(k)_{A=3} = 1 - \frac{i\,.283\,k}{.54 + i\,k} \qquad (3.4)$$

where the 2-dimensional equation is Theodorsen's function.

Jones' gust functions as given by the inverse wavelength transform of Eq. (28) of Reference 3-2 may be written

$$G(k)_{A=\infty} = 1 - \frac{i\,.236\,k}{.058 + i\,k} - \frac{i\,.513\,k}{.364 + i\,k} - \frac{i\,.171\,k}{2.42 + i\,k}$$

$$G(k)_{A=6} = 1 - \frac{i\,.448\,k}{.29 + i\,k} - \frac{i\,.272\,k}{.725 + i\,k} - \frac{i\,.193\,k}{3 + i\,k}$$

$$G(k)_{A=3} = 1 - \frac{i\,.679\,k}{.558 + i\,k} - \frac{i\,.227\,k}{3.2 + i\,k} \qquad (3.5)$$

where the 2-dimensional equation is Stark's function and Bisplinghoff's Eq. (5-376), Reference 3-4, except for phase reference; Jones references phase to the orbital angle at the leading edge while Sears and Bisplinghoff reference the orbital angle at the half-chord.

k is the reduced inverse wavelength, defined as

$$k = \frac{\pi}{\lambda/c} \tag{3.6}$$

k' is the reduced frequency, defined as

$$k' = \omega \frac{c}{2V}$$

$$= 2\pi \frac{V_e}{\lambda} \frac{c}{2V} = \frac{\pi}{\lambda/c} \frac{V \pm c_w}{V}$$

$$= k \left(1 \pm \frac{c_w}{V}\right) \tag{3.7}$$

Heave, pitch, flap deflection, and orbital angle are vectors. The orbital angle at the incidence hinge is the reference phase. The lift curve slope is also a vectorial function of depth but the non-linearity introduced by the lift curve slope is not explored in this volume.

The components of Eqs. (3.1) - (3.3) are considered in detail in the three following sections.

3.1 REFERENCES

3-1 T. Theodorsen, "General Theory of Aerodynamic Instability and the Mechanism of Flutter," NACA Report 496, 1935. Currently available in AIAA Selected Reprints, "Aerodynamic Flutter," I. E. Garrick, Editor, March 1969.

3-2 R. T. Jones, "The Unsteady Lift of a Wing of Finite Aspect Ratio," NACA Report 681, 1939.

3-3 "USAF Stability and Control Methods" (DATCOM), Douglas Aircraft Co., 1965.

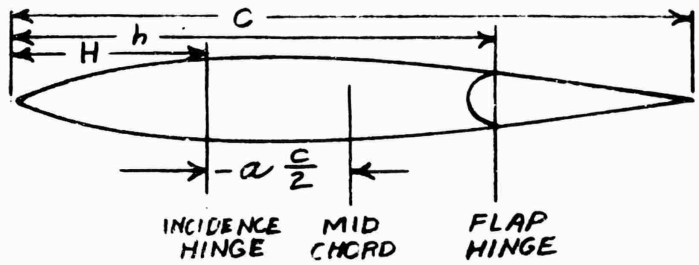
3-4 Bisplinghoff, Ashley, and Halfman, "Aeroelasticity," Addison-Wesley, 1957.

TABLE 3-1 VALUES OF T

$\frac{c_f}{c}$	$\frac{h}{c}$	$-\frac{T_1}{\pi}$	$-T_2/\pi$ & $-T_6/\pi$	$-\frac{T_3}{\pi}$	$-\frac{T_4}{\pi}$	$-\frac{T_5}{\pi}$	$\frac{T_7}{\pi}$	$\frac{T_8}{\pi}$	$T_9 - \frac{a}{2}T_4$	T_{10}/π NOTE 1	$\frac{T_{11}}{\pi}$	T_{12}/π NOTE 2
0	1	0	0	0	0	0	0	0	0	0	0	0
.05	.95	.000751	.000560	.0000281	.01869	.01259	.000316	.00804	.01380	.2823	.03777	.0003838
.1	.9	.00420	.00443	.000445	.05204	.04976	.001439	.01872	.03600	.3958	.1063	.002195
.15	.85	.01145	.01480	.002235	.09406	.1106	.003018	.02720	.06070	.4805	.1942	.006121
.2	.8	.02322	.03469	.00700	.1424	.1941	.004285	.03110	.08533	.5498	.2975	.01272
.25	.75	.0401	.0669	.01693	.1955	.2991	.004218	.02883	.10825	.6090	.4135	.02249
.3	.7	.0624	.1142	.03478	.2523	.4246	.001607	.01924	.12831	.6607	.5406	.03595
.4	.6	.1249	.2637	.1077	.3735	.7317	-.01672	-.02509	.15677	.7478	.8229	.07586
.5	.5	.2122	.5	.2573	.5	1.1037	-.06250	-.1061	.16667	.8183	1.1366	.1366
.6	.4	.3249	.8358	.5210	.6265	1.5263	-.1483	-.2251	.15677	.8760	1.4759	.2229
.7	.3	.4625	1.2781	.9402	.7477	1.9808	-.2866	-.3808	.12831	.9227	1.8359	.3406
.75	.25	.5401	1.5392	1.2215	.8045	2.2124	-.3792	-.4712	.10825	.9423	2.0225	.4135
.8	.2	.6232	1.8255	1.5576	.8576	2.4411	-.4893	-.5689	.08533	.9595	2.2127	.4975
.85	.15	.7115	2.1348	1.9533	.9059	2.6612	-.6180	-.6728	.06070	.9741	2.4061	.5942
.9	.1	.8042	2.4632	2.4128	.9480	2.8643	-.7664	-.7813	.03600	.9861	2.6022	.7063
.95	.05	.9008	2.8040	2.9394	.9813	3.0367	-.9353	-.8920	.01380	.9952	2.8004	.8378
1	0	1	π	3.5343	1	π	-1.1250	-1	0	1	3	1

NOTES: 1. $T_{10}/\pi = d\alpha/d\delta$

2. $T_{12}/\pi = -\frac{2}{\pi}\left(\frac{c_f}{c}\right)^2 C_{h_\alpha}$ which is substituted for T_{12}/π in this report.



$T_6 = T_2$

$T_9 - \frac{a}{2}T_4 = T_9 - \left(\frac{H}{c} - \frac{1}{2}\right)T_4$

$T_{13} = -\frac{1}{2}\left[T_7 + 2\left(\frac{h}{c} - \frac{H}{c}\right)T_1\right] = -\frac{1}{2}T_7 - \left(\frac{h}{c} - \frac{H}{c}\right)T_1$

$T_{14} = \frac{1}{2}\left(2\frac{H}{c} - 1\right)\left(2\frac{h}{c} - 1\right) + \frac{1}{16} = 2\left(\frac{H}{c} - \frac{1}{2}\right)\left(\frac{h}{c} - \frac{1}{2}\right) + \frac{1}{16}$

Theodorsen's $c = 2\frac{h}{c} - 1$

Theodorsen's $a = 2\frac{H}{c} - 1$

4. TRIM CHARACTERISTICS

4.1 LIFT CURVE SLOPE

Reference 4-1 is employed to estimate the lift and pitching moment characteristics of the foil/pod combination. Theoretically this reference is valid only for blunt-based bodies but experience has shown that the pod does contribute lift in excess of that corresponding to the shrouded foil area and that excess cannot be accounted for by the potential characteristics of the streamlined body. Similarly, Reference 4-1 has provided correlation for the pitching moment characteristics for configurations similar to the AG(EH). Experience indicates, then, that the blunt based pod provides a practical approximation for the streamlined pod with its wake for the pitch case.

The section lift curve slope presents a more serious unknown, particularly for the 16-series section. The 16-section characteristics employed here are from Reference 4-2 but all of the data of Reference 4-2 except that at a Reynolds number of $.85 \times 10^6$ is subject to obvious Mach number effects while any laminar flow section data is subject to Reynolds number effects at Reynolds numbers of less than about one million. Thus the use of section data measured at .85 million RN and model data measured at 3 - 4 million RN to predict prototype performance at 30 - 40 million RN reflects significant uncertainties throughout the prototype foil characteristics.

Reference 4-1 presents the pitch lift curve slope as the sum of foil, body, and nose slopes:

$$C_{L_\alpha} = C_{L_\alpha}{}_{foil} + C_{L_\alpha}{}_{pod} + C_{L_\alpha}{}_{nose}$$

$$= \frac{S'}{S} K_{W(B)} C'_{L_\alpha} + \frac{S'}{S} K_{B(W)} C'_{L_\alpha} + \frac{S_N}{S} C_{L_\alpha}{}_{B} \qquad (4.1.1)$$

where:

S = reference area = area of complete foil

S' = area of exposed foil

S_N = pod frontal area = $\pi D^2/4$

C_{L_α}' = exposed foil lift curve slope

D/b = pod diameter/foil span ratio

$C_{L_{\alpha_B}}$ = blunt based pod lift curve slope based on frontal area = 2 from classic potential theory

$K_{W(B)}$ = pod lift carry-over to foil, Chart 1, Reference 4-1

$K_{B(W)}$ = foil lift carry-over to pod, Chart 1, Reference 4-1

Eq. (4.1.1) is evaluated in Table 4-1 for the AG(EH) forward and aft configurations. The results differ from that for the complete foil neglecting the pod by 3.37% fwd and 1.5% aft which is not significant but the values of Eq. (4.1.1) are assumed hereafter for consistency with the moment calculations.

Reference 4-1 presents the incidence lift curve slope as the sum of foil and body slopes:

$$C_{L_i} = C_{L_{i_{foil}}} + C_{L_{i_{pod}}}$$

$$= \frac{S'}{S} k_{W(B)} C_{L_\alpha}' + \frac{S'}{S} k_{B(W)} C_{L_\alpha}' \qquad (4.1.2)$$

where $k_{W(B)}$ and $k_{B(W)}$ are from Chart 1 of Reference 4-1

The incidence lift curve slopes are also evaluated in Table 4-1. The incidence lift curve slopes differ from the pitch lift slopes by 16% fwd and 22% aft which is a significant difference and one which must be observed as required. It is to be noted, however, that the AG(EH) aft foil and pod are rigidly attached, the incidence control motion is between pod and strut, so that the incidence lift curve slope is never required for this configuration.

For the 20% chord, sealed gap flaps proposed for the fwd foils, a flap effectiveness of .47 was taken from Figure 18 of Reference 4-3 and the flap curve slope becomes:

$$C_L = \frac{d\alpha}{d\delta} C_{L_i}$$

$$= .47 \times 2.49$$

$$= 1.17 \qquad (4.1.3)$$

The lift curve slopes of Eqs. (4.1.1) - (4.1.3) are aerodynamic; i.e., infinite depth. The hydrodynamic pitch lift curve slopes were measured for the fwd and aft foils at three depths and two speeds each for Reference 4-4 with the results presented in Figures I-30 and I-31 of that Reference and on Figure 4-1 of this report. Also presented on Figure 4-1 are the free surface effect predictions of References 4-5 - 4-8. These four predictions present distinctive aerodynamic (infinite depth) lift curve slopes which have been adjusted to the lift curve slope of Eq. (4.1.1) on Figure 4-1; i.e., each prediction has been employed in the form $C_{L_\alpha}/C_{L_{\alpha_\infty}}$.

In considering these slopes, it must be recognized that hydrodynamic lift curve slopes can only be measured with a precision on the order of $\pm$ 5% so the entire spread of predictions on Figure 4-1 is scarcely significant. Nevertheless the 50-knot forward foil results of Figure 4-1 appear doubtful and this reflects on the other characteristics associated with these measurements.

The incidence lift curve slope was measured only for the fwd foil in Reference 4-4 but there are independent measurements at two depths in Reference 4-9 and these are compared with the predictions on Figure 4-2.

The tapered, swept foil free surface effect has received inadequate attention in the literature and the incidence lift case, particulary, presents a problem in selecting the reference chord for depth effect. The MAC is preferred over the MGC as a reference in this report and on Figure 4-2 the MAC for the entire foil is employed rather than the exposed foil MAC simply because it provides a better comparison with the predictions.

From Figures 4-1 and 4-2 the Panchenkov free surface effect has been selected as the definition for this effect. By employing a common definition for pitch and incidence lift free surface effect, the ratio between the two lift curve slopes becomes independent of depth and for the AG(EH) fwd foil is defined by:

$$\frac{C_{L_i}}{C_{L_\alpha}} = \frac{C_{L_{i_\infty}}}{C_{L_{\alpha_\infty}}} = \frac{2.49}{2.97} = .838 \qquad (4.1.4)$$

The lift curve slope is independent of camber so the experimental results considered thus far can be expected to be representative of the prototype except for the unknown Reynolds number effect. In the consideration of foil and flap angles below, however, we must recognize that the model and prototype have different cambers.

4.2 RESIDUAL LIFT

In the linear lift range the lift curve is conveniently expressed in slope-intercept form where the intercept may be on the angle of attack scale at the zero lift angle of attack or on the lift coefficient scale at the residual lift; i.e., the lift when pitch, incidence, and flap are zero. The slope-residual lift form of the lift curve is most convenient where there is more than one angle involved and in this report the lift curve is considered in the form

$$C_L = C_{L_\alpha}\alpha + C_{L_i} i + C_{L_\delta}\delta + C_{L_0}$$

$$= C_{L_\alpha}\left[\alpha + \frac{C_{L_i}}{C_{L_\alpha}}\left(i + \frac{d\alpha}{d\delta}\delta\right)\right] + C_{L_{i_{eff.}}} + C_{L_{pod}} \qquad (4.2.1)$$

$C_{L_{i_{eff}}}$ is not known, in general, in the presence of a pod and particularly in the presence of a free surface. It is approximated in this report by

$$C_{L_{i_{eff}}} = -C_{L_i}\alpha_{c_\ell=0} \qquad (4.2.2)$$

where the section zero lift angle of attack for most sections is available in Reference 4-10. The only comparable source available to this report for the 16-series sections was Reference 4-2 and the zero lift angles in this report are from an unpublished summary of the data of Reference 4-2 for a .3 Mach number and $.85 \times 10^6$ Reynolds number.

$C_{L_{pod}}$ is the lift due to pod asymmetry and to the pod/foil asymmetry in theory but includes difficiencies in the approximation of Eq. (4.2.2) in practice.

For the fwd. foil model of Reference 4-4, Eq. (4.2.1) becomes

$$C_L = C_{L_\alpha}\left(\alpha + \frac{C_{L_i}}{C_{L_\alpha}} i\right) - C_{L_i}\,\alpha_{c_\ell = 0} + C_{L_{pod}}$$

$$\frac{C_L}{C_{L_\alpha}} = \alpha + \frac{C_{L_i}}{C_{L_\alpha}} i - \frac{C_{L_i}}{C_{L_\alpha}}\,\alpha_{c_\ell = 0} + \frac{C_{L_{pod}}}{C_{L_\alpha}} \qquad (4.2.3)$$

and at zero lift

$$i_{C_{L=0}} = \alpha_{c_\ell = 0} - \frac{C_{L_{pod}}}{C_{L_i}} - \frac{C_{L_\alpha}}{C_{L_i}}\,\alpha \qquad (4.2.4)$$

The measured zero lift incidence angles of Reference 4-4 are presented in the form of Eq. (4.2.4) on Figure 4-3. The difference between the 35 and 50 knot results on Figure 4-3 is incredible, particularly for deep submergence, and the 50-knot results are discarded because they are suspect on Figure 4-1. The 35-knot results indicate that the pod lift is a function of depth in the same way that C_{L_i} is; i.e., $C_{L_{pod}}/C_{L_i}$ is a constant and the pod lift can be expressed as

$$C_{L_{pod}} = -\,C_{L_i}(\alpha\, C_{L_{pod}} = 0) \qquad (4.2.5)$$

where

$$\alpha\, C_{L_{pod}} = 0 = -2.25 - (-2.92)$$

$$= .67^o$$

and where this angle is assumed to be independent of the foil camber.

For the aft foil model of Reference 4-4 Eq. (4.2.1) becomes

$$C_L = C_{L_\alpha} \alpha - C_{L_i} \alpha_{c_\ell = 0} + C_{L_{pod}}$$

$$\frac{C_L}{C_{L_\alpha}} = \alpha - \frac{C_{L_i}}{C_{L_\alpha}} \alpha_{c_\ell = 0} + \frac{C_{L_{pod}}}{C_{L_\alpha}} \qquad (4.2.6)$$

and at zero lift

$$\alpha_{C_L = 0} = \frac{C_{L_i}}{C_{L_\alpha}} \alpha_{c_\ell = 0} - \frac{C_{L_{pod}}}{C_{L_\alpha}} \qquad (4.2.7)$$

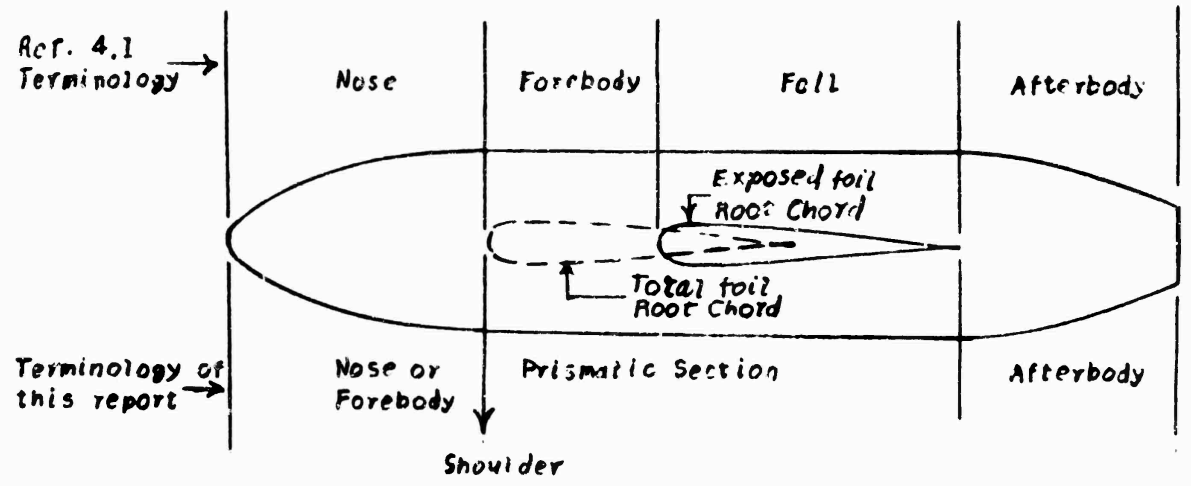
The measured zero lift angles of Reference 4-4 for the aft foil model are presented on Figure 4-4 in the form of Eq. (4.2.7). The results are rather badly scattered and for this report it is assumed from Figure 4-4 that the pod lift is zero.

The foil lift curve results are summarized in Table 4-1.

4.3 FOIL PITCHING MOMENT SLOPE

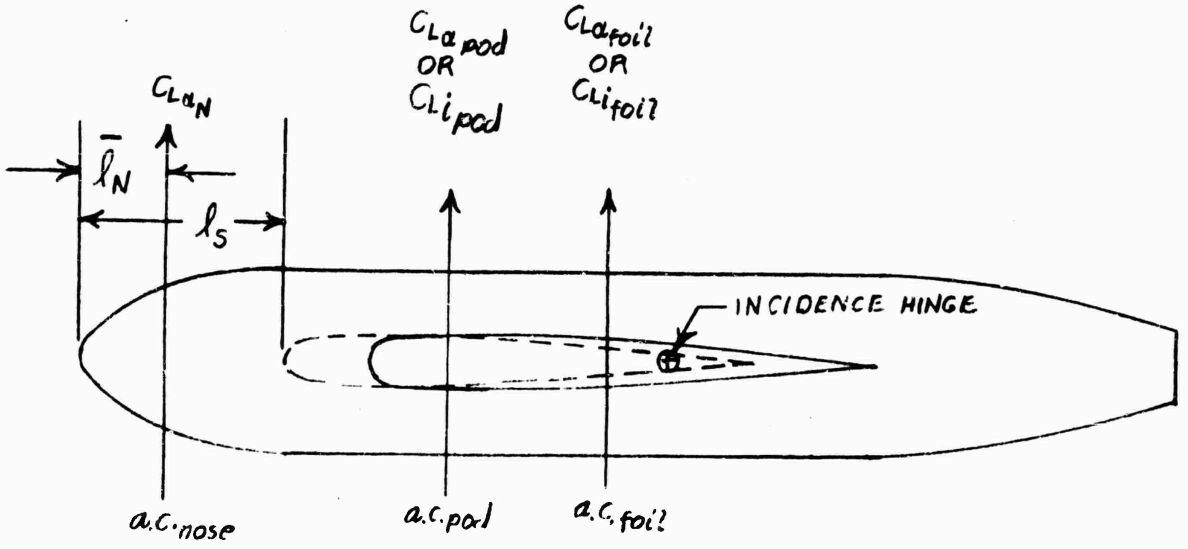
Grumman Aerospace Corporation practice with pods is to locate the shoulder, the first point of maximum diameter, at the foil root chord leading edge (center of pod). Whether that practice is reflected in the "as-built" AG(EH) or not is uncertain. Undefined pod changes are noted in the design history (Reference 4-11) and Figures 1 and I.1 of the model test report (Reference 4-4) conflict on this point. Prototype production prints available to date do not clarify the issue. It must be noted that the methods of Reference 4-1 are invalid if the shoulder is not forward of the exposed foil root chord leading edge.

In this report the terms "forebody" and "nose" are considered synonymous and the pod is divided into a forebody, prismatic section, and afterbody. Thus Reference 4-1 terminology is related to the terminology of this note as follows:



It must be noted that the "centers of pressure" of Reference 4-1 are centers of pressure only for foils of symmetric section or in the context of the thin airfoil theory of that reference. In the more general case of the cambered foil, the centers of pressure of Reference 4-1 must be designated as aerodynamic centers and they are so regarded in this report.

Reference 4-1 defines the moments acting on the total configuration by locating the aerodynamic center associated with each of the three loads identified by Eqs. (4.1.1) and (4.1.2).



Reference 4-1 states that the aerodynamic center for the foil lift is unknown in the general case and is best approximated by employing the aerodynamic center for the exposed foil. Referring to Figures 1-2 and 1-3, then, the AG(EH) foil lift aerodynamic centers are located on the total foil mean aerodynamic chord at

$$\text{a.c.}_{\text{foil}_1} = \frac{8.10 - 4.93}{9.33} = \frac{3.17}{9.33} = .340$$

$$\text{a.c.}_{\text{foil}_2} = \frac{4.167 - 2.245}{4.81} = \frac{1.622}{4.81} = .337 \qquad (4.3.1)$$

In general the nose lift aerodynamic center is located by

$$\bar{\ell}_N = \ell_S - V_S/S_N \qquad (4.3.2)$$

Reference 4-1 gives the aerodynamic center for ogival noses in Chart 9. Ellipsoidal noses were specified for the AG(EH) and are assumed here though the "as built" nose lines were not available for this report. For ellipsoidal noses, the aerodynamic center is located 1/3 of the nose length aft of the leading edge. Referring to Figures 1-2 and 1-3, the AG(EH) nose aerodynamic centers are located on the total foil mean aerodynamic chord at

$$\text{a.c.}_{\text{nose}_1} = -\left(\frac{4.93 + 2/3 \times 3.766}{9.33}\right) = -\frac{4.93 + 2.51}{9.33} = -\frac{7.44}{9.33} = -.797$$

$$\text{a.c. nose}_2 = -\left(\frac{2.545 + 2/3 \times 2.867}{4.81}\right) = -\frac{2.545 + 1.91}{4.81} = -\frac{4.555}{4.81} = -.925$$

(4.3.3)

The location for the body lift aerodynamic center is a tedious calculation, particularly for low aspect ratio foils. These calculations are presented in Appendix A where Eq. (A16) gives the result:

$$\text{a.c.}_{\text{pod}_1} = .1325$$

$$\text{a.c.}_{\text{pod}_2} = .163 \qquad (4.3.4)$$

In general these aerodynamic centers in combination with the lift curve slopes of Table 4-1 produce a total aerodynamic center defined by

$$\text{a.c.} = \frac{H}{c} - \frac{\sum \left(\frac{H}{c} - \text{a.c.}\right) \left(C_{L_\alpha} \text{ or } C_{L_i}\right)}{\sum \left(C_{L_\alpha} \text{ or } C_{L_i}\right)} \tag{4.3.5}$$

where the terms of the numerator and denominator are determined by the type of lift involved and by the application to be made of the aerodynamic center and where the terms of numerator and denominator do not necessarily correspond.

Noting that

$$C_{H_\alpha} = \left(\frac{H}{c} - \text{a.c.}\right) C_{L_\alpha} \quad \text{or} \quad C_{H_i} = \left(\frac{H}{c} - \text{a.c.}\right) C_{L_i}$$

$$C_{H_{C_L}} = \frac{dC_H}{dC_L} = \frac{H}{c} - \text{a.c.} \tag{4.3.6}$$

Eq. (4.3.5) simply states that

$$\text{total } C_{H_{C_L}} = \frac{\sum \text{component } C_{H_\alpha}}{\sum \text{component } C_{L_\alpha}} \tag{4.3.7}$$

The forward foil hinge moment slopes of interest to the AG(EH) are numerically evaluated in Table 4-2 which illustrates the application of Eq. (4.3.7) for the case where incidence lift control is achieved by moving the foil relative to the pod. For the AG(EH) aft foil, where foil and pod are rigidly attached, there is no "incidence lift" case and Eq. (4.3.7) becomes simply:

$$C_{H_{C_L}} = \frac{\left(\frac{H}{c} - \text{a.c.}_{\text{foil}}\right) C_{L_\alpha}{}_{\text{foil}} + \left(\frac{H}{c} - \text{a.c.}_{\text{pod}}\right) C_{L_\alpha}{}_{\text{pod}} + \left(\frac{H}{c} - \text{a.c.}_{\text{nose}}\right) C_{L_\alpha}{}_{\text{nose}}}{C_{L_\alpha}}$$

$$= \frac{(.336 - .337)\,2.385 + (.336 - .163)\,.501 + (.336 + .925)\,.1326}{3.015}$$

$$= \frac{-\,.001 \times 2.385 + .173 \times .501 + 1.261 \times .1326}{3.015}$$

$$= \frac{-\,.002385 + .0868 + .1671}{3.015} = \frac{.2515}{3.015}$$

$$= .0834 \qquad (4.3.8)$$

The hinge moment slopes of Figures I-8 through I-17 of Reference 4-4 are presented on Figure 4-5 as aerodynamic center for this case from Table 4-2. Figure 13 of Reference 4-15 indicates that there is an uncertainty range of about + 5%, - 1% of MAC associated with the aerodynamic center prediction and this range has bracketed previous experience with this characteristic. Figure 4-5 indicates, however, that the prediction error in this case barely lies within even the more conservative uncertainty range of Reference 4-1.

The hinge moment aerodynamic center prediction for pitch lift of Table 4-2 is compared with the measured slopes of Figures B1 through B6 of Appendix B on Figure 4-6. The result is the same as for incidence lift; the two cases present about the same a.c., as theory indicates, but both aerodynamic centers are well forward of the expected position. Similarly, the measured aft foil aerodynamic center measured by the slopes of Figures I-4 through I-7 of Reference 4-4 lie well ahead of the predicted position as shown on Figure 4-7.

The suspect term in these calculations is the exposed foil aerodynamic center and the "measured" characteristics of Table 4-2 proceed from the measured characteristics by appropriate adjustment to the exposed foil aerodynamic center. It is proposed that this aerodynamic center location be estimated by integrating the pitch and incidence spanwise load distributions outboard the pod. This is not a difficult procedure but time does not permit such a procedure for this report.

4.4 RESIDUAL FOIL PITCHING MOMENT

The moment about the aerodynamic center is assumed to be

$$C_{M_{a.c._{eff}}} = \frac{MAC'}{MAC}\frac{S'}{S} C_{M_{a.c.}}$$

$$= \frac{-MAC'}{MAC}\frac{S'}{S} c_{\ell_{i_{eff}}} \qquad (4.4.1)$$

where, from an unpublished compilation of the .3 Mach Number, $.85 \times 10^6$ Reynolds number data of Reference 4-2, the effective design lift coefficient for an 8% 16-series is taken to be 83% of the design lift coefficient.

Then the hinge moment for the AG(EH) aft foil may be written:

$$C_H = C_{H_\alpha}\,\alpha + C_{H_0} \qquad (4.4.2)$$

where

$$C_{H_0} = C_{M_{a.c._{eff}}} + C_{M_{pod}}$$

$C_{M_{pod}}$ is the unpredictable pod effect.

To account for depth effect on the lift curve slope, this equation must be employed in the form:

$$C_H = C_{L_\alpha}\left(\frac{H}{c} - a.c.\right)\alpha + C_{H_0} \qquad (4.4.3)$$

At zero lift the aft foil hinge moment is:

$$C_{H_{C_L = 0}} = C_{L_\alpha}\left(\frac{H}{c} - a.c.\right)\left(-\frac{C_{L_0}}{C_{L_\alpha}}\right) + C_{H_0}$$

$$= -\left(\frac{H}{c} - a.c.\right) C_{L_0} + C_{H_0} = C_{M_{a.c._{eff}}} + C_{M_{pod}}$$

(4.4.4)

This equation is compared with the measured model zero lift hinge moments on the lowest graph of Figure 4-8. The reduction in hinge moment indicated on that plot for a fixed transition is in the expected direction but the possibility of premature transition on the prototype has profound implications for drag and cavitation, as well as for incidence and flap moments, which are beyond the scope of the present study.

The systematic variation of zero lift hinge moment with depth is of interest here. In an attempt to account for this variation, Eq. (4.4.4) was considered in the form:

$$\frac{C_{L_{\alpha_\infty}}}{C_{L_\alpha}} C_{H_{C_{L=0}}} = C_{M_{a.c._{eff.}}} + C_{M_{pod}} \qquad (4.4.5)$$

The result, also presented on Figure 4-8, indicates that the moment coefficient about the aerodynamic center is subject to the same free surface effect as the lift curve slope; i.e., $C_{M_{a.c.}}/C_{M_{a.c._\infty}} = C_{L_\alpha}/C_{L_{\alpha_\infty}}$. From Figure 4-8 a value of $-.0055$ is taken as $C_{M_{pod}}$.

For the more general case with incidence motion relative to the pod, the hinge moment is

$$C_H = C_{H_\alpha}\,\alpha + C_{H_i}\,i + C_{H_0}$$

$$= C_{H_\alpha}\,\alpha + C_{H_i}\,i + C_{M_{a.c._{eff}}} + C_{M_{pod}} + C_{H_{C_{L_i}}} C_{L_0} \qquad (4.4.6)$$

where:

$$C_{M_{a.c._{eff}}} = \frac{S'}{S} C_{M_{a.c.}}$$

$$= \frac{S'}{S}(-\tfrac{1}{4} C_{L_{i_{eff}}}) \text{ for a = 1.0 chord line}$$

$$C_{L_{i_{eff}}} = .83\, C_{L_i} \text{ for 8\% 16-series section on a = 1.0}$$

$$C_{M_{pod}} = \text{unpredictable pod effect}$$

For the purpose of examining the model data Eq. (4.4.6) may be written:

$$C_H = C_{L_\alpha}\left(\frac{H}{c} - a.c._{\alpha_H}\right)\alpha + C_{L_i}\left(\frac{H}{c} - a.c._{i_H}\right) i + C_{H_0}$$

$$C_{H_{C_L = 0}} = C_{L_\alpha}\left(\frac{H}{c} - a.c._{\alpha_H}\right)\alpha + C_{L_i}\left(\frac{H}{c} - a.c._{i_H}\right) i_{C_L = 0} + C_{H_0} \tag{4.4.7}$$

where:

$$C_L = C_{L_\alpha}\,\alpha + C_{L_i}\, i + C_{L_0} = 0$$

$$C_{L_i}\, i_{C_L = 0} = - C_{L_0} - C_{L_\alpha}\,\alpha$$

$$i_{C_L = 0} = - \frac{C_{L_0}}{C_{L_i}} - \frac{C_{L_\alpha}}{C_{L_i}}\,\alpha \tag{4.4.8}$$

Then Eq. (4.4.7) may be written:

$$C_{H_{C_L = 0}} = C_{L_\alpha}\left(\frac{H}{c} - a.c._{\alpha_H}\right)\alpha + C_{L_i}\left(\frac{H}{c} - a.c._{i_H}\right)\left(- \frac{C_{L_0}}{C_{L_i}} - \frac{C_{L_\alpha}}{C_{L_i}}\,\alpha\right) + C_{H_0}$$

$$= \left[\left(\frac{H}{c} - a.c._{\alpha_H}\right) - \left(\frac{H}{c} - a.c._{i_H}\right)\right](C_L)_\alpha - C_{H_{C_{L_i}}} C_{L_0} + C_{M_{a.c._{eff}}}$$

$$+ C_{M_{pod}} + C_{H_{C_{L_i}}} C_{L_0}$$

$$= (a.c._{i_H} - a.c._{\alpha_H})\,(C_L)_\alpha + C_{M_{a.c._{eff}}} + C_{M_{pod}} \tag{4.4.9}$$

For the purpose of evaluating the residual hinge moment from the towing tank data, Eq. (4.4.9) was considered in the form (which assumes that C_{H_0} is subject to $C_{L_\alpha}/C_{L_{\alpha_\infty}}$):

$$C_{M_{a.c._{eff}}} + C_{M_{pod}} = \frac{C_{L_{\alpha_\infty}}}{C_{L_\alpha}} \left[C_{H_{C_L = 0}} - (a.c._{i_H} - a.c._{\alpha_H}) C_{L_\alpha} \alpha \right]$$

$$= \frac{C_{L_{\alpha_\infty}}}{C_{L_\alpha}} C_{H_{C_L = 0}} - (a.c._{i_H} - a.c._{\alpha_H}) C_{L_{\alpha_\infty}} \alpha \qquad (4.4.10)$$

The towing tank data is presented in the form of Eq. (4.4.10) on Figure 4-9 which contradicts the results of Figure 4-8 with respect to the effects of the pod and of the fixed transition. From Figure 4-9 a value of + .0151 is taken as $C_{M_{pod}}$.

4.5 COMPARISON WITH PROTOTYPE DATA

Reference 4-14 provided independent measures for the AG(EH) forward and aft lift and hinge moment curves which can be compared with theory and with the towing tank results. On the craft, however, the forward and aft lift and hinge moment are all interdependent and the buoyancy for the submerged configuration becomes of some interest.

Foil buoyancy is given by

$$B_{foil} = \frac{4}{3} K \frac{t}{c} \frac{S^{3/2}}{\sqrt{A}} \frac{1 + \lambda + \lambda^2}{(1 + \lambda)^2} \rho g$$

$$C_{B_{foil}} = \frac{8}{3} \frac{K}{V^2} \frac{t}{c} \frac{b}{A} \frac{1 + \lambda + \lambda^2}{(1 + \lambda)^2} g \qquad (4.5.1)$$

where K = section area/ct

The buoyancy coefficient is a function of the configuration size, b, and is negligible in model scale but of some significance on the prototype.

For the AG(EH) the numerical evaluation for Eq. (4.5.1) is:

$$C_{B_{foil}} = \frac{8}{3} \times \frac{.735}{V^2} \times .08 \times \frac{b}{3} \times \frac{1.39}{1.69} g$$

$$= 1.384 \frac{b}{V^2}$$

$$C_{B_{foil_1}} = 1.384 \times 26/V^2 = 35.95/V^2$$

$$C_{B_{foil_2}} = 1.384 \times 13.416/V^2 = 18.58/V^2 \qquad (4.5.2)$$

Much of the interior of the prisimatic portion of the pod, excluding the foil structure, is wet. Consequently, the buoyancy for the prismatic portion of the pod is approximated here by employing the buoyancy of the total foil and neglecting the prismatic pod portion entirely.

The pod buoyancy employed here, then is

$$B_{pod} \approx 2/3 \times \frac{\pi}{4} D^2 (1 - \ell_{prism}) \rho g$$

$$= \frac{\pi D^2}{6} (1 - c_r) \rho g$$

$$C_{B_{pod}} = \frac{\pi D^2}{2 S V^2} (1 - c_r)$$

$$C_{B_{pod_1}} = \frac{\pi (3\ 1/3)^2 g}{3 \times 225 V^2} (26.812 - 13.314) = 22.5/V^2$$

$$C_{B_{pod_2}} = \frac{\pi (2\ 1/4)^2 g}{3 \times 60 V^2} (13 - 6.868) = 17.45/V^2 \qquad (4.5.3)$$

By reference to Sheet 22 of Reference 4-16 and to Foil Contract Guidance Plan (AG(EH) 800-2068282, Hydrofoil System Geometry - Structural Arrangement, it was determined that:

$$d_1 = 16.32 - \text{height} \qquad \text{(any pitch)}$$

$$d_2 = 14.82 - \text{height} \qquad \text{(pitch = 0)} \tag{4.5.4}$$

The pitch reference axis is assumed. For the conditions of Figures 1 - 3 of Reference 4-14, then, the foil depths are:

$$d_1 = 11.32 = 1.215 \text{ MAC}$$

$$d_2 = 9.82 + 125.87/57.3 = 12.015 = 2.495 \text{ MAC} \tag{4.5.5}$$

The average submerged strut thickness ratio is

$$\left(\frac{t}{c}\right)_1 = .1 + .002265\left(d - \frac{D}{2}\right)$$

$$\left(\frac{t}{c}\right)_2 = .1 + .00238\left(d - \frac{D}{2}\right) \tag{4.5.6}$$

Then the strut buoyancy is given by

$$B_{strut} = K c^2 \left(\frac{t}{c}\right)_{avg} \rho g \left(d - \frac{D}{2}\right)$$

$$C_{B_{strut}} = \frac{2Kc^2 \frac{t}{c}_{avg} g}{V^2 s}\left(d - \frac{D}{2}\right)$$

$$C_{B_{strut_1}} = \frac{2 \times .735(11.75)2g}{225V^2}(11.32 - 1.667)[.1 + .002265(11.32 - 1.667)] = 34.15/V^2$$

$$C_{B_{strut_2}} = \frac{2 \times .735(6)2g}{60V^2}(12.015 - 1.125)[.1 + .00238(12.015 - 1.125)] = 38.9/V^2 \tag{4.5.7}$$

and the total buoyancy coefficients become

$$C_{B_1} = (35.95 + 22.50 + 34.15)/V^2 = 92.6/V^2 = 32.5/V_K^2$$

$$C_{B_2} = (18.58 + 17.45 + 38.9)/V^2 = 74.9/V^2 = 26.3/V_K^2 \qquad (4.5.8)$$

With the buoyancy coefficient defined, the balance of lift forces on the craft may be written:

$$L_1 + B_1 + L_2 + B_2 = W$$

$$\frac{S_1}{S} C_{L_1} + \frac{S_2}{S} C_{L_2} = \frac{W}{q S} - \frac{S_1}{S} C_{B_1} - \frac{S_2}{S} C_{B_2}$$

$$\frac{S_1}{S}(C_{L_{\alpha_1}} \theta + C_{L_{i_1}} i_1 + C_{L_{0_1}}) + \frac{S_2}{S}(C_{L_{\alpha_2}} \theta + C_{L_{\alpha_2}} i_2 + C_{L_{0_2}}) = \frac{W}{q S} - C_B$$

$$\frac{S_1}{S} C_{L_{i_1}} i_1 + \frac{S_2}{S} C_{L_{\alpha_2}} i_2 = \frac{W}{q S} - C_B - \left(\frac{S_1}{S} C_{L_{\alpha_1}} + \frac{S_2}{S} C_{L_{\alpha_2}}\right) \theta - \left(\frac{S_1}{S} C_{L_{0_1}} + \frac{S_2}{S} C_{L_{0_2}}\right)$$

$$= \frac{W}{q S} - C_B - C_{L_\alpha} \theta - C_{L_0}$$

$$\frac{S_1}{S} C_{L_{i_1}} i_1^{\circ} + \frac{S_2}{S} C_{L_{\alpha_2}} i_2^{\circ} = \frac{57.3 W}{q S} - 57.3\, C_B - C_{L_\alpha} \theta^{\circ} - 57.3\, C_{L_0} \qquad (4.5.9)$$

The moment balance, neglecting the thrust/drag moment, may be written:

$$\ell_1(L_1 + B_1) + M_{H_{trim_1}} - \ell_2(L_2 + B_2) + M_{H_2} = 0$$

$$\frac{\ell_1}{\ell} \frac{S_1}{S}(C_{L_1} + C_{B_1}) + \frac{MAC_1}{\ell} \frac{S_1}{S} C_{H_{trim_1}} - \frac{\ell_2}{\ell} \frac{S_2}{S}(C_{L_2} + C_{B_2}) + \frac{MAC_2}{\ell} \frac{S_2}{S} C_{H_2} = 0$$

$$\frac{\ell_1}{\ell}\frac{S_1}{S}C_{L_1} + \frac{MAC_1}{\ell}\frac{S_1}{S}C_{H_{trim_1}} - \frac{\ell_2}{\ell}\frac{S_2}{S}C_{L_2} + \frac{MAC_2}{\ell}\frac{S_2}{S}C_{H_2}$$

$$= -\left(\frac{\ell_1}{\ell}\frac{S_1}{S}C_{B_1} - \frac{\ell_2}{\ell}\frac{S_2}{S}C_{B_2}\right)$$

$$\frac{\ell_1}{\ell}\frac{S_1}{S}(C_{L_{\alpha_1}}\theta + C_{L_{i_1}}i_1 + C_{L_{0_1}}) + \frac{MAC_1}{\ell}\frac{S_1}{S}(C_{H_{\alpha_{trim_1}}}\theta + C_{H_{i_{trim_1}}}i_1 + C_{H_{0_1}})$$

$$-\frac{\ell_2}{\ell}\frac{S_2}{S}(C_{L_{\alpha_2}}\theta + C_{L_{\alpha_2}}i_2 + C_{L_{0_2}}) + \frac{MAC_2}{\ell}\frac{S_2}{S}(C_{H_{\alpha_2}}\theta + C_{H_{\alpha_2}}i_2 + C_{H_{0_2}}) = -C_{M_B}$$

$$\frac{S_1}{S}\left(\frac{\ell_1}{\ell}C_{L_{i_1}} + \frac{MAC_1}{\ell}C_{H_{i_{trim_1}}}\right)i_1 - \frac{S_2}{S}\left(\frac{\ell_2}{\ell}C_{L_{\alpha_2}} - \frac{MAC_2}{\ell}C_{H_{\alpha_2}}\right)i_2$$

$$= -C_{M_B} - \left(\frac{\ell_1}{\ell}\frac{S_1}{S}C_{L_{\alpha_1}} - \frac{\ell_2}{\ell}C_{L_{\alpha_2}}\right)\theta - \left(\frac{\ell_1}{\ell}\frac{S_2}{S}C_{L_{0_1}} - \frac{\ell_2}{\ell}\frac{S_2}{S}C_{L_{0_2}}\right)$$

$$-\left(\frac{MAC_1}{\ell}\frac{S_1}{S}C_{H_{\alpha_{trim_1}}} + \frac{MAC_2}{\ell}\frac{S_2}{S}C_{H_{\alpha_2}}\right)\theta - \left(\frac{MAC_1}{\ell}\frac{S_1}{S}H_{H_{0_1}} + \frac{MAC_2}{\ell}\frac{S_2}{S}C_{H_{0_2}}\right)$$

$$= -C_{M_B} - C_{M_\alpha}\theta - C_{M_{0_L}} - C_{M_{0_M}} - \left[\frac{MAC_1}{\ell}\frac{S_1}{S}\left(\frac{H}{c} - a.c.\right)_{\alpha_{trim_1}}C_{L_{\alpha_1}}\right.$$

$$\left. + \frac{MAC_2}{\ell}\frac{S_2}{S}\left(\frac{H}{c} - a.c.\right)_2 C_{L_{\alpha_2}}\right]\theta$$

then:

$$\frac{S_1}{S}\left[\frac{\ell_1}{\ell} + \frac{MAC_1}{\ell}\left(\frac{H}{c} - a.c.\right)_{i_{trim_1}}\right]C_{L_{i_1}}i_1^{\circ}$$

$$-\frac{S_2}{S}\left[\frac{\ell_2}{\ell} - \frac{MAC_2}{\ell}\left(\frac{H}{c} - a.c.\right)_2\right]C_{L_{\alpha_2}}i_2^{\circ}$$

$$= - C_{M_\alpha} \theta^o - \left[\frac{MAC_1}{\ell} \frac{S_1}{S} \left(\frac{H}{c} - a.c. \right)_{\alpha_{trim_1}} C_{L_{\alpha_1}} \right.$$

$$\left. + \frac{MAC_2}{\ell} \frac{S_2}{S} \left(\frac{H}{c} - a.c. \right)_2 C_{L_{\alpha_2}} \right] \theta^o$$

$$- 57.3 (C_{M_B} + C_{M_{0_L}} + C_{M_{0_M}}) \qquad (4.5.10)$$

For many purposes, Eqs. (4.5.9) and (4.5.10) may be employed in a form which neglects buoyancy and hinge moment:

$$\frac{S_1}{S} C_{L_{i_1}} i_1^o + \frac{S_2}{S} C_{L_{\alpha_2}} i_2^o = \frac{57.3W}{q S} - C_{L_\alpha} \theta^o - 57.3 C_{L_0}$$

$$\frac{\ell_1}{\ell} \frac{S_1}{S} C_{L_{i_1}} i_1^o - \frac{\ell_2}{\ell} \frac{S_2}{S} C_{L_{\alpha_2}} i_2^o = - C_{M_\alpha} \theta^o - 57.3 C_{M_{0_L}} \qquad (4.5.11)$$

The parameters required for Eqs. (4.5.9) - (4.5.11) are evaluated numerically in Table 4-4 for the weight and balance of Figures 1 - 3 of Reference 4-14 and four forms of the equations are presented in numerical form for the same weight and balance in Table 4-5.

The variation of forward and aft incidence angle with speed was calculated for each of the four sets of equations of Table 4-5 with the result presented on Figure 4-10. The results demonstrate that foil moment and buoyancy are both significant to craft of this size compared with craft of the PGH size, for example, where neither effect had any practical significance. The measured foil angles of Reference 4-14 are also shown on Figure 4-10 where agreement with theory, and the towing tank, is reasonable forward and negative aft.

For the theoretical incidence angles of Figure 4-10, with foil moment and buoyancy, the corresponding hinge moment variation with speed was calculated by the methods of Tables 4-2 and 4-3 with the result presented on Figures 4-11 and 4-12. Two theoretical hinge moments appear on these figures because the towing tank aero-

dynamic centers do not agree with theory. The prototype measured hinge moments are also shown on these figures and the agreement with theory is not satisfactory for the forward or aft foil.

A negative increment in hinge moment due to buoyancy could be added to the theoretical curves of Figures 4-11 and 4-12. There is a mean buoyant chord just as there is a mean aerodynamic chord. The mean buoyant chord may be defined as the chord of a rectangular foil having the same area and buoyancy as the total foil, i.e.,

$$K\frac{t}{c}MBC\ S\ \rho\ g = \frac{4}{3}K\frac{t}{c}\frac{S^{3/2}}{\sqrt{A}}\frac{1+\lambda+\lambda^2}{(1+\lambda)^2}\rho\ g$$

$$MBC = \frac{4}{3}\sqrt{\frac{S}{A}}\frac{1+\lambda+\lambda^2}{(1+\lambda)^2} \qquad (4.5.12)$$

The MBC is located on the semi-span at

$$\eta_{MBC} = \frac{1-\frac{A}{2b}(1+\lambda)\,MBC}{1-\lambda}$$

$$= \frac{1-\frac{A}{ab}(1+\lambda)\ x\ \frac{4}{3}\sqrt{\frac{S}{A}}\frac{1+\lambda+\lambda^2}{(1+\lambda)^2}}{1-\lambda}$$

$$= 1/3\,\frac{1+\lambda-2\lambda^2}{1-\lambda^2} \qquad (4.5.13)$$

It will be noted that the MBC is located at mid-semi-span on a rectangular foil, evaluated by taking first derivative of numerator and denominator with respect to λ, and at 1/3 the semi-span for a zero taper ratio as would be expected.

The effect of the pod nose and afterbody buoyancy on the aft hinge moment are neglected here but would have to be examined on a larger craft of this configuration. Similarly the section center of gravity would have to be established on a larger craft but it is assumed to lie at mid-chord here.

As the foil buoyancy is approximated here, therefore, the forward and aft centers of buoyancy are identically located at 48.6% of the MAC and contribute hinge moments of

$$M_{H_B} = C_{H_B}\, q\, SMAC$$

$$= C_{B_{foil}} \left(\frac{H}{c} - b.c.\right) q\, SMAC$$

$$= \frac{35.95}{V^2}(.385 - .486) \times .995V^2 \times 225 \times 9.33 = -7,580 = -.091 \times 10^{6''}\ \#\ \text{fwd}$$

$$= \frac{18.58}{V^2}(.336 - .486) \times .995V^2 \times 60 \times 4.81 = -800 = -.0096 \times 10^{6''}\ \#\ \text{aft} \qquad (4.5.14)$$

Neither of these results is significant to the results of Figures 4-11 and 4-12.

The towing tank and prototype lift and hinge moment results are summarized on Figures 4-13 and 4-14 and on these figures the prototype weight, less buoyancy, has simply been distributed on the hinge location to conserve time. The forward foil results of Figure 4-13 indicate reasonable agreement between theory, towing tank, and prototype for lift but poor for hinge moment. The towing tank hinge moments are low and outside the range of previous experience with theory. The aft foil prototype lift results of Figure 4-14 are high and of suspect slope and zero lift angle. The prototype hinge moments are higher and the towing tank moments lower than theory with both sets of results being outside the prediction error results for previous results with the theory.

4.6 FLAP HINGE MOMENT

In the nomenclature of this Volume, Theodorsen's Eq. XIX of Reference 4-17 becomes, for steady state incidence and flap deflections:

$$\frac{M_f}{b} = -\rho \frac{c^2 V^2}{4\pi}(T_5 - T_4 T_{10})\,\delta - \rho \frac{c^2 V}{4} T_{12}\left(V\alpha + \frac{T_{10}}{\pi} V\delta\right)$$

$$= -\frac{\rho}{2} V^2 c^2 \times \frac{T_5 - T_4 T_{10}}{2\pi} \delta - \frac{\rho}{2} V^2 c^2 \times \frac{1}{2} T_{12} \left(\alpha + \frac{T_{10}}{\pi} \delta \right)$$

$$C_h = \frac{M_f}{q S_f c_f} = \frac{M_f}{q Sc} \left(\frac{c}{c_f} \right)^2 = \left[- \frac{T_5 - T_4 T_{12}}{2\pi} \delta - \frac{T_{12}}{2} \left(\alpha + \frac{T_{12}}{\pi} \delta \right) \right] \left(\frac{c}{c_f} \right)^2$$

$$= - \frac{1}{2} \left(\frac{c}{c_f} \right)^2 T_{12} \alpha - \frac{(c/c_f)^2}{2\pi} \left[T_5 - (T_4 - T_{12}) T_{10} \right] \delta$$

$$= C_{h_\alpha} \alpha + C_{h_\delta} \delta \,. \qquad (4.6.1)$$

Eq. (4.6.1) provides 2-dimensional, thin airfoil flap hinge moment slopes which are compared on Figures 4-15 and 4-16 with two other predictions for these slopes which provide accountability for the section thickness. The DATCOM prediction of these figures is from Reference 4-12 and Toll's prediction is from Reference 4-3. The 16-series $c_{\ell_\alpha} / c_{\ell_\alpha}$ theoretical employed was from an unpublished compilation of the lowest Mach Number data of Reference 4-2; that for the 65-series section was derived from Section 4.1.1 of the DATCOM. Figures 4-15 and 4-16 provide identification for Theodorsen's "T" parameters in terms of practical coefficients.

Three procedures for converting the 2-dimensional flap moment slopes to 3-dimensional are considered in Appendix C. The state-of-the-art provides little guidance in this particular area and Perkin's and Hage's procedure was adopted simply because it is the simplest procedure and the most satisfying intuitively.

For C_{h_α}, Perkins and Hage simply employ

$$C_{h_\alpha} = \frac{C_{L_i}}{c_{\ell_\alpha}} c_{h_\alpha} \qquad (4.6.2)$$

and in consideration of the uncertainty associated with this derivative there is no real loss of accuracy if the theoretical section slope is employed.

$$C_{h_\alpha} = C_{L_i} C_{h_\alpha} / 2\pi \qquad (4.6.3)$$

For C_{h_δ} Perkins and Hage add the difference between the 2- and 3-dimensional C_{h_α}'s, reduced by the flap effectiveness, to the 2-dimensional flap effectiveness and that procedure is adopted here without further comment:

$$C_{h_\delta} = c_{h_\delta} + \frac{d\alpha}{d\delta}(C_{h_\alpha} - c_{h_\alpha}) \qquad (4.6.4)$$

For the residual flap hinge moment this volume simply employs:

$$C_{h_0} = - C_{L_{i_{eff}}}/2 \qquad (4.6.5)$$

noting that this value is very probably an upper (negative) bound for the true value and that a better approximation might be provided by:

$$C_{h_0} = - C_{L_{i_{eff}}} \Big/ 6 \left(1 - \frac{c_f/c}{2}\right) \text{ (for triangular load distribution)} \qquad (4.6.6)$$

It must be recognized that the flap hinge moment, being an intimate function of the boundary layer characteristics at the foil trailing edge, is the most uncertain of all the foil characteristics and this remains true with or without model test guidance.

The AG(EH) flap hinge moment is numerically evaluated in Table 4-6. These characteristics were measured in the towing tank but the results are not available at this writing.

4.7 FOIL PITCHING MOMENT DUE TO FLAP

In the nomenclature of the volume, Theodorsen's Eq. XX of Reference 4-17 becomes for a steady-state flap deflection:

$$\frac{M_H}{b} = - \rho \frac{c^2}{4}(T_4 + T_{10}) V^2 \delta + 2\pi \rho V \frac{c^2}{4}\left(2\frac{H}{c} - \frac{1}{2}\right) \times \frac{T_{10}}{\pi} V \delta$$

$$= - \frac{\rho}{2} c^2 V^2 \times \frac{T_4 + T_{10}}{2} \delta + 2\pi \frac{\rho}{2} c^2 V^2 \left(\frac{H}{c} - \frac{1}{4}\right) \frac{T_{10}}{\pi} \delta$$

$$C_H = \left(\frac{H}{c} - \frac{1}{4}\right) \times 2\pi \times \frac{T_{10}}{\pi} \delta - \frac{1}{2}(T_4 + T_{10}) \delta \qquad (4.7.1)$$

The 2π coefficient of the first term is the aerodynamic, 2-dimensional lift curve slope and Eq. (4.7.1) may be written more generally as:

$$C_H = \left(\frac{H}{c} - \frac{1}{4}\right) \times C_{L_\alpha} \times \frac{T_{10}}{\pi} \delta - \frac{1}{2}(T_4 + T_{10})\,\delta \qquad (4.7.2)$$

Eq. (4.7.2) presents flap lift as the sum of two chordwise load distributions, one identical with the load distribution associated with the section angle of attack and having its center of pressure at the section aerodynamic center and the other being concentrated on the flap hinge line. The principle is employed in Section 6 of this volume to calculate the pressure distribution over the flapped foil and it is discussed in good detail in Reference 4-18.

The first term of Eq. (4.7.2), then, is the product of the lift coefficient due to flap deflection and the distance between the foil incidence hinge and the aerodynamic center for one component of the flap lift. Where the flap extends the full span of the exposed foil that aerodynamic center is identical with the aerodynamic center for incidence lift.

Theodorsen's T_{10}/π is obviously the theoretical flap effectiveness, $d\alpha/d\delta$, graphically presented for example on Figure 18 of Reference 4-3 which also presents practical values for the flap effectiveness.

As Theodorsen defines T_4 and T_{10} in References 4-17, the second term of Eq. (4.7.2) may be written:

$$-\frac{1}{2}(T_4 + T_{10})\,\delta = -2\sqrt{\frac{c_f}{c}\left(1 - \frac{c_f}{c}\right)^3}\,\delta$$

$$= \frac{\partial C_{M_{a.c.}}}{\partial \delta}\,\delta \qquad (4.7.3)$$

which is the approximation employed in Eq. 6.1.2.1-a of Reference 4-12, for example, for the moment slope. The approximation is 2-dimensional and the 3-dimensional slope is unknown but reduction of the 2-dimensional slope by the ratio $C_{L_i}/C_{L_{\alpha_{2\text{-}D}}}$ should provide a reasonable approximation for the 3-dimensional effect.

With these considerations incorporated, a practical representation for Eq. (4.7.2) becomes

$$(C_H)_\delta = C_{L_i} \frac{d\alpha}{d\delta}\left(\frac{H}{c} - a.c._{i_H}\right)\delta - \frac{C_{L_i}}{2\pi} \times \frac{\pi}{2}\left(\frac{T_4}{\pi} + \frac{T_{10}}{\pi}\right)\delta$$

$$= C_{L_i} \frac{d\alpha}{d\delta} C_{H_{C_{L_i}}} \delta - C_{L_i} \times \frac{1}{4}\left(\frac{T_4}{\pi} + \frac{T_{10}}{\pi}\right)\delta$$

$$= C_{L_i}\left[\frac{d\alpha}{d\delta} C_{H_{C_{L_i}}} - \frac{1}{4}\left(\frac{T_4}{\pi} + \frac{T_{10}}{\pi}\right)\right]\delta$$

$$= C_{L_i} C_{H_{C_{L_\delta}}} \delta \qquad (4.7.4)$$

For the proposed AG(EH) flap system, the hinge moment slope for flap deflection becomes

$$C_{H_{C_{L_\delta}}} = .47\, C_{H_{C_{L_i}}} - \frac{1}{4}(-.1424 + .5498)$$

$$= .47\, C_{H_{C_{L_i}}} - .1018 \qquad (4.7.5)$$

which is evaluated in Table 4-3.

The incidence hinge moment due to flap deflection for the proposed AG(EH) flap system has been measured in the towing tank but the results are not available at this writing.

4.8 REFERENCES

4-1 Pitts, Nielsen, & Kaattari, "Lift and Center of Pressure of Wing-Body-Tail Combinations at Subsonic, Transonic, and Supersonic Speeds", NACA Report 1307, 1959

4-2 Lindsey, Stevenson, & Daley, "Aerodynamic Characteristics of 24 NACA 16-Series Airfoils at Mach Numbers Between 0.3 and 0.8", NACA TN 1546, September 1948

4-3 T. Toll, "Summary of Lateral-Control Research", NACA Report 868, 1947

4-4 Richter & Palmer, "AG(EH) Hydrofoil Research Ship Hydrodynamic Report of Model Test Program", Grumman Aerospace Corporation, Report M23.77, 8/21/62, Rev. 1/15/63

4-5 J. Feldman, "Experimental Investigation of Near-Surface Hydrodynamic Force Coefficients for a Systematic Series of Tee Hydrofoils, DTMB Series HG-1", DTMB Report 1801, December 1963

4-6 "Hydrofoil Handbook", Vol. II, Gibbs & Cox, Inc., 1954

4-7 A. N. Panchenkov, "Approximate Analysis of Lifting Forces on a Wing Near a Free Surface", BuShips Translation 825, August 1963, translated from Zh. Prikl, Mekh. Fix. (PMTF) no. 4 (Nov/Dec 1960) pp 67-68 by Scripta Technica, Inc.

4-8 Wadlin, Shuford, & McGehee, "A Theoretical and Experimental Investigation of the Lift and Drag Characteristics of Hydrofoils at Subcritical and Supercritical Speeds", NACA Report 1232, 1955

4-9 W. C. O'Neill, "Unsteady Lift and Hinge Moment Characteristics of the AG(EH) Main Foil and Strut Assembly", NSRDC Report 2805, July, 1968

4-10 Abbott, von Doenhoff, & Stivers, "Summary of Airfoil Data", NACA Report 824, 1945

4-11 F. G. Smith, "Design History of the Hydrofoil Research Ship AG(EH)", Grumman Aerospace Corporation, Report M23.12, 2/16/62

4-12 "USAF Stability and Control Methods" (DATCOM), Douglas Aircraft Company, 1965

4-13 H. R. Lawrence, "The Lift Distribution on Low Aspect Ratio Wings at Subsonic Speeds", Journal of the Aeronautical Sciences, Vol. 18, No. 10, October 1951

4-14 W. E. Wright, "Post-RAV Foilborne Trial Results", PLAINVIEW AG(EH)-1 Technical Note TN-A-8, November 1971

4-15 DeYoung & Harper, "Theoretical Symmetric Span Loading at Subsonic Speeds for Wings Having Arbitrary Plan Form", NACA Report 921, 1948

4-16 "Recommendations for Operating Restrictions for Initial Smooth Water Trials", PLAINVIEW AG(EH)-1 Technical Note TN-2 (Revision A), December 1970

4-17 T. Theodorsen, "General Theory of Aerodynamic Instability and the Mechanism of Flutter", NACA Report 496, 1935. Currently available in AIAA Selected Reprints, "Aerodynamic Flutter", I. E. Garrick, Editor, March 1969

4-18 Allen, "Calculation of the Chordwise Load Distribution Over Airfoil Sections with Plain, Split, or Serially Hinged Trailing-Edge Flaps", NACA Report 634, 1938

4-19 Perkins & Hage, "Airplane Performance, Stability, and Control", Wiley, 1956

TABLE 4-1 AG(EH) FOIL LIFT CHARACTERISTICS

CHARACTERISTIC	SYMBOL	DERIVATION	FWD. FOIL	AFT FOIL
GEOMETRY				
Foil area ratio	S'/S	S'/S	.813	.757
Pod area ratio	S_N/S	S_N/S	.0388	.0663
PITCH LIFT				
Foil lift factor	$K_{W(B)}$	Chart 1, Ref. 4.7.1	1.11	1.14
Pod lift factor	$K_{B(W)}$	Chart 1, Ref. 4.7.1	.165	.24
Foil lift curve slope	$C_{L_{\alpha_{foil}}}$	$\frac{S'}{S} K_{W(B)} C_{L'_\alpha}$	2.52	2.385
Pod lift curve slope	$C_{L_{\alpha_{pod}}}$	$\frac{S'}{S} K_{B(W)} C_{L'_\alpha}$	.374	.501
Nose lift curve slope	$C_{L_{\alpha_{nose}}}$	$\frac{S_N}{S} C_{L_{\alpha_B}} = 2\frac{S_N}{S}$	.0776	.1326
Total lift curve slope	C_{L_α}	$C_{L_{\alpha_{foil}}} + C_{L_{\alpha_{pod}}} + C_{L_{\alpha_{nose}}}$	2.97	3.015
INCIDENCE LIFT				
Foil lift factor	$k_{W(B)}$	Chart 1, Ref. 4.7.1	.96	.94
Pod lift factor	$k_{B(W)}$	Chart 1, Ref. 4.7.1	.135	.18
Foil lift curve slope	$C_{L_{i_{foil}}}$	$\frac{S'}{S} k_{W(B)} C_{L'_\alpha}$	2.175	1.965
Pod lift curve slope	$C_{L_{i_{pod}}}$	$\frac{S'}{S} k_{B(W)} C_{L'_\alpha}$	.306	.501
Total lift curve slope	C_{L_i}	$C_{L_{i_{foil}}} + C_{L_{i_{pod}}}$	2.49	2.34

TABLE 4-1 (Continued)

CHARACTERISTIC	SYMBOL	DERIVATION	FWD. FOIL		AFT FOIL
Lift curve slope ratio	C_{L_i}/C_{L_α}	C_{L_i}/C_{L_α}	.838		.777
FLAP LIFT					
Flap lift curve slope	C_{L_δ}	$\frac{d\alpha}{d\delta} C_{L_i}$	1.17		Not applicable
RESIDUAL LIFT					
Section zero lift angle, deg.	$\alpha_{C_\ell = 0}$	Section characteristic	-2.92^o model	-3.22 prototype	-2.92^o
Residual foil lift	$C_{L_{i_{eff}}}$	$- C_{L_i} \alpha_{C_\ell = 0}$	.127 model	.140 prototype	.119
Pod zero lift angle, deg.	$*\alpha_{C_{L_{pod}} = 0}$	Emperical	$.67^o$		0
Residual pod lift	$C_{L_{pod}}$	$- C_{L_i} \alpha_{C_{L_{pod}} = 0}$	-.029		0
Residual lift	C_{L_0}	$C_{L_{i_{eff}}} + C_{L_{pod}}$	.098* model	.111* prototype	.119*

$$C_{L_1} = C_{L_\alpha} \alpha + C_{L_i} i + C_{L_\delta} \delta + C_{L_0}$$

$$C_{L_2} = C_{L_\alpha} \alpha + C_{L_0}$$

$$C_{L_0} = \frac{C_{L_\alpha}}{C_{L_{\alpha_\infty}}} \times C_{L_{0_\infty}}$$

* Aerodynamic

TABLE 4-2 AG(EH) FOIL MOMENT SLOPES

		PREDICTED				MEASURED		
COMPONENT	H/c	a.c.	$\frac{H}{c}$ - a.c. = $C_{H_{C_L}}$	C_{L_α}	$C_{H_\alpha} = C_{H_{C_L}} C_{L_\alpha}$	C_{H_α}	$C_{H_{C_L}}$	a.c.
PITCH LIFT - FWD FOIL								
Foil	.385	.340	.045	2.52	.1135	.2375	.0943	.291
Pod		.1325	.2525	.374	.0945	.0945		
Nose		- .797	1.182	.0776	.0918	.0918		
Foil + pod + nose = $C_{H_{\alpha_{trim}}}$				$C_{H_{\alpha_{trim}}}$	.2998	.4238		
Used to trim craft moments				C_{L_α}	2.97	2.97		
				$C_{H_{C_{L_{trim}}}}$	.101	.1427		
				a.c.$_{\alpha_{trim}}$	.284	.2423		
Foil only				C_{H_α}	.1135	.2375		
Control force hinge moment slope				C_{L_α}	2.97	2.97		
				$C_{H_{C_L}}$	.0382	.080		
				a.c.$_{\alpha_H}$	.3468	.315		
COMPONENT	H/c	a.c.	$\frac{H}{c}$ - a.c. = $C_{H_{C_L}}$	C_{L_i}	$C_{H_i} = C_{H_{C_L}} C_{L_i}$	C_{H_i}	$C_{H_{C_L}}$	a.c.
INCIDENCE LIFT - FWD FOIL								
Foil	.385	.340	.045	2.175	.0979	.1745	.0801	.305
Pod		.1325	.2525	.306	.0773	.0773		
Foil + pod = $C_{H_{i_{trim}}}$				$C_{H_{i_{trim}}}$	.1752	.2518		
Used to trim craft moments				C_{L_i}	2.49	2.49		
				$C_{H_{C_{L_{trim}}}}$	.0705	.1012		
				a.c.$_{i_{trim}}$	.3145	.2838		

TABLE 4-2 (Continued)

COMPONENT	H/c	PREDICTED a.c.	PREDICTED $\frac{H}{c}$ - a.c. = $C_{H_{C_L}}$	PREDICTED C_{L_i}	PREDICTED $C_{H_i} = C_{H_{C_L}} \times C_{L_i}$	MEASURED C_{H_i}	MEASURED $C_{H_{C_L}}$	MEASURED a.c.
Foil only = C_{H_i}				C_{H_i}	.0979	.1745		
Control force hinge moment slope				C_{L_i}	2.49	2.49		
(Note that a.c.$_{i_H}$ = a.c.$_{foil}$ for incidence lift)				$C_{H_{C_L}}$	.0393	.070		
				a.c.$_{i_H}$	.3457	.315		
AFT FOIL (SEE EQ. 4.3.8)								
	$\frac{H}{c}$ = .336			C_{H_α}	.2515	.588		
				C_{L_α}	3.015	3.015		
				$C_{H_{C_L}}$	.0834	.195		
				a.c.	.2526	.141		

TABLE 4-3 AG(EH) FOIL MOMENTS

FWD. FOIL										
$C_H =$	$\left(\frac{H}{C} - a.c.\right)_\alpha C_{L_\alpha}$		$+\left(\frac{H}{C} - a.c.\right)_i C_{L_i}$		$-\left(\frac{d\sigma}{d\delta} C_{H_{C_{L_i}}} - \frac{T_4 + T_{10}}{4\pi}\right) C_{L_i}$		$+ C_{H_0}$			
	$C_{H_{C_{L_\alpha}}} (C_L)_\alpha$		$+ C_{H_{C_{L_i}}} (C_L)_i$		$- C_{H_{C_{L_\delta}}} C_{L_i}$					
	$C_{H_{C_{L_\alpha}}} = \frac{H}{C} - a.c._\alpha$		$C_{H_{C_{L_i}}} = \frac{H}{C} - a.c._i$		$- C_{H_{C_{L_\delta}}} = \frac{d\sigma}{d\delta} C_{H_{C_{L_i}}} - \frac{T_4 + T_{10}}{4\pi}$		C_{H_0}			
							MODEL		PROTOTYPE	
	THEORY	TOW TANK	THEORY	TOW TANK	THEORY	TOW TANK	THEORY	TOW TANK	THEORY	TOW TANK
For trim	.1[illegible]	.1427	.0705	.1012	- .0686	- .0542	- .0551	- .040	- .0608	- .0457 NOTE 3
For hinge moment	.0382	.080	.0393	.070	- .0833	- .0689	- .0551	- .040	- .0608	- .0457 NOTE 3

NOTES: 1. For most practical purposes $C_{H_\alpha} = C_{H_i}$ and $C_{H_{C_{L_\alpha}}} = C_{H_{C_{L_i}}}$.

2. Results from table are aerodynamic; multiply by $C_{L_\alpha}/C_{L_{\alpha_\infty}}$.

3. Prototype camber not tested in tow tank; this value is model result plus theoretical effect of camber increase.

AFT FOIL: $C_H = \left(\frac{H}{C} - a.c.\right) C_{L_\alpha} + C_{H_0} = C_{H_{C_L}} (C_L)_\alpha + C_{H_0}$

$= .0834(C_L)_\alpha - .0500 \frac{C_{L_\alpha}}{C_{L_{\alpha_\infty}}}$ (Theoretical)

$= .195(C_L)_\alpha - .0555 \frac{C_{L_\alpha}}{C_{L_{\alpha_\infty}}}$ (Tow Tank)

TABLE 4-4 NUMERICAL EVALUATION FOR TRIM PARAMETERS

$\ell_1 = 95.4 - 81.6 = 13.8$

THEORY/TOW TANK

$S_1 = 450$ $\quad \ell_1 = 13.8$ $\quad MAC_1 = 9.33$ $\quad C_{H_{C_{L_{\alpha_{trim_1}}}}} = .101/.1427$

$S_2 = 60$ $\quad \ell_2 = 112.1$ $\quad MAC_2 = 4.81$ $\quad C_{H_{C_{L_{t_{trim_1}}}}} = .0705/.1012$

$S = 519$ $\quad \ell = 125.9$ $\quad \frac{MAC_1}{\ell} = .0741$ $\quad C_{H_{C_{L_2}}} = .0834/.195$

$\frac{S_1}{S} = 382$ $\quad \frac{\ell_1}{\ell} = .1095$ $\quad \frac{MAC_2}{\ell} = .03825$

$\frac{S_2}{S} = .1176$ $\quad \frac{\ell_2}{\ell} = .891$

$d_1 = 11.32$ $\quad C_{L_{\alpha_1}} = 2.8$ $\quad \frac{C_{L_{\alpha_1}}}{C_{L_{\alpha_\infty}}} = .943$ $\quad C_{L_{0_1}} = .1044$ $\quad C_{B_1} = 32.5/v_k^2$

$d_2 = 12.02$ $\quad C_{L_{t_1}} = 2.35$ $\quad \frac{C_{L_{t_1}}}{C_{L_{t_{1_\infty}}}} = .943$ $\quad C_{L_{0_2}} = .1165$ $\quad C_{B_2} = 29.1/v_k^2$

$\frac{d_1}{MAC_1} = 1.214$ $\quad C_{L_{\alpha_2}} = 2.95$ $\quad \frac{C_{L_{\alpha_2}}}{C_{L_{\alpha_{2_\infty}}}} = .979$ $\quad C_{H_{0_1}} = -.0573/-.0431$

$\frac{d_2}{MAC_2} = 2.495$ $\quad C_{H_{0_2}} = -.0490/-.0543$

$$\frac{57.3W}{qS} = \frac{57.3 \times 2240 \times 295}{2.84 \times 510\, V_K^2} = 26{,}100/V_K^2$$

Craft lift curve slope, $C_{L_\alpha} = \frac{S_1}{S} C_{L_{\alpha_1}} + \frac{S_2}{S} C_{L_{\alpha_2}} = .882 \times 2.8 + .1176 \times 2.95 = 2.47 + .347 = 2.82$

Static stability, $C_{M_\alpha} = \frac{\ell_1}{\ell}\frac{S_1}{S} C_{L_{\alpha_1}} - \frac{\ell_2}{\ell}\frac{S_2}{S} C_{L_{\alpha_2}} = .1095 \times 2.47 - .891 \times .347 = .2705 - .3095 = -.039$

Craft residual lift, $C_{L_0} = \frac{S_1}{S} C_{L_{0_1}} + \frac{S_2}{S} C_{L_{0_2}} = .882 \times .1044 + .1176 \times .1165 = .09208 + .0137 = .1058$

Craft residual lift moment, $C_{M_{0_L}} = \frac{\ell_1}{\ell}\frac{S_1}{S} C_{L_{0_1}} - \frac{\ell_2}{\ell}\frac{S_2}{S} C_{L_{0_2}} = .1095 \times .09208 - .891 \times .0137 = .01008 - .01221 = -.00213$

Craft residual moment, $C_{M_{0_M}} = \frac{MAC_1}{\ell}\frac{S_1}{S} C_{H_{0_1}} + \frac{MAC_2}{\ell}\frac{S_2}{S} C_{H_{0_2}} = .0741 \times .882 \begin{pmatrix} -.0573 \\ -.0431 \end{pmatrix} + .03825 \times .1176 \begin{pmatrix} -.0490 \\ -.0543 \end{pmatrix}$

$= -.00375 - .0002205 = -.00397$ Theory

$-.00282 - .000244 = -.003064$ Towing Tank

Craft buoyancy coefficient, $C_B = \frac{S_1}{S} C_{B_1} + \frac{S_2}{S} C_{B_2} = (.882 \times 32.5 + .2276 \times 29.1)/V_K^2 = (2.87 + 3.42)/V_K^2 = \frac{32.12}{V_K^2}$

Craft buoyant moment, $C_{M_B} = \frac{\ell_1}{\ell} \frac{S_1}{S} C_{B_1} - \frac{\ell_2}{\ell}\frac{S_2}{S} C_{B_2} = (.1095 \times 28.7 - .891 \times 3.42)/V_K^2$

$= (3.143 - 3.047)/V_K^2 = .096/V_K^2$

TABLE 4-5 NUMERICAL EVALUATION FOR TRIM EQUATIONS

NO FOIL MOMENT OR BUOYANCY

$$\underline{\text{LIFT:}}\quad \frac{S_1}{S} C_{L_{i_1}} i_1^{o} + \frac{S_2}{S} C_{L_{\alpha_2}} i_2^{o} = \frac{57.3W}{q\,S} - C_{L_\alpha}\theta^{o} - 57.3\,C_{L_0}$$

$$.882 \times 2.35\, i_1^{o} + .1176 \times 2.95\, i_2^{o} = 26{,}100/V_K^{2} - 2.82 \times 1 - 57.3 \times .1058$$

$$2.07\, i_1^{o} + .347\, i_2^{o} = 26{,}100/V_K^{2} - 2.82 - 6.07$$

$$= 26{,}100/V_K^{2} - 8.89$$

$$\underline{\text{MOMENT:}}\quad \frac{\ell_1}{\ell}\frac{S_1}{S} C_{L_{i_1}} i_1^{o} - \frac{\ell_2}{\ell}\frac{S_2}{S} C_{L_{\alpha_2}} i_2^{o} = - C_{M_\alpha}\theta^{o} - 57.3\,C_{M_{0_L}}$$

$$.1095 \times 2.07\, i_1^{o} - .891 \times .347\, i_2^{o} = .039 \times 1 + 57.3 \times .00213$$

$$.227\, i_1^{o} - .3095\, i_2^{o} = .039 + .122$$

$$= .161$$

PREDICTED FOIL MOMENT - NO BUOYANCY

$$\underline{\text{LIFT:}}\quad \frac{S_1}{S} C_{L_{i_1}} i_1^{o} + \frac{S_2}{S} C_{L_{\alpha_2}} i_2^{o} = \frac{57.3W}{q\,S} - C_{L_\alpha}\theta^{o} - 57.3\,C_{L_0}$$

$$2.07\, i_1^{o} + .347\, i_2^{o} = 26{,}100/V_K^{2} - 8.89$$

$$\underline{\text{MOMENT:}}\quad \frac{S_1}{S}\left[\frac{\ell_1}{\ell} + \frac{MAC_1}{\ell} C_{H_{C_{L_{i_{trim_1}}}}}\right] C_{L_{i_1}} i_1^{o} - \frac{S_2}{S}\left[\frac{\ell_2}{\ell} - \frac{MAC_2}{\ell} C_{H_{C_{L_2}}}\right] C_{L_{\alpha_2}} i_2^{o}$$

$$= - C_{M_\alpha}\theta^{o} - \left[\frac{MAC_1}{\ell}\frac{S_1}{S} C_{H_{C_{L_{\alpha_{trim_1}}}}} C_{L_{\alpha_1}} + \frac{MAC_2}{\ell}\frac{S_2}{S} C_{H_{C_{L_2}}} C_{L_{\alpha_2}}\right]\theta^{o}$$

$$- 57.3(C_{M_{0_L}} + C_{M_{0_M}})$$

$$.882\,[.1095 + .0741 \times .0705] \times 2.35\, i_1^{o} - .1176\,[.891 - .03825 \times .0834] \times 2.95\, i_2^{o}$$

$$= .039 - [.0741 \times .882 \times .101 \times 2.8 + .03825 \times .1176 \times .0834 \times 2.95] \times 1$$

$$- 57.3(- .00213 - .00397)$$

$$.882(.1095 + .0052) \times 2.35\, i_1^{o} - .1176(.891 - .003) \times 2.95\, i_2^{o} = .039 - (.01852 + .00110) + .349$$

$$.882 \times .1147 \times 2.35\, i_1^{o} - .1176 \times .888 \times 2.95\, i_2^{o} = .039 - .01962 + .349$$

$$.2375\, i_1^{o} - .308\, i_2^{o} = .3684$$

TABLE 4-5 (Continued)

PREDICTED FOIL MOMENT WITH BUOYANCY

LIFT: $\frac{S_1}{S} C_{L_{i_1}} i_1^o + \frac{S_2}{S} C_{L_{\alpha_2}} i_2^o = \frac{57.3W}{q S} - C_{L_\alpha} \theta^o - 57.3\, C_{L_0} - 57.3\, C_B$

$$2.07\, i_1^o + .347\, i_2^o = 26,100/V_K^2 - 8.89 - 57.3 \times 32.12/V_K^2$$

$$= (26,100 - 1837)/V_K^2 - 8.89$$

$$= 24,260/V_K^2 - 8.89$$

MOMENT: SUBTRACT $57.3\, C_{M_B}$ FROM RIGHT SIDE OF PREVIOUS EQUATION

$$.2375\, i_1^o - .308\, i_2^o = .3684 - 57.3 \times .096/V_K^2$$

$$= .3684 - 5.49/V_K^2$$

TOWING TANK FOIL MOMENT WITH BUOYANCY

LIFT: UNCHANGED

$$2.07\, i_1^o + .347\, i_2 = 24,260/V_K^2 - 8.89$$

MOMENT: $\frac{\ell_1}{\ell} + \frac{MAC_1}{\ell} C_{H_{C_{L_{i_{trim_1}}}}} = .1095 + .0741 \times .1012 = .1095 + .0075 = .1170$

$$\frac{\ell_2}{\ell} - \frac{MAC_2}{\ell} C_{H_{C_{L_2}}} = .891 - .03825 \times .195 = .891 - .00746 = .884$$

$$\frac{MAC_1}{\ell}\frac{S_1}{S} C_{H_{C_{L_{\alpha_{trim_1}}}}} C_{L_{\alpha_1}} + \frac{MAC_2}{\ell}\frac{S_2}{S} C_{H_{C_{L_2}}} C_{L_{\alpha_2}}$$

$$= .0741 \times .882 \times .1427 \times 2.8 + .03825 \times .1176 \times .195 \times 2.95$$

$$= .0261 + .00259 = .02869$$

$$.882 \times .117 \times 2.35\, i_1^o - .1176 \times .884 \times 2.95\, i_2^o$$

$$= .039 \times 1 - .02869 \times 1 - 57.3(-.00213 - .003064) - 57.3 \times .096/V_K^2$$

$$.2425\, i_1^o - .306\, i_2^o = .039 - .02869 + 57.3 \times .00519 - 5.49/V_K^2$$

$$= .01031 + .297 - 5.49/V_K^2$$

$$= .3073 - 5.49/V_K^2$$

TABLE 4-6 FLAP HINGE MOMENT - FWD. ONLY

$$\underline{C_h} = \underline{C_{h_\alpha}}\,\alpha + \underline{C_{h_\delta}}\,\delta + \underline{C_{h_0}}$$

$$= \underline{C_{h_\alpha}}\,\alpha + \left[C_{h_\delta} - \frac{d\alpha}{d\delta}\left(C_{h_\alpha} - \underline{C_{h_\alpha}}\right)\right]\delta - C_{L_{i_{eff.}}}/2$$

$$= \frac{C_{L_i}}{2\pi} C_{h_\alpha}\,\alpha + \left[C_{h_\delta} - \frac{d\alpha}{d\delta}\left(C_{h_\alpha} - \frac{C_{L_i}}{2\pi} C_{h_\alpha}\right)\right]\delta - C_{L_{i_{eff.}}}/2$$

$$= \frac{C_{L_i}}{2\pi} C_{h_\alpha}\,\alpha + \left[C_{h_\delta} - \frac{d\alpha}{d\delta} C_{h_\alpha}\left(1 - \frac{C_{L_i}}{2\pi}\right)\right]\delta - C_{L_{i_{eff.}}}/2$$

C_{h_α} is from Figure 4-15

C_{h_δ} is from Figure 4-16

$C_{h_{i_{eff}}}$ is from Table 4-1

$$\underline{C_h} = -.043\frac{C_{L_i}}{2\pi}\,\alpha + \left[-.54 + .47 \times .043\left(1 - \frac{C_{L_i}}{2\pi}\right)\right]\delta - C_{L_{i_{eff.}}}/2$$

$$= -.043\frac{C_{L_i}}{2\pi}\,\alpha + \left(-.52 - .0202\frac{C_{L_i}}{2\pi}\right)\delta - C_{L_{i_{eff.}}}/2$$

$$= -.043\frac{C_{L_i}}{2\pi}\,\alpha - \left(.52 + .0202\frac{C_{L_i}}{2\pi}\right)\delta - .0635 \text{ (for model)}$$

$$= -.043\frac{C_{L_i}}{2\pi}\,\alpha - \left(.52 + .0202\frac{C_{L_i}}{2\pi}\right)\delta - .070 \text{ (for prototype)}$$

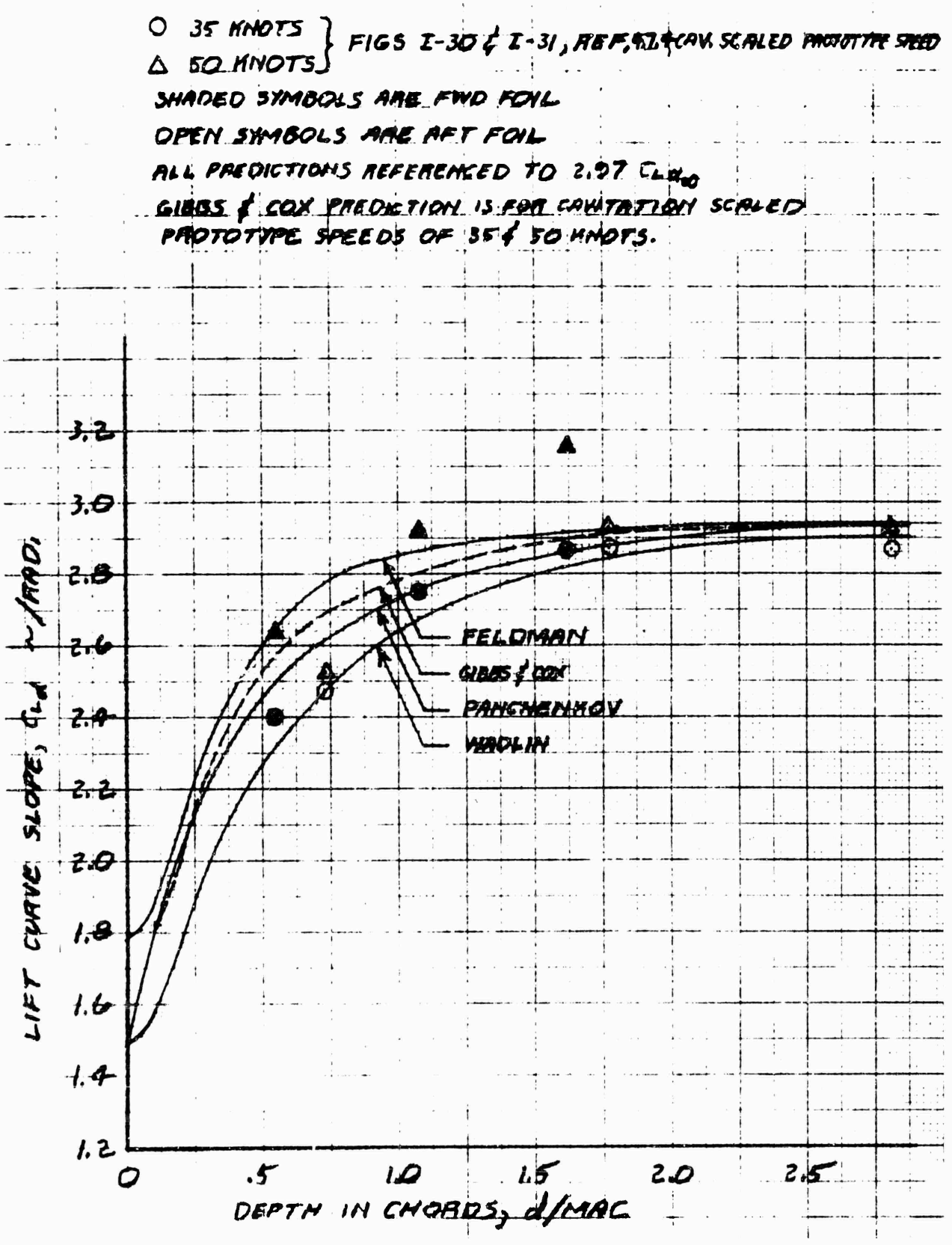


Figure 4-1. Pitch Lift Curve Slope

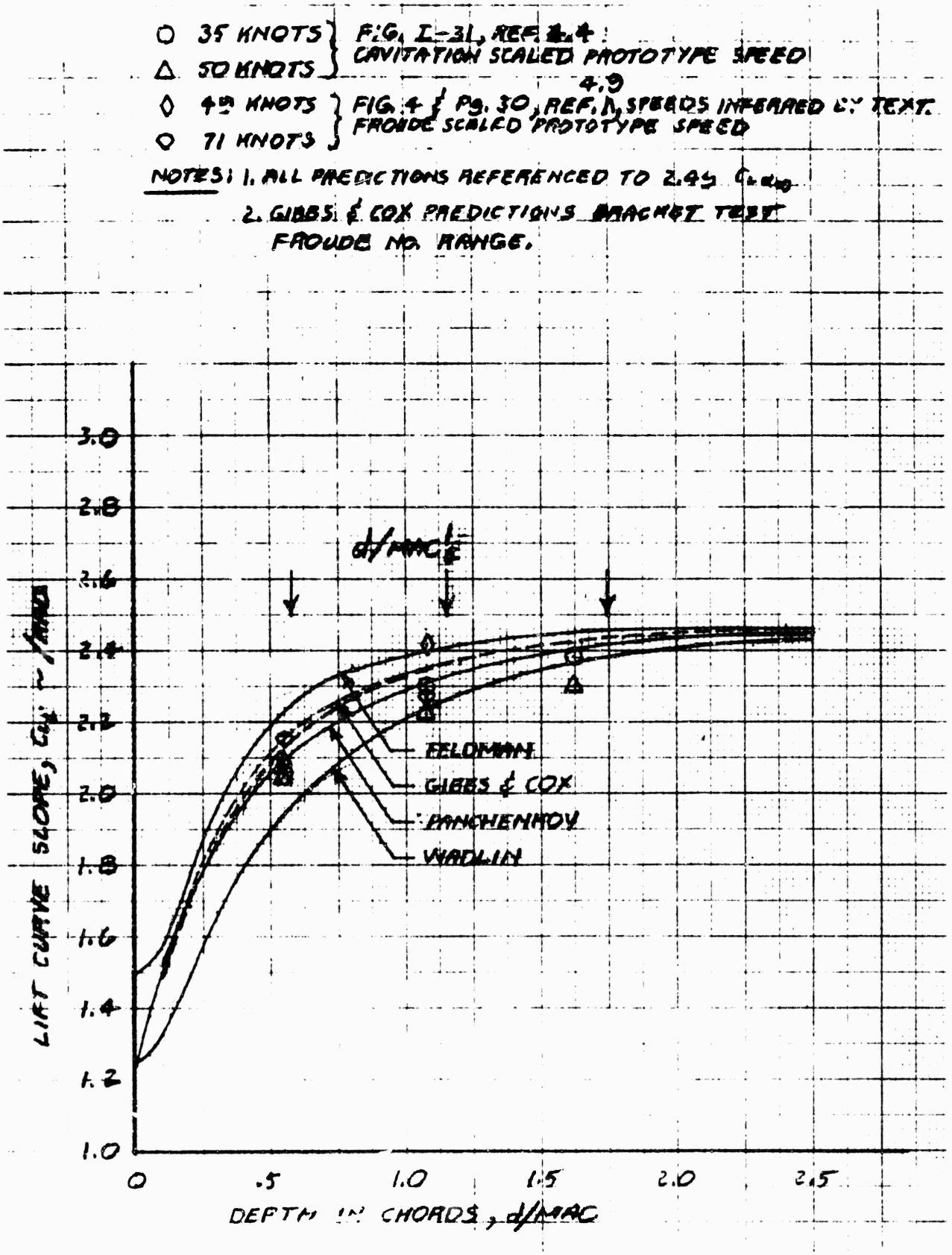


Figure 4-2. Incidence Lift Curve Slope

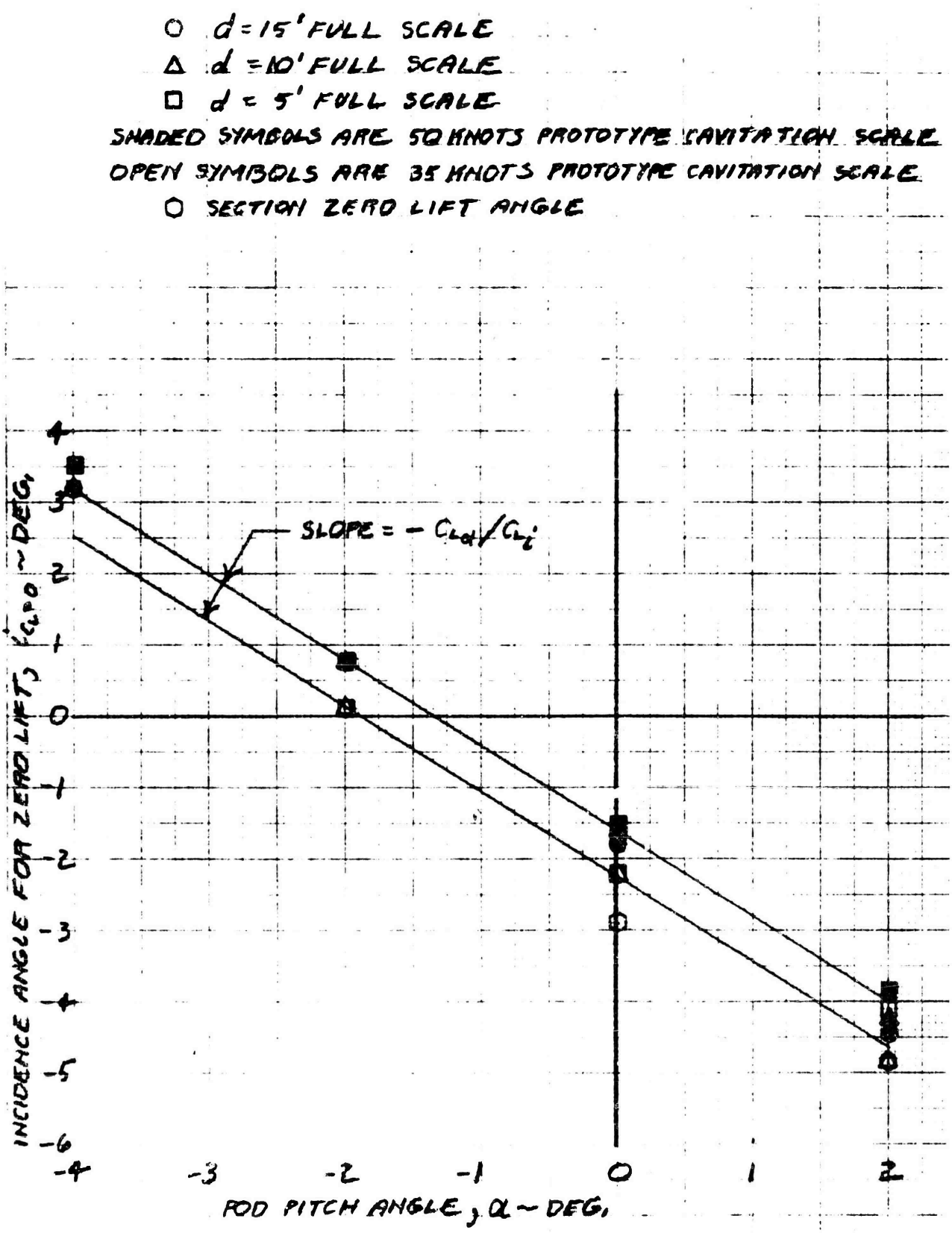


Figure 4-3. Fwd. Foil Zero Lift Angle

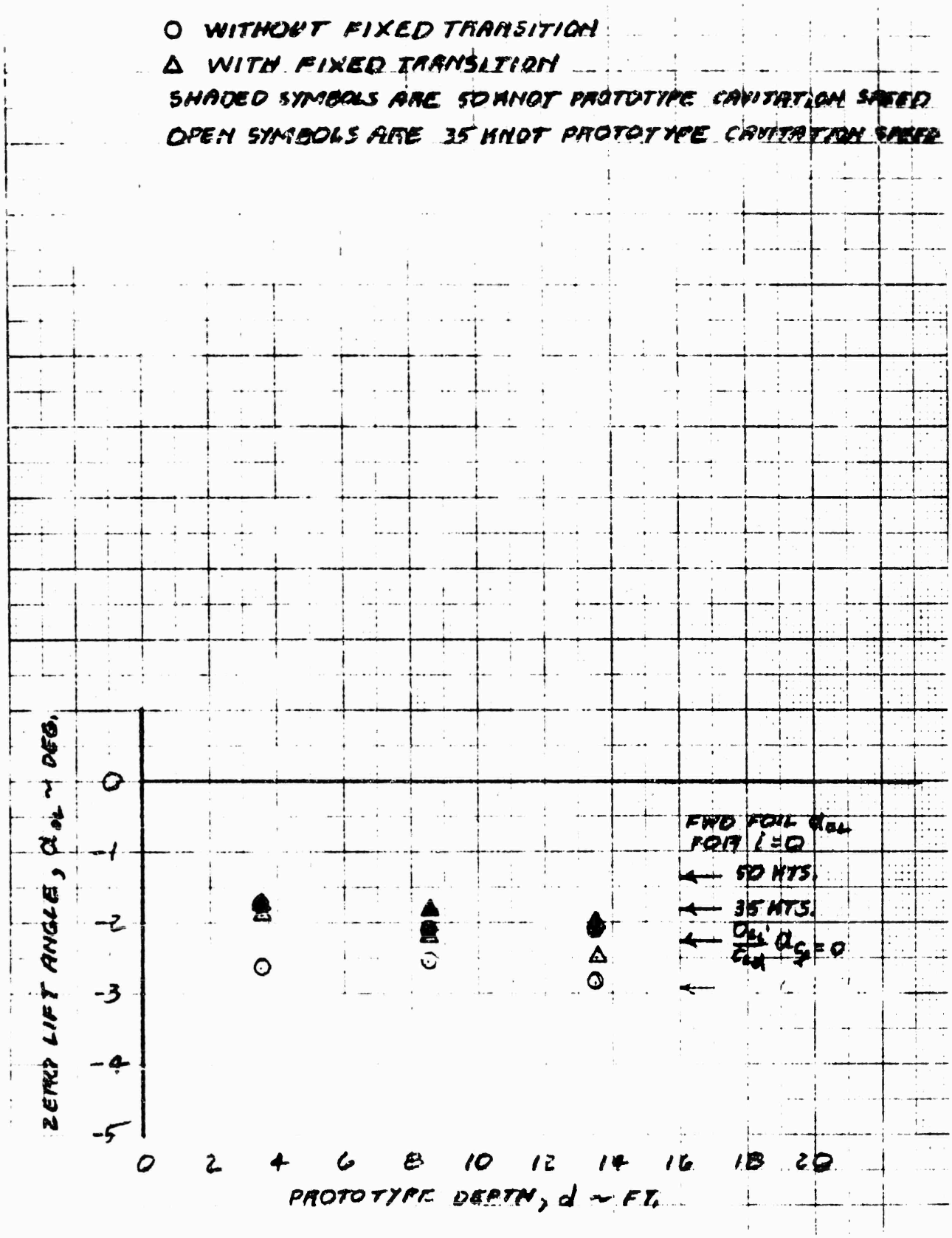


Figure 4-4. Aft Foil Zero Lift Angle

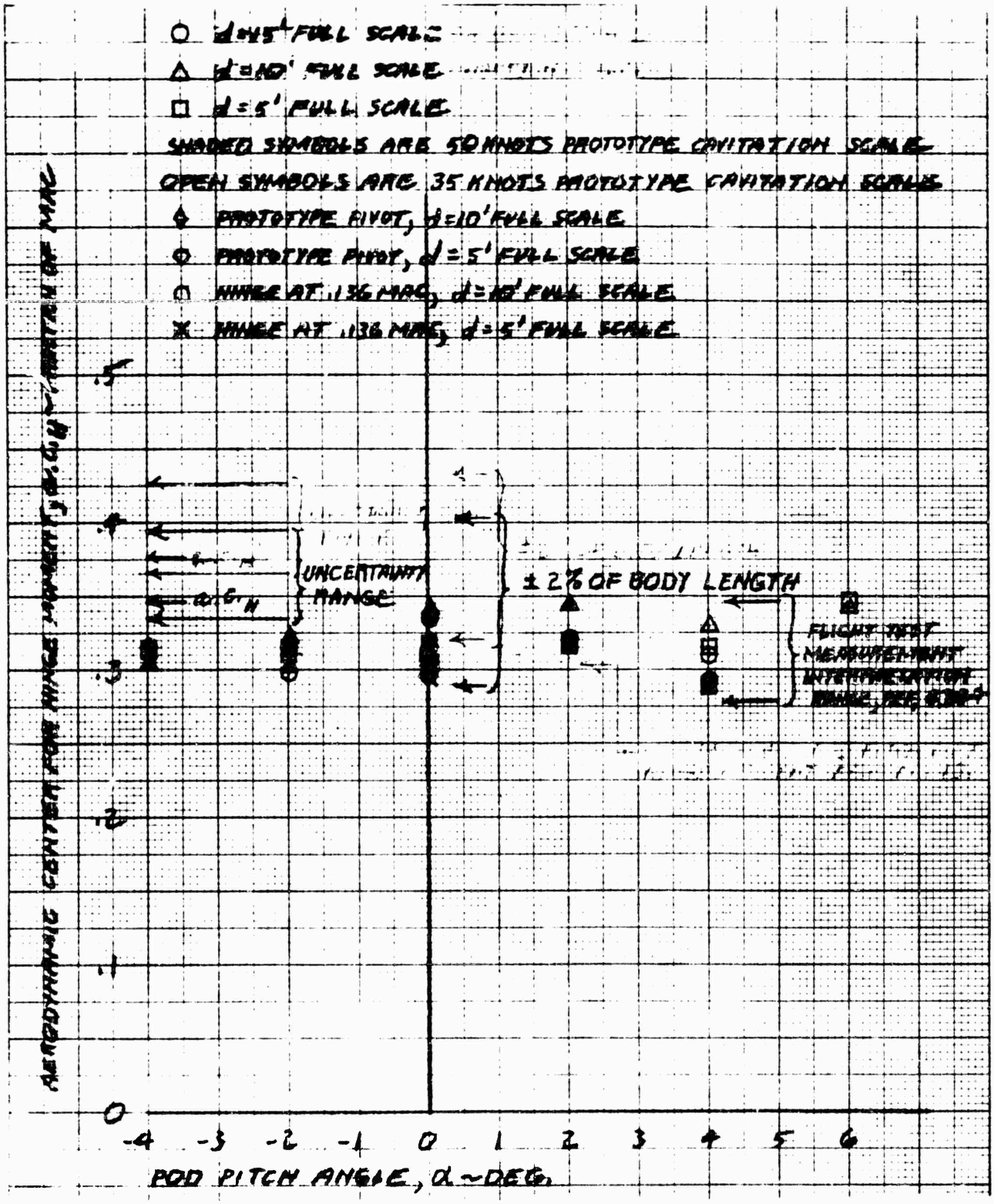


Figure 4-5. Fwd. Foil Aerodynamic Center, Incidence Lift Hinge Moment

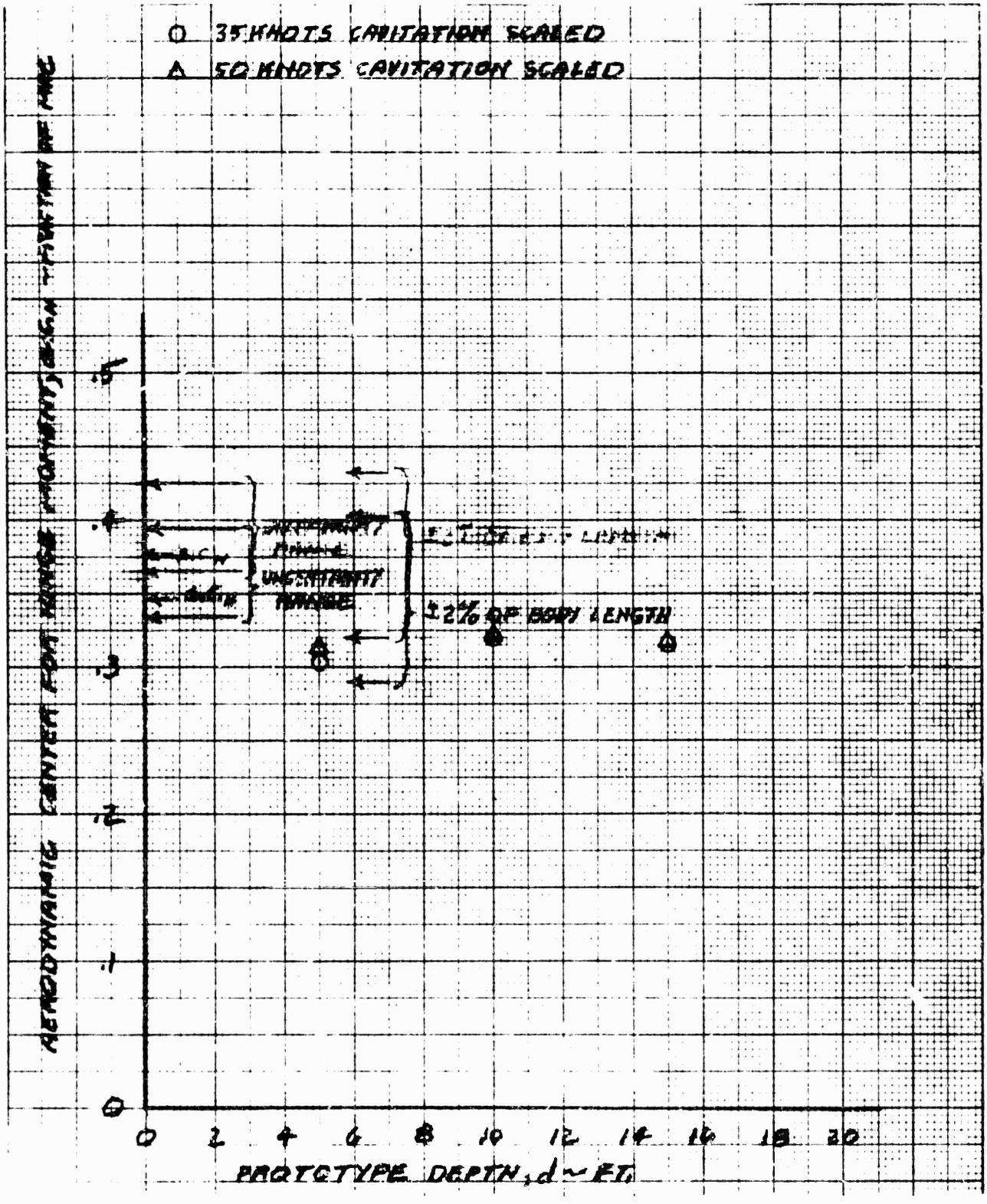


Figure 4-6. Fwd. Foil Aerodynamic Center, Pitch Lift Hinge Moment

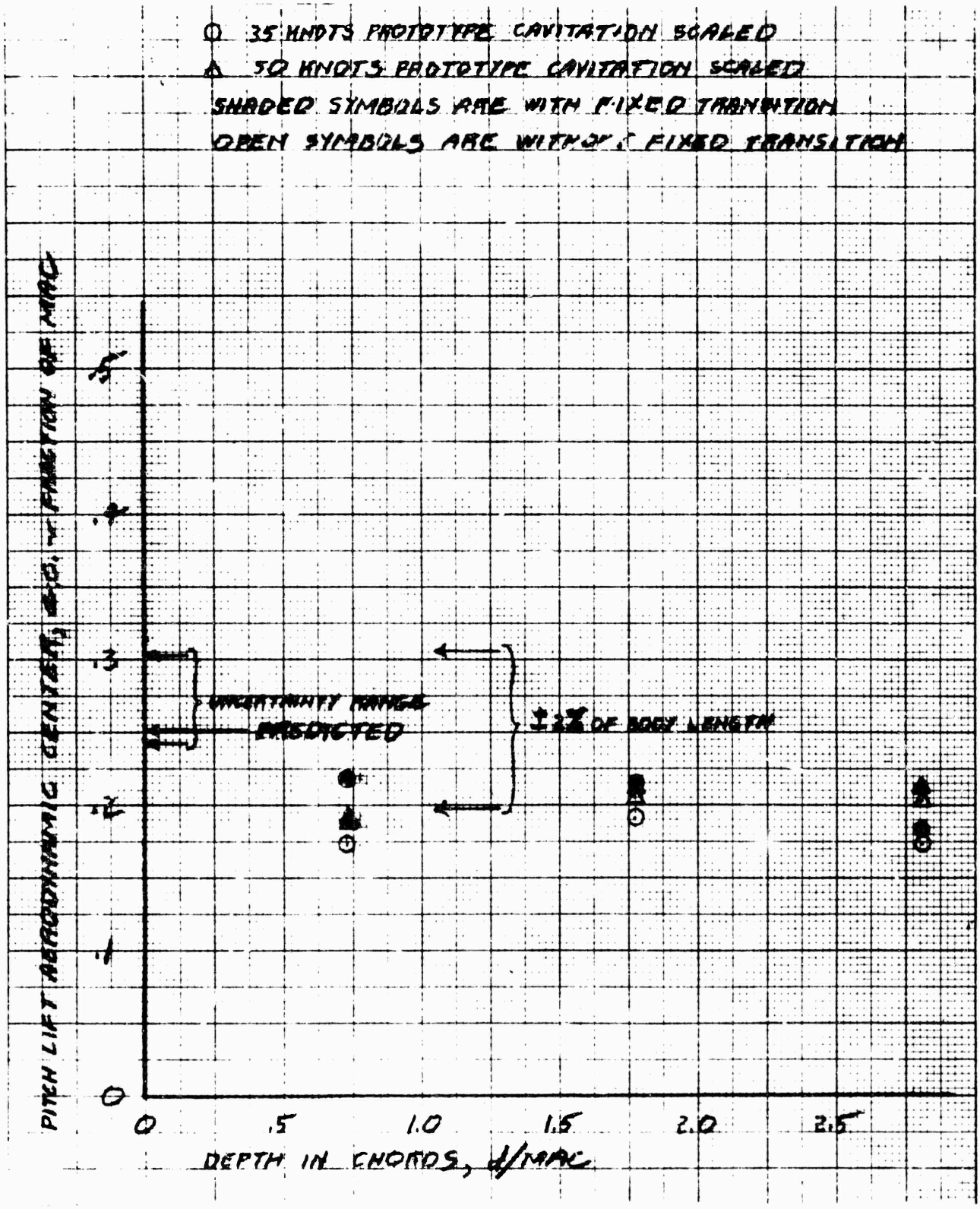


Figure 4-7. Aft Foil Aerodynamic Center, Pitch Lift

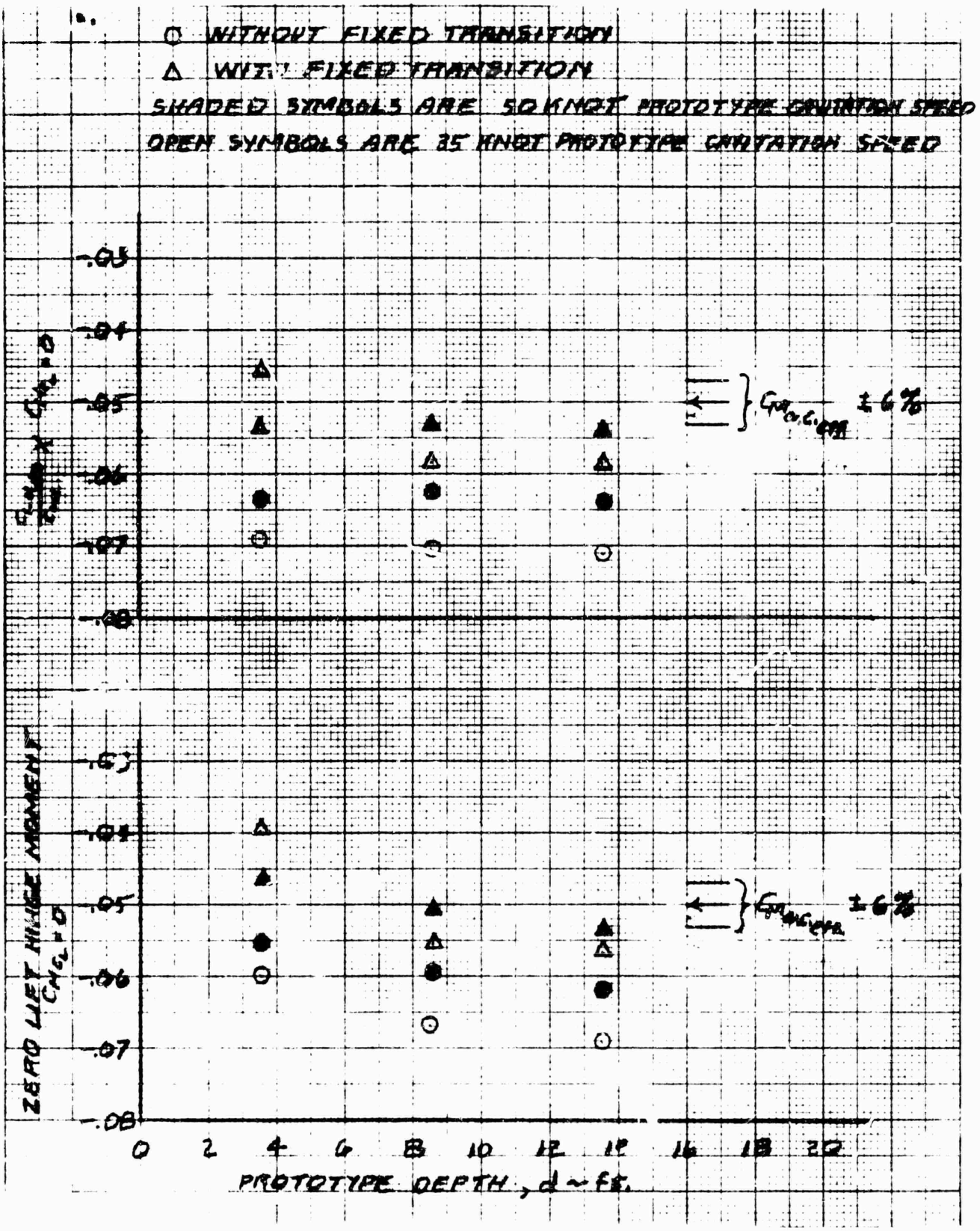


Figure 4-8. Aft Foil Residual Hinge Moment Pitch Lift

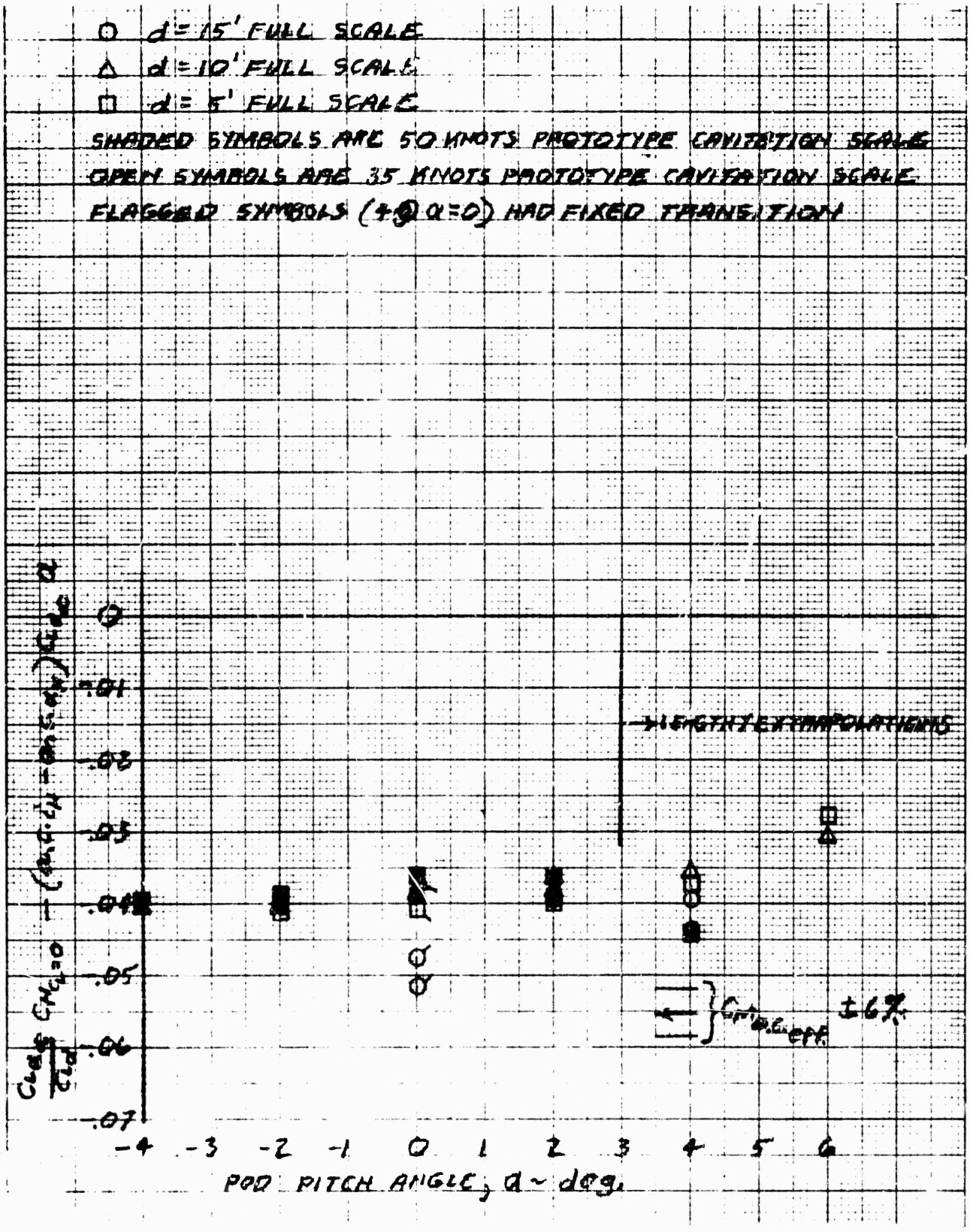


Figure 4-9. Fwd. Foil Residual Hinge Moment

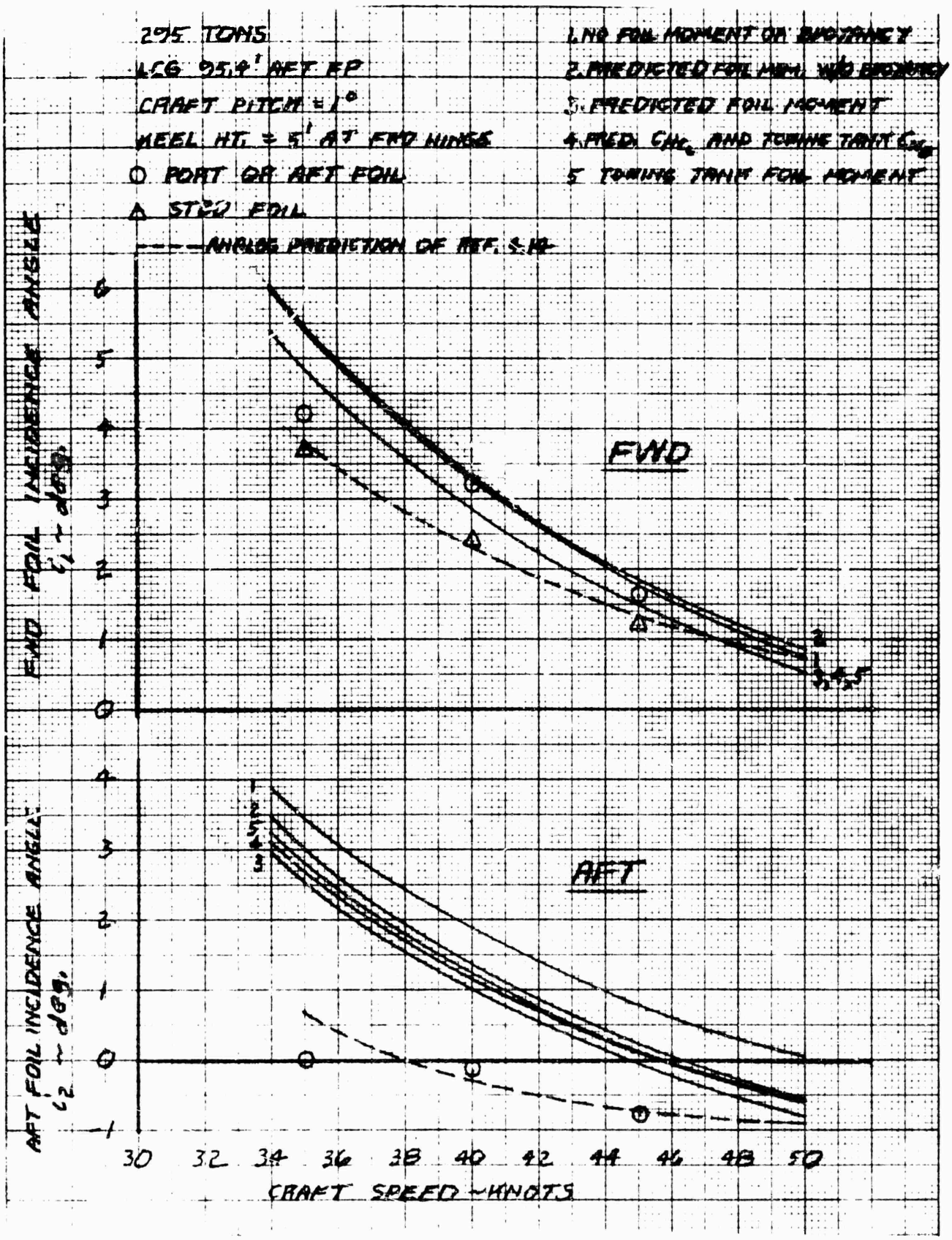


Figure 4-10. Prototype Foil Angles

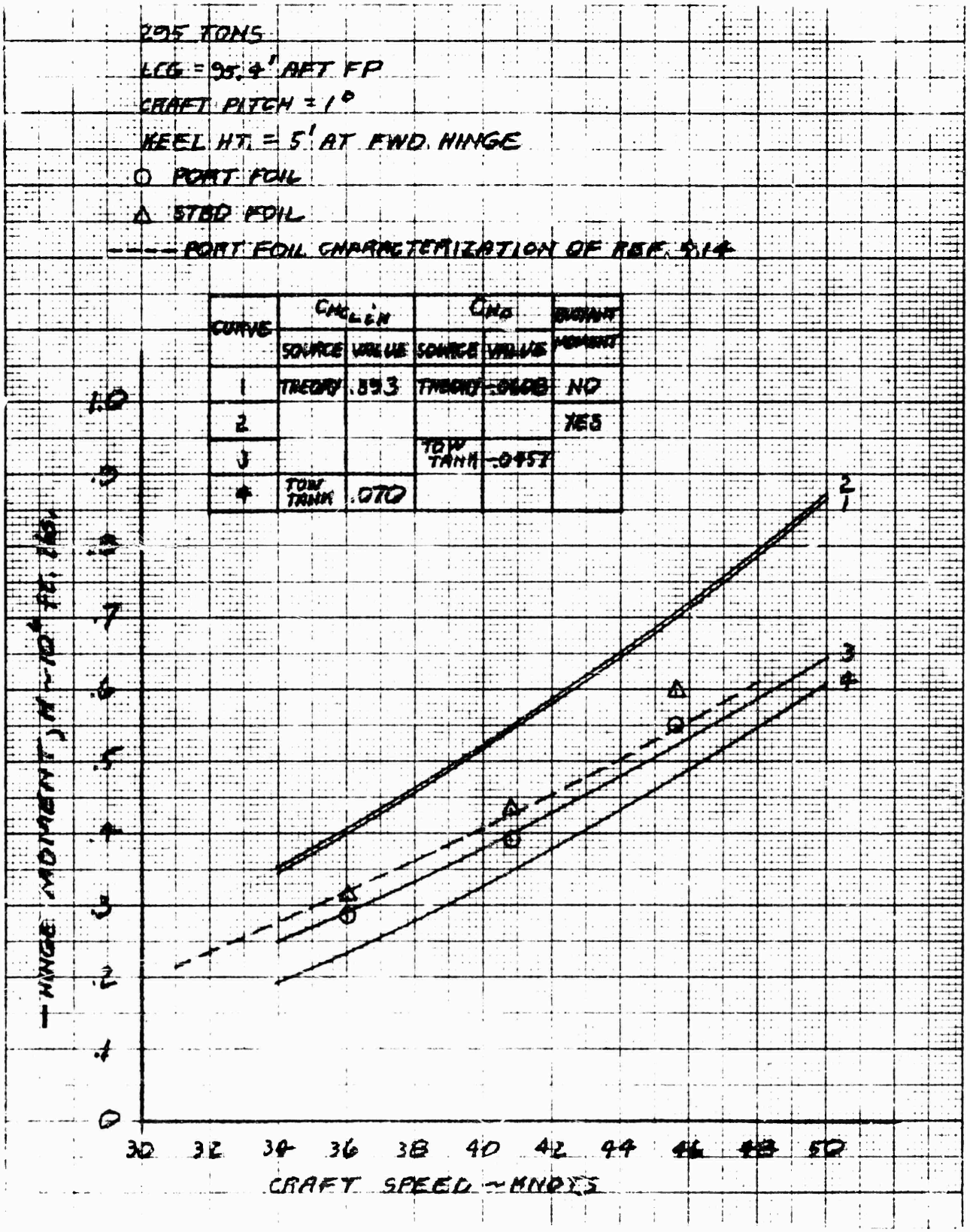


Figure 4-11. Prototype Fwd. Foil Hinge Moment

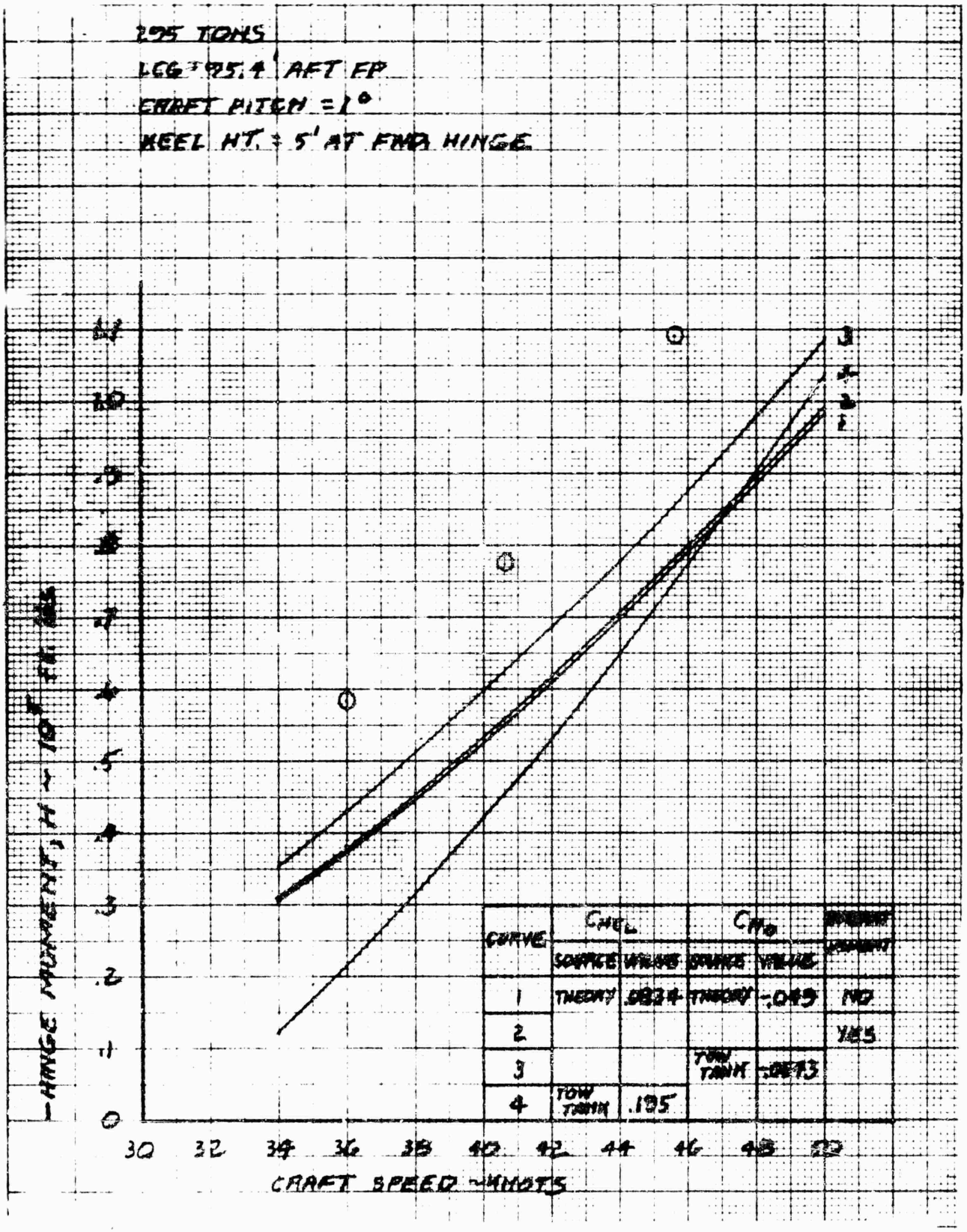


Figure 4-12. Prototype Aft Foil Hinge Moment

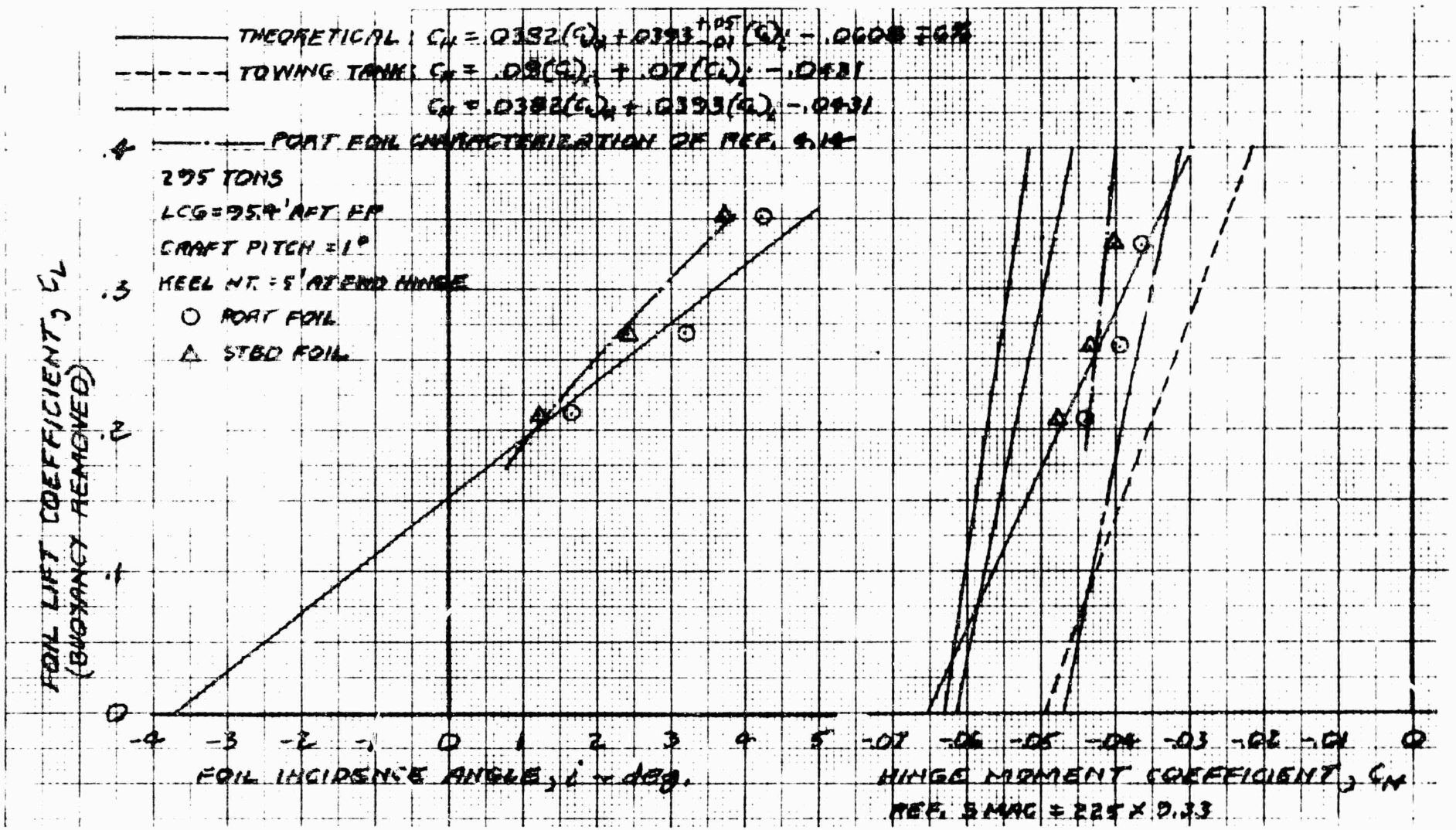


Figure 4-13. Prototype Fwd. Foil Lift and Hinge Moment

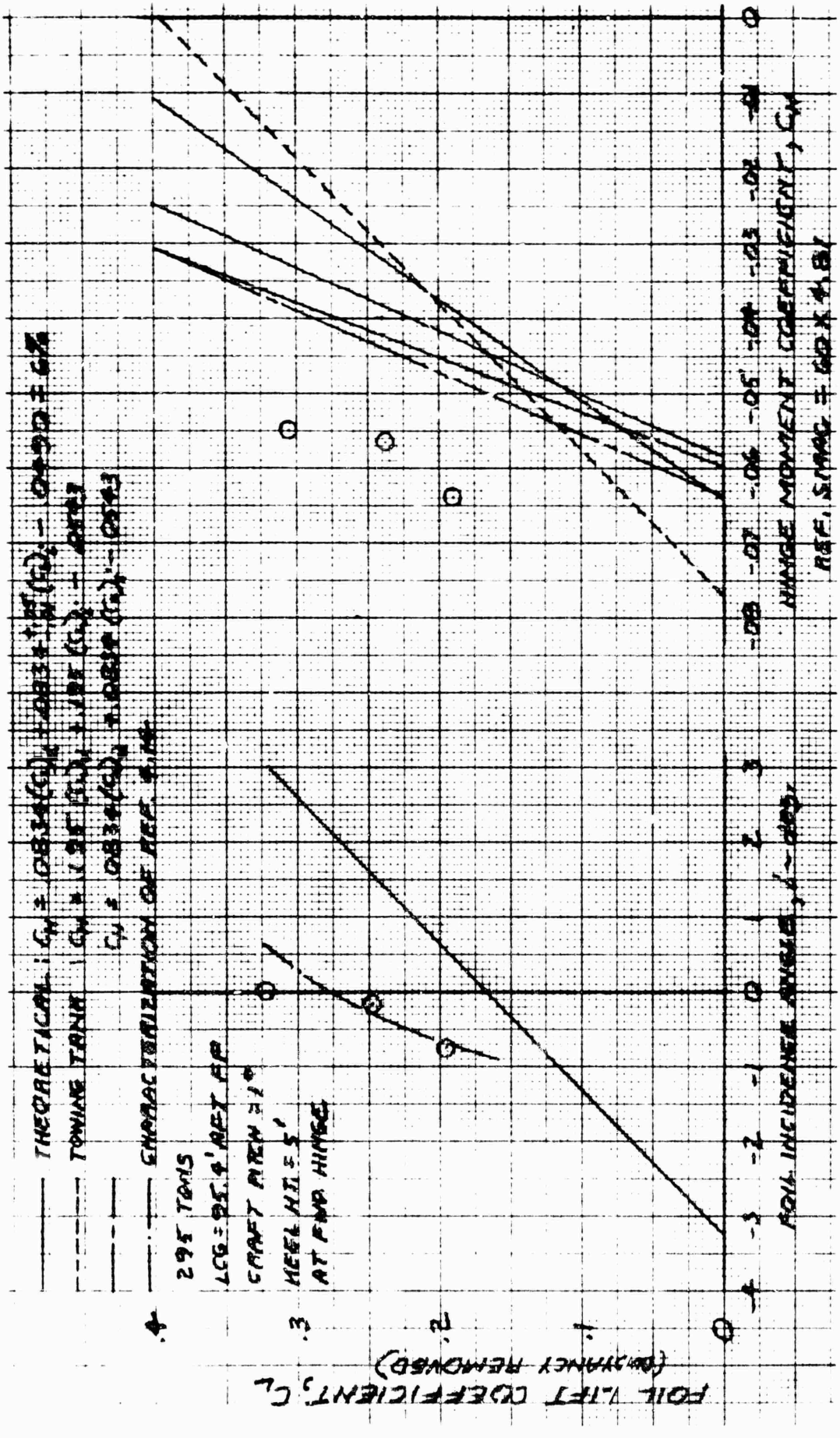


Figure 4-14. Prototype Aft Foil Lift and Hinge Moment

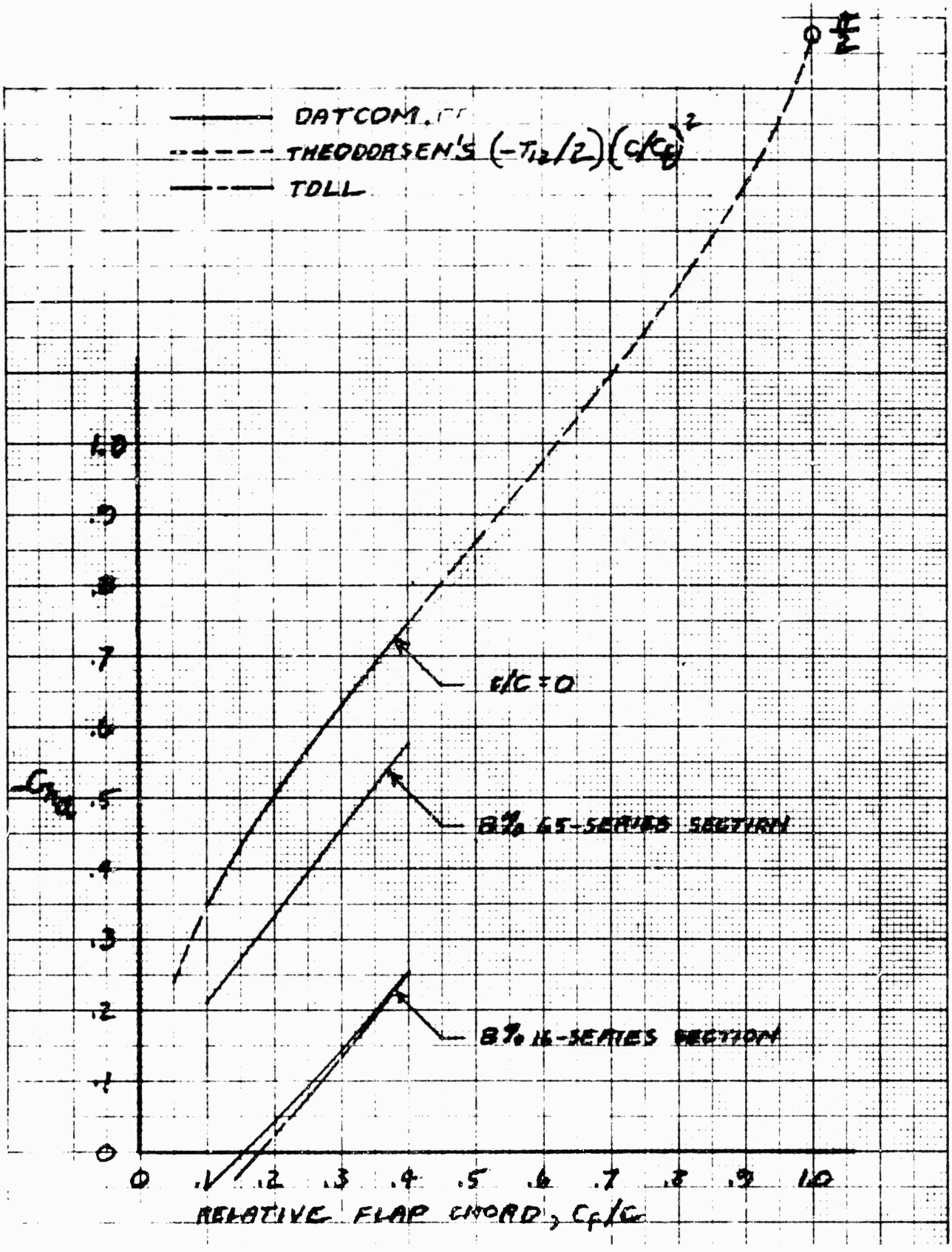


Figure 4-15. Flap Hinge Moment Derivative, C_{h_α}, 2-Dimensional

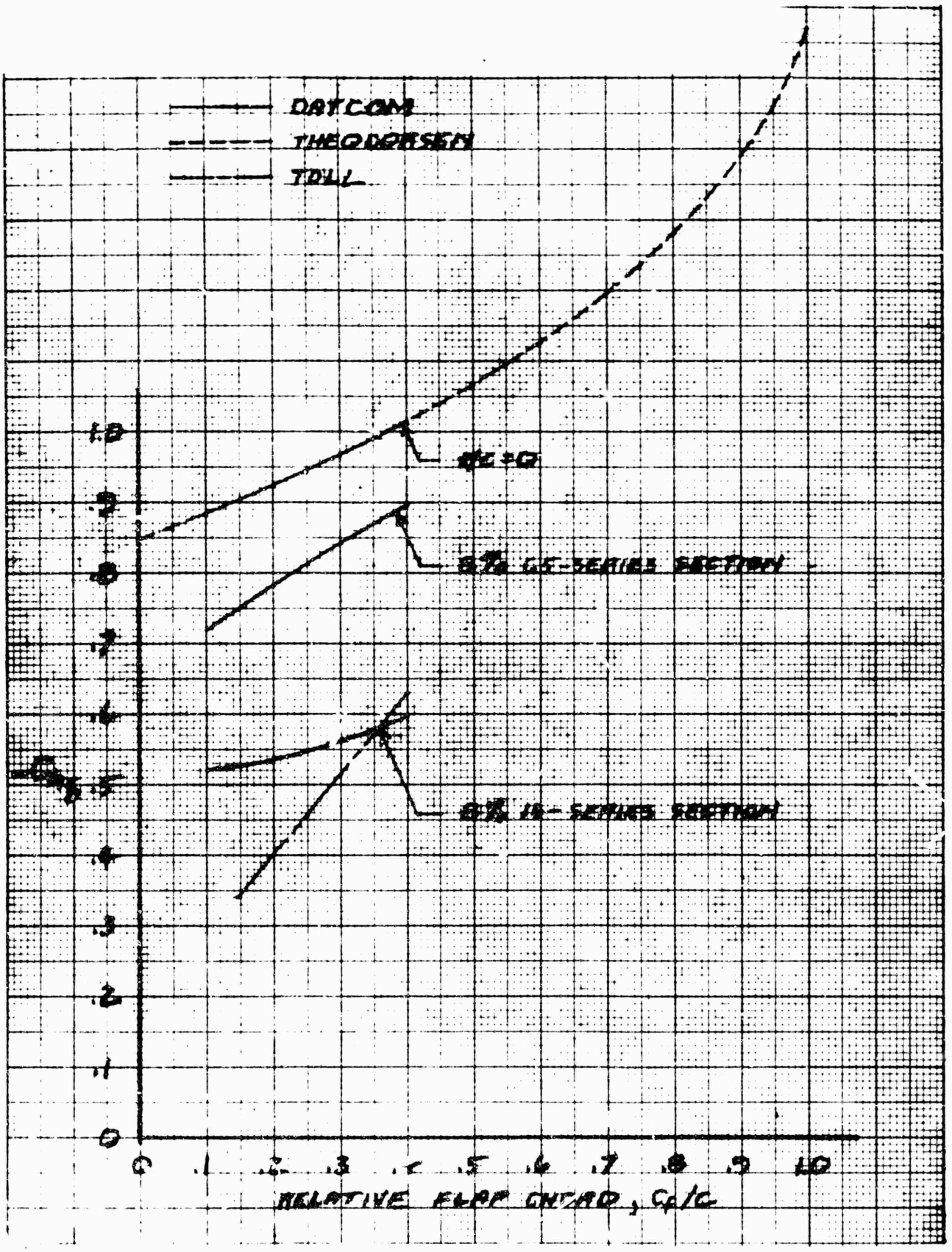


Figure 4-16. Flap Hinge Moment Derivative, C_{h_δ}, 2-Dimensional

5. UNSTEADY LOAD CHARACTERISTICS

Unsteady load effects present significant attenuations and rather large phase shifts. Reference 5-9 demonstratesthat these effects can extend to wavelengths of significance to the hydrofoil craft.

The hydrofoil can present from nine to twenty unsteady load responses, depending upon configuration. The AG(EH), fitted with flap lift control and variable incidence, requires evaluation of all twenty of these responses for autopilot and/or structural considerations. The unsteady load review of this section is not intended to be an exhaustive theoretical review of the subject or to contribute to the state-of-the-art. It is only intended to review the predictions available for unsteady load response and to measure the confidence level associated with those predictions in order to provide the best possible representation for unsteady lift for the concurrent optimal control program development reported in Volume II of this report.

In one area it was necessary to proceed beyond classic aircraft practice for unsteady load. In aircraft practice, there is no wave celerity and wavelength and frequency are inversely proportional. Hydrofoils never encounter a zero wave celerity and it was necessary to consider the spatial (circulatory) and inertial terms separately. For foil motion responses this presents no problem because Theodorsen has displayed these two effects. In the case of orbital motion only Leehey and Nishayama, of the literature reviewed, have recognized the significance of the difference between wavelength and frequency and neither of them displayed the spatial and inertial terms in a manner convenient to modification to a particular 3-dimensional case. Greenberg was therefore employed to derive Leehey's result with an intermediate step displaying the two terms of interest. The final lift result, however, presents a contradiction with Leehey which remains to be resolved.

The significance of the wavelength/frequency distinction is not considered in this report. Efforts now underway are directed to examining the significance of every unsteady load term to the autopilot design in order to minimize the complexity which these effects introduce into the optimal control program.

The particular unsteady load responses, predictions, and experimental results considered in this section are listed in Tables 5-1, 5-2, and 5-3, respectively. The sub-section and figures associated with each response are listed in Table 5-4 and a judgment of the confidence level for each response is presented in Table 5-5. The 1972 AG(EH) flapped model test results are not considered in the main body of this report; they are presented in an appendix.

5.1 JONES' FOIL MOTION AND GUST FUNCTIONS

Jones' Eqs. (29) and (30) of Reference 5-1 may be written

$$C(S)_{A=\infty} = 1 - .165\, e^{-.045S} - .335\, e^{-.300S}$$

$$C(S)_{A=6} = 1 - .361\, e^{-.381S}$$

$$C(S)_{A=3} = 1 - .283\, e^{-.54S}$$

$$\text{where } C(S) = C_{L_{\alpha_U}} / C_{L_{\alpha}} \qquad (5.1.1)$$

These are approximate expressions, in a form convenience to analysis, which reconcile conflicting distinct theories at zero S. A significant amount of smoothing is involved for distances less than 3/4 chord, where the starting vortex lies in the foil, and perhaps extending to as much as two chord lengths.

The inverse wavelength form of (5.1.1) is

$$C(k)_{A=\infty} = 1 - \frac{i.165k}{.045 + ik} - \frac{i.335k}{.3 + ik}$$

$$C(k)_{A=6} = 1 - \frac{i.361k}{.381 + ik}$$

$$C(k)_{A=3} = 1 - \frac{i.283k}{.54 + ik} \qquad (5.1.2)$$

of which the last two are Jones' Eq. (39) divided by the ratio of the 2-dimensional to the finite aspect ratio lift curve slope. The two-dimensional form of Eq. (5.1.2) is

virtually identical with Theodorsen's function. All three forms of the equation present the circulatory portion of the unsteady lift; the inertial portion remains to be accounted for. Eq. (5.1.2) is presented graphically on Figure 5-1 for reference.

Jones' Eq. (45) gives the lift transient response to a gust as

$$G(S)_{A=\infty} = 1 - .236\, e^{-.058S} - .513\, e^{-.364S} - .171\, e^{-2.42S}$$

$$G(S)_{A=6} = 1 - .448\, e^{-.29S} - .272\, e^{-.725S} - .193\, e^{-3S}$$

$$G(S)_{A=3} = 1 - .679\, e^{-.558S} - .227\, e^{-3.2S}$$

$$\text{where } G(S) = C_{L_{\alpha_w}} / C_{L_\alpha} \qquad (5.1.3)$$

which are analytically convenient approximations for the rationally derived response curves of his Figure 9. Eq. (5.1.3) assumes a rectangular planform and S = 0 represents the penetration of a sharp-edged gust by the leading edge. The inverse wavelength equivalent of Eq. (5.1.3) is

$$G(k)_{A=\infty} = 1 - \frac{i.236k}{.058 + ik} - \frac{i.513k}{.364 + ik} - \frac{i.171k}{2.42 + ik}$$

$$G(k)_{A=6} = 1 - \frac{i.448k}{.29 + ik} - \frac{i.272k}{.725 + ik} - \frac{i.193k}{3 + ik}$$

$$G(k)_{A=3} = 1 - \frac{i.679k}{.558 + ik} - \frac{i.227k}{3.2 + ik} \qquad (5.1.4)$$

The total lift response, inciuding inertial effects, is included in Eq. (5.1.4) but only for the case where the reduced inverse wavelength and reduced frequency are identical; i.e., only when k = k'. For this particular case, Jones' 2-dimensional result is virtually identical with Sears' function and with Bisplinghoff's representation (Eq. 5-376 of Reference 5-2), except that both of the alternative forms reference the response phase to the angle of attack at mid-chord rather than to the angle of attack at the leading edge.

Eq. (5.1.4) is presented graphically on Figure 5-2 for reference but is only an approximation for the hydrofoil case where k and k' cannot be equal. More appropriate forms for the hydrofoil case are considered in Section 5.11.

5.2 HEAVE LIFT

For a foil heaving in smooth water, k and k' are identically given by Eq. (3.7) and Eq. (3.1) degenerates to

$$C_{L_h} = \frac{2\pi}{c} k^2 h - i \frac{2}{c} khC_{L_\alpha} C(k)$$

$$= \frac{2\pi}{c} \times \frac{\omega c}{2V} hk - i \frac{2}{c} \frac{\omega c}{2V} hC_{L_\alpha} C(k)$$

$$= \left[C_{L_\alpha} C(k)\right] + i\pi k \left(-\frac{\dot{h}}{V}\right) \qquad (5.2.1)$$

The instantaneous angle of attack is $-\dot{h}/V$ and Eq. (5.2.1) is conveniently expressed as

$$\Lambda_h = \frac{C_{L_{\alpha_h}}}{C_{L_\alpha}} = \frac{C_{L_h}/(-\dot{h}/V)}{C_{L_\alpha}} = C(k) + i \frac{\pi}{C_{L_\alpha}} k \qquad (5.2.2)$$

Theodorsen's prediction is aerodynamic and a first order approximation for free surface effect is made in Eq. (5.2.2) by applying a classic free surface effect correction to the steady-state lift curve slope, C_{L_α}.

The only heave unsteady lift measurements considered for this report were those of Pattison in Reference 5-3. Pattison compares theory and experiment in the form (noting that the heave sign convention here reverses that of Pattison):

$$C_{L_T} = \frac{L_h}{\pi \rho V^2 k^2 (-h) b} = \frac{L_h}{-\frac{\rho}{2} V^2 \pi k \frac{c}{V} \omega h b}$$

$$= \frac{L_h}{-\frac{\rho}{2} V^2 \pi k b c i \left(-\frac{\dot{h}}{V}\right)} = \frac{C_{L_h}}{-i\pi k \left(-\frac{\dot{h}}{V}\right)}$$

$$= i \frac{C_{L_{\alpha_h}}}{\pi k} \qquad (5.2.3)$$

Then Pattison's results are related to Theodorsen's prediction in the form of Eq. (5.2.2) by

$$C_{L_{\alpha_h}} = i \pi k C_{L_T}$$

$$\Lambda_h = \frac{C_{L_h} / \frac{-\dot{h}}{V}}{C_{L_\alpha}} = -i \frac{\pi k}{C_{L_\alpha}} C_{L_T}$$

$$= \frac{\pi k}{C_{L_\alpha}} C_{L_T} \angle -\frac{\pi}{2} \qquad (5.2.4)$$

Pattison's measured steady-state lift curve slopes are presented on Figure 5-3 where they are compared with the Geising-Smith prediction of Pattison's report, with Feldman's prediction of Reference 5-4, and the Gibbs & Cox prediction of Reference 5-5. The Feldman and Gibbs & Cox represent the extreme range of a number of classic slope predictions available. The low measured slopes of Figure 5-3 reflect doubt on the unsteady lift results as well and only one set of Pattison's results is presented in this report.

Figures 5-4 and 5-5 compare Pattison's measured heave unsteady lift at one chord submergence with several predicted heave responses and are typical of the results throughout the depth range tested except that the 5^0 α effect at 6.32 Froude number is not apparent at the other depths.

The Widnall predictions of Figures 5-4 and 5-5 are from Pattison's report. Theodorsen's unsteady lift is compared with the Theodorsen function on the figures to display the wavelength at which the inertial terms become significant; that wavelength

would be increased in head seas and reduced in following seas. The Smullin & Bender predictions are from Figure 10 of Reference 5-6. The Stark program prediction is from a Saab Aircraft flutter analysis program which is not particularly well suited to this purpose since the lift results are an intermediate step; a program modification and a substantial hand calculation effort were required to display those lift results. Stark's Reference 5-7 has been received since the derivation of the predictions of this report and would provide for a more convenient evaluation of the aerodynamic case. Of course, the Widnall and Bolt, Beranek, & Newman work present the best potential for the hydrofoil case.

In view of the questionable precision of the data, the Pattison results present no practical necessity for any more sophisticated prediction procedure for the heave lift case than that of Theodorsen's Reference 5-8.

5.3 HEAVE MOMENT

For a foil heaving in smooth water, k and k' are identically given by Eq. (3.7) and Eq. (3.2) degenerates to

$$C_{H_h} = \frac{2\pi}{c}\frac{S'}{S}\frac{MGC'}{c}\left(\frac{H}{c}-\frac{1}{2}\right)k^2 h - i\frac{2}{c}C_{L_\alpha}C(k)\left(\frac{H}{c}-\frac{1}{4}\right)k\,h$$

$$= \frac{2\pi}{c}\frac{S'}{S}\frac{MGC'}{c}\left(\frac{H}{c}-\frac{1}{2}\right)\frac{\omega^2}{2V}k\,h - i\frac{2}{c}C_{L_\alpha}C(k)\left(\frac{H}{c}-\frac{1}{4}\right)\frac{\omega c}{2V}h$$

$$= \left[C_{L_\alpha}\left(\frac{H}{c}-\frac{1}{4}\right)C(k) + i\pi\frac{S'}{S}\frac{MGC'}{c}\left(\frac{H}{c}-\frac{1}{2}\right)k\right]\left(-\frac{\dot{h}}{V}\right) \qquad (5.3.1)$$

which is conveniently evaluated as

$$H_h = \frac{C_{H_{\alpha_h}}}{C_{H_\alpha}} = \frac{C_{H_h}/(-\dot{h}/V)}{C_{H_\alpha}}$$

$$= \frac{1}{C_{H_\alpha}} \left[C_{L_\alpha} \left(\frac{H}{c} - \frac{1}{4} \right) C(k) + i\pi \frac{S'}{S} \frac{MGC'}{c} \left(\frac{H}{c} - \frac{1}{2} \right) k \right] \qquad (5.3.2)$$

For the steady state case, the hinge moment coefficient slope is

$$C_h = \left(\frac{H}{c} - \frac{1}{4} \right) C_{L_\alpha} (-\dot{h}/V)$$

$$C_{h_\alpha} = \left(\frac{H}{c} - \frac{1}{4} \right) C_{L_\alpha} \qquad (5.3.3)$$

which is a classic relationship and which reduces Eq. (5.3.2) to

$$H_h = C(k) + i \frac{\pi}{C_{L_\alpha}} \frac{S'}{S} \frac{MGC'}{c} \frac{\frac{H}{c} - \frac{1}{2}}{\frac{H}{c} - \frac{1}{4}} k \qquad (5.3.4)$$

For the 2-dimensional case there is a further reduction to

$$H_h = C(k) + i \frac{\pi}{c_{\ell_\alpha}} \frac{\frac{H}{c} - \frac{1}{2}}{\frac{H}{c} - \frac{1}{4}} k \qquad (5.3.5)$$

The amplitude for H_h is unbounded for the general case and carries little intuitive significance, therefore Theodorsen's incidence hinge moment is compared with Pattison's data in the 2-dimensional form of Eq. (5.3.1):

$$C_{H_{\alpha_h}} = C_{\ell_\alpha} \left(\frac{H}{c} - \frac{1}{4} \right) C(k) + i\pi \left(\frac{H}{c} - \frac{1}{2} \right) k \qquad (5.3.6)$$

and that comparison is made with reference to the quarter-chord station:

$$C_{H_{\alpha_h}}{}_{c/4} = -i\frac{\pi}{4}k \tag{5.3.7}$$

Note that, for the aerodynamic case, all of the heave quarter chord moment is produced by the inertial load acting at the half-chord. The hydrodynamic case alters this relationship only slightly by modifying the circulatory chordwise pressure distribution.

Theodorsen's unsteady moment is related to Pattison's form of the coefficient by (again noting a reversal for the heave sign convention):

$$C_{M_T} = \frac{M_H}{\pi \rho V^2 \frac{c}{2} k^2 (-h)} = \frac{M_H/q\,S}{-\pi k^2 \frac{c}{2Vk}(-\dot{h})}$$

$$= \frac{M_H/q\,Sc}{-i\pi\frac{k}{2}\left(-\frac{\dot{h}}{V}\right)} = \frac{C_{H_{\alpha_h}}}{-i\pi\frac{k}{2}}$$

$$C_{H_{\alpha_h}}{}_{c/4} = \pi\frac{k}{2}\left|C_{M_T}\right| \angle\left(\phi_{M_T} - \frac{\pi}{2}\right) \tag{5.3.8}$$

which, for Pattison's data, is related to the quarter-chord station by

$$C_{H_{\alpha_h}}{}_{c/4} = C_{H_{\alpha_h}}{}_{.4165} + C_{L_{\alpha_h}}(.25 - .4165)$$

$$= C_{H_{\alpha_h}}{}_{.4165} - .1665\,C_{L_{\alpha_h}} \tag{5.3.9}$$

A typical comparison between the Pattison data and the predictions considered here is shown on Figures 5-5 and 5-6. The validity of these comparisons for the Stark result is doubtful because the Stark result was derived for the AG(EH) foil planform and adjusted to the 2-dimensional case only by changing the reference lift curve slope. As for the heave lift, the Pattison data will not support a necessity for any more sophisticated analysis than that of Theodorsen.

5.4 PITCH LIFT

For a foil pitching in smooth water, k and k' are identically given by Eq. (3.7) and Eq. (3.1) degenerates to:

$$C_{L_P} = \left[1 + i\,2\left(\frac{3}{4} - \frac{H}{c}\right)k\right]\left(\theta + \frac{C_{L_i}}{C_{L_\alpha}}\,i\right) C_{L_\alpha} C(k) + \pi k\left[2\left(\frac{H}{c} - \frac{1}{2}\right)k + i\right]\left(\theta + \frac{S'}{S}\,i\right) \qquad (5.4.1)$$

Further reduction depends upon whether it is the pitch or incidence lift case which is presented:

$$\Lambda_\theta = \frac{C_{L_{P_\theta}}/\theta}{C_{L_\alpha}} = \left[1 + i\,2\left(\frac{3}{4} - \frac{H}{c}\right)k\right] C(k) + \frac{\pi}{C_{L_\alpha}}\,k\left[2\left(\frac{H}{c} - \frac{1}{2}\right)k + i\right] \qquad (5.4.2)$$

$$\Lambda_i = \frac{C_{L_{P_i}}/i}{C_{L_i}} = \left[1 + i\,2\left(\frac{3}{4} - \frac{H}{c}\right)k\right] C(k) + \frac{\pi}{C_{L_i}}\,\frac{S'}{S}\,k\left[2\left(\frac{H}{c} - \frac{1}{2}\right)k + 1\right] \qquad (5.4.3)$$

The difference between the coefficients for the inertial terms is scarcely significant since S'/S is a reasonably good approximation for C_{L_i}/C_{L_α}; e.g., the area ratio for the AG(EH) forward foil is .813 and the lift curve slope ratio is .838. The hinge location, however, has not been defined for the incidence lift case. Intuitively it seems that the hinge should be located on the exposed foil MAC for this case rather than on the total foil MAC and it is so defined in this report. For this definition Eqs. (5.4.2) and (5.4.3) are virtually identical and it is the incidence lift form which is presented on Figures 5-8 through 5-11 with spot comparisons with the pitch lift result at two wavelengths.

Submergence enters Eqs. (5.4.2) and (5.4.3) as a steady-state lift curve slope but the significance is slight. The 1.14 MGC submergence slope is presented in the figures with spot comparisons with the .57 MGC submergence result at two wavelengths.

The test applied to Theodorsen's pitch lift, which is aerodynamic, for the hydrodynamic case is that provided by O'Neill's data of Reference 5-9 which presents the incidence lift case. Two other predictions are compared with Theodorsen and with O'Neill's data on Figures 5-8 through 5-11.

- Widnall's hydrodynamic lifting surface program. This is not the 2-dimensional prediction of Reference 5-9 but a later 3-dimensional prediction supplied by the Contracting Officer
- The Stark aerodynamic lifting surface program previously mentioned.

The Smullin and Bender hydrodynamic lifting surface program is of particular interest because it provides flap effects but the unsteady pitch lift of Figure 13 of Reference 5-6 is 2-dimensional and referenced to a quarter-chord hinge location; therefore not comparable with O'Neill's data. The Smullin and Bender result is related to O'Neill's data here, though remotely, by comparison with the 2-dimensional form of Eq. (5.4.1) with a quarter-chord hinge on Figures 5-12 and 5-13. For this case the Theodorsen equation reduces to:

$$\Lambda_P = \frac{C_{L_P}/\theta}{C_{L_\alpha}} = (1 + i\,k)\,C(k) + \frac{k}{2}\left(-\frac{k}{2} + i\right) \quad \text{aerodynamic}$$

$$= (1 + i\,k)\,C(k) + 1.208\,\frac{k}{2}\left(-\frac{k}{2} + i\right) \text{ for } \frac{h}{c} = \frac{1}{2} \qquad (5.4.4)$$

Figures 5-8 through 5-11 do not indicate any practical requirement for resort to the added complexity of the lifting surface theory.

5.5 PITCH MOMENT

For a foil pitching in smooth water, k and k' are identically given by Eq. (3.7) and Eq. (3.2) degenerates to

$$C_H = \left(\frac{H}{c} - \frac{1}{4}\right)\left[1 + i\,2\left(\frac{3}{4} - \frac{H}{c}\right)k\right]\left(\theta + \frac{C_{L_i}}{C_{L_\alpha}}\,i\right) C_{L_\alpha}\,C(k)$$

$$+ 2\pi \frac{S'}{S} \frac{MAC'}{MAC} k \left\{ \left[\frac{1}{32} + \left(\frac{H}{c} - \frac{1}{2} \right)^2 \right] k - i \frac{1}{2} \left(\frac{3}{4} - \frac{H}{c} \right) \right\} i$$

$$+ 2\pi k \left\{ \left[\frac{1}{32} + \left(\frac{H}{c} - \frac{1}{2} \right)^2 \right] k - i \frac{1}{2} \left(\frac{3}{4} - \frac{H}{c} \right) \right\} \theta \qquad (5.5.1)$$

where it must be understood that the final term is inferred in Eq. (3.2)

All of the parenthetical terms containing the hinge location are from 2-dimensional theory and none have been defined for the practical case. In one instance the $\left(\frac{H}{c} - \frac{1}{4} \right)$ term becomes identifiable if the circulatory term is written in the form:

$$(C_{H_{C_L}})_C = C_{H_C} \Big/ \left(\theta + \frac{C_{L_i}}{C_{L_\alpha}} i \right) C_{L_\alpha}$$

$$= \left(\frac{H}{c} - \frac{1}{4} \right) C(k) + i\, 2 \left(\frac{H}{c} - \frac{1}{4} \right) \left(\frac{3}{4} - \frac{H}{c} \right) k\, C(k)$$

$$= C_{H_{C_L}} C(k) + i\, 2 \left(\frac{H}{c} - \frac{1}{4} \right) \left(\frac{3}{4} - \frac{H}{c} \right) k\, C(k) \qquad (5.5.2)$$

where the measured $C_{H_{C_L}}$'s of Table 4-2 are employed in this study.

It is not so obvious, and in fact it is unlikely, that the second occurence of $\left(\frac{H}{c} - \frac{1}{4} \right)$ is $C_{H_{C_L}}$. Throughout this study, except for the one use of $C_{H_{C_L}}$, the hinge has been related to the total foil MAC for pitch lift and to the exposed foil MAC for incidence lift. The chord reference stations -- 1/4, 1/2, and 3/4 -- are employed unchanged. Actually for the 3-dimensional case the fractional terms require redefinition.

O'Neill's data is compared with Theodorsen, Widnall, and Stark on Figures 5-14 through 5-17 where the following comments are in order.

Theodorsen's prediction correlates well with O'Neill's data throughout except for phase for the 32% hinge on the shortest waves. The indication is that the camber term

of the circulatory terms or, more likely, the pitch acceleration term needs more attention. Note that it is the experimental $C_{H_{C_L}}$ of Section 4 which correlates the data of Figures 5-14 and 5-15. The theoretical $C_{H_{C_L}}$ of that section does not produce as good a correlation, inferring good consistency between the measured steady-state and unsteady hinge moments. The relative insignificance of the circulatory term is encouraging because elimination of this term would eliminate a troublesome cross product, $\alpha\, C_{L_\alpha}\, C(k)$, in the equations of motion.

The Widnall prediction has overemphasized the steady-state moment slope for the 32% hinge with a consequential effect on the phase. The effect is not so evident for the 6.2% hinge where $C_{H_{C_L}}$ is not critical but the practical case is the low $C_{H_{C_L}}$, preferably zero, case. Note that one disadvantage of the lifting surface programs is the accessability of individual characteristics for modification.

The Stark program also missed the steady-state hinge moment and is presented on the figures as the product of gain and the measured steady-state hinge moment. The procedure is not really valid for amplitude, however, and does not affect phase so the result is not satisfactory.

Smullin and Bender's prediction is not available in 3-dimensions and is compared with Theodorsen's 2-dimensional result on Figures 5-18 and 5-19. The aerodynamic result only indicates that Smullin and Bender produce Theodorsen at infinite submergence.

For the 2-dimensional case, Theodorsen's unsteady moment about the quarter-chord reduces to

$$C_{H_{\theta_P}} = \frac{\pi}{2}\, k(.375\, k - i) \qquad (5.5.3)$$

having no circulatory contribution. What the lifting surface programs can provide, which is not yet available in analytic form, is the steady-state moment, i.e., the

chordwise load distribution, which must vanish relative to the quarter-chord in Theodorsen's unsteady lift. Comparison of Smullin and Bender's Figures 13 and 14 indicate an aerodynamic center shift of almost 2% of the chord forward at a steady-state submergence of 1/2 chord. The effect on the moment amplitude on Figure 5-18 is small, but there is a significant effect on the phases of Figure 5-19.

In summary, Theodorsen provides reasonably good correlation for O'Neill's hinge moment data and better correlation than is available at present with the lift surface theories, though Theodorsen does not provide the understanding of free surface effect that will become available with a fully-developed lifting surface theory.

5.6 FLAP LIFT

For flap motion on a 2-dimensional airfoil in smooth water, k and k' are identically given by Eq. (3.7) and Eq. (3.1) degenerates to

$$C_L = \left(\frac{d\alpha}{d\delta} + i\frac{1}{2}\frac{T_{11}}{\pi}k\right) C_{L_\alpha}\,\delta\, C(k) + \pi k\left(\frac{T_1}{\pi}k - i\frac{T_4}{\pi}\right)\delta$$

$$\Lambda_F = \frac{C_L/\delta}{\frac{d\alpha}{d\delta}C_{L_\alpha}} = \left(1 + i\frac{1}{2}\frac{T_{11}/\pi}{d\alpha/d\delta}\cdot k\right) C(k) + \frac{\pi}{C_{L_\alpha}}\frac{k}{d\alpha/d\delta}\left(\frac{T_1}{\pi}k - i\frac{T_4}{\pi}\right) \qquad (5.6.1)$$

For the theoretical, thin airfoil, case $d\alpha/d\delta$ is Theodorsen's T_{10}/π, given here in Table 3-1. For the practical case, the flap effectiveness may be taken from Toll's Reference 5-10 or equivalent or from model tests. Eq. (5.6.1) is aerodynamic but a first order approximation to the hydrodynamic case may be obtained by making the classic adjustment to the lift curve slope.

Eq. (5.6.1) is compared with Smullin and Bender's Figure 16 on Figures 5-20 and 5-21. Also shown on these figures is Theodorsen's equation for the AG(EH) forward foil at 1/2 chord submergence:

$$C_{L_\delta} = \left(\frac{d\alpha}{d\delta} + i\frac{1}{2}\frac{T_{11}}{\pi}k\right) C_{L_j}\, C(k) + \pi\frac{S'}{S}k\left(\frac{T_1}{\pi}k - i\frac{T_4}{\pi}\right)$$

$$A_F = \left(1 + i\frac{1}{2}\frac{T_{11}/\pi}{d\alpha/d\delta}k\right) C(k) + \frac{\pi}{C_{L_\delta}}\frac{S'}{S}k\left(\frac{T_1}{\pi}k - i\frac{T_4}{\pi}\right)$$

$$= \left(1 + i\frac{1}{2} \times \frac{.2975}{.47}k\right) C(k) + \frac{\pi}{.47 \times 2.06} \times .813\,k(-.02322\,k + i\,.1424)$$

$$= (1 + i\,.3165\,k)\,C(k) - .0611\,k(k - i\,6.14) \qquad (5.6.2)$$

The AG(EH) foil response has been measured in the towing tank but the results are still being analyzed at this writing and will be reviewed in an appendix to this volume.

Figures 5-20 and 5-21 indicate that this response is probably insignificant to the AG(EH) though significant for foils of higher aspect ratio.

5.7 FLAP HINGE MOMENT

For flap motion on a 2-dimensional airfoil in smooth water, k and k' are identically given by Eq. (3.7) and Eq. (3.3) degenerates to:

$$C_h = \frac{M_h}{q\,S_f\,c_f} = \frac{S}{S'}\left(\frac{c}{c_f}\right)^2\frac{M_h}{q\,Sc}$$

$$= C_{h_\alpha}\left(\frac{d\alpha}{d\delta} + i\frac{1}{2}\frac{T_{11}}{\pi}k\right)\delta\,C(k)$$

$$= \left[C_{h_\delta} - \frac{d\alpha}{d\delta}C_{h_\alpha} - \frac{1}{2}\left(\frac{c}{c_f}\right)^2\frac{T_3}{\pi}k^2 + i\frac{\pi}{4}\left(\frac{c}{c_f}\right)^2\frac{T_4}{\pi} - \frac{T_{11}}{\pi}k\right]\delta \qquad (5.7.1)$$

For the theoretical, thin airfoil, case the flap hinge moment derivative C_{h_α} is related to Theodorsen's T_{12} and may be taken from Table 3-1. The practical case is more difficult and uncertain. For this report the 2-dimensional value of this derivative has been evaluated by the methods of References 5-10 and 5-11, which are quite similar for two sections of interest to hydrofoils with the results presented on Figure 5-22. The 3-dimensional derivative may practically be evaluated as:

$$\underline{C}_{h_\alpha} = \frac{C_{L_i}}{C_{\ell_\alpha}} C_{h_\alpha} \approx \frac{C_{L_i}}{2\pi} C_{h_\alpha} \qquad (5.7.2)$$

which is essentially the 3-dimensional evaluation of Perkins & Hage in Reference 5-12.

The thin airfoil, 2-dimensional flap hinge moment derivative C_{h_δ} can be related to Theodorsen's "T" coefficients by writing the steady-state form of Eq. XIX) of Reference 5-8 for flap deflection:

$$\frac{M_h}{b} = \rho V \frac{c^2}{4} T_{12} \frac{1}{\pi} T_{10} V \delta - \rho \frac{c^2}{4} \frac{1}{\pi} V^2 (T_5 - T_4 T_{10}) \delta$$

$$C_{h_\delta} = \frac{M_h/\delta}{q b c_f^2} = \frac{(c/c_f)^2}{2} \left[\frac{T_5}{\pi} - \left(\frac{T_4}{\pi} - \frac{T_{12}}{\pi} \right) \frac{T_{10}}{\pi} \pi \right] \qquad (5.7.3)$$

which is compared with the practical values of Toll and the Datcom on Figure 5-23.

Toll does not give a conversion to the 3-dimensional case for this derivative and the Datcom conversion is not very convenient. The following conversion is adapted from Perkins and Hage and is presented without theoretical justification.

$$\underline{C}_{h_\delta} = C_{h_\delta} + \frac{d\alpha}{d\delta} \left(\underline{C}_{h_\alpha} - C_{h_\alpha} \right)$$

$$= C_{h_\delta} + \frac{d\alpha}{d\delta} \left(\frac{C_{L_i}}{2\pi} - 1 \right) C_{h_\alpha} \qquad (5.7.4)$$

Smullin and Bender's flap moment response is compared with Theodorsen's on Figures 5-24 and 5-25 which indicate little practical difference between the two predictions. The comparison is worsened when the Smullin and Bender steady-state derivatives are substituted for Theodorsen's in the Theodorsen equation. Presumably this is because Theodorsen's coefficients are so interrelated that changes in any coefficient reflect changes in others. It would be desirable to identify all of Theodorsen's "T" coefficients in order to adapt his equations to the practical case with more confidence. The 20% chord Theodorsen result is shown on Figures 5-24 and 5-25 to relate these figures to the following two figures.

The Stark program, which was for the AG(EH) foil, is compared with Theodorsen on Figures 5-24 and 5-25. The Stark 3-dimensional and Smullin and Bender 2-dimensional results are quite similar and both differ rather significantly from the 3-dimensional Theodorsen result.

The AG(EH) flap moment response has been measured in the towing tank but the results are still being analyzed at this writing and will be reviewed in an appendix to this volume.

5.8 FLAP MOTION FOIL HINGE MOMENT

For flap motion in smooth water, k and k' are identically given by Eq. (3.7) and Eq. (3.2) degenerates to:

$$C_{H_{\delta_F}} = \left(\frac{H}{c} - \frac{1}{4}\right)\left(\frac{d\alpha}{d\delta} + i\frac{1}{2}\frac{T_{11}}{\pi}k\right)C_{L_i}C(k)$$

$$- \frac{\pi}{2}\frac{S'}{S}\frac{MAC'}{MAC}\left\{\frac{T_4}{\pi} + \frac{d\alpha}{d\delta} + \left[\frac{T_7}{\pi} + 2\left(\frac{h}{c} - \frac{H}{c}\right)\frac{T_1}{\pi}\right]k^2\right.$$

$$\left. + i\left[\frac{T_1}{\pi} - \frac{T_8}{\pi} - 2\left(\frac{h}{c} - \frac{H}{c}\right)\frac{T_4}{\pi} + \frac{1}{2}\frac{T_{11}}{\pi}\right]k\right\} \qquad (5.8.1)$$

which reduces for the steady-state case to:

$$C_{H_\delta} = \left(\frac{H}{c} - \frac{1}{4}\right)\frac{d\alpha}{d\delta}C_{L_i} - \frac{\pi}{2}\frac{S'}{S}\frac{MAC'}{MAC}\left(\frac{T_4}{\pi} + \frac{d\alpha}{d\delta}\right) \qquad (5.8.2)$$

which holds academic as well as practical interest and which is discussed further in Section 4. The numerical evaluations considered here employ for $\left(\frac{H}{c} - \frac{1}{4}\right)$ the measured incidence lift $C_{H_{C_L}}$ of Table 4-2.

Two forms of Eq. (5.8.1) are compared with Figure 18 of Reference 5-6 on Figures 5-28 and 5-29; the Stark program output is not available for this response. There are no significant differences between any of the responses considered and

this particular response may be negligible for the practical case, depending upon the sensitivity of the closed loop system to phase shift.

This response has been measured in the towing tank on the AG(EH) model but the results are still being analyzed at this writing and will be reviewed in an appendix to this volume.

5.9 FOIL HEAVE FLAP HINGE MOMENT

For a foil heaving in smooth water, k and k' are identically given by Eq. (3.7) and Eq. (3.3) degenerates to:

$$C_{h_h} = - i \frac{2}{c} C_{h_\alpha} k h C(k) + \frac{\pi}{c} \left(\frac{c}{c_f} \right)^2 \frac{T_1}{\pi} k^2 h \qquad (5.9.1)$$

and where

$$\dot{h} = i \frac{2V}{c} k h$$

$$k h = i \frac{c}{2} \left(- \frac{\dot{h}}{V} \right)$$

Eq. (5.9.1) may be written

$$C_{h_h} = C_{h_\alpha} \left(- \frac{\dot{h}}{V} \right) C(k) + i \frac{\pi}{2} \left(\frac{c}{c_f} \right)^2 \frac{T_1}{\pi} k \left(- \frac{\dot{h}}{V} \right)$$

$$\lambda_h = \frac{C_{h_h} \Big/ \left(- \frac{\dot{h}}{V} \right)}{C_{h_\alpha}}$$

$$= C(k) + i \frac{\pi}{2} \left(\frac{c}{c_f} \right)^2 \frac{T_1/\pi}{C_{h_\alpha}} k \qquad (5.9.2)$$

For the theoretical, thin airfoil case the denominator of the second term may be replaced by its Theodorsen equivalent of Note 2 of Table 3-1:

$$\lambda_h = C(k) + i \frac{T_1/\pi}{\frac{2}{\pi} \left(\frac{c}{c_f} \right)^2 C_{h_\alpha}} k$$

$$= C(k) + i \frac{T_1/\pi}{(-T_{12}/\pi)} k \qquad (5.9.3)$$

Theodorsen's response is compared with Figure 12 of Reference 5-6 on Figures 5-30 and 5-31 which indicate that this will be a troublesome response. The two sets of results differ substantially in the hinge moment slope with respect to foil angle of attack, C_{h_α}, and in the inertial, quadrature component. The quadrature component can be examined by writing Eq. (5.9.3) in the form

$$\lambda_h - C(k) = i \frac{T_1/\pi}{\frac{2}{\pi}\left(\frac{c_f}{c}\right)^2 C_{h_\alpha}} k$$

$$= i \frac{T_1/\pi}{(-T_{12}/\pi)} k \qquad (5.9.4)$$

where the first form may be expected to represent actual practice while the second form is Theodorsen's 2-dimensional, thin airfoil result. The left side of the equation is appropriate for Smullin and Bender's aerodynamic case but only approximate for the finite depth case.

Smullin and Bender's predictions are plotted in the form of Eq. (5.9.4) on Figure 5-32. The corresponding phases are nearly in quadrature and inconsequential to this analysis. The Theodorsen predictions in this form are straight lines of slope determined by the relative flap chord and by the denominator, of Eq. (5.9.4), employed. Obviously, Theodorsen and Smullin & Bender differ substantially in quadrature component, as well as in-phase component, and the problem is going to be particularly difficult for the practical case where the sections employed produce low and uncertain C_{h_α}'s.

No data has been located to test this response and the Stark program was not employed for this case.

5.10 FOIL PITCH FLAP HINGE MOMENT

For a foil pitching in smooth water, k and k' are identically given by Eq. (3.7) and Eq. (3.3) degenerates to

$$C_{h_\theta} = \left[1 + i\,2\left(\frac{3}{4} - \frac{H}{c}\right) k\right] C_{h_\alpha} C(k)$$

$$+ \pi \left(\frac{c}{c_f}\right)^2 k \left\{\frac{T_{13}}{\pi} k + i\,\frac{1}{2}\left[\frac{2}{\pi}\left(T_9 - \frac{a}{2} T_4\right) + \frac{1}{2}\,\frac{T_4}{\pi} + \frac{T_1}{\pi}\right]\right\} \qquad (5.10.1)$$

where the incidence lift case is not being considered here.

Eq. (5.10.1) is compared with Figure 15 of Reference 5-6 on Figures 5-33 and 5-34 which indicate much the same difficulty associated with the flap hinge moment response to foil heaving motion except that there are several more effects associated with the pitching motion.

No data has been located to this response and the Stark program was not employed for this case.

5.11 ORBITAL MOTION LIFT

In the notation of this volume, Eq. (12) of Greenberg's Reference 5.13 is

$$\frac{L'_C}{b} = 2\pi \rho \frac{c}{2} V^2 \frac{w_g}{V} C(k) \left[J_0(k) + J_1(k)\right] \qquad (5.11.1)$$

where the subscript, C, indicates circulatory lift.

The 2π coefficient is the 2-dimensional lift curve slope and Eq. (5.11.1) is arbitrarily generalized by writing

$$G'_C = \frac{C_{L_{\alpha_C}}}{C_{L_\alpha}} = \frac{C_{L_C} \Big/ \frac{w_g}{V}}{C_{L_\alpha}}$$

$$= \left[J_0(k) - i\,J_1(k)\right] C(k) \qquad (5.11.2)$$

where the prime indicates that the lift phase reference is the orbital angle of attack at the half-chord position.

Greenberg's Eq. (B8) in the notation of this volume may be written

$$\frac{L'_{NC}}{b} = i\,2\pi\,\rho\,\frac{c^2}{4}\,V\,\frac{w_g}{V}\,\frac{\omega}{k}\,J_1(k) \qquad (5.11.3)$$

where the subscript, NC, indicates non-circulatory (inertial) lift.

Greenberg reduced this equation for the case of a zero wave celerity but a more general reduction follows from the relationship:

$$\omega = 2\pi\,\frac{V}{\lambda} = \frac{2}{c}\,\frac{\pi}{\lambda/c}\,\frac{V + C_w}{V}\,V$$

$$= \frac{2V}{c}\,k\left(1 + \frac{C_w}{V}\right)$$

$$= \frac{2V}{c}\,k' \qquad (5.11.4)$$

Then Eq. (5.11.3) may be written

$$\frac{L'_{NC}}{b} = i\,2\pi\,\rho\,\frac{c^2}{4}\,V \times \frac{2V}{c}\,\frac{k'}{k}\,\frac{w_g}{V}\,J_1(k)$$

$$= i\,\pi\,\rho\,c\,V^2\,\frac{w_g}{V}\,\frac{k'}{k}\,J_1(k) \qquad (5.11.5)$$

This is an inertial term and the π coefficient is not related to the lift curve slope but to a fluid volume, therefore the reduction proceeds:

$$C_{L'_{NC}} = \frac{L'_{NC}}{\frac{\rho}{2}V^2\,b\,c} = i\,2\pi\,\frac{w_g}{V}\,\frac{k'}{k}\,J_1(k)$$

$$G'_{NC} = \frac{C_{L_{\alpha_{NC}}}}{C_{L_\alpha}} = \frac{C_{L_{NC}} \Big/ \frac{w_g}{V}}{C_{L_\alpha}}$$

$$= i \frac{2\pi}{C_{L_\alpha}} \frac{k'}{k} J_1(k) \qquad (5.11.6)$$

Then the total lift is given by

$$G' = G'_C + G'_{NC}$$

$$= \left[J_0(k) - i J_1(k) \right] C(k) + i \frac{2\pi}{C_{L_\alpha}} \frac{k'}{k} J_1(k) \qquad (5.11.7)$$

For the 2-dimensional case Eq. (5.11.7) reduces to

$$G' = \left[J_0(k) - i J_1(k) \right] C(k) + i \frac{k'}{k} J_1(k) \qquad (5.11.8)$$

which is to be compared with Eq. (8.26) of Leehey's Reference 5.14 and with the identical Eq. (6) of Steele's Reference 5.15:

$$G' = \left[J_0(k) - i J_1(k) \right] C(k') + i \frac{k'}{k} J_1(k) \qquad (5.11.9)$$

which makes Theodorsen's function a temporal rather than a spatial function.

For waves of zero celerity, Eqs. (5.11.8) and (5.11.9) both reduce to

$$G' = \left[J_0(k) - i J_1(k) \right] C(k) + i J_1(k) \qquad (5.11.10)$$

which is Eq. (5-376) of Bisplinghoff's Reference 5-2 and which is virtually identical numerically with Sear's function.

Eqs. (5.11.7), (5.11.8), and (5.11.10) may be shifted in phase to reference the orbital angle at the leading edge by

$$G = C' \angle -\frac{\pi}{\lambda/c}$$

$$= C' \angle -k \qquad (5.11.11)$$

and for this reference phase Eq. (5.11.10) is virtually identical numerically with Jones' 2-dimensional gust function; only Jones offers a 3-dimensional version of this function though in the volume Eq. (5.11.7) is employed with Jones' 3-dimensional C(k) and with the 3-dimensional hydrodynamic lift curve slope to approximate 3-dimensional and free-surface effects.

O'Neill offers an adjustment to the results above which accounts for the variation in dynamic pressure through the wave cycle. From Reference 5-9 that adjustment has the form

$$\Delta C_L = 2 C_L' \frac{w_g}{V} \angle -\frac{\pi}{2}$$

$$\Delta G = \frac{\Delta C_{L_\alpha}}{C_{L_\alpha}} = \frac{\Delta C_L \Big/ \frac{w_g}{V}}{C_{L_\alpha}} = 2 \frac{C_L'}{C_{L_\alpha}} \angle -\frac{\pi}{2} \qquad (5.11.12)$$

where C_L' is the steady-state lift coefficient. This q effect increment was tested in the preparation of this volume but the assumption of a fixed reference C_L' should be reexamined in the future.

In deep water gravity waves the ratio of the wave celerity to craft velocity, for head and following waves, is given by

$$\frac{C_w}{V} = \frac{1}{V}\sqrt{\frac{\lambda g}{2\pi}}$$

$$= \frac{1}{F_h}\sqrt{\frac{\lambda/c}{2\pi\, d/c}}$$

$$\text{or} = 1/F_h \sqrt{2k\frac{d}{c}} \qquad (5.11.13)$$

so the lift response, G, is a rather complex function of Froude Number, depth, and wavelength.

For Reference 5-15, Steele ran an aspect ratio 6-1/4, rectangular foil under head and following seas at the zero lift angle of attack. Wave length/height ratios were very long, ranging from 24 to 226. Measured wave celerities checked well with theoretical. Orbital velocities varied from .8% to 7.5% of model speed introducing the possibility of q variations to 15%.

For this report, Steele's data was reduced directly from his Tables 2-5 by:

$$G = \frac{L_M}{q\, S \frac{w_g}{V}\, C_{L_\alpha}} \left| - \left(k \pm \frac{\pi}{2} \right) \right. \qquad (5.11.14)$$

The following numerical values were employed

$$\rho = 1.938$$

$$S = 25 \text{ sq. in.}$$

$$\left.\begin{aligned} C_L &= 4.01 \text{ at 4" depth} \\ &= 3.68 \text{ at 2" depth} \end{aligned}\right\} \text{ Wadlin's free-surface effect}$$

to obtain

$$G = 1.485 \frac{L_M}{V w_g} \left| - \left(k \pm \frac{\pi}{2} \right) \right. \text{ at 4" depth}$$

$$= 1.62 \frac{L_M}{V w_g} \left| - \left(k \pm \frac{\pi}{2} \right) \right. \text{ at 2" depth} \qquad (5.11.15)$$

Steele's data is compared with Eq. (5.11.7), shifted in phase by Eq. (5.11.11), on Figures 5-35 and 5-36. Jones' gust function for aspect ratio 6, which is an aerodynamic result, is also shown on these figures.

Leehey notes that Eq. (5.11.10) approaches the value of C(k) for sufficiently long waves and likens the orbital lift response to the heave response on long waves. The heave response is therefore compared with Steele's data and with the predictions of Figures 5-35 and 5-36. The analogy is not good in the wavelengths of interest to the control system and is theoretically weak anyway; actually, all the unsteady load responses approach each other on long waves because they all approach unity.

O'Neill's form of the q effect is not applicable to Steele's data. The effect of the sinusoidal variation in submergence was considered briefly and should be considered in more detail in the future. The effect on the steady-state lift curve slope could produce a substantial phase shift but only a 5% change in amplitude. The effect on the instantaneous orbital angle was not examined. In summary, no accountability was found for Steele's following sea amplitude or head sea phase. The low Froude Number for Steele's data should be noted.

The data presented by Conolly in Reference 5-16 was examined but found inconclusive because of data scatter. Conolly's following sea lift responses on 24 chord-length waves, corrected for q effect, present attenuations to 1.1 with a mean at about .9. The head sea responses range to an attenuation of 1.45 with a mean at about 1.1 so the data qualitatively reverses the indication of Steele's data but with a low level of confidence.

For Reference 5-9, O'Neill ran the AG(EH) foil model under head seas at two speeds (with distinct angles of attack), two foil hinge locations (insignificant to lift data), and at a single depth. Wave length to height ratios were very long, ranging from 30 to 125. Orbital velocities do not exceed 1.5% of model speed but the model was at prototype angle of attack, introducing the possibility of q effect.

O'Neill's data is in terms of $\Delta C_{L_{\frac{c}{ht.}}}$ and is referenced to the wave peak at the mean geometric quarter chord. O'Neill's data, then, is considered here in the form

$$G = \frac{\left(\Delta C_{L_{\frac{c}{ht.}}}\right)}{\frac{w_g}{V} C_{L_\alpha \frac{c}{ht.}}} \left| - \left(\frac{\pi/2}{\lambda/c} + \frac{\pi}{2}\right)\right.$$

$$= \frac{V}{w_g} \frac{ht.}{c} \frac{1}{C_{L_\alpha}} \left(\Delta C_L \frac{c}{ht.}\right) \Big| -\left(\frac{k}{2} + \frac{\pi}{2}\right)$$

$$= \frac{V}{w_g} \frac{\lambda/c}{\lambda/ht.} \frac{1}{C_{L_\alpha}} \left(\Delta C_L \frac{c}{ht.}\right) \Big| -\frac{1}{2}(k + \pi) \qquad (5.11.16)$$

Orbital motion acts on the pitch lift curve slope which was not measured in Reference 5-9. The steady-state lift curve slope employed here was the 2.75 value which appears at 1.07 MAC on Figure 4-1. The data reduction for this report proceeded from O'Neill's tabulated values and the attenuations do not correspond to O'Neill's gains. O'Neill's q effect has been subtracted from the data and from the Leehey prediction appearing on his curves and the correction tended to reduce the scatter in his data.

O'Neill's data is compared with several predictions on Figures 5-39 and 5-40. The comparison generally presents one group of 2-dimensional predictions and another group of 3-dimensional predictions spaced neatly on opposite sides of the data. Basically the difference between the 2-D and 3-D predictions can be seen in the Jones foil motion function of Figure 5-1 and the Jones gust functions of Figure 5-2. O'Neill's data, then, simply indicates inadequate accountability for planform effects in the presence of a free surface. The accountability for planform and depth are obviously inadequate in Eq. (5.11.7) since the inertial term is assumed to be independent of both. Figures 5-39 and 5-40 indicate, by comparing Eq. (5.11.7) and the Jones gust function, that this particular inadequancy has significance in phase but not in amplitude.

It is interesting to note that if Smullin and Bender's aerodynamic curve is matched with the three dimensional curves, their hydrodynamic curve falls through the data; i.e., the prospects for a 3-dimensional version of the Smullin and Bender program appear promising.

In summary, the lift response to the orbital angle still presents theoretical and experimental contradictions of considerable academic significance. The question of the sensitivity of the autopilot design to this response therefore assumes considerable practical importance.

5.12 ORBITAL MOTION MOMENT

In the notation of this volume, Eq. (13) of Greenberg's Reference 5-13 is

$$\frac{M'_{a_c}}{b} = -2\pi \rho V^2 \frac{c^2}{4} \frac{w_g}{V} \left[\frac{1}{2} - \left(a + \frac{1}{2}\right) C(k)\right] \left[J_0(k) - i J_1(k)\right]$$

$$= -\frac{\rho}{2} V^2 C^2 \times \pi \frac{w_g}{V} \left[\frac{1}{2} - \left(a + \frac{1}{2}\right) C(k)\right] \left[J_0(k) - i J_1(k)\right]$$

$$C'_{M_{a_C}} = -\pi \frac{w_g}{V} \left[\frac{1}{2} - \left(a + \frac{1}{2}\right) C(k)\right] \left[J_0(k) - i J_1(k)\right] \qquad (5.12.1)$$

If the hinge moment reference is expressed as a chord station and identified as the foil hinge, "a" becomes

$$a = \frac{\frac{H}{c} - \frac{c}{2}}{\frac{c}{2}}$$

$$= 2\frac{H}{c} - 1 \qquad (5.12.2)$$

and (5.12.1) becomes

$$C'_{H_C} = -\pi \frac{w_g}{V} \left[\frac{1}{2} - \left(2\frac{H}{c} - 1 + \frac{1}{2}\right) C(k)\right] \left[J_0(k) - i J_1(k)\right]$$

$$= -2\pi \frac{w_g}{V} \left[\frac{1}{4} - \left(\frac{H}{c} - \frac{1}{4}\right) C(k)\right] \left[J_0(k) - i J_1(k)\right]$$

$$C'_{H_{\alpha_C}} = \frac{C'_{H_C}}{w_g/V} = -2\pi \left[\frac{1}{4} - \left(\frac{H}{c} - \frac{1}{4}\right) C(k)\right] \left[J_0(k) - i J_1(k)\right]$$

$$= -C_{L_\alpha} \left[\frac{1}{4} - \left(\frac{H}{c} - \frac{1}{4}\right) C(k)\right] \left[J_0(k) - i J_1(k)\right] \qquad (5.12.3)$$

It is interesting to note that for the steady-state case this coefficient vanishes for a hinge at half-chord; i.e., the center of pressure for the steady-state circulatory lift is at the half-chord position.

Greenberg's Eq. (B15) in the notation of this volume may be written

$$\frac{M'_{a_{NC}}}{b} = \frac{2\pi\rho\frac{c^2}{4}V^2\frac{w_g}{V}}{k}J_1(k) + \frac{i\,2\pi\rho\frac{c^3}{8}a\omega V\frac{w_g}{V}}{k}J_1(k)$$

$$- \frac{\pi\rho\frac{c^3}{8}\omega V\frac{w_g}{V}}{k}J_2(k)$$

$$= \frac{\rho}{2}V^2c^2\frac{w_g}{V} \times \frac{\pi}{k}J_1(k) + i\frac{\rho}{2}V^2c^2\frac{w_g}{V} \times \frac{\pi}{2}\frac{c}{V}\frac{a}{k}\omega J_1(k)$$

$$- \frac{\rho}{2}V^2c^2\frac{w_g}{V} \times \frac{\pi}{4}\frac{c}{k}\frac{\omega}{V}J_2(k)$$

$$C'_{M_{\alpha_{a_{NC}}}} = \frac{\pi}{k}J_1(k) + i\frac{\pi c a\omega}{2Vk}J_1(k) - \frac{\pi c\omega}{4kV}J_2(k) \qquad (5.12.4)$$

At this point Greenberg assumed a zero wave celerity, which is still aerodynamic practice but which cannot be the case for gravity waves. For the hydrodynamic case

$$\frac{\omega c}{2V} = k'$$

and (5.12.4) may be written

$$C'_{M_{\alpha_{a_{NC}}}} = \frac{\pi}{k}J_1(k) + i\,a\pi\frac{k'}{k}J_1(k) - \frac{\pi}{2}\frac{k'}{k}J_2(k) \qquad (5.12.5)$$

From the recurrence relationship for Bessel functions:

$$C'_{M_{\alpha_{a_{NC}}}} = \frac{\pi}{k}J_1(k) + i\,a\pi\frac{k'}{k}J_1(k) + \frac{\pi}{2}\frac{k'}{k}J_0(k) - \frac{\pi}{2}\frac{k'}{k} \times \frac{2}{k}J_1(k)$$

$$= \frac{\pi}{2}\frac{k'}{k} J_0(k) + \frac{\pi}{k}\left(1 - \frac{k'}{k} + i a k'\right) J_1(k) \qquad (5.12.6)$$

Referenced to a hinge chord station by Eq. (5.12.2):

$$C'_{H_{\alpha_{NC}}} = \frac{\pi}{2}\frac{k'}{k} J_0(k) + \frac{\pi}{k}\left(1 - \frac{k'}{k}\right) J_1(k) + i\pi\left(2\frac{H}{c} - 1\right)\frac{k'}{k} J_1(k)$$

$$= \frac{\pi}{2}\frac{k'}{k} J_0(k) + \frac{\pi}{k}\left(1 - \frac{k'}{k}\right) J_1(k) + i\,2\pi\left(\frac{H}{c} - \frac{1}{2}\right)\frac{k'}{k} J_1(k) \qquad (5.12.7)$$

Note that in smooth water this equation reduces to

$$C'_{H_{\alpha_{NC}}} = \frac{\pi}{2} = \frac{1}{4} \times 2\pi \qquad (5.12.8)$$

which is a pure couple or a moment about the aerodynamic center. Added to the smooth water form of the circulatory moment, Eq. (5.12.3), Eq. (5.12.8) produces the classical quarter-chord center of pressure for the aerodynamic section:

$$C_{H_\alpha} = C_{H_{\alpha_C}} + C_{H_{\alpha_{NC}}}$$

$$= -2\pi\left[\frac{1}{4} - \left(\frac{H}{c} - \frac{1}{4}\right)\right] + \frac{1}{4} \times 2\pi$$

$$= \left(\frac{H}{c} - \frac{1}{4}\right) \times 2\pi \qquad (5.12.9)$$

Eqs. (5.12.3) and (5.12.7) give the total moment for the unsteady case:

$$C'_{H_{\alpha_w}} = C'_{H_{\alpha_C}} + C'_{H_{\alpha_{NC}}}$$

$$= -C_{L_\alpha}\left[\frac{1}{4} - \left(\frac{H}{c} - \frac{1}{4}\right) C(k)\right]\left[J_0(k) - i J_1(k)\right]$$

$$+ \frac{\pi}{2}\frac{k'}{k} J_0(k) + \frac{\pi}{k}\left(1 - \frac{k'}{k}\right) J_1(k) + i\,2\pi\left(\frac{H}{c} - \frac{1}{2}\right)\frac{k'}{k} J_1(k)$$

(5.12.10)

The reduction is trivial but is given in detail to conserve the time of the interested reader:

$$C'_{H_{\alpha_w}} = \left(\frac{H}{c} - \frac{1}{4}\right) C_{L_\alpha} C(k) \left[J_0(k) - i J_1(k)\right] - \frac{1}{4} C_{L_\alpha} J_0(k) + i \frac{1}{4} C_{L_\alpha} J_1(k)$$

$$+ i 2\pi \left(\frac{H}{c} - \frac{1}{2}\right)\frac{k'}{k} J_1(k) + \frac{1}{4} \times 2\pi \frac{k'}{k} J_0(k) + \frac{\pi}{k} \left(1 - \frac{k'}{k}\right) J_1(k)$$

$$= \left(\frac{H}{c} - \frac{1}{4}\right) C_{L_\alpha} C(k) \left[J_0(k) - i J_1(k)\right] - \frac{1}{4} C_{L_\alpha} \left[J_0(k) - i J_1(k)\right]$$

$$+ i \left(\frac{H}{c} - \frac{1}{4}\right) \times 2\pi \frac{k'}{k} J_1(k) + \frac{1}{4} \times 2\pi \frac{k'}{k} J_0(k) - i \frac{1}{4} \times 2\pi \frac{k'}{k} J_1(k)$$

$$+ \frac{\pi}{k} \left(1 - \frac{k'}{k}\right) J_1(k)$$

$$= \left(\frac{H}{c} - \frac{1}{4}\right) \left\{ C_{L_\alpha} \left[J_0(k) - i J_1(k)\right] C(k) + i 2\pi \frac{k'}{k} J_1(k) \right\}$$

$$- \frac{1}{4} C_{L_\alpha} \left[J_0(k) - i J_1(k)\right] + \frac{1}{4} \times 2\pi \frac{k'}{k} \left[J_0(k) - i J_1(k)\right]$$

$$+ \frac{\pi}{k} \left(1 - \frac{k'}{k}\right) J_1(k)$$

$$= \left(\frac{H}{c} - \frac{1}{4}\right) C'_{L_{\alpha_w}} + \frac{1}{4} \left(2\pi \frac{k'}{k} - C_{L_\alpha}\right) \left[J_0(k) - i J_1(k)\right]$$

$$+ \frac{\pi}{k} \left(1 - \frac{k'}{k}\right) J_1(k) \qquad (5.12.11)$$

With reference to the aerodynamic center the lift term drops:

$$C'_{H_{\alpha_{a.c.}}} = \frac{1}{4} \left(2\pi \frac{k'}{k} - C_{L_\alpha}\right) \left[J_0(k) - i J_1(k)\right] + \frac{\pi}{k} \left(1 - \frac{k'}{k}\right) J_1(k) \qquad (5.12.12)$$

and for the 2-dimensional foil there is a further reduction to

$$C'_{H_{\alpha}}{}_{a.c.} = \frac{\pi}{2}\left(\frac{k'}{k} - 1\right)\left[J_0(k) - i\,J_1(k)\right] - \frac{\pi}{k}\left(\frac{k'}{k} - 1\right) J_1(k)$$

$$= \frac{\pi}{2}\left(\frac{k'}{k} - 1\right)\left[J_0(k) - \left(\frac{2}{k} + i\right) J_1(k)\right] \qquad (5.12.13)$$

Leehey's Eq. (8.29') in the notation of this volume becomes

$$M'_{a.c.} = -\rho\,\frac{c^2}{4}\,V\pi\,w_g\left(1 - \frac{k'}{k}\right)\left[J_0(k) - \left(\frac{2}{k} + i\right) J_1(k)\right]$$

$$= -\frac{\rho}{2}\,V^2\,c^2\,\frac{w_g}{V}\,\frac{\pi}{2}\left(1 - \frac{k'}{k}\right)\left[J_0(k) - \left(\frac{2}{k} + i\right) J_1(k)\right]$$

$$C'_{H_{\alpha}}{}_{a.c.} = \frac{\pi}{2}\left(\frac{k'}{k} - 1\right)\left[J_0(k) - \left(\frac{2}{k} + i\right) J_1(k)\right] \qquad (5.12.14)$$

which is identical with (5.12.13). The uncertainty with regard to the proper form for Theodorsen's function does not enter the moment prediction then, except to transfer the moment to hinge positions away from the aerodynamic center.

For zero wave celerities the moment about the aerodynamic center vanishes, hence Bisplinghoff, e.g., concludes that the lift in sinusoidal gusts acts through the aerodynamic center (quarter-chord). Leehey appears to be the only author who has recognized the significance of the wave celerity to the moment about the aerodynamic center and this prediction must be credited to him. Note, however, that Leehey's result is only for the 2-dimensional, aerodynamic case and that Eq. (5.12.12) is the more general form.

There are many problems associated with Eq. (5.12.12) for the 3-dimensional case and very little experimental guidance. None of the coefficients, the π terms, or the Bessel function terms have been examined for three dimensions or in the presence of a free surface. For this volume only the lift curve slope is modified to suit the hydrodynamic, 3-dimensional case.

Only O'Neill's experimental results are examined for this volume. His results for the two hinge positions have been shifted to the aerodynamic center by the relationship:

$$C_{M_{\alpha_{a.c.}}} = C_{H_\alpha} - \left(\frac{H}{c} - a.c.\right) C_{L_\alpha} \qquad (5.12.15)$$

where the .0801 $C_{H_{C_L}}$ of Table 4-2 was employed for $\frac{H}{c}$ - a.c. for the .32 MGC hinge position and where that distance for the .062 MGC hinge was

$$\frac{H}{c} - a.c. = .0801 - (.32 - .062)\frac{MGC}{MAC}$$

$$= .0801 - .258 \times \frac{8.65}{9.33}$$

$$= -.1589$$

The data has been compared with several predictions in the form $C_{M_{\alpha_{a.c.}}}/C_{L_{\alpha_w}}$ on Figures 5-41 - 5.43. This form of presentation has the disadvantage that the lift response uncertainties are brought into the moment comparison but it has the advantage of relating the moment about the aerodynamic center to the moment, about any other hinge position, produced by the lift; the ratio of moment/lift is, in fact, a distance as a fraction of the chord.

The moment/lift ratio for the data was derived directly from O'Neill's data in the form

$$\frac{C_{M_{\alpha_{a.c.}}}}{C_{L_\alpha}} = \frac{\Delta C_H \frac{c}{ht}}{\Delta C_L \frac{c}{ht}} - \left(\frac{H}{c} - a.c.\right) \qquad (5.12.16)$$

The predictions presented are:

- The Leehey prediction of Reference 5-9, read from the graphs of that reference. Presumably these are 2-dimensional predictions differing from the Leehey prediction below principally in inclusion of q effect

- The 2-D Leehey prediction of Eqs. (5.11.9) and (5.12.14) with the k'/k ratio corresponding to an F_h of 5 and a one chord depth
- The 3-D Leehey prediction of Eqs. (5.11.7) and (5.12.12) for $F_h = 5$, $d/c = 1$, and $C_L = 2.75$
- The Smullin and Bender prediction of Figures 7 and 9 of Reference 5-6. This is a 2-dimensional prediction for $F_h = 10$ and $d/c = 1/2$.

The comparison of Figures 5-41 through 5-43 are not encouraging. The principal difficulty appears to lie in a classic small difference between two large numbers, best illustrated by example. For a wavelength of 32 chords, k is .0982 and for an F_h of 5 at one chord depth:

$$\frac{k'}{k} - 1 = \frac{1}{7.07\sqrt{k}} = .451$$

Then Eq. (5.12.14) becomes

$$C'_{H_{\alpha_{a.c.}}} = \frac{\pi}{2}\left(\frac{k'}{k} - 1\right)\left[J_0(k) - \frac{2}{k}J_1(k) - iJ_1(k)\right]$$

$$= \frac{\pi}{2} \times .451 \left[.998 - \frac{2}{.0982} \times .0490 - i\,.0490\right]$$

$$= .708 \left[.998 - .99796 - i\,.0490\right]$$

This is the characteristic arithmetic and, in fact, for wavelengths greater than 10 chords the moment slope may be written

$$C'_{H_{\alpha_{a.c.}}} = \frac{\pi}{2}\left(\frac{k'}{k} - 1\right)\left(-i\frac{k}{2}\right)$$

$$= \frac{\pi}{4}\left(\frac{k'}{k} - 1\right)k \Big\lfloor -\frac{\pi}{2}$$

$$\approx \frac{\pi}{4} \times \frac{k}{2} \Big\lfloor -\frac{\pi}{2}$$

which is sufficiently small so that practical considerations; such as 3 dimensions, sweep, q effect, etc.; overwhelm the effect of Eq. (5.12.14).

The moment problem appears so forbidding that it would seem most advisable in this case to establish the precision required first, by trending studies from the autopilot end of the loop, before further attacks upon the moment itself.

In the meantime Figures 5-41 and 5-42 indicate that for the AG(EH) a $C_{M_{a.c}}$ of 10% of the lift can be employed. That $C_{M_{a.c.}}$ is in quadrature with the lift, presumably leading on head seas and lagging on following seas.

5.13 ORBITAL MOTION FLAP MOMENT

Since steady-state flap hinge moment is proportional to lift, the aerodynamic foil lift attenuation, G, might be expected to furnish an approximation for the flap moment attenuation in orbital motion. This presumption is supported by comparison of Jones' 2-dimensional gust function with the aerodynamic flap moment response of Figure 7 of Reference 5-6 as shown on Figures 5-44 and 5-45. Three effects are not accounted for, however:

1. The effect of wave celerity for which we have only the 2-D, aerodynamic effect of Leehey and that analysis does not include flap load. The two previous sections indicate poor agreement with experiment, particularly for foil moment which is closely related with flap moment.

2. Free surface effect which further redistributes the chordwise load. The effect in two dimensions is indicated by the two Smullin and Bender curves of Figures 5-44 and 5-45.

3. Planform effect which, presumably, modifies the relative importance of the circulatory and inertial terms. This effect is illustrated by the two Jones' functions of Figures 5-44 and 5-45.

These effects are not available in combination yet by an theoretical means and no experimental data on this effect has been examined. For the present the Jones' 3-dimensional gust function, operating on the steady-state hinge moment slope, is being employed to represent the unsteady flap hinge moment.

5.14 SUMMARY

It is to be noted that one of the most significant limitations upon the confidence level for moment response to unsteady motion is the steady-state response to displace-

ment. Errors here can have a substantial effect upon the response phase and a lesser effect upon the amplitude. This is true of the incidence moment where the steady-state moment is minimized to reduce control load and of the 16-series section flap which presents a vanishingly small and unpredictable moment slope. A second limitation, on the rational analytical (non-lifting surface) methods is a convenient accountability for chordwise load redistribution under a free surface. Both of these limitations are significant to the steady-state case as well as to the unsteady case and both are currently under review.

The measure of unsteady load prediction accuracy is its significance to the autopilot design problem. Therefore, current effort is directed to approaching Table 5-5 from the autopilot end of the control loop, employing the optimal control program to establish the unsteady load accuracy required for confident autopilot design practice. This will limit further effort to improve the confidence levels of Table 5-5 to those responses where good confidence levels are a practical necessity. At the same time, the necessity for accounting for the circulatory and/or inertial terms of each response and for distinguishing between wavelength and frequency will be examined. Wherever possible, the circulatory portion of the response will be dropped and the inertial portion accounted for by modifying the craft mass and inertia.

5.15 REFERENCES

5-1 R. T. Jones, "The Unsteady Lift of a Wing of Finite Aspect Ratio", NACA Rpt. 681, 1939

5-2 Bisplinghoff, Ashley, & Halfman, "Aeroelasticity", Addison-Wesley, 1957

5-3 J. H. Pattison, "Unsteady Hydrodynamic Loads on a Two-Dimensional Hydrofoil", NSRDC Report 3245, November 1970

5-4 J. Feldman, "Experimental Investigation of Near-Surface Hydrodynamic Force Coefficients for a Systematic Series of Tee Hydrofoils, DTMB Series HF-1", DTMB Report 1801, December 1963

5-5 "Hydrofoil Handbook", Vol. II, Gibbs & Cox, Inc., 1954

5-6 Smullin & Bender, "The Unsteady Hydrodynamics and Control of Hydrofoils Near A Free Surface", Bolt, Beranek and Newman Report No. 1970, January 1971

5-7 Stark, "A Subsonic Oscillating-Surface Theory for Wings with Partial-Span Controls", AIAA Paper 72-61, January 1972

5-8 T. Theodorsen, "General Theory of Aerodynamic Instability and the Mechanism of Flutter", NACA Report 496, 1935. Currently available in AIAA Selected Reprints, "Aerodynamic Flutter", I. E. Garrick, Editor, March 1969

5-9 W. C. O'Neill, "Unsteady Lift and Hinge Moment Characteristics of the AG(EH) Main Foil and Strut Assembly", NSRDC Report 2805, July 1968

5-10 Toll, "Summary of Laterial Control Research", NACA Rpt. 868, 1947

5-11 "USAF Stability and Control Methods" (DATCOM), Douglas Aircraft Co., 1965

5-12 Perkins & Hage, "Airplane Performance, Stability, and Control", Wiley, 1956

5-13 J. M. Greenberg, "Some Considerations on an Airfoil in an Oscillating Stream", NACA TN 1372, August 1947

5-14 P. Leehey, "The Hilbert Problem for an Airfoil in Unsteady Flow", DTMB Report 1077, January 1957

5-15 J. M. Steele, "The Unsteady Lift Force on a Restrained Hydrofoil in Regular Waves", NSRDC Report 3386, November 1970

5-16 A. C. Conolly, "Flapped Hydrofoils in Waves, Subcavitating Flow", General Dynamics/Convair Report 63-032, May 1963

TABLE 5-1 UNSTEADY LOAD RESPONSE TERMINOLOGY

RESPONSES / MOTIONS	LIFT	PITCHING MOMENT FOIL + POD (FOR CRAFT TRIM)	INCIDENCE MOMENT FOIL ONLY (CONTROL LOAD IF FOIL MOVES RELATIVE TO POD)	FLAP MOMENT
HEAVE	Λ_h $= C_{L_{\alpha_h}} / C_{L_\alpha}$ $= \dfrac{C_{L_h} / \left(-\frac{\dot{h}}{V}\right)}{C_{L_\alpha}}$	$H_h = C_{H_{\alpha_h}} / C_{H_\alpha}$ $C_{H_h} = C_{H_h} / \left(-\frac{\dot{h}}{V}\right)$ Sometimes with subscript to locate H	$I_h = C_{H_{i_h}} / C_{H_\alpha}$ $C_{H_{i_h}} = C_{H_i} / \left(-\frac{\dot{h}}{V}\right)$ Sometimes with subscript to locate H	$\eta_h = C_{h_{\alpha_h}} / C_{h_\alpha}$ $= \dfrac{C_{h_h} / \left(-\frac{\dot{h}}{V}\right)}{C_{h_\alpha}}$
PITCH (Pod moving with foil)	Λ_P $= C_{L_{\alpha_P}} / C_{L_\alpha}$ $= \dfrac{C_{L_P} / \alpha}{C_{L_\alpha}}$	$H_P = C_{H_{\alpha_P}} / C_{H_\alpha}$ $= \dfrac{C_{H_P} / \alpha}{C_{H_\alpha}}$	$I_P = C_{H_{i_P}} / C_{H_\alpha}$ $= \dfrac{C_{H_P} / i}{C_{H_\alpha}}$	$\eta_P = C_{h_{\alpha_P}} / C_{h_\alpha}$ $= \dfrac{C_{h_P} / \alpha}{C_{h_\alpha}}$

TABLE 5-1 (Continued)

RESPONSES / MOTIONS	LIFT	PITCHING MOMENT FOIL + POD (FOR CRAFT TRIM)	INCIDENCE MOMENT FOIL ONLY (CONTROL LOAD IF FOIL MOVES RELATIVE TO POD)	FLAP MOMENT
INCIDENCE (Foil moving relative to pod)	Λ_i $= C_{L_{\alpha_i}} / C_{L_i}$ $= \frac{C_{L_{i_P}} / i}{C_{L_i}}$	$H_i = C_{H_{\alpha_i}} / C_{H_i}$ $= \frac{C_{H_{i_P}} / i}{C_{H_i}}$	$I_i = C_{H_{i_i}} / C_{H_\alpha}$ $= \frac{C_{H_{i_P}} / i}{C_{H_i}}$	$\eta_i = C_{h_{i_i}} / C_{h_i}$ $= \frac{C_{h_{i_P}} / i}{C_{h_i}}$
FLAP	Λ_F $= C_{L_{\delta_F}} / C_{L_\delta}$ $= \frac{C_{L_F} / \delta}{C_{L_\delta}}$	$H_F = C_{H_{\delta_F}} / C_{H_\delta}$ $= \frac{C_{H_F} / \delta}{C_{H_\delta}}$	$I_F = C_{H_{\delta_F}} / C_{H_\delta}$ $= \frac{C_{H_F} / \delta}{C_{H_\delta}}$	$\eta_F = C_{h_{\delta_F}} / C_{h_\delta}$ $= \frac{C_{H_F} / \delta}{C_{h_\delta}}$

TABLE 5-1 (Continued)

RESPONSES / MOTIONS	LIFT	PITCHING MOMENT FOIL + POD (FOR CRAFT TRIM)	INCIDENCE MOMENT FOIL ONLY (CONTROL LOAD IF FOIL MOVES RELATIVE TO POD)	FLAP MOMENT
ORBITAL VELOCITY	$\Lambda_w = G$	$H_w = \dfrac{C_{H_w} / \frac{w_g}{V}}{C_{H_\alpha}}$	$I_w = \dfrac{C_{H_w} / \frac{w_g}{V}}{C_{H_\alpha}}$	$\eta_F = C_{h_{\delta_w}} / C_{h_\delta}$
(Normal phase reference is orbital angle at L.E. but c/4, c/2, and a.c. sometimes used)	$= \dfrac{C_{L_w} / \frac{w_g}{V}}{C_{L_\alpha}}$		Other forms employed for a.c. moment reference	$= \dfrac{C_{h_w} / \frac{w_g}{V}}{C_{h_\delta}}$

TABLE 5-2 UNSTEADY LOAD RESPONSE PREDICTIONS

1. THEODORSEN, REFERENCE 5-8

   2-D, aerodynamic, thin airfoil, C_w = 0 lift, foil and flap moment response to heave, pitch, and flap motion. Incorporation of practical steady-state moments essential. Inertial terms displayed. Extend to 3-D, hydrodynamic with appropriate steady-state derivatives; inertial accountability uncertain. Employ k' with inertial terms for C_w. For 3-D employ Jones' C(k).

2. JONES, REFERENCE 5-1

   3-D, aerodynamic, C_w = 0 lift response to orbital motion.

3. LEEHEY, REFERENCE 5-14

   2-D, aerodynamic lift and foil moment response to orbital motion with C_w accountability.

4. WIDNALL LIFTING SURFACE PROGRAM

   3-D, hydrodynamic. 2-D lift and moment response to heave and pitch over wide range of d/C and F_h appear in Reference 5.3. 2-D lift and moment response to pitch appear in Reference 5.9. 3-D AG(EH) lift and moment response to pitch available but unpublished.

5. SMULLIN AND BENDER LIFTING SURFACE PROGRAM

   2-D, hydrodynamic, C_w = 0, with flap. All responses to all motions presented in Reference 5.6 for aerodynamic and one hydrodynamic case.

6. STARK LIFTING SURFACE PROGRAM

   3-D, aerodynamic, with flap but without orbital motion. Predictions of this note are intermediate output of flutter program; see Reference 5.7 for more suitable program.

TABLE 5-3 UNSTEADY LOAD DATA REVIEWED

1. PATTISON - REFERENCE 5-3

   Lift, moment, and drag response to heave and pitch for model between walls (2-D) without flap. Steady-state lift curve slope is not 2-D.

2. STEELE - REFERENCE 5-15

   Lift response to head and following seas, 2 depths, several speeds. Aspect ratio 6.25 foil without flap. Lift amplificiations to 1.5 in 30 chord length following seas.

3. CONOLLY - REFERENCE 5-16

   Lift response to head and following seas for various flap configurations. Number of wavelengths measured too limited for data scatter encountered.

4. O'NEILL - REFERENCE 5-9

   Lift and incidence moment response to incidence motion and to head seas for AG(EH) fwd foil/pod/strut. Good data precision and steady-state characteristics.

NOTE: This is not an exhaustive listing of the data available in the literature. Time did not permit further data analysis.

TABLE 5-4 UNSTEADY LOAD COMPARISON

RESPONSES / MOTIONS	LIFT	PITCHING MOMENT	INCIDENCE MOMENT	FLAP MOMENT
HEAVE	Sect. 5.2 Figs. 5-4 & 5-5 Pattison data Theodorsen Widnall Stark Smullin & Bender	Sect. 5.3 Figs. 5-6 & 5-7 Pattison data Theodorsen Widnall Stark Smullin & Bender		Sect. 5.9 Figs. 5-30 - 5-32 No data Theodorsen Smullin & Bender
PITCH	Sect. 5.4 Figs. 5-12 & 5-13 No data Theodorsen Smullin & Bender	Sect. 5.5 Figs. 5-18 & 5-19 No data Theodorsen Smullin & Bender		Sect. 5.10 Figs. 5-33 & 5-34 No data Theodorsen Smullin & Bender
INCIDENCE	Sect. 5.4 Figs. 5-8 - 5-11 O'Neill data Theodorsen Widnall Stark	Sect. 5.5	Sect. 5.5 Figs. 5-14 - 5-17 O'Neill data Theodorsen Widnall Stark	
FLAP	Sect. 5.6 Figs. 5-20 & 5-21 No data Theodorsen Smullin & Bender Stark NOTE 1	Sect. 5.8 Figs. 5-28 & 5-29 No data Theodorsen Smullin & Bender	NOTE 1	Sect. 5.7 Figs. 5-24 - 5-27 No data Theodorsen Smullin & Bender Stark NOTE 1

TABLE 5-4 (Continued)

RESPONSES / MOTIONS	LIFT	PITCHING MOMENT	INCIDENCE MOMENT	FLAP MOMENT
ORBITAL VELOCITY	Sect. 5.11 Figs. 5-35 - 5-40 Steele's data O'Neills data Jones Leehey Smullin & Bender Heave response	Sect. 5.12 Figs. 5-41 - 5-43 O'Neill's data Leehey Smullin & Bender		Sect. 5.13 Figs. 5-44 & 5-45 No data Smullin & Bender Jones

1. AG(EH) lift, incidence & flap moment response to flap motion were measured for this study; analysis is presented in appendix to this report.

TABLE 5-5 UNSTEADY LOAD CONFIDENCE LEVELS

RESPONSES / MOTIONS	LIFT	PITCHING MOMENT	INCIDENCE MOMENT	FLAP MOMENT
HEAVE	Doubtful data Fair prediction comparisons Amplitude - fair Phase - good	Doubtful data Amplitude - good Phase - N.G. No confidence level	No data See heave/pitching moment	No data Contradictory predictions. No confidence level NOTE 1
PITCH	See incidence/ lift case.	Presumed adequate from incidence/ incidence moment case. NOTE 1	Presumed adequate from incidence/ incidence moment case. NOTE 1	No data Contradictory predictions No confidence level NOTE 1
INCIDENCE	Amplitude - fair Phase - good	Presumed adequate from incidence/ incidence moment case. NOTE 1	Can be correlated well with Theodorsen. Difficult case for lifting surface programs. NOTE 1 Adequate	No data. More difficult than pitch/ flap moment. No confidence level
FLAP	No data or comparable predictions. No confidence level NOTE 2	No data or comparable predictions. No confidence level	No data or comparable predictions. No confidence level NOTE 2	No data or comparable predictions. No confidence level NOTE 2

TABLE 5-5 (Continued)

RESPONSES / MOTIONS	LIFT	PITCHING MOMENT	INCIDENCE MOMENT	FLAP MOMENT
ORBITAL VELOCITY	Theory deficient. Correlation poor/ fair. May be negligible response. Poor/fair	Theory deficient. No correlation. Negative confidence level NOTE 1	More difficult than w_g/ pitching moment. Negative confidence level	Theory dificient. No data No confidence level

1. Lifting surface theories do not produce practical C_{H_α} or C_{h_α}.
2. Measured for this program with appended results.
3. Judgements subjective and subject to review following optimal control program trending analysis.

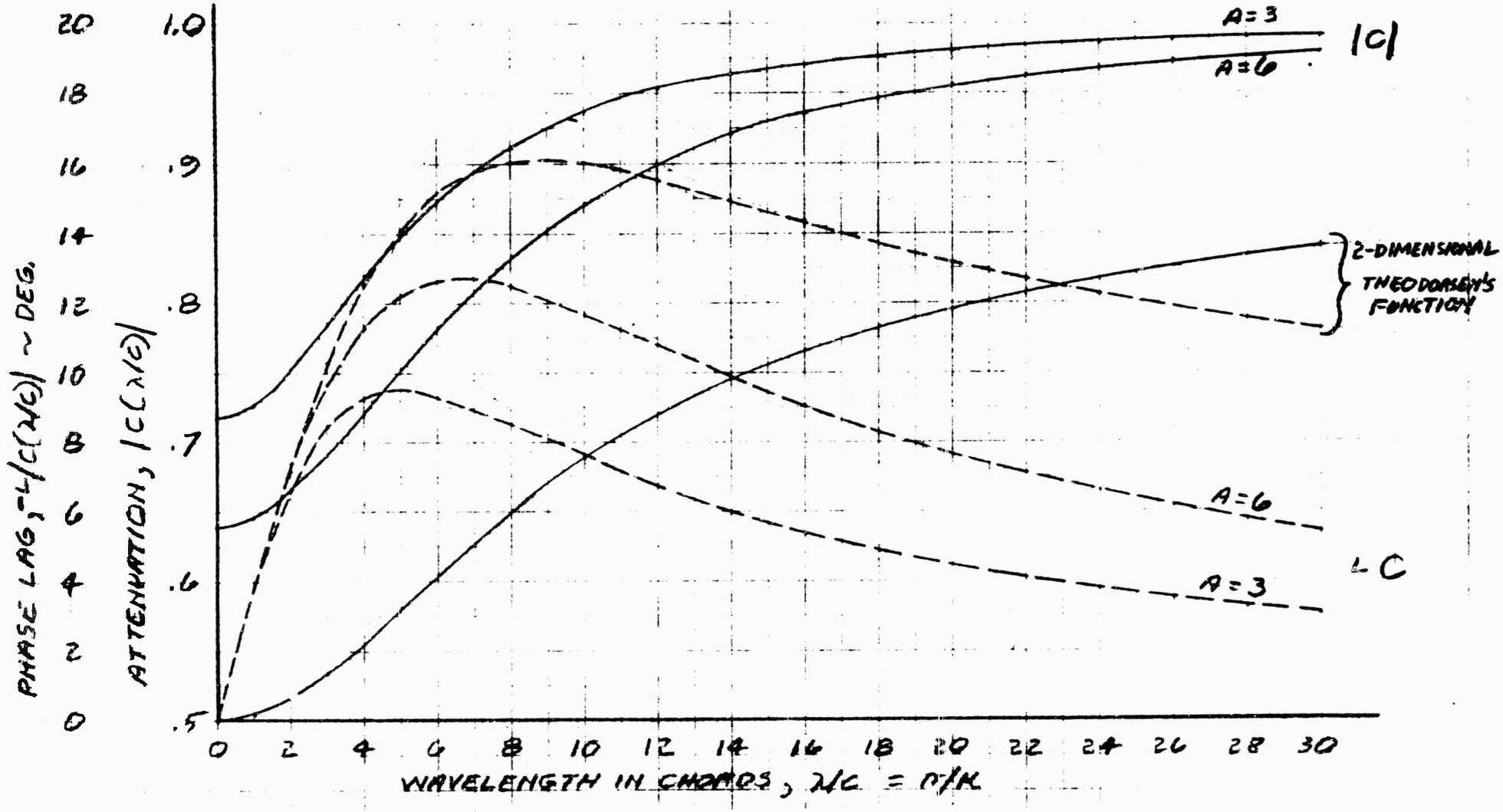


Figure 5-1. Jones' Foil Motion Function

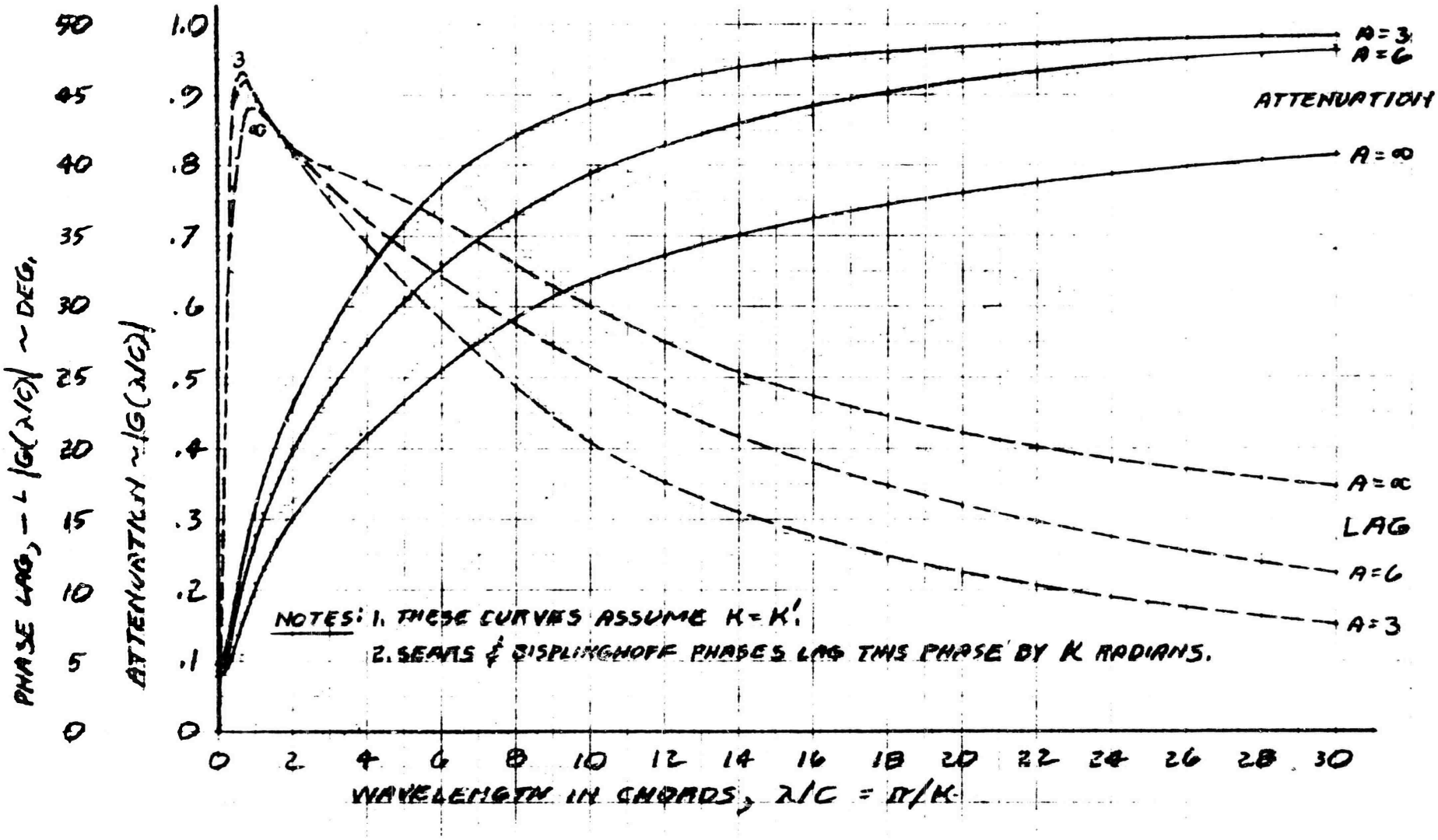


Figure 5-2. Jones' Gust Function

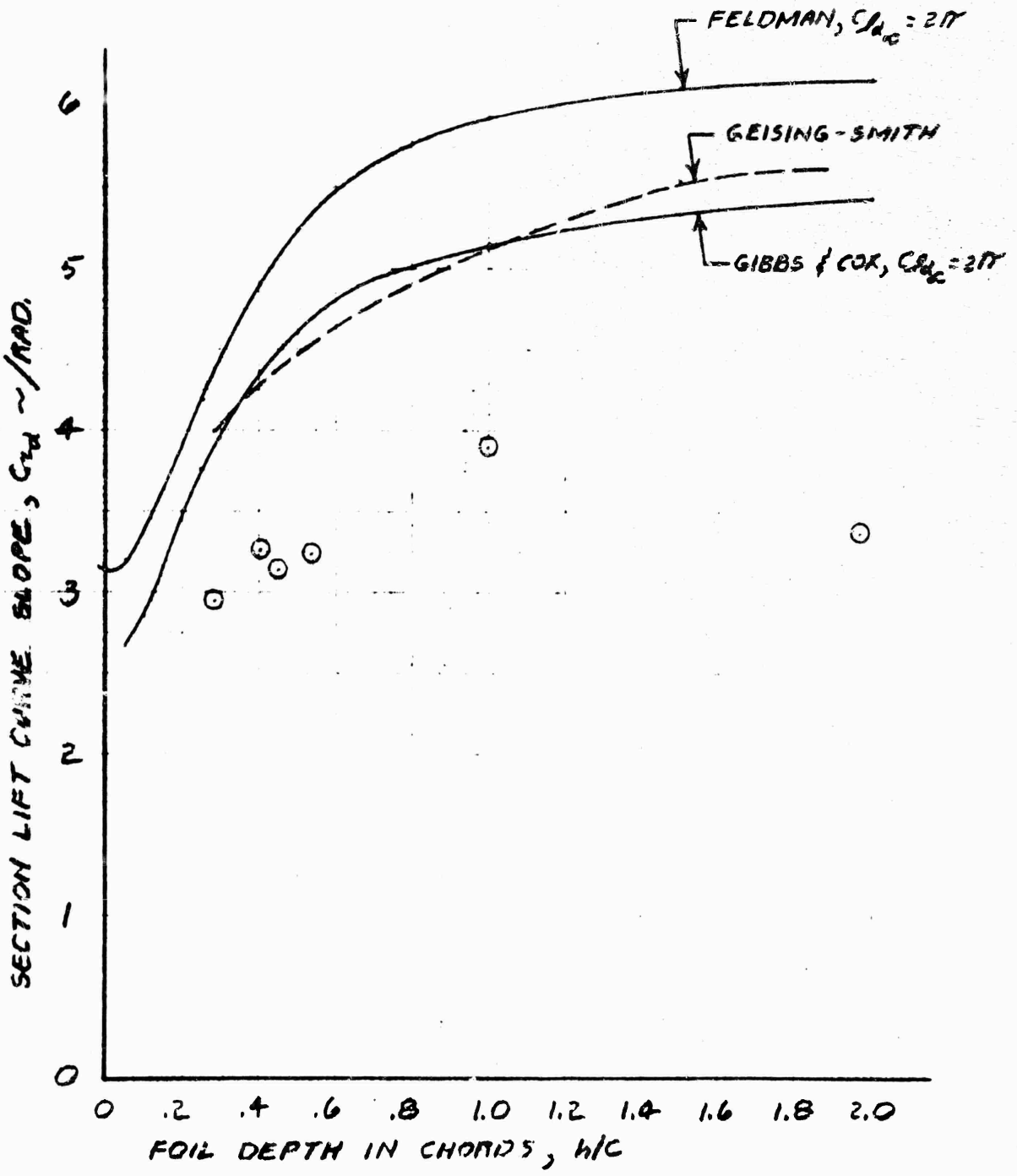


Figure 5-3. Pattison's Steady State Lift Curve Slope, 2-D

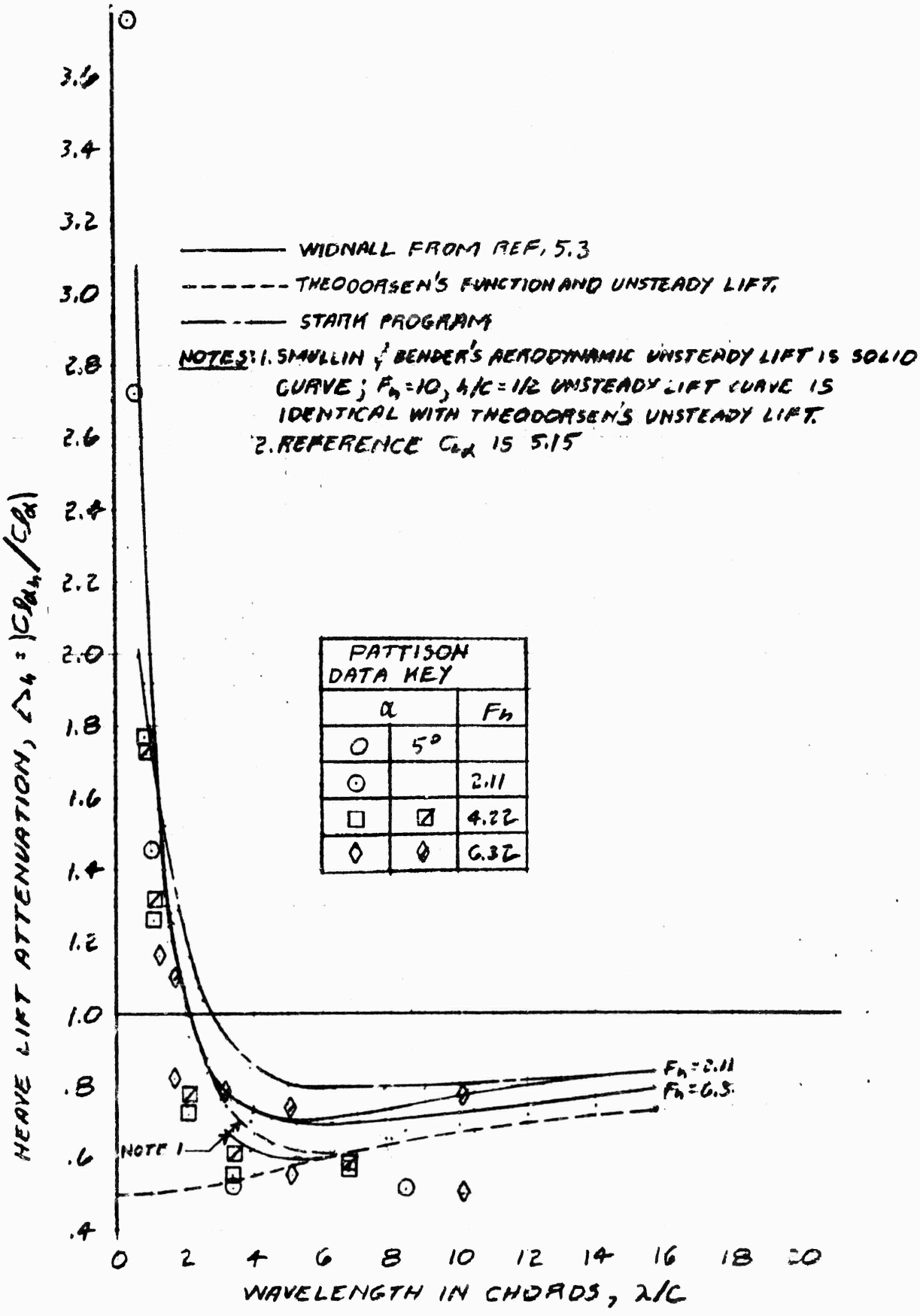


Figure 5-4. Heave Lift Attenuation, 2-D, d/c = .995

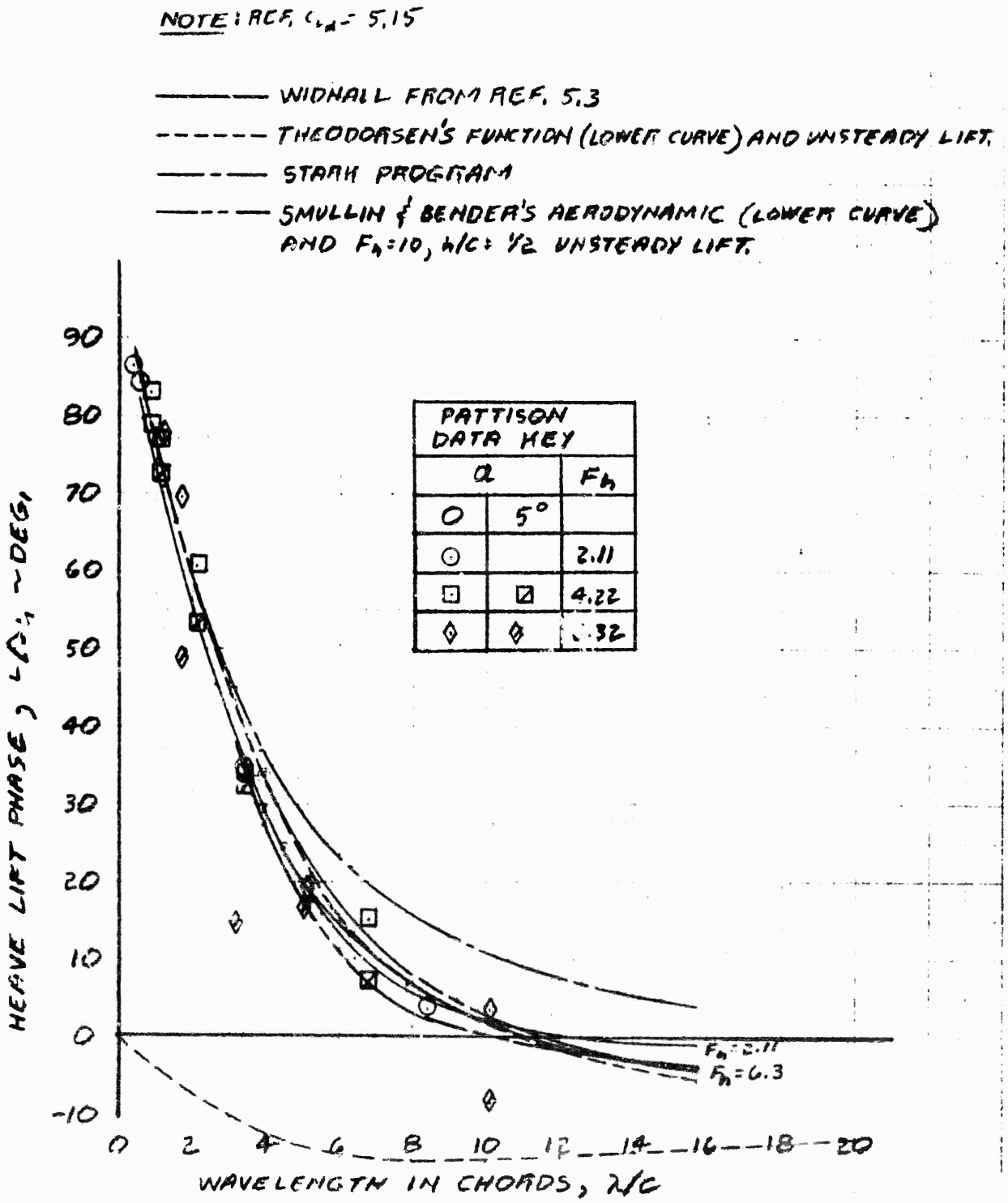


Figure 5-5. Heave Lift Phase, 2-D, d/c = .995

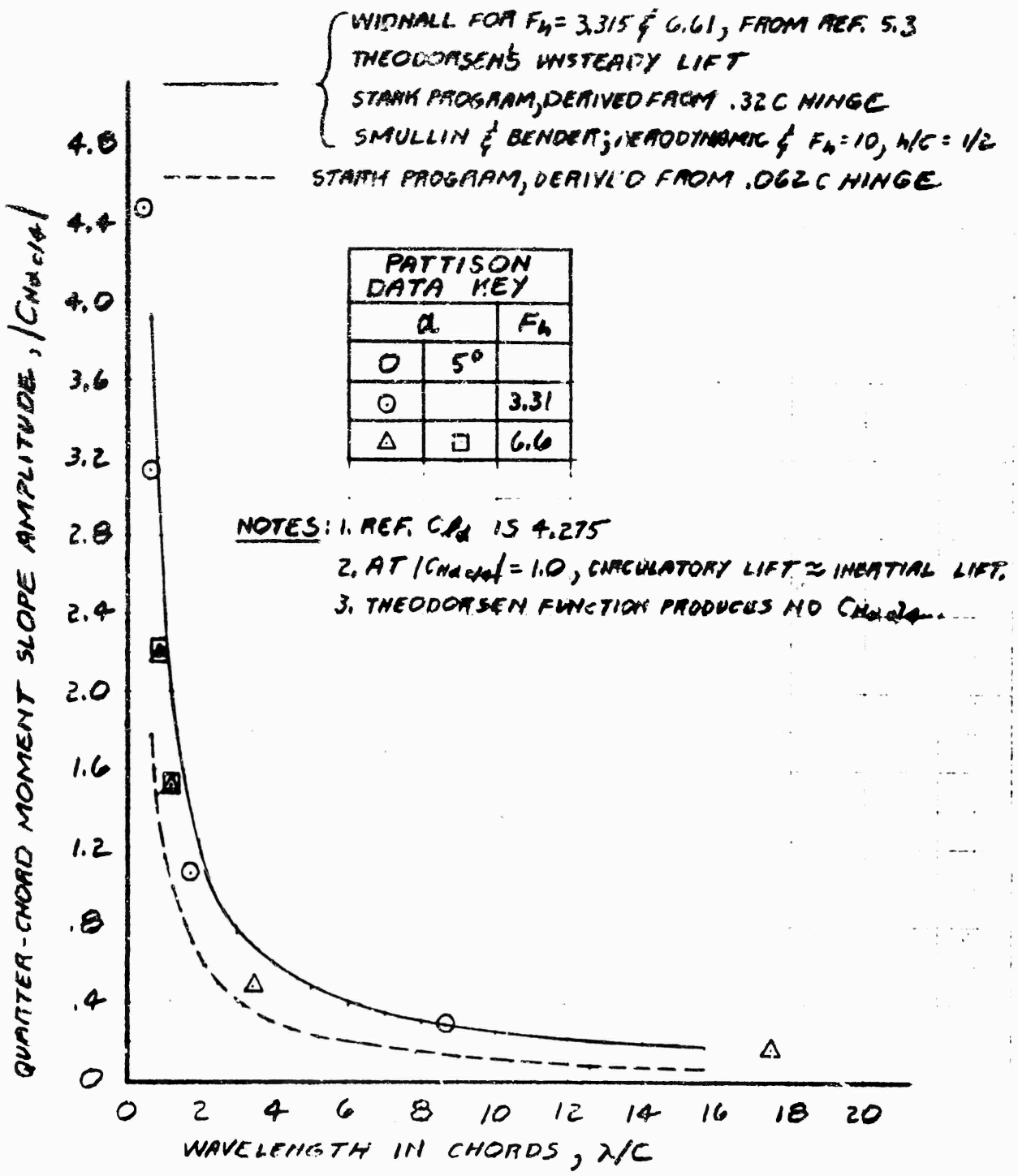


Figure 5-6. Heave Moment Amplitude, 2-D, d/c = .405

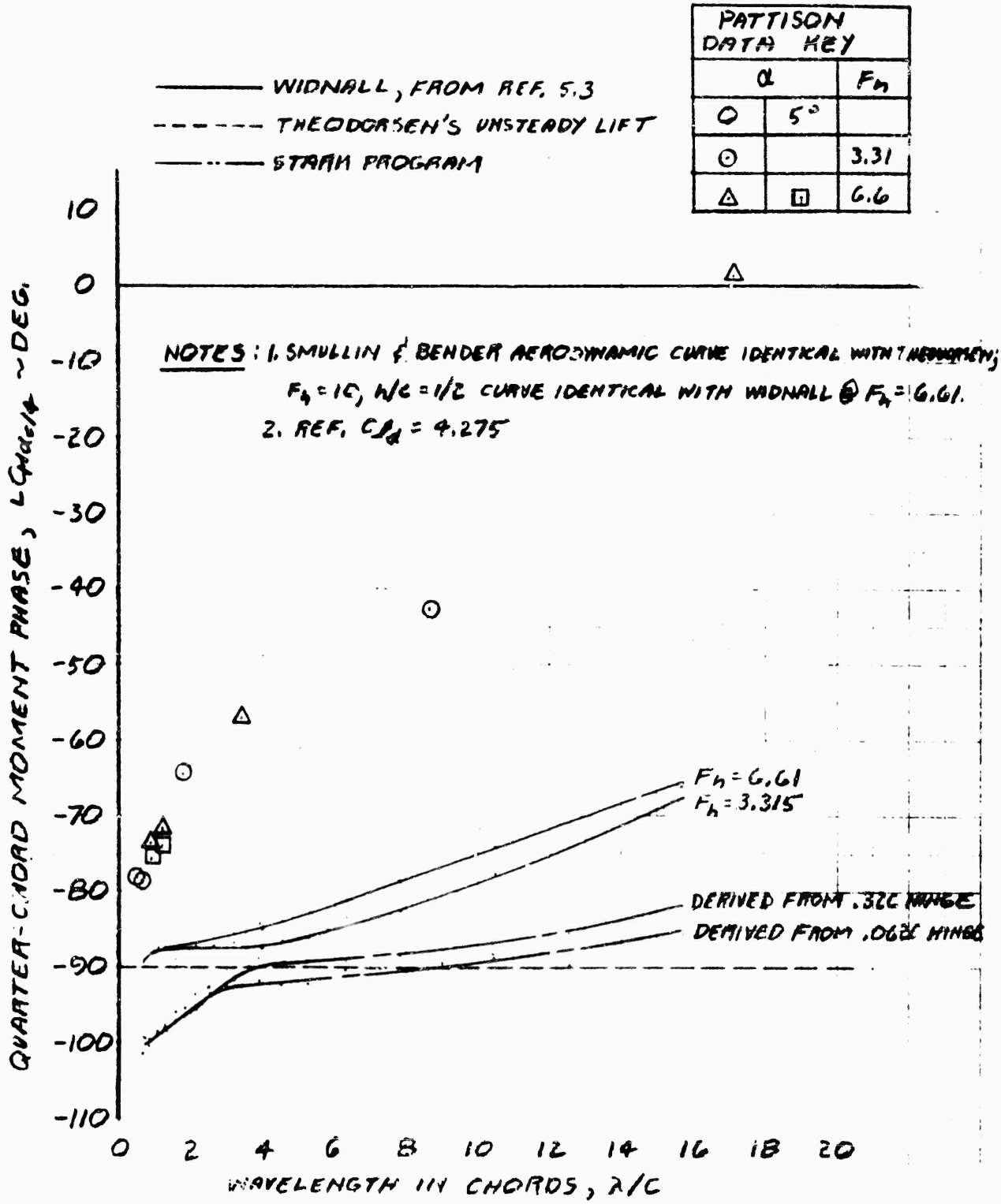


Figure 5-7. Heave Moment Phase, 2-D, d/c = .405

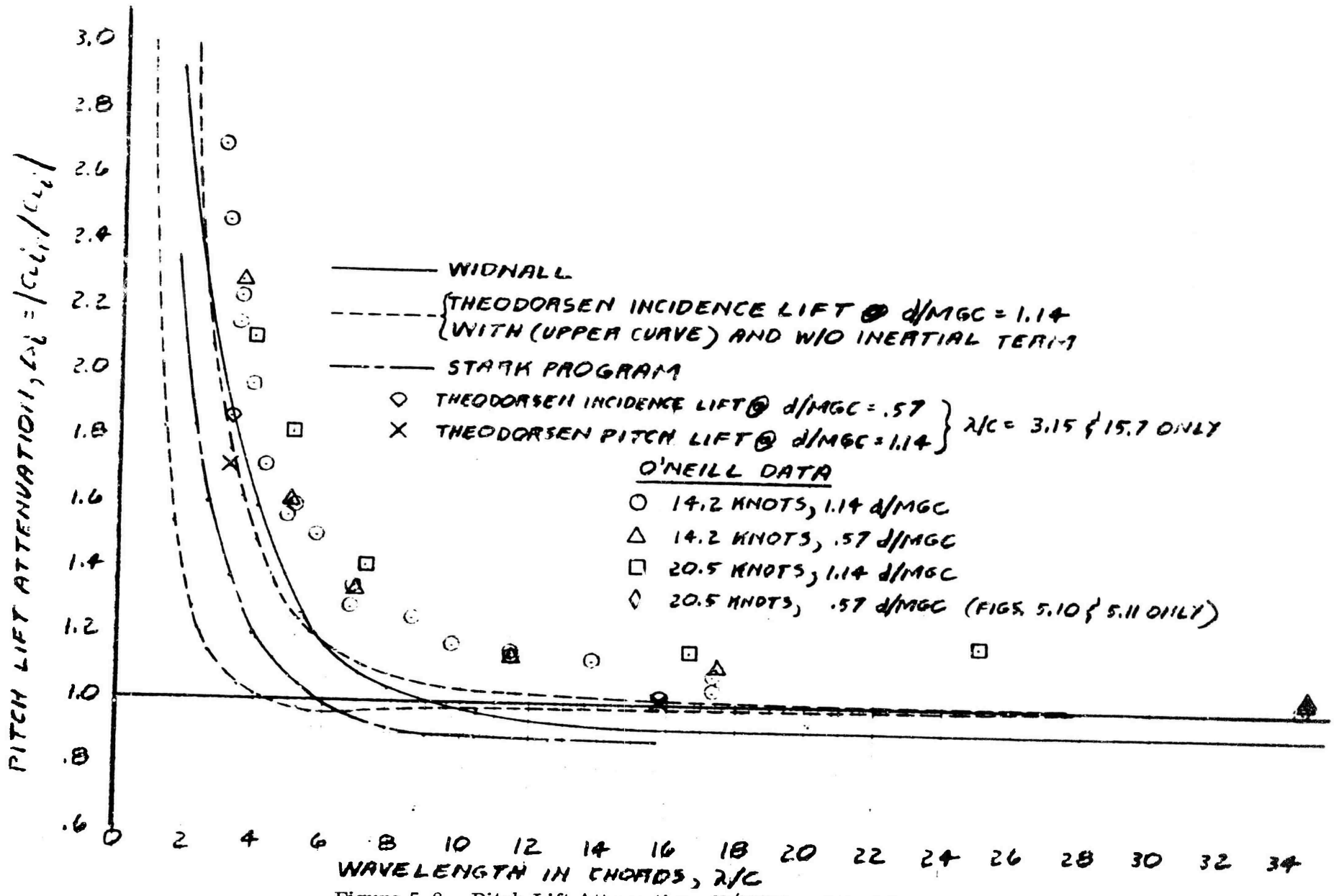


Figure 5-8. Pitch Lift Attenuation, H/MGC = .32, AG(EH) Fwd. Foil

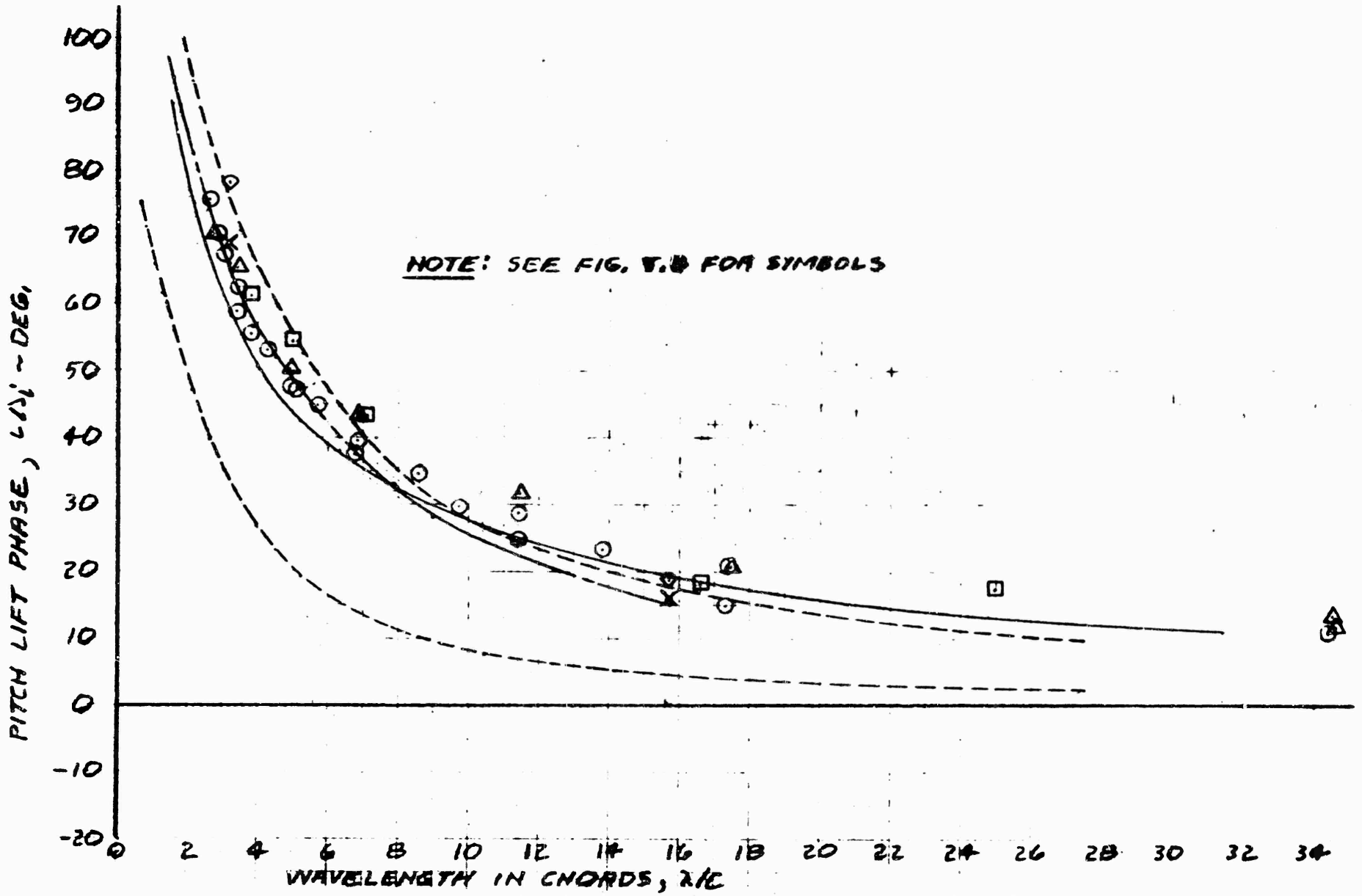


Figure 5-9. Pitch Lift Phase, H/MGC = .32, AG(EH) Fwd. Foil

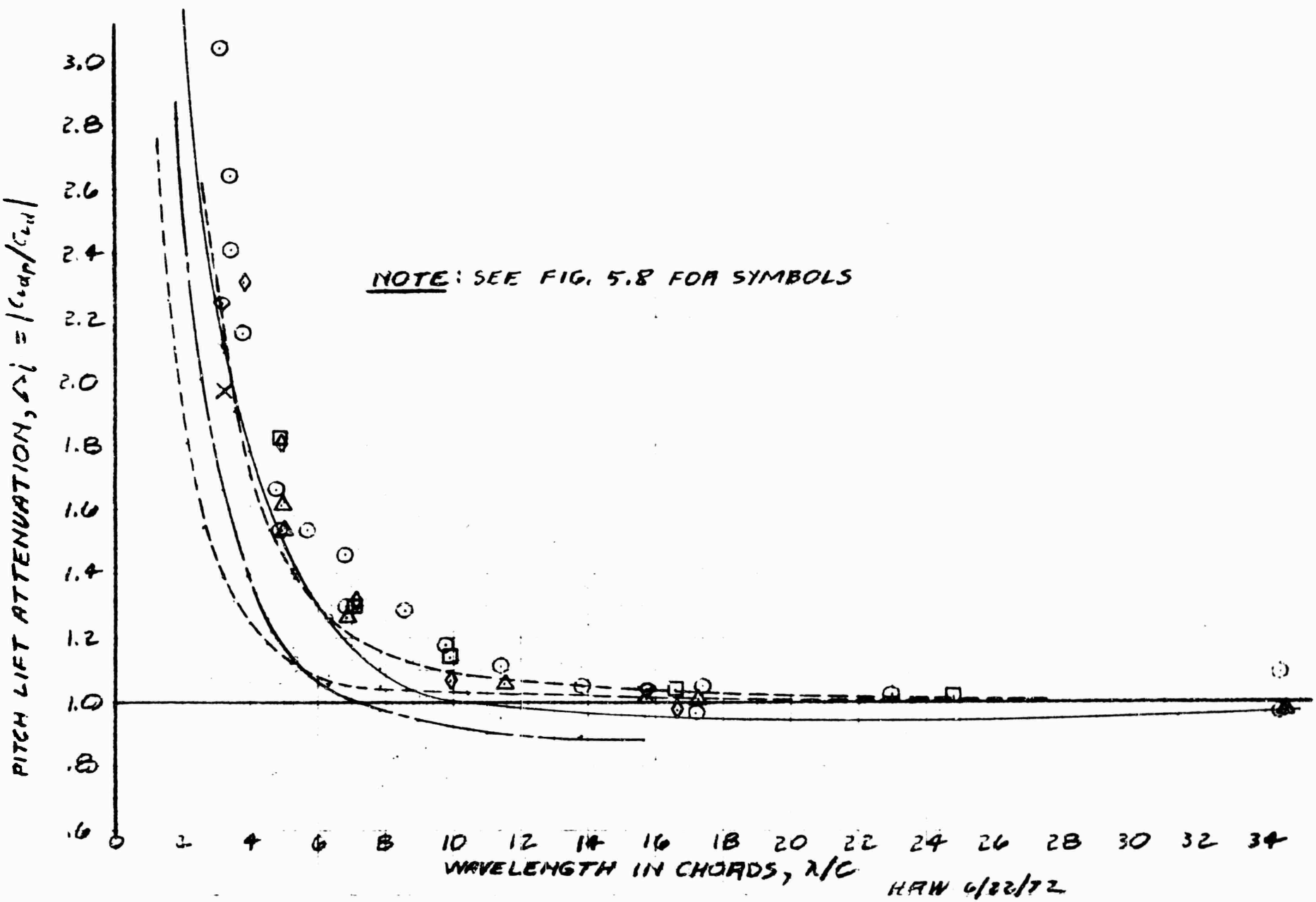


Figure 5-10. Pitch Lift Attenuation, H/MGC = .062, AG(EH) Fwd. Foil

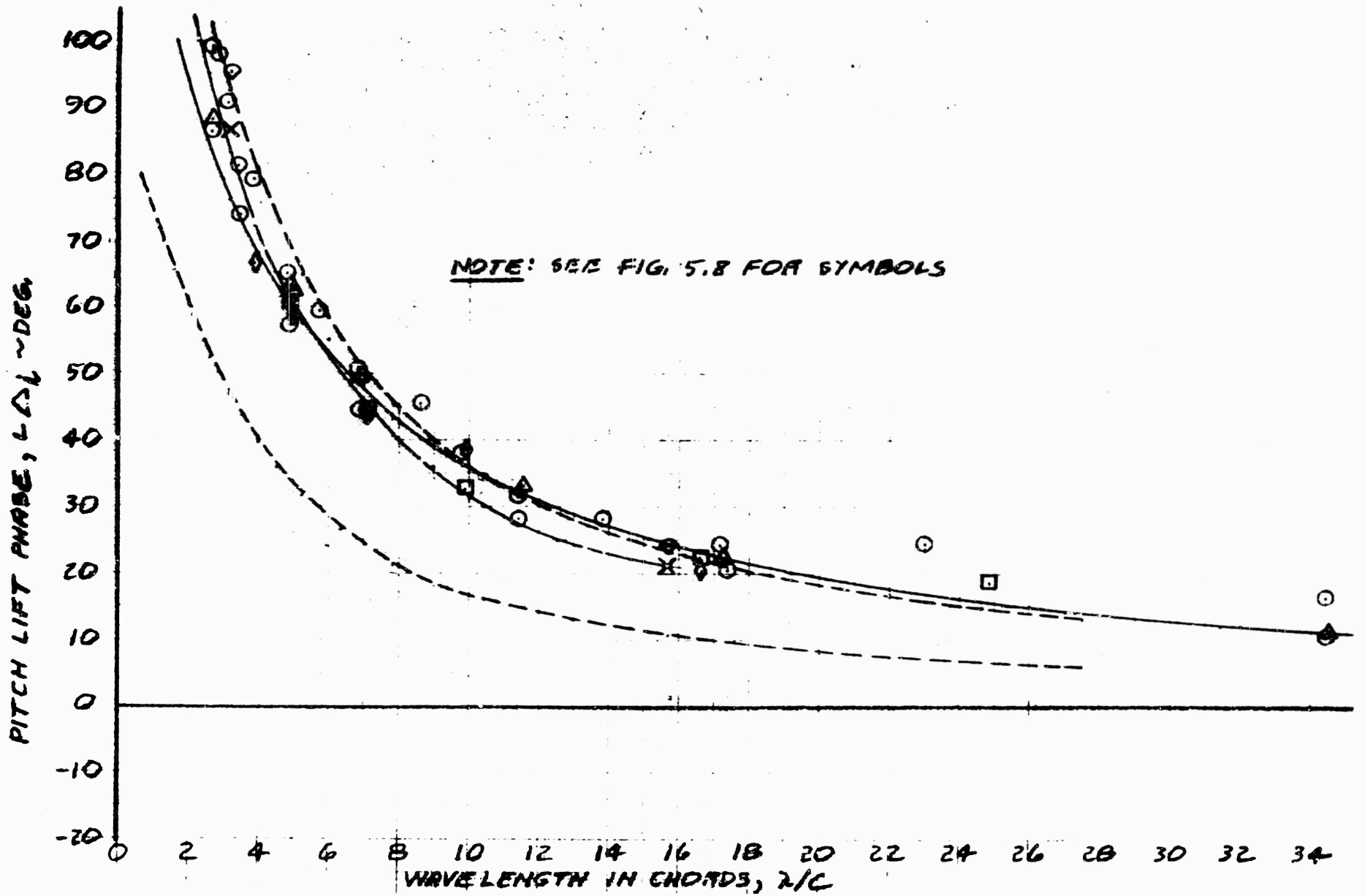


Figure 5-11. Pitch Lift Phase, H/MGC = .062, AG(EH) Fwd. Foil

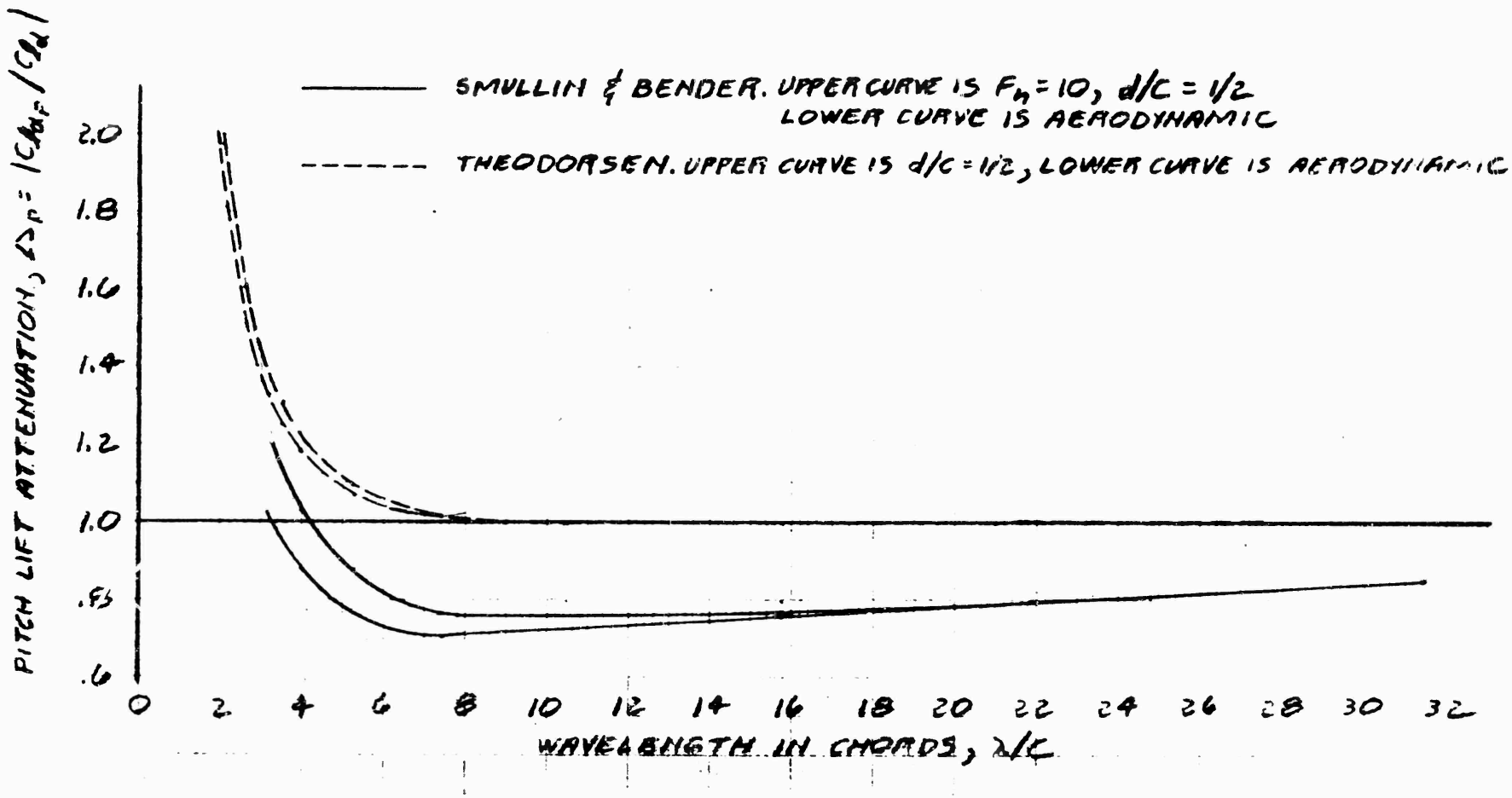


Figure 5-12. Pitch Lift Attenuation, H/c = 1/4, 2-D

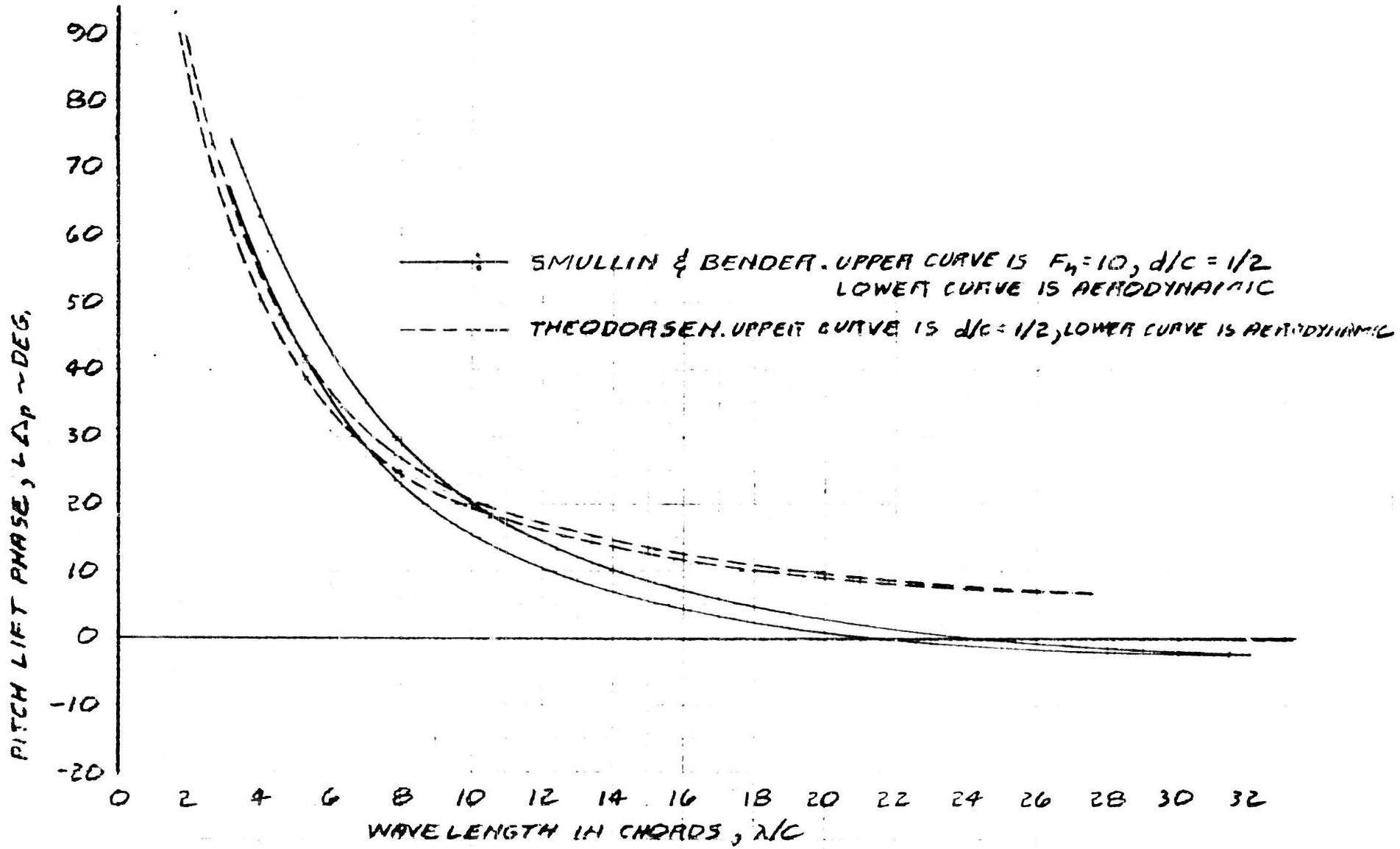


Figure 5-13. Pitch Lift Phase, H/c = 1/4, 2-D

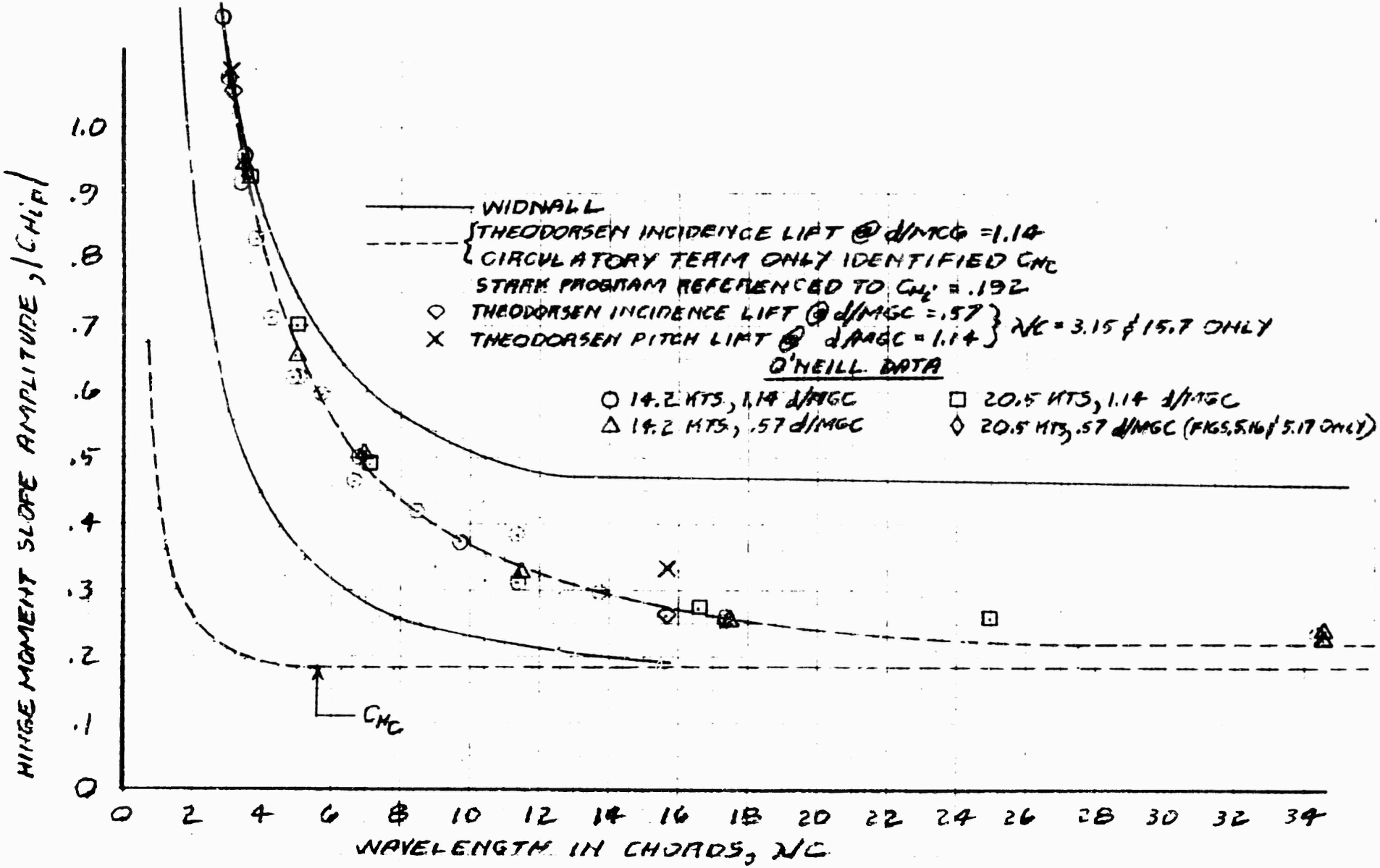


Figure 5-14. Pitch Moment Slope, H/MGC = .32, AG(EH) Fwd. Foil

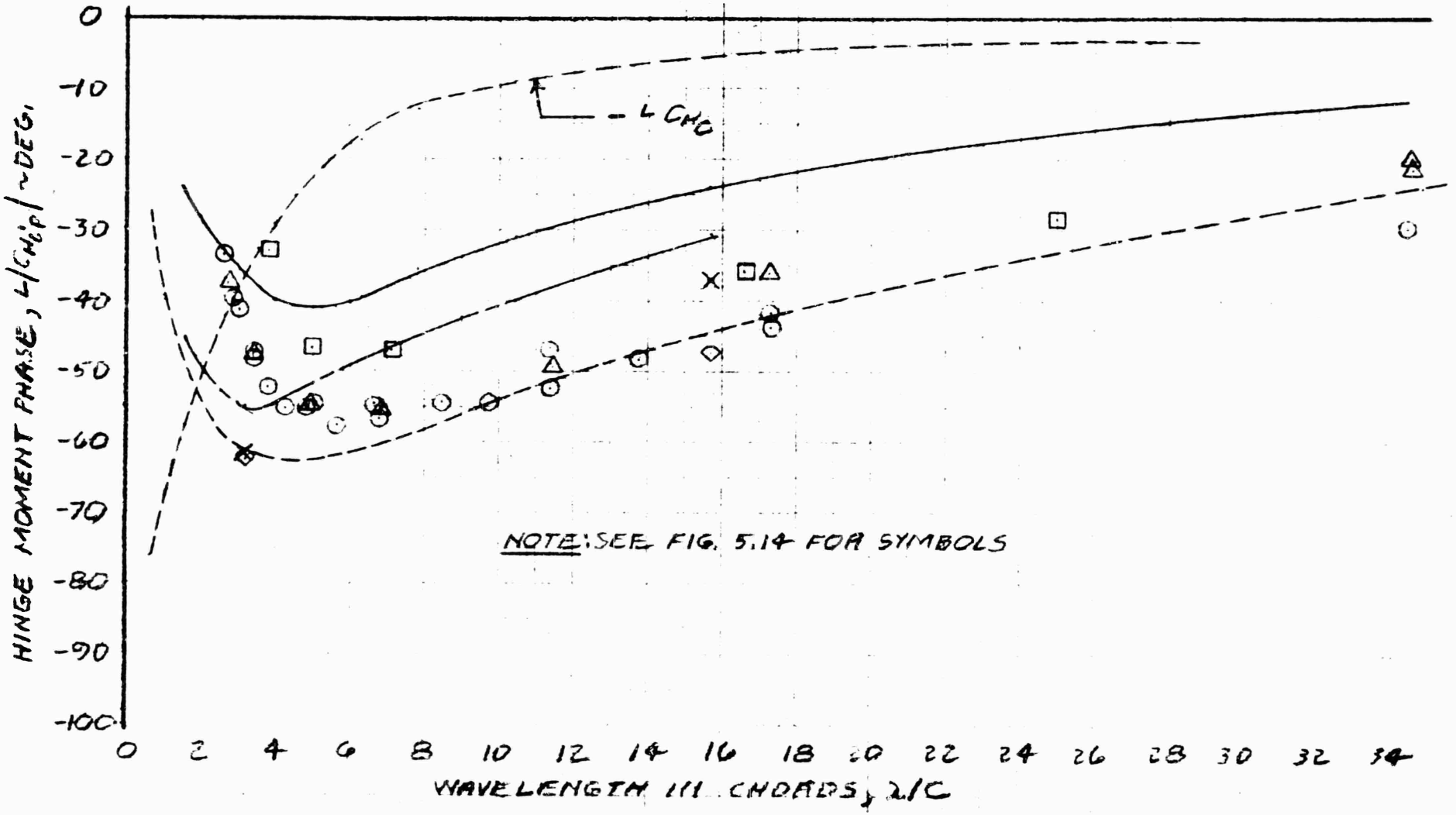


Figure 5-15. Pitch Moment Phase, H/MGC = .32, AG(EH) Fwd. Foil

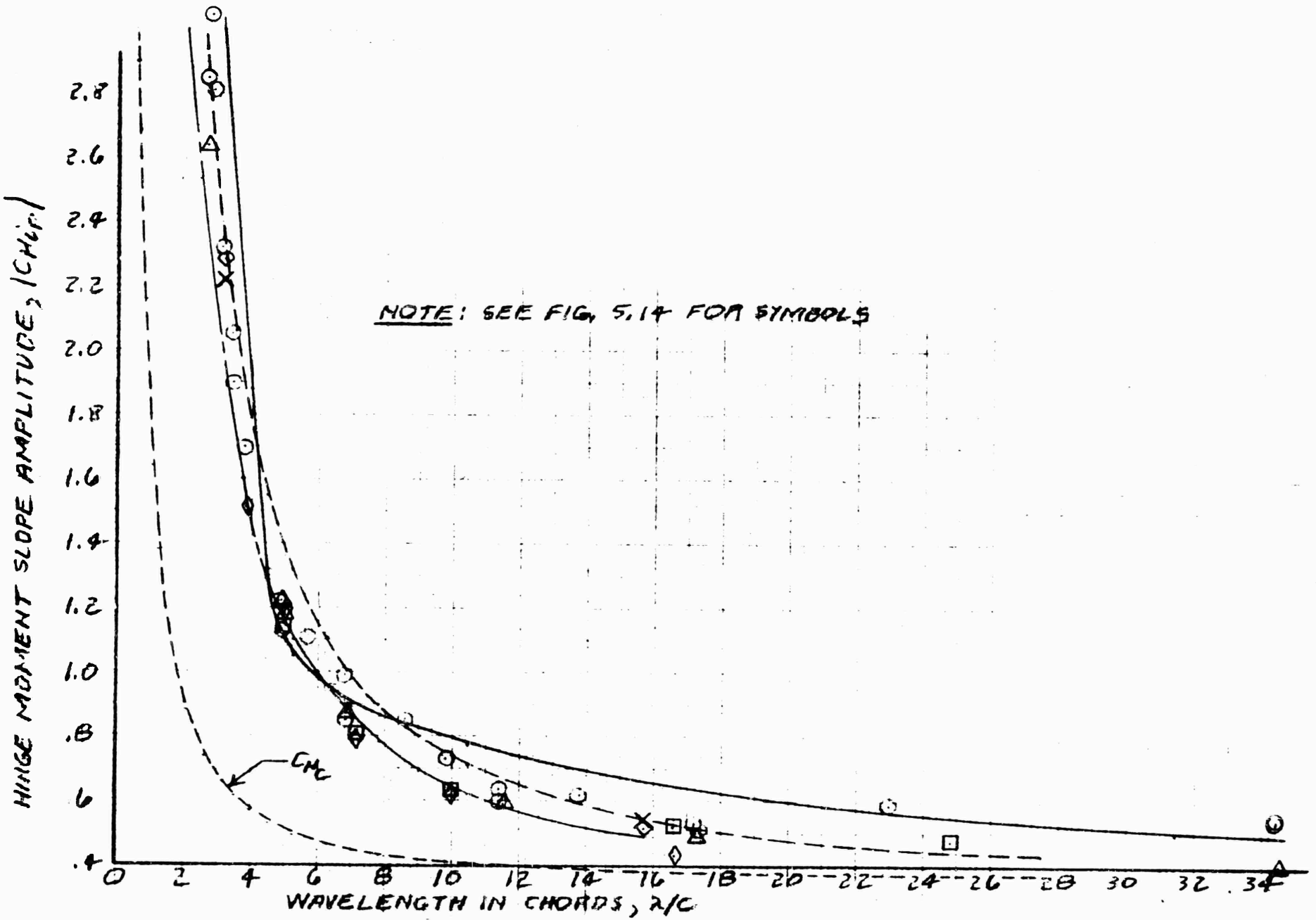


Figure 5-16. Pitch Moment Slope, H/MGC = .062, AG(EH) Fwd. Foil

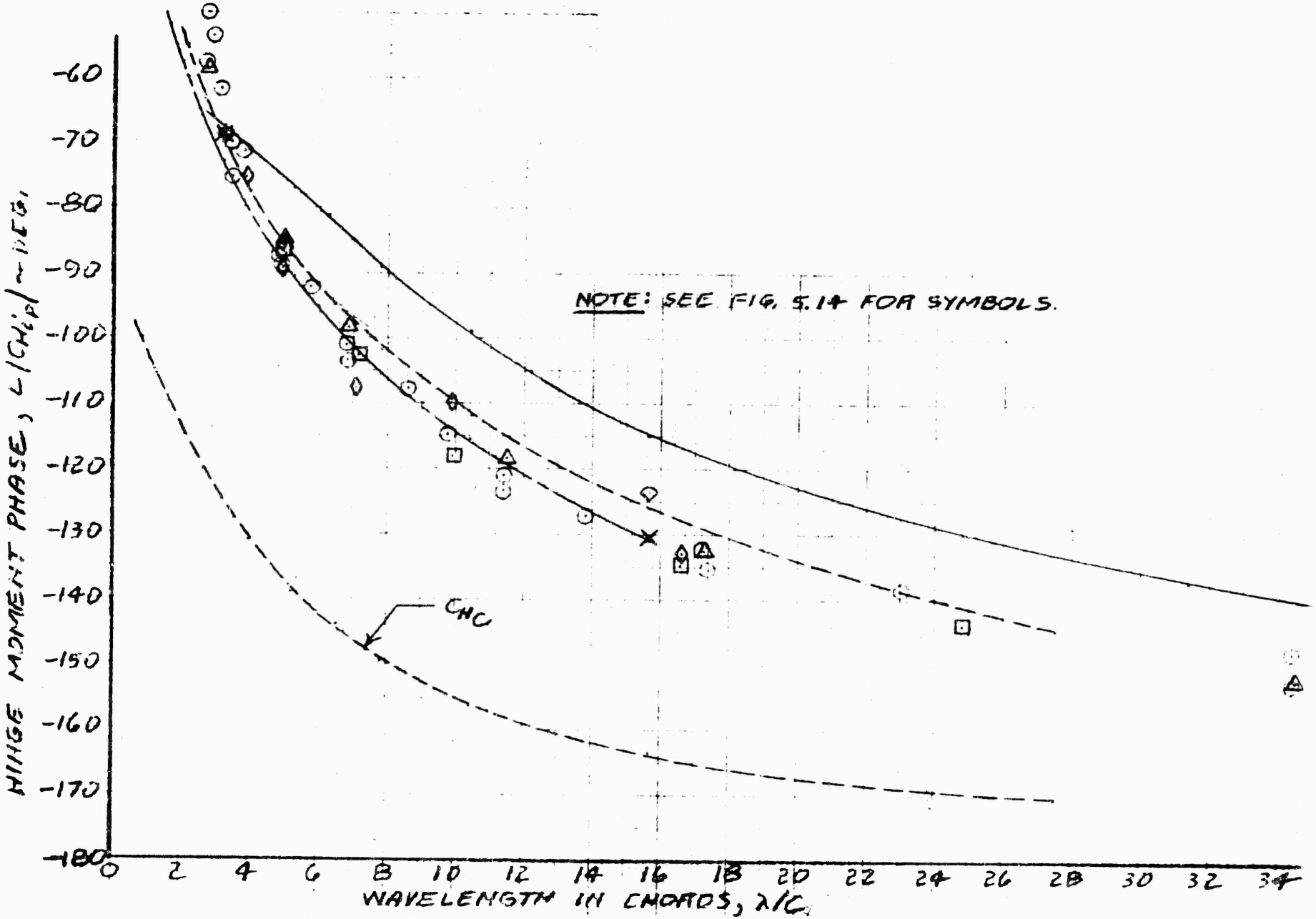


Figure 5-17. Pitch Moment Phase, H/MGC = .062, AG(EH) Fwd. Foil

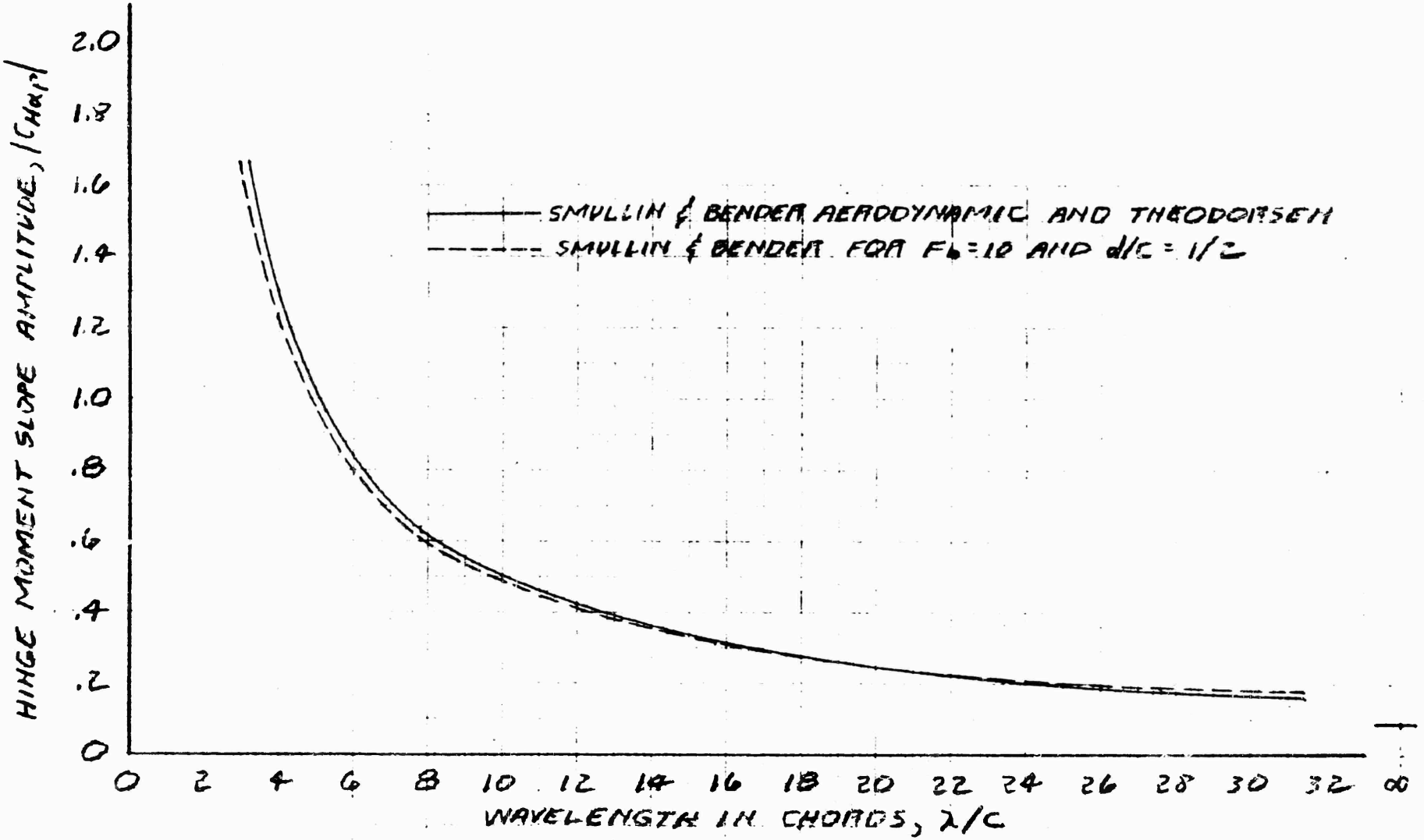


Figure 5-18. Pitch Moment Amplitude, 2-D, H/c = 1/4

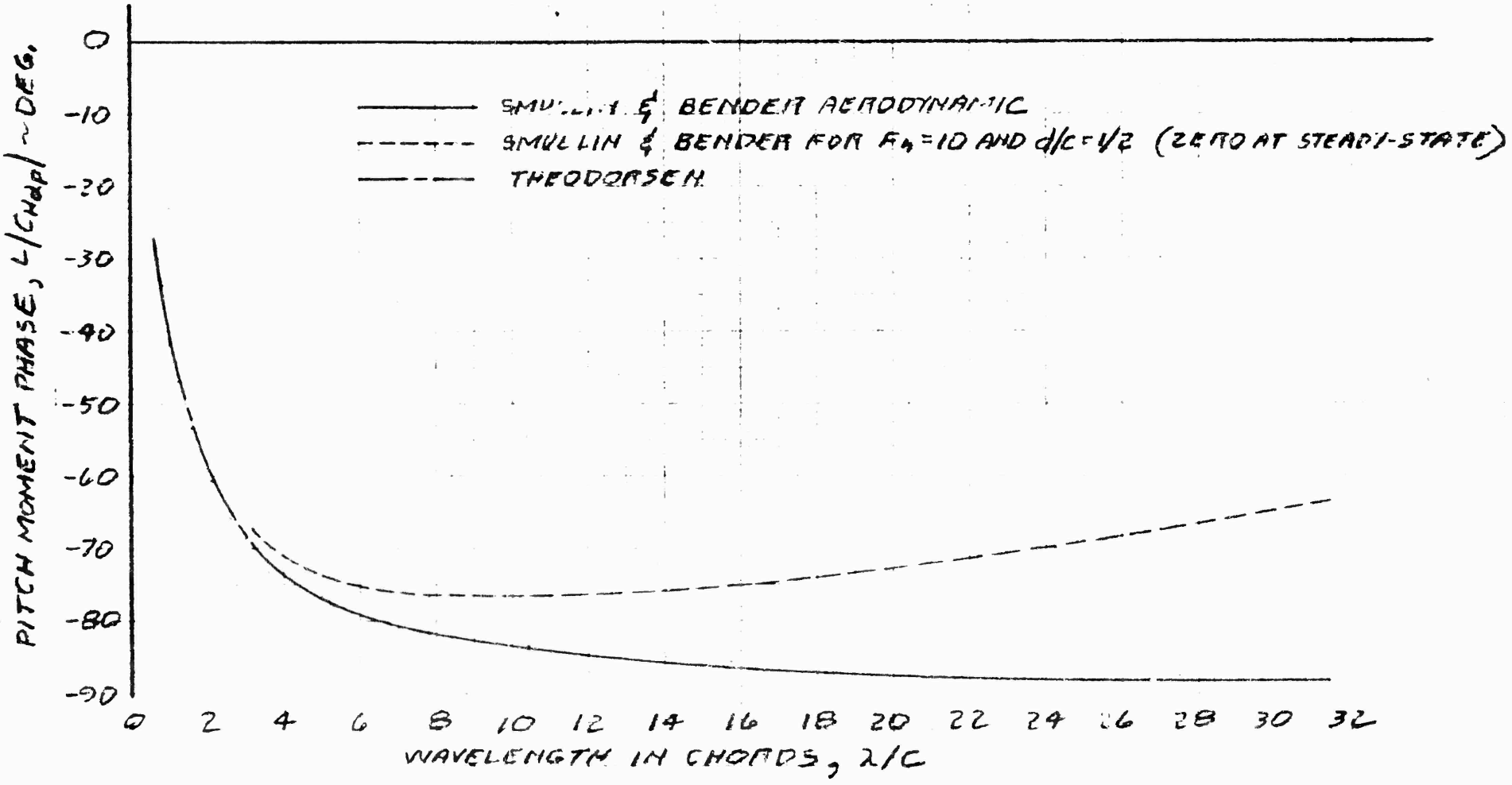


Figure 5-19. Pitch Moment Phase, 2-D, H/c = 1/4

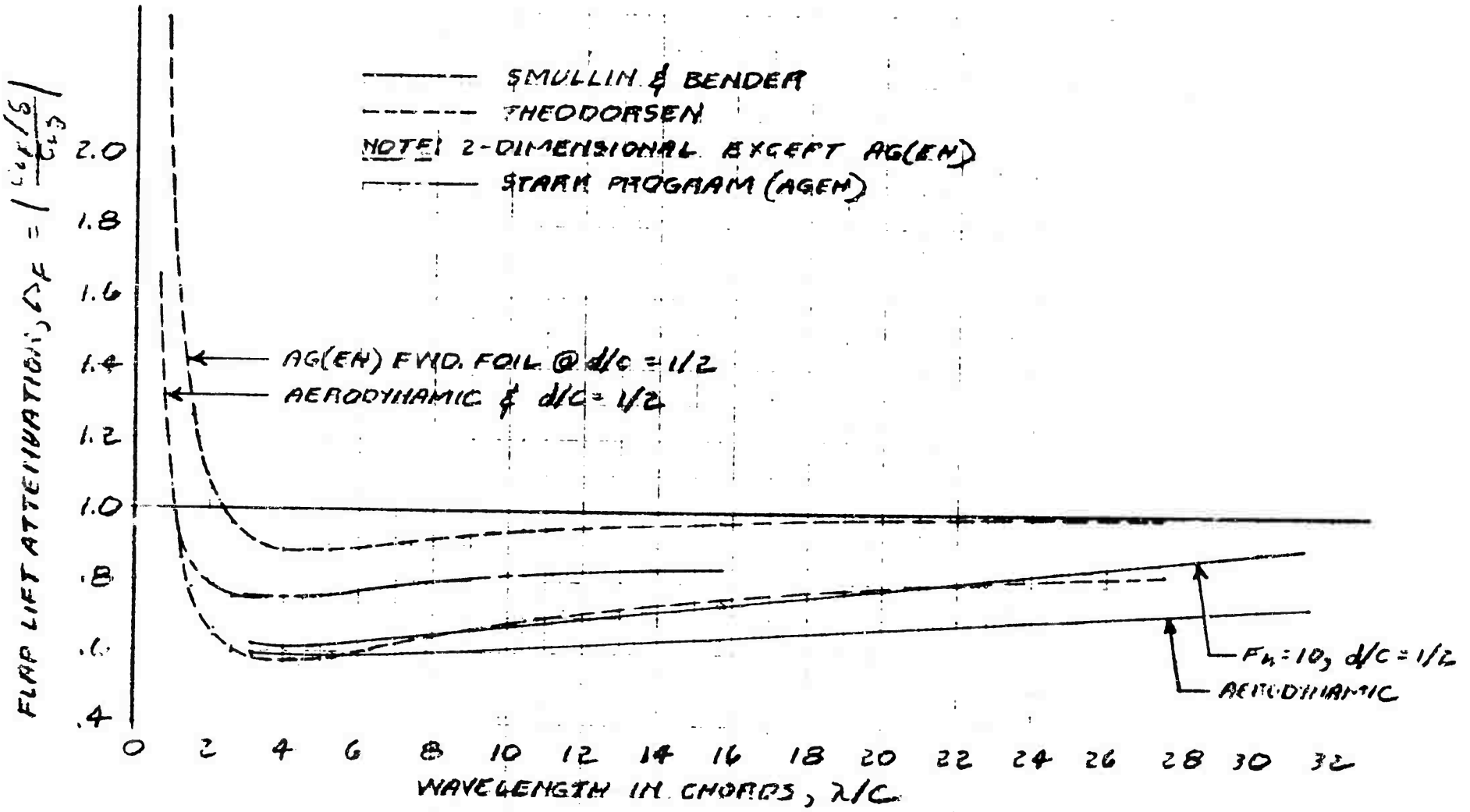


Figure 5-20. Flap Lift Attenuation

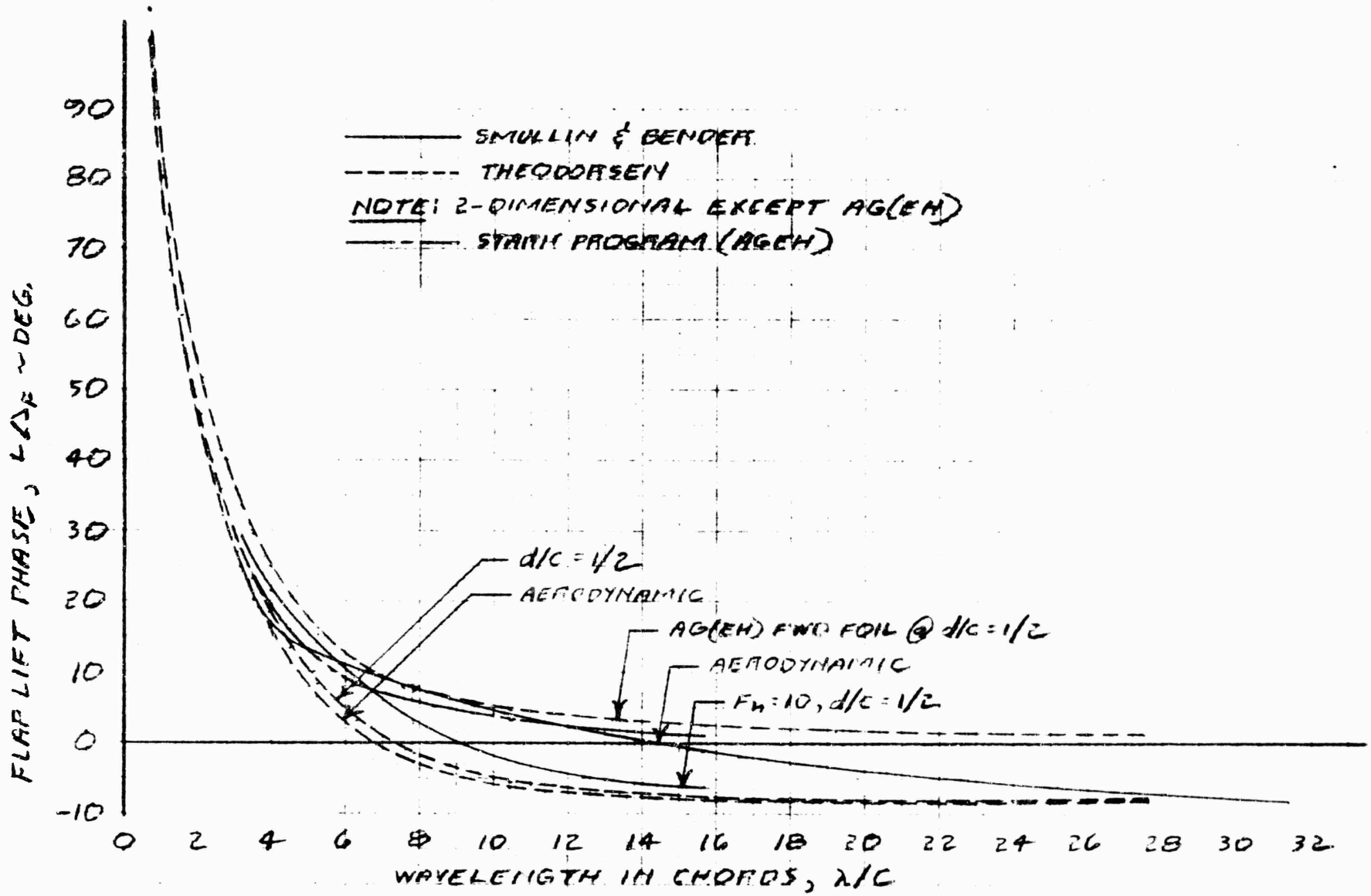


Figure 5-21. Flap Lift Phase

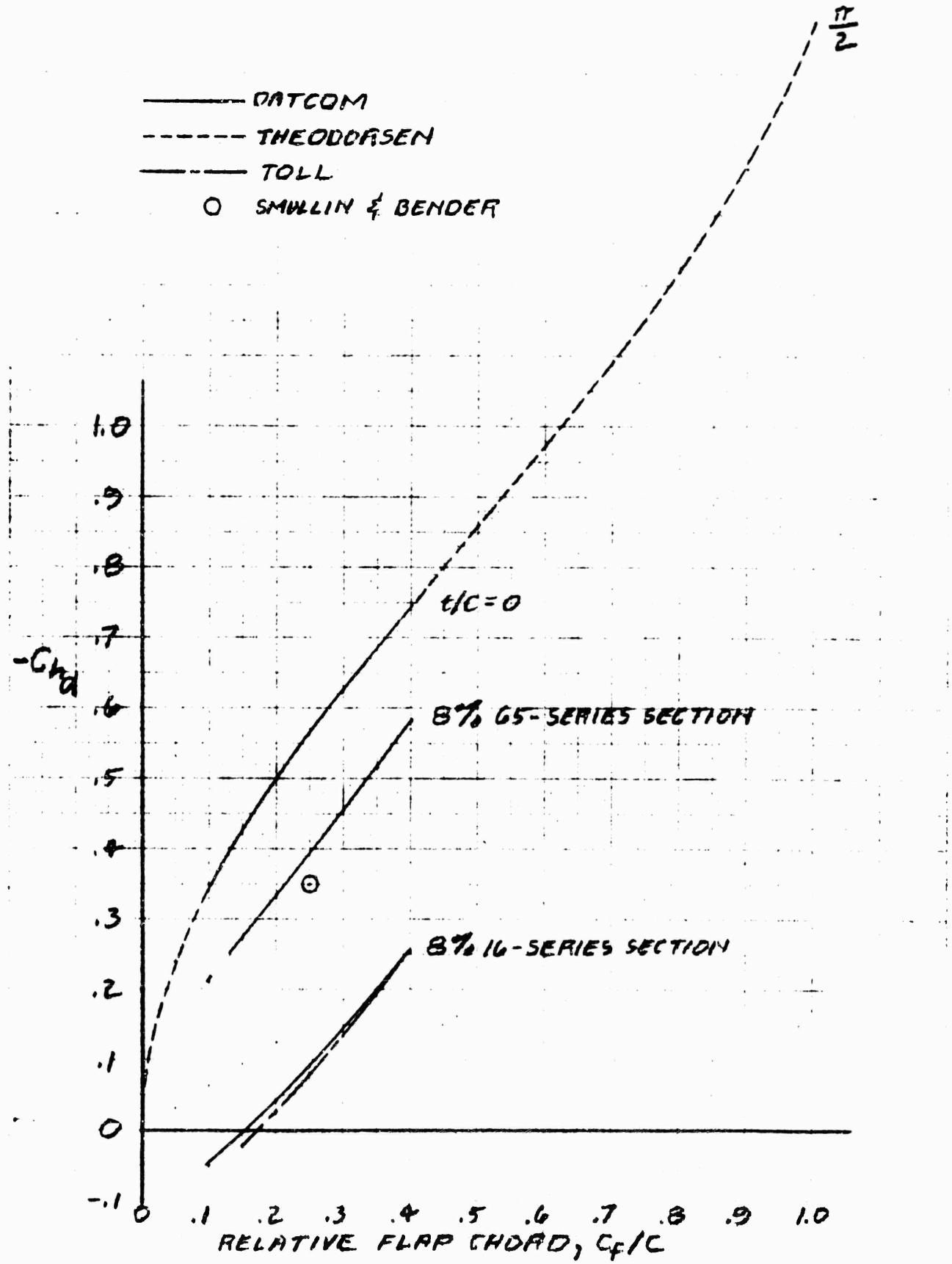


Figure 5-22. Flap Hinge Moment Derivative C_{h_α}, 2-D

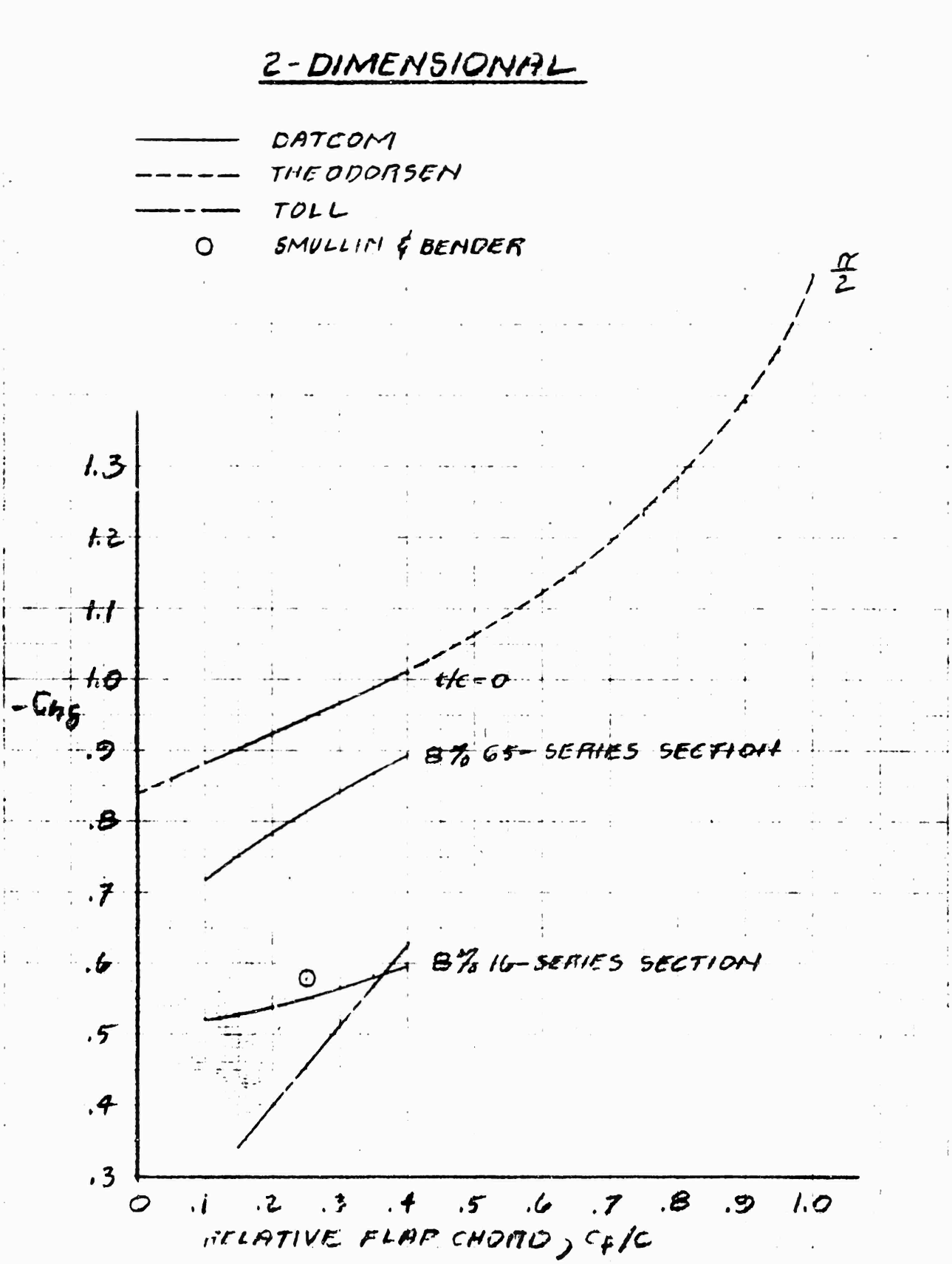


Figure 5-23. Flap Hinge Moment Derivative C_{h_δ}

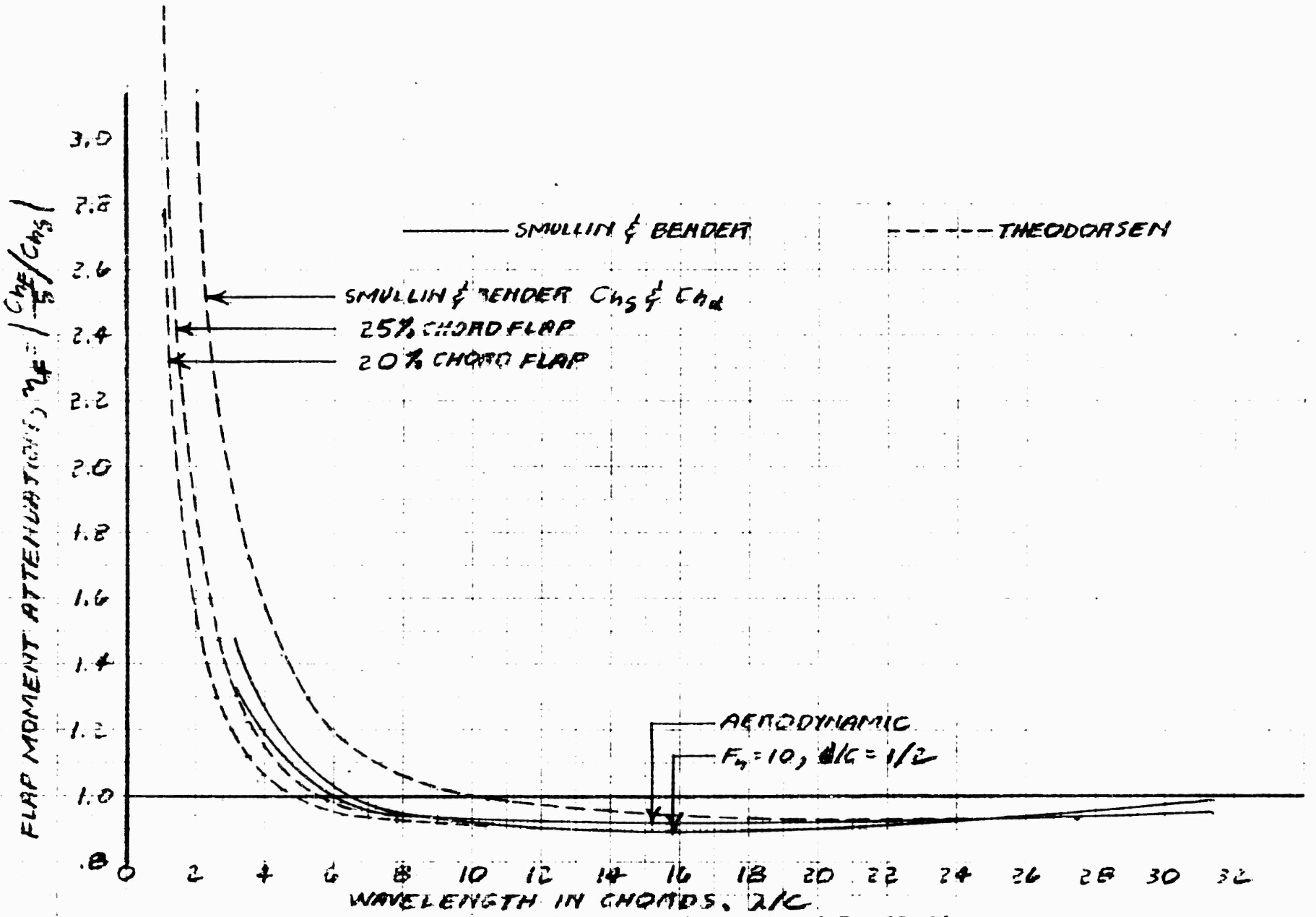


Figure 5-24. Flap Moment Attenuation, 2-D, .25c Flap

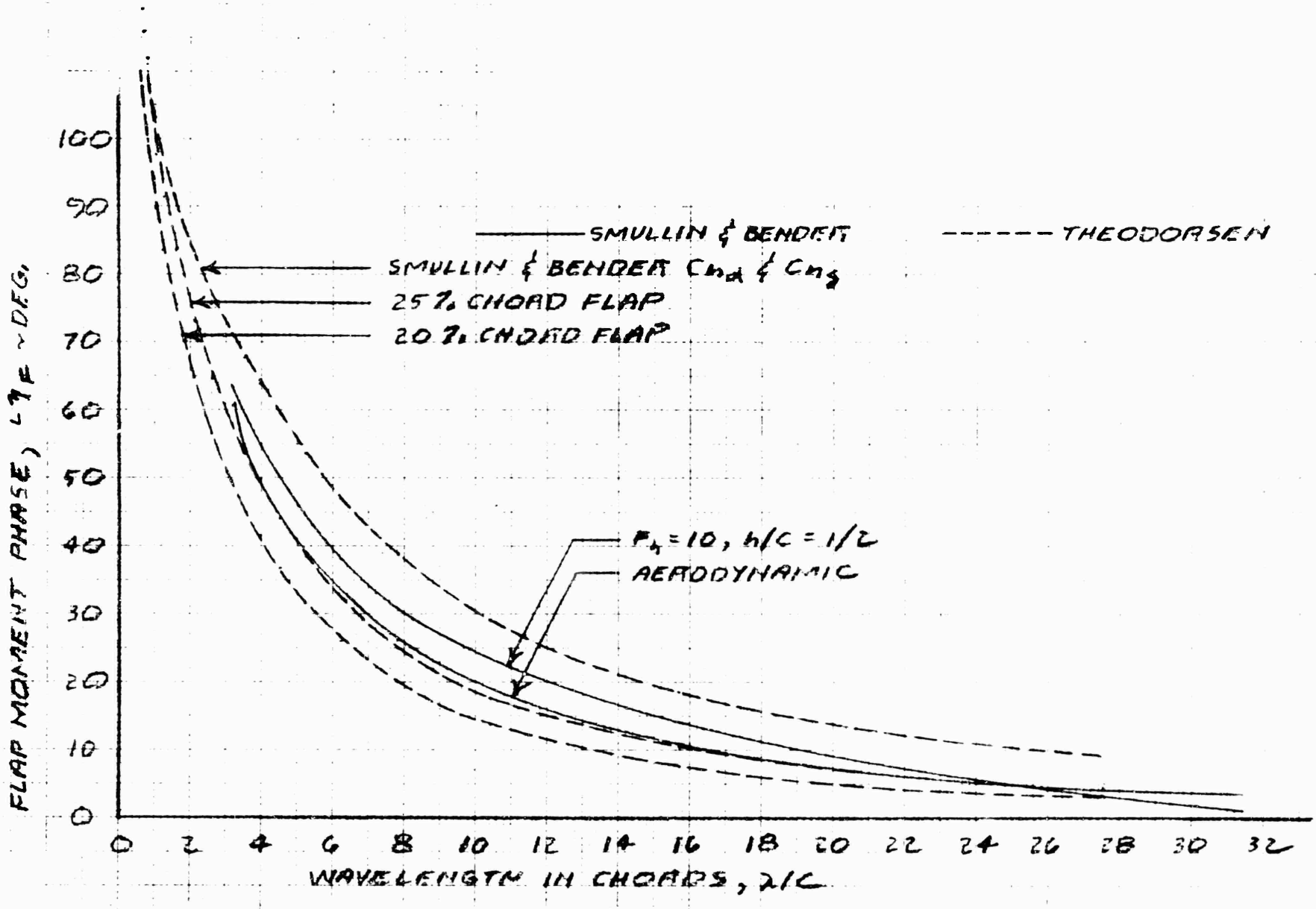


Figure 5.25. Flap Moment Phase, 2-D, .25c Flap

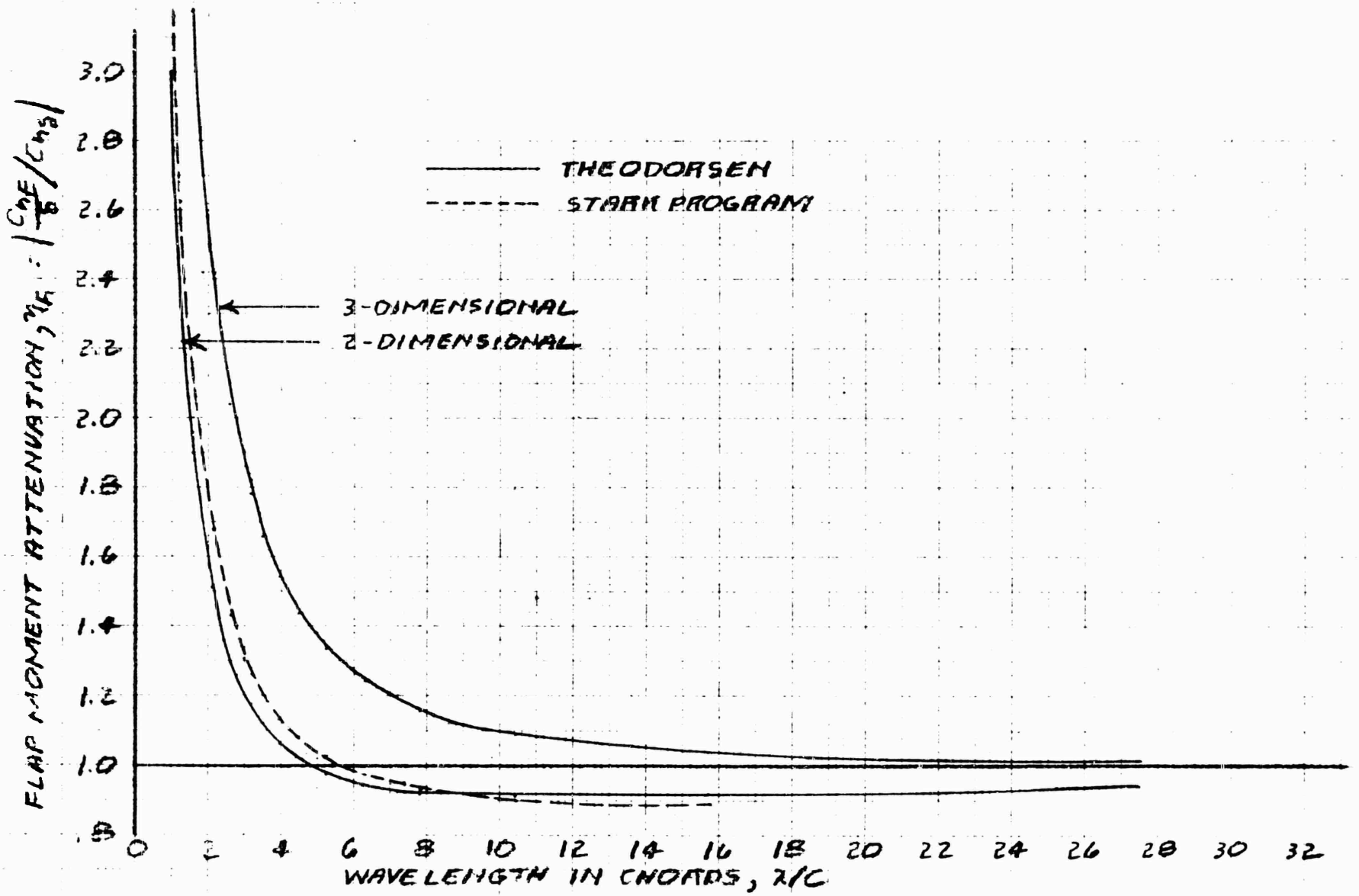


Figure 5-26. Flap Moment Attenuation, AG(EH) Fwd. Foil

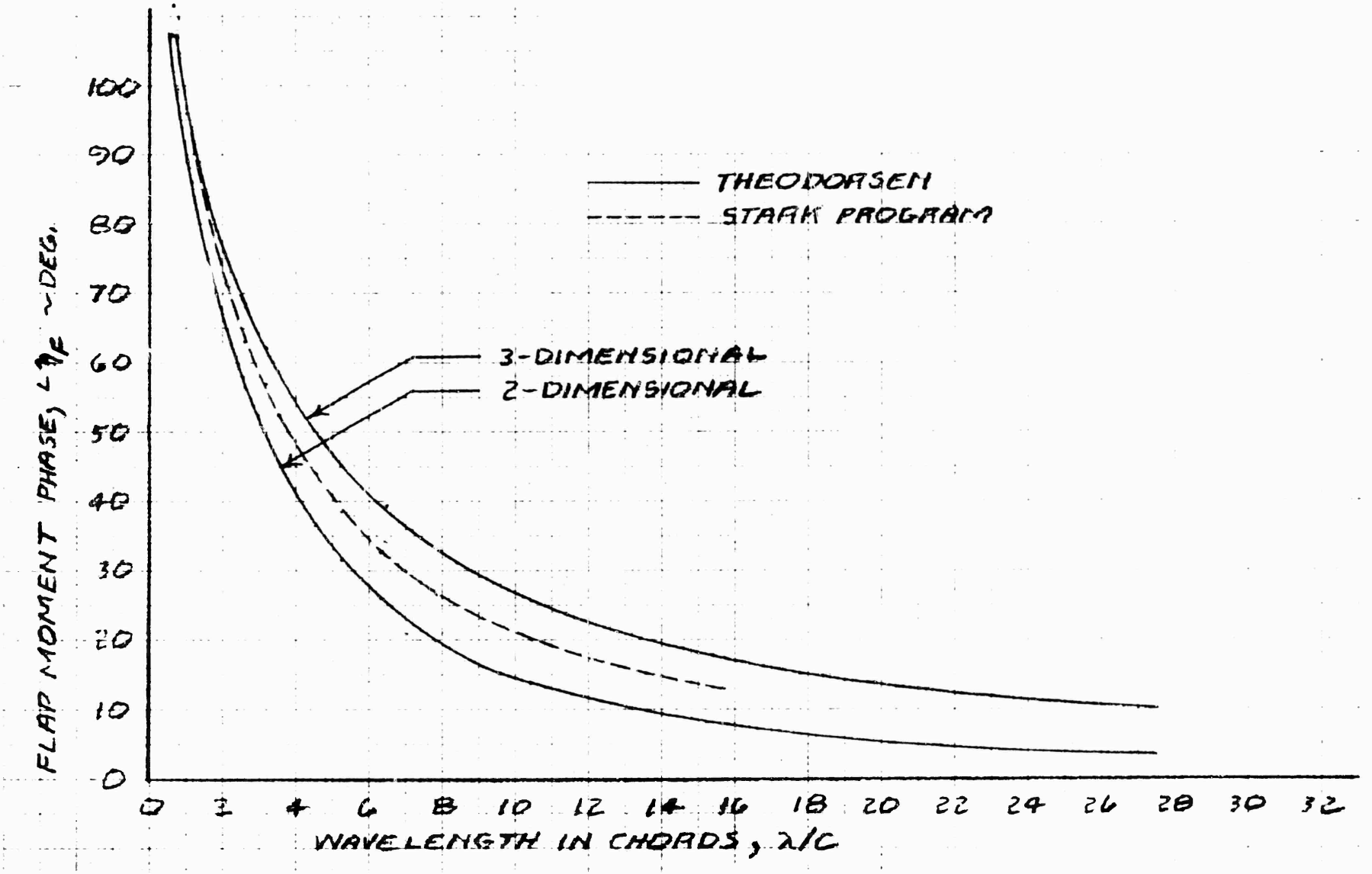


Figure 5-27. Flap Moment Phase, AG(EH) Fwd. Foil

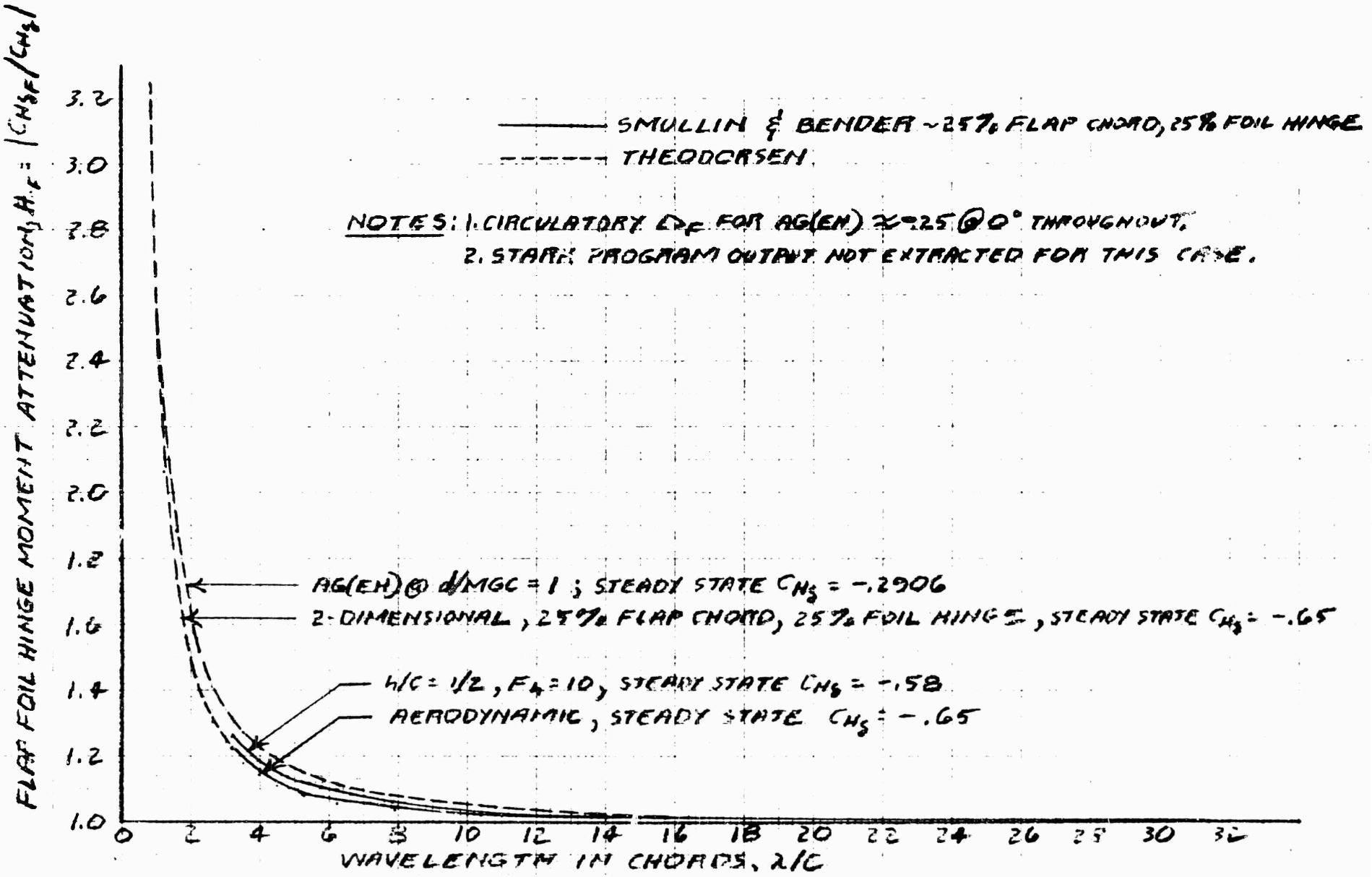


Figure 5-28. Flap Foil Hinge Moment Attenuation

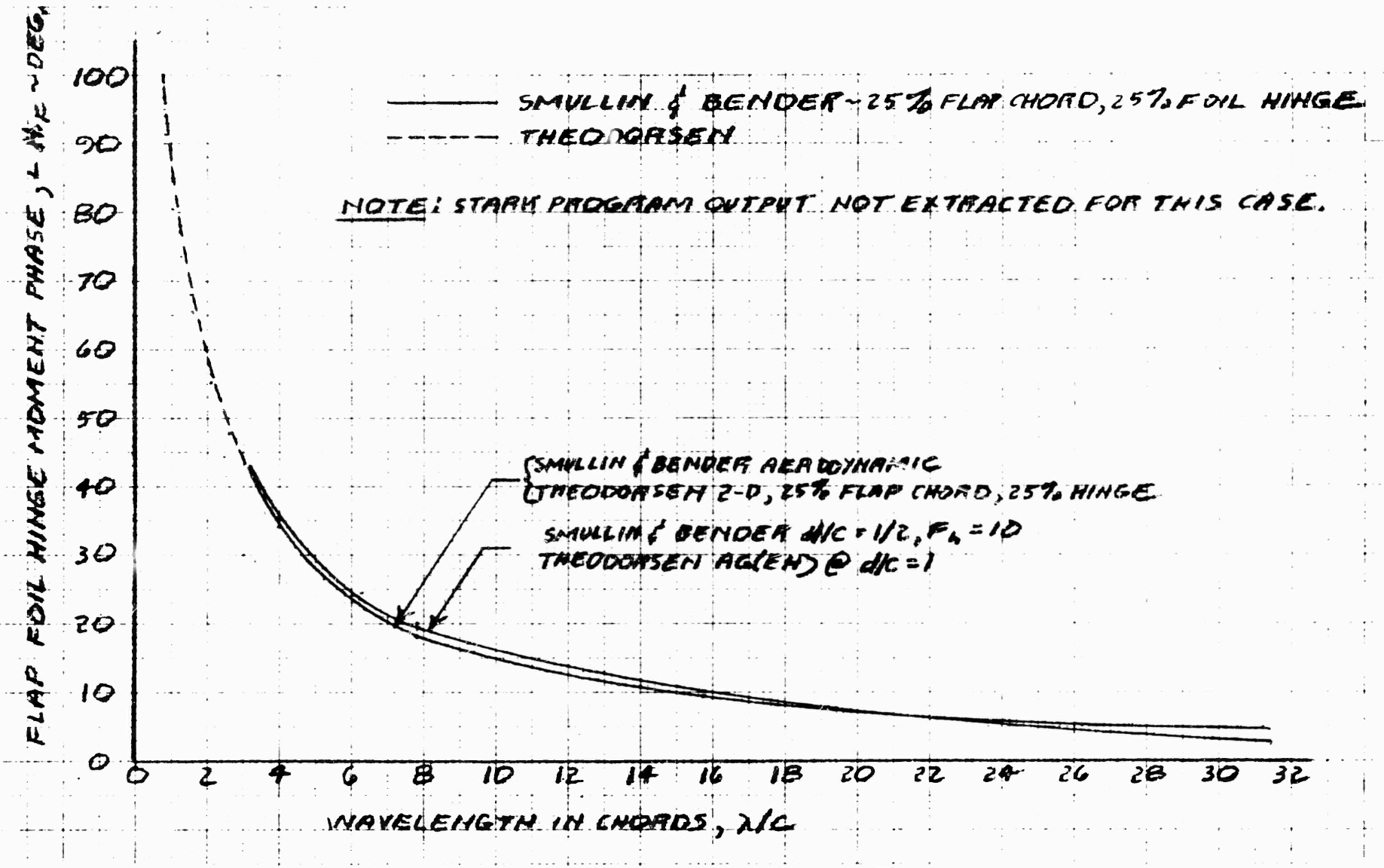


Figure 5-29. Flap Foil Hinge Moment Phase

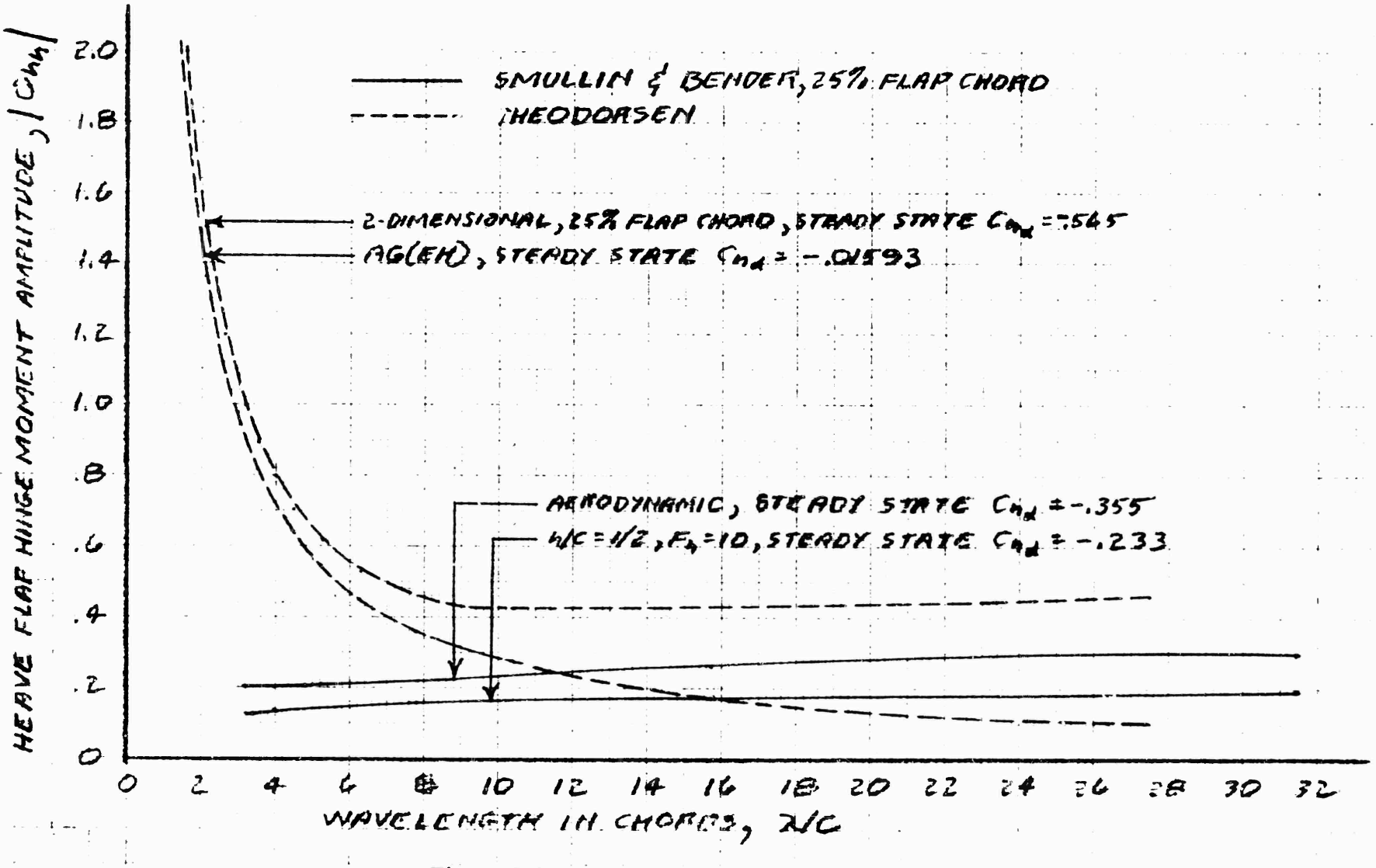


Figure 5-30. Heave Flap Hinge Moment Amplitude

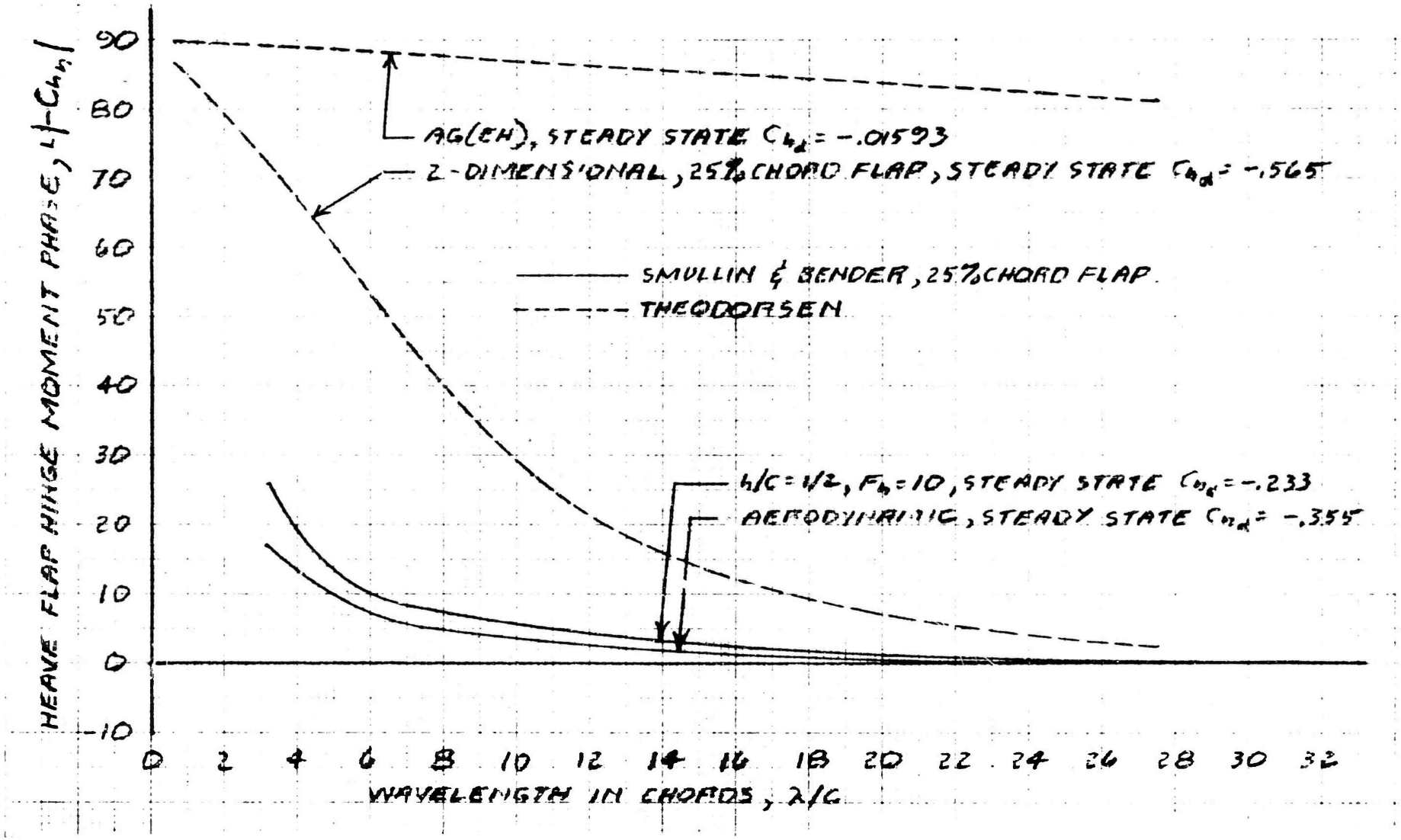


Figure 5-31. Heave Flap Hinge Moment Phase

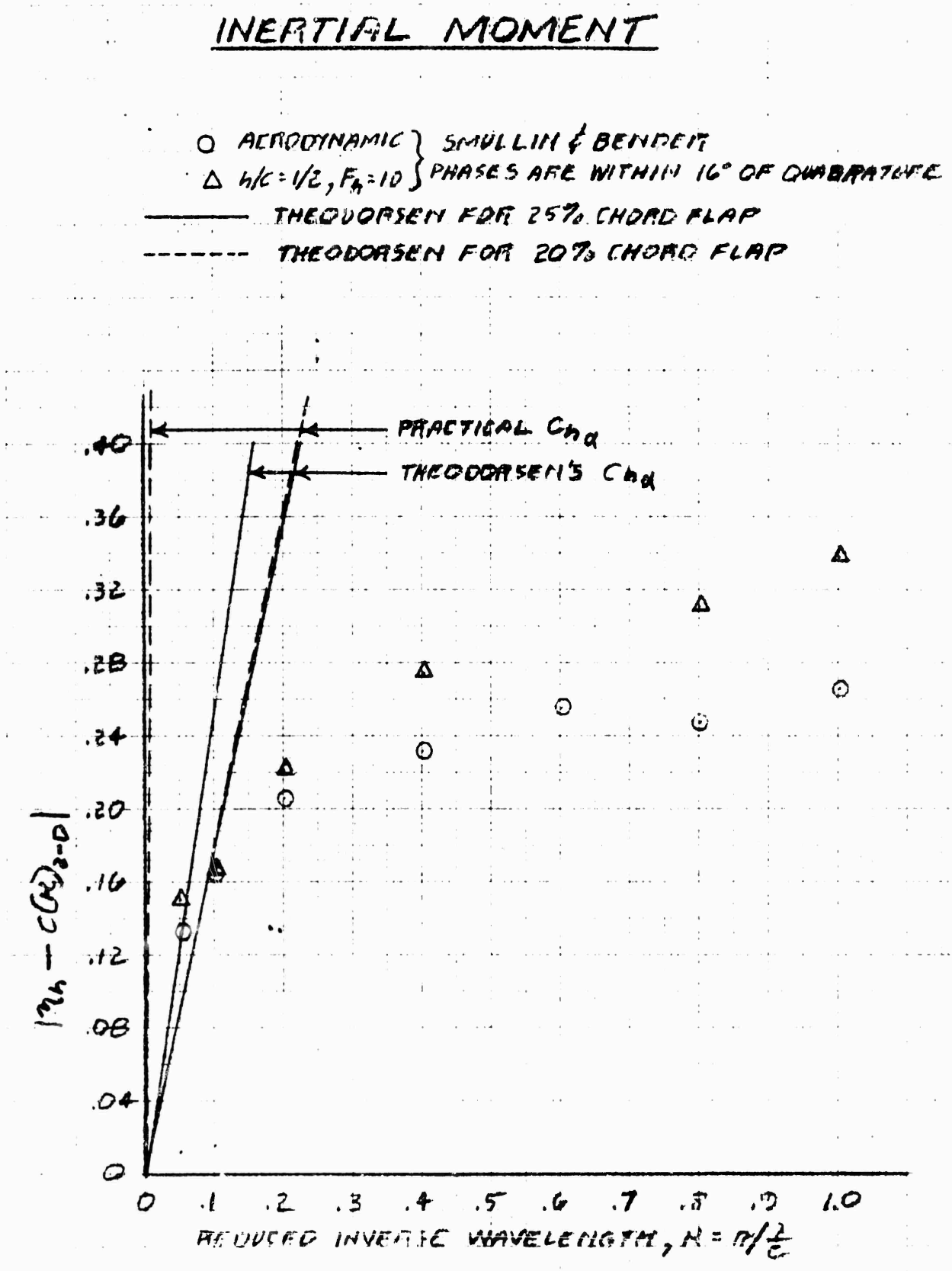


Figure 5-32. Heave Flap Hinge Moment Analysis

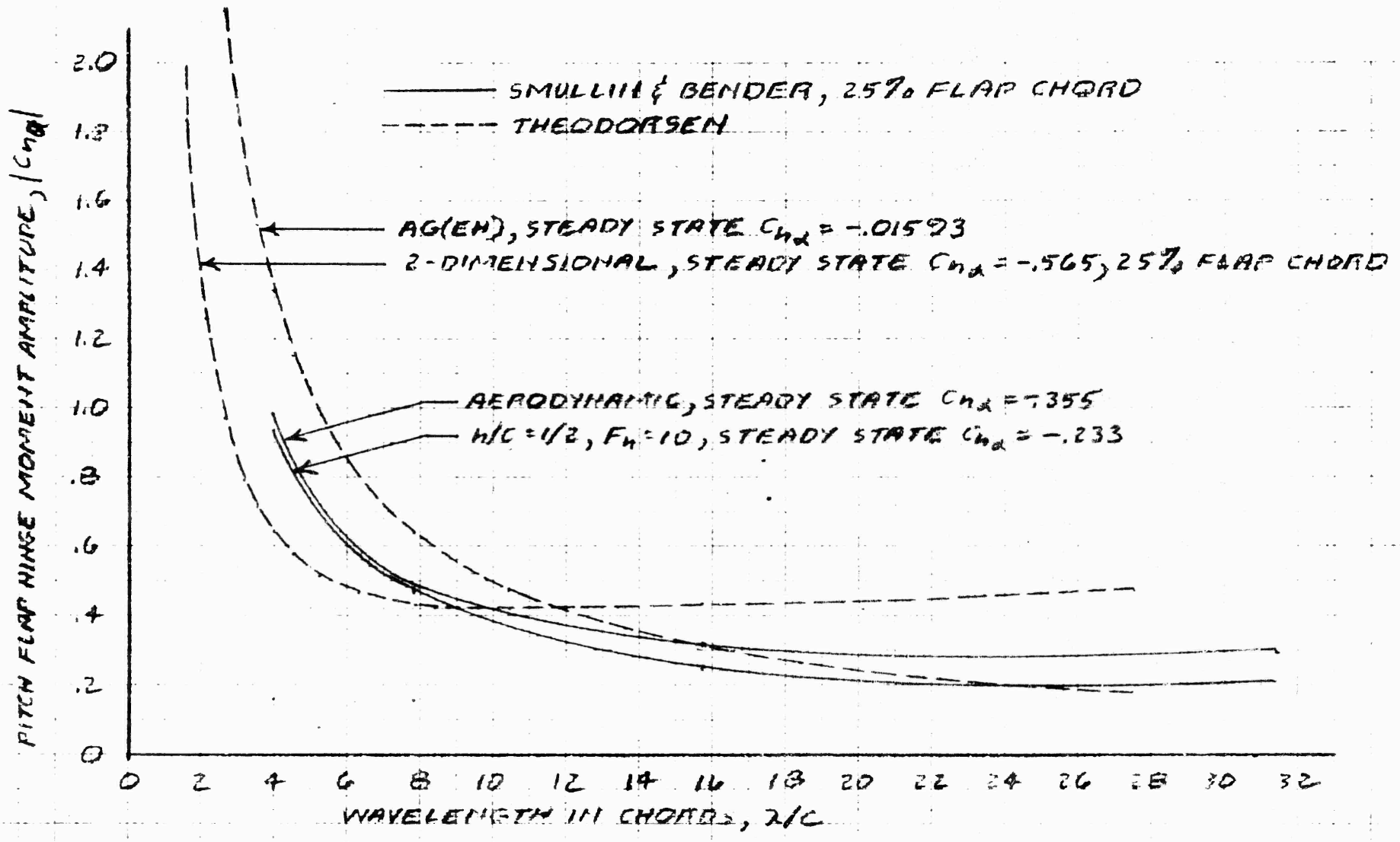


Figure 5-33. Pitch Flap Hinge Moment Amplitude

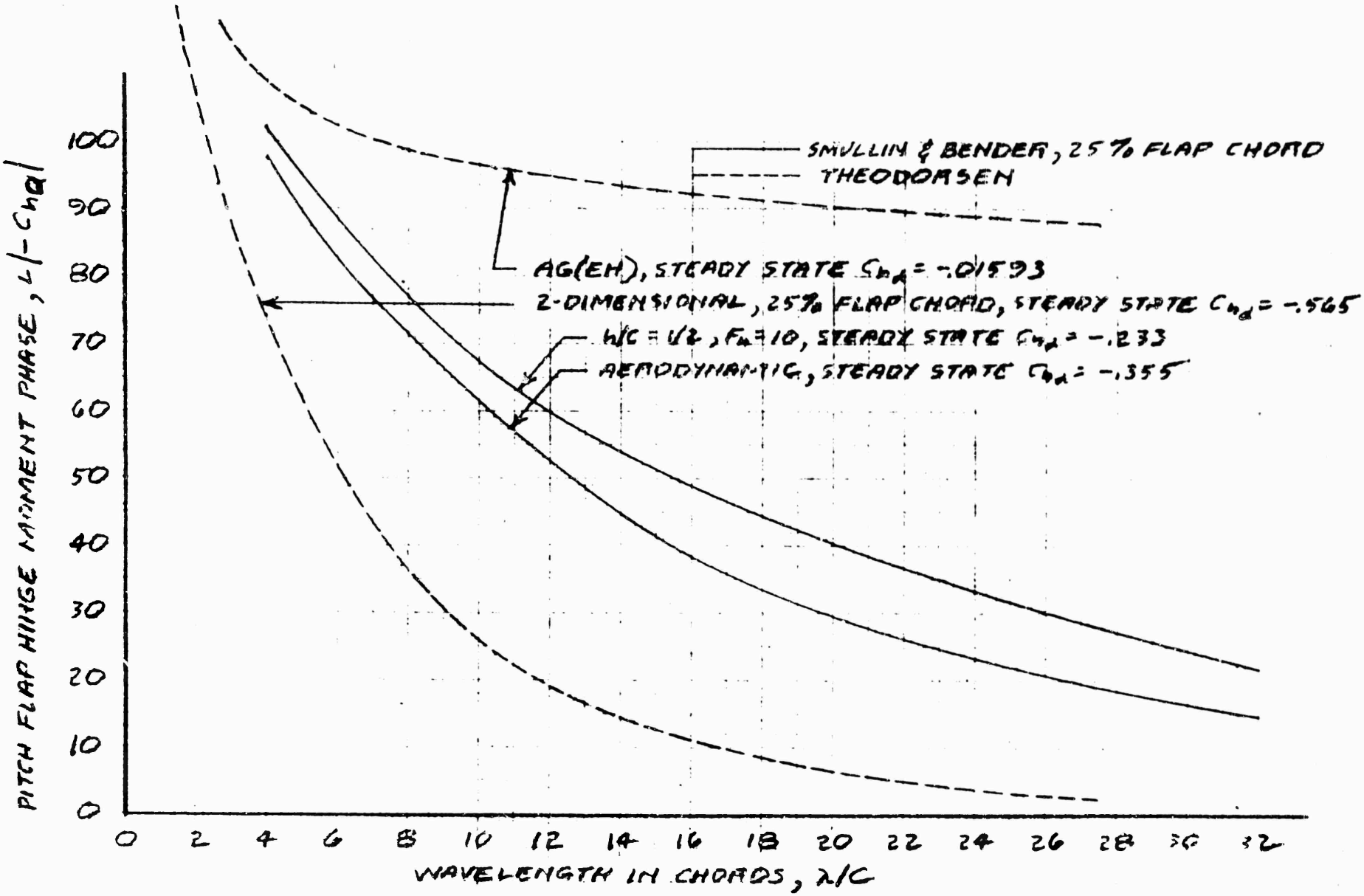


Figure 5-34. Pitch Flap Hinge Moment Phase

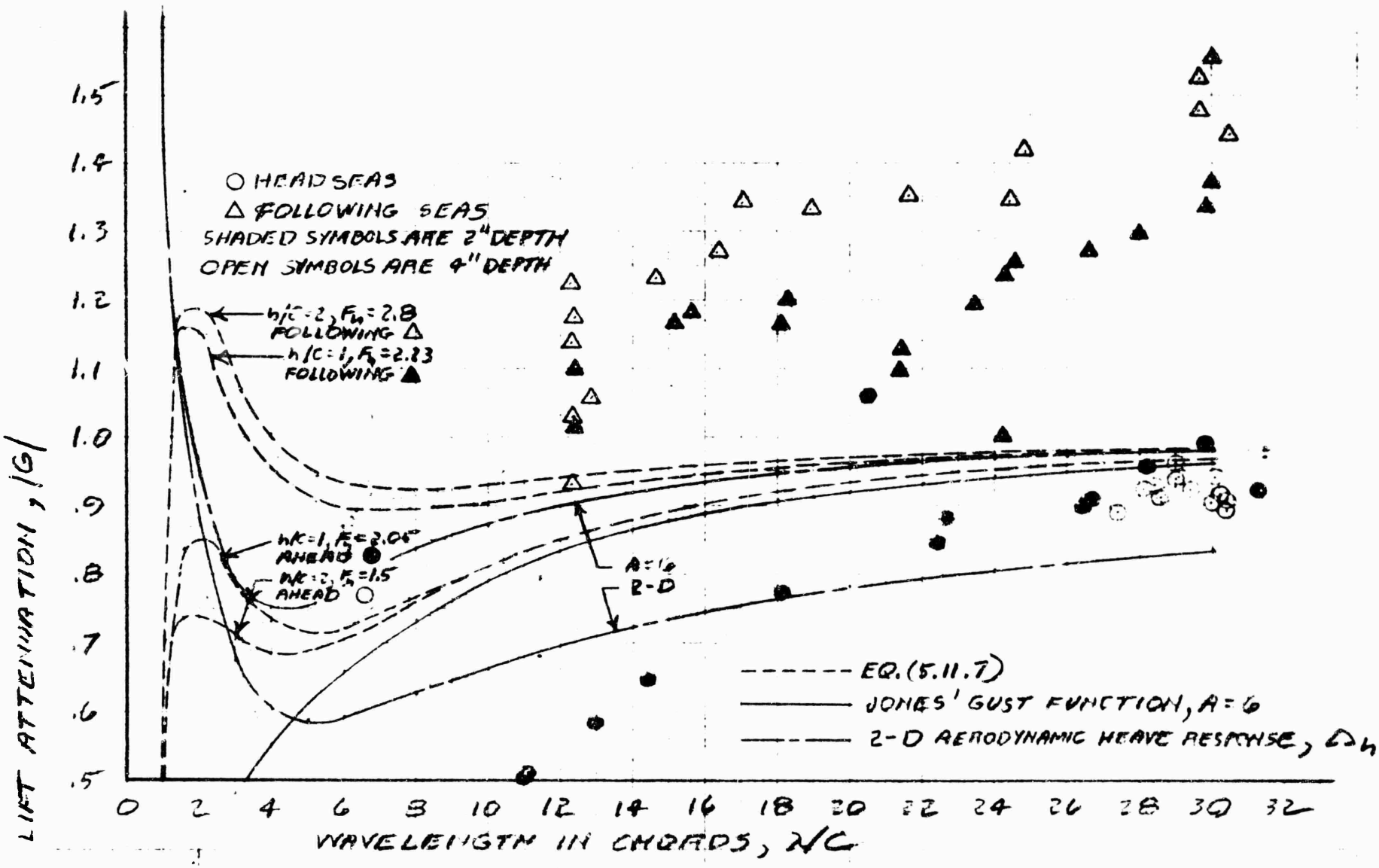


Figure 5-35. Orbital Motion, Steele's Data, Attenuation

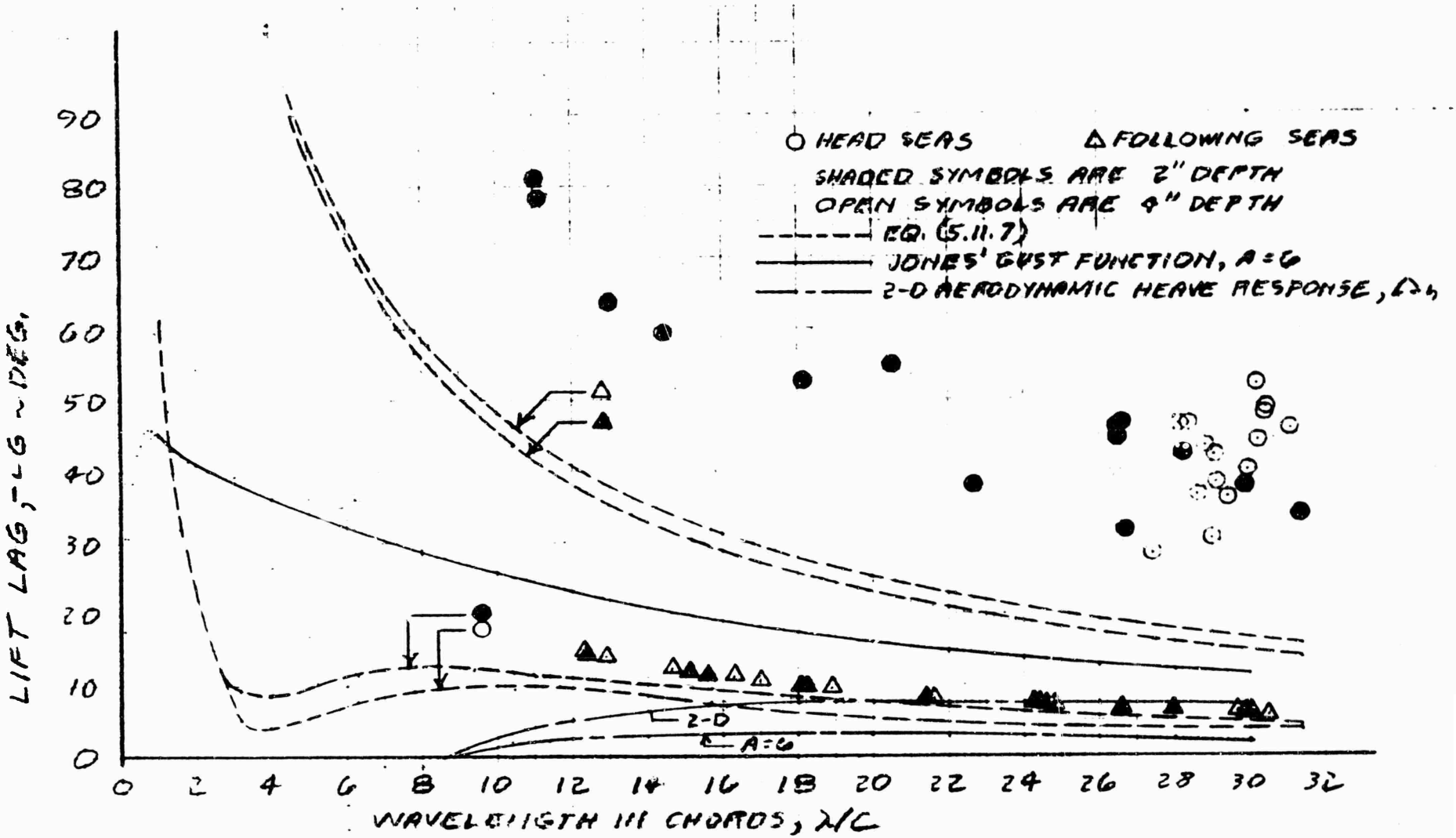


Figure 5-36. Orbital Motion, Steele's Data, Phase

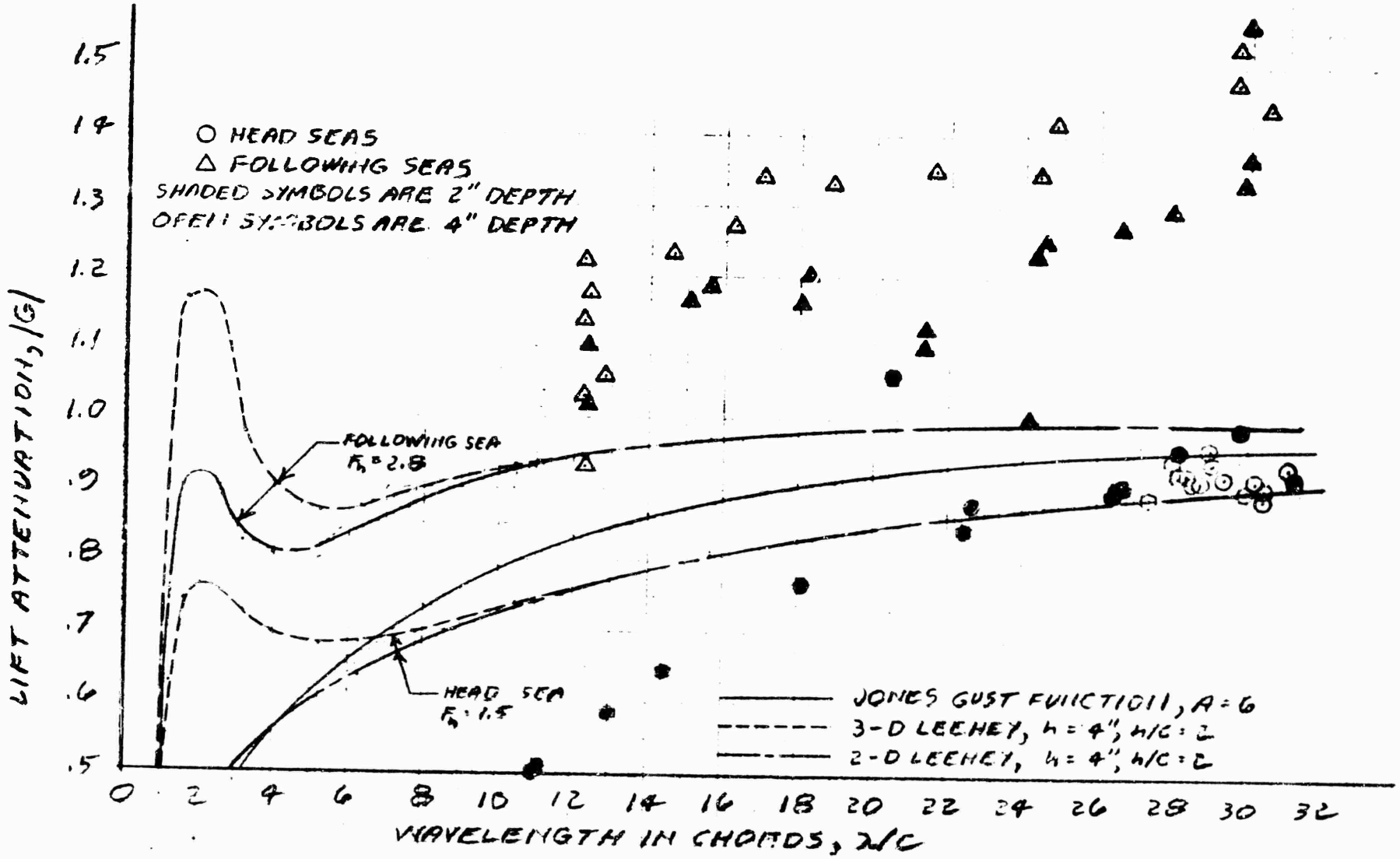


Figure 5-37. Orbital Motion, Steele's Data, Attenuation

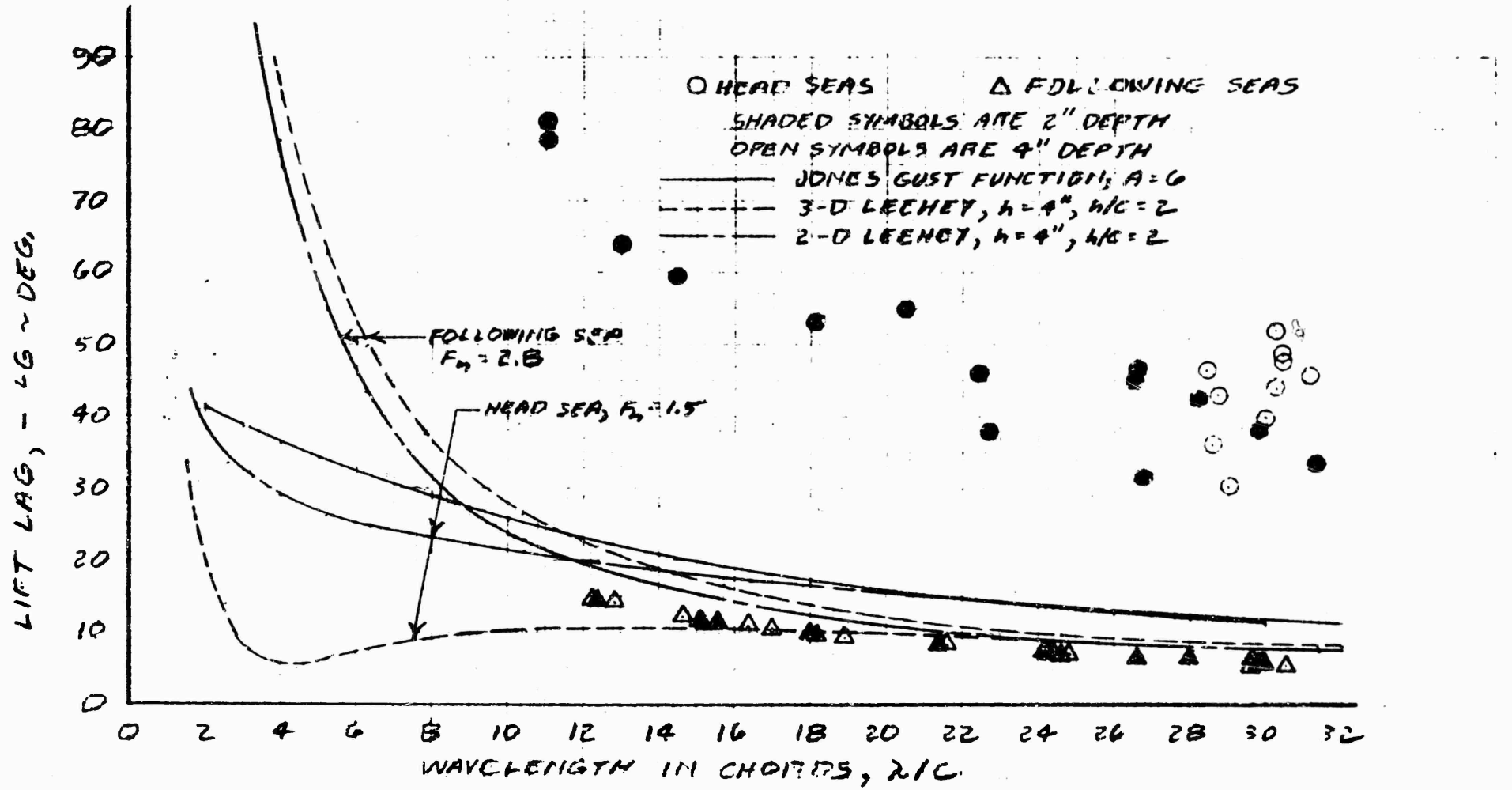


Figure 5-38. Orbital Motion, Steele's Data, Phase

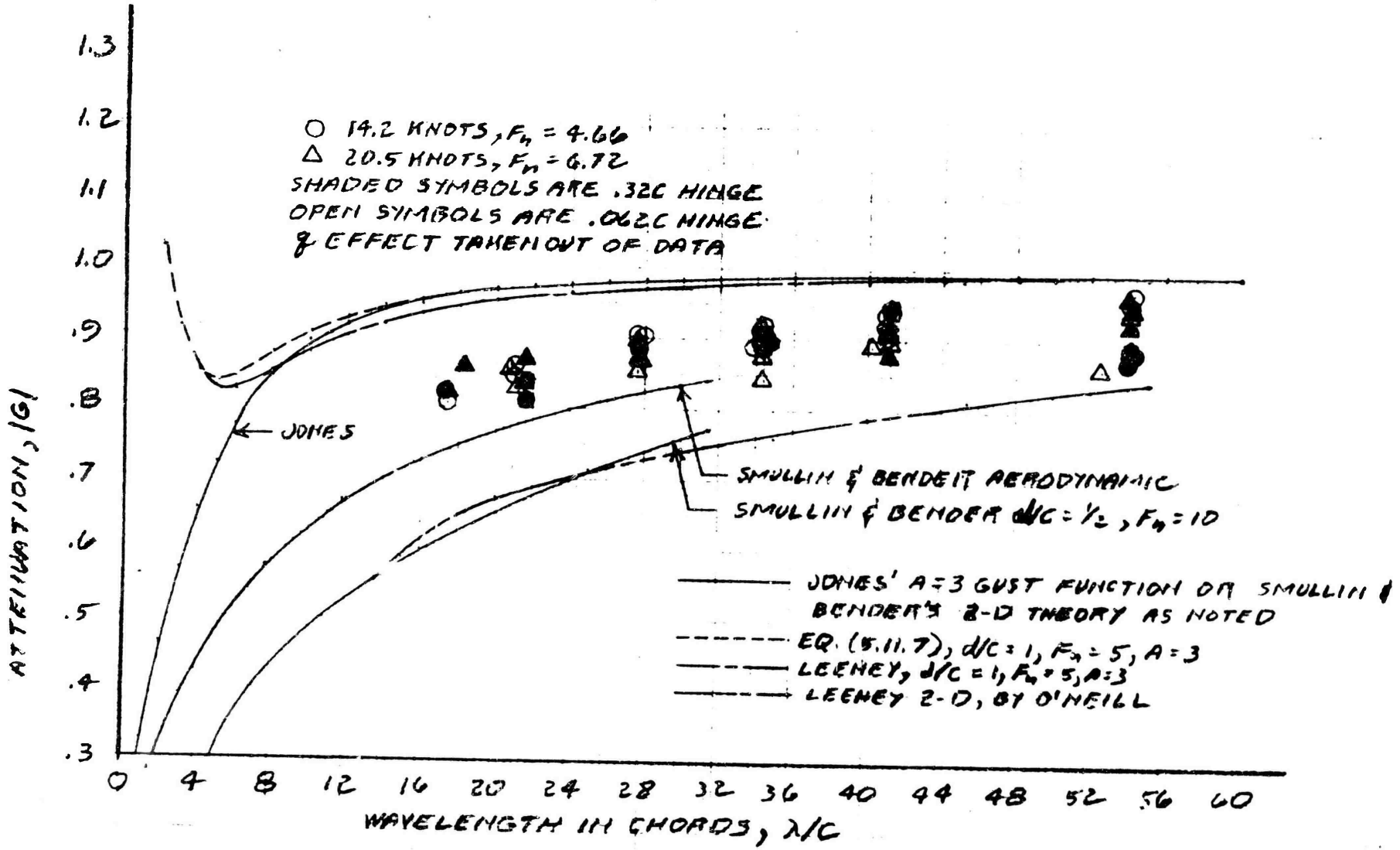


Figure 5-39. Orbital Motion, O'Neill's Data, Attenuation

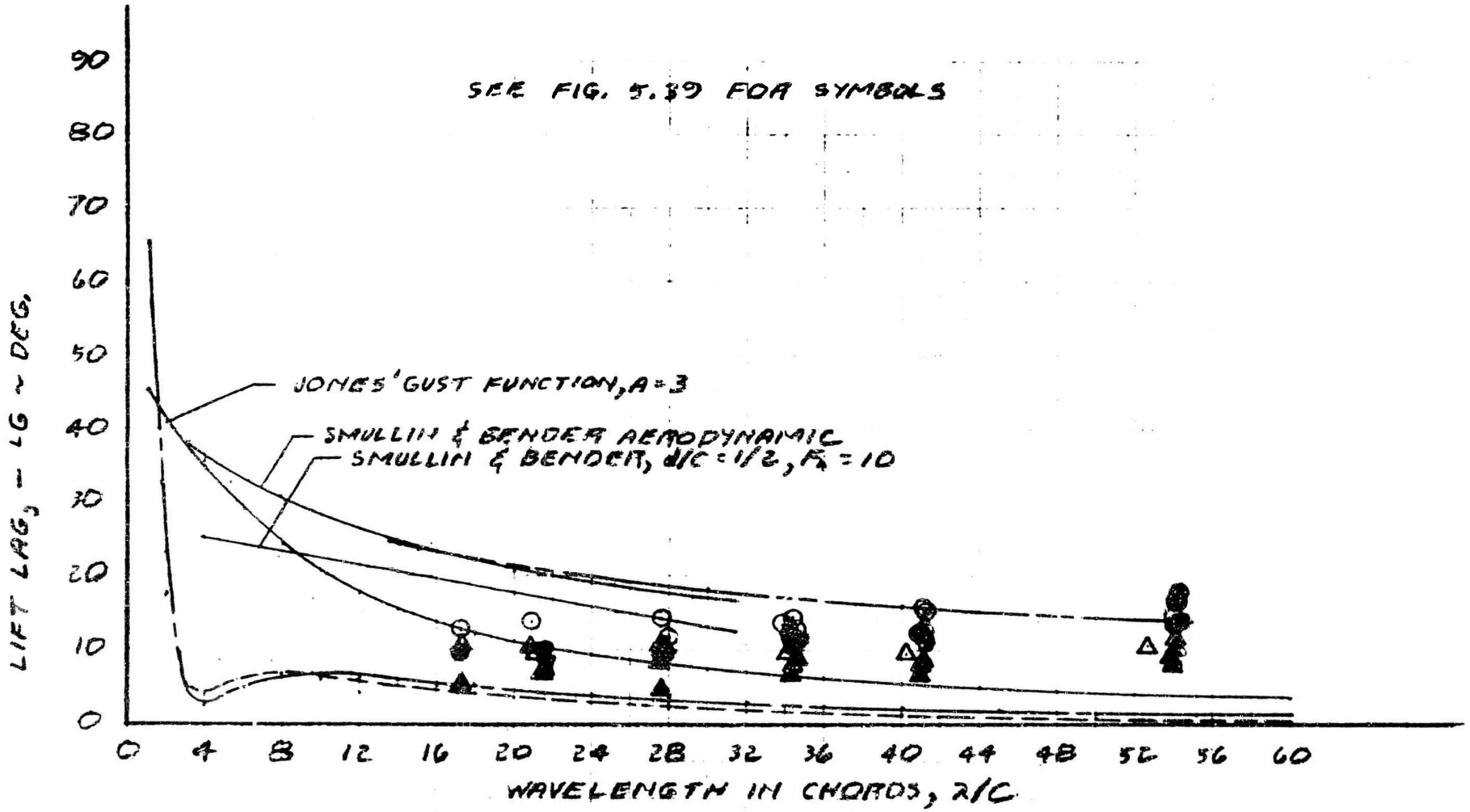


Figure 5-40. Oribtal Motion, O'Neill's Data, Phase

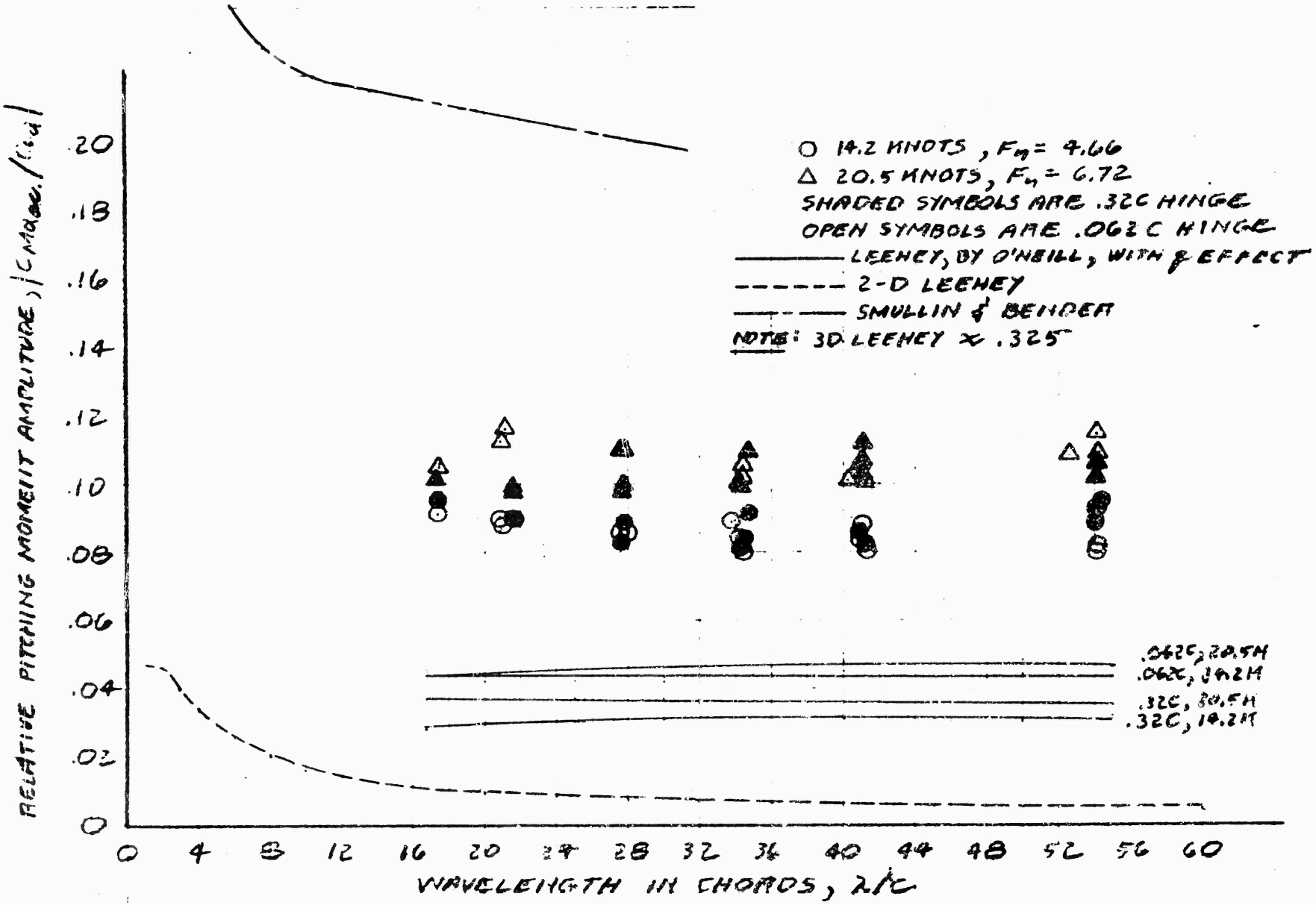


Figure 5-41. Orbital Motion Foil Pitching Moment Amplitude

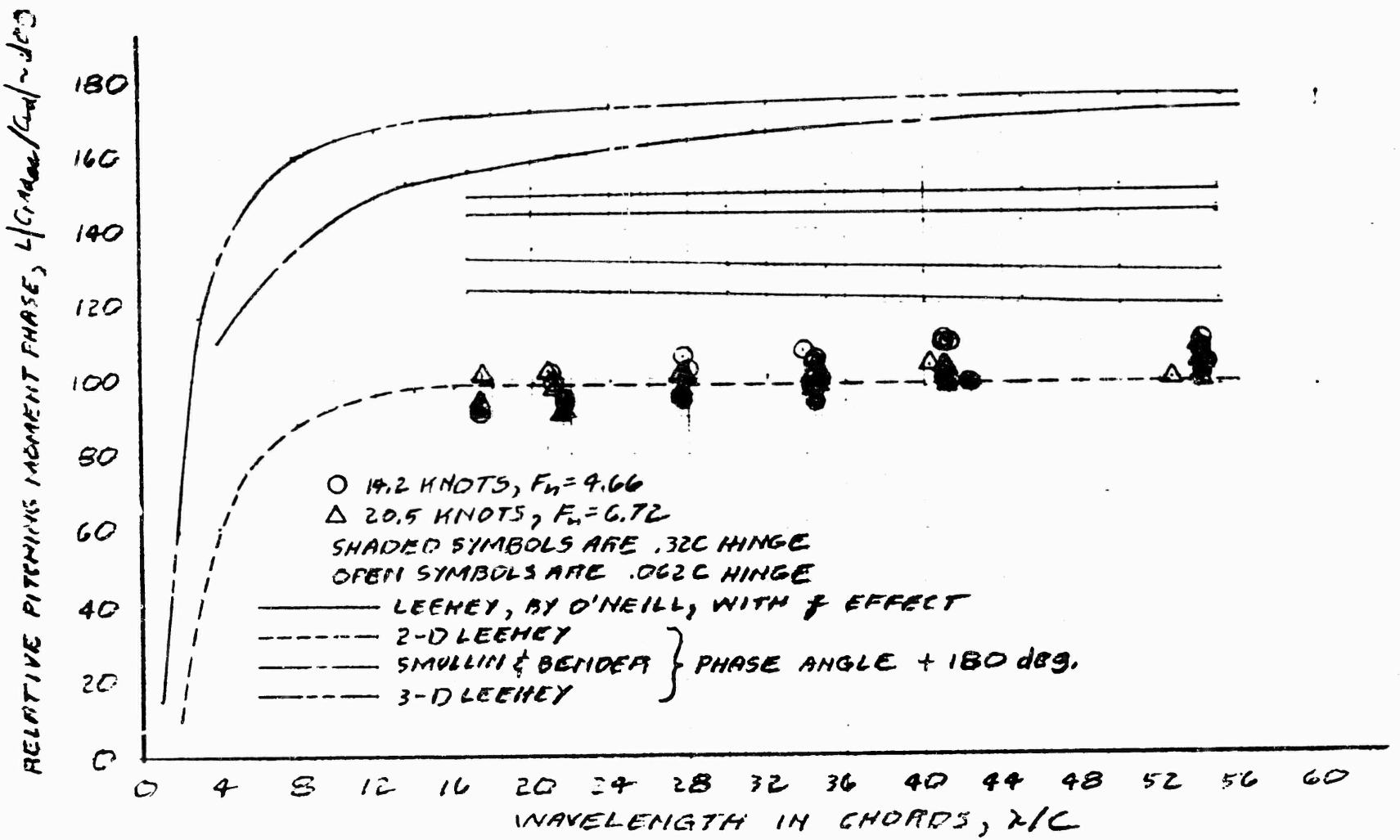


Figure 5-42. Orbital Motion Foil Pitching Moment Phase

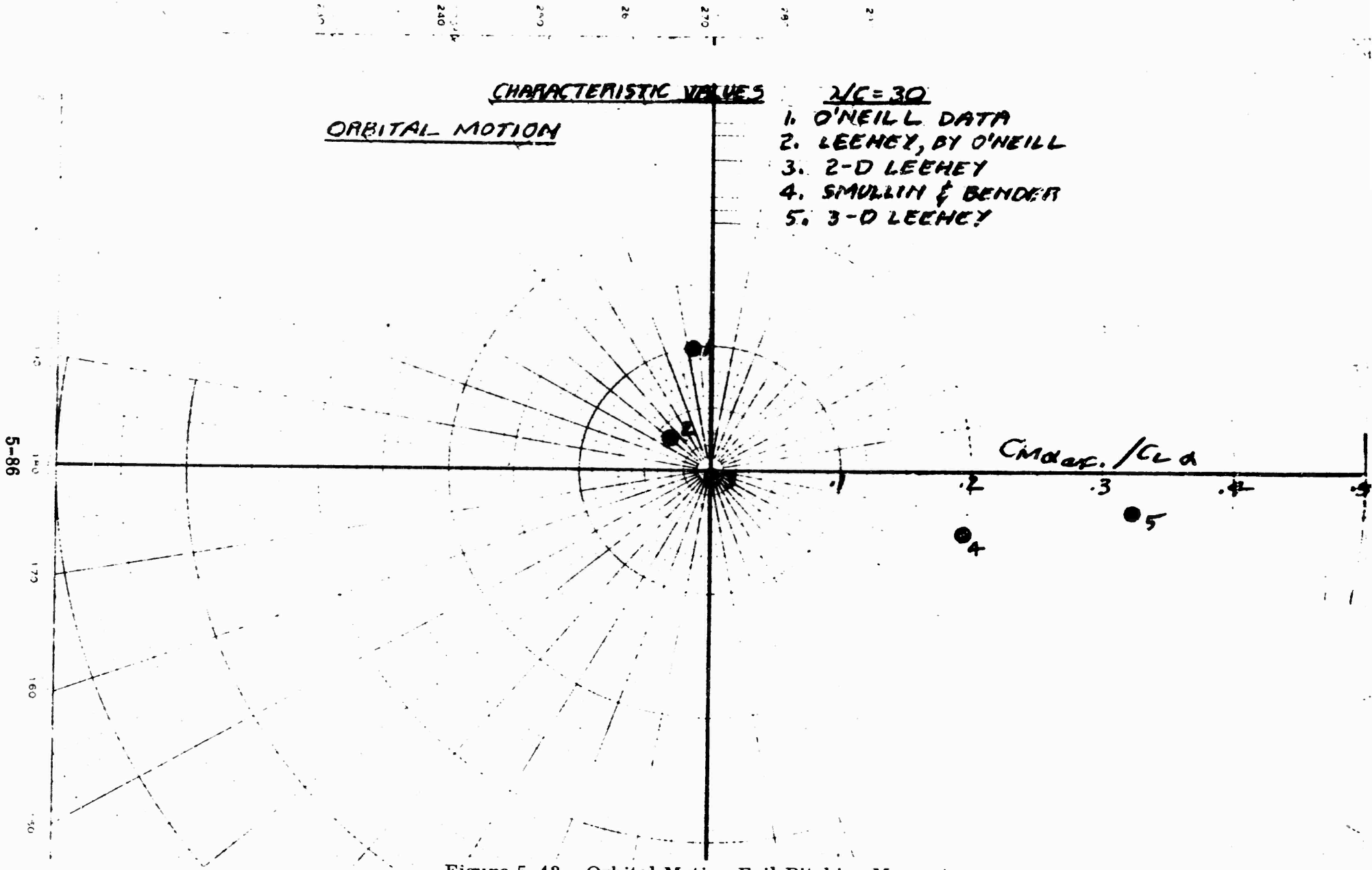


Figure 5-43. Orbital Motion Foil Pitching Moment

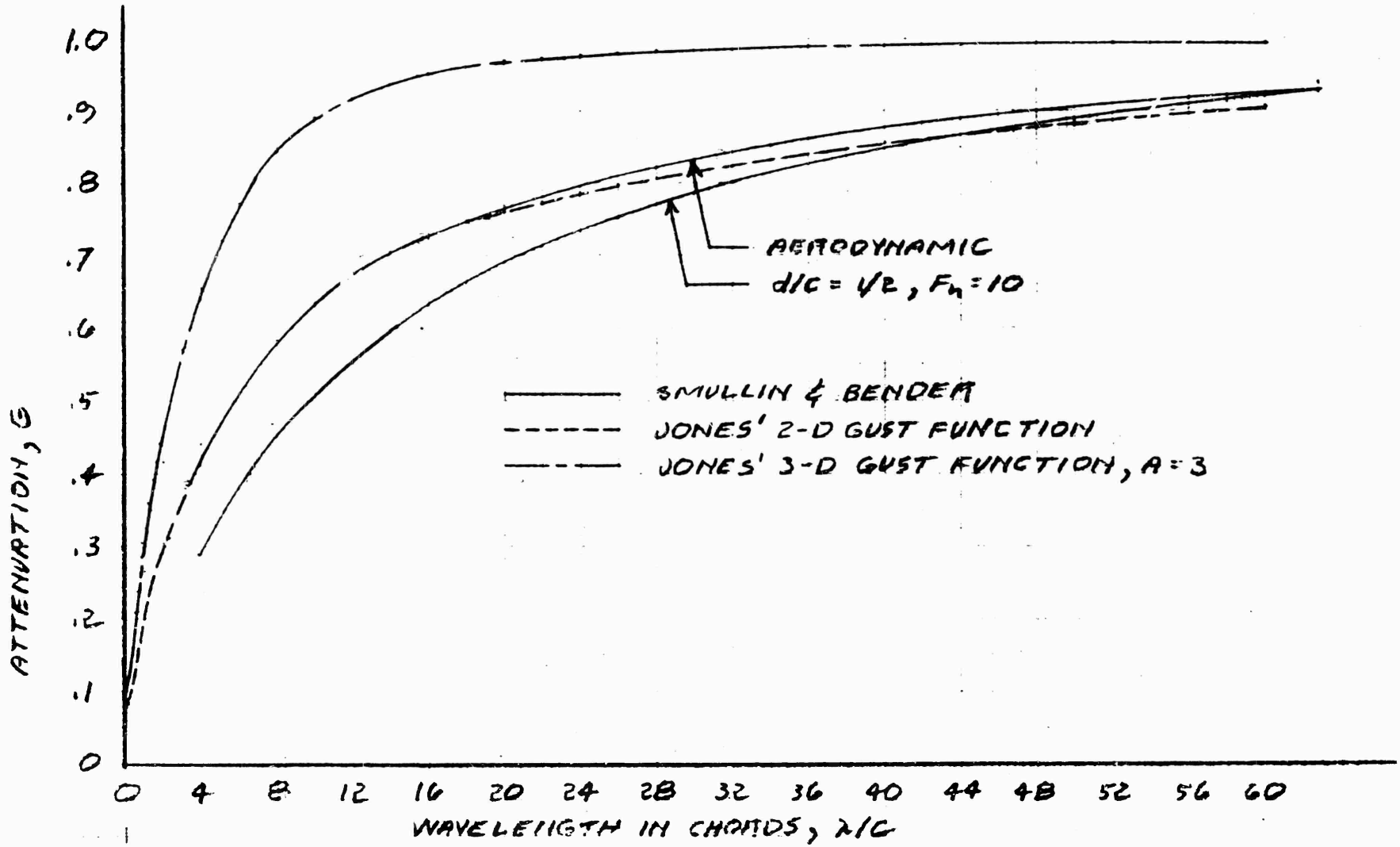


Figure 5-44. Orbital Motion Flap Hinge Moment Attenuation

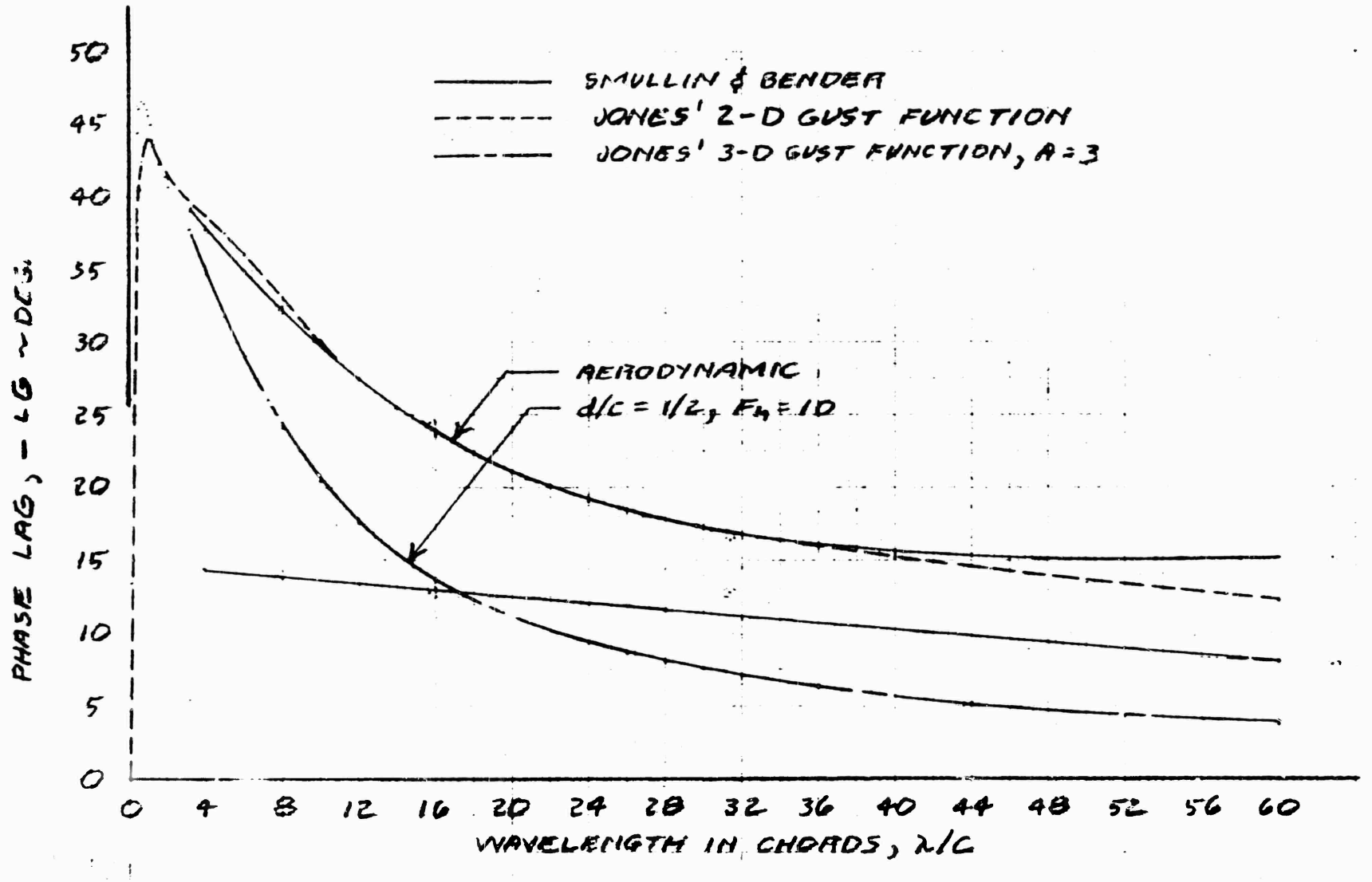


Figure 5-45. Orbital Motion Flap Hinge Moment Phase

6. CAVITATION CHARACTERISTICS

6.1 INCIDENCE LIFT CAVITATION

The cavitation bucket prediction employed in this report is given in some detail because it is not entirely classic. In particula , it should be noted that no theoretical accountability is taken of the flow conditions at the plane of symmetry or "kink" region.

The theoretical spanwise lift d ribution for the AG(EH) fwd foil for the pitch lift and incidence lift cases are prese ted in Figure 6.1. These distributions were derived by the methods of DeYoung's Reference 6.1 where the pitch lift case becomes a trivial special case and the incidence lift case can be presented as a full chord, partial span flap. The two lift cases produce significantly, measurably different cavitation buckets. The maximum and minimum (at pod) lift coeffieients on this figure provide the station and foil loading for initial upper and lower surface cavitation respectively for the two lift cases.

The total velocity ratio for the section is

$$\sqrt{S} = \frac{v}{V} \pm \frac{\Delta v}{V} \pm \frac{\Delta v_a}{V} \left(c_\ell - c_{\ell_{i_{eff}}}\right) \qquad (6.1.1)$$

where S = pressure coefficient, $1 + \frac{P_0 - P}{q}$

$\frac{v}{V}$ = increment due to thickness, function of chord station

$\frac{\Delta v}{V}$ = increment due to camber

$\frac{\Delta v_a}{V}\left(c_\ell - c_{\ell_{i_{eff}}}\right)$ = increment due to angle of attack, function of chord station

$\frac{v}{V}$, $\frac{\Delta v}{V}$, & $\frac{\Delta v_a}{V}$ may all be taken from Reference 6-2

Upper and lower signs refer to upper and lower surface respectively. The effective design lift coefficient is a section function and is a little more uncertain. The value employed here, 83% of the design lift coefficient, is from an unpublished analysis of the data of Reference 6-3.

The square root of the pressure coefficient is a linear function of the section lift coefficient:

$$\sqrt{S} = \left(\frac{v}{V} \pm \frac{\Delta v}{V} \mp c_{\ell_{i_{eff}}} \frac{\Delta v_a}{V} \right) \pm \frac{\Delta v_a}{V} c_\ell$$

$$= \Psi \pm \frac{\Delta v_a}{V} c_\ell \qquad (6.1.2)$$

and a family of such lines outlines the section cavitation bucket as shown on Figure (6.2).

Cavitation takes place when the local pressure drops to vapor pressure; i.e., when:

$$S - 1 = \frac{P_0 - P}{q} = \frac{P_0 - P_V}{q} = \sigma$$

$$S - 1 = \frac{P_{cav}}{\frac{\rho}{2} V'^2} = \frac{P_{cav}}{\frac{\rho}{2} \times 2.85 \, V_K'^2}$$

$$V_K' = \frac{1}{1.689} \sqrt{\frac{P_{cav}}{\frac{\rho}{2}(S-1)}}$$

$$= .592 \sqrt{\frac{P_{cav}}{\frac{\rho}{2}(S-1)}} \qquad (6.1.3)$$

The most convenient way to proceed for pitch and incidence lift control is to calculate the cavitation speed, V_K', for arbitrary lift coefficients on the section bucket of Figure (6.2). Then the corresponding foil lift coefficient is $c_\ell / (C_\ell / C_L)$ for the maximum or minimum local c_ℓ ratio as appropriate. Then the foil loading is $C_L q'$. Finally, the entire process is identified as having taken place in the plane perpendicular to the quarter-chord line and the craft speed is identified as $V_K' / \cos \Lambda$.

This process proceeds quite conveniently in tabular manner under the following headings:

1. List arbitrary c_ℓ's over the range of Figure 6-2, particularly select the values at the corners of the bucket.
2. List the corresponding coefficients, $\sqrt{S}$
3. Compute V_K' from Eq. 6.1.3
4. Compute $C_L = c_\ell / (c_\ell / C_L)_{\max \text{ or } \min}$ from Figure 6-1
5. Compute foil loading, $W/S = (W/S)' = q' C_L$
6. Compute craft speed, $V_K = V_K' / \cos \Lambda$

The result is the foil cavitation bucket of Figure 6-3.

Alternatively, the relationships of Eq. (6.1.3) may be expressed as:

$$S - 1 = \sigma'$$

$$\left(\Psi \pm \frac{\Delta v_a}{V} c_\ell\right)^2 - 1 = \sigma'$$

$$\Psi \pm \frac{\Delta v_a}{V} c_\ell = \sqrt{1 + \sigma'}$$

$$\pm \frac{\Delta v_a}{V}\left(\frac{c_\ell}{C_L}\right) C_L = \sqrt{1 + \sigma'} - \Psi$$

$$C_L = \frac{\sqrt{1 + \sigma'} - \Psi}{\pm \frac{\Delta v_a}{V}\left(\frac{c_\ell}{C_L}\right)}$$

$$\frac{W}{S} = \left(\frac{W}{S}\right)' = q' C_L = \frac{q'}{\pm \frac{\Delta v_a}{V}\left(\frac{c_\ell}{C_L}\right)} \left(\sqrt{1 + \sigma'} - \Psi\right) \qquad (6.1.4)$$

But q' in the plane perpendicular to the quarter chord is:

$$q' = q \cos^2 \Lambda = \frac{\rho}{2} \times 2.85 \cos^2 \Lambda V_K^2$$

$$= 1.425 \cos^2 \Lambda \rho V_K^2 \qquad (6.1.5)$$

and (6.1.4) may be written

$$\frac{W}{S} = \frac{1.425 \cos^2 \Lambda \rho V_K^2}{\pm \frac{\Delta v_a}{V}\left(\frac{c_\ell}{C_L}\right)} \left(\sqrt{1+\sigma'} - \psi\right)$$

$$= \frac{1.425 \cos^2 \Lambda \rho V_K^2}{\pm \frac{\rho v_a}{V}\left(\frac{c_\ell}{C_L}\right)} \sqrt{1 + \frac{P_A + \rho g d - P_V}{1.425 \cos^2 \Lambda \rho V_K^2}} - \psi \qquad (6.1.6)$$

where the (+) sign goes with upper surface velocity distributions and with the $(c_\ell/C_L)_{max}$, and the (-) sign goes with lower surface velocity distributions and with the $(c_\ell/C_L)_{min}$.

This equation provides the variation of incipient cavitation speed with foil loading for any chord station.

The effect of cavitation on foil lift as measured in the Grumman Whirling Tank is shown on Figure 6-4. Figure 6-4 was measured with the AG(EH) fwd foil model; the PGH foil model results were similar though fewer speeds were tested. The PGH model exhibited the zero lift angle shift at higher speeds shown on Figure 6-4. The source of this characteristic has not yet been identified. The central and lower region of these characteristics has not yet been adequately mapped.

The significant characteristics of Figure 6-4 are the initiation of the cavitation lift effect, which is important to control considerations, and the lift "plateau". For the aspect ratio 6 PGH foil model the lift "plateau" was a well defined peak lift which was not again attained for many degrees angle of attack. That peak lift coefficient could confidently be employed as a limit load for the PGH. There appear to be no significant lift reversals on the AG(EH) curves, but in consideration of the cavitation drag, it appears likely that the plateau would still present a limit load condition.

The effect of cavitation on foil drag is presented on Figure 6-5 which is characteristic. The extreme drags associated with cavitation insure that operation will not extend much beyond the initiation of this effect under any conditions.

Figures 6-4 and 6-5 are summarized and compared with the theoretical cavitation

inception bucket on Figure 6-6. There appears to be no difficulty with operation to the effective cavitation boundary. The lift effect boundary marks the end of the linear portion of the lift curve and is significant to the control problem, the drag boundary limits normal operation, and the lift plateau marks the probable limit load. It is to be noted that there is apparently no significant effect, except visible caviation, associated with the cavitation inception but that there is at present no way to predict the position of the effective cavitation boundaries.

It is to be recognized that there are objections to the benefit taken of sweep in Eq. (6.1.6) and that Reference 6-4 presents conclusions in contradiction of Figure 6-6 for an identical planform. The derivation of Eq. (6.1.6) is essentially that of Reference 6-5 and the method has served well in predicting the $C_{L_{max}}$ for highly swept airfoils. Appendix D of this report draws support for Figure 6-6 from the same data from which Spangler drew a contradictory conclusion in Reference 6-4. Nevertheless, more experimental data directed to the question of sweep effect is required.

6.2 FLAP LIFT CAVITATION

In Reference 6-6, Allen presents the effect of the flap on the velocity distribution over the section as an increase in the increment due to angle of attack plus an increment in the basic distribution similar to that associated with camber. He presents the flap basic loading distribution in his Table III for various flap configurations and displacement ranges. Allen's parameter is employed here with the designation:

$$\left(\frac{\Delta v}{V}\right)_F = \frac{1}{4}\,\frac{P_{\rho\delta}}{C_{m_{b\delta}}} \qquad (6.2.1)$$

Allen's chordwise stations are somewhat awkward to use, so his distribution for the 20% chord flap at small displacements is presented graphically on Figure 6-7 for convenience.

Allen tabulates the centroids for the flap basic load distributions, relative to the section aerodynamic center, as G in his Table IV. Therefore:

$$G c_{\ell_b} = c_{m_{a.c.}}$$

$$= d \frac{c_{m_{a.c.}}}{d\delta} \delta \qquad (6.2.2)$$

$$= c_{H_\delta} \delta$$

The flap angle is related to the flap lift by

$$c_{\ell_F} = c_{\ell_\alpha} \frac{d\alpha}{d\delta} \delta$$

$$\delta = \frac{c_{\ell_F}}{c_{\ell_\alpha} \frac{d\alpha}{d\delta}} \qquad (6.2.3)$$

and Eq. (6.2.2) may be written:

$$G c_{\ell_b} = \frac{C_{H_\delta}}{G c_{\ell_\alpha} \frac{d\alpha}{d\delta}} c_{\ell_F} \qquad (6.2.4)$$

$$c_{\ell_b} = \frac{c_{H_\delta}}{G c_{\ell_\alpha} \frac{d\alpha}{d\delta}} c_{\ell_F}$$

It is convenient to define the parameter:

$$\zeta = c_{H_\delta} / G c_{\ell_\alpha} \frac{d\alpha}{d\delta} \qquad (6.2.5)$$

and write (6.2.4) as

$$c_{\ell_b} = \zeta c_{\ell_F} \qquad (6.2.6)$$

where ζ serves to proportion the total flap lift between that part producing the basic load distribution and that part producing additional (type) load distribution.

It must be noted that the parameter ζ presents several uncertainties and thus

becomes critical to the prediction of flapped foil cavitation characteristics. The foil moment derivitive has already introduced uncertainties into the steady-state incidence moment at Eq. (4.7.3) and into the unsteady lift response at Eq. (5.8.2). There is some uncertainty with respect to all four components of ζ in 2-dimensions and a great deal of uncertainty with respect to their application in 3-dimensions. For the purpose of this note, and pending some experimental evidence for flapped foil cavitation, the following evaluations are employed:

c_{H_δ} - the 2-dimensional, thin airfoil theory value, $-2\sqrt{\frac{c_f}{C}\left(1 - \frac{c_f}{C}\right)^3}$

G - Allen's value is employed

c_{ℓ_α} - the theoretical, 2-dimensional value, 2π, is employed

$d\alpha/d\delta$ - the practical value, .47 for 20% chord, is employed

The remainder of the lift coefficient due to flap produces additional type loading:

$$c_{\ell_a} = c_{\ell_F} - c_{\ell_b} \qquad (6.2.7)$$

$$= (1 - \zeta)\, c_{\ell_F}$$

Now Eq. (6.1.1) can be written in the more general form:

$$\sqrt{S} = \frac{v}{V} \pm \frac{\Delta v}{V} \pm \left(\frac{\Delta v}{V}\right)_F c_{\ell_b} \pm \left(c_{\ell_x} + c_{\ell_a} - c_{\ell_{i_{eff}}}\right) \frac{\Delta v_a}{V}$$

$$= \Psi \pm \left(\frac{\Delta v}{V}\right)_F c_{\ell_b} \pm \left(c_{\ell_x} + c_{\ell_a}\right) \frac{\Delta v_a}{V} \qquad (6.2.8)$$

where c_{ℓ_x} designates the lift coefficient due to angle of attack and where the total lift coefficient will be designated without subscript; i.e.

$$c_\ell = c_{\ell_x} + c_{\ell_F} = c_{\ell_w} + c_{\ell_0} + (c_\ell)_i + c_{\ell_F} \qquad (6.2.9)$$

It is convenient to express Eq. (6.2.8) in terms of the lift c_{ℓ_x} and total lift:

$$\sqrt{S} = \Psi \pm \left(\frac{\Delta v}{V}\right)_F \zeta c_{\ell_F} \pm \left[c_{\ell_x} + (1-\zeta)\, c_{\ell_F}\right] \frac{\Delta v_a}{V}$$

$$= \Psi \pm \left(\frac{\Delta v}{V}\right)_F \zeta (c_\ell - c_{\ell_x}) \pm \left[c_{\ell_x} + (1-\zeta)(c_\ell - c_{\ell_x})\right] \frac{\Delta v_a}{V}$$

$$= \Psi \pm \zeta \left(\frac{\Delta v}{V}\right)_F c_{\ell_x} \pm \zeta \left(\frac{\Delta v}{V}\right)_F c_\ell \pm \zeta \frac{\Delta v_a}{V} c_{\ell_x} \pm (1-\zeta) \frac{\Delta v_a}{V} c_\ell$$

$$= \Psi \pm \zeta \left[\frac{\Delta v_a}{V} - \left(\frac{\Delta v}{V}\right)_F\right] c_{\ell_x} \pm \left[\zeta \frac{\Delta v_a}{V} - \zeta \left(\frac{\Delta v}{V}\right)_F - \frac{\Delta v_a}{V}\right] c_\ell$$

$$= \Psi \pm \zeta \left[\frac{\Delta v_a}{V} - \left(\frac{\Delta v}{V}\right)_F\right] c_{\ell_x} \pm \left[\zeta \left[\frac{\Delta v_a}{V} - \left(\frac{\Delta v}{V}\right)_F\right] - \frac{\Delta v_a}{V}\right] c_\ell \qquad (6.2.10)$$

The parameter ω is defined for convenience:

$$\omega = \zeta \left[\frac{\Delta v_a}{V} - \left(\frac{\Delta v}{V}\right)_F\right] \qquad (6.2.11)$$

Then Eq. (6.2.10) becomes

$$\sqrt{S} = \Psi \pm \omega\, c_{\ell_x} \pm \left(\omega - \frac{\Delta v_a}{V}\right) c_\ell \qquad (6.2.12)$$

For this more general case, Eq. (6.1.4) becomes:

$$S - 1 = \sigma'$$

$$\left[\Psi \pm \omega\, c_{\ell_x} \pm \left(\omega - \frac{\Delta v_a}{V}\right) c_\ell\right]^2 - 1 = \sigma'$$

$$\Psi \pm \omega\, c_{\ell_x} \pm \left(\omega - \frac{\Delta v_a}{V}\right) c_\ell = \sqrt{1 + \sigma'} \qquad (6.2.13)$$

At this point, it is necessary to provide for orbital motion and to distinguish the lift curve slopes upon which the incidence control, flap control, and orbital motion act:

$$c_{\ell_x} = \left(\frac{c_\ell}{C_L}\right)_i C_L' + \left(\frac{c_\ell}{C_L}\right)_\alpha C'_{L_w} \qquad (6.2.14)$$

where C_L' is a more convenient symbol for $C_{L_0} + (C_L)_i$

$$c_\ell = c_{\ell_x} + c_{\ell_F}$$

$$= \left(\frac{c_\ell}{C_L}\right)_i C_L' + \left(\frac{c_\ell}{C_L}\right)_\alpha C'_{L_w} + \left(\frac{c_\ell}{C_L}\right)_F C_{L_F}$$

$$= \left(\frac{c_\ell}{C_L}\right)_i C_L' + \left(\frac{c_\ell}{C_L}\right)_\alpha C'_{L_w} + \left(\frac{c_\ell}{C_L}\right)_F \left(C_L - C_L' - C'_{L_w}\right)$$

$$= \left[\left(\frac{c_\ell}{C_L}\right)_i - \left(\frac{c_\ell}{C_L}\right)_F\right] C_L' + \left(\frac{c_\ell}{C_L}\right)_F C_L + \left[\left(\frac{c_\ell}{C_L}\right)_\alpha - \left(\frac{c_\ell}{C_L}\right)_F\right] C'_{L_w} \qquad (6.2.15)$$

Then the reduction of Eq. (6.2.13) proceeds:

$$w \pm w\left[\left(\frac{c_\ell}{C_L}\right)_i C_L' + \left(\frac{c_\ell}{C_L}\right)_\alpha C'_{L_w}\right]$$

$$\pm \left(w - \frac{\Delta v_a}{V}\right)\left\{\left[\left(\frac{c_\ell}{C_L}\right)_i - \left(\frac{c_\ell}{C_L}\right)_F\right] C_L' + \left(\frac{c_\ell}{C_L}\right)_F C_L + \left[\left(\frac{c_\ell}{C_L}\right)_\alpha - \left(\frac{c_\ell}{C_L}\right)_F\right] C'_{L_w}\right.$$

$$= \sqrt{1 + \sigma'} \qquad (6.2.16)$$

which may be written

$$\left(w - \frac{\Delta v_a}{V}\right) C_L = \pm \left(\sqrt{1 + \sigma'} - w\right) \Big/ \left(\frac{c_\ell}{C_L}\right)_F$$

$$+ \left\{w + \frac{\Delta v_a}{V}\left[\frac{(c_\ell/C_L)_i}{(c_\ell/C_L)_F} - 1\right]\right\} C_L'$$

$$+ \left\{w + \frac{\Delta v_a}{V}\left[\frac{(c_\ell/C_L)_\alpha}{(c_\ell/C_L)_F} - 1\right]\right\} C'_{L_w} \qquad (6.2.17)$$

The parameter ξ is defined for convenience:

$$\xi_i = \frac{(c_\ell/C_L)_i}{(c_\ell/C_L)_F} - 1$$

$$\xi_\alpha = \frac{(c_\ell/C_L)_\alpha}{(c_\ell/C_L)_F} - 1 \qquad (6.2.18)$$

Then Eq. (6.2.17) will reduce to

$$(\omega - \frac{\Delta v_a}{V})\, C_L = \mp (\sqrt{1+\delta'} - v)/\left(\frac{c_\ell}{C_L}\right)_F + (\omega + \frac{\Delta v_a}{V}\,\xi_i)\, C_L' + (\omega + \frac{\Delta v_a}{V}\,\xi_\alpha)\, C_{L_w}'$$

$$C_L = [\mp (\sqrt{1+\delta'} - v)/\left(\frac{c_\ell}{C_L}\right)_F - (\omega + \frac{\Delta v_a}{V}\,\xi_i)\, C_L' - (\omega + \frac{\Delta v_a}{V}\,\xi_\alpha)\, C_{L_w}']/(\frac{\Delta v_a}{V} - \omega)$$

$$\frac{W}{S} = q' C_L = [\mp (\sqrt{1+\delta'} - v)\, q'/\left(\frac{c_\ell}{C_L}\right)_F - (\omega + \frac{\Delta v_a}{V}\,\xi_i)\left(\frac{W}{S}\right)_{ref} - (\omega + \frac{\Delta v_a}{V}\,\xi_\alpha)\, C_{L_w}'\, q']/(\frac{\Delta v_a}{V} - \omega) \qquad (6.2.19)$$

where $\left(\frac{W}{S}\right)_{ref}$ is related to incidence angle by

$$\left(\frac{W}{S}\right)_{ref} = (C_{L_i}\, i + C_{L_0})\, q = C_L'\, q'$$

$$C_L' = (C_{L_i}\, i + C_{L_0})/\cos^2 \Lambda = C_{L_{ref}}/\cos^2 \Lambda$$

implying that $C_{L_w}' = \frac{C_{L_\alpha}}{\cos^2 \Lambda}\,\frac{w_g}{V} \qquad (6.2.20)$

For the case where the incidence and flap lift curves slopes are the same, as for the AG(EH), Eq. (6.2.19) reduces to:

$$\frac{W}{S} = [\mp (\sqrt{1+\sigma'} - v)\, q'/\left(\frac{c_\ell}{C_L}\right)_F - \omega \left(\frac{W}{S}\right)_{ref} - (\omega + \frac{\Delta v_a}{V}\,\xi_a)\, C_{L_w}'\, q']/(\frac{\Delta v_a}{V} - \omega) \qquad (6.2.21)$$

Eq. (6.2.21) provides the variation of incipient cavitation foil loading with speed for any chord station with flap lift control on an arbitrary incidence foil loading. The parameters required for the AG(EH) models for the stations of interest are given in Table 6-1.

Eq. (6.2.21) is not as awkward numerically as algerbraically. For example, the foil loading for upper surface hinge line cavitation in smooth water with the incidence fixed at 1435 psf foil loading at 50 knots is

$$\frac{W}{S} = \left[\left(\sqrt{1 + \frac{1365}{2500}} - 1.118 \right) \times \frac{1.895 \times 2500}{1.31} + .559 \times 1435 \right] / .635$$

$$= 1975 \qquad (6.2.22)$$

For this particular case the leading edge is more restricted at 1470 psf.

6.3 FLAP OPERATION MODES

Where there is variable incidence supplied with the flap, as for the AG(EH), there is the question of the optimum schedule for the incidence. The first schedule examined here was that for the design foil loading; i.e., the incidence is varied with the speed so that the flap is always neutral for 1g operation. The corresponding cavitation bucket is shown on Figure 6.8.

The speed for incipient cavitation for the basic incidence control bucket is the corss-over point when comparing the incidence control and flap buckets for the fixed incidence loading mode of operation. Above this speed, the upper surface leading edge boundary is expanded because the hinge line is carrying a greater share of the load. Below this point, the leading edge boundary is reduced because the flap is not as effective as incidence in unloading the leading edge. Since operation at these lower speeds is outside the bucket in either case, it is not clear whether this is a disadvantage or not.

A second possible mode of operation is to employ the flap as a cavitation control device, i.e., the incidence can be scheduled so that, at any speed, when cavitation

occurs, it will occur at the leading edge and hinge line simultaneously. On Figure 6-8, for example, it is evident that the best possible boundary at 55 knots occurs when the incidence is set to carry a 1435 psf foil loading.

The simultaneous solution for Eq. (6.2.21) written for the leading edge and hinge line will yield the foil loading and reference foil loading for this optimum bucket and the result for the AG(EH) fwd. foil is shown on Figure 6-9. Note, however, that Eq. (6.2.21) may be written in the form:

$$\left(\frac{\Delta V_a}{V} - \omega\right)\frac{W}{S} + \omega\left(\frac{W}{S}\right)_{ref} = \left(\sqrt{1+\sigma'} - \psi\right)\frac{q'}{(c_\ell/C_L)_F}$$

$$\left(\frac{\Delta V_a}{V} - \omega\right) C_L + \omega\, C_{L_{ref}} = \left(\sqrt{1+\sigma'} - \psi\right) / (c_\ell/C_L)_F$$

$$\left(\frac{\Delta V_a}{V} - \omega\right) C_L + \omega\left[(C_L)_i + C_{L_0}\right] = \left(\sqrt{1+\sigma'} - \psi\right) / (c_\ell/C_L)_F$$

$$\left(\frac{\Delta V_a}{V} - \omega\right) C_L + \omega\,(C_L)_i = \frac{\sqrt{1+\sigma'} - \psi}{(c_\ell/C_L)_F} + \omega\, C_{L_0} \qquad (6.3.1)$$

It follows that the "optimum" incidence angle is independent of speed except for the variation of the cavitation number with speed and, in fact, the foil loading variation for a constant lift coefficient is practically indistinguishable from the optimum, as shown on Figure 6-9.

The .167 $C_{L_{ref}}$ of Figure 6-9 requires flap at 50 knots, but it would be desirable to carry neutral or negative flap at high speed in order to reduce the flap required at low speed. For this reason Figure 6-10 was prepared to show the effect of an increased $C_{L_{ref}}$ on the cavitation bucket. The $C_{L_{ref}}$ selected for the comparison was .202, providing the design 1435 $(W/S)_{ref}$ at 50 knots (trim flap).

6.4 ORBITAL MOTION EFFECT

For the flapped foil operating at optimum incidence angle, both cycles of the

orbital angle in seas must reduce the right boundary of the cavitation bucket because they both produce non-optimum angles of attack. The "optimum" incidence angle is defined for the right boundary of the bucket without regard to the incidence effect upon the upper-mid-chord and lower surface boundaries; therefore the orbital angle does not necessarily restrict these two boundaries. This inefficient method for neutralyzing the orbital angle is the most distinctive hydrodynamic characteristic of the flap lift control system and is the characteristic which produces the only significant reservation about the system. It is a very difficult characteristic to judge in real seas and, in fact, quantitative judgement does not yet exist.

The effect of orbital motion on the flap lift control cavitation bucket is illustrated on Figure 6.11 which was derived for the AG(EH) fwd foil from Eq. (6.2.21) and Tables 4.1, 4.3, and 6.1. The 10 X 200 ft. wave train was arbitrarily selected for illustration. The classic orbital velocity for a 10-ft. depth was assumed.

Platforming (lg) the 10 X 200 ft. train of regular waves, the flapped foil cavitation bucket cycles from the smooth water bucket through each of the extreme buckets alternately. Flying through such a wave train at 50 knots, the cavitation pattern on the foil would cycle from clear through upper surface leading edge and hinge line cavitation alternately. In heavier seas, the margin to the cavitation boundary is the lift margin available for the normal accelerations required to negotitate the seas before cavitation takes place.

As for the incidence lift control, the existence of cavitation is not significant, it is the lift and drag effect boundaries which are significant and these boundaries are not predictable. Towing tank cavitation tests of the AG(EH) flapped foil conducted in connection with this study were intended to measure the cavitation effect boundary for several angles of attack and the results are discussed in Appendix E of this report.

The incidence lift control bucket is shown in Figure 6.11 for comparison. This bucket is not affected by seas; the cavitation bucket is a function only of section geometry. The comparison of the incidence lift bucket and smooth water flap bucket on Figure 6.11 indicates that in incidence lift control system employing a flap only for cavitation control would make the most effective possible lift control system.

The effect of increasing the fixed incidence angle to reduce the flap deflections required is illustrated on Figure 6-12. If the incidence angle is set to provide a trimmed flap at 50 knots, a significant lift and drag effect on the positive orbital angles is indicated by this figure. Further, there are only 2 degrees of flap deflection to be gained with the increased angle.

Figure 6.13 presents the variation of flap angle for $1 \pm 1/8$ g with speed for the two fixed incidence angles considered. These curves assume a .47 flap effectiveness throughout. The curves and the flap cavitation bucket, through ζ, are both adversely affected by separation. The aerodynamic literature anticipates such separation at flap angles of 5 - 20 degrees and the hydrodynamic case is no more predictable, thus this question also introduces a significant undertainty into the characteristics of the flapped foil. The AG(EH) flapped foil towing tank model tests were also directed to this questions but it must be noted that this separation, even more than that associated with angle of attack, is strongly influenced by Reynolds Number.

6.5 REFERENCES

6-1 DeYoung, "Theoretical Symmetric Span Loading Due to Flap Deflection for Wings of Arbitrary Planform at Subsonic Speeds," NACA Report 1071, 1952.

6-2 Abbott, von Doenhoff, and Stivers, "Summary of Airfoil Data," NACA Report 824, 1945.

6-3 Lindsey, Stevenson, and Daley, "Aerodynamic Characteristics of 24 NACA 16 - Series Airfoils at Mach Numbers Between 0.3 and 0.8," NACA TN 1546, September 1948.

6-4 P. Spangler, "Model Test Results for the Hystad Strut - Nacelle - Foil Combination," DTMB Report 2138, January 1966.

6-5 "Effects of Sweepback on Boundary Layer and Separation," NACA Report 884.

6-6 H. J. Allen, "Calculation of the Chordwise Load Distribution Over Airfoil Sections with Plain, Split, or Serially Hinged Trailing Edge Flaps," NACA Report 634, 1938.

TABLE 6-1

CAVITATION PARAMETERS

16 - (.353) 08 SECTION

STATION	.0125c	.025c	.6c	.7c	.8c
v/V	1.025	1.051	1.092	1.087	1.067
$\Delta v/V$	.073				
$c_{\ell_i}{}_{eff}$	.293				
$\Delta v_a/V$	1.346	.970	.131	.103	.076
Ψ	.704 1.346	.840 1.262	1.127 1.057	1.130 1.044	1.118 1.016
$(\Delta v/V)_F$	.015	.0275	.2825	.4025	1.1
ζ	$\frac{C_{H_\delta}}{G\, c_{\ell_\alpha} \frac{d\alpha}{d\delta}} = \frac{-.64}{-.397 \times 2\pi \times .47} = .545$				
$1 - \zeta$	.455				
ω	.726	.514	-.0824	-.1635	-.559
$\cos \Lambda$	.817				
$\cos^2 \Lambda$	.668				
q'	$\frac{\rho}{2} V^2 \cos^2 \Lambda = 2.84\, V_K^2 \times .668 = 1.895\, V_K^2$				
P_{cav}	$P_A - P_V + \rho gh = 2116 - 72 + 64 \times 8.5 = 2588$				
des. W/S	1435				
$\frac{\Delta v_a}{V} - \omega$	.620	.456	.2134	.2665	.635

Table 6-1 (Continued)

STATION	.0125c	.025c	.6c	.7c	.8c
$\left(\frac{c_\ell}{C_L}\right)_\alpha$	1.169 .880				
$\left(\frac{c_\ell}{C_L}\right)_i$	1.310 .710				
$\left(\frac{c_\ell}{C_L}\right)_F$	1.310 .710				
$\frac{(c_\ell/C_L)_\alpha}{(c_\ell/C_L)_F}$	.891 1.240				
C_{L_α}	2.75				
$C_{L_\alpha}/\cos\Lambda$	3.37				
σ'	$P_{cav}/q' = 2588/1.895\ V_K^2 = 1365/\ V_K^2$				
C_{L_0}	.111 (Prototype from Table 4.1				

For dual numbers $\binom{a}{b}$; upper number is for upper surface, lower number is for lower surface.

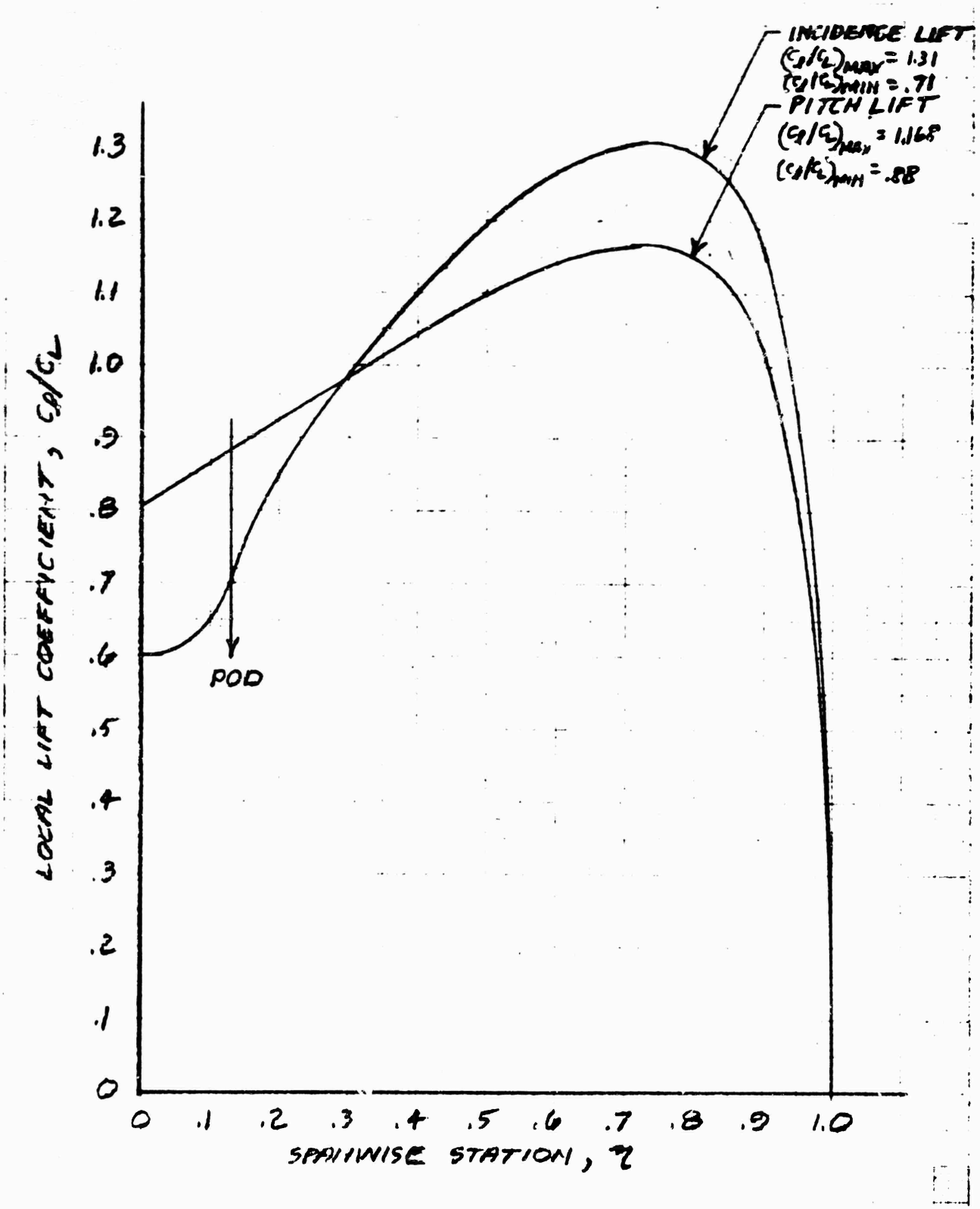


Figure 6-1. Spanwise Lift Distribution

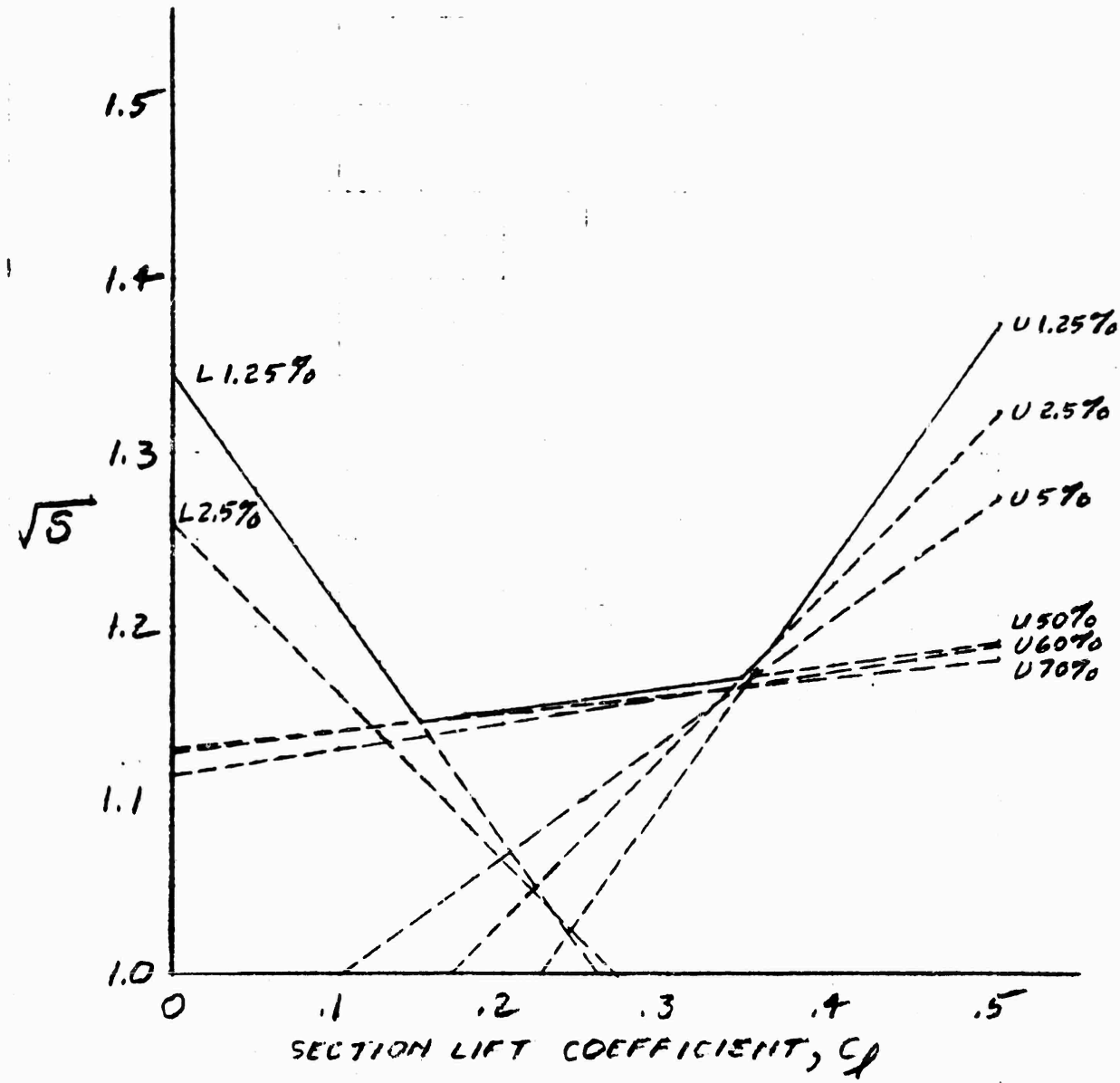


Figure 6-2. Pressure Coefficient Distribution

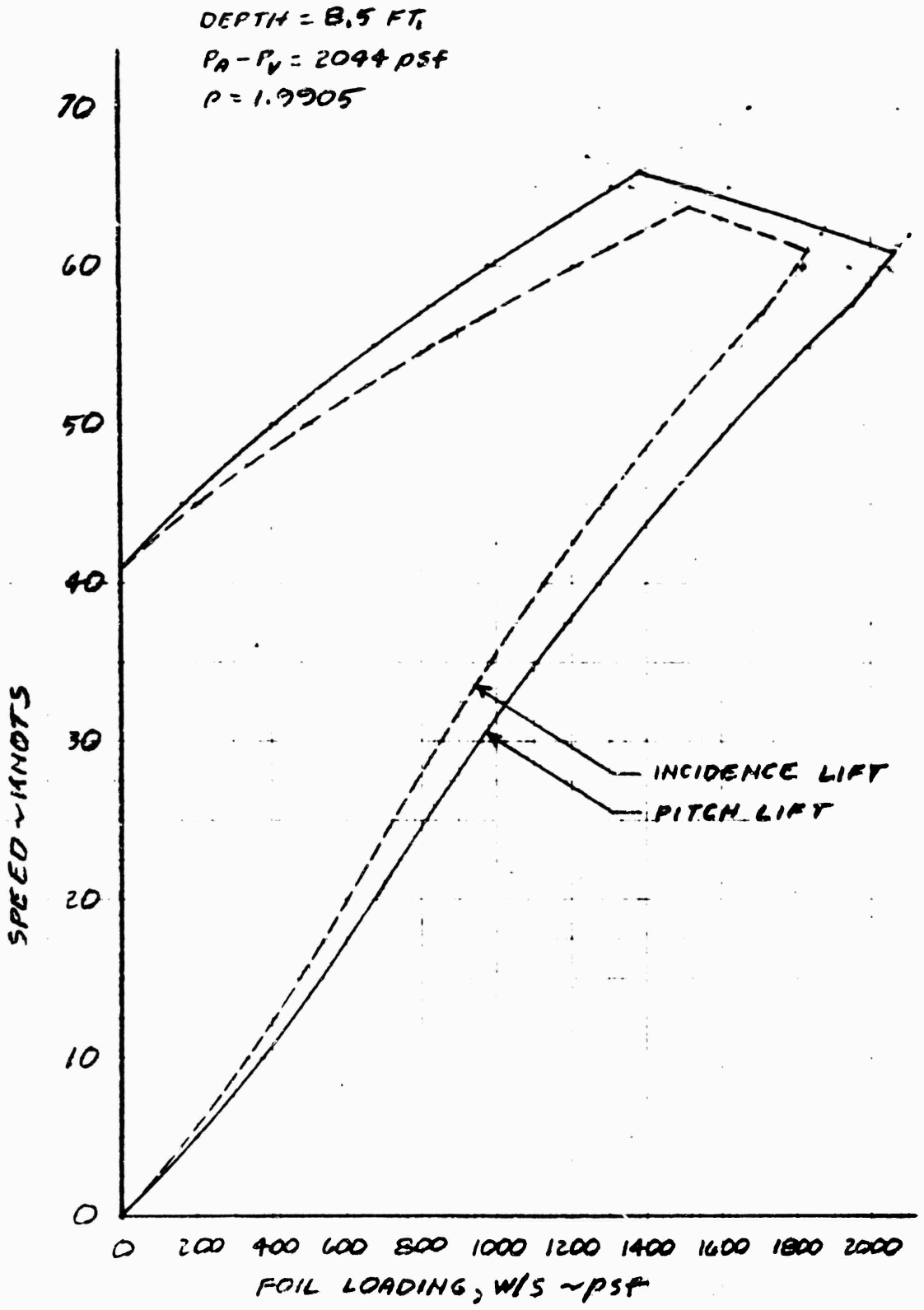


Figure 6-3. Foil Cavitation Buckets

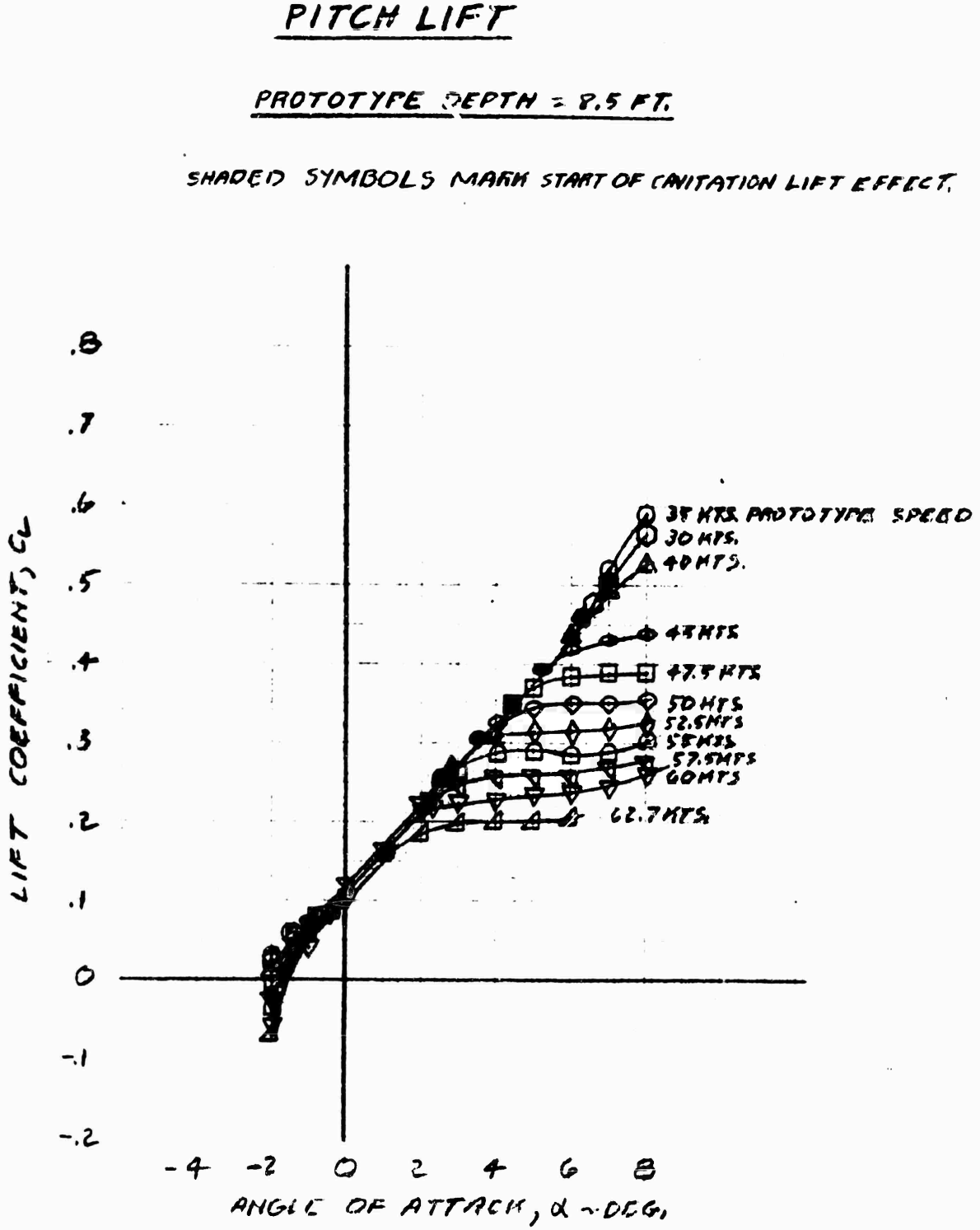


Figure 6-4. Cavitation Lift Effect

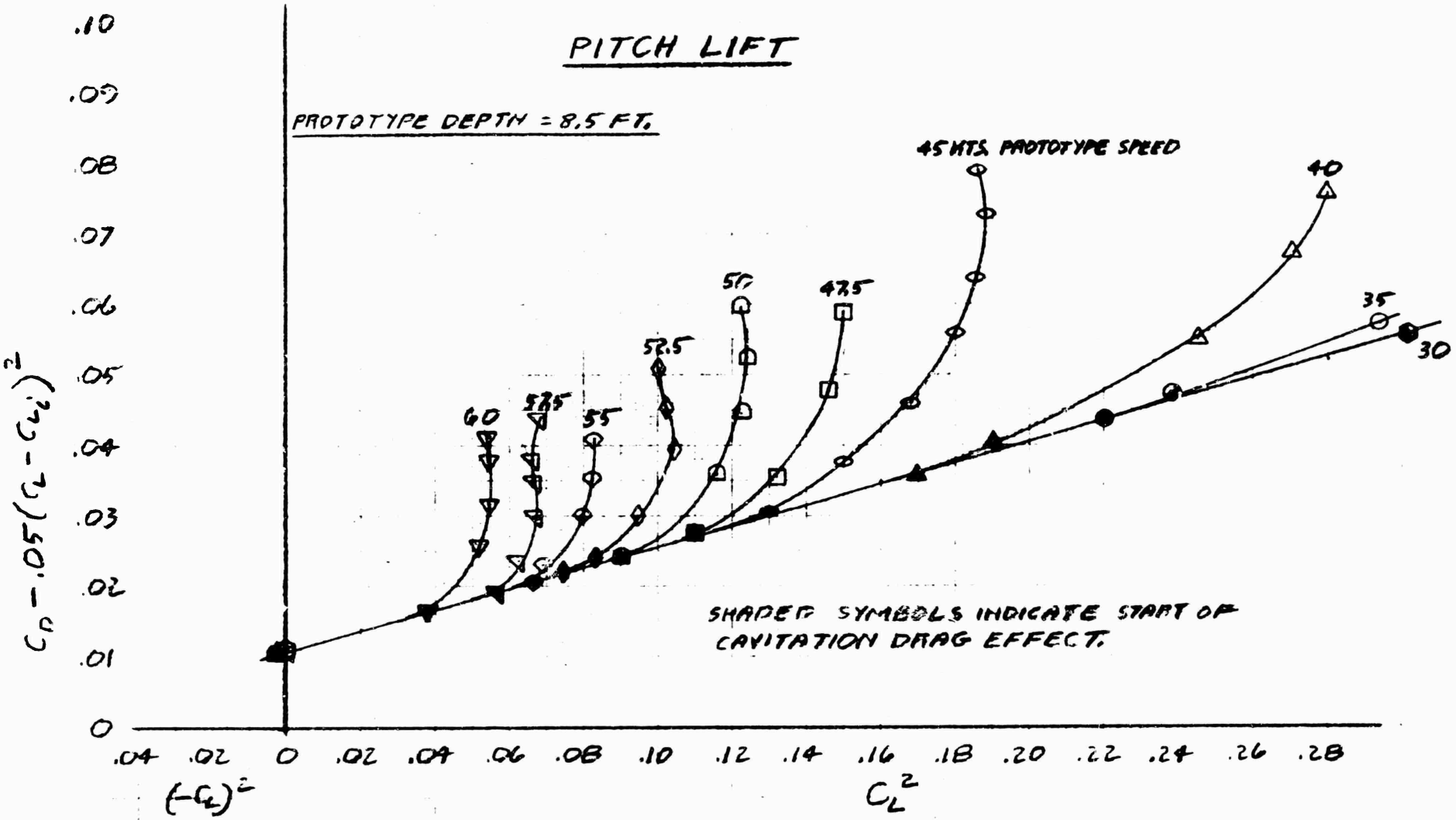


Figure 6-5. Cavitation Drag Effect

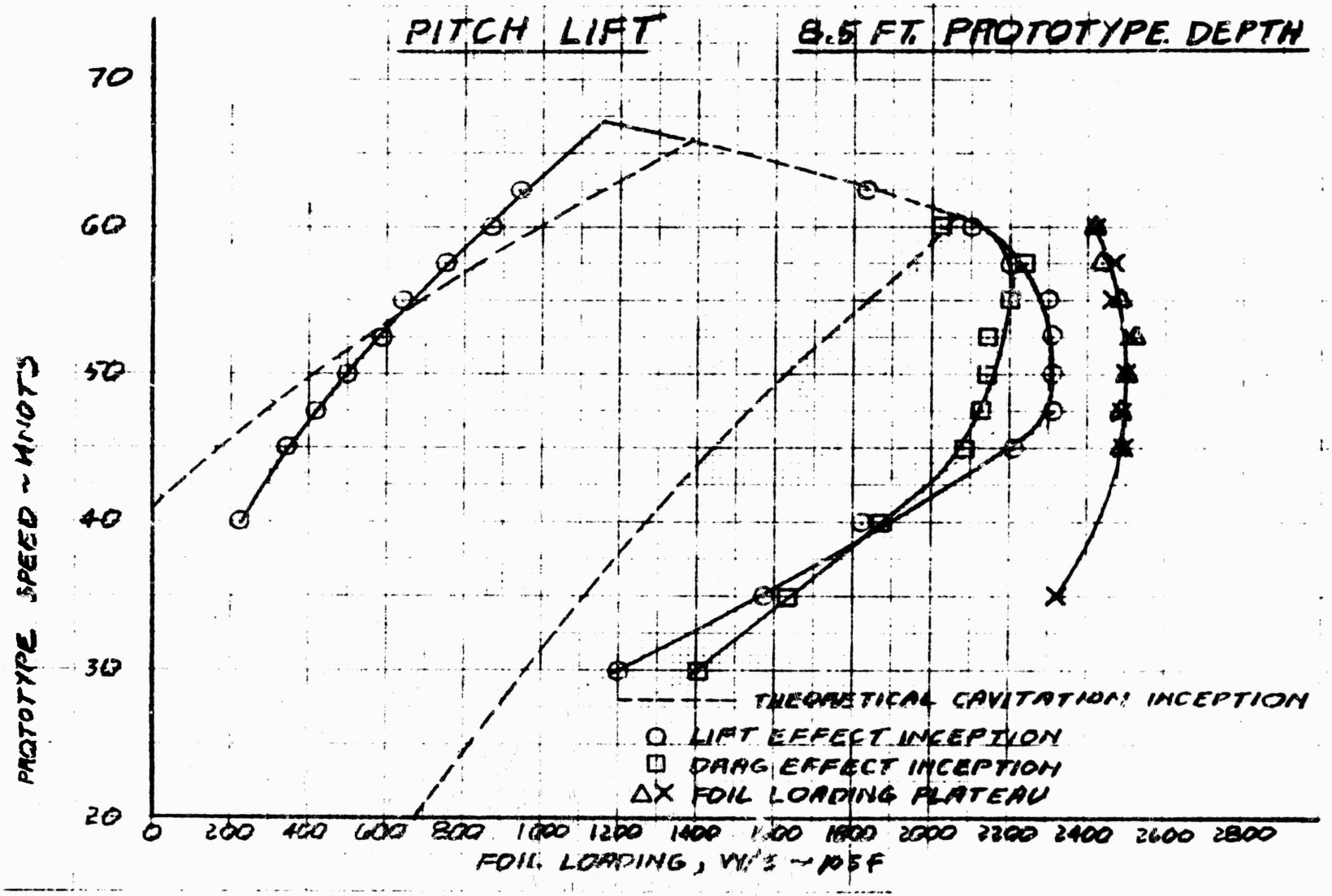


Figure 6-6. Cavitation Effect Boundaries

.2 C FLAP δ LESS THAN 20°

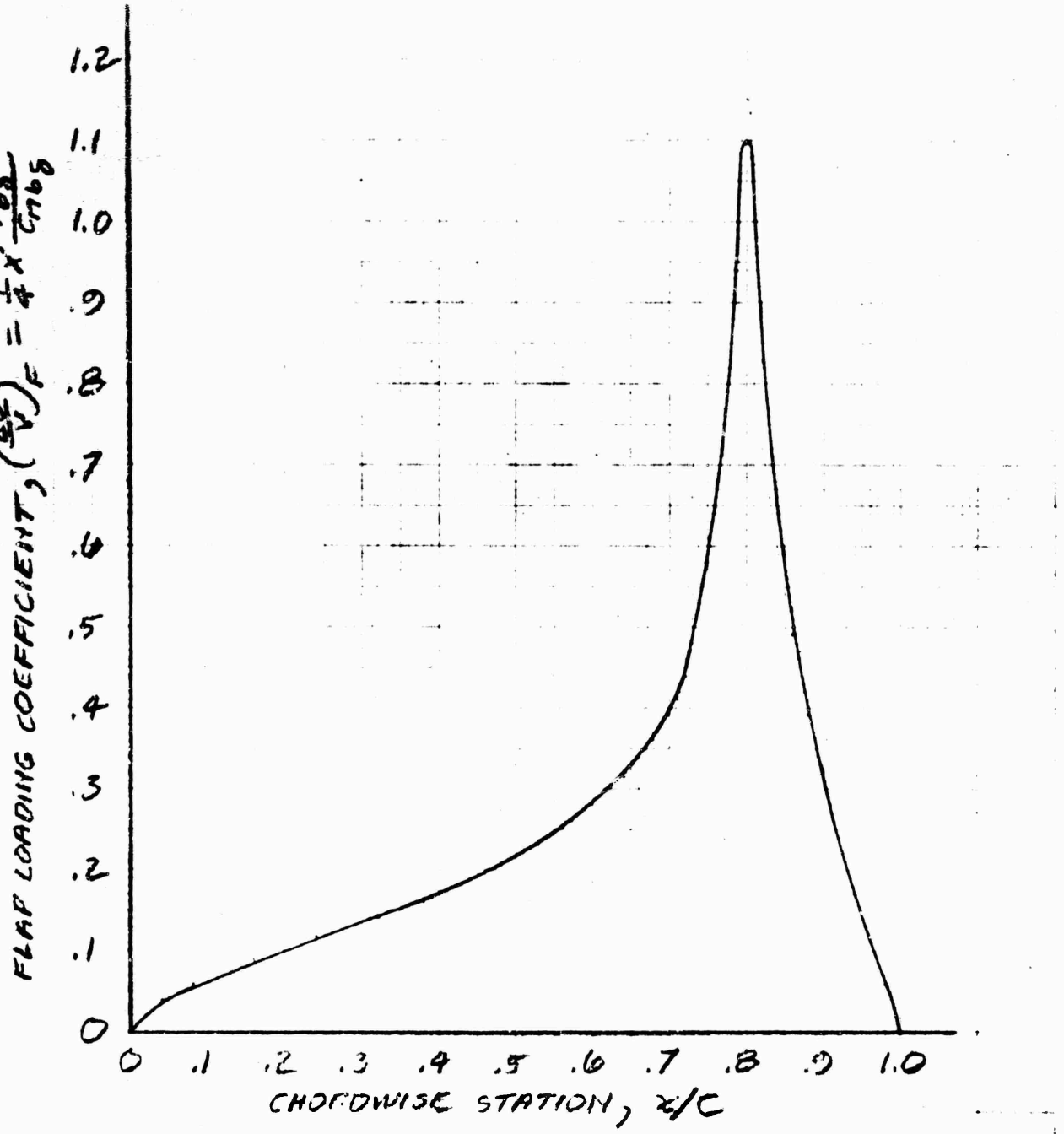


Figure 6-7. Flap Basic Load Distribution

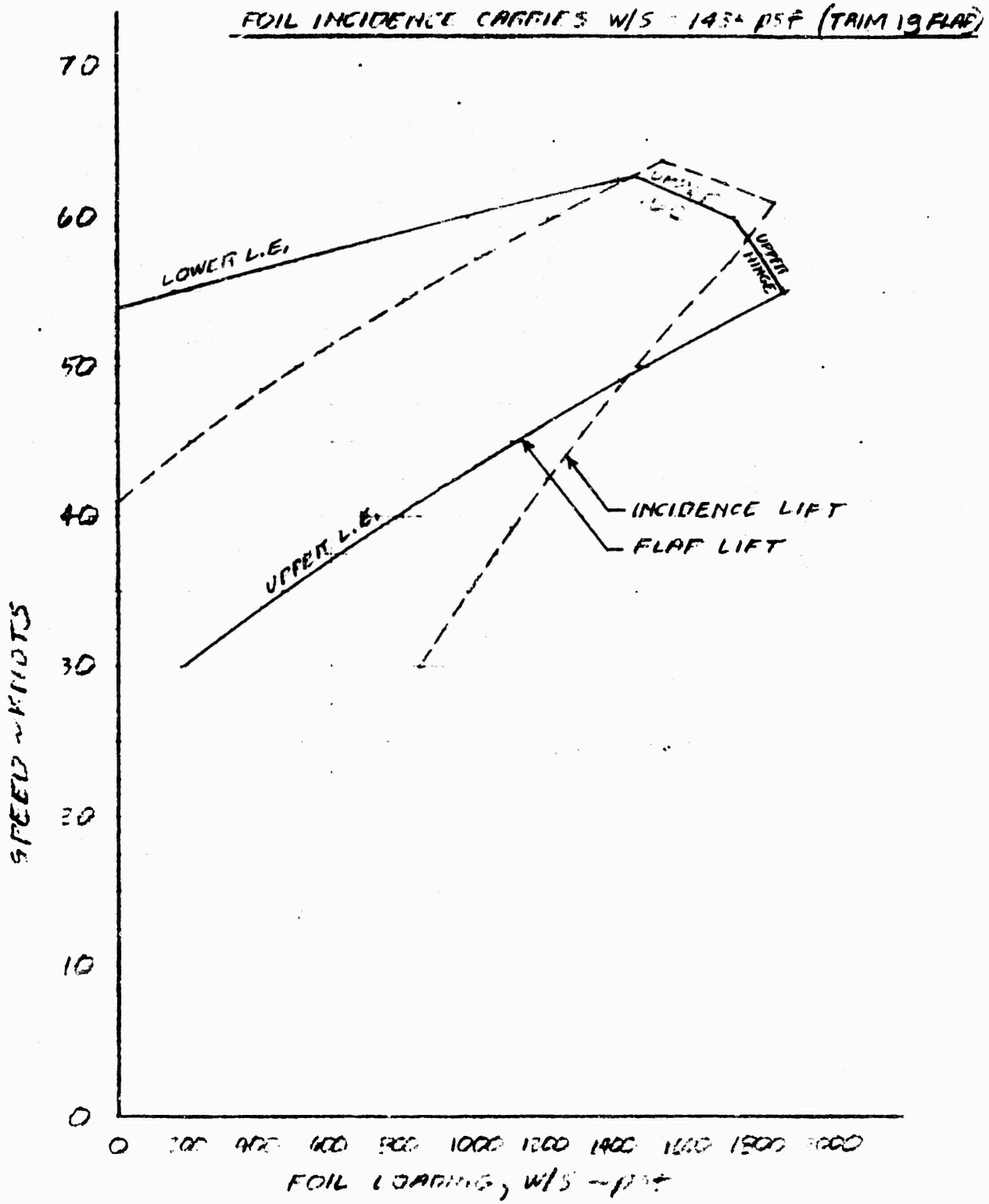


Figure 6-8. Flap Cavitation Bucket, Fixed Foil Incidence

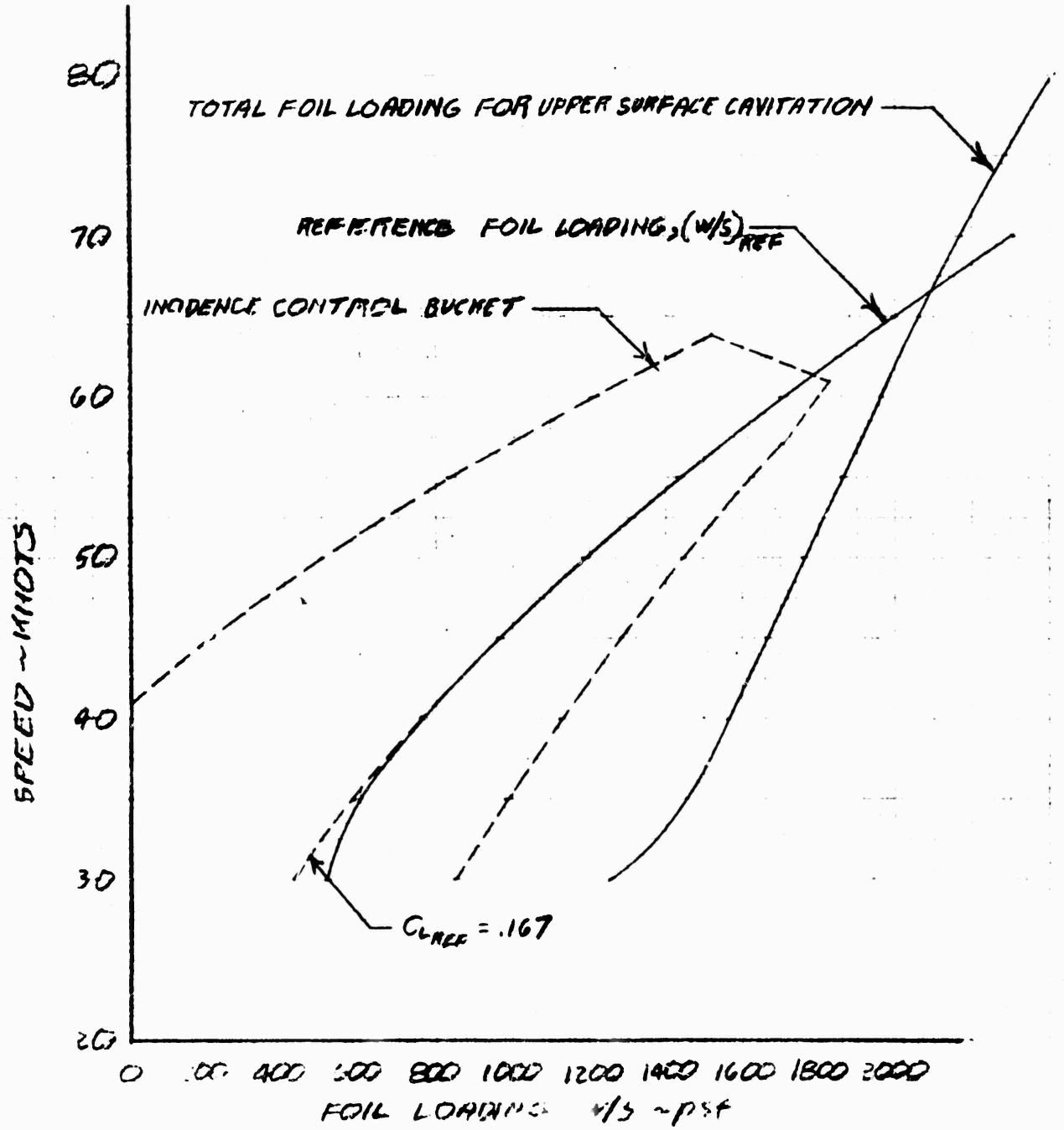


Figure 6-9. Optimum Flap Cavitation Bucket

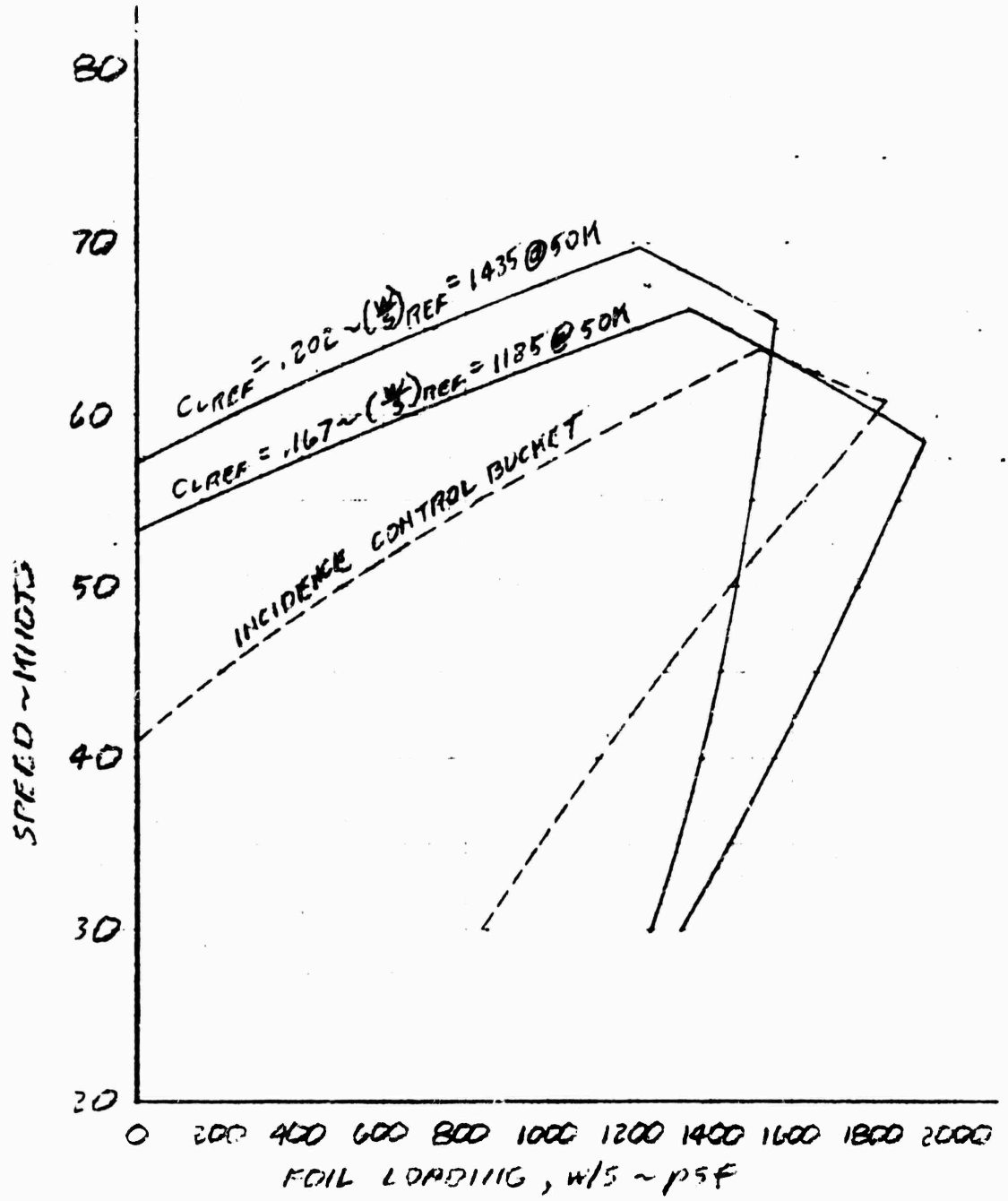


Figure 6-10. Effect of $C_{L_{ref}}$ on Cavitation Bucket

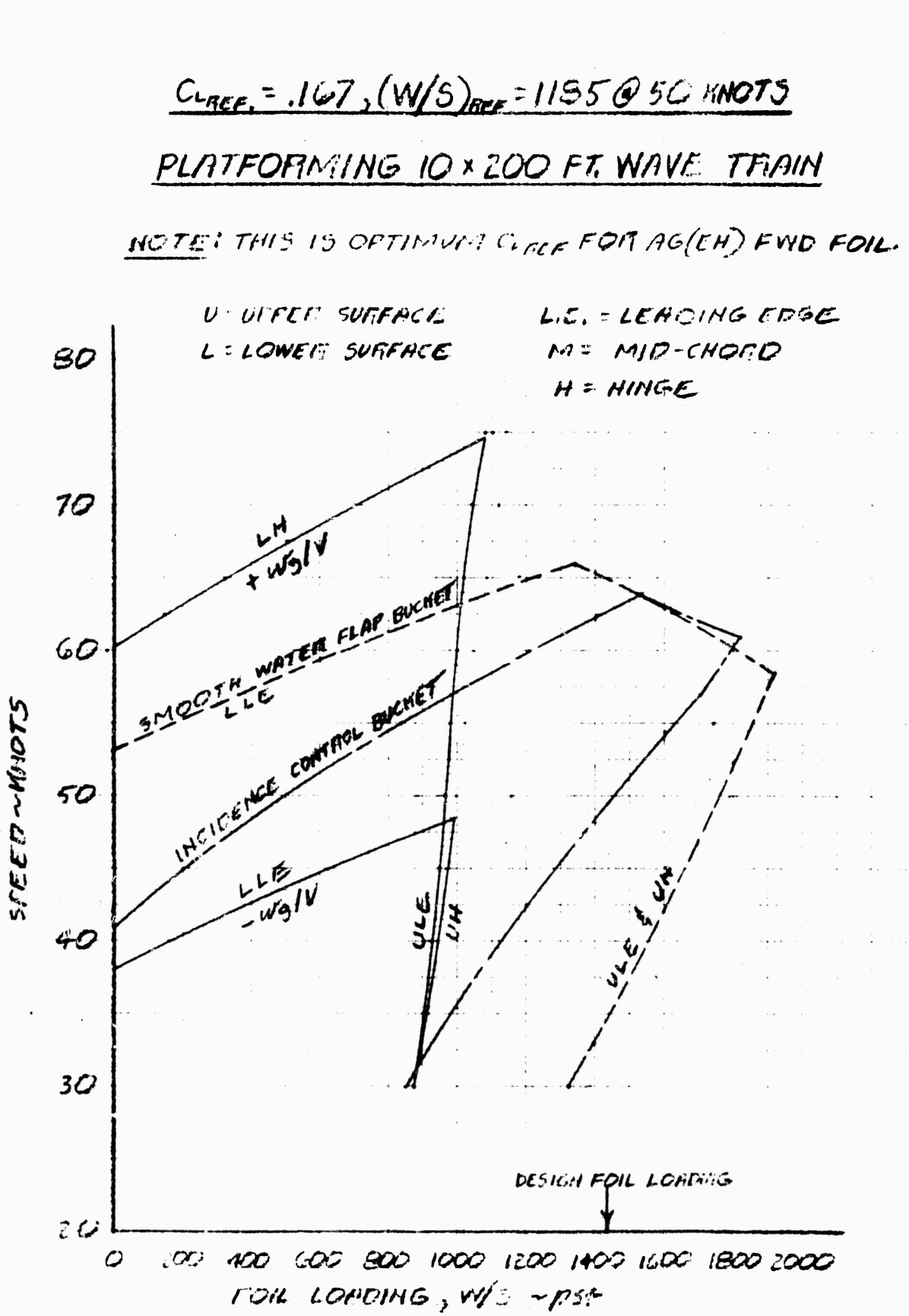


Figure 6-11. Flapped Cavitation Bucket in Seas, $C_{L_{ref}} = .167$

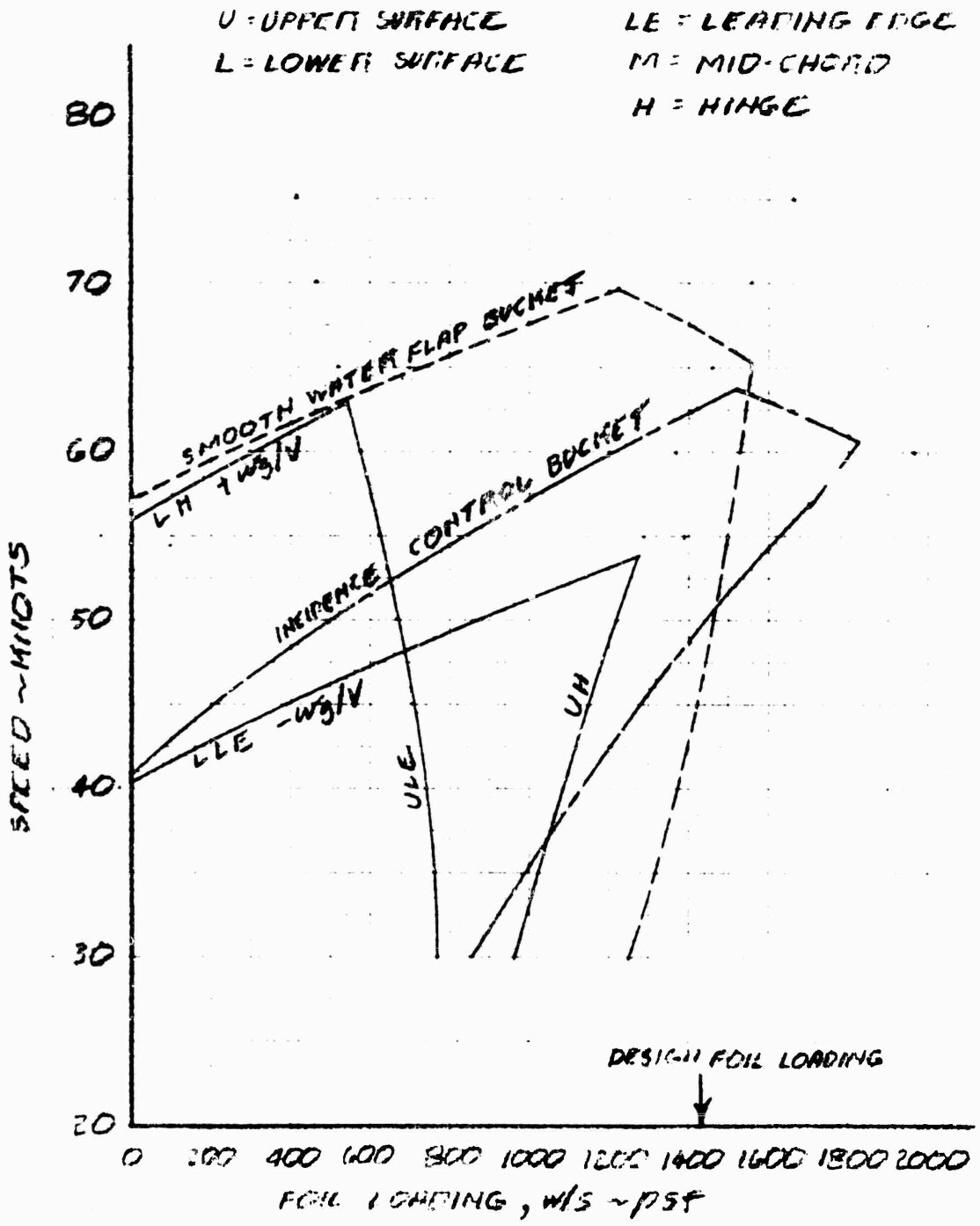


Figure 6-12. Flapped Cavitation Bucket in Seas, $C_{L_{ref}}$ = .202

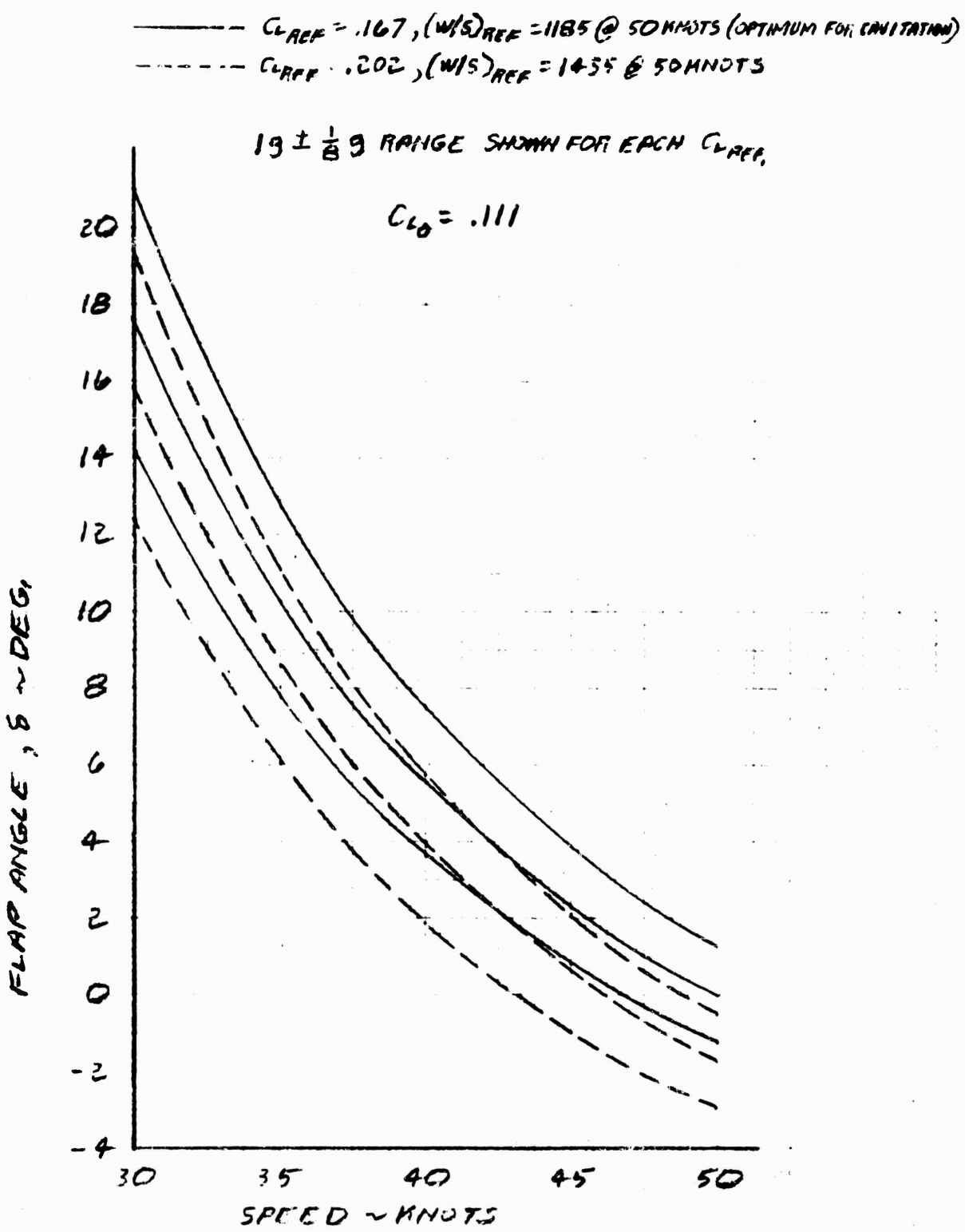


Figure 6-13. Flap Deflection vs. Speed

APPENDIX A

BODY LIFT AERODYNAMIC CENTER

For foil aspect ratios greater than or equal to 4, the body aerodynamic center is located on the exposed foil root chord by Eq. (D6) of Reference 4-1 which may be written

$$\frac{\bar{x}_{B(W)}}{c'_r} = \frac{1}{4} + \frac{A}{4} \times \frac{1+\lambda}{1 - \frac{D}{b}(1-\lambda)} \tan \Lambda \, f\left(\frac{D}{b}\right) \quad A \text{ or } A' \gtrsim 4 \tag{A1}$$

where $f\left(\frac{D}{b}\right)$ is

$$f\left(\frac{D}{b}\right) = \frac{\sqrt{1-2\frac{D}{b}} \ln\left[\frac{(1-\frac{D}{b}) + \sqrt{1-2\frac{D}{b}}}{D/b}\right] - (1-\frac{D}{b}) + \frac{\pi}{2}\frac{D}{b}}{\frac{D/b}{\sqrt{1-2\frac{D}{b}}} \ln\left[\frac{(1-\frac{D}{b}) + \sqrt{1-2\frac{D}{b}}}{D/b}\right] + \frac{1-\frac{D}{b}}{D/b} - \frac{\pi}{2}} - \frac{D}{b} \tag{A2}$$

Note that Eq. (A1) can be referred to the sweep of any chord station on the foil:

$$\frac{\bar{x}_{B(W)}}{c'_r} = \frac{1}{4} + \frac{A}{4} \times \frac{1+\lambda}{1 - \frac{D}{b}(1-\lambda)} \left(\tan \Lambda_{x/c} - \frac{1-4\frac{x}{c}}{A} + \frac{1-\lambda}{1+\lambda} \right) f\left(\frac{D}{b}\right) \tag{A3}$$

and, in particular, if the chord line at x/c has no sweep:

$$\frac{\bar{x}_{B(W)}}{c'_r} = \frac{1}{4} - \left[\frac{1}{4} - \left(\frac{x}{c}\right)_{\Lambda = o}\right] \frac{1-\lambda}{1 - \frac{D}{b}(1-\lambda)} f\left(\frac{D}{b}\right) \quad A \text{ or } A' \gtrsim 4 \tag{A4}$$

Thus in the general case given by Eq. (A1) the body lift aerodynamic center is a function of foil aspect ratio but for the particular family of foils laid out on a straight x/c chord line the body lift aerodynamic center is independent of aspect ratio. It is this particular family of planforms, significant only to the interpolation procedure below, which is referred to in Reference 4-1 as having body lift aerodynamic centers independent of aspect ratio.

The total foil taper ratio is related to the exposed foil taper ratio by

$$\lambda = \frac{(1 - \frac{D}{b})\lambda'}{1 - \frac{D}{b}\lambda'} \tag{A5}$$

so that in terms of the exposed foil geometry Eq. (A4) would be written

$$\frac{\bar{x}_{B(W)}}{c_r'} = \frac{1}{4} - \left[\frac{1}{4} - \left(\frac{x}{c}\right)_{\Lambda=o}\right] \frac{1 - \lambda'}{1 - \frac{D}{b}} \quad f\left(\frac{D}{b}\right) \quad A \text{ or } A' \gtrsim 4 \tag{A6}$$

and this is the form presented on Chart 16 of Reference 4-12. This is implied in the text for Reference 4-1. It is specified for aspect ratio in Reference 4-12 but there is a contrary implication there in the use of the symbol " λ " where " λ_e " would be more suitable.

For the aspect ratios less than about 4 the body lift aerodynamic center must be interpolated between the value given by (A4) or (A6) and the theoretical location for zero aspect ratio, given in Figure 4.3.2.1 - 10b of Reference 4-12 as

$$\frac{\bar{x}_{B(W)}}{c_r'} = \frac{1}{8} A' (1 + \lambda') \tan \Lambda_{L.E.} \; ; \; \frac{1}{4} A' (1 + \lambda') \tan \Lambda_{L.E.} \leq 1$$

$$= .5 \qquad ; \; \frac{1}{4} A' (1 + \lambda') \tan \Lambda_{L.E.} > 1 \tag{A7}$$

For a foil having a straight chord line at x/c, the leading edge sweep is given by

$$\tan \Lambda_{L.E.} = \frac{4}{A} \left(\frac{x}{c}\right)_{\Lambda = o} \frac{1 - \lambda}{1 + \lambda} \tag{A8}$$

so that it may be more convenient to employ Eq. (A7) in the form

$$\frac{\bar{x}_{B(W)}}{c_r'} = \frac{1}{2} \left(\frac{x}{c}\right)_{\Lambda = o} (1 - \lambda') \; ; \left(\frac{x}{c}\right)_{\Lambda = o} (1 - \lambda') \leq 1$$

$$= .5 \qquad ; \left(\frac{x}{c}\right)_{\Lambda = o} (1 - \lambda') > 1 \tag{A9}$$

where any foil has a straight chord line at

$$\left(\frac{x}{c}\right)_{\Lambda = o} = \frac{1}{4} + \frac{A}{4}\,\frac{1+\lambda}{1-\lambda}\tan\Lambda \qquad \text{(A10)}$$

The required interpolation may be guided by the aerodynamic center for the root chord loading for the D/b = 0 case; i.e., for the foil alone. Only the root chord loadings of Reference 4-1, presented here on Figure A2, were available for this report though Reference 4-1 reports that the subject is treated in some detail in Reference 4-13.

For the AG(EH) foils the chord line of zero sweep is

$$\left(\frac{x}{c}\right)_{\Lambda = 0} = \frac{1}{4} + \frac{3}{4} \times \frac{1.3}{.7} \times .706 = 1.234 \qquad \text{(A11)}$$

The function $f\left(\frac{D}{b}\right)$ is presented graphically on Figure A1. Referring to Figures 1-2, 1-3, and A1, Eq. (A6) becomes for the AG(EH) fwd and aft foils:

$$\left(\frac{\bar{x}_{B(W)}}{c_r'}\right)_1 = \frac{1}{4} - \left(\frac{1}{4} - 1.234\right) \times \frac{1 - .339}{1 - .1283} \times .1525 = .3655$$

$$\left(\frac{\bar{x}_{B(W)}}{c_r'}\right)_2 = \frac{1}{4} - \left(\frac{1}{4} - 1.234\right) \times \frac{1 - .339}{1 - .1675} \times .167 = .3805 \qquad \text{(A12)}$$

$A \text{ or } A' \lesssim 4$

The parameter of Eq. (A9) becomes:

$$\text{FWD } \left(\frac{x}{c}\right)_{\Lambda = o} (1 - \lambda') = 1.234 \times .671 = .828$$

$$\text{AFT } \left(\frac{x}{c}\right)_{\Lambda = o} (1 - \lambda') = 1.234 \times .661 = .816 \qquad \text{(A13)}$$

and the zero aspect ratio body lift aerodynamic centers become

$$\left[\frac{\bar{x}_{B(W)}}{c_r'}\right]_1 = .414$$

$$\left[\frac{\bar{x}_{B(W)}}{c_r'}\right]_2 = .408 \qquad A = 0 \qquad \text{(A14)}$$

The interpolations required are shown on Figure A2 where the final aerodynamic centers selecter were

$$\text{FWD} \quad \frac{\bar{x}_{B(W)}}{c_r'} = .371$$

$$\text{AFT} \quad \frac{\bar{x}_{B(W)}}{c_r'} = .385 \qquad \text{(A15)}$$

which are located on the total foil mean aerodynamic chord at

$$\text{FWD: a.c.}_{pod} = \frac{1.665 + .371 \times 12.12 - 4.93}{9.33} = \frac{1.235}{9.33} = .1325$$

$$\text{AFT: a.c.}_{pod} = \frac{.994 + .385 \times 6.07 - 2.545}{4.81} = \frac{.784}{4.81} = .163 \qquad \text{(A16)}$$

$$f\left(\frac{D}{b}\right) = \frac{\sqrt{1-2\frac{D}{b}}\,\ln\left[\frac{\left(1-\frac{D}{b}\right)+\sqrt{1-2\frac{D}{b}}}{D/b}\right]-\left(1-\frac{D}{b}\right)+\frac{\pi}{2}\frac{D}{b}}{\frac{D/b}{\sqrt{1-2\frac{D}{b}}}\,\ln\left[\frac{\left(1-\frac{D}{b}\right)+\sqrt{1-2\frac{D}{b}}}{D/b}\right]+\frac{1-\frac{D}{b}}{D/b}-\frac{\pi}{2}} - \frac{D}{b}$$

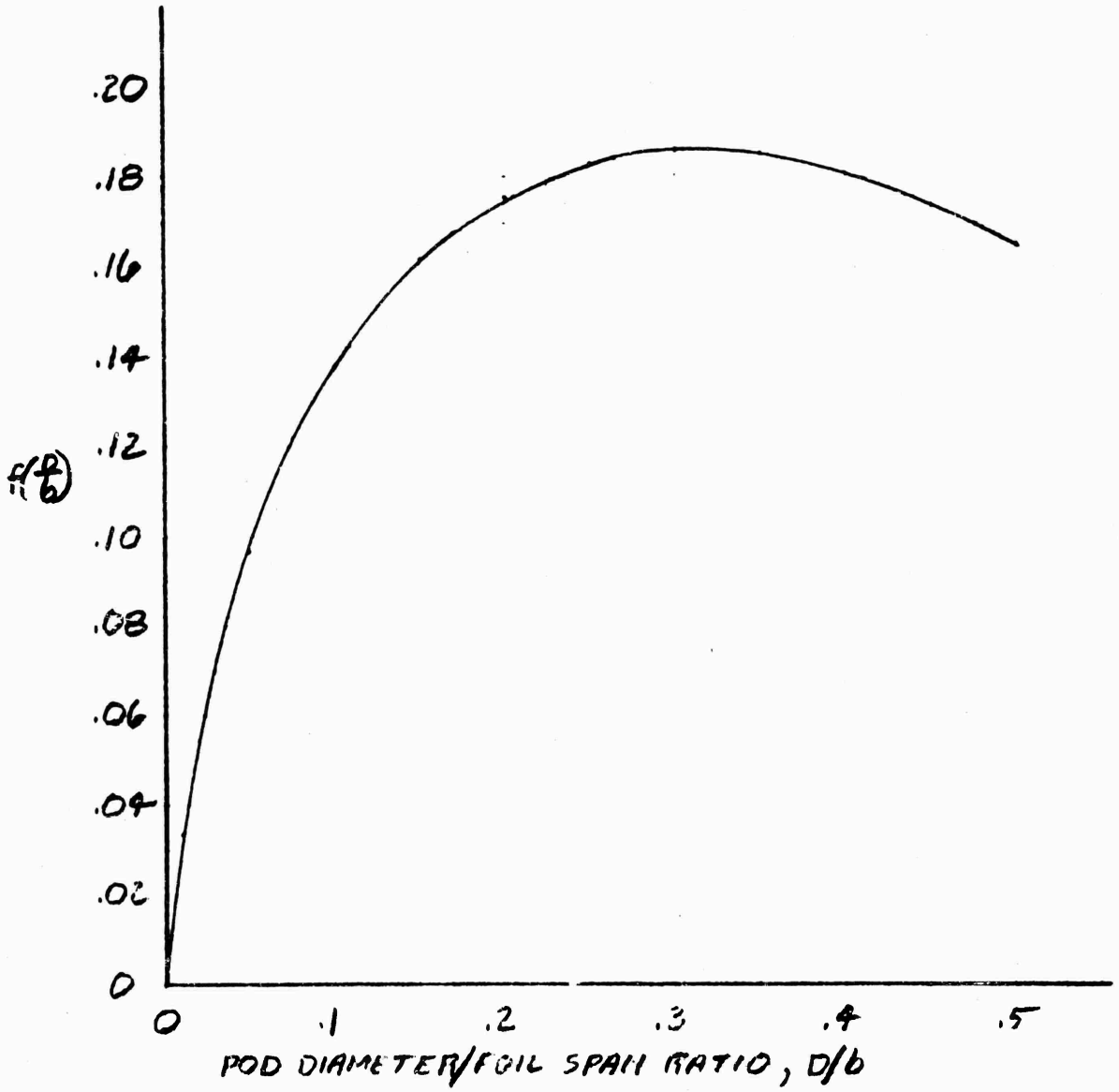


Figure A1. Body Aerodynamic Center Parameter, $f\left(\frac{D}{b}\right)$

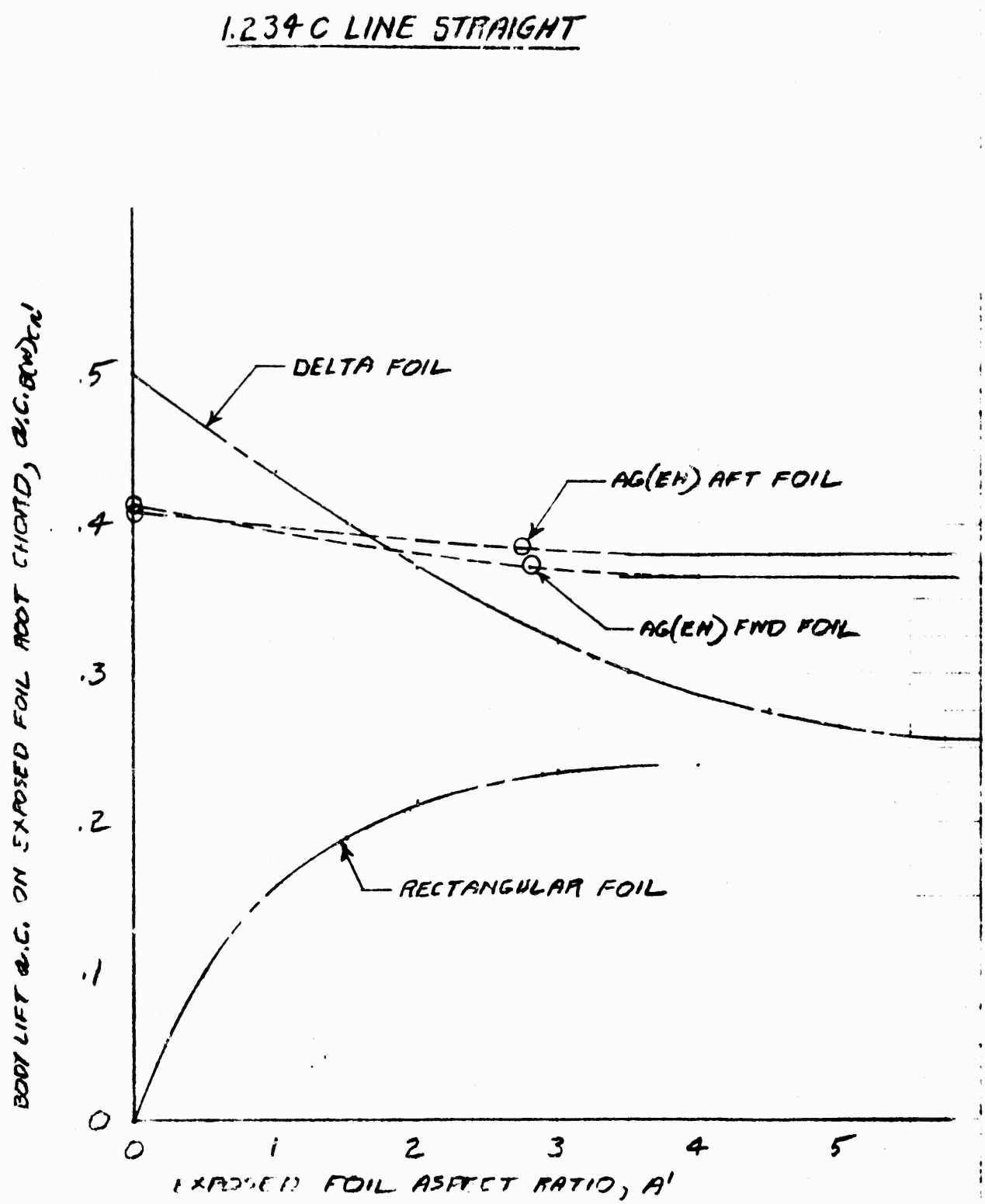


Figure A2. Body Lift Aerodynamic Center, AG(EH) Foils

APPENDIX B

AG(EH) FWD FOIL DATA CROSSPLOTS

The forward foil data of Figures I-8 through I-17 of Reference 4-4 are presented as lift, drag, and moment curves over a range of incidence angles for five pod pitch angles. That data is cross-plotted on Figures B1-B6 to examine the lift and moment slopes as a function of pitch angle for various incidence angles. The cross-plots are smoothed to the extent that not all of the data was measured at integral incidence angles and the coefficients of the cross-plots are taken from the curves of Reference 4-4 where necessary and in most instances; some of the moment curves of Reference 4-4 were reinterpreted for these cross-plots. The cross-plots do not include the cavitated points of Reference 4-4.

The predicted lift curve slopes shown on the cross-plots are the Panchenkov slopes of Figure 4-4 which are in reasonable agreement with the data throughout the speed and depth ranges. It is possible that the 50-knot pitch lift curve slopes of Reference 4-4 were measured in the vicinity of the lower end of the linear portion of the lift curve where there is a characteristic slope increase.

The residual lift of Figures B1-B6 is the .098 of Table 4-1. To that has been added the Panchenkov incidence lift slope of Figure 4-2 to tick off the zero pitch for each incidence angle. These residual lifts (zero pitch lifts) agree reasonable well with the data only for the two deepest 35-knot plots. The 50-knots disagreement is considered to be the pod cavitation effect discussed in Section 6.

These cross-plots were prepared in support of the moment study of Section 4 of this report and are considered further in that section. These cross-plots did not influence the lift considerations of Section 4 which were based entirely upon the plots presented in Reference 4-4.

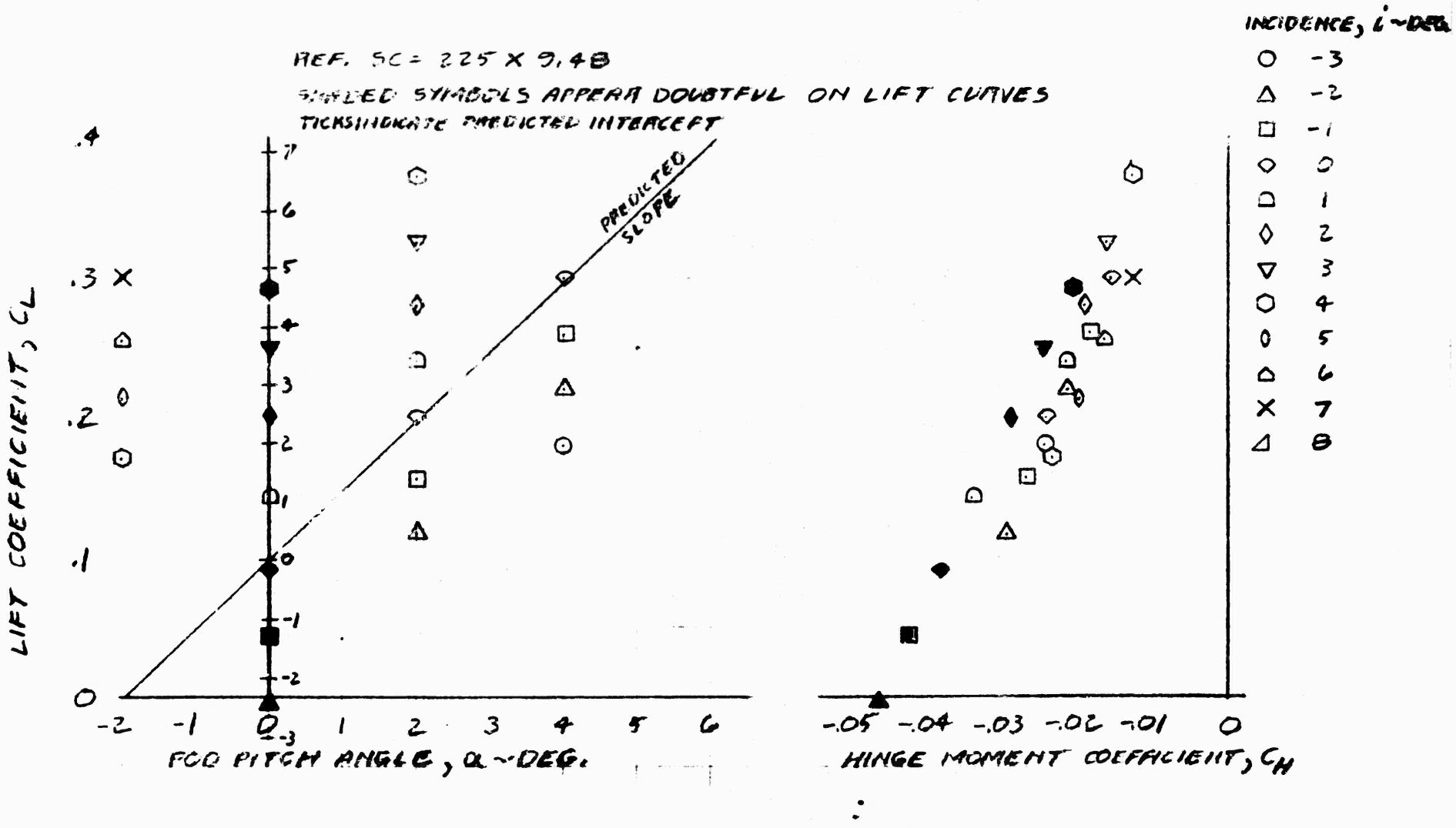


Figure B1. Lift and Hinge Moment vs. Pod Pitch, AG(EH) Forward Foil, 15-ft Depth at 35K for Prototype

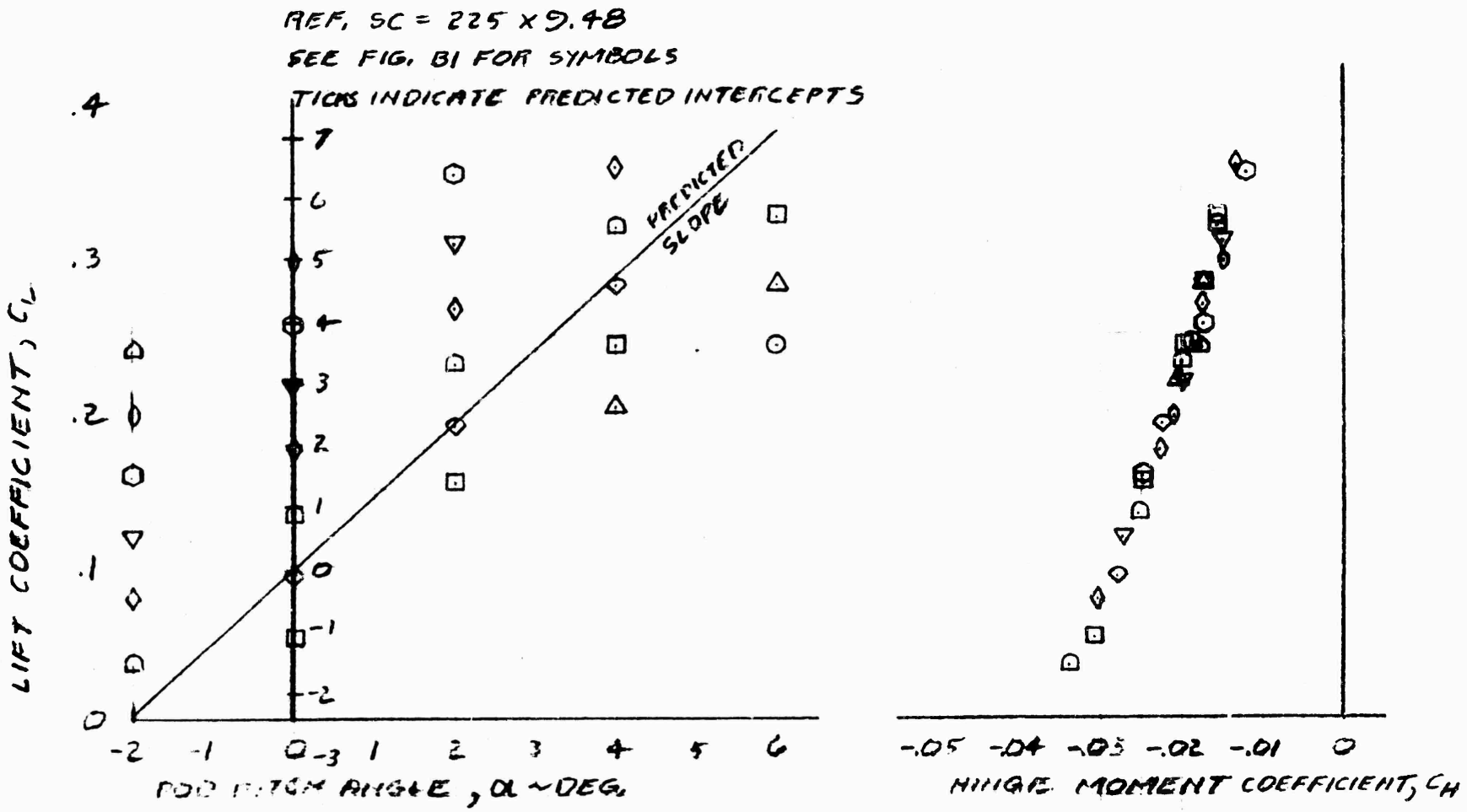


Figure B2. Lift and Hinge Moment vs. Pod Pitch, AG(EH) Forward Foil, 10-ft Depth at 35K for Prototype

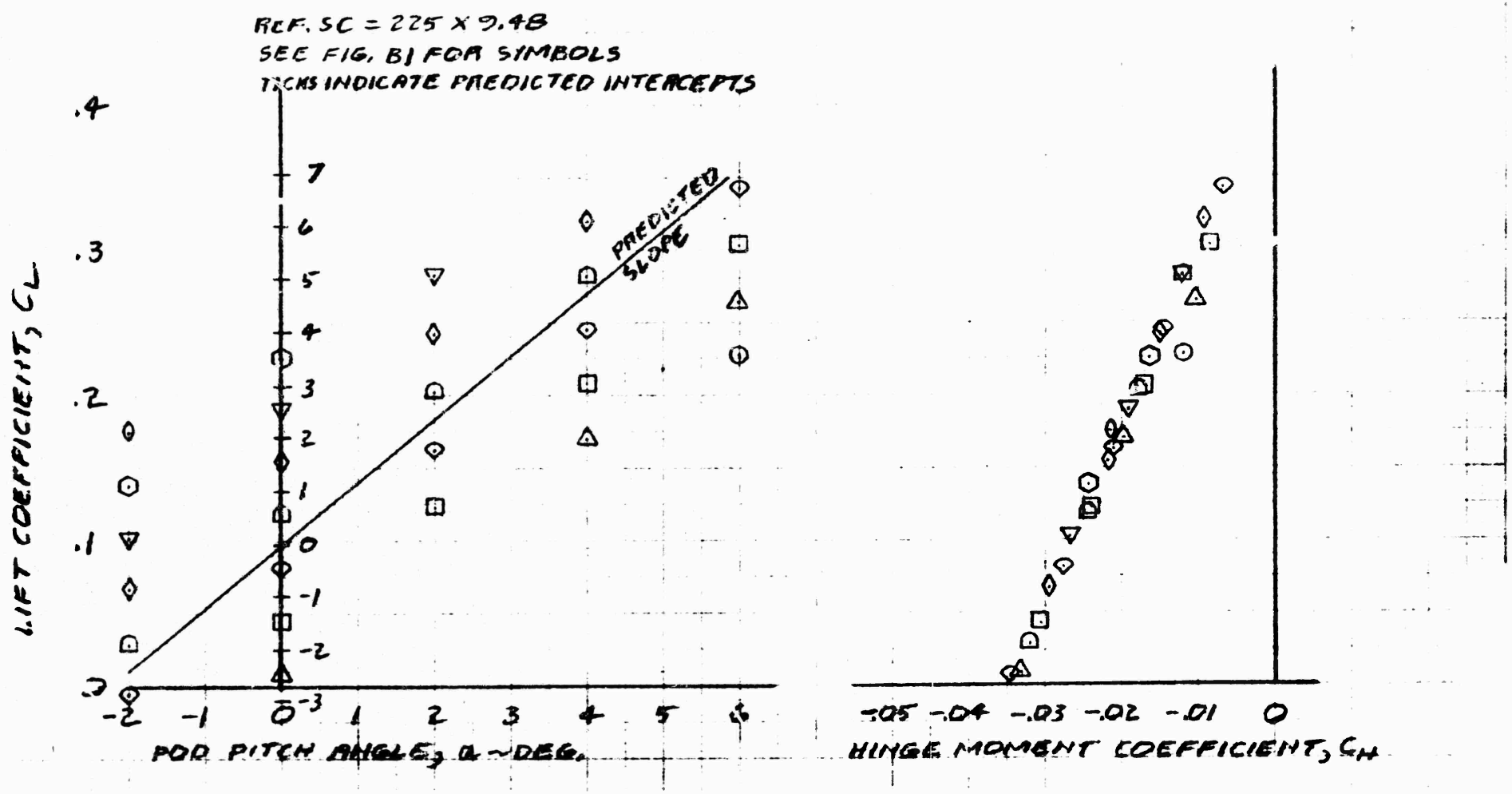


Figure B3. Lift and Hinge Moment vs. Pod Pitch, AG(EH) Forward Foil, 5-ft Depth at 35K for Prototype

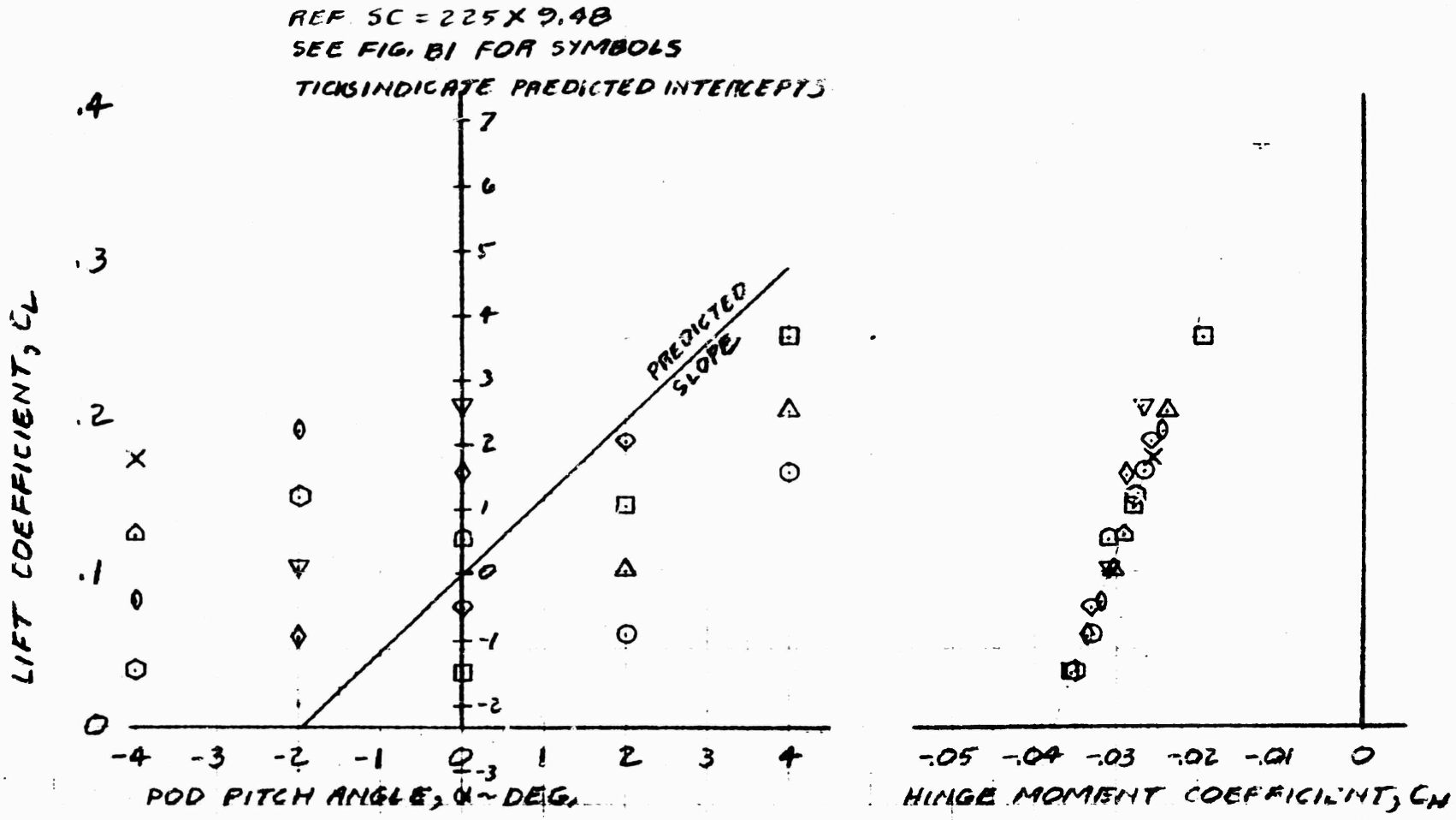


Figure B4. Lift and Hinge Moment vs. Pod Pitch, AG(EH) Forward Foil, 15-ft Depth at 50K for Prototype

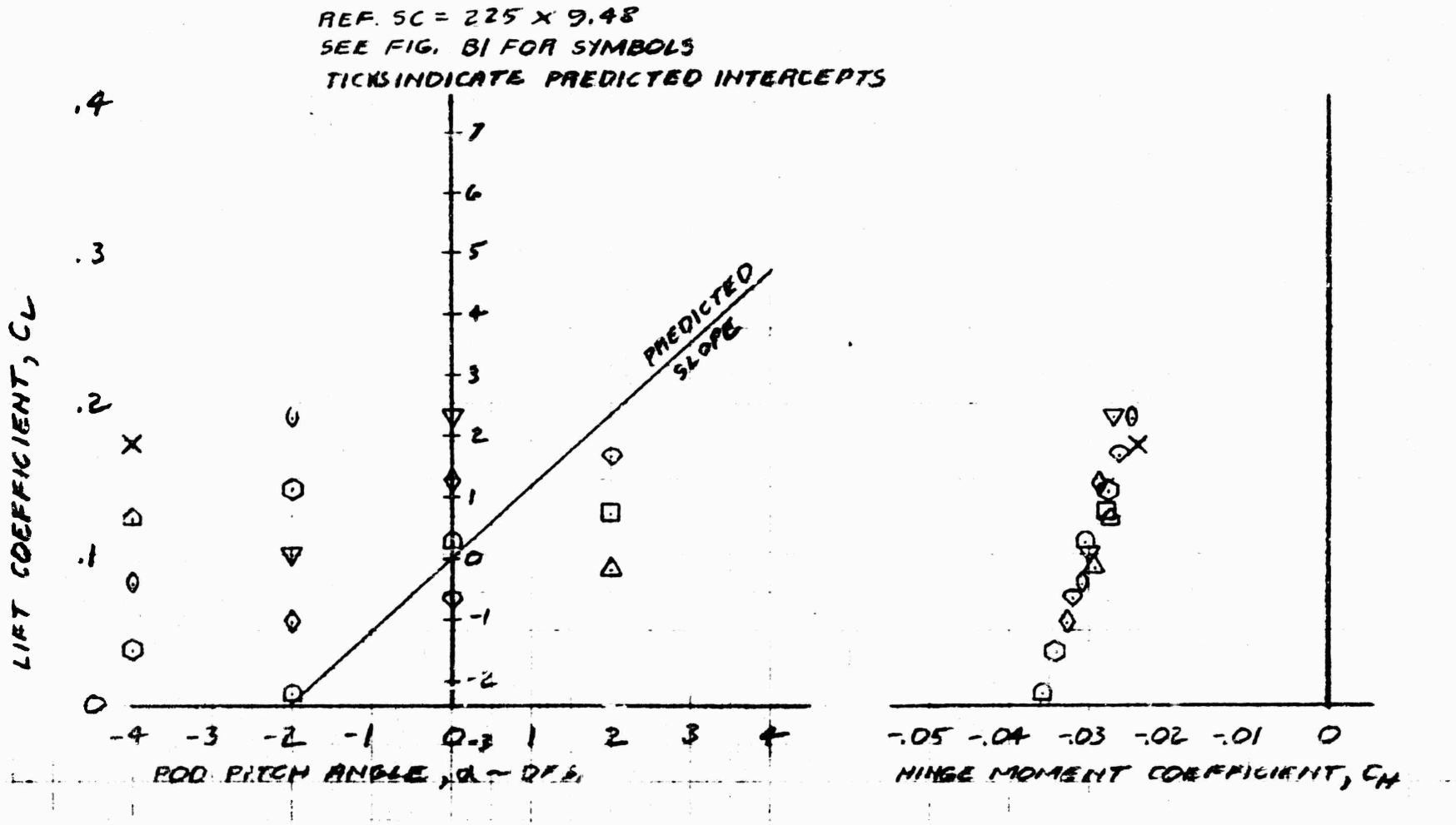


Figure B5. Lift and Hinge Moment vs. Pod Pitch, AG(EH) Forward Foil, 10-ft Depth at 50K for Prototype

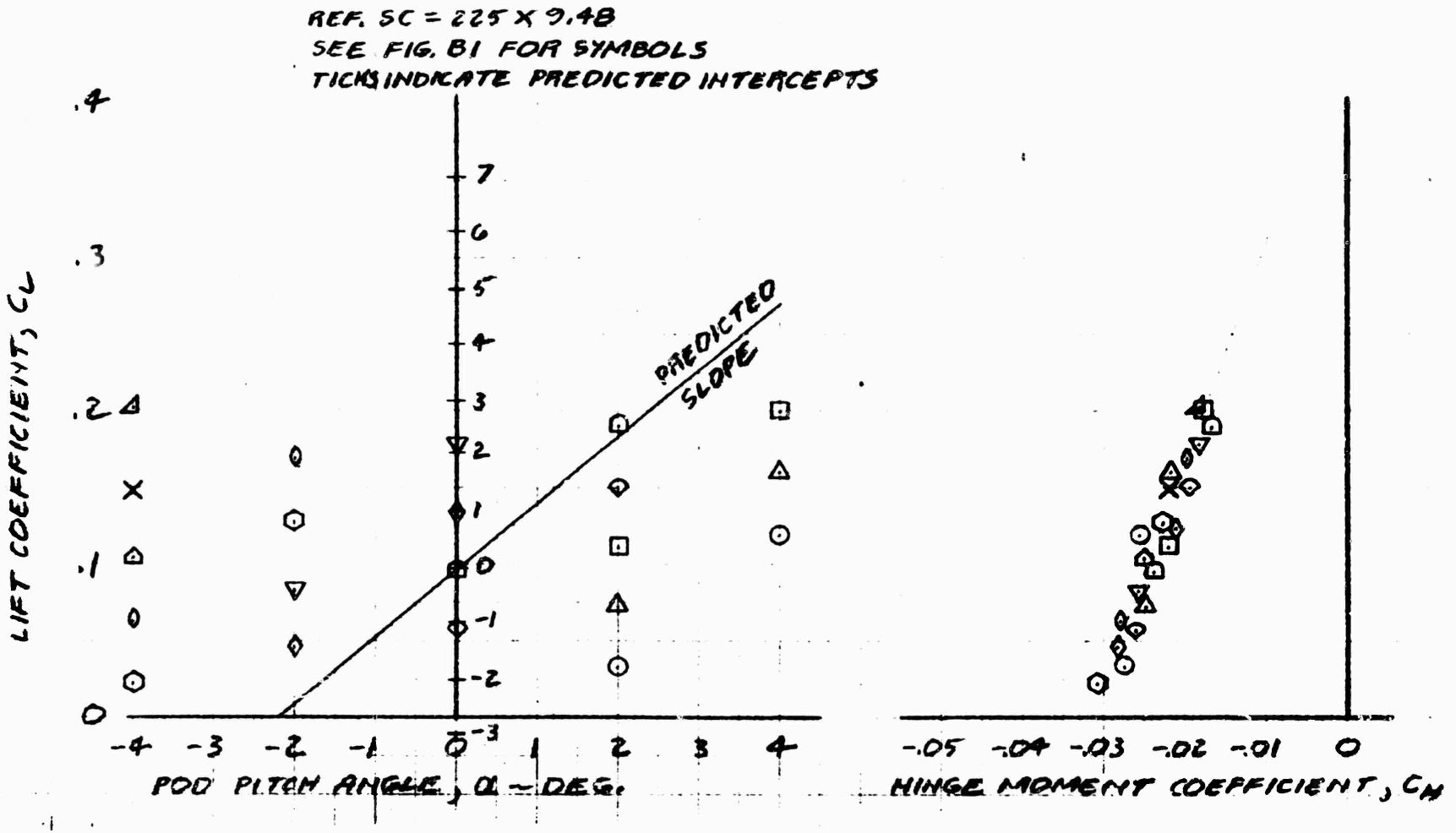


Figure B6. Lift and Hinge Moment vs. Pod Pitch, AG(EH) Forward Foil, 5-ft Depth at 50K for Prototype

APPENDIX C

EVALUATION OF FLAP HINGE MOMENT DERIVATIVES

C_{h_α} AND C_{h_δ}

GENERAL

Three methods for predicting the three dimensional derivatives from the two dimensional derivatives are compared:

1 Perkins & Hage, Reference 4-19, which is the simplest,

2 Toll, Reference 4-3,

3 DATCOM, Reference 4-12

The AG(EH) configuration is assumed. Figures 4-15 and 4-16 present two new sets of section derivitives for this configuration and Perkins and Hage would contribute a third. For the purpose of comparing the conversions to three dimensions, however, the DATCOM section derivitives were employed:

$$C_{h_\alpha} = -.043$$

$$C_{h_\delta} = -.54$$

PERKINS AND HAGE

Perkins and Hage's $\underline{C}_{h_\alpha}$ may be interpreted as

$$\underline{C}_{h_\alpha} = C_{L_i} \frac{c_{h_\alpha}}{c_{\ell_\alpha}} \approx \frac{C_{L_i}}{2\pi} c_{h_\alpha} = \frac{2.75 \times .845}{2\pi} c_{h_\alpha} = .37\ c_{h_\alpha} = -.01593$$

and their $\underline{C}_{h_\delta}$ is practically

$$\underline{C}_{h_\delta} = c_{h_\delta} + \frac{d\alpha}{d\delta}(\underline{C}_{h_\alpha} - C_{h_\alpha}) = c_{h_\delta} + \frac{d\alpha}{d\delta}\left(\frac{C_{L_i}}{2\pi} - 1\right) c_{h_\alpha}$$

$$= c_{h_\delta} - .47 \times .63\ c_{h_\alpha} = c_{h_\delta} - .296\ c_{h_\alpha}$$

$$= -.54 + .296 \times .043$$

$$= -.527$$

TOLL

$B_2 = .915$ (Figure 11 of Reference 4-3 for no overhang)

$$\frac{(\Delta c_{h_\alpha})_{LS}}{B_2} = .0015 \times 57.3 = .086 \quad \text{(Fig. 11 of Ref. 4-3 for .1283 D/b)}$$

$$(\Delta c_{h_\alpha})_{LS} = .0786$$

$$C_{h_\alpha} = \frac{C_{L_\alpha}}{c_{\ell_\alpha}} c_{h_\alpha} + (\Delta c_{h_\alpha})_{LS} \approx \frac{C_{L_\alpha}}{2\pi} c_{h_\alpha} + (\Delta c_{h_\alpha})_{LS}$$

$$= \frac{2.75}{2\pi} c_{h_\alpha} + (\Delta c_{h_\alpha})_{LS}$$

$$= .438\ (-.043) + .0786$$

$$= .0598$$

Toll suggests model tests for C_{h_δ} in Reference 4-3 through he was an author for one of the DATCOM sources and the DATCOM C_{h_α} is essentially Toll's.

DATCOM

$$\frac{\Delta c_{h_\alpha}}{c_{\ell_\alpha} B_2 K_\alpha \cos \Lambda} = .014 \qquad \text{(Figure 6.1.6.1 - 4, Reference 4-12)}$$

$c_{\ell_\alpha} = 2\pi$ (assumed)

$B_2 = .915$ (Figure 6.1.6.1 - 4, Reference 4.12)

$K_d = 1.2$ (Figure 6.1.6.1 - 4, Reference 4.12)

$$\cos \Lambda = \cos 35.2^{o} = .818$$

$$\Delta c_{h_{\alpha}} = .014 \times 2\pi \times .915 \times 1.2 \times .818 = .079$$

$$C_{h_{\alpha}} = .529\, c_{h_{\alpha}} + .079$$

$$= -.529 \times .043 + .079$$

$$= .0563$$

$$\frac{\Delta c_{h_{\delta}}}{c_{\ell_{\delta}} B_2 K_{\delta} \cos \Lambda} = .025 \qquad \text{(Figure 6.1.6.1, Reference 4-12)}$$

$$c_{\ell_{\delta}} = \frac{d\alpha}{d\delta}\, c_{\ell_{\alpha}} = .47 \times 2\pi = 2.95$$

$$B_2 = .915 \qquad \text{(Figure 6.1.6.1, Reference 4-12)}$$

$$K_{\delta} = 1.15 \qquad \text{(Figure 6.1.6.1, Reference 4-12)}$$

$$\cos \Lambda = .818$$

$$\Delta c_{h_{\delta}} = .0635$$

$$\tan \Lambda_{HL} = \tan \Lambda + \frac{1 - 4 \times .8}{A} \frac{1 - \lambda}{1 - \lambda}$$

$$= .706 + \frac{1 - 3.2}{3} \times \frac{1 - .3}{1 + .3}$$

$$= .311$$

$$\Lambda_{HL} = 17.27^{o}$$

$$C_{h_{\delta}} = \cos \Lambda \cos \Lambda_{HL} \left(c_{h_{\delta}} - \frac{d\alpha}{d\delta}\, c_{h_{\alpha}} \frac{2 \cos \Lambda}{A + 2 \cos \Lambda} + \Delta c_{h_{\delta}}\right)$$

$$= .818 \times .955 \left[-.54 - .47 (-.043) \times \frac{2 \times .818}{3 + 1.636} + .0635 \right]$$

$$= -.367$$

SUMMARY

	2-D	Perkins & Hage	Toll	DATCOM
$\underline{C}_{h_\alpha}$	-.043	-.01593	.0598	.0563
$\underline{C}_{h_\delta}$	-.54	-.527	--	-.367

The highly empirical nature of these procedures and the scatter illustrated here generates little confidence. The Perkins & Hage procedure is adopted in this volume because of its simplicity.

APPENDIX D

ANALYSIS OF HYSTAD MODEL CAVITATION CHARACTERISTICS

DTMB Report 2138, "Model Test Results for the Hystad Strut-Nacelle-Foil Combination" by Peter Spangler, January 1966 presents on Figure 3 a "measured cavitation bucket" at variance with that predicted at Grumman and with that measured in the NSRDC towing tank and in the Grumman Whirling Tank for the AG(EH) planform. The Hystad and AG(EH) planforms are identical so this appendix examines the Hystad results to account for the apparent discrepancy.

Note that the Hystad and AG(EH) planforms are identical and that the Hystad foil pitches relative to the pod so that the Hystad lift is "incidence lift," comparable with the NSRDC AG(EH) forward foil model. No incidence lift version of the AG(EH) foil was tested in the Whirling Tank. Note, too, that the Hystad section is 16-407 while the AG(EH) model sections are 16- (.353)08.

The data of Figure 3 of the Spangler report are plotted as lift curves for various speeds on Figure D1. This plot is analogous with Figure 6-4 of the main body of this volume, though Figure 6-4 presents pitch lift characteristics. By reference to Figure 4-2 of this volume, it may be seen that the Hystad lift curve slopes are substantially in agreement with those measured at NSRDC and in the Whirling Tank.

The AG(EH) and Hystad lift curve slopes should be identical, but the effects of cavitation on the lift curve slope are not because of the different design lift coefficients.

Figure D2 presents the Hystad drag curves plotted against C_L^2 and with the estimated separation drag removed to linearize the fully wetted portion of the drag curve. The wetted slopes of Figures 6-5 and D2 should be similar but differ by 25%. The subject of induced drags lies outside the scope of this report and no attempt is made here to reconcile the two sets of drag curves.

The significant cavitation characteristics of Figures D1 and D2 are the initial effects on the lift and drag and the maximum lift and these effects are plotted as speed versus foil loading on Figure D3 where they are compared with the theorectical incipient

cavitation bucket for the model. The results are consistent with previous experience with these characteristics; the upper surface leading edge effects leave the theoretical bucket in the vicinity of its right-hand corner, bow out to the right, and tend to suck back in at lower speeds. Lower surface cavitation effect lies outside and generally paralle! with the theoretical bucket.

The prototype incipient cavitation bucket is also shown on Figure D3. Since the effective boundaries are functions of lift coefficient and cavitation number, they can be expected to shift to the same position relative to the theoretical prototype bucket that they hold for the model test condition, i.e., the significant scales on Figure D3 are cavitation number and C_L which may be expressed as model speed and model foil loading or as prototype speed and prototype foil loading.

Spangler's observed cavitation bucket of his Figure 3 is also shown on Figure D3. Note that Spangler has identified 66 fps as first observed cavitation at 4°, which lies between photographs (a) and (b) of his Figure 9 and was the first speed at which the leading edge cavitation on the one semi-span was observed. The difference between the two semi-spans is evidently due to the difference in depths between the two semi-spans and evidently the model is rolled to port rather than starboard as the text states. This roll angle obscures the identification of first observed cavitation to some extent but that effect is not significant to our discussion here.

The significant point is that the starboard cavitation of Figure 9, like the cavitation of both semi-spans on Figure 8, is classic leading edge cavitation and corresponds to the right boundary of the incipient cavitation bucket. Now, on Figure 10, note that Spangler has identified first observed cavitation with a disturbance at the foil/pod intersection which has no relationship with the incipient cavitation bucket and which looks more like the result of a surface imperfection.

The foil trailing edge disturbances of Figure 10 have no obvious explanation, though they do have the classic shape for cavitation originating at a point surface imperfection. Only if those disturbances are located at 80-90% of the semi-span could they be associated with classic leading edge or mid-chord cavitation. Then the

indication of Spangler's Figures 10-13 is that no classic leading edge or mid-chord cavitation was encountered at 0-3° just as the theoretical bucket would indicate. Such a conclusion cannot be certain, however, without extending the low angle of attack range to a speed which would conclusively display the appearance of the mid-chord cavitation.

If the observed cavitation boundaries are redrawn from the photographs for the classic cavitation pattern, the "preferred" observed cavitation bucket of Figure D3 is obtained and it is interesting to note that there are cases where the lift and drag are affected before there is visible evidence of classic cavitation. A case in point is the 86.4 fps photograph of Spangler's Figure 10 for which the lift curve slope is significantly reduced though there is no visible leading edge cavitation even in the next photograph.

Note on Spangler's Figures 14-16 that the lower surface cavitation is all of classic inboard, leading edge type.

Finally, the theoretical incipient bucket for the AG(EH) prototype 10 ft. depth is compared with that for Spangler's model test depth to illustrate the substantial difference in top-of-the-bucket speeds and foil loading for the two cases. This difference is particularly significant to the tow tank; the Whirling Tank speeds may be greater or less than prototype speed and never differ from prototype cavitation speed by any substantial amount. Discussions of cavitation speeds, then, must differentiate model and prototype speeds carefully.

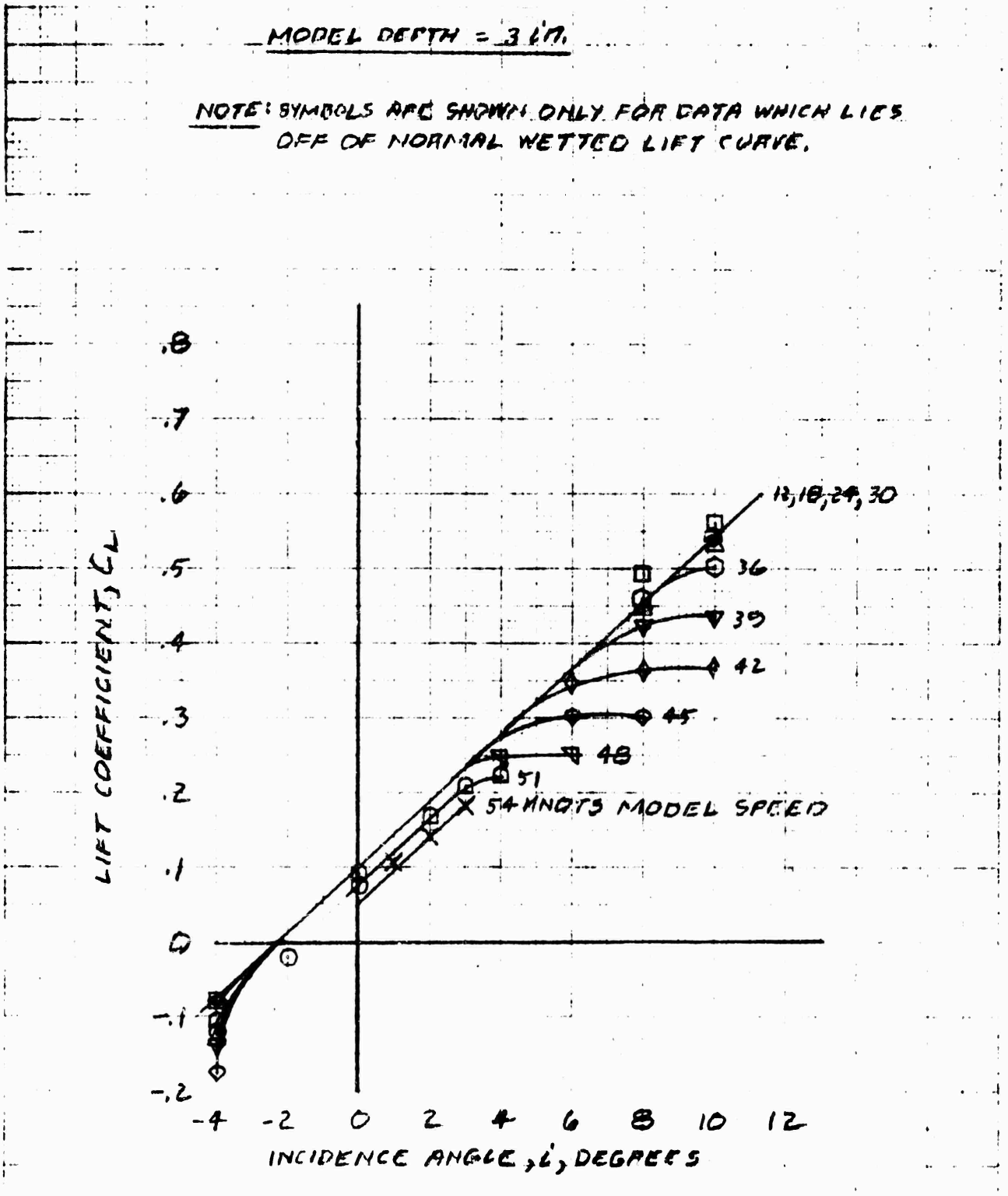


Figure D1. Hystad Model Incidence Lift Curves

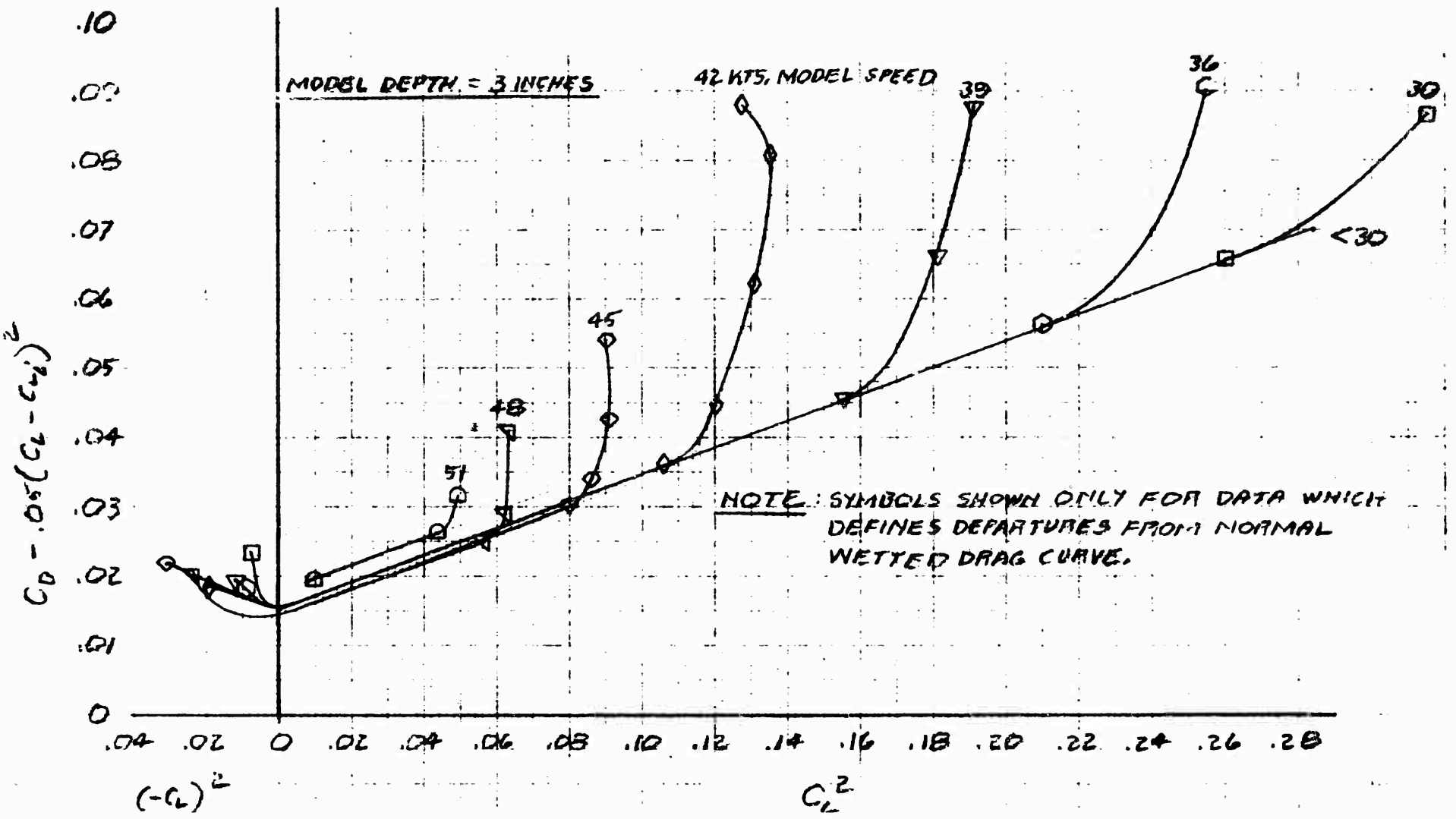


Figure D2. Hystad Model Cavitation Drag Effect

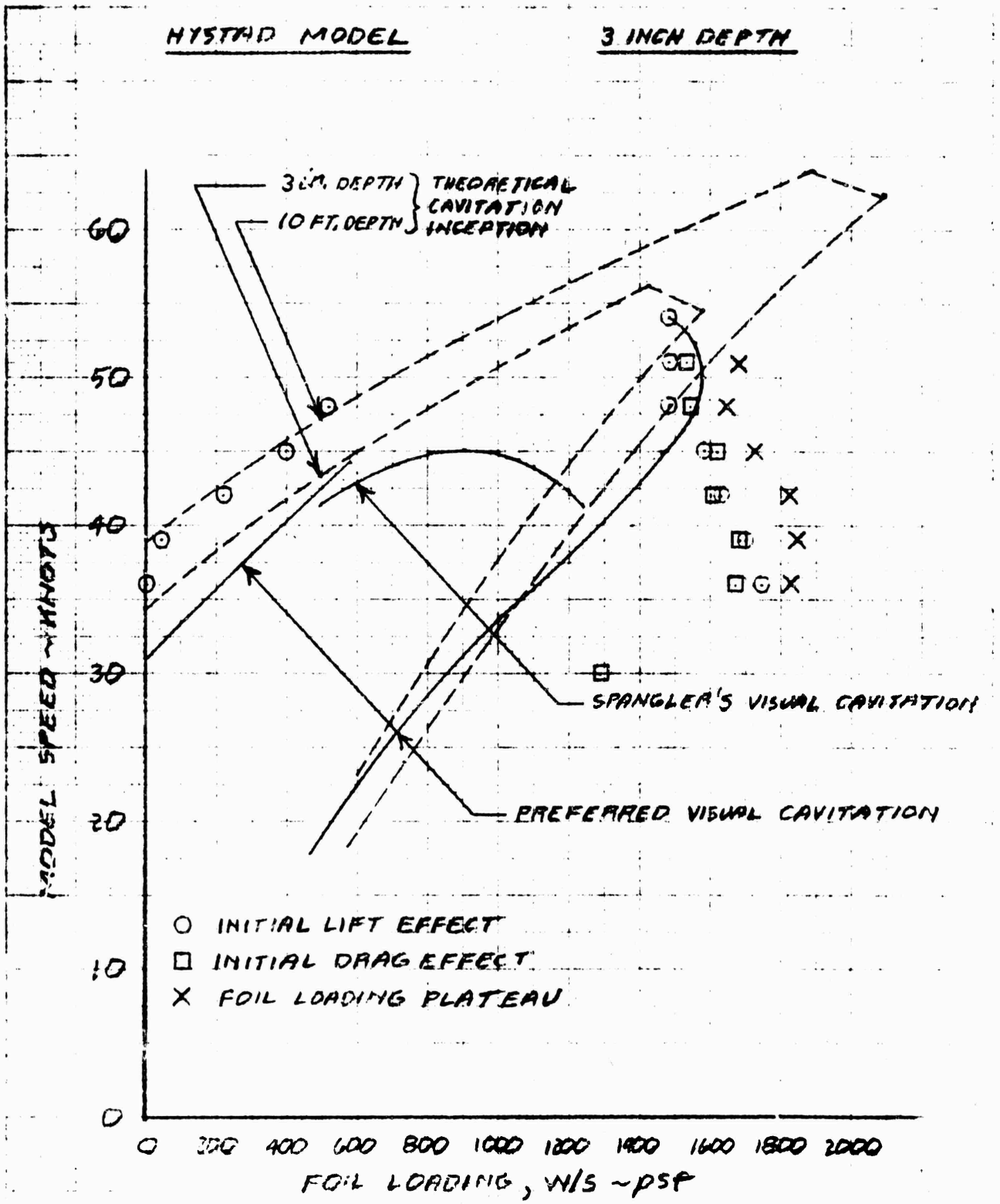


Figure D3. Hystad Model Cavitation Effect Boundaries, Incidence Lift

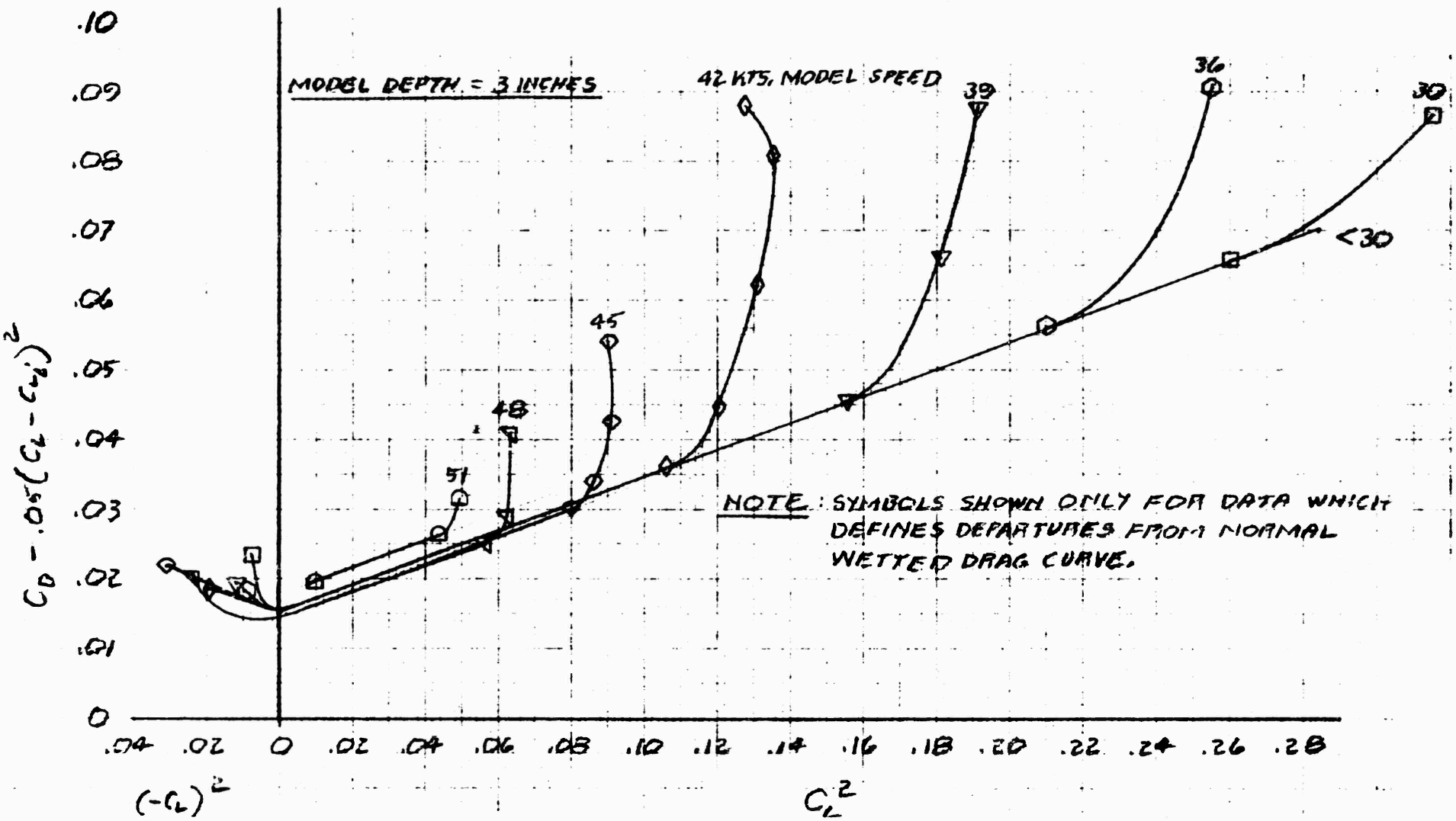


Figure D2. Hystad Model Cavitation Drag Effect

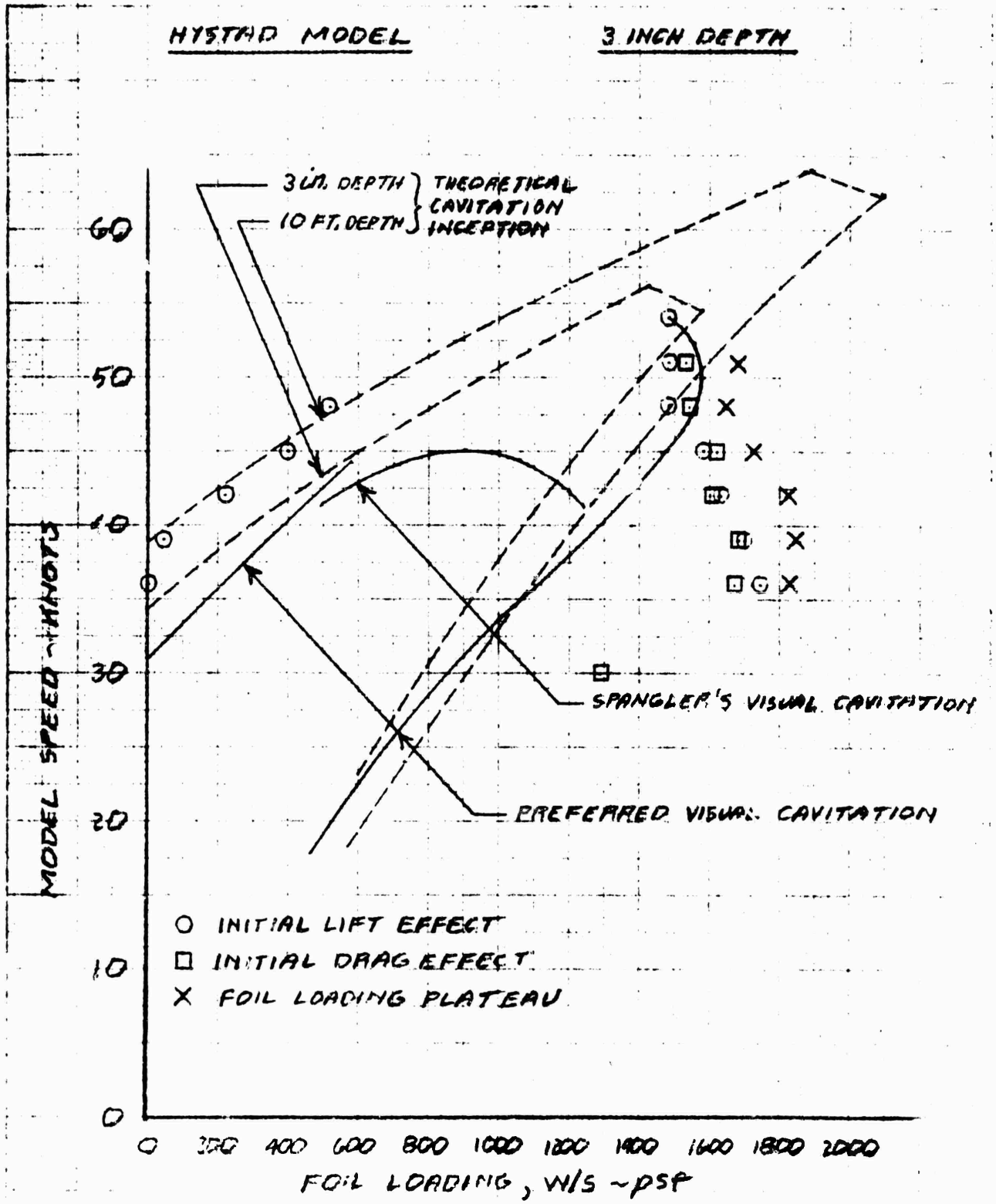


Figure D3. Hystad Model Cavitation Effect Boundaries, Incidence Lift

INDEX, APPENDIX E

PAGE

SUMMARY E-1

CONCLUSIONS AND RECOMMENDATIONS E-2

DISCUSSION E-5

- Steady-State Data - General E-5
- Lift Characteristics E-6
- Foil Hinge Moment E-8
- Flap Hinge Moment E-11
- Cavitation E-12
- Dynamic Hinge Friction Characteristics E-14
- Air Calibration E-17
- Static Calbirations E-19
- Unsteady Load Responses - General E-23
- Flap Lift Response E-24
- Flap Hinge Moment Response E-26
- Foil Pitching Moment Response E-27

REFERENCES E-30

TABLES

- E1 Steady-State Lift Data, 1.14 MAC Depth E-31
- E2 Flap Hinge Moment Air Calibration E-32
- E3 Air Calibrations E-33
- E4 Static Calibrations E-35
- E5 Flap Lift Response E-36
- E6 Flap Hinge Moment Response E-40
- E7 Foil Pitching Moment Response E-41

FIGURES

		Page
E1	Froude Scaled Test Results, 14.7 Knots, Lost Sandpaper	E-48
E2	Froude Scaled Test Results, 14.7 Knots, No Sandpaper	E-49
E3	Froude Scaled Test Results, 14.7 Knots, With Sandpaper	E-50
E4	Froude Scaled Test Results, 20.9 Knots	E-51
E5	Cavitation Scaled Test Results, 27.5 Knots, $\alpha = 0$	E-52
E6	Cavitation Scaled Test Results, 32 Knots, $\alpha = 0$	E-53
E7	Cavitation Scaled Test Results, 36.5 Knots, $\alpha = 0$	E-54
E8	Cavitation Scaled Test Results, 40.9 Knots, $\alpha = 0$	E-55
E9	Cavitation Scaled Test Results, 44.9 Knots, $\alpha = 0$	E-56
E10	Cavitation Scaled Test Results, 32 Knots, $\alpha = -1.5^{o}$	E-57
E11	Cavitation Scaled Test Results, 36.5 Knots, $\alpha = -1.5^{o}$	E-58
E12	Cavitation Scaled Test Results, 44.9 Knots, $\alpha = -1.5^{o}$	E-59
E13	Cavitation Scaled Test Results, 32 Knots, $\alpha = -3^{o}$	E-60
E14	Cavitation Scaled Test Results, 36.5 Knots, $\alpha = -3^{o}$	E-61
E15	Cavitation Scaled Test Results, 44.9 Knots, $\alpha = -3^{o}$	E-62
E16	Cavitation Scaled Test Results, 32 Knots, $\alpha = 1.5^{o}$	E-63
E17	Cavitation Scaled Test Results, 36.5 Knots, $\alpha = 1.5^{o}$	E-64
E18	Cavitation Scaled Test Results, 44.9 Knots, $\alpha = 1.5^{o}$	E-65
E19	Cavitation Scaled Test Results, 32 Knots, $\alpha = 3^{o}$	E-66
E20	Cavitation Scaled Test Results, 36.5 Knots, $\alpha = 3^{o}$	E-67
E21	High Aspect Ratio Foil Flap Cavitation	E-68
E22	Flap Effectiveness	E-69
E23	Residual Lift	E-70
E24	Foil Moment Characteristics	E-71
E25	Flap Hinge Moment Slope	E-72
E26	Residual Flap Hinge Moment	E-73
E27	Flap Hinge Moment, $\alpha = 2^{o}$, $i = 1.25^{o}$	E-74
E28	Flap Hinge Moment, $\alpha = 2^{o}$, $i = -1.45^{o}$	E-75

FIGURES (Continued)

		Page
E29	Flap Hinge Moment, $\alpha = 0$, $i = 4.5^{o}$	E-76
E30	Flap Hinge Moment, $\alpha = -1.5^{o}$, $i = 4.5^{o}$	E-77
E31	Flap Hinge Moment, $\alpha = -3^{o}$, $i = 4.5^{o}$	E-78
E32	Flap Hinge Moment, $\alpha = 1.5^{o}$, $i = 4.5^{o}$	E-79
E33	Flap Hinge Moment, $\alpha = 3^{o}$, $i = 4.5^{o}$	E-80
E34	Joined Flap Hinge Moment Curves	E-81
E35	Evaluation of Twist C_2	E-82
E36	Normal Cavitation Bucket, $\alpha = 0$	E-83
E37	Cavitation Characteristics, $\alpha = 0$	E-84
E38	Cavitation Characteristics, $\alpha = -1.5^{o}$	E-85
E39	Cavitation Characteristics, $\alpha = -3^{o}$	E-86
E40	Cavitation Characteristics, $\alpha = 1.5^{o}$	E-87
E41	Cavitation Characteristics, $\alpha = 3^{o}$	E-88
E42	Cavitation Drag Effect, 44.9 Knots, $\alpha = 0$	E-89
E43	Cavitation Drag Effect, 36.5 Knots, $\alpha = 3^{o}$	E-90
E44	Flap System Inertia In Air	E-91
E45	Flap Hinge Friction In Air	E-92
E46	Flap Hinge Moment Air Calibration	E-93
E47	Lift Amplitude In Air	E-94
E48	Lift Phase In Air	E-95
E49	Foil Lift Air Calibration	E-96
E50	Drag Amplitude In Air, as Function of δ^2	E-97
E51	Drag Amplitude In Air	E-98
E52	Drag Phase In Air	E-99
E53	Foil Drag Air Calibration	E-100
E54	Foil Hinge Moment In Air, Real Part	E-101
E55	Foil Hinge Moment In Air, Imaginary Part	E-102

FIGURES (Continued)

		Page
E56	Foil Hinge Moment Air Calibration, After Freeing-Up Hinge	E-103
E57	Foil Hinge Moment Air Calibration, Before Freeing-Up Hinge	E-104
E58	Static Calibration, Flap Hinge Moment	E-105
E59	Static Calibration, Foil Hinge Moment	E-106
E60	Static Calibration, Lift	E-107
E61	Calibration Effect, Flap Lift Amplitude	E-108
E62	Calibration Effect, Flap Lift Phase	E-109
E63	Flap Lift Amplitude	E-110
E64	Flap Lift Phase	E-111
E65	Calibration Effect, Flap Hinge Moment Amplitude	E-112
E66	Calibration Effect, Flap Hinge Moment Phase	E-113
E67	Flap Hinge Moment Amplitude	E-114
E68	Flap Hinge Moment Phase	E-115
E69	Calibration Effect, Foil Pitching Moment Amplitude	E-116
E70	Calibration Effect, Foil Pitching Moment Phase	E-117
E71	Foil Pitching Moment Amplitude	E-118
E72	Foil Pitching Moment Phase	E-119

SUMMARY

The measurement of unsteady load responses requires light, friction-free mechanisms throughout, while the measurement of cavitation characteristics require sturdy structure and positive sealing against air leakage. The attempt of this program to satisfy both requirements with the same model has demonstrated the impracticality of such an approach. The air sealing provisions were not adequate but those seals, with the hinge required for cavitation scaled loads, presented excessive friction during the measurement of unsteady load responses.

The measured cavitation characteristics indicate a substantial effective "wash-in" outboard on the foil and are consistent with a root wash-out by air leakage. The foil pitching moments contradicted previous results with the same model throughout and were consistent with the presence of abnormally high pressure (i.e., air leakage) aft of the foil hinge. These indications persisted down to Froude scaled speeds and preclude confident acceptance of any of the data obtained.

Analysis of the data obtained from this program indicate areas, principally in data reduction, in which improved procedures are required to improve the effectiveness of future programs of this type.

CONCLUSIONS AND RECOMMENDATIONS

The most obvious observations from this test program are the remarkable sensitivity of the AG(EH) configuration to air leakage from the strut and the difficulties introduced by friction into the interpretation of unsteady load measurements. Both observations indicate that cavitatior scaled and Froude-scaled testing should proceed with separate models specifically designed to the requirements peculiar to these two objectives. Analysis of the cavitation scaled data obtained during this program further indicates that the interpretation of such data and the probability of displaying all the characteristics of interest would be much improved by substantially expanding the test matrix. It is therefore recommended that the mapping of civitation characteristics be conducted in continuous flow facilities capable of providing 10-100 times the high-speed data available to this program.

Consistent with the observation that it is impractical to measure cavitation characteristics and unsteady load responses with the same model, the current plan is to modify themodel of this test program for the measurement of unsteady load responses at Froude-scaled speeds. To aid the conduct of that test program, the recommend ations below summarize the experience gained with the past program in some detail.

1. The indications are that the air leakage problem persists down to the Froude-scaled speeds and with significant effect. Further improvement in the provisions for sealing the strut are therefore required.

2. There can be no assurance that the air calibration presents the submerged friction forces and all of the friction forces confuse interpretation of the air calibration and distort the flap motion. The planned isolation of the flap moment strain gages from the flap hinge will aid this problem but every advantage possible must be taken of the reduced load requirement to reduce the friction forces throughout the system.

3. There was confusion about the phase relationships throughout this program. Some of this confusion resulted from an internal misunderstanding at Grumman which identified positive phase with lag and that identification appears through-

out Reference E1. Further confusion resulted from data transmission through illdefined procedures and, possibly, from two questionable practices which have appeared in the general literature:

a. Specifying the phase associated with a negative amplitude

b. Relating the phase to a derived quantity; e.g., a rate or acceleration.

It is recommended that all responses to flap motion be related in phase to the flap deflection and that all responses to waves be related in phase to the instantaneous surface height (positive above MWL) at any convenient, but specified, point on the foil chord. It is understood that amplitudes are half-peak-to-peak, absolute (plus) quantities and that plus phases are leading.

4. Data reduction, transmittal, and analysis time must be reduced. Each run of the proposed program represents several objectives and there is considerable risk of losing a run which has not been analyzed within twenty-four hours.

5. The Grumman pre-test report for the new test program must define the transmittal of data in an explicit and detailed manner. The data requirements of the Aero Test and Marine groups must be distinguished as to content and timing; a data identification system must be established; data transmittal duplications, as for data reduction corrections, must be explained.

6. The air calibration smoothing procedure of Reference E1 was not satisfactory because it reproduces the data scatter and because it does not distinguish the friction and inertial sources in the calibration. Each of the responses for these calibrations should be considered individually, their inertial component estimated, the results plotted in appropriate manner and smoothed by eye. For this purpose the inertias of all moving parts should be estimated and documented in the pre-test report. The air

calibrations are the first and best test of the data reduction for phase relationships.

7. The programmed static (submerged zero speed) runs are intended to test Theodorsen's inertial coefficients but the validity of this test is not yet certain; this data is academic rather than practical.

8. If the phase relationships are well defined and the air calibrations are reasonable, the analysis of the response data is routine.

9. Some consideration, not yet defined, should be given to the unsteady responses at harmonics of the flap motion to test the flap motion waveform achieved, test the superposition of the responses, and extend the test frequency range.

DISCUSSION

Steady State Data - General

The reduced steady state data available at this writing is presented graphically on Figures E1 - E20 and the corresponding test conditions are tabulated in Table E1. All reduced data is from Reference E1 except the zero pitch cavitation data of Figures E5 - E9. That data is incorrect in Reference E1 and hand reduced data recorded on the carriage is employed here.

It must be recognized that this data presents fragments of a very complex and unfamiliar set of characteristics; Figure E21 is from data obtained from the Grumman Whirling Tank for a high aspect ratio flapped foil model and the test conditions were extended well into the upper and lower surface cavitation ranges to aid interpretation. This data is cross-plotted from fixed flap angle pitch curves which have not yet been analyzed and may change in final form. Note that the combination of high aspect ratio and double struts has produced almost 2-dimensional lift characteristics for this model.

Note that no portion of Figure E21 is predictable at present. There is a predictable slope between 2° and 6° flap angle at the 35-knot speed. At the lower speeds there is a characteristic but unpredictable slope increase and at higher speeds a characteristic slope reduction due to cavitation. The zero lift angle for the normal slope has been radically altered by some still unknown effect so that even this portion of the lift curve is unpredictable. The separated flow slope for positive flap angles at low speed is normal; the supercavitated slopes are higher than normal. The positive flap separated and supercavitated slopes are repeated for negative flap at 25 and 55 knots; at intermediate speeds the negative flap slopes are still in transition. A fragmentary view of these characteristics would pose a substantial data analysis problem.

The data of Figures E1 - E20 present such a problem and one which has been complicated by the fact that these are abnormal results. The lift, drag, and moments are interrelated and are all related to the cavitation characteristics. Thus interpretations given the lift data of Figures E1 - E20 are hypothetical until they have been shown consistent with the other measured characteristics at their own and at all the other test

conditions. The final results of this Appendix evolved from several iterations of this process but remain hypothetical in nature because of the uncertain character of the abnormality involved.

Figure E22 was employed for guidance in the interpretation of the lift results. It was assumed that separation effect was of the order of the difference between small and large deflections of a plain flap while flap cavitation was of the order of the split flap effect on Figure E22.

Lift Characteristics

The total lift coefficient may be expressed in the form:

$$C_L = C_{L_\alpha}\,\alpha + C_{L_i}\,i + C_{L_\delta}\,\delta + C_{L_0}$$

$$= C_{L_\alpha}\left(\alpha + \frac{C_{L_i}}{C_{L_\alpha}}\,i + \frac{d\alpha}{d\delta}\,\frac{C_{L_i}}{C_{L_\alpha}}\,\delta\right) + C_{L_0} \qquad \text{(E.1)}$$

which, for a trimmed flap, becomes:

$$C_{L_{\delta=0}} = C_{L_\alpha}\left(\alpha + \frac{C_{L_i}}{C_{L_\alpha}}\,i\right) + C_{L_0} \qquad \text{(E.2)}$$

and from the results of Section 4, for the AG(EH) forward foil this becomes (at 10 ft. submergence):

$$C_{L_{\delta=0}} = 2.75\,(\alpha + .838i) + .090 \qquad \text{(E.3)}$$

If various combinations of pitch and incidence are tested, Eq. (E.3) will test pitch lift curve slope, incidence lift curve slope, and residual lift simultaneously. Further, the flap lift curve slope is tested by the C_L at zero flap. The lift curve results of Figure E1 - E20 are tested in this manner on Figure E23.

The slopes upon which Figure E23 are based are tabulated in Table E1. It was not possible to employ a common slope through the lift data and the slopes of Table E1 and Figure E23 are the solid lift curves of Figures E1 - E20. The corresponding flap effectivenesses are listed in Table E1 and are disappointing; only the lowest speed Froude scaled tests presented a normal flap effectiveness. Flap effectiveness appears to be subject to incidence, pitch, and speed but not in any usefully systematic manner.

The residual lift discrepancy of Figure E23 was noted early in the test program and initiated a substantial effort to control air leakage over the foil. Elimination of the air leakage, visually and under pressure test, increased the residual lift but not to the expected value. Investigation disclosed that the incidence angles of Reference E2 were relative. The subject is not specified in Reference E3 though it is standard operating procedure for the Grumman model shop to provide a template locating the foil plane. Nevertheless these tests proceeded on what now appears to have been a mistaken assumption that this was the first absolute measure of the residual lift for the model. Note on Figure E23 that the residual lift is, in some cases, speed dependent though the residual lift for the Froude scaled tests is as low as that for the cavitation scaled tests. Only the lowest, zero pitch speed presented a residual lift approaching that of the 1962 model tests.

While the assumption of a common slope and intercept does violence to the measured lift data, it is essential that this be done for performance and control studies. The flap effectivenesses for the cavitation data of Table E1 seem grouped about values of .37 and .31, which may indicate distinct boundary layer conditions. For the purpose of characterizing these results an effectiveness of .34 and a residual lift of .04 were employed and the resulting lift curves are shown as dotted lines on Figures E5 - E20. The corresponding lift description is

$$C_L = C_{L_\alpha}\,\alpha + C_{L_i}\,i + C_{L_{\frac{d\alpha}{d\delta}}}\,\delta + C_{L_0}$$

$$= .048\alpha^\circ + .0402i^\circ + .0402 \times .34\delta^\circ + .040$$

$$= .048\alpha^\circ + .0402i^\circ + .0137\delta^\circ + .040 \qquad \text{(E.4)}$$

The result provides a rather good correlation for the cavitation lift data.

Foil Hinge Moment

Foil hinge moments were measured only on the Froude scaled runs and do not provide a measure of C_{H_α} and C_{H_i}. If the towing tank derivatives of Table 4-3 are assumed, the foil hinge moments of Figures E1 - E4 can be compared with each other as on Figure E24. Only one set of four points on Figure E24 display the expected slope and they are associated with a profound change in residual moment. From Figures E23 and E24 the 1962 and 1972 tests can be compared as:

$$C_{H_{C_{L_\Delta}}} = \frac{\Delta C_{H_0}}{\Delta C_{L_0}} = \frac{-.035-(-.01)}{.09-.04} = \frac{-.025}{+.05} = -.5$$

or

$$= \frac{-.035-(-.0215)}{.09-.04} = \frac{-.0135}{-.05} = -.27 \qquad \text{(E.5)}$$

That is, the loss in residual lift apparently had a centroid 50% aft of the hinge on the total foil MAC or at 88.5% of the MAC for the four points of normal slope. For most of the points, however, that centroid is at 65.5% of the MAC with an indication, discussed below, that it is located laterally at the pod.

For the flap effectiveness above the $C_{H_{C_L}}$'s of Table 4-3 produce foil hinge moment slopes of:

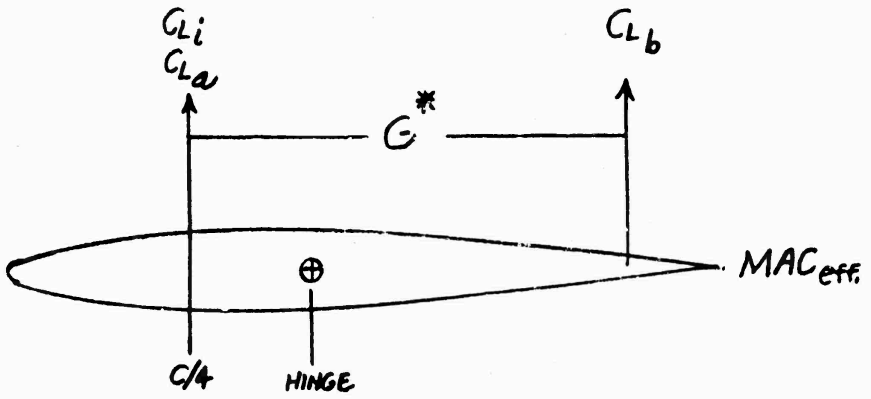
$$C_{H_\delta} = C_{H_{C_{L_\delta}}} C_{L_\delta} = .0402 \times .34\, C_{H_{C_{L_\delta}}} = .01367\, C_{H_{C_{L_\delta}}}$$

$$= .01367(-.0985) = -.001347/\text{deg (theoretical)}$$

$$= .01367(-.0689) = -.000942/\text{deg (tow tank)} \qquad \text{(E.6)}$$

and these slopes are shown on Figure E24 with their associated residual hinge moments of Table 4-3.

On some "effective mean aerodynamic chord" for pitch moment the flap load distribution is described by:



$$\frac{MAC}{MAC_{eff}} C_{H_\delta} = \left(\frac{H}{MAC_{eff}} - \frac{1}{4}\right) C_{L_{a_\delta}} - \left[G^* - \left(\frac{H}{MAC_{eff}} - \frac{1}{4}\right) \right] C_{L_{b_\delta}}$$

$$= \left(\frac{H}{MAC_{eff}} - \frac{1}{4}\right) (1 - \zeta) C_{L_\delta} - \left[G^* - \left(\frac{H}{MAC_{eff}} - \frac{1}{4}\right) \right] \zeta C_{L_\delta}$$

$$\frac{MAC}{MAC_{eff}} C_{H_{C_{L_\delta}}} = \frac{H}{MAC_{eff}} - \frac{1}{4} - G^* \zeta \qquad \text{(E.7)}$$

where G* denotes the absolute value of Allen's G to avoid associating a sign with distance.

A problem in symbols arises here because

$$\frac{MAC_{eff}}{MAC} \times \frac{H}{MAC_{eff}} \neq \frac{H}{MAC}$$

$\frac{H}{MAC_{eff}}$ is the chord station for the hinge on the effective MAC, given by

$$\frac{H}{MAC_{eff}} = \frac{\frac{H}{c_r} - \frac{1}{4} \eta_{eff} (1 - \lambda) \left(1 + A \frac{1 + \lambda}{1 - \lambda} \tan \Lambda\right)}{1 - \eta_{eff} (1 - \lambda)} \qquad \text{(E.8)}$$

The ratio, MAC/MAC_{eff}, is given by

$$\frac{MAC}{MAC_{eff}} = \frac{1 - \eta_{MAC} (1 - \lambda)}{1 - \eta_{eff} (1 - \lambda)} \qquad \text{(E.9)}$$

Substituting (E.8) and (E.9) in Eq. (E.7) and rearranging, the spanwise station for the effective mean chord is identified as:

$$\eta_{eff} = \frac{\frac{H}{c_r} - [1 - \eta_{MAC}(1-\lambda)]\, C_{H_{C_{L_\delta}}} - (G^* \zeta + \frac{1}{4})}{[\frac{1}{4}(1 + A\frac{1+\lambda}{1-\lambda}\tan\Lambda) - (G^* \zeta + \frac{1}{4})](1-\lambda)} \qquad (E.10)$$

and for the AG(EH)

$$\eta_{eff} = \frac{.639 - [1 - .429 \times .7]\, C_{H_{C_{L_\delta}}} - (.397 \times .545 + .25)}{[\frac{1}{4}(1 + 3 \times \frac{1.3}{.7} \times .706) - (.397 \times .545 + \frac{1}{4})] \times .7}$$

$$= .322 - 1.304\, C_{H_{C_{L_\delta}}} \qquad (E.11)$$

For the three slopes of Figure E24 the corresponding effective spanwise sections are:

η_{eff} = .332-1.304(-.0985) = .322 + .1285 = .450 (theoretical)

η_{eff} = .322-1.304(-.0689) = .322 + .09 = .412 (1962 towing tank result and four points of 1972 result)

η_{eff} = .322-1.304(-.0032/.0137) = .322-1.304(-.2335) = .322 + .304

= .626 (1972 towing tank results)

There are too many uncertainties involved here for confident, quantitative interpretation but the qualitative indication that the effective MAC for pitch moment has been moved outboard some 20% of the semi-span is very significant. The effect of the 7% shift of MAC shift of MAC on Figure 1-2 on the $(c_\ell/C_L)_{max}$ is shown on Figure 6-1.

The effect here is one which "washes-out" some portion of the foil at the root. If the upper four foil hinge moment points of Figure E4 really present a normal condition, rather than scatter, the lift curve of that figure indicates that the lift curve slope is not affected. Thus Figure E4 indicates that this "wash out" is independent of flap angle and all of the lift curves demonstrate that the effect is practically independent of speed.

Therefore the effect is one of foil twist, in a direction to wash out the center section.

In summary, these results present two possible foil hinge moment curves:

$$C_H = .00384\alpha^\circ + .002815i^\circ - .000942\delta^\circ - .01$$

$$C_H = .00384\alpha^\circ + .002815i^\circ - .0032\delta^\circ - .0215$$

where neither residual moment and only the lower C_{H_δ} are in agreement with the 1962 model test results. Both of these curves are shown on Figures E1 - E4; the first as a solid curve and the second as a dashed curve.

Flap Hinge Moment

The flap hinge moment data for common pitch and incidence angles is presented on Figures E27-E33. On these figures the moment slopes and trimmed flap hinge moments as judged by eye were plotted against pitch angle on Figures E25 and E26. No quantitative effort is made to judge these results because the lift disturbance is centered in the region of the flap and must have had a direct effect on the residual flap hinge moment by unloading the flap. A further effect on the residual flap hinge moment and upon the hinge moment slope would result from the apparent redistribution of the spanwise loading associated with the lift disturbance. There are significant qualitative indications to be considered in these results however.

It is to be noted that the steep slopes of Figure E25 are associated with the extreme angles of attack; i.e., the effect is opposite that to be expected as a result of flow separation. The view is clarified only a little by presenting the hinge moments plotted directly against flap angle as on Figure E34. Here it was necessary to present faired results; the actual curves are much more complex because an interruption in the lift or hinge moment curve porduces an effect in the C_L-δ curve.

Figure E34 presents either a non-symmetric slope; i.e., different slopes for positive and negative displacements, or a symmetric discontinuity about a shallow slope in the region of the test data. Interpretation is hampered by the lift disturbance known to be in the data and by the foil camber. In either event, the slope discontinuities of Figure E34 are of considerable significance to the control design.

These slope discontinuities are modified by the lift disturbance but they are not introduced by it. Similar discontinuities are evident in Figures 48-51 of Reference E6 which presents data for a 16-309 section. It is to be noted that the camber for the AG(EH) model is the equivalent of 20.7 degrees of flap which introduces a substantial assymetry into whatever boundary layer effects are at work. Note that most of the literature on plain flap hinge moments is for symmetric sections. It may be necessary to obtain comparable hydrodynamic data before attempting to quantitatively analyze hydrodynamic data for cambered sections.

This hinge moment provides no useful quantitative result for prototype application and the flap hinge moment prediction of Section 4 will continue to be employed except that it does now seem to be advisable to reduce the residual hinge moment to $C_{l_{i\,eff}}/6$ rather than the $C_{l_{i\,eff}}/2$ of Section 4. This prediction is compared with the faired measured hinge moments on Figures E1-E20.

Cavitation

For zero pitch Eq. (6.2.19) may be written

$$C_L\left(\frac{\Delta v_a}{V} - \alpha\right) = \frac{\sqrt{1+\sigma'} - \Psi}{(c_\ell/C_L)_F}\cos^2\Lambda - \alpha C_{L_{ref}}$$

$$= \frac{\sqrt{1+\sigma'} - \Psi}{(c_\ell/C_L)_F} - \alpha\left(C_{L_i} + C_{L_0} + C_{L_T}\right) \qquad \text{(E.14)}$$

where C_{L_T} is proportional to the local lift coefficient increment at 75% of the semi-span due to the lift disturbance.

Eq. (E.14) may be written

$$\frac{\frac{\Delta v_a}{V} - \alpha}{\alpha} C_{L_c} + C_{L_{ref}} = \frac{1}{(c_\ell/C_L)_F}\,\frac{(\sqrt{1+\sigma'} - \Psi)\cos^2\Lambda}{\alpha} - C_{L_T} \qquad \text{(E.15)}$$

where C_{L_c} is the foil lift coefficient for incipient cavitation.

For the upper surface leading adge Eq. (E15) becomes

$$.854C_{L_c} + .221 = \frac{1}{(c_\ell/C_L)_F} \left[.92 \left(\sqrt{1+\sigma'} - .704\right)\right] - C_{L_T} \qquad \text{(E.16)}$$

The incipient cavitation coefficients of Figures E5 thru E9 are plotted in this manner on Figure E35. Assuming the validity of the cavitation prediction, Figure E35 indicates that the lift disturbance is not a stable, or consistent, condition though it is assumed so in the calculations to follow. There is an indication that the lift disturbance does not affect the spanwise distribution associated with angle of attack since it could only be expected to increase c_ℓ/C_L and this would be inconsistent with the results on Figure E35.

From Figure E35 it is assumed that the C_L ref is effectively increased by .118 at 75% of the semi-span which is equivalent to about 2-1/2 degrees of "wash-in" at this point. Only one test condition, shown on Figure E15, presented a measure of the inboard effective twist. A direct solution of Eq. (E14) for this condition indicated a C_{L_T} of -.00344 which is quite low and indicates either that the lift disturbance is widespread or that it is concentrated on the pod at the strut intersection.

Figure E36 compares the zero pitch cavitation characteristics with the expected cavitation bucket to indicate the severity of the problem encountered in this data. The incidence control bucket is compared with the flap bucket on this figure and the upper surface leading edge boundaries are identical for the two buckets when the flap is trimmed. The incidence control bucket has been confirmed by the 1962 tests so at the test speed of Figure E36 for a 45.7 knot prototype speed there is a direct comparison of the 1962 and 1972 model cavitation characteristics. The low speed case of Figure E36 presents a fertile field for speculation. If this is a normal case flaps will present rather poor drag characteristics and, from Figure E29, a monumental non-linearity problem. It is more likely, however, that at 1150 prototype W/S on Figure E36 air displaced a separated boundary layer over some portion of the flap span and produced

the drag and flap hinge moment disturbances.

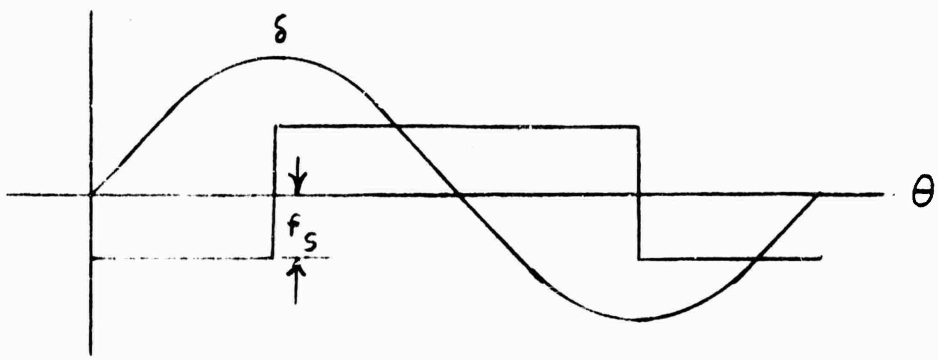
Figures E37-E41 compare the incipient cavitation bucket for the assumed foil twist with the observed cavitation characteristics at each of the pitch angles tested and indicate a reasonable consistency for the assumed nature of the difficulty. Figure E42 presents a typical drag result. The one out-of-line hand reduced point is clearly identified on Figure E9 as ventilation and demonstrates that, at least intermittently, there was air in the strut available to the foil. Figure E43 presents one of two cases where the minimum drag was affected without effect on the induced drags and might present a case where an entire run was affected as was one point on Figure E42.

Figures E37-E41 indicate remarkable penetration of the leading edge cavitation boundary with a minimal lift and drag disturbance. This characteristic of the effectively twisted AG(EH) foil is similar to the transit foil and, in fact, physical twist would be another way to achieve transit foil characteristics. The cavitation objective for this test program, however, was to demonstrate the cavitation characteristics when the chordwise and spanwise load distributions were more uniform than was available for these results. Figure E39 presents the only anticipated case which was achieved and then not at the anticipated pitch angle.

In summary, the cavitation test results do not achieve the test objective but instead demonstrate a remarkable sensitivity of those characteristics to foil root ventilation.

Dynamic Hinge Friction Characteristics

With reference to the flap angle as a sine wave, the sliding hinge friction is assumed to have the shape of a square wave:



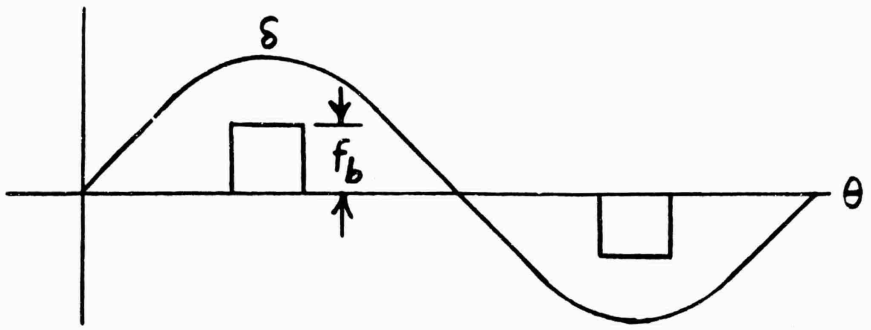
Where only one term of the series defining the friction is employed, as in these results, the sliding friction is a cosine wave of amplitude:

$$a_1 = \frac{2}{\pi}\left[\int_0^{\pi/2} (-f_s)\cos x\, dx + \int_{\frac{\pi}{2}}^{\pi} f_s \cos x\, dx\right]$$

$$= -\frac{4}{\pi} f_s \qquad \text{(E.17)}$$

so that this idealized sliding friction, as the dynamic data is reduced, lags the flap deflection by 90°.

For the same reference, the breakaway friction is assumed to have the shape of a pulse:

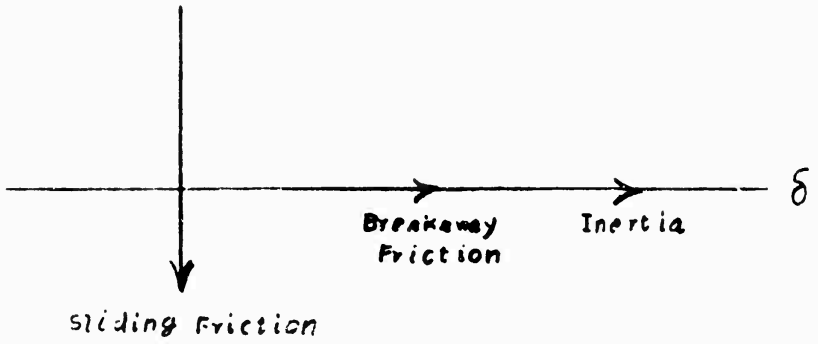


The breakaway friction, then, can be defined as a sine function having a first term of amplitude:

$$a_1 = \frac{2}{\pi}\int_{\frac{\pi}{2}}^{\frac{\pi}{2}+w} f_b \sin x\, dx$$

$$= \frac{2}{\pi} f_b \sin w \qquad \text{(E.18)}$$

which is in phase with the flap deflection. The inertial loads are in phase with the flap deflection so that the moments measured in the air calibration have the relationship.



The flap hinge moments measured during the air calibration are listed in Table E2 and it was necessary to invert the phases supplied by NSRDC to obtain an interpretation with physical significance.

The real part of the measured hinge moment while cycling the flaps in air is shown on Figure E44 which displays the inertial effect. Removing the inertial effect from the real part of the measured hinge moment produces the measured friction moments of Figure E45 which indicates that the "freeing up" process on the flap hinge actually increased the hinge friction. Figure E45 indicates friction moment amplitudes of 2.47 in. lbs. before freeing up the hinge and 3.97 in. lbs. after freeing up the hinge. These are interpretations, of course, which place a considerable strain upon the data precision for these measurements.

Figures E44 and E45 indicate hinge moments in air of

$$h_a = .000485\omega^2 \delta \quad -.1-i.18 \qquad \text{before free-up}$$

$$= .000485\omega^2 \delta \quad -.1-i.315 \qquad \text{after free-up} \qquad \text{(E.19)}$$

Figure E46 compares Eq. (E.19) with the smoothed calibration of Table II of Reference E1. The smoothing process of Reference E1 produces a better set of results for a given set of points but with no relation to the physical mechanisms involved and with no flexibility for new deflections and frequencies.

Air Calibration

Eq. (E.19) constitutes the air calibration assumed in this note for the flap hinge moment.

The entire flap control mechanism rests upon the lift gage blocks so the friction forces do not appear in the measured lift which should present an amplitude proportional to ω^2 and 180° out of phase with the flap displacement. The measured amplitudes are shown on Figure E47 and the change in slope after freeing up the hinge has not been explained. The inertia producing the lift force of Figure E47 is due to all the moving parts of the flap control system of Figure 2 of Reference E1. The inertia has not been estimated though it is obviously substantially greater than that of Figure E44 which presents only the inertia below the flap moment dynamometer. The weights of Figure E47 assume all of the moving mass to be concentrated on a one inch arm for qualitative comparison with the dotted line which presents the estimated three pound weight below the flap dynamometer. No masses were changed when the flap was freed up and the indication is that one or the other of the two sets of calibrations is in error.

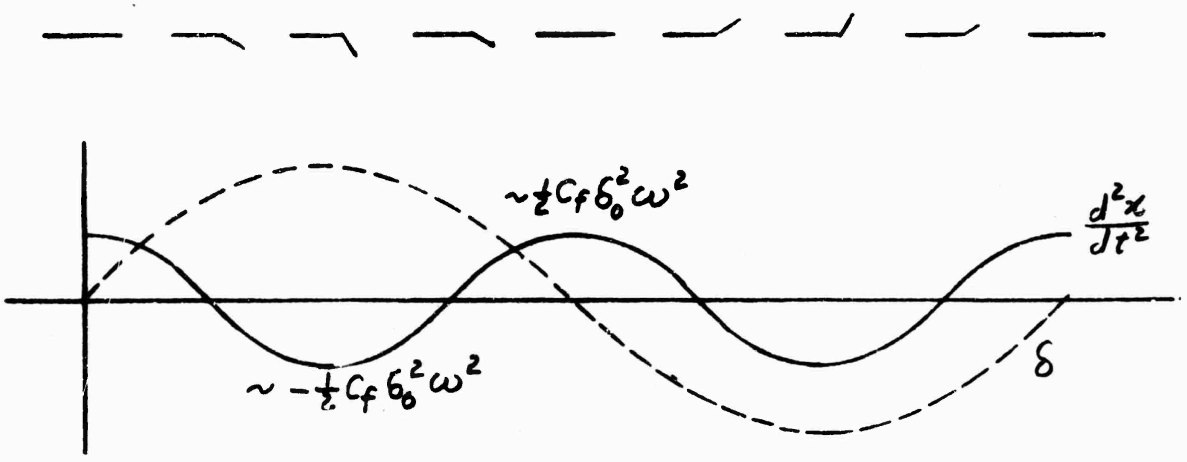
The measured lift phases are presented on Figure E48 which does not provide any reliable variation of phase with frequency. Note that it was necessary to invert the reported phase to give physical meaning to the result.

From Figures E47 and E48 the calibration assumed was

$$\begin{aligned} L_a &= .0224\omega^2 \delta \quad 161^\circ \qquad \text{before freeing-up hinge} \\ &= .05\,\omega^2 \delta \quad 161^\circ \qquad \text{after freeing-up hinge} \end{aligned} \tag{E.20}$$

which is compared with the calibration after freeing the hinge and with the smoothed calibration of Table II of Reference E1 on Figure E49. In this instance the machine smoothed calibration was led into significant error by the inclusion of wild points.

As with lift, the friction forces do not register on the drag gages but the data reduction procedure eliminates most of the drag response to flap motion. The analysis here proceeded only far enough to indicate a form for the air calibration.



Only the flap mass is considered for illustration though Figure 2 of Reference E1 indicates that other masses are in motion, some countering the effect of the flap mass. Assuming the flap mass concentrated at mid-flap-chord, that mass is located on x at

$$x = \frac{1}{2} c_f - \frac{1}{2} c_f \cos \delta$$

$$\text{where} \quad \delta = \delta_0 \sin \omega t \tag{E.21}$$

so (E.21) may be written

$$x = \frac{1}{2} c_f \cos (\delta_0 \sin \omega t) \tag{E.22}$$

The acceleration on x may be written

$$\frac{d^2x}{dt^2} = \frac{1}{2} c_f \delta_0 \omega^2 [\delta_0 \cos^2 \omega t \cos (\delta_0 \sin \omega t) - \sin \omega t \sin (\delta_0 \sin \omega t)] \tag{E.23}$$

One extreme is given at t = 0:

$$\frac{d^2x}{dt^2} = \frac{1}{2} c_f \delta_0^2 \omega^2 \cos \delta_0 \tag{E.24}$$

The other extreme is given at $\sin \omega t = \pm 1$, $\cos \omega t = 0$:

$$\frac{d^2x}{dt^2} = -\frac{1}{2} c_f \delta_0 \omega^2 \sin \delta_0 \tag{E.25}$$

If $\cos \delta_0$ is approximated by unity and $\sin \delta_0$ is approximated by δ_0, the acceleration is bounded by:

$$-\frac{1}{2} c_f \delta_0^2 \omega^2 \leq \frac{d^2x}{dt^2} \leq \frac{1}{2} c_f \delta_0^2 \omega^2 \qquad \text{(E.26)}$$

Eq. (E.23) is quite a complex function having a fundamental frequency double that of the flap motion, indicated by the $\cos^2$ term, and a distorted sinusoidal wave form. From the form of Eq. (E.26) the air calibration was first examined in terms of D/δ^2 on Figure E50 but the systematic variation with flap amplitude indicates that this is an unwise procedure. Evidently the amplitude at the fundamental frequency is a function of δ^2 while the amplitude at the flap frequency, provided by the data reduction procedure, is more a function of δ.

At the flap frequency, the first harmonic of the basic inertial frequency for drag, only the distortions in the fundamental wave form are viewed and measurement precision can be expected to suffer in amplitude and, especially, in phase. Therefore the calibration is defined here purely in emperical terms. The amplitude is presented on Figure E51 in terms of D/δ and has arbitrarily been fit to a quadratic in ω^2 for convenience. The phase is presented on Figure E52 where the low frequency phases are questionable because of the low amplitudes with which they are associated. Two forms of curve fit were examined and that which neglects the lowest frequency points is preferred because it appears to provide better correlation for those points of significant amplitude.

From Figures E51 and E52 the drag calibration in air which was adopted was

$$\left|\frac{D}{\delta}\right|_a = 4.44 - 8.99 \frac{\omega^2}{1,000} = 4.56 \left(\frac{\omega^2}{1,000}\right)^2$$

$$\angle D_a = 253.89 - 4.565 \frac{\omega^2}{1,000} - 1.6625 \left(\frac{\omega^2}{1,000}\right)^2 \text{ (degrees)} \qquad \text{(E.27)}$$

The calibrations of this appendix and of Reference E.1 are compared with the measured points on Figure E53. There is no objective measure of the relative validity of the two smoothed phase calibrations.

Note that time does not permit the very elaborate analysis required to provide physical significance to the drag phase at flap frequency: the measured phases have been reversed here only because that reversal was physically required for the other three air calibrations.

Time limitations also prevent analysis of the physical significance of the foil hinge moment calibration. Normally the foil hinge moment would be related to a flap load and moment by

$$H_a = h_a - c \left(\frac{h}{c} - \frac{H}{c}\right) L \qquad \text{(E.28)}$$

but in this case there are masses and frictions in the foil hinge moment case which are not in the flap moment calibration and the analysis of the air calibration is complicated by the model linkage arrangement provided to transmit hydrodynamic flap load and moment to the foil pivot. Eq. (E.28) has been employed, then only to provide a logical form in which to display the foil moment calibration.

Related to the exposed foil mean aerodynamic chord, for convenience, Eq. (E.28) becomes

$$H_a = h_a - .348\ L_a \qquad \text{(E.29)}$$

and from Eq. (E.19) and (E.20) the numerical evaluation is

$$H_a = [.01694\ \omega^2 \delta - .1] + i\left[-.00566\ \omega^2 \delta - \frac{.18}{.315}\right] \qquad \text{(E.30)}$$

where .18 = before freeing-up hinge

.315 = after freeing-up hinge

The real part of the air calibration is shown on Figure E54 where the scatter practically precludes interpretation. From the results after freeing-up the hinge, the slope of Eq. (E.30) is employed for Figure E54 and curves are drawn for two of the calibrations. The scatter is still worse for the imaginary terms on Figure E55 and one curve is drawn to represent two of the calibrations.

The solid lines of Figures E54 and E55 represent the calibrations:

$$H_a = \left[.00224\,\omega^2\,\delta - \frac{1.84}{1.25}\right] - i\left[.00568\,\omega^2\,\delta + .5\right]$$

where 1.84 = before freeing-up hinge

1.25 = after freeing-up hinge (E.31)

which are compared with their respective measured calibrations on Figures E56 and E57. The result is most unsatisfactory on Figure E56 but that measured case appears to be in conflict with the flap moment and lift calibrations, individually, and with the foil moment case of Figure E.57.

It should be noted that calibrations over frequency and amplitude ranges simultaneously hamper considerations of the result. A better procedure would be a range over frequency at two or three amplitudes followed by a range over amplitude at two or three frequencies.

In summary, the air calibrations assumed for the freed-up hinge are

$$h_a = .000485\,\omega^2\,\delta - .1 - i\begin{matrix}.180 & \text{before freeing-up hinge}\\ .315 & \text{after freeing-up hinge}\end{matrix}$$

$$H_a = \left[.00224\,\omega^2\,\delta - \frac{1.84}{1.25}\right] + i\left[-.00568\,\omega^2\,\delta - .5\right]$$

$$L_a = \begin{matrix}.0224\\ .05\end{matrix}\,\omega^2\,\delta \;\underline{/161^\circ}$$

$$\left|\frac{D}{\delta}\right|_a = 4.44 - 8.99\,\frac{\omega^2}{1,000} + 4.56\left(\frac{\omega^2}{1,000}\right)^2$$

$$\angle\, D_a = 253.89 - 4.565\,\frac{\omega^2}{1,000} - 1.6625\left(\frac{\omega^2}{1,000}\right)^2 \qquad \text{(E.32)}$$

The measured flap hinge moments in air are tabulated in Table E2. The measured foil hinge moment, lift, and drag in air are presented in Table E3.

Static Calibrations

No zero speed, submerged runs were made after the hinge was freed up and the results of only one of the three static calibrations made was available to this study with the results tabulated in Table E4.

For a zero speed, Theodorsen's equation for flap hinge moment reduces to:

$$h = -\frac{\pi}{4}\rho Sc^3 T_3 cps^2\delta$$

$$= -\frac{1}{1/16\pi}\rho Sc^3 T_3 \omega^2\delta$$

where $\rho = 1.9384$ (assumed)

$S = 1.27$ = exposed foil area

$c = .719$ = exposed MGC

$T_3 = -.007\pi$ from Table 3-1 (E.33)

For these values Eq. (E.33) reduces to

$$h = .000396\omega^2\delta \qquad \text{(E.34)}$$

This equation is compared with the raw measured data and with that data corrected for the friction of Table II of Reference E.1 and of Eq. (E.19) of this appendix on Figure E58. The applicability of Theodorsen's equation to the 3-dimensional case is questionable, particularly at finite sumbergence, so the scatter of Figure E58 precludes conclusive judgement. Figure E58 might indicate that Theodorsen's T_3 coefficient does not apply to this case or that the hinge friction was increased some 17% in water. No significant difference between the two friction calibrations is indicated but the result does confirm that the Phases supplied are inverted.

For a zero speed, Theodorsen's equation for foil hinge moment reduces to:

$$H = \frac{1}{16}\rho Sc^3\left[T_7 + \left(\frac{h}{c} - \frac{H}{c}\right)T_\ell\right]\omega^2\delta$$

where ρ, S, and c are as for Eq. (E.33)

$$T_7 = .00428\pi \text{ from Table 3.1}$$

$$T_1 = -.02322\pi \text{ from Table 3.1} \qquad \text{(E.35)}$$

For these values Eq. (E.35) reduces to

$$H = .00523\omega^2\delta \qquad \text{(E.36)}$$

which is compared with the raw data and with two sets of corrected data on Figure E59. As for flap hinge moment, the applicability of Theodorsen's coefficients in 3-dimensions at finite submergence is in question but Figure E59 is inconclusive because of data scatter. The Reference E1 calibration appears to be preferable for amplitude but neither air calibration is adequate for phase unless there is a substantial free surface effect.

For a zero speed, Theodorsen's equation for foil lift reduces to:

$$L = \frac{1}{8}\rho S c^2 T_1 \omega^2 \delta \qquad \text{(E.37)}$$

which, for the values of Eqs. (E.33) and (E.35), reduces to

$$L = -.01161\omega^2\delta$$

$$= .01161\omega^2\delta \ \underline{/180^\circ} \qquad \text{(E.38)}$$

Eq. (E.38) is compared with the raw data and with two sets of corrected data on Figure E.60. Little choice between the air calibrations is indicated but there is an indication here that the Theodorsen coefficient does not describe the case tested. Note that for this case it was necessary to employ the phase as reported to derive a creditable result.

Unsteady Load Responses - General

The steady-state characteristics considered in the cavitation study were not of adequate confidence level to provide a basis for the measurement of unsteady load response. Those responses are considered here only to provide guidance for a new unsteady load test series. Two subjects are of particular interest in this connection:

1. The reliability of the data reduction and transmittal procedures, with particular reference to the phase angles,

2. The significance of the air calibration, including friction effects, to the measured hydrodynamic responses.

Flap Lift Response

The lift responses transmitted from NSRDC through Grumman Aero Test are presented in Table E5. The phases have been inverted and the sign reversed. Reversing the sign accounts for the difference in sign convention between Reference E.1 and this report but the source for the phase inversion has not been identified.

The data supplied has had the air calibration removed in accordance with the relationship:

$$\frac{C_{L_\delta}}{C_{L_\delta}}_{ss} = \left(\frac{C_{L_\delta}}{C_{L_\delta}}_{ss}\right)_{meas.} - \frac{C_{L_{\delta_a}}}{C_{L_\delta}}_{ss} \qquad (E.39)$$

where, from Eq. (E.32)

$$\frac{C_{L_{\delta_a}}}{C_{L_\delta}}_{ss} = \frac{L_a/qS\delta}{C_{L_\delta}}_{ss}$$

$$= \frac{.0224}{\frac{.05}{m}^2 qS\, C_{L_\delta}}_{ss} \quad \angle 161^\circ \quad \text{Before Freeing-up Hinge}$$
$$\text{After Freeing-up Hinge}$$

$$= \frac{.0224}{\frac{.05}{} \times 4\, V^2 k^2/c^2} \quad \angle 161^\circ$$
$$\frac{\rho}{2} V^2 S\, C_{L_\delta}{}_{ss}$$

$$= \frac{8 \times .05}{\rho S c^2 C_{L_{\delta_{ss}}}} \frac{.0224}{k^2} \underline{|161^\circ}$$

$$= \frac{8 \times .05}{1.938 \times 1.56 \ (.72)^2 C_{L_{\delta_{ss}}}} \frac{.0224}{k^2} \underline{|161^\circ}$$

$$= \frac{.255}{C_{L_{\delta_{ss}}}} \frac{.1142}{k^2} \underline{|161^\circ} \qquad \text{(E.40)}$$

where, from Table I of Reference E1, $C_{L_{\delta_{ss}}}$ is .0198/deg. for the low speed run and .0167/deg. for the high speed run.

The data with and without the air calibration removed are compared with the final result of Reference E1 on Figures E61 and E.62 which should also be compared with Figure 22 of Reference E1. The solid line of Figures E61 and E62 attempts to represent both test speeds after freeing up the hinge and does so on a gain/frequency plot which exaggerates the scatter at high frequency. The attenuation/wavelength presentation is preferred here because it identifies that scatter with the unbounded inertial effect at wavelengths of questionable significance. Figures E61 and E62 do, nevertheless, idicate that the air calibrations of Reference E1 and this appendix do differ substantially in their effect on the measured amplitudes though not on phase.

Figures E63 and E64 compare the flap lift hydrodynamic responses (measured less air calibration) for four runs with the result of Reference E1 and with the most appropriate predictions of Section 5 of this report. Figures E63 and E64 should be examined in connection with Figures 5-20 and 5-21. The persistent attenuation to long wavelengths may indicate the presence of air leakage. The experimental phase agreement with Theodorsen on Figure E64 is about as good as could be hoped for with this

type measurement. The various Theodorsen predictions of Figure 5-21 indicate that a 3-dimensional version of Smullin & Bender's program might well coincide with the measurements and with Theodorsen on Figure E64.

Flap Hinge Moment Response

The flap hinge moment responses transmitted from NSRDC through Grumman Aero Test are presented in Table E6. For this case it was necessary to employ the phase as reported to obtain a reasonable result.

The data supplied has had the air calibration removed in accordance with the relationship:

$$\frac{C_{h_\delta}}{C_{h_\delta}}_{ss} = \left(\frac{C_{h_\delta}}{C_{h_\delta}}_{ss}\right)_{meas} - \frac{C_{h_{\delta_a}}}{C_{h_\delta}}_{ss} \qquad (E.41)$$

where, from Eq. (E.32):

$$\frac{C_{h_{\delta_a}}}{C_{h_\delta}}_{ss} = \frac{h_a}{\frac{\rho}{2} V^2 S c \delta C_{h_\delta}}_{ss}$$

$$= \frac{.000485\, \omega^2 \delta - .1 - i\, .315^{.18}}{\frac{\rho}{2} V^2 S c \delta C_{h_\delta}}_{ss}$$

$$= \frac{8 \times .000485}{\rho S c^3 C_{h_\delta}}_{ss} k^2 - \frac{.1 + i\, .315^{.18}}{\frac{\rho}{2} V^2 S c \delta C_{h_\delta}}_{ss}$$

$$= \frac{8 \times .000485}{1.938 \times 1.56\,(.72)^3\, C_{h_{\delta_{ss}}}} k^2 - \frac{.18}{.1 + i\,.315} \Big/ .969 \times 1.56 \times .72\, V^2 \delta\, C_{h_{\delta_{ss}}}$$

$$\frac{.00344}{C_{h_{\delta_{ss}}}} \cdot^2 - \frac{.092}{C_{h_{\delta_{ss}}} V^2 \delta} - i \frac{.1656}{C_{h_{\delta_{ss}}} V^2 \delta} \quad \begin{matrix} \text{Before Freeing-up Hinge} \\ \text{After Freeing-up Hinge} \end{matrix} \qquad \text{(E.42)}$$

where, from Table I of Reference E1, $C_{h_{\delta_{ss}}}$ is -.01175/rad. for the low speed run and -.0109/rad. for the high-speed runs.

The data with and without the air calibration removed are compared with the final result of Reference E1 on Figures E65 and E66 which should also be compared with Figure 23 of Reference E1. In this case, again, a significant difference between the air calibrations of Reference E1 and of this appendix appears in amplitude but not in phase. For the flap hinge moment, however, the air calibration has a very substantial effect upon the response indicating excessive friction in comparison with the measurement.

Figures E67 and E68 compare the flap hinge moment hydrodynamic responses (measured less air calibration) for four runs with the result of Reference E1 and with the Theodorsen prediction of Section 5 of this report. Figures E67 and E68 should be compared with Figures 5-24 - 5-27. The results are totally inconclusive because of the persistent attenuation at low frequencies which might be due to differing hinge frictions in air and water (also indicated on Figure E58 or to air leakage over the flap during the steady-state and/or unsteady runs. No confident interpretation can be given the unsteady result unless the air calibration and static submerged calibration can be interpreted confidently.

Foil Pitching Moment Response

The foil pitching moment responses transmitted from NSRDC through Grumman Aero Test are presented in Table E7. For this case it was necessary to employ the phase as reported to obtain a reasonable result.

The data supplied has had the air calibration removed in accordance with the relationship:

$$\frac{C_{H_\delta}}{C_{H_{\delta_{ss}}}} = \left(\frac{C_{H_\delta}}{C_{H_{\delta_{ss}}}}\right)_{meas.} - \frac{C_{H_{\delta_a}}}{C_{H_{\delta_{ss}}}} \qquad \text{(E.43)}$$

where, from Eq. (E.32):

$$C_{H_{\delta_a}} = \frac{H_a}{qSc\delta}$$

$$= \frac{1.84}{\frac{[.00224 - 1.25]}{} + i\left[-.00568\,\omega^2\delta - .5\right]}{qSc\delta}$$

$$= \left[\frac{8 \times .00224\,k^2}{\rho S c^3} - \frac{\frac{1.84}{1.25}}{\frac{\rho}{2}V^2 S c\delta}\right] + i\left[-\frac{8 \times .00568\,k^2}{\rho S c^3} - \frac{.5}{\frac{\rho}{2}V^2 S c\delta}\right]$$

$$= \left[\frac{8 \times .00224}{1.938 \times 1.56\,(.72)^3}\,k^2 - \frac{\frac{1.84}{1.25}}{.969 \times 1.56 \times .72} \times \frac{1}{V^2\delta}\right]$$

$$+ i\left[-\frac{8 \times .00568}{1.938 \times 1.56\,(72)^3}\,k^2 - \frac{.5}{.969 \times 1.56 \times .72} \times \frac{1}{V^2\delta}\right]$$

$$= \left[.01592\,k^2 - \frac{1.69}{1.15}\right] + i\left[-.0404\,k^2 - \frac{.46}{V^2\delta}\right] \quad \begin{matrix}\text{Before Freeing-up Hinge}\\ \text{After Freeing-up Hinge}\end{matrix}$$

(E.44)

and where, from Table I of Reference E1, $C_{H_{\delta_{ss}}}$ is -.2825/rad. for the low speed run and -.275/rad. for the high speed runs.

The data with and without the air calibration removed are compared with the final result of Reference E1 on Figures E-69 and E-70 which should also be compared with

Figure 21 of Reference E1 and with Figure E56 of this appendix. For this case the air calibration has a very substantial effect upon the hydrodynamic response and the smoothed calibrations of Reference E1 and of this note produce substantially different hydrodynamic amplitudes and phases.

Figures E71 and E72 compare the foil pitching moment hydrodynamic responses (measured less air calibations) for four runs with the result of Reference E1 and with the Theodorsen prediction of Section 5 of this report. Figures E71 and E72 should be compared with Figures 5-28 and 5-29. The results are not contributory in any sense and only present a scatter about a steady-state value which has been offset by random friction values (in calibration and data runs) and/or by air leakage. The very poor results of Figures E71 and E72 give some indication that the foil pitching moment response to flap motion presents the most difficult measurement problem of those presented though it is also possible that the phase angle confusion throughout has produced an erroneous final result.

REFERENCES

E1 W. McAllister, "Results of NSRDC Tow Tank Tests on a 1/12 Scale Flapped Version of the AG(EH) Main Foil and Strut Assembly", GAC report in preparation

E2 W. C. O'Neill, "Unsteady Lift and Hinge Moment Characteristics of the AG(EH) Main Foil and Strut Assembly", NSRDC Report 2805, July 1968

E3 Richter & Palmer, "AG(EH) Hydrofoil Research Ship Hydrodynamic Report of Model Test Program", Grumman Aerospace Corporation Report M23.77, 8/21/62, Rev. 1/15/63

E4 DeYoung & Harper, "Theoretical Symmetric Span Loading at Subsonic Speeds for Wings Having Arbitrary Plan Form", NACA Report 921, 1948

E5 H. J. Allen, "Calculation of the Chordwise Load Distribution Over Airfoil Sections with Plain, Split, or Serially Hinged Trailing Edge Flaps", NACA Report 634, 1938

E6 C. E. Jones, "Flapped Hydrofoils in Smooth Water", General Dynamics/ Convair Report ZH-153, 11/61

Table E1

Steady-state Lift Data

1.14 MGC Depth

Runs	Fig.	V_{K_M}	V_K (Cav. Scale)	i deg.	α deg.	Wetted			Disturbed Slope				$\alpha^\circ + .838i^\circ$	$C_{L_\alpha}{}^\circ \times (\alpha^\circ + .838i^\circ)$	C_{L_0}	Stream-wise $d\alpha/d\delta$
						$C_{L_\delta}{}^\circ$	$d\alpha/d\delta$	$C_{L_{\delta=0}}$	Initial C_L	Initial δ°	$C_{L_\delta}{}^\circ$	$d\alpha/d\delta$				
249-253	E.1	14.7	16.4	1.25	2	.0189	.47	.183					3.048	.146	.186	.492
259-265	E.2					.0193	.48	.190	.4	11.25	.01	.249				.502
289-299	E.3					.0177	.44	.183								.46
300-308	E.4	20.9	23.3	-1.45		.0164	.408	.065					.785	.38	.42	.427
118-127	E.5	27.5	30.7	4.5	0	.0127	.316	.251					3.77	.181	.221	
128-136	E.6	32	35.7			.0154	.383	.227	.345	7.25	.0104	.259				
137-142	E.7	36.5	40.7			.0145	.361	.22								
143-150	E.8	40.9	45.7			.0122	.303	.216								
151-158	E.9	44.9	50.1			.0125	.311	.217								
183-189	E.10	32	35.7		-1.5	.0137	.341	.150					2.27	.109	.149	
190-199	E.11	36.5	40.7			.0152	.378	.138	.305	11	.0088	.219				
200-206	E.12	44.9	50.1			.0146	.363	.140								
159-166	E.13	32	35.7		-3.0	.0132	.328	.090					.77	.037	.077	
167-175	E.14	36.5	40.7			.013	.323	.090	.27	13.5	.0065	.162				
176-182	E.15	44.9	50.1			.0137	.341	.069	.187	8.5	.0062	.154				
207-213	E.16	32	35.7		1.5	.0153	.380	.290					5.27	.253	.253	
214-219	E.17	36.5	40.7			.0161	.400	.295								
220-227	E.18	44.9	50.1						$C_{L_{\delta=0}}$	=.266	.0088	.219				
228-233	E.19	32	35.7		3.0	.01665	.414	.370					6.77	.325	.365	
234-239	E.20	36.5	40.7			.0153	.381	.370								

Table E2

Flap Hinge Moment Air Calibration

BF or AF	Run No.	cps	ω $\frac{rad}{sec.}$	ω^2 $(\frac{rad}{sec})^2$	$\lvert h \rvert$ ft.-lbs.	$\angle h$ deg	$\mathcal{R}h$ ft.-lbs.	$\mathcal{I}h$ ft.-lbs.	$\lvert \delta \rvert$ deg	$\lvert \delta \rvert$ rad
BF	19	.5	3.142	9.87	.2062	-118.0	-.0968	-.1821	1.8	.0314
	20	4	25.15	632	.1992	-115.8	-.0867	-.1793	1.8	.0314
	21	6	37.7	1421	.1921	-112.1	-.0723	-.1780	1.4	.02445
	8	8.02	50.5	2550	.191	-109.8	-.0647	-.1797	1.4	.02445
	15	9	56.6	3204	.1829	-104.0	-.0442	-.1775	1.45	.0253
	9 or 10	10 or 10.01	63	3969	.1826	-101.1	-.03515	-.1792	1.35?	.02355
	11	12	75.5	5700	.1845	-90.7	-.00225	-.1845	1.2	.0209
	12	13.01	82	6724	.1829	-93.0	-.00957	-.1826	1.1?	.0192
	23	.5	3.142	9.87	.272	-114.8	-.1141	-.2469	10.4	.1815
	24	4	25.15	632	.2264	-109.8	-.0767	-.2130	8	.1395
	25	6	37.7	1421	.4044	-98.5	-.0598	-.4000	7	.1222
	26	9	56.6	3204	.187	-77.1	.0418	-.1823	5.7	.0995
	28	10.99	69	4761	.1981	-58.6	.1032	-.1691	5.1	.089
	27	12.98	81.5	6642	.2392	-46.7	.1640	-.1741	4.6	.0803
AF	241	.25	1.572	2.471	.2743	-103.6	-.0645	-.2666	3.66	.0639
	242	2.015	12.67	160.5	.3114	-105.3	-.0822	-.3004	3.625	.0632
	243	4	25.15	632	.3203	-104.1	-.0780	-.3106	2.995	.0523
	244	6	37.7	1421	.3231	-101.3	-.0633	-.3168	2.963	.0518
	245	8	50.3	2530	.315	-97.6	-.0417	-.3122	2.732	.0476
	246	10	62.85	3950	.3267	-85.1	.02791	-.3255	2.612	.0455
	247	12	75.5	5700	.3272	-80.2	.0557	-.3224	2.448	.0428
	248	13	81.7	6675	.3279	-79.3	.0609	-.3222	2.29	.04

BF = Before Freeing-up Hinge

AF = After Freeing-up Hinge

NSRDC Phase Has Been Inverted (ϕ - 180°)

Table E3

Air Calibrations

BF or AF	Run	cps	ω $\frac{rad}{sec}$	ω^2 $(\frac{rad}{sec})^2$	$\lvert H \rvert$ ft-lbs	$\angle H$ deg	$\lvert L \rvert$ lbs	$\angle L$ deg	D lbs	$\angle D$ deg	$\lvert \delta^\circ \rvert$ deg	$\lvert \delta \rvert$ rad	
	19	.5	3.142	9.87	1.613	-114.1	.0165	207.8	.0269	-281.9	1.8	.0314	
	20	4	25.15	632	1.843	-117.6	.0321	193.5	.13	-113	1.8	.0314	
	21	6	37.7	1421	2.136	-117.2	.0554	166.3	.1635	-163.3	1.4	.02445	
Before	8	8.02	50.5	2550	2.588	-118.8	1.19	157	.0406	-114.7	1.4	.02445	NSRDC
Freeing	15	9	56.6	3204	2.861	-118.2	1.785	151.9	.773	-254	1.45	.0253	Phase
Up	11	12	75.5	5700	2.523	-111.8	2.558	151.8	1.625	-188	1.2	.02095	has
Hinge	12	13.01	82	6724	3.185	-113.5	4.74		3.044	-204	1.1	.0192	been
													Inverted
	1	.505	3.175	10.08		-108.3	.01867	155.9	.00841	-252	3.7	.0646	$\phi - 180^\circ$
	2	3.01	18.92	358		-111	.0546	219.5	.123	-270.4	3.7	.0646	
	3	4.01	25.2	635		-115.4	.0568	166.9	.2423	-126.5	2.9	.0506	
	4	6.01	37.8	1429		-114.5	1.093	149.8	.183	-103.5	2.9	.0506	
	6	8.04	50.5	2550			2.735	156.2			2.7	.0471	
	7	10.03	63.1	3982		-117.9	4.35	158.1			2.5	.0436	
	17	11.02	69.4	4816		-123.9	3.48	162.7			2.55	.0445	
	18	12	75.5	5700		-119.9	5.11	164.1	3.167	-184.1	2.3	.0401	
	14	13.01	82	6724		-104.7	9.33	142.1			2.3	.0401	
	23	.5	3.142	9.87	1.715	-153.7	.0379	185.2	.0146	-311.6	10.4	.1815	

Table E3 (Continued)

BF or AF	Run	cps	ω $\frac{rad}{sec}$	ω^2 $(\frac{rad}{sec})^2$	|H| ft-lbs	$\angle$ H deg	| L| lbs	$\angle$ L deg	D lbs	$\angle$ D deg	$\|\delta^o\|$ deg	$\|\delta\|$ rad	
BF	24	4	25.15	632	2.379	-102.7	1.561	170.9	.0699	-184	8	.1397	
	25	6	37.7	1421	2.556	-148.7	6.31	172.8	.467	-119.2	7	.1223	
	26	9	56.6	3204	2.916	-108.3	6.82	169.2	1.164	-154	5.7	.0995	
	28	10.99	69	4761	2.996	-111.8	5.98	166.9	9.1	-176.1	5.1	.089	NSRDC
	27	12.98	81.5	6642	3.618	-104.3	14.13	136.8	13.53	-216.5	4.6	.0803	Phase has
After Freeing Up Hinge	241	.25	1.572	2.471	2.643	-102.5	.2797		.1325	-322.9	3.66	.0639	been
	242	2.015	12.67	160.5	2.808	-109.2	.6135	160.9	.1179		3.625	.0633	Inverted
	243	4	25.15	632	3.019	-112.8	1.516	160.9	.2288	-162.2	2.995	.0522	$\phi - 180^o$
	244	6	37.7	1421	3.339	-108.7	3.98	174.8	.2243	-139.7	2.963	.0517	
	245	8	50.3	2530	3.206	-119.4	6.37	162	.4522	-109.6	2.732	.0476	
	246	10	62.85	3950	1.672	-122.9	14.77	156.1	2.121	-60	2.612	.0455	
	247	12	75.5	5700	1.103	-129.2	11.86	163.7	4.555	-181.5	2.448	.0428	
	248	13	81.7	6675	1.04	-128.4	12.74	126.6	6.05	-281.4	2.29	.03995	

Table E4

Static Calibrations

h/c = 1.14						Before Freeing-up Hinge						
Run	cps	ω $\frac{rad}{sec}$	ω^2 $(\frac{rad}{sec})^2$	$\lvert\delta^\circ\rvert$ deg	$\lvert\delta\rvert$ rad	$\omega^2\delta$ sec^{-2}	$\lvert h\rvert$ ft. lbs.	$\angle_h$ deg *	$\lvert H\rvert$ ft. lbs	$\angle_H$ deg *	$\lvert L\rvert$ lbs.	$\angle_L$ deg
38	.5	3.142	9.87	1.85	.0323	.319	.179	-114.3	2.22	-112.4	.0718	-52.3
39	4	25.15	632	1.8[illegible]	.032	20.2	.190	-108.7	2.34	-114.3	.437	143.1
40	6	37.7	1421	1.41	.0246	35	.1845	-104.8	2.48	-116.2	.921	160
41	10	62.8	3940	1.48	.02585	101.9	.1955	-9[illegible].7	2.26	-124.9	4.71	137.6
42	13	81.7	6675	1.04	.01816	121.2	.1965	-74.1	2.38	-108.3	5.55	147.6
43	13	81.7	6676	1.39	.0243	162.3	.218	-68.5	2.43	-108.5	7.33	150.5

* Phases Supplied Have Been Inverted

Table E5

Flap Lift Response

Before Freeing-up Hinge

Comp. Run	k	h/c	V_K	Gain	MEAS $\left\|\frac{C_{L_\delta}}{C_{L_\delta}}\right\|_{ss}$	MEAS $\frac{\angle C_{L_\delta}}{C_{L_\delta}}_{ss}$ deg *	k^2	$\left\|\frac{C_{L_{\delta_a}}}{C_{L_\delta}}\right\|_{ss}$	$\frac{\angle C_{L_{\delta_a}}}{C_{L_\delta}}_{ss}$ deg	$\left\|\frac{C_{L_\delta}}{C_{L_\delta}}\right\|_{ss}$	$\frac{\angle C_{L_\delta}}{C_{L_\delta}}_{ss}$ deg	$\frac{\lambda}{c}$
228	.0326	1.14	20.5	-1.372	.854	3.81	.001064	.000127	161	.854	3.81	96.4
229	.064			-1.22	.869	4.39	.0041	.00049		.869	4.38	49
230	.1275			-1.56	.836	6.91	.01626	.00194		.838	6.85	24.6
231	.1909			-1.979	.796	6.61	.03644	.00436		.800	6.47	16.45
232	.2533			-1.066	.884	7.81	.0642	.00767		.891	7.59	12.38
233	.3180			-1.756	.817	8.09	.1011	.0121		.828	7.71	9.38
234	.3842			-1.325	.858	9.51	.1476	.0176		.873	8.96	8.4
235	.4477			-1.347	.856	7.49	.2004	.024		.877	6.79	7.01
236	.576			-.2304	.974	13.89	.3318	.0397		1.007	12.66	5.45
237	.707			-.1021	.988	14.89	.5	.0598		1.038	13.05	4.44
238	.833			-.523	.942	46.31	.694	.0829		.979	41.90	3.77
239	.032	.57		-1.771	.815	4.49	.00102	.000122		.815	4.49	98
240	.0639			-1.821	.811	4.91	.00408	.000488		.811	4.90	49.1
241	.1277			-2.206	.776	5.29	.01631	.00195		.778	5.23	24.6
242	.19			-2.317	.766	5.59	.0361	.00431		.770	5.46	16.53
243	.254			-1.973	.797	5.51	.0645	.00771		.804	5.28	12.37

Table E5 (Continued)

Comp. Run	k	h/c	V_K	Gain	MEAS $\left\|\frac{C_{L_\delta}}{C_{L_\delta}}\right\|_{ss}$	MEAS $\angle\frac{C_{L_\delta}}{C_{L_\delta}}_{ss}$ deg *	k^2	$\left\|\frac{C_{L_{\delta_a}}}{C_{L_\delta}}\right\|_{ss}$	$\angle\frac{C_{L_{\delta_a}}}{C_{L_\delta}}_{ss}$ deg	$\left\|\frac{C_{L_\delta}}{C_{L_\delta}}\right\|_{ss}$	$\angle\frac{C_{L_\delta}}{C_{L_\delta}}_{ss}$ deg	$\frac{\lambda}{c}$
244	.3343	.57	20.5	-1.263	.865	4.89	.1118	.01337	161	.877	4.54	9.38
245	.3846			-2.413	.757	8.61	.1479	.01765		.773	8.00	8.15
246	.4462			-1.869	.806	5.19	.1991	.0238		.828	4.51	7.04
247	.5762			-.908	.901	9.91	.332	.0397		.936	8.73	5.45
248	.7019			-1.288	.862	12.39	.493	.0589		.913	10.46	4.46

* Reported Phase Inverted and Sign Reversed.

$$\frac{C_{L_{\delta_a}}}{C_{L_\delta}}_{ss} = \frac{.1142}{.255}\,k^2\ \angle -161^\circ \qquad \text{(Eq. E.40)}$$

Before Freeing-up Hinge
After Freeing-up Hinge

where C_{L_δ} = 1.135 for runs 400 - 423
.957 for runs 228 - 248 and 444 - 454

$$\frac{C_{L_\delta}}{C_{L_\delta}}_{ss} = \left(\frac{C_{L_\delta}}{C_{L_\delta}}\right)_{ss\ MEAS} - \frac{C_{L_{\delta_a}}}{C_{L_\delta}}_{ss}$$

$$\frac{\lambda}{c} = \frac{\pi}{k}$$

Table E5 (Continued)

Flap Lift Response

After Freeing-up Hinge

Comp. Run	k	h/c	V_K	Gain	MEAS $\left\|\frac{C_{L_\delta}}{C_{L_\delta}}\right\|_{ss}$	MEAS $\frac{\angle C_{L_\delta}}{C_{L_\delta}}_{ss}$ deg *	k^2	$\left\|\frac{C_{L_{\delta_a}}}{C_{L_\delta}}\right\|_{ss}$	$\frac{\angle C_{L_{\delta_a}}}{C_{L_\delta}}_{ss}$ deg.	$\left\|\frac{C_{L_\delta}}{C_{L_\delta}}\right\|_{ss}$	$\frac{\angle C_{L_\delta}}{C_{L_\delta}}_{ss}$ deg	$\frac{\lambda}{c}$
400	.0256	1.14	14.2	-.1115	.987	1.81	.00066	.0001485	161	.987	1.81	122.5
401	.0459			.2264	1.026	3.31	.00211	.000474		1.026	3.30	68.5
402	.0923			-.3486	.961	4.79	.00852	.001915		.963	4.74	34
403	.1388			-.3204	.964	5.09	.01927	.00434		.968	4.98	22.6
404	.1848			-.513	.943	4.31	.03415	.00767		.950	4.13	17
405	.23			-.447	.950	3.39	.0529	.0119		.961	3.12	13.65
406	.275			-.862	.905	2.89	.0756	.017		.921	2.50	11.4
407	.3217			-.677	.925	4.61	.1035	.0233		.946	4.04	9.77
408	.3668			-.758	.916	2.49	.1345	.03025		.944	1.82	8.55
409	.4087			-1.013	.890	7.09	.1670	.0376		.924	6.06	7.68
410	.4548			-.605	.933	6.81	.2068	.0465		.975	5.62	6.9
411	.5021			-.896	.902	4.89	.2521	.0566		.954	3.51	6.25
412	.5473			-1.102	.881	7.41	.2995	.0674		.942	5.59	5.74
413	.5913			-.662	.927	6.21	.3496	.0785		.999	4.29	5.3
414	.6354			-.4027	.955	6.89	.4037	.0907		1.037	4.70	4.95
415	.7262			-.3979	.955	2.69	.5274	.1187		1.066	.33	4.31

Table E5 (Continued)

Comp. Run	k	h/c	V_K	Gain	MEAS $\frac{C_{L_\delta}}{C_{L_\delta}}_{ss}$	MEAS $\frac{\angle C_{L_\delta}}{C_{L_\delta}}_{ss}$ deg *	k^2	$\left\|\frac{C_{L_{\delta_a}}}{C_{L_\delta}}\right\|_{ss}$	$\frac{\angle C_{L_{\delta_a}}}{C_{L_{\delta_a}}}_{ss}$ deg	$\left\|\frac{C_{L_\delta}}{C_{L_\delta}}\right\|_{ss}$	$\frac{\angle C_{L_\delta}}{C_{L_\delta}}_{ss}$ deg	$\frac{\lambda}{c}$
416	.8211	1.14	14.2	.1675	1.019	5.21	.674	.1515	161	1.159	2.14	3.82
417	.9127			-.917	.900	20.39	.833	.187		1.051	13.91	3.44
418	1			-1.598	.832	10.31	1	.225		1.034	4.19	3.14
419	.8203			.2152	1.025	4.91	.673	.1513		1.165	1.89	3.83
420	.9152			-.905	.901	21.41	.838	.1885		1.052	14.74	3.43
421	1.005			-1.575	.834	7.69	1.010	.227		1.042	2.07	3.12
422	1.095			.2078	1.024	11.49	1.199	.27		1.264	5.27	2.87
423	1.192			.605	1.072	25.61	1.421	.32		1.319	15.8	2.63
444	.0315		20.5	-1.285	.862	4.61	.00099	.000264		.862	4.60	99.7
445	.0642			-.9	.902	7.11	00412	.0011		.903	7.08	48.9
446	.1288			-1.503	.841	4.99	.01659	.00443		.845	4.87	24.4
447	.1918			-1.873	.806	8.41	.03679	.00983		.815	8.09	16.37
448	.2546			-1.077	.883	14.51	.0648	.0173		.897	13.90	12.34
449	.3199			-1.67	.825	9.71	.1023	.02735		.849	8.82	9.8
450	.3833			-1.333	.858	9.91	.1469	.0392		.892	8.69	8.2
451	.447			-.902	.901	8.09	.1998	.0534		.948	7.48	7.03
452	.5758			.2451	1.029	13.81	.3315	.0885		1.104	11.32	5.45
453	.704			-1.161	.875	17.29	496	.1325		.985	12.72	4.46
454	.833			-.483	.946	46.81	.694	.185		1.036	37.43	3.77

Table E6

Flap Hinge Moment Response

Before Freeing-up Hinge

Comp. Run	k	h/c	V_K	Gain	MEAS $\left\lvert \frac{C_{h_\delta}}{C_{h_{\delta_{ss}}}} \right\rvert$	MEAS $\frac{\angle C_{h_\delta}}{C_{h_{\delta_{ss}}}}$ deg *	$\frac{\Re C_{h_{\delta_a}}}{C_{h_{\delta_{ss}}}}$	$\frac{\Im C_{h_{\delta_a}}}{C_{h_{\delta_{ss}}}}$	$\left\lvert \frac{C_{h_\delta}}{C_{h_{\delta_{ss}}}} \right\rvert$	$\frac{\angle C_{h_\delta}}{C_{h_{\delta_{ss}}}}$	$\frac{\lambda}{c}$	Flap Ampl $\lvert\delta\rvert$ deg
228	.0326	1.14	20.5	1.918	1.247	32.30	.2137	.3845	.8863	18.54	96.4	1.8
229	.064			1.899	1.244	24.60	.2127		.928	8.26	49	
230	.1275			2.096	1.273	32.00	.2089		.918	18.43	24.6	
231	.1909			1.706	1.217	35.50	.2025		.852	22.23	16.45	
232	.2533			2.325	1.307	37.80	.1938		.937	26.41	12.38	
233	.3180			2.24	1.294	40.50	.1821		.922	29.62	9.88	
234	.3842			3.51	1.498	44.00	.228	.494	1.010	32.76	8.4	1.4
235	.4477			3.378	1.475	47.10	.2112		.986	36.49	7.01	
236	.576			3.789	1.547	54.43	.1697		1.057	46.31	5.45	
237	.707			4.274	1.636	62.13	.1381	.532	1.108	55.57	4.44	1.3
238	.833			4.1	1.603	69.70	.077		1.083	63.75	3.77	
239	.042	.57		1.075	1.132	29.70	.2957		.6882	2.40	98	
240	.0639			1.113	1.137	30.50	.2947		.686	3.76	49.1	
241	.1277			1.759	1.224	33.40	.2908		.745	10.98	24.6	
242	.19			1.187	1.146	34.70	.2846		.668	10.37	16.53	
243	.254			1.467	1.184	38.10	.2756		.685	16.84	12.37	

Table E6 (Continued)

Comp. Run	k	h/c	V_K	Gain	MEAS $\left\lvert \frac{C_{h_\delta}}{C_{h_{\delta_{ss}}}} \right\rvert$	MEAS $\angle \frac{C_{h_\delta}}{C_{h_{\delta_{ss}}}}$ deg *	$\Re \frac{C_{h_{\delta_a}}}{C_{h_{\delta_{ss}}}}$	$\Im \frac{C_{h_{\delta_a}}}{C_{h_{\delta_{ss}}}}$	$\left\lvert \frac{C_{h_\delta}}{C_{h_{\delta_{ss}}}} \right\rvert$	$\angle \frac{C_{h_\delta}}{C_{h_{\delta_{ss}}}}$	$\frac{\lambda}{c}$	Flap Ampl $\lvert\delta\rvert$ deg
244	.3343	.57	20.5	2.976	1.409	39.50	.2607	.532	.903	23.78	9.38	1.3
245	.3846			2.928	1.401	42.20	.2094	.46	.958	30.14	8.15	1.5
246	.4462			3.39	1.477	43.73	.1931		1.039	32.69	7.04	
247	.5762			3.539	1.472	49.46	.1512		1.041	39.19	5.45	
248	.7019			3.629	1.519	55.70	.1005		1.097	46.45	4.46	

* Reported Phase

$$\frac{C_{h_{\delta_a}}}{C_{h_{\delta_{ss}}}} = \frac{.00344}{C_{h_{\delta_{ss}}}} k^2 - \frac{.092}{C_{h_{\delta_{ss}}} V^2\delta} - i \frac{\begin{matrix}.1656 \\ .29\end{matrix}}{C_{h_{\delta_{ss}}} V^2\delta}$$ Before Freeing Hinge / After Freeing Hinge (Eq. E.42)

where $C_{h_{\delta_{ss}}}$ = -.0109 for runs 228 - 248 and 444 - 454.
$C_{h_{\delta_{ss}}}$ = -.01175 for runs 400 - 423

$$\frac{C_{h_\delta}}{C_{h_{\delta_{ss}}}} = \left(\frac{C_{h_\delta}}{C_{h_{\delta_{ss}}}}\right)_{meas} - \frac{C_{h_{\delta_a}}}{C_{h_{\delta_{ss}}}}$$

$$\frac{\lambda}{c} = \frac{\pi}{k}$$

Table E6 (Continued)

Flap Hinge Moment Response

After Freeing-up Hinge

Comp Run No.	k	h/c	V_K	Flap Ampl $\lvert\delta\rvert$ deg	Gain	MEAS $\left\lvert \frac{C_{h_\delta}}{C_{h_{\delta_{ss}}}} \right\rvert$	MEAS $\frac{\angle C_{h_\delta}}{C_{h_{\delta_{ss}}}}$ deg *	$\Re\frac{C_{h_{\delta_a}}}{C_{h_{\delta_{ss}}}}$	$\Im\frac{C_{h_{\delta_a}}}{C_{h_{\delta_{ss}}}}$	$\left\lvert \frac{C_{h_\delta}}{C_{h_{\delta_{ss}}}} \right\rvert$	$\frac{\angle C_{h_\delta}}{C_{h_{\delta_{ss}}}}$	$\frac{\lambda}{c}$
400	.0256	1.14	14.2	3.7	1.422	1.178	19.3	.1963	.620	.944	-14.14	122.5
401	.0459				2.319	1.306	30.8	.1959		.927	3.01	68.5
402	.0923				2.984	1.410	35.33	.1940		.976	11.55	34.0
403	.1388				3.327	1.467	38.6	.1909		1.000	17.17	22.6
404	.1848				3.693	1.530	39.1	.1865		1.059	19.02	17.0
405	.23				3.66	1.524	41.4	.1810		1.037	21.95	13.65
406	.275				3.707	1.532	42.3	.1744		1.043	23.21	11.40
407	.3217				4.004	1.586	45.2	.1662		1.077	27.98	9.77
408	.3668			2.9	4.23	1.826	51	.2117	.790	1.129	33.86	8.55
409	.4087				5.29	1.839	51.6	.2021		1.144	34.71	7.68
410	.4548				5.13	1.805	52.8	.1905		1.109	35.72	6.90
411	.5021				5.48	1.879	54.83	.1773		1.173	39.50	6.25
412	.5473				5.5	1.884	55.2	.1635		1.185	39.70	5.74
413	.5913				5.5	1.884	57	.1460		1.183	41.91	5.30
414	.6354				5.31	1.843	59.9	.1330		1.128	45.47	4.95
415	.7262				5.92	1.977	60.23	.0970		1.281	46.31	4.31

Table E6 (Continued)

Comp Run No.	k	h/c	V_K	Flap Ampl $\lvert\delta\rvert$ deg	Gain	MEAS $\left\lvert \frac{C_{h_\delta}}{C_{h_{\delta_{ss}}}} \right\rvert$	MEAS $\angle \frac{C_{h_\delta}}{C_{h_{\delta_{ss}}}}$ deg *	$\Re \frac{C_{h_{\delta_a}}}{C_{h_{\delta_{ss}}}}$	$\lambda \frac{C_{h_{\delta_a}}}{C_{h_{\delta_{ss}}}}$	$\left\lvert \frac{C_{h_\delta}}{C_{h_{\delta_{ss}}}} \right\rvert$	$\angle \frac{C_{h_\delta}}{C_{h_{\delta ss}}}$	$\frac{\lambda}{c}$
416	.8211	1.14	14.2	2.9	6.21	2.044	63.9	.0540	.790	1.344	51.05	3.82
417	.9127				6.22	2.046	66.53	.0080		1.353	53.41	3.44
418	1				6.28	2.061	68.8	-.0415		1.378	55.19	3.14
419	.8203			2.4	6.79	2.185	65.5	.1073	.956	1.305	52.27	3.83
420	.9152				6.79	2.185	67.8	.0590		1.314	54.30	3.43
421	1.005				7.13	2.272	68.93	.0090		1.417	55.24	3.12
422	1.095				7.12	2.270	70.5	-.0460		1.431	55.82	2.87
423	1.192				6.82	2.193	76.2	-.1120		1.334	61.58	2.63
444	.0315		20.5	1.8	.616	1.073	33.8	.2137	.675	.682	-6.57	99.7
445	.0642				1.339	1.167	34	.2010		.767	-1.68	48.9
446	.1288				2.681	1.362	37.9	.1620		.927	10.04	24.4
447	.1918				2.49	1.332	41.5	.2024		.822	14.63	16.37
448	.2546				2.833	1.386	41.8	.1935		.876	16.50	12.34
449	.3199				3.041	1.419	42.2	.1817		.913	17.74	9.80
450	.3833			1.4	4.3	1.641	46	.2281	.866	.964	19.03	8.20
451	.447				4.37	1.654	49.9	.2115		.943	25.06	7.03
452	.5758				4.78	1.734	52	.1698		1.028	29.13	5.45
453	.704				4.88	1.754	56	.1180		1.044	34.28	4.46
454	.833				4.32	1.644	63.4	.0555		.910	41.59	3.77

Table E7

Foil Pitching Moment Response

Before Freeing-up Hinge

Comp. Run No.	k	h/c	V_K	Flap Ampl $\lvert\delta\rvert$ deg	Gain	MEAS $\left\lvert \frac{C_{H_\delta}}{C_{h_\delta}} \right\rvert_{ss}$	* MEAS $\angle \frac{C_{H_\delta}}{C_{h_\delta}}{}_{ss}$ deg	$\left\lvert \frac{C_{H_{\delta_a}}}{C_{H_\delta}} \right\rvert_{ss}$	$\angle \frac{C_{H_{\delta_a}}}{C_{H_\delta}}{}_{ss}$	$\left\lvert \frac{C_{H_\delta}}{C_{H_\delta}} \right\rvert_{ss}$	$\angle \frac{C_{H_\delta}}{C_{H_\delta}}{}_{ss}$ deg	$\frac{\lambda}{c}$
228	.0326	1.14	20.5	1.8	-1.245	.866	-5.1	.1612	15.28	.717	-9.59	96.4
229	.064				-1.504	.841	-16.7	.161	15.47	.710	-23.63	49.0
230	.1275				-1.8	.813	-11.1	.1608	16.15	.674	-17.37	24.6
231	.1909				-2.466	.753	-12.4	.1608	17.27	.618	-19.79	16.45
232	.2533				-1.828	.810	-12.0	.1608	18.83	.677	-18.99	12.38
233	.3180				-1.604	.831	-13.1	.1603	20.91	.704	-20.42	9.88
234	.3842			1.4	-1.516	.840	-13.0	.206	21.69	.681	-22.92	8.40
235	.4477				-1.849	.808	-11.4	.206	24.03	.651	-21.97	7.01
236	.576				-1.513	.840	-12.0	.208	29.76	.699	-23.43	5.45
237	.707			1.3	-2.176	.778	-7.7	.2285	35.32	.630	-22.01	4.44
238	.833				-2.378	.760	-17.6	.2375	42.43	.673	-35.39	3.77
239	.032	.57			-1.296	.861	-5.8	.2235	15.27	.657	-12.52	98.0
240	.0639				-1.653	.827	-8.0	.223	15.40	.629	-16.10	49.1
241	.1277				-1.587	.833	-7.5	.2225	15.90	.614	4.46	24.6
242	.19				-1.71	.821	-10.3	.2225	16.70	.609	7.93	16.52

Table E7 (Continued)

Comp. Run No.	k	h/c	V_K	Flap Ampl $\lvert\delta\rvert$ deg	Gain	MEAS $\left\lvert \frac{C_{H_\delta}}{C_{h_\delta}} \right\rvert_{ss}$	* MEAS $\angle \frac{C_{H_\delta}}{C_{h_\delta}}$ deg	$\left\lvert \frac{C_{H_{\delta_a}}}{C_{H_\delta}} \right\rvert_{ss}$	$\angle \frac{C_{H_{\delta_a}}}{C_{H_\delta}}$	$\left\lvert \frac{C_{H_\delta}}{C_{H_\delta}} \right\rvert_{ss}$	$\angle \frac{C_{H_\delta}}{C_{H_\delta}}$ deg	$\frac{\lambda}{c}$
243	.254	.57	20.5	1.3	-1.912	.802	-9.2	.2220	17.84	.613	-18.68	12.37
244	.3343				-.333	.962	-7.6	.2220	19.76	.772	-15.20	9.38
245	.3846			1.5	-1.632	.829	-2.3	.1925	22.10	.658	-9.24	8.15
246	.4462				-1.167	.874	-10.6	.1925	24.56	.725	-19.39	7.04
247	.5762				-.562	.937	-7.2	.1950	30.71	.792	-15.90	5.45
248	.7019				-1.234	.868	-8.1	.2005	37.85	.743	-19.29	4.46

* Reported Phase

$$C_{H_{\delta_a}} = \left[.01592k^2 - \frac{1.69}{1.15 V^2_\delta} \right] + i \left[-.0404k^2 - \frac{.46}{V^2_\delta} \right]$$

Before Freeing-up Hinge
After Freeing-up Hinge

(Eq. E.44)

$C_{H_\delta}{}_{ss}$ = -.275 for runs 228 - 248 and 444 - 454

$C_{H_\delta}{}_{ss}$ = -.2825 for runs 400 - 423

$$\frac{C_{H_\delta}}{C_{H_\delta}{}_{ss}} = \left(\frac{C_{H_\delta}}{C_{H_\delta}{}_{ss}} \right)_{meas} - \frac{C_{H_{\delta_a}}}{C_{H_\delta}{}_{ss}}$$

$$\frac{\lambda}{c} = \frac{\pi}{k}$$

Table E7 (Continued)

Foil Pitching Moment Response

After Freeing-up Hinge

Comp. Run No.	k	h/c	V_K	Flap Ampl $\lvert\delta\rvert$ deg	Gain	MEAS $\left\lvert \frac{C_{H_\delta}}{C_{H_\delta}} \right\rvert_{ss}$	MEAS $\angle \frac{C_{H_\delta}}{C_{H_\delta}}_{ss}$ deg	$\left\lvert \frac{C_{H_{\delta_a}}}{C_{H_\delta}} \right\rvert_{ss}$	$\angle \frac{C_{H_{\delta_a}}}{C_{H_\delta}}_{ss}$ deg	$\left\lvert \frac{C_{H_\delta}}{C_{H_\delta}} \right\rvert_{ss}$	$\angle \frac{C_{H_\delta}}{C_{H_\delta}}_{ss}$ deg	$\frac{\lambda}{c}$
400	.0256	1.14	14.2	3.7	-.524	.941	-6.9	.1100	21.84	.846	-10.48	122.5
401	.0459				-.3039	.966	-7.0	.1100	21.94	.871	-10.50	68.5
402	.0923				-.4500	.949	-6.6	.1103	22.45	.854	-10.19	34.0
403	.1388				-.3728	.958	-7.4	.1103	23.33	.865	-11.14	22.6
404	.1848				-.457	.949	-7.4	.1103	24.51	.857	-11.30	17.0
405	.2300				-.499	.944	-6.7	.1105	25.99	.853	-10.71	13.65
406	.2750				-.545	.939	-6.0	.1108	27.81	.837	3.18	11.40
407	.3217				-.2993	.966	-7.0	.1113	30.00	.880	-11.37	9.77
408	.3668			2.9	-1.384	.853	-8.3	.1420	30.14	.747	-15.09	8.55
409	.4087				-1.254	.866	-6.8	.1430	32.13	.760	-13.59	7.68
410	.4548				-1.200	.871	-9.0	.1440	34.54	.773	-16.37	6.90
411	.5021				-1.087	.882	-7.5	.1460	37.17	.785	-15.01	6.25
412	.5473				-1.025	.889	-7.3	.1480	39.90	.797	-15.69	5.74
413	.5913				-1.139	.877	-8.0	.1510	42.68	.790	-16.50	5.30
414	.6354				-1.211	.870	-6.6	.1537	45.56	.785	-15.49	4.95
415	.7262				-.85	.907	-2.5	.1623	51.70	.823	-11.71	4.31

Table E7 (Continued)

Comp. Run No.	k	h/c	V_K	Flap Ampl $\lvert\delta\rvert$ deg	Gain	MEAS $\lvert \frac{C_{H_\delta}}{C_{H_\delta}} \rvert_{ss}$	MEAS $\angle \frac{C_{H_\delta}}{C_{H_\delta}}_{ss}$ deg	$\lvert \frac{C_{H_{\delta_a}}}{C_{H_\delta}} \rvert_{ss}$ deg	$\angle \frac{C_{H_{\delta_a}}}{C_{H_\delta}}_{ss}$ deg	$\lvert \frac{C_{H_\delta}}{C_{H_{\delta_{ss}}}} \rvert$	$\angle \frac{C_{H_\delta}}{C_{H_\delta}}_{ss}$ deg	$\frac{\lambda}{c}$
416	.8211	1.14	14.2	2.9	-.1518	.983	-2.1	.1750	58.04	.909	-11.71	3.82
417	.9127				-1.244	.86	-5.2	.1905	63.97	.819	-17.76	3.44
418	1				-.414	.953	1.0	.2055	68.86	.896	-11.26	3.14
419	.8203			2.4	-.768	.915	-3.1	.2015	52.28	.817	-14.80	3.83
420	.9152				-2.226	.774	-6.0	.2135	58.91	.710	-21.80	3.43
421	1.005				-.915	.900	1.2	.2305	64.13	.821	-13.27	3.12
422	1.095				1.294	1.161	-1.6	.2495	69.77	1.107	-13.93	2.87
423	1.192				1.110	1.136	-8.8	.2775	73.78	1.134	-22.84	2.63
444	.0315		20.5	1.8	-1.941	.800	2.7	.1138	21.90	.693	-.39	99.7
445	.0642				-1.170	.874	-180.0	.1138	22.15	.980	-177.49	48.9
446	.1288				-.937	.898	.3	.1138	23.13	.794	-2.89	24.4
447	.1918				-1.946	.799	-.2	.1140	24.74	.697	-4.15	16.37
448	.2546				-1.289	.862	-3.0	.1144	26.95	.765	-7.28	12.34
449	.3199				-.804	.912	-7.0	.1152	29.88	.823	-11.82	9.89
450	.3833			1.4	-1.597	.832	-4.0	.1482	30.84	.715	-10.80	8.20
451	.4470				-1.858	.807	-1.8	.1500	33.98	.691	-9.09	7.05
452	.5758				-.496	.944	1.0	.1560	41.47	.831	-5.99	5.45
453	.7040				-.1354	.984	.4	.1663	49.91	.885	-7.81	4.16
454	.8330				-1.172	.874	-8.0	.1830	58.48	.818	-19.83	3.77

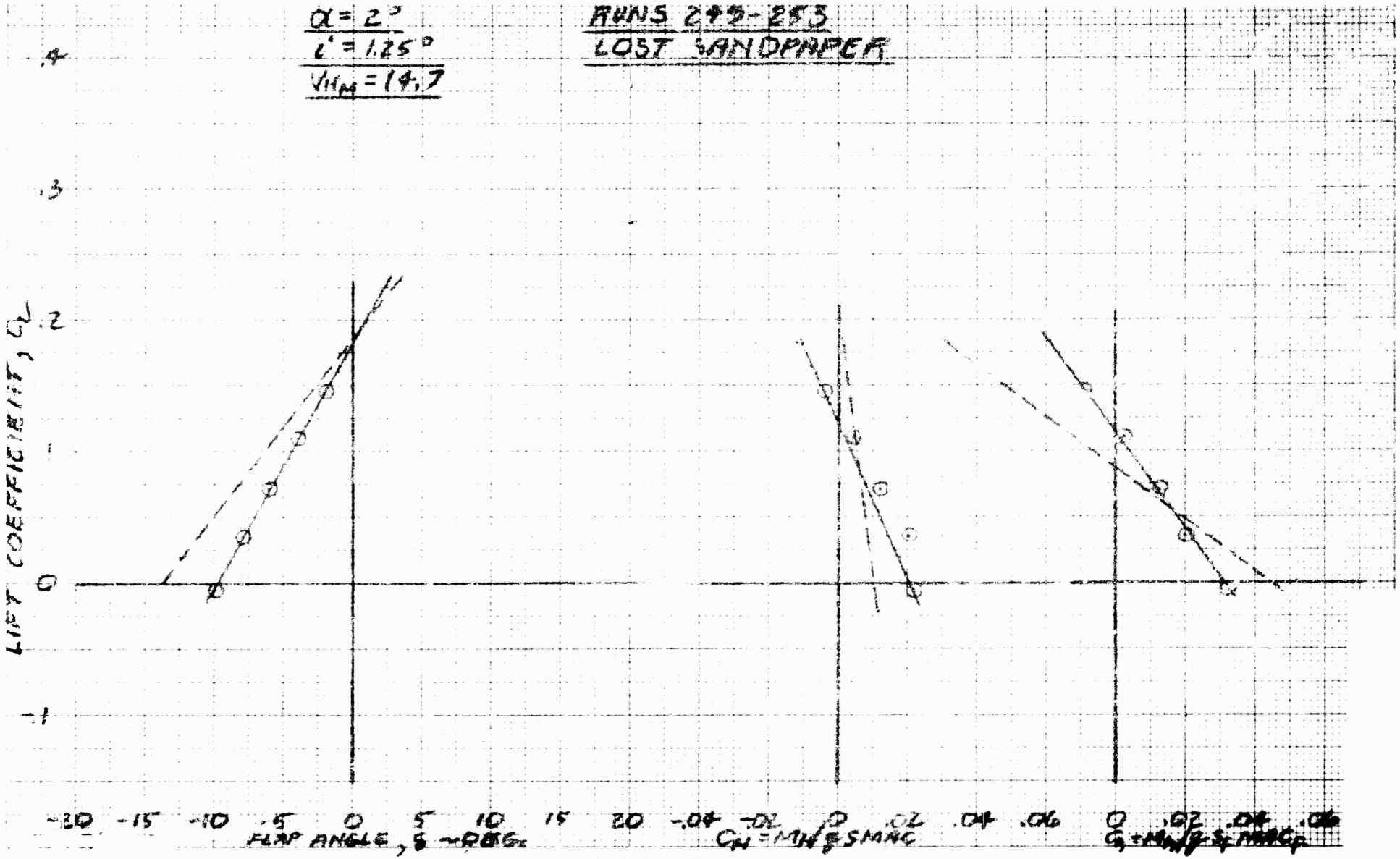


Figure E1. Froude Scaled Test Results, 14.7 Knots, Lost Sandpaper

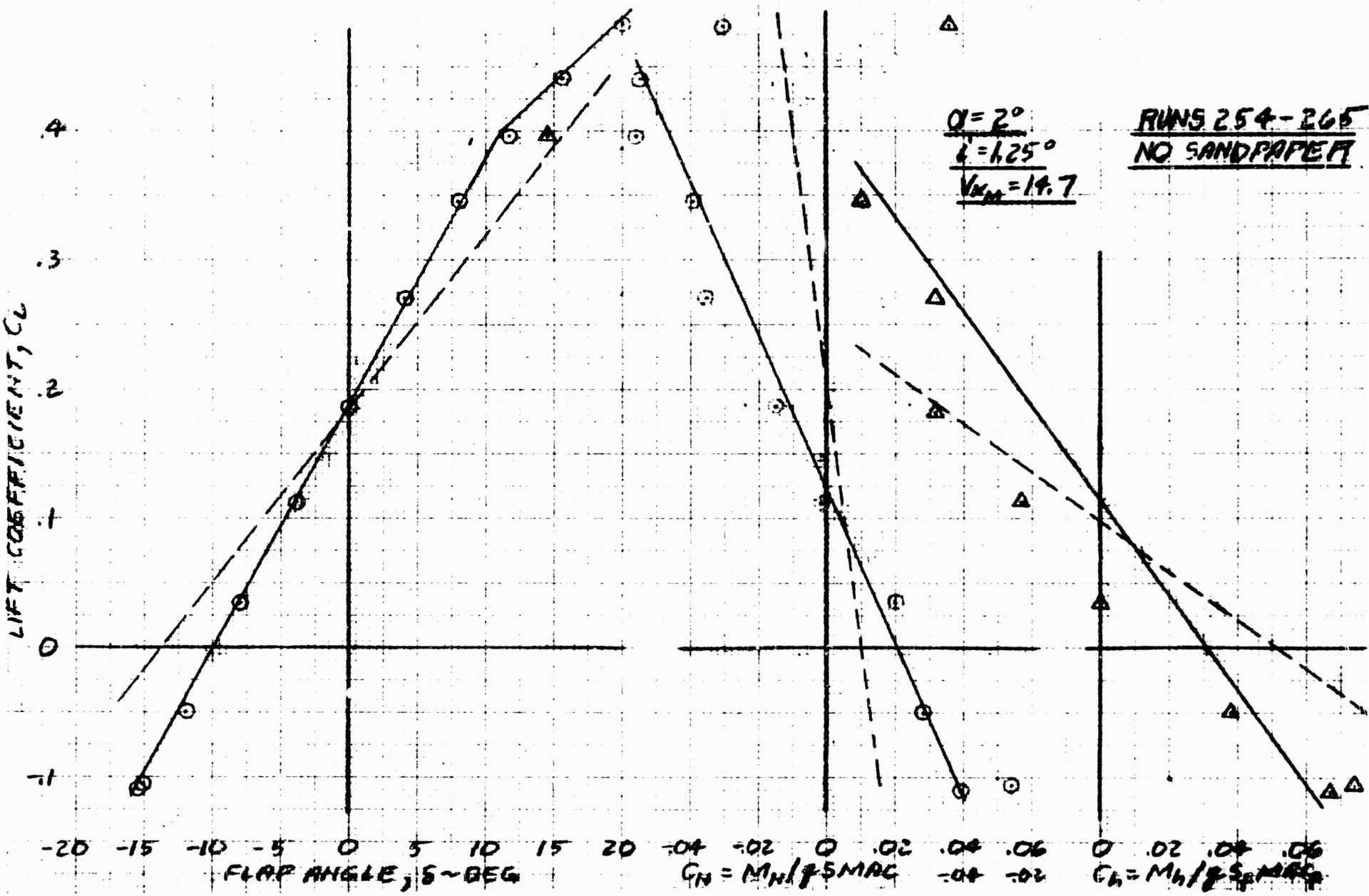


Figure E-. Froude Scaled Test Results, 14.7 Knots, No Sandpaper

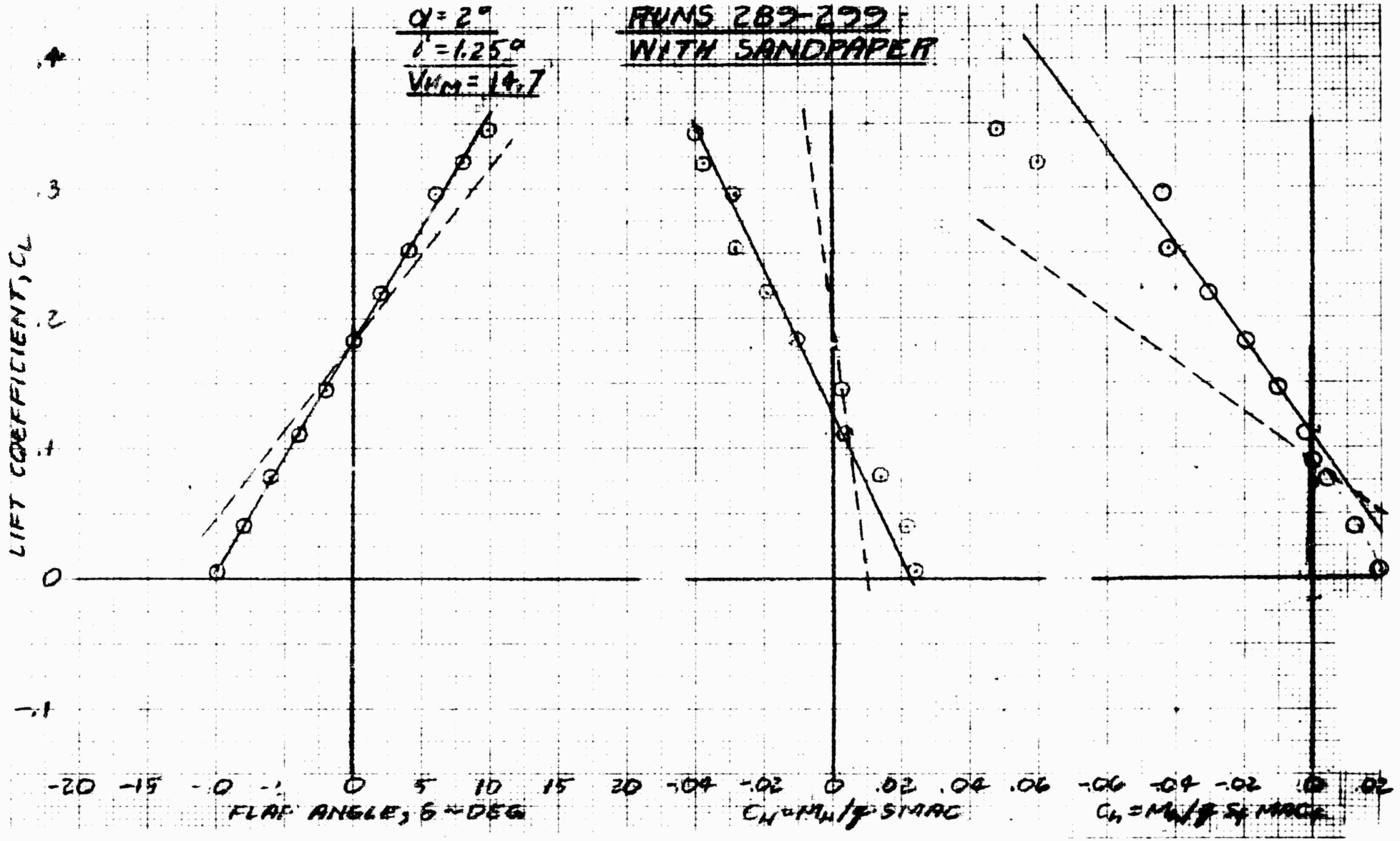


Figure E3. Froude Scaled Test Results, 14.7 Knots, With Sandpaper

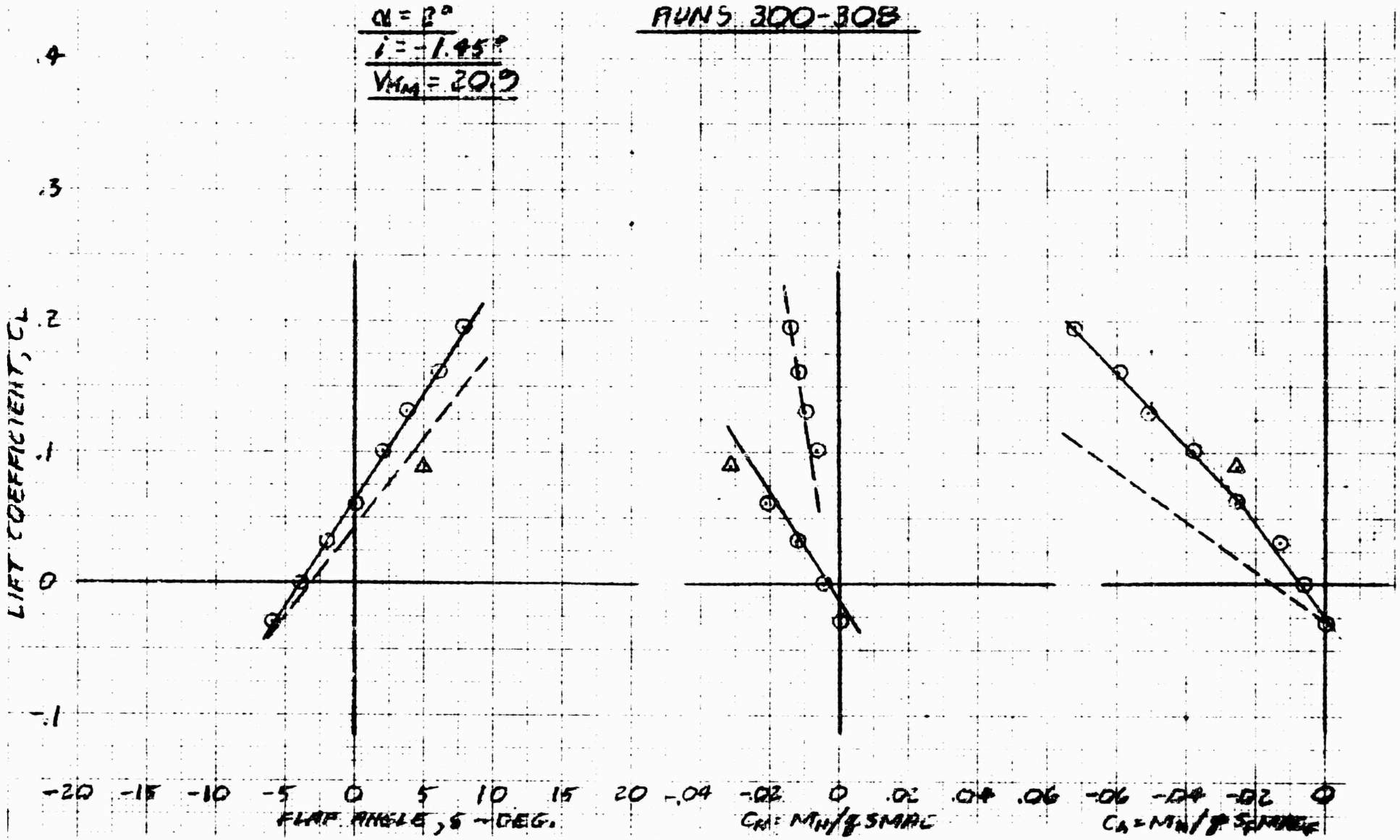


Figure E4. Froude Scaled Test Results, 20.9 Knots

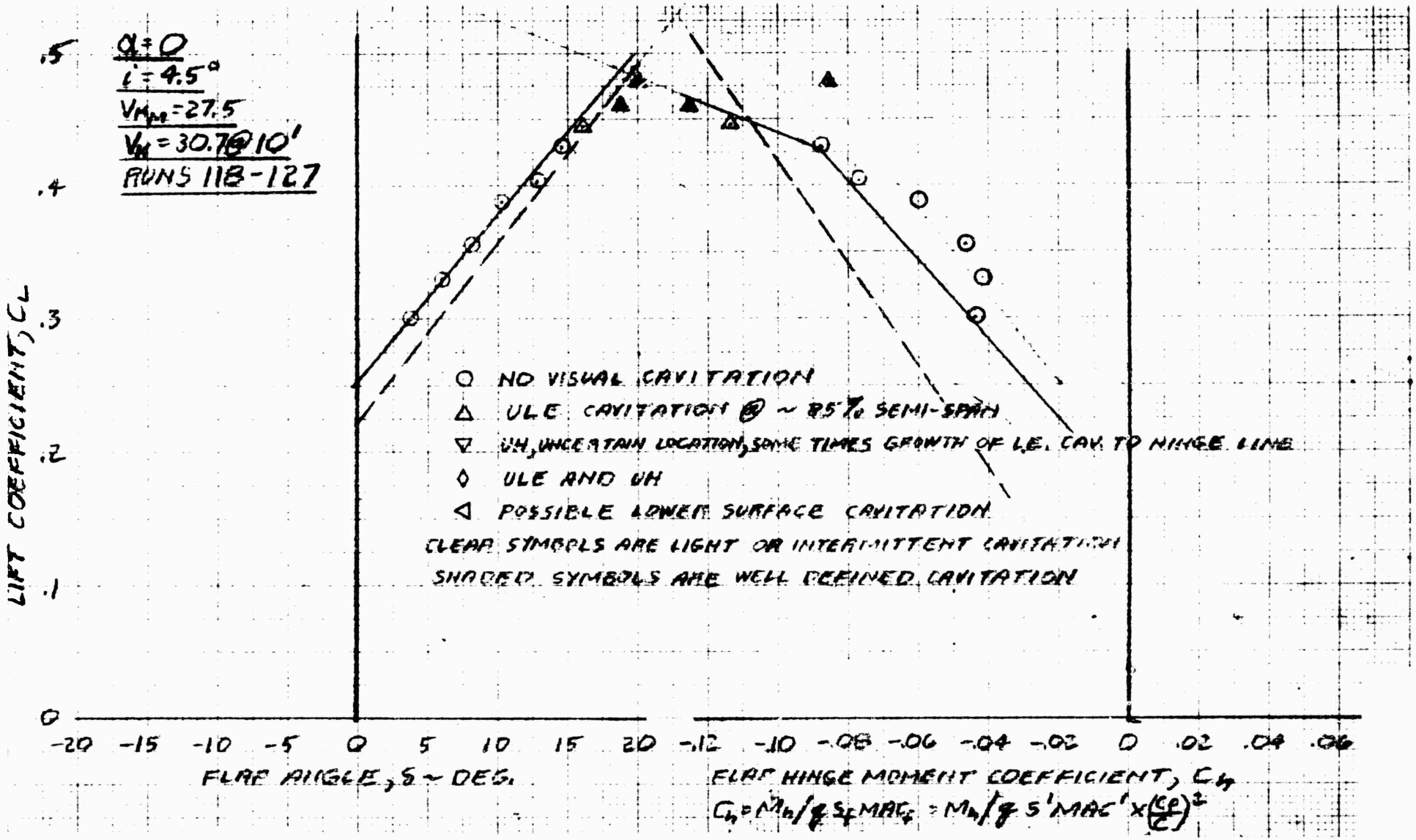


Figure E5. Cavitation Scaled Test Results, 27.5 Knots, $\alpha = 0$

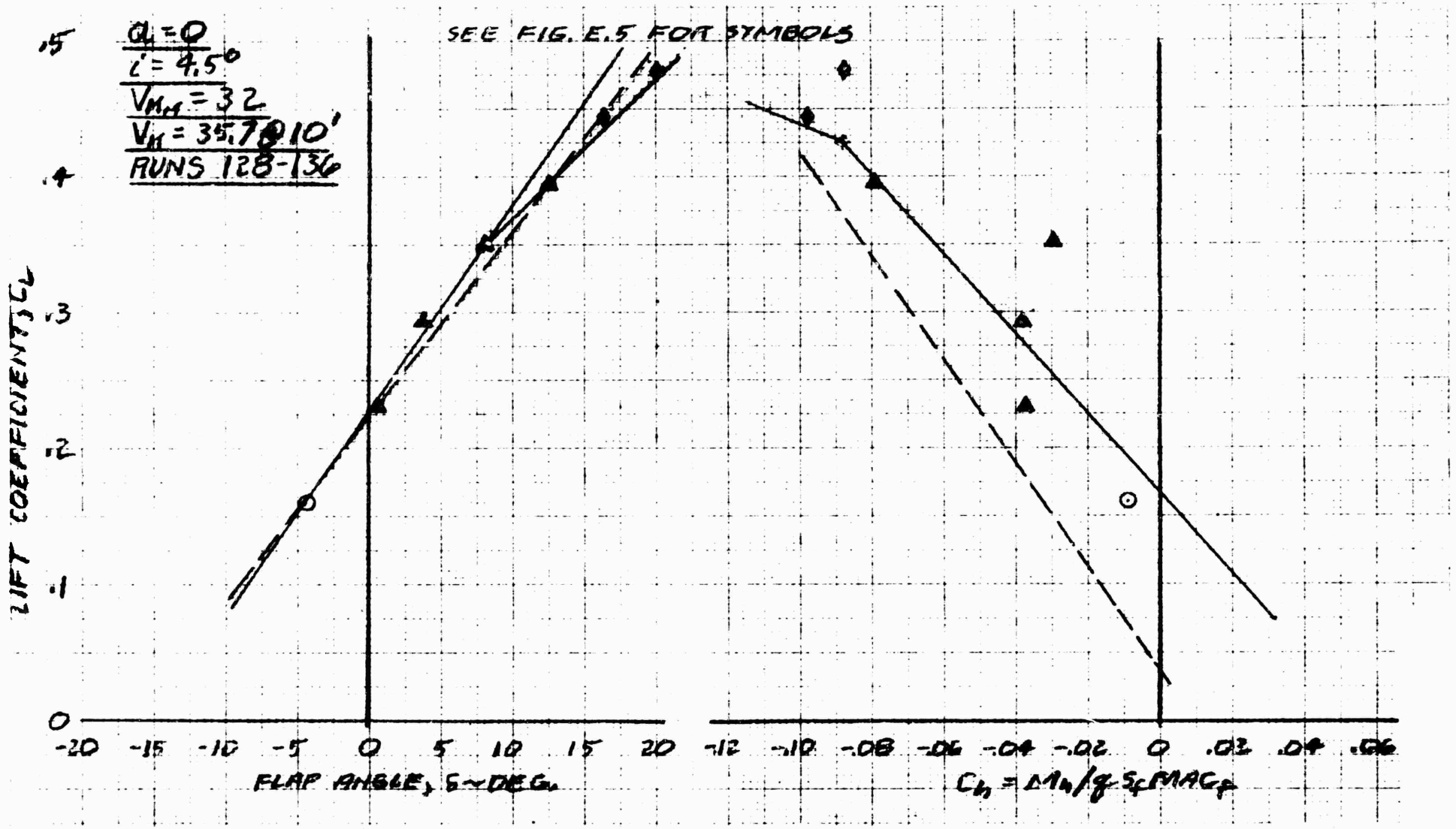


Figure E6. Cavitation Scaled Test Results, 32 Knots, $\alpha = 0$

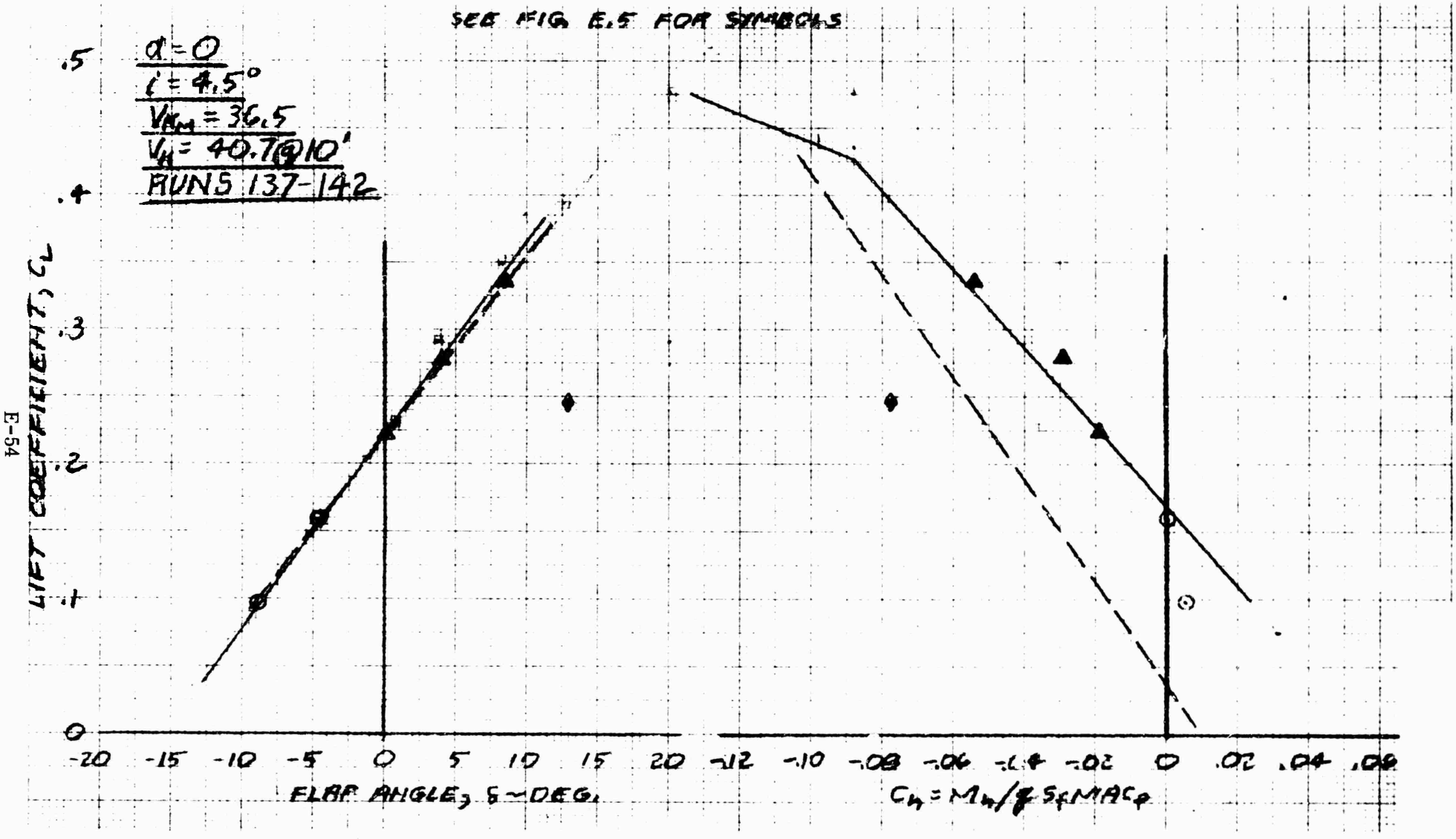


Figure E7. Cavitation Scaled Test Results, 36.5 Knots, $\alpha = 0$

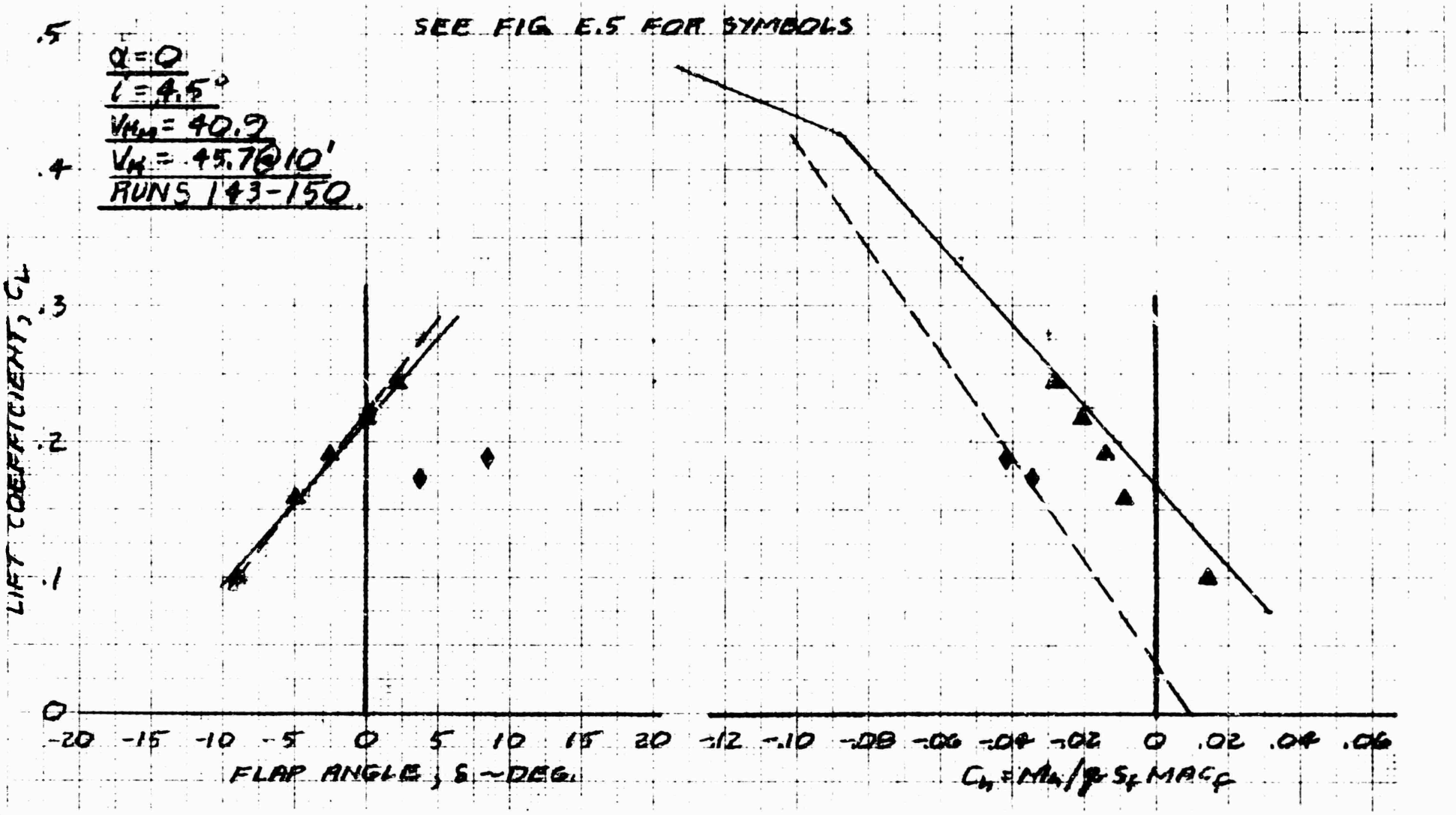


Figure E8. Cavitation Scaled Test Results, 40.9 Knots, $\alpha = 0$

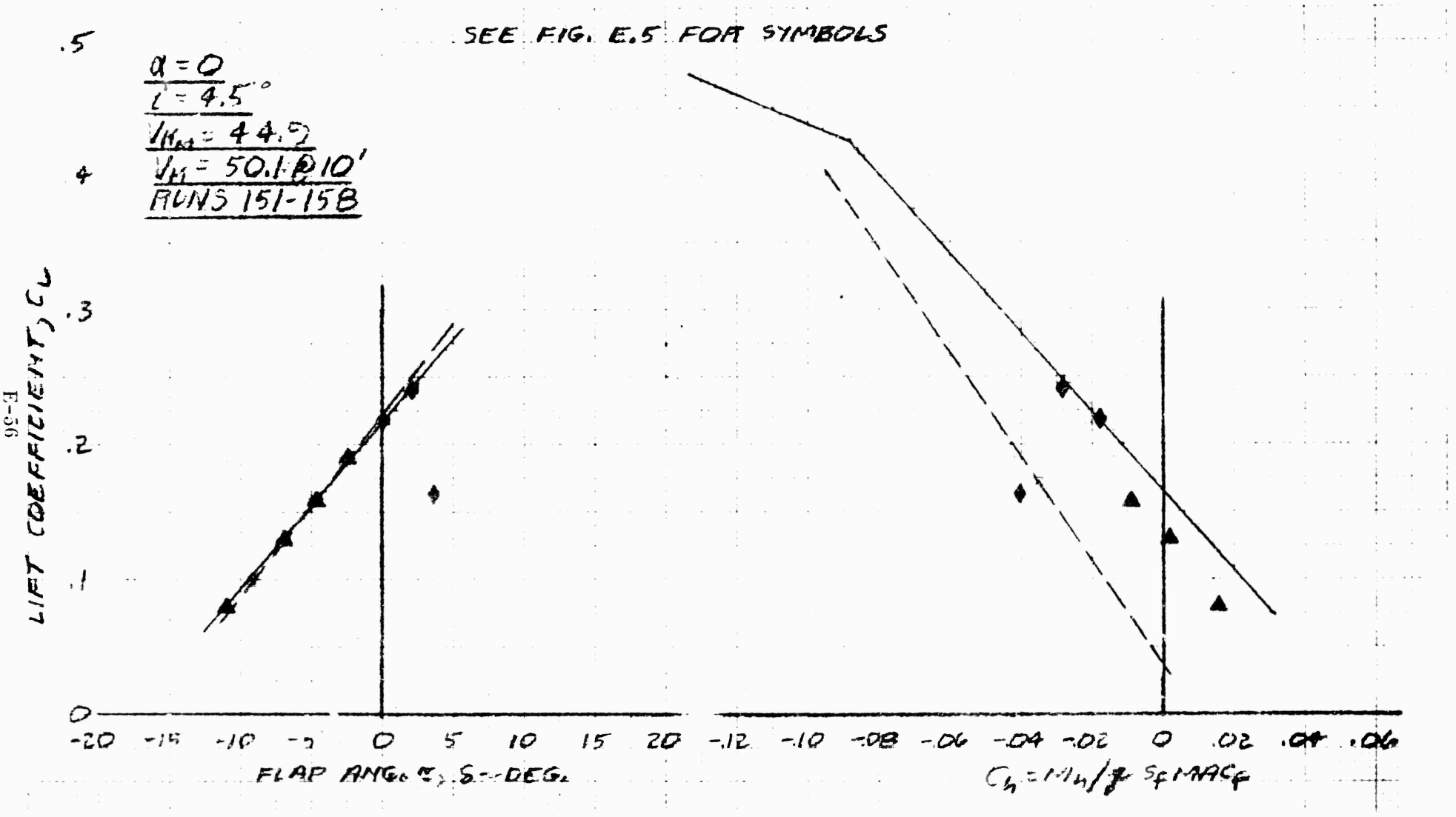


Figure E9. Cavitation Scaled Test Results, 44.9 Knots, $\alpha = 0$

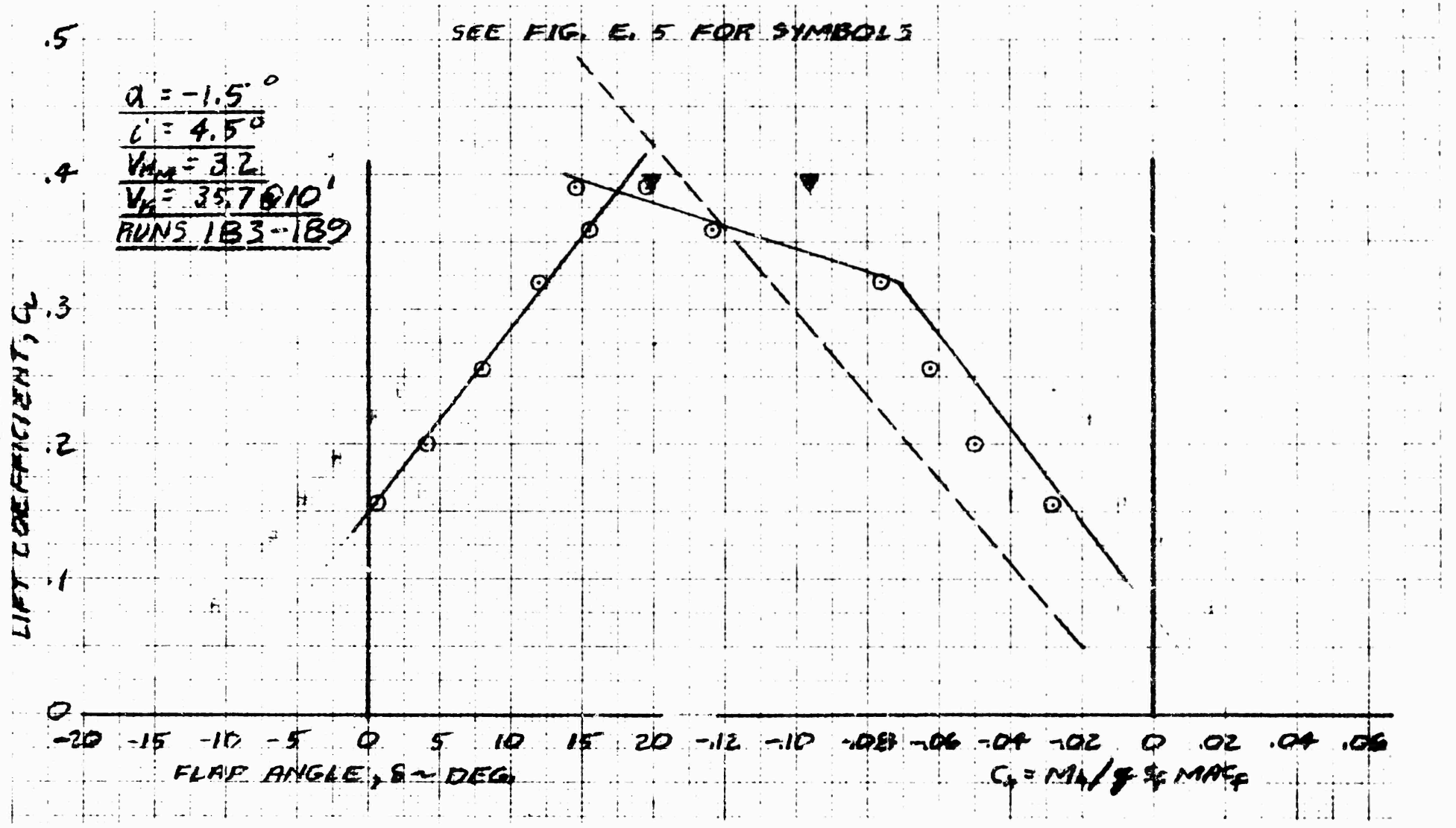


Figure E10. Cavitation Scaled Test Results, 32 Knots, $\alpha = -1.5^{\circ}$

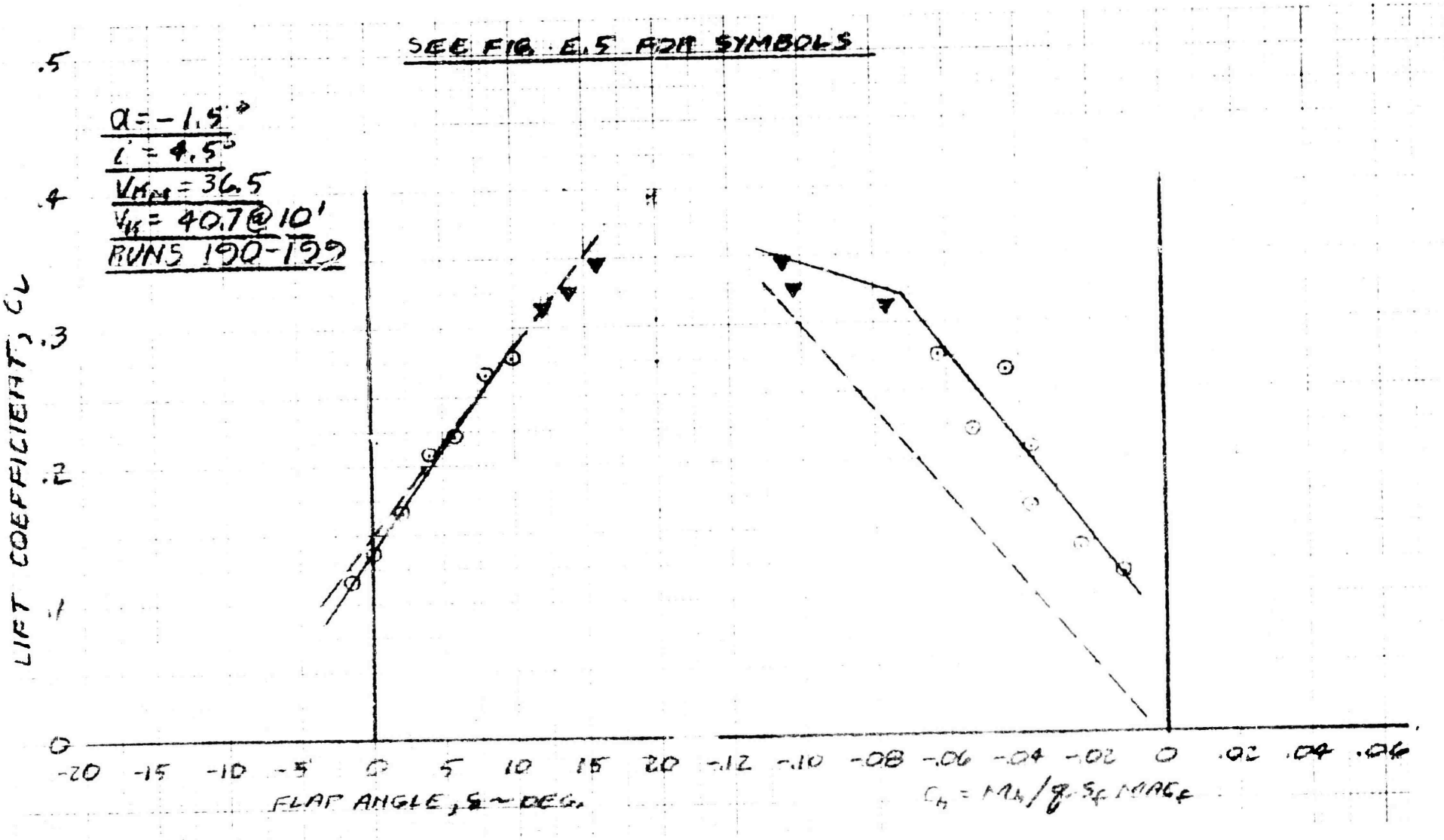


Figure E11. Cavitation Scaled Test Results, 36.5 Knots, $\alpha = -1.5^{\circ}$

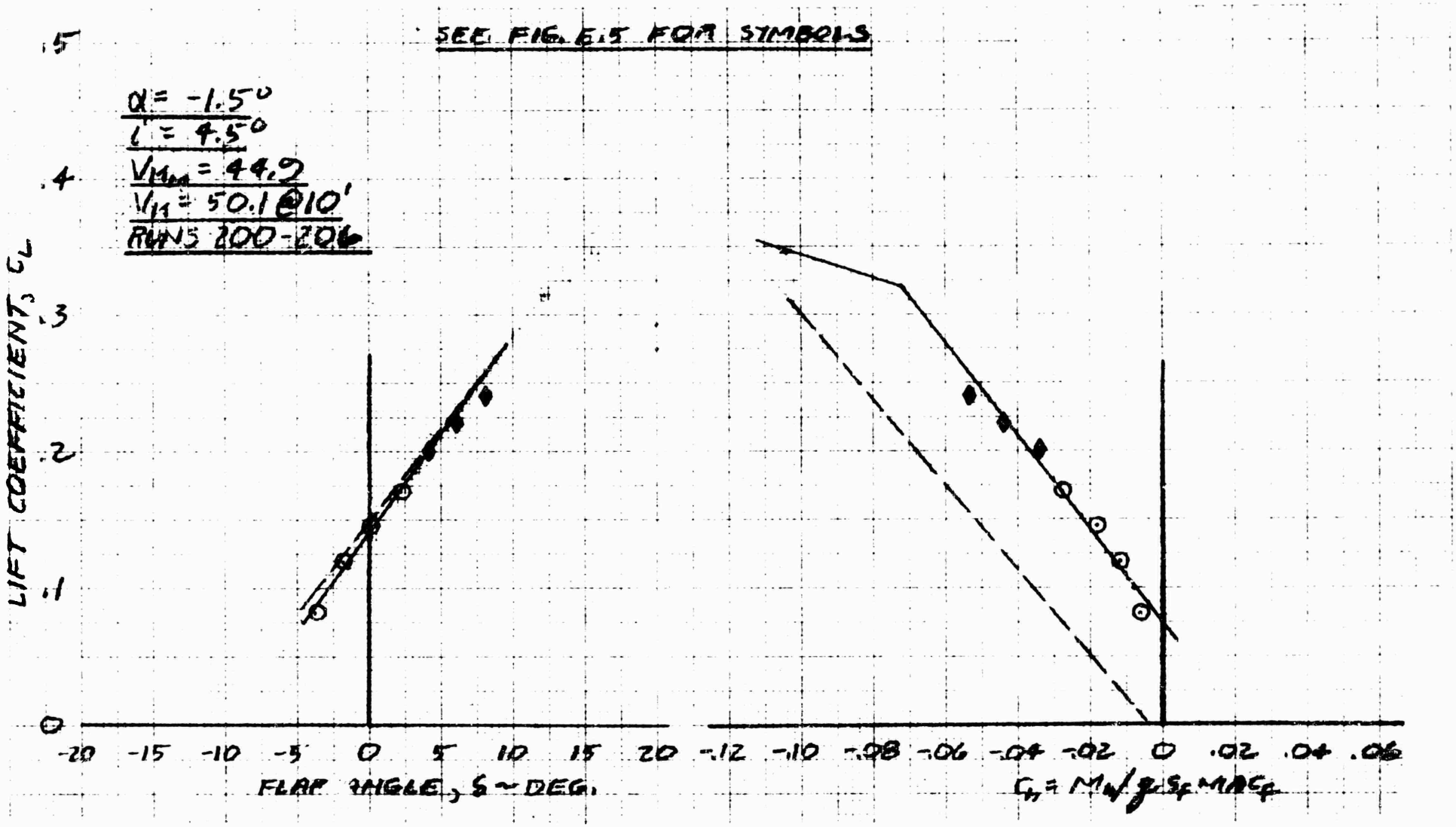


Figure E12. Cavitation Scaled Test Results, 44.9 Knots, $\alpha = -1.5^{\circ}$

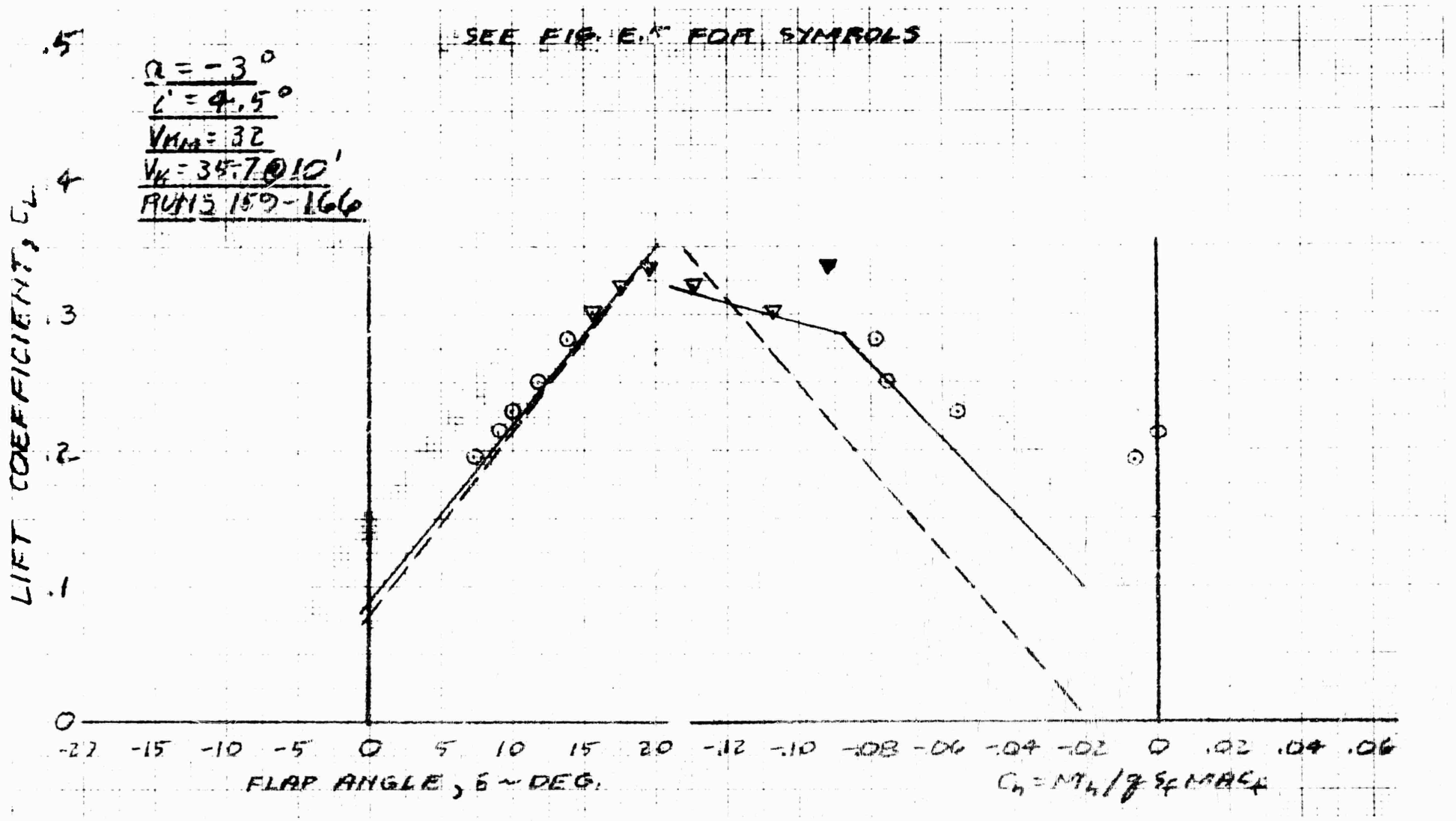


Figure E13. Cavitation Scaled Test Results, 32 Knots, $\alpha = -3^{0}$

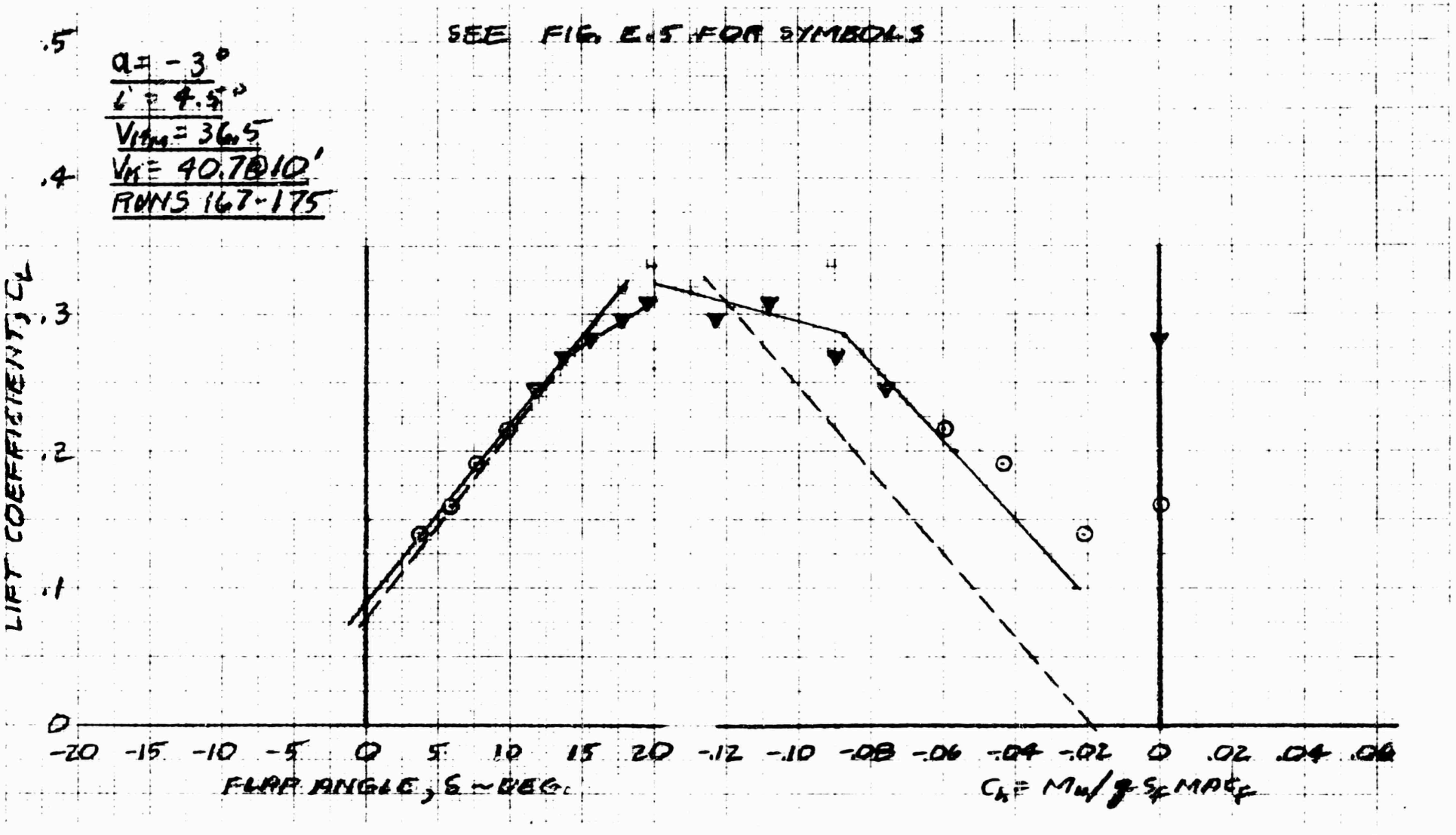


Figure E14. Cavitation Scaled Test Results, 36.5 Knots, $\alpha = -3^{\circ}$

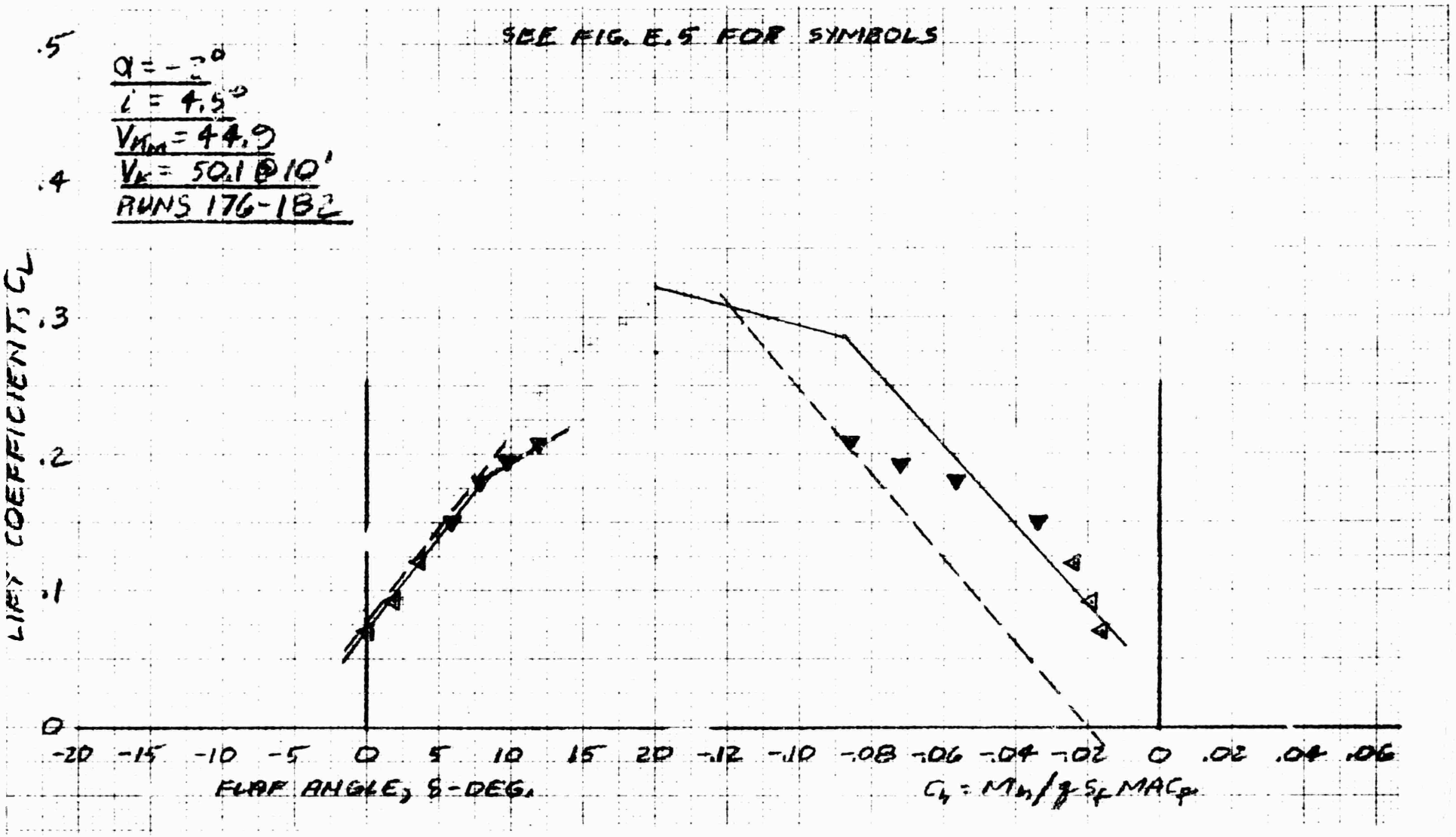


Figure E15. Cavitation Scaled Test Results, 44.9 Knots, $\alpha = -3^{\circ}$

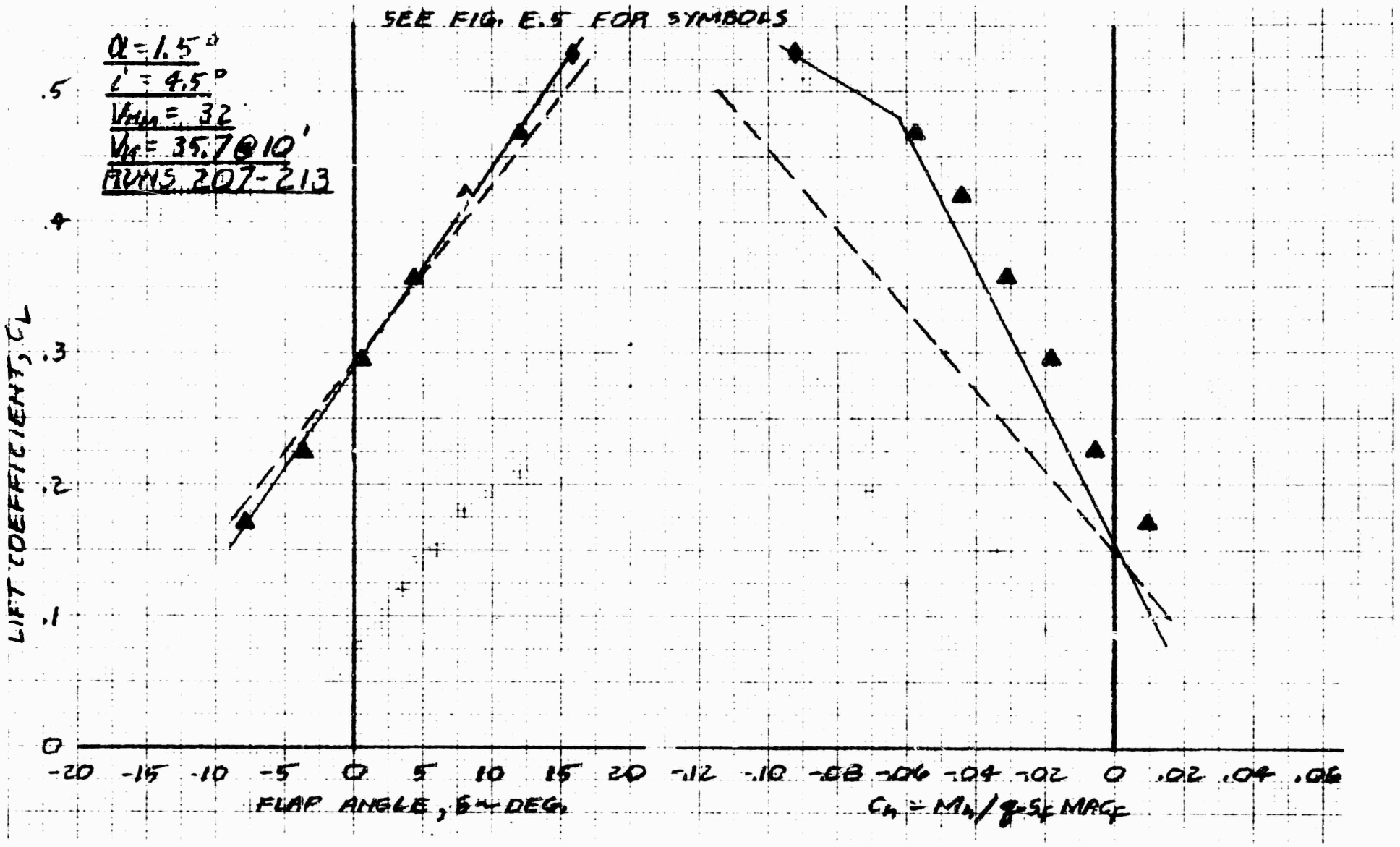


Figure E16. Cavitation Scaled Test Results, 32 Knots, $\alpha = 1.5^{o}$

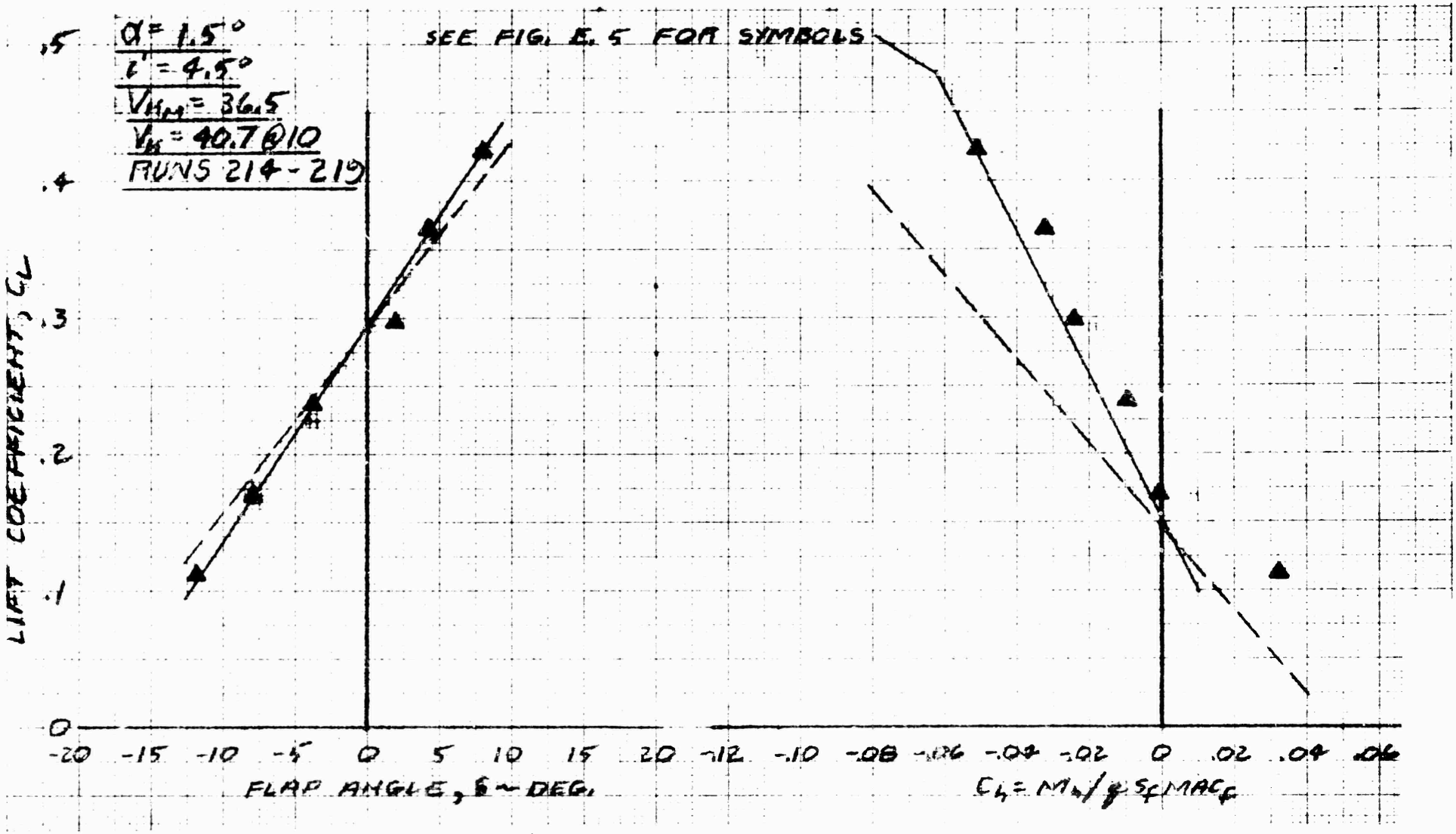


Figure E17. Cavitation Scaled Test Results, 36.5 Knots, $\alpha = 1.5^{o}$

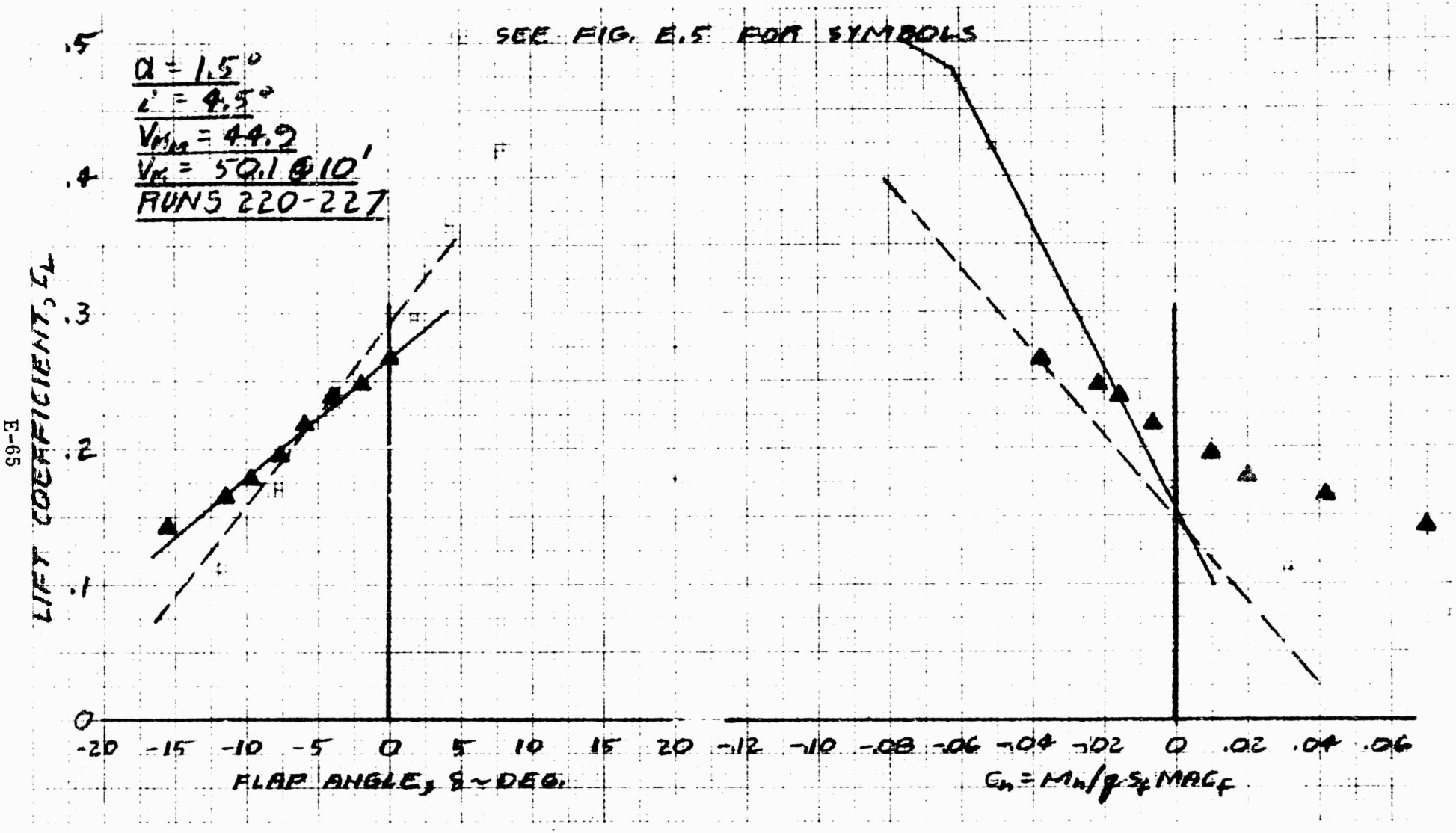


Figure E18. Cavitation Scaled Test Results, 44.9 Knots, $\alpha = 1.5^{o}$

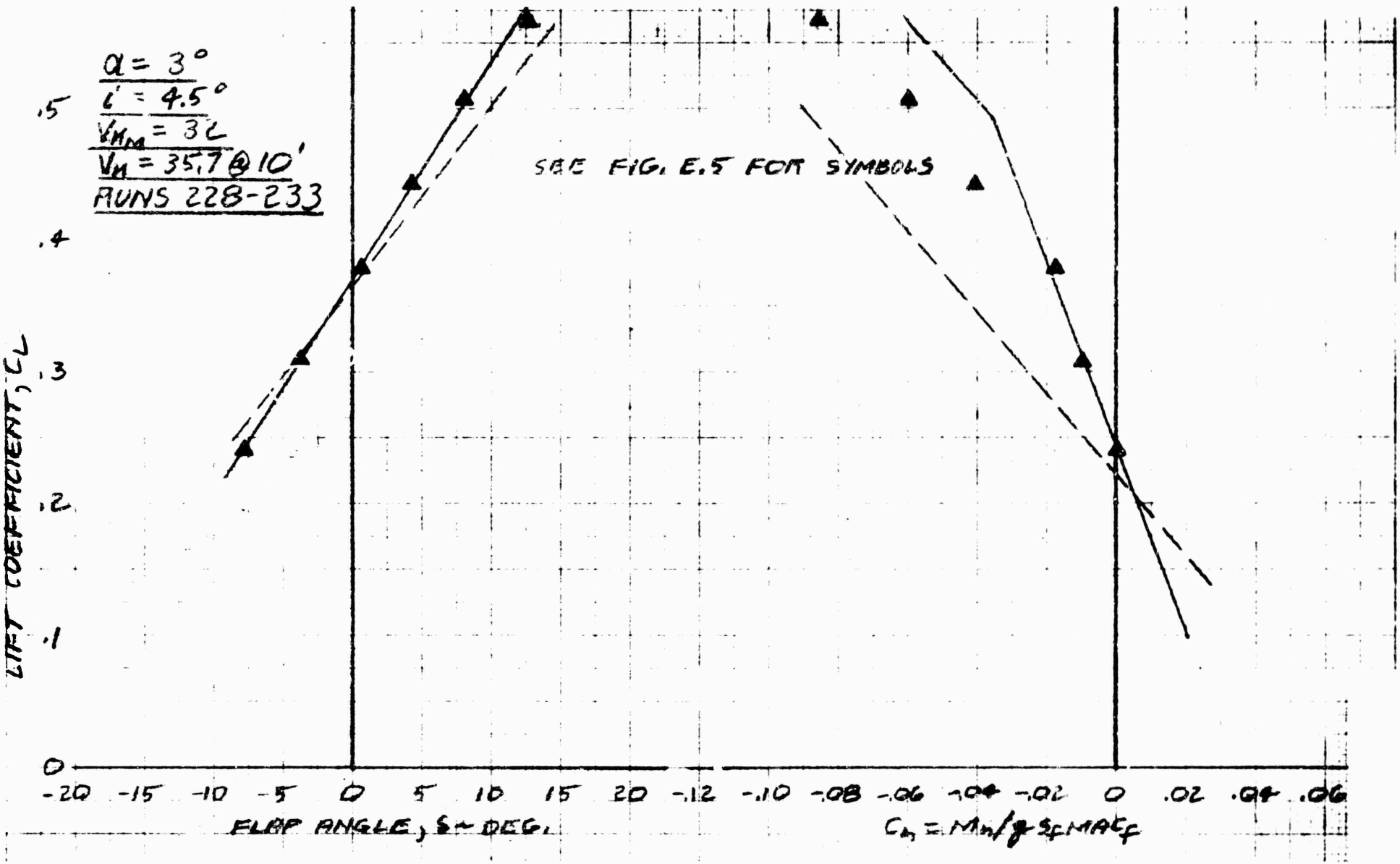


Figure E19. Cavitation Scaled Test Results, 32 Knots, $\alpha = 3^{o}$

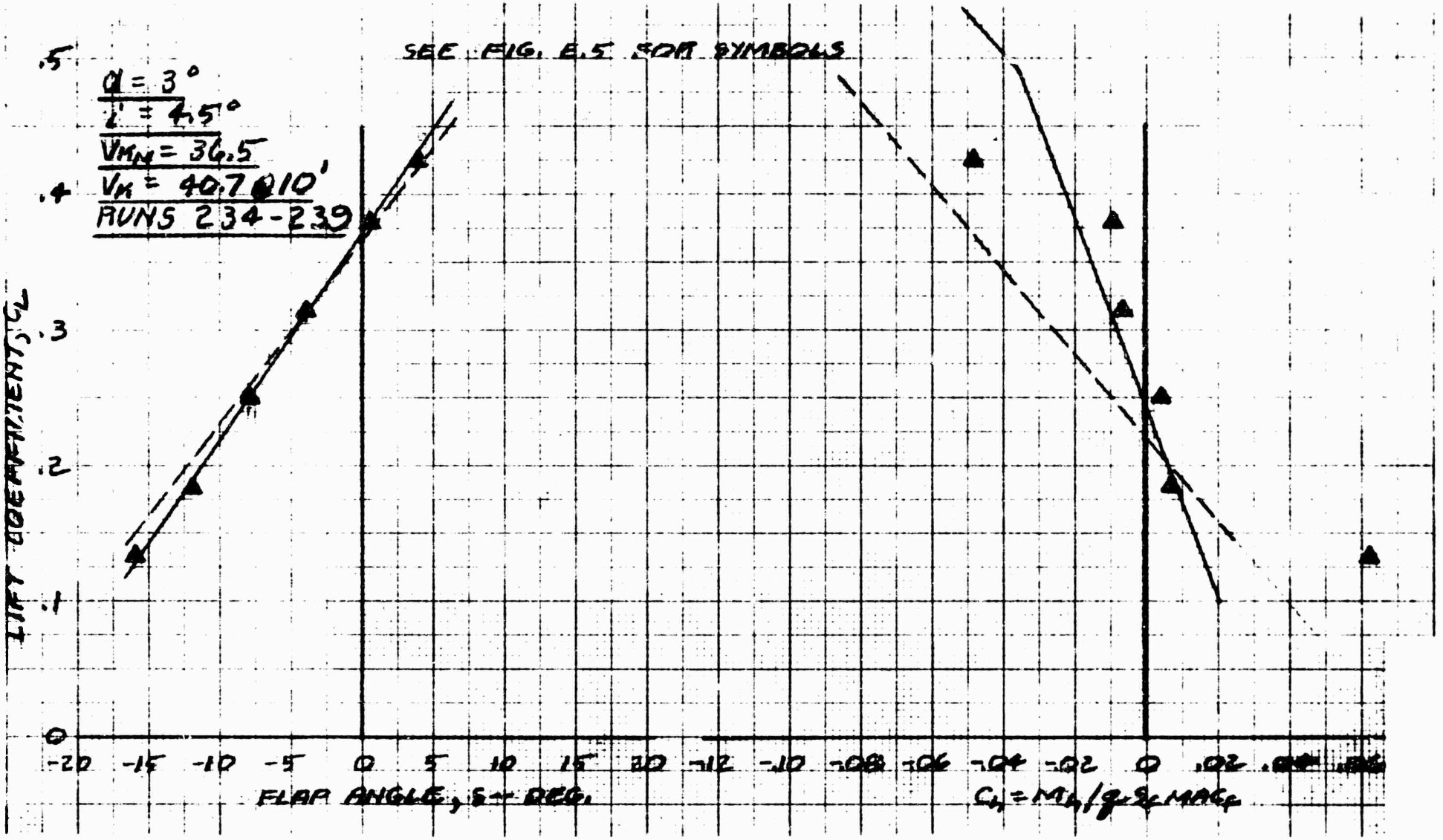


Figure E20. Cavitation Scaled Test Results, 36.5 Knots, $\alpha = 3^{o}$

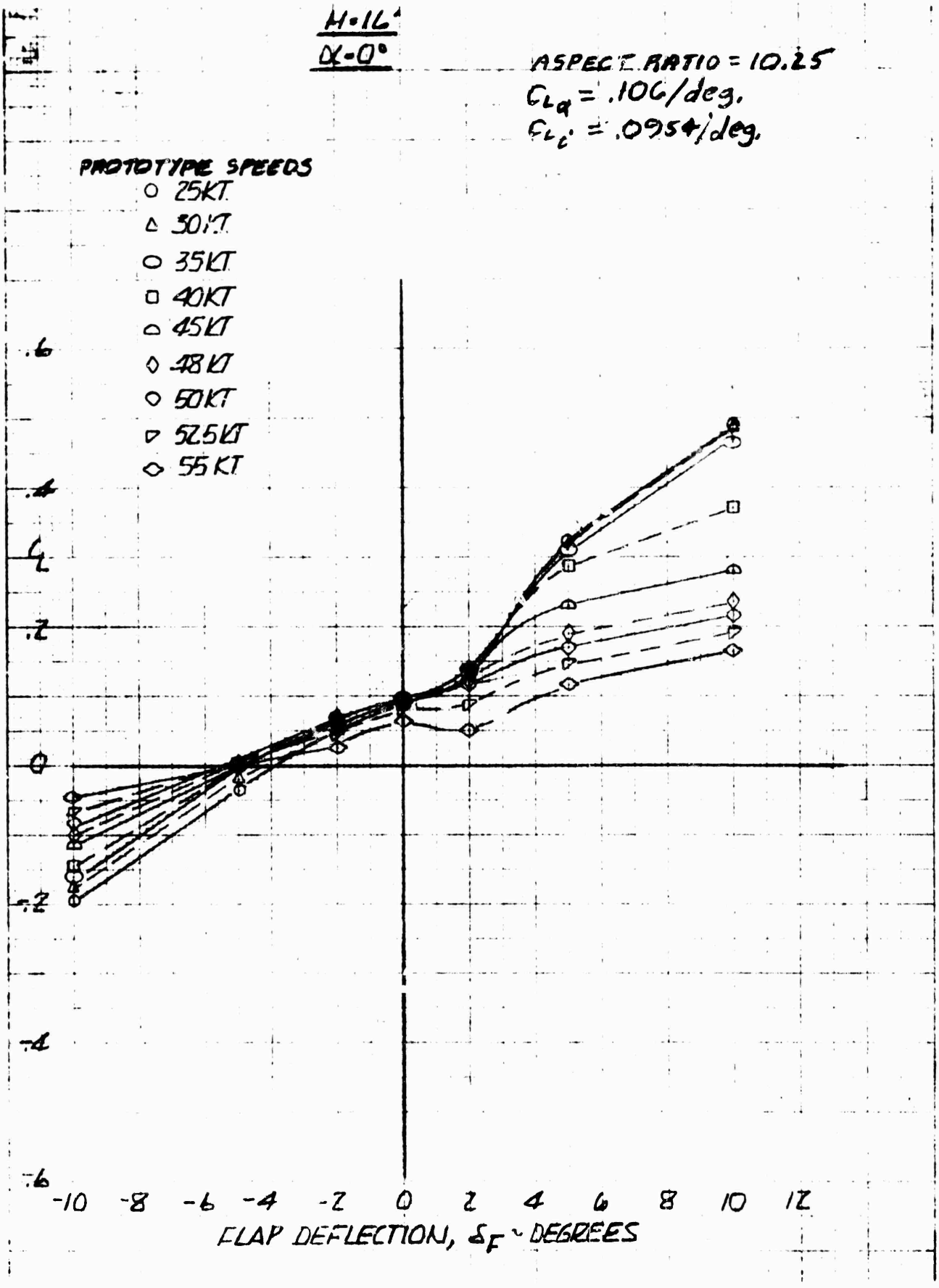


Figure E21. High Aspect Ratio Foil Flap Cavitation

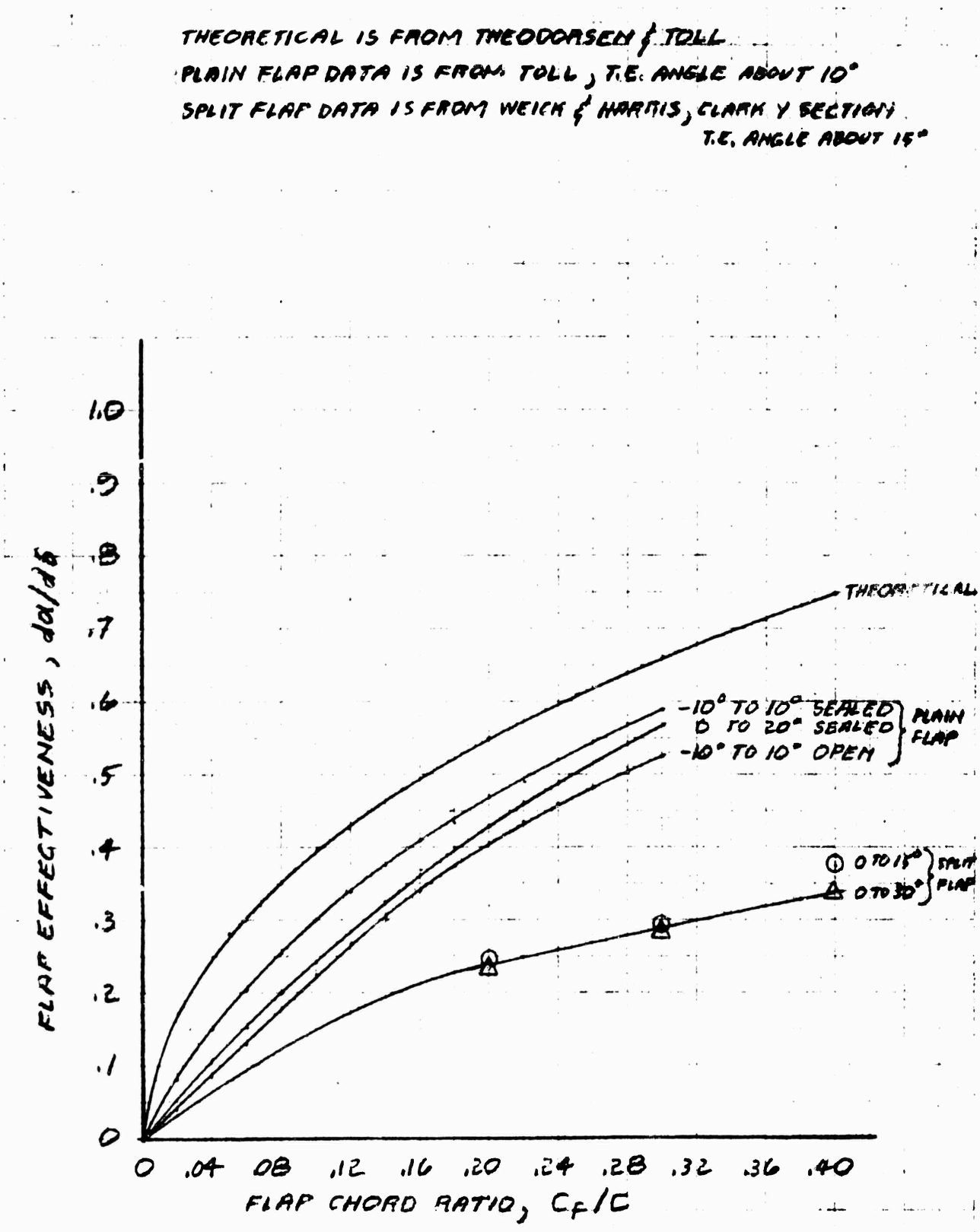


Figure E22. Flap Effectiveness

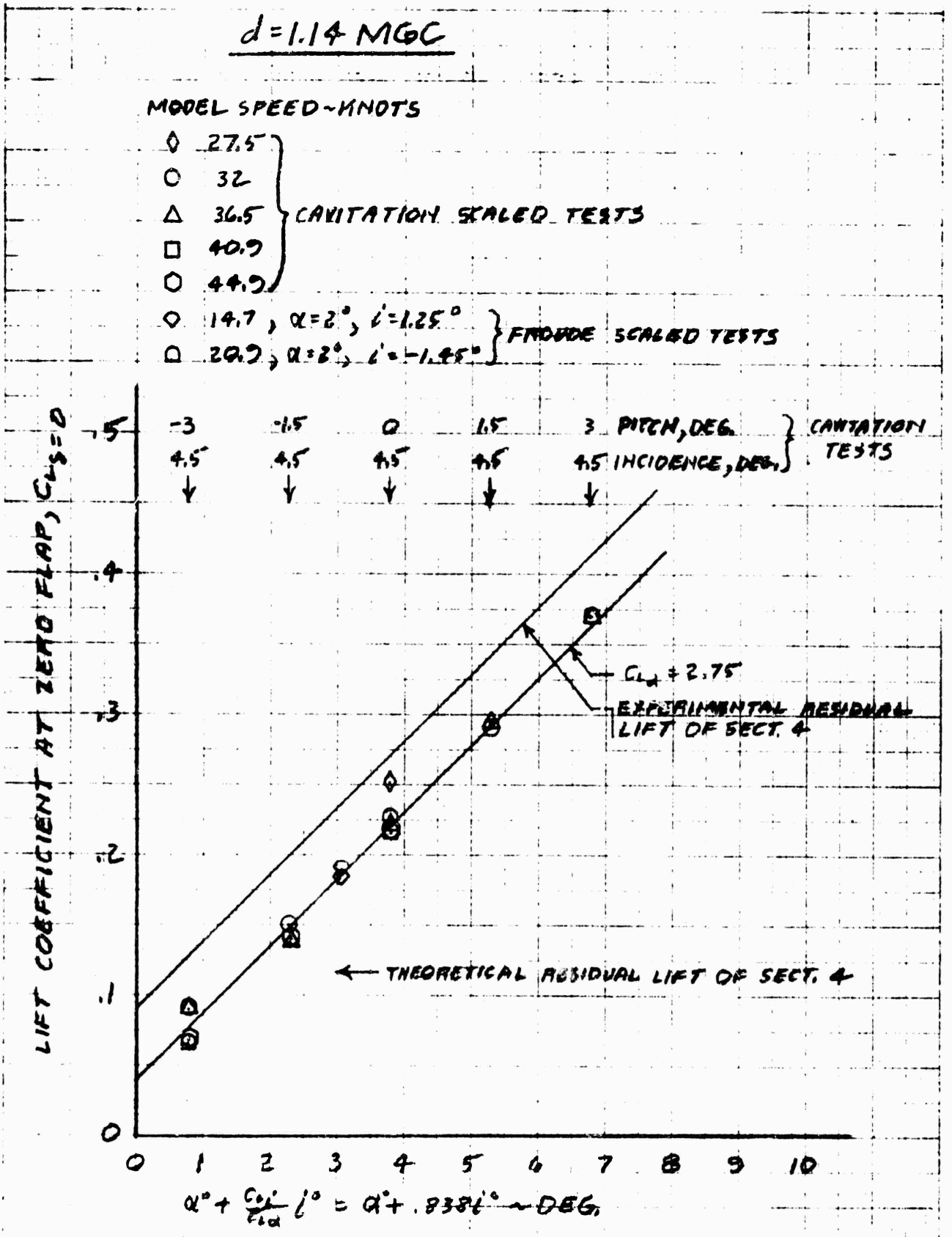


Figure E23. Residual Lift

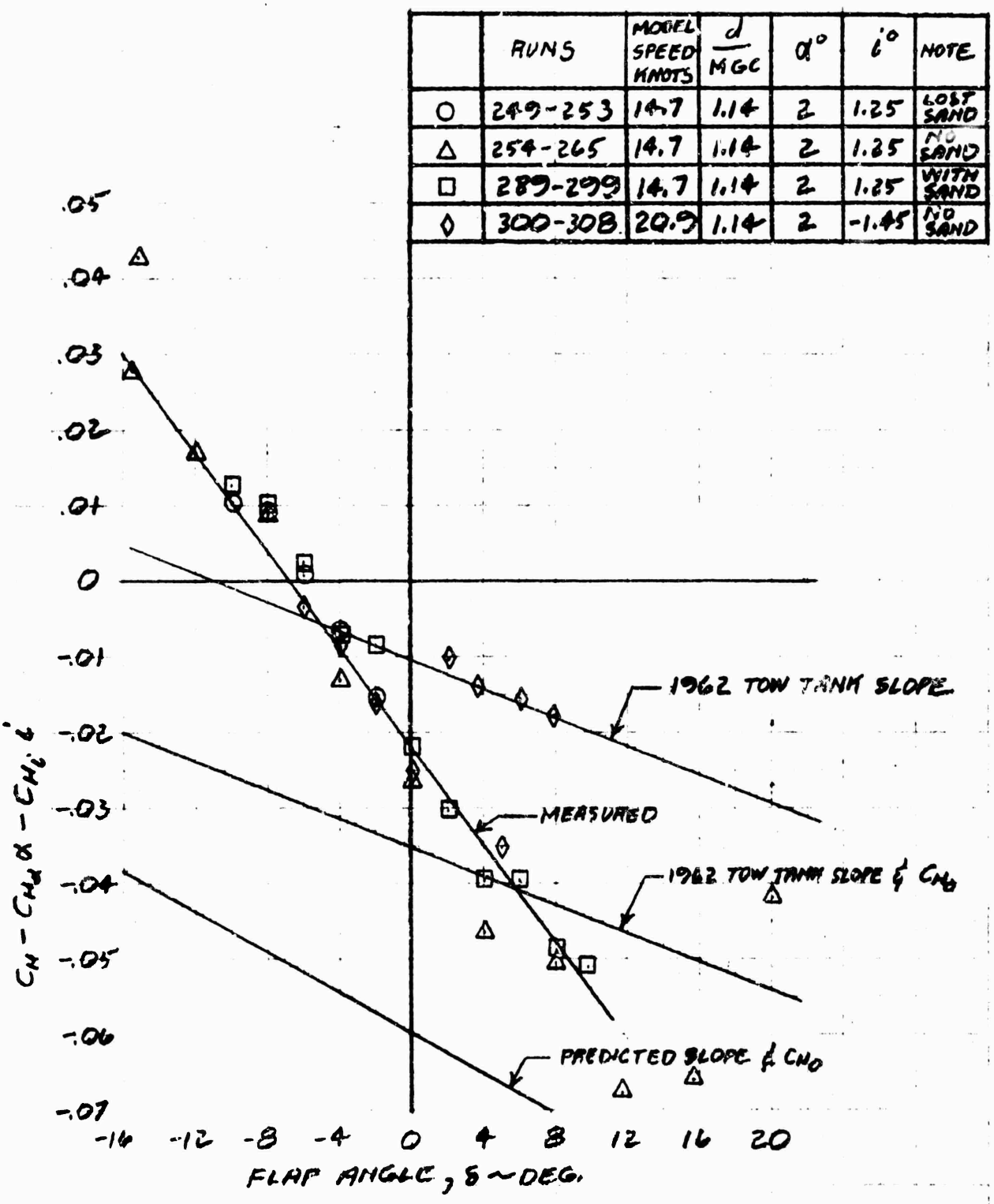


Figure E24. Foil Moment Characteristics

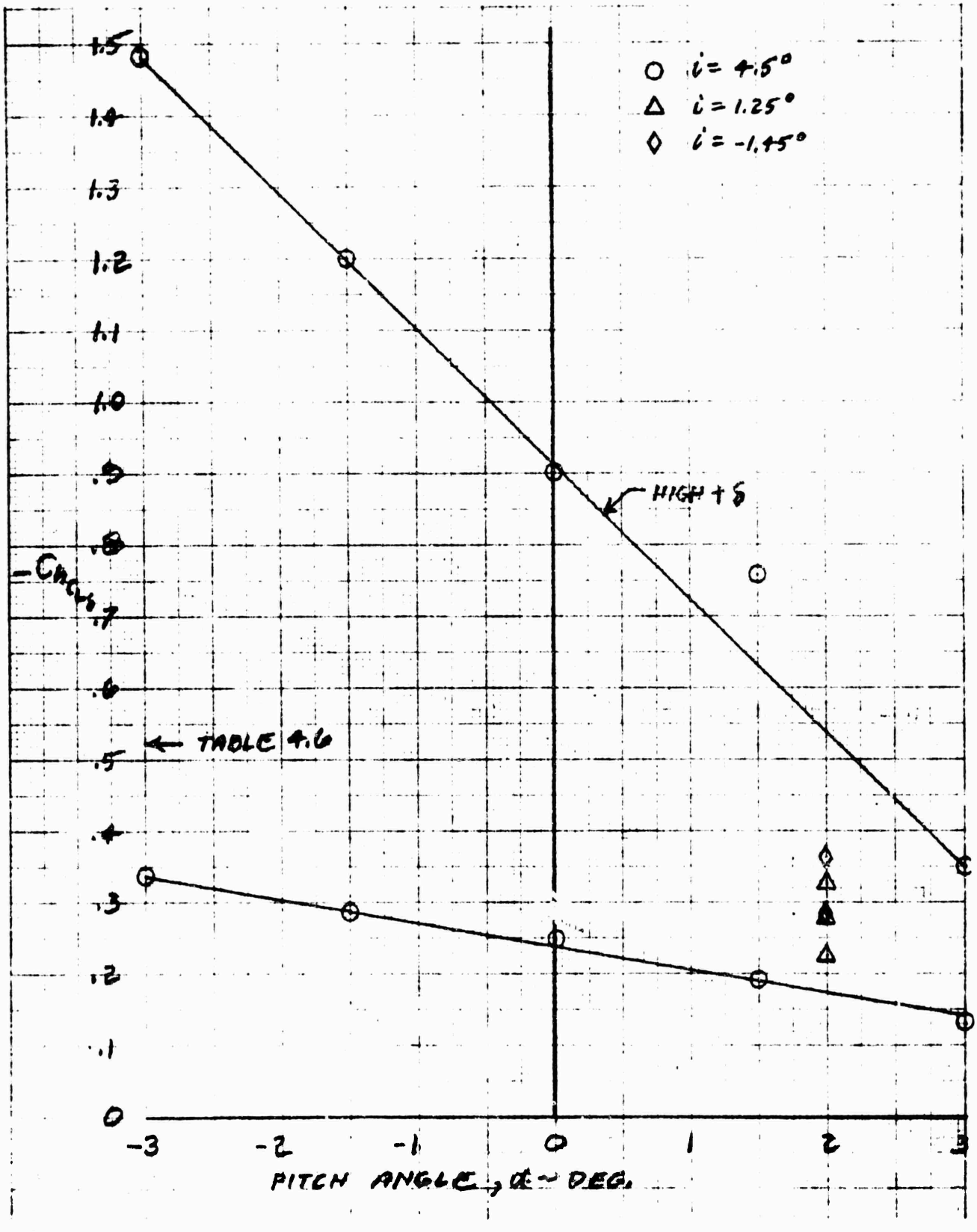


Figure E25. Flap Hinge Moment Slope

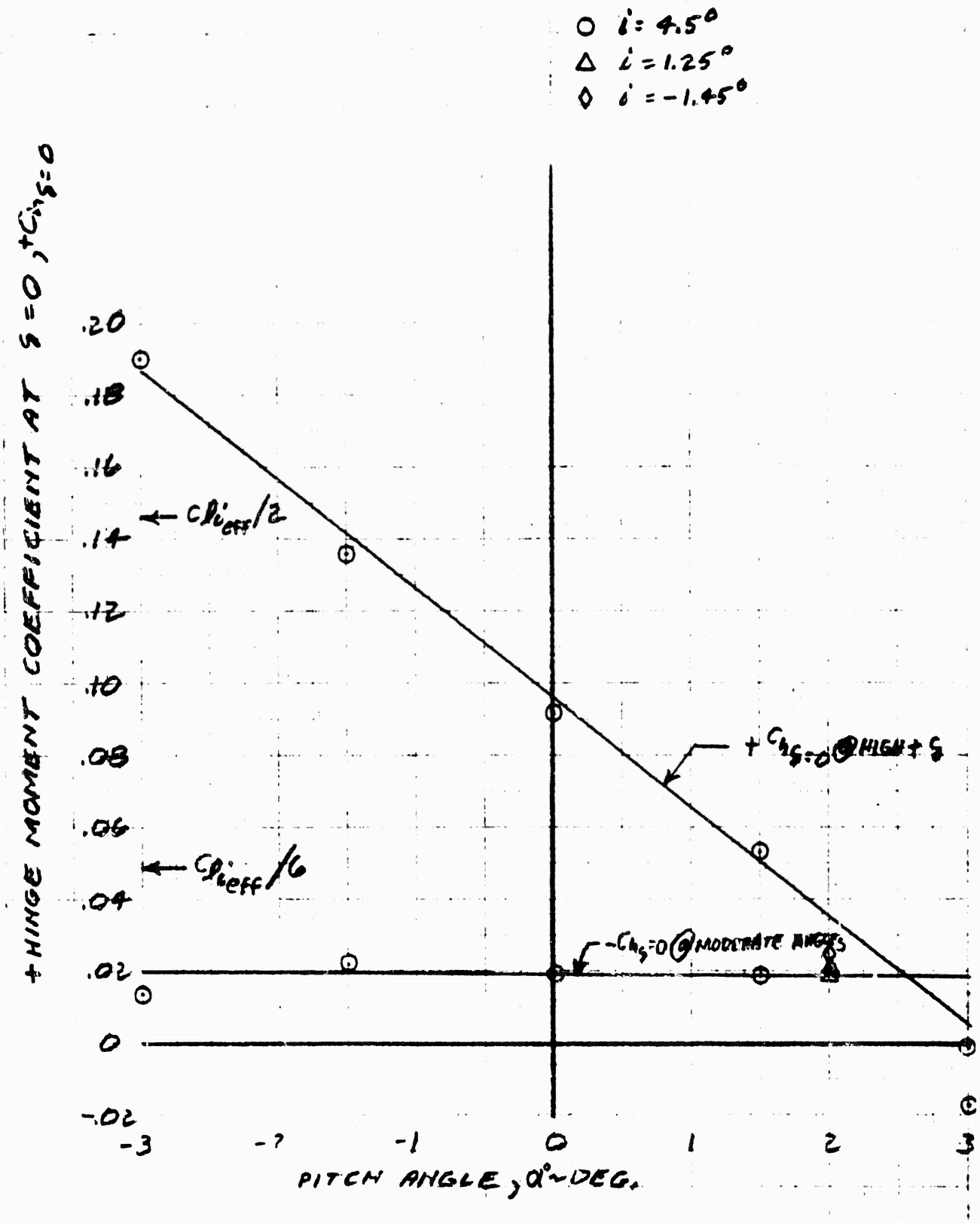


Figure E26. Residual Flap Hinge Moment

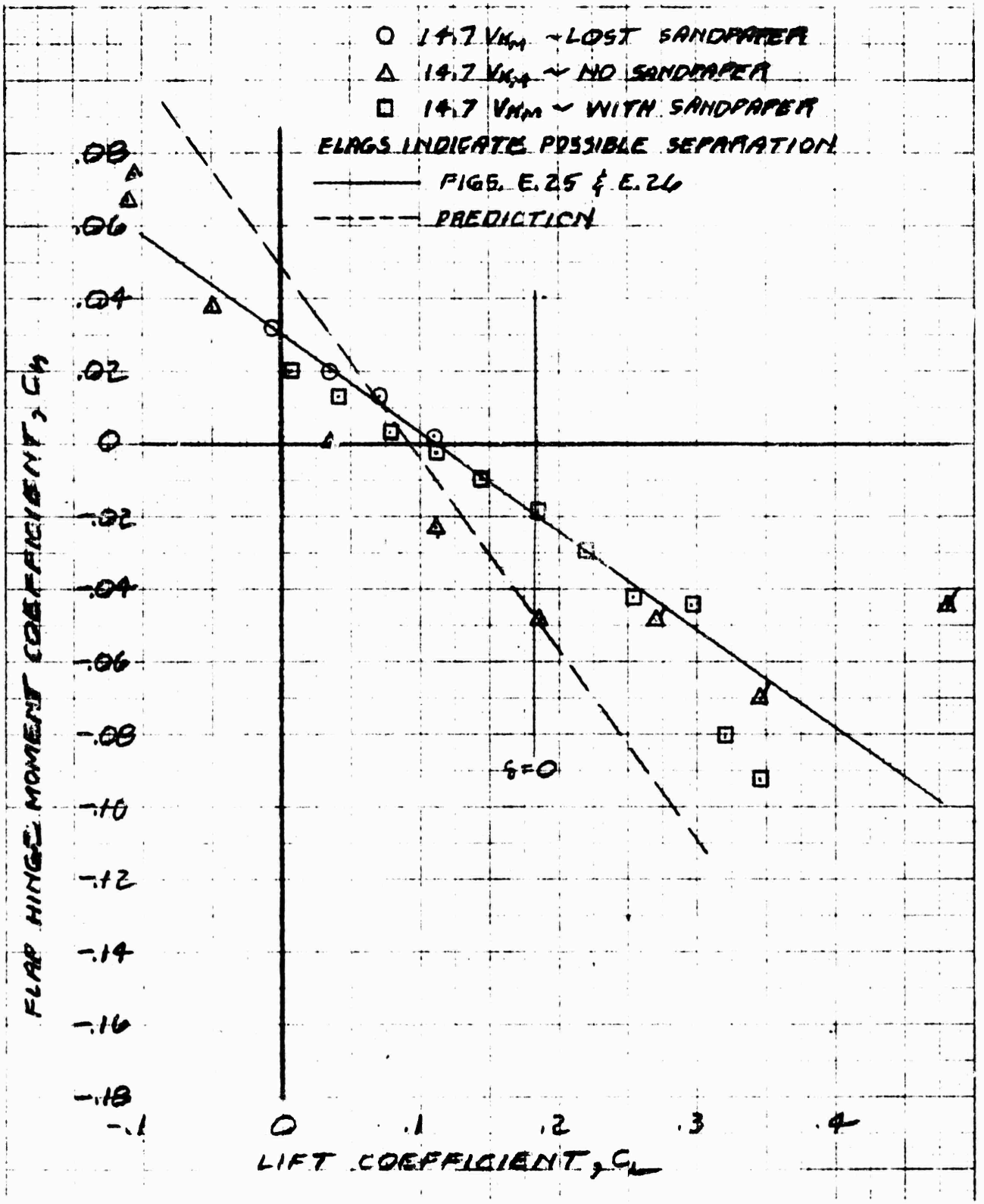


Figure E27. Flap Hinge Moment, $\alpha = 2^{o}$, $i = 1.25^{o}$

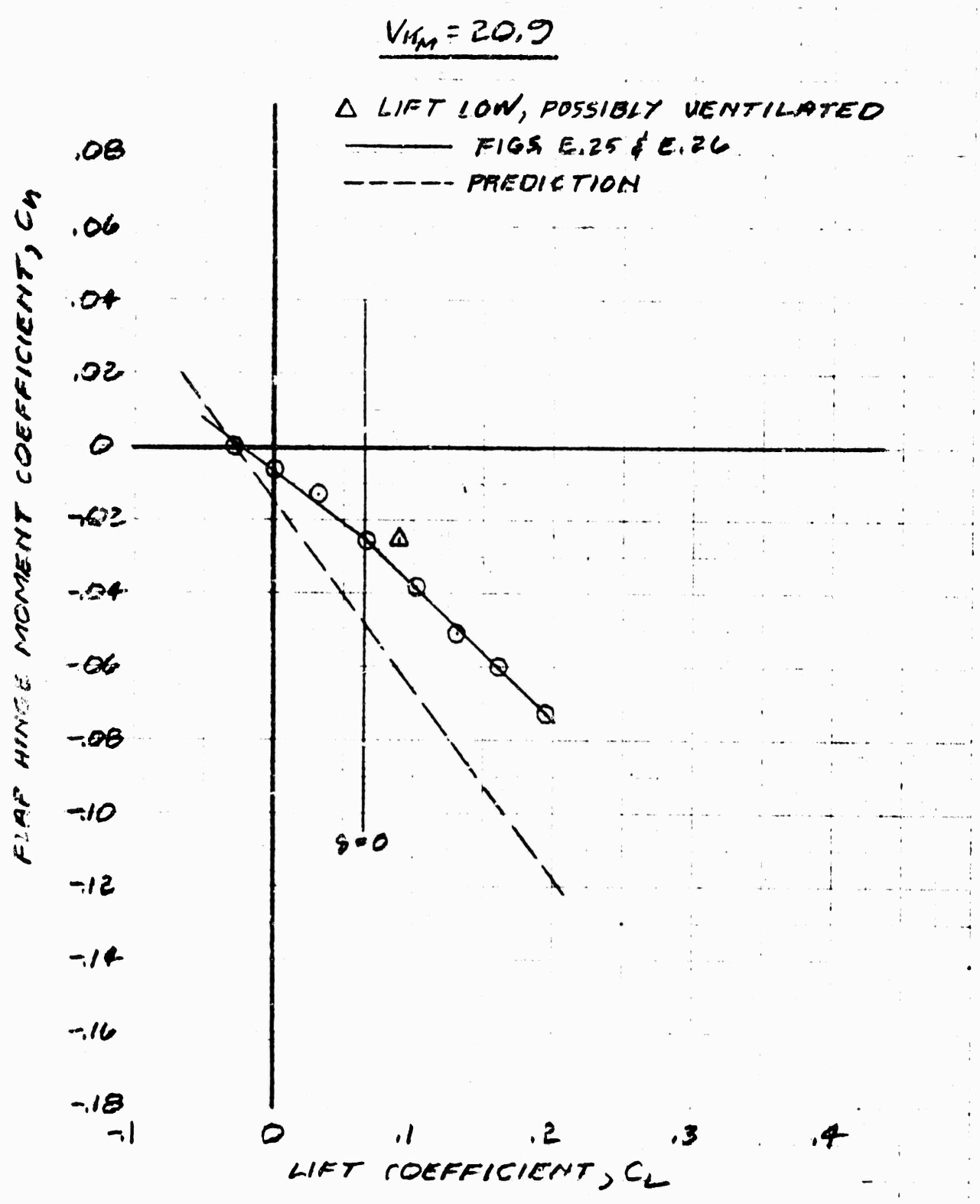


Figure E28. Flap Hinge Moment, $\alpha = 2^{\circ}$, $i = -1.45^{\circ}$

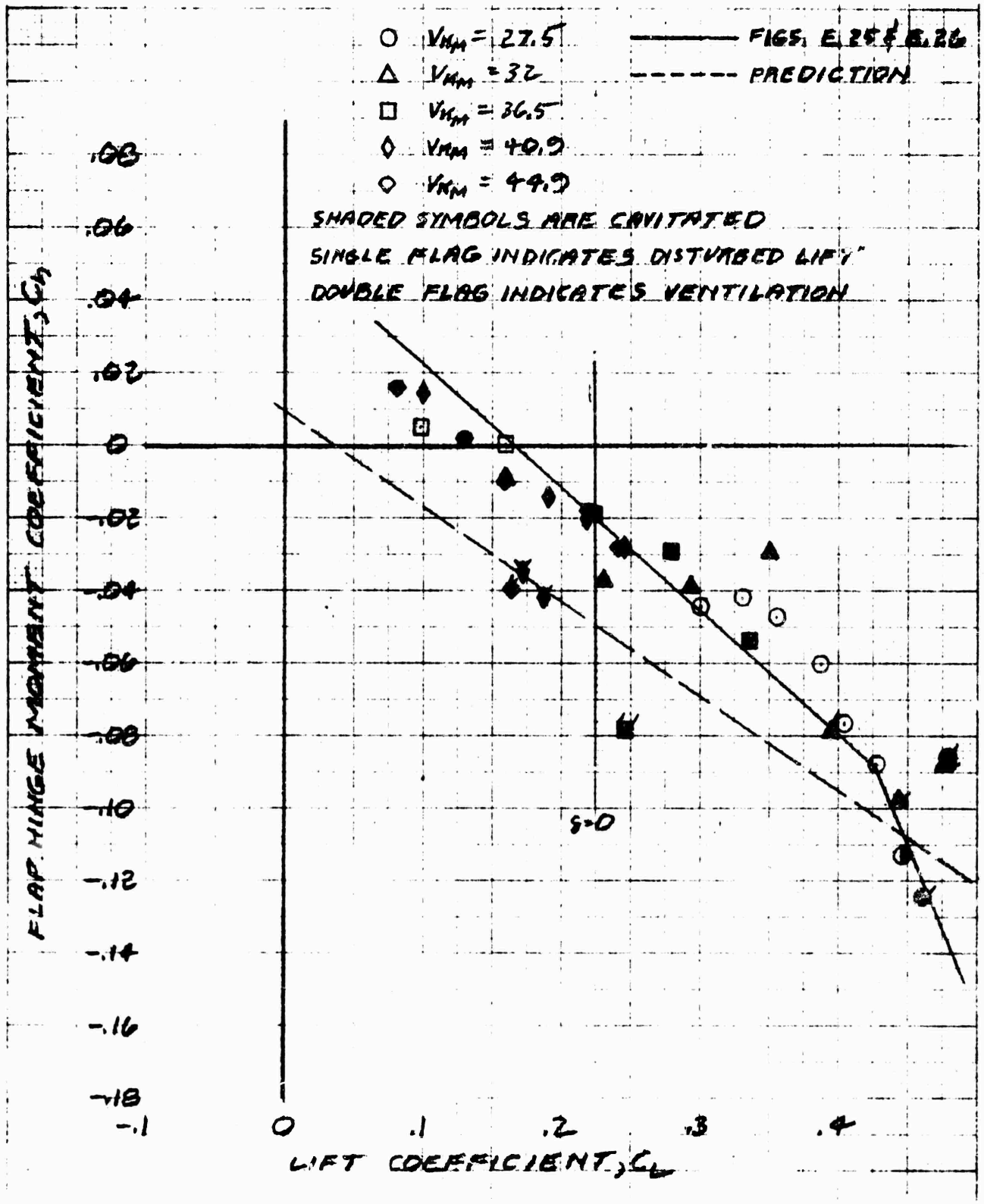


Figure E29. Flap Hinge Moment, α = 0, i = 4.5°

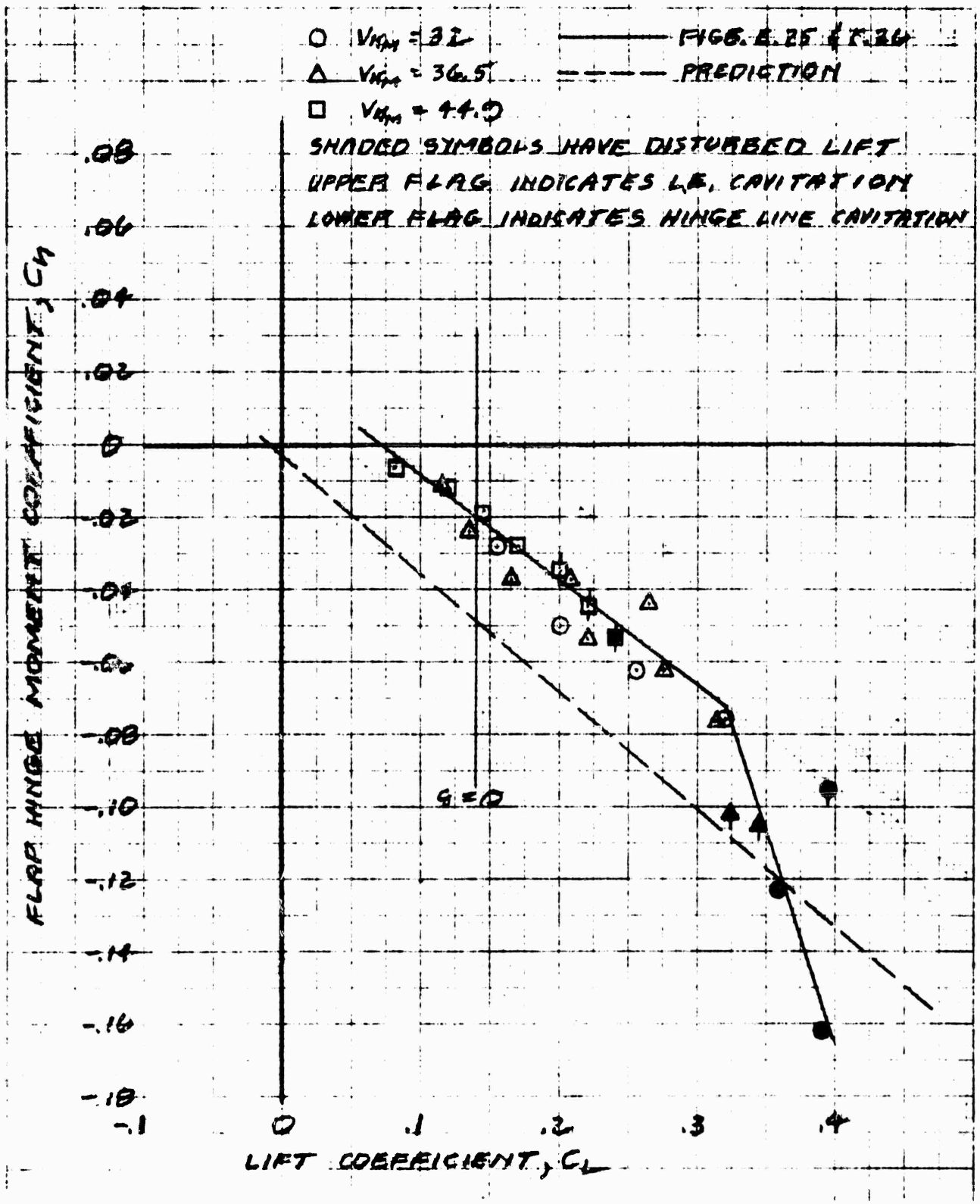


Figure E30. Flap Hinge Moment, $\alpha = -1.5^{o}$, $i = 4.5^{o}$

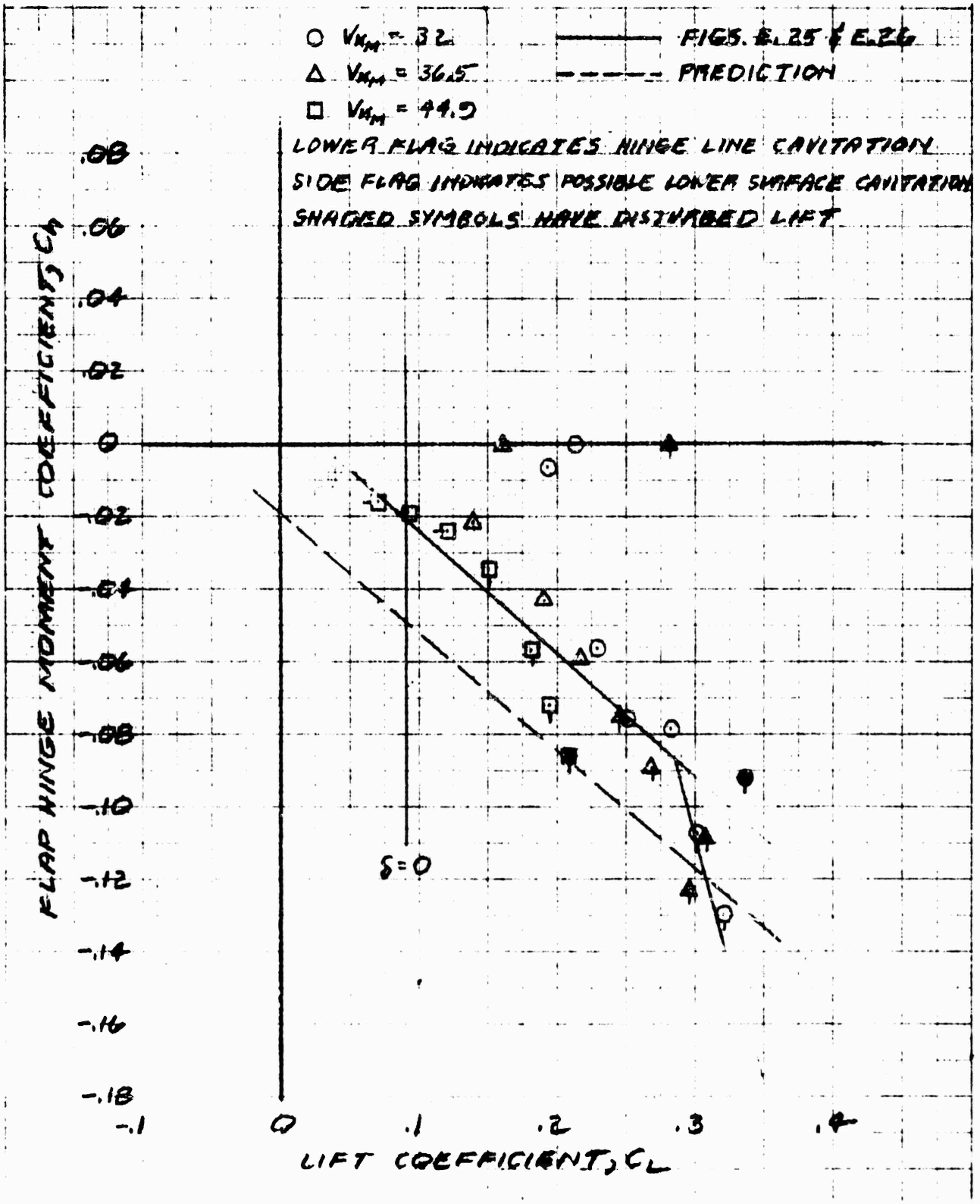


Figure E31. Flap Hinge Moment, $\alpha = -3^{o}$, $i = 4.5^{o}$

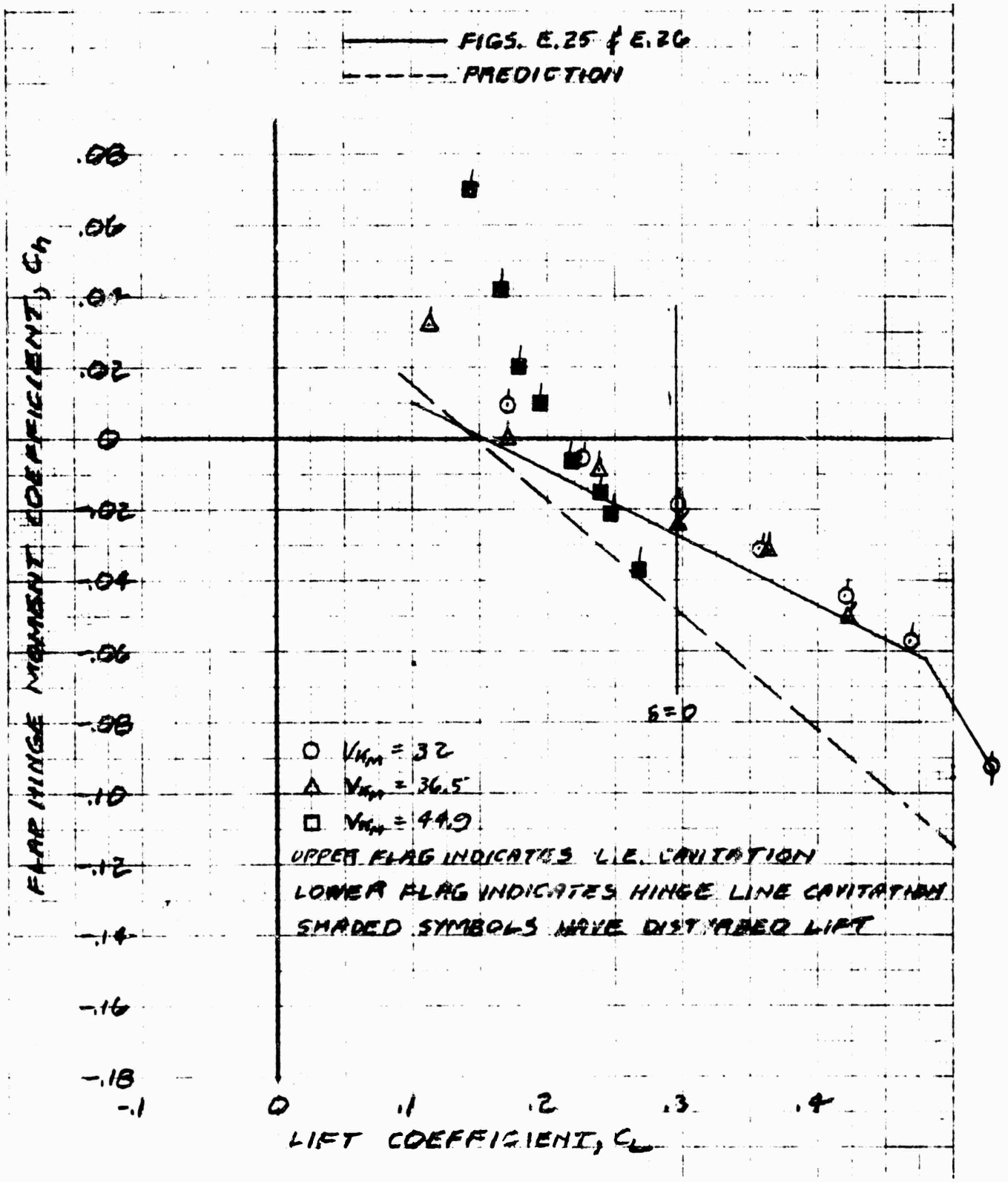


Figure E32. Flap Hinge Moment, $\alpha = 1.5^{o}$, $i = 4.5^{o}$

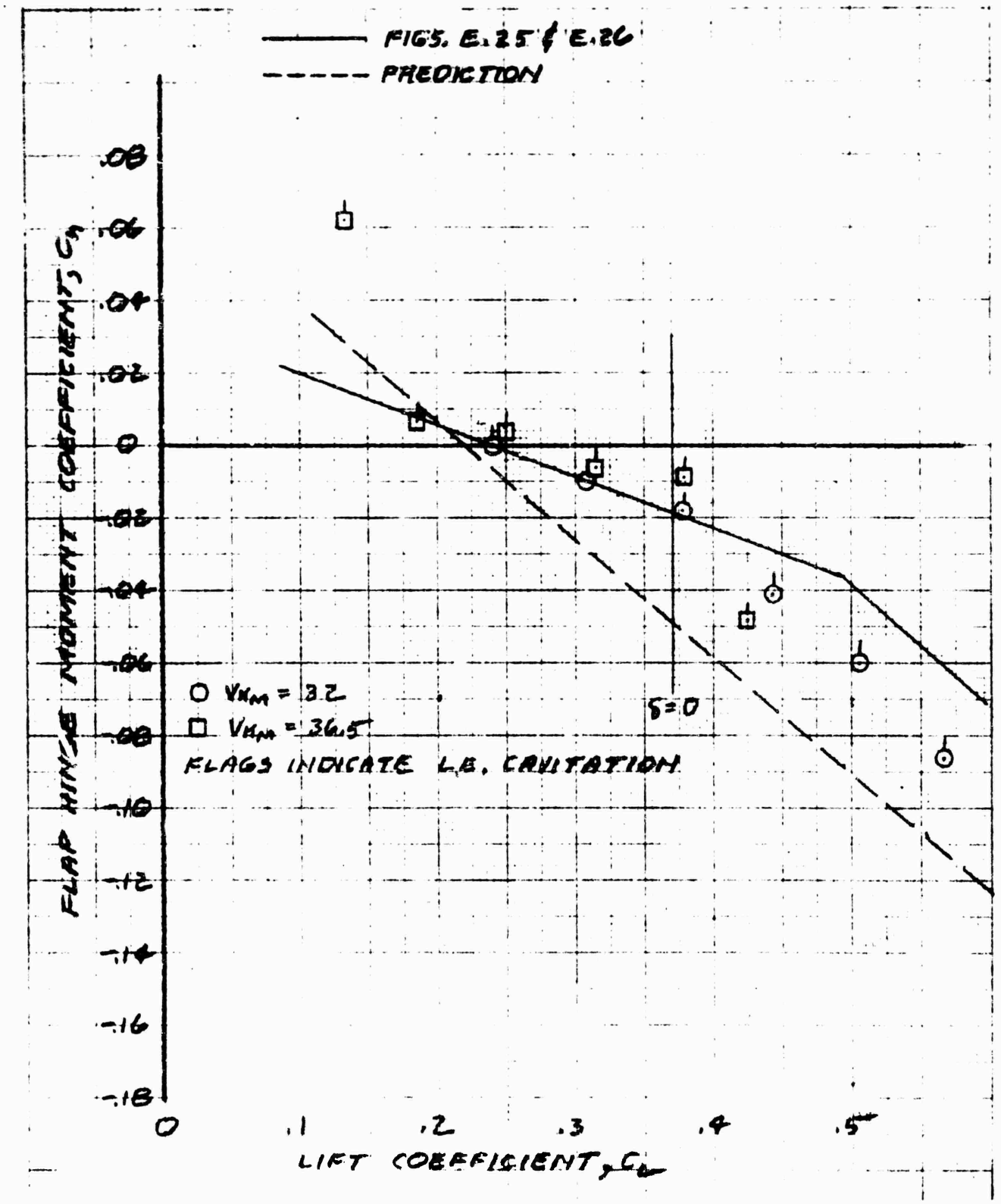


Figure E33. Flap Hinge Moment, $\alpha = 3^{o}$, $i = 4.5^{o}$

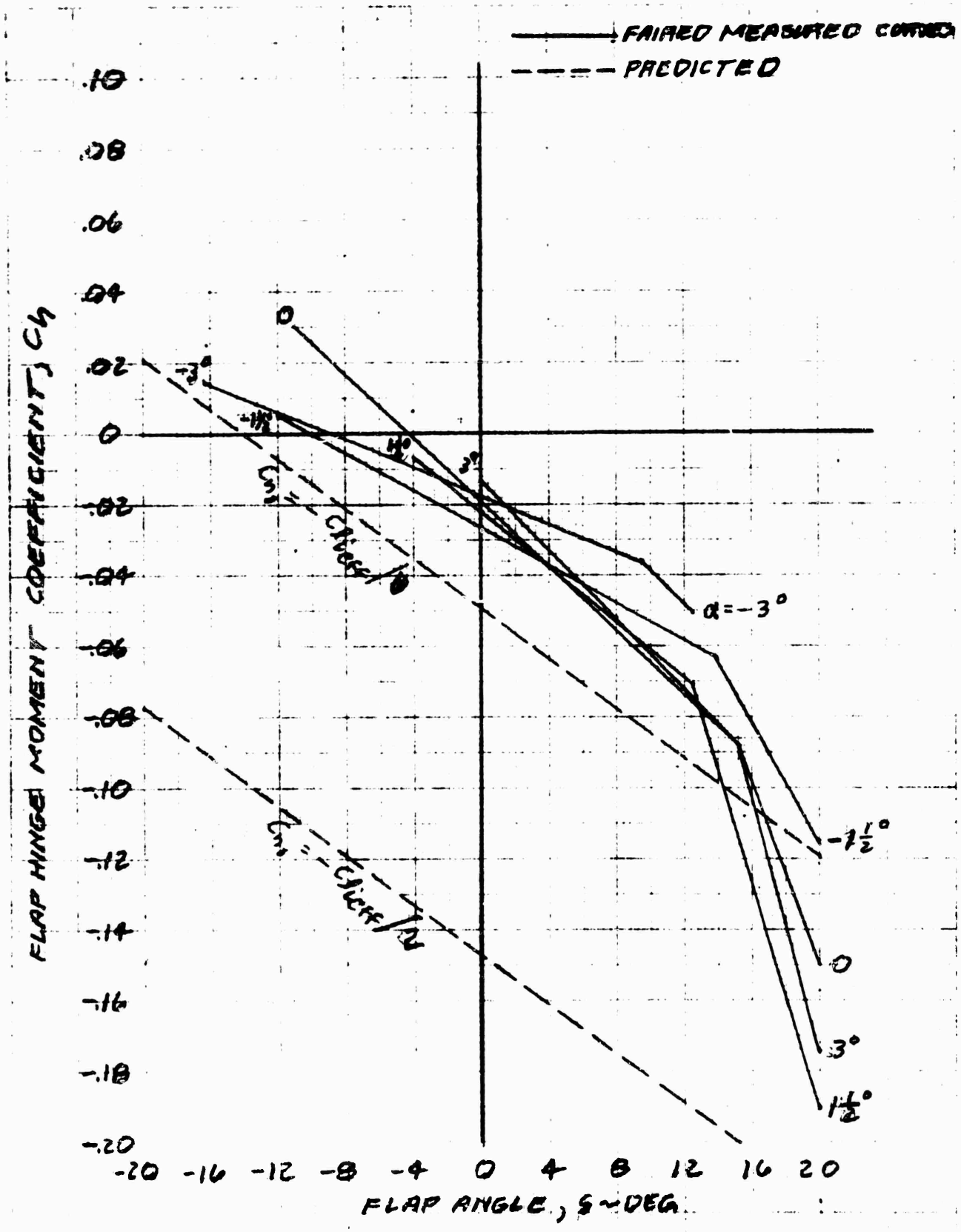


Figure E34. Faired Flap Hinge Moment Curves

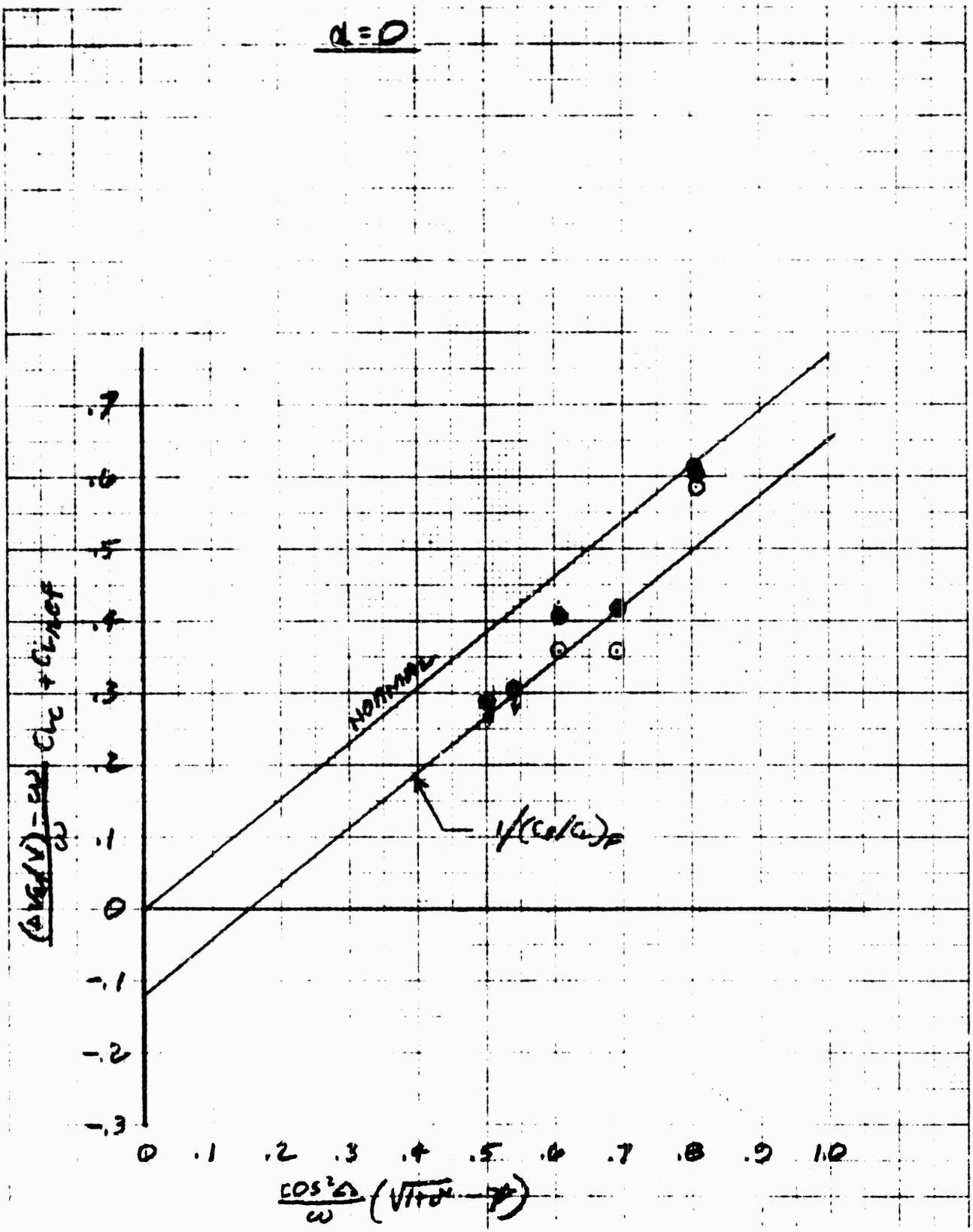


Figure E35. Evaluation of Twist C_L

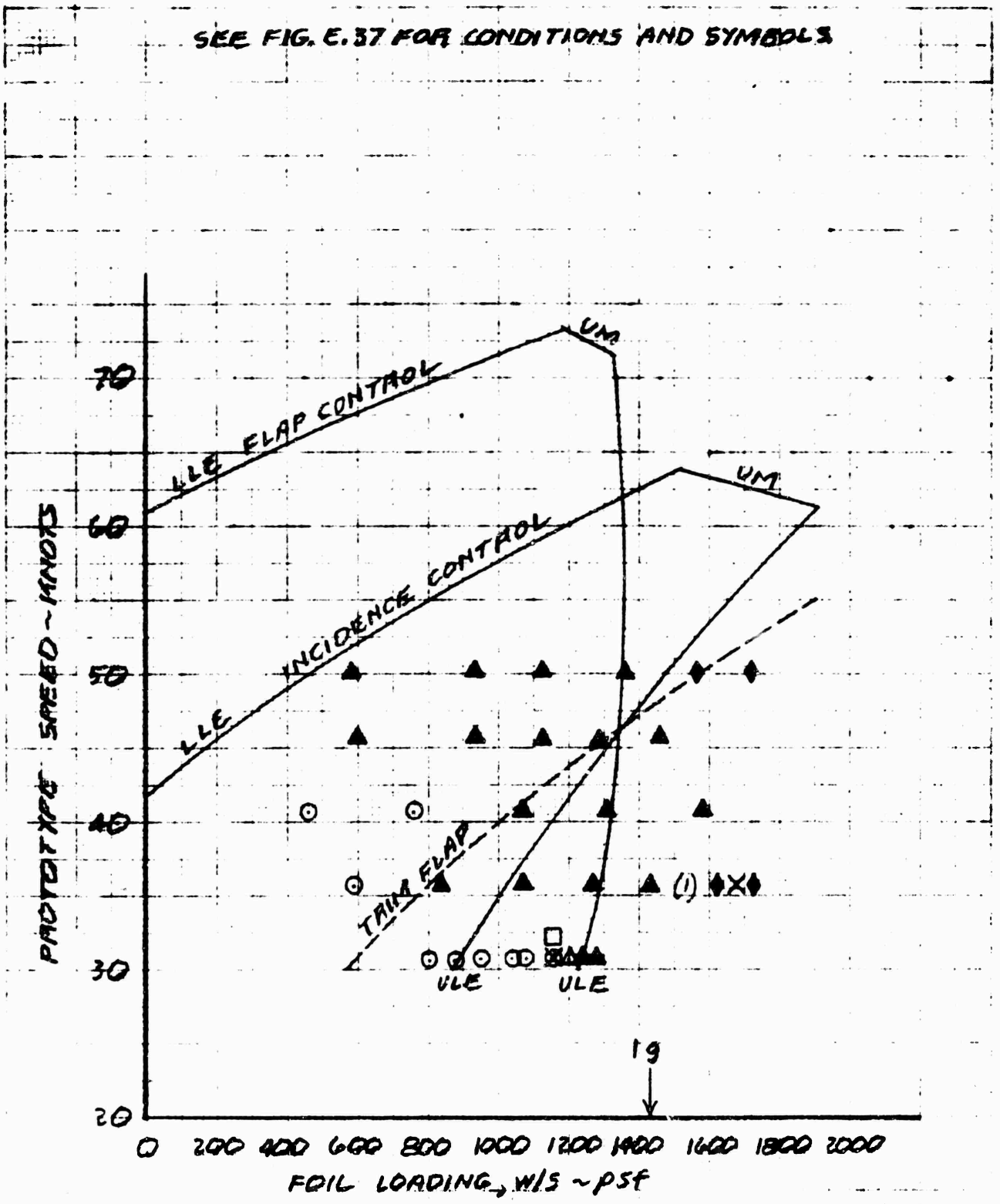


Figure E36. Normal Cavitation Bucket, $\alpha = 0$

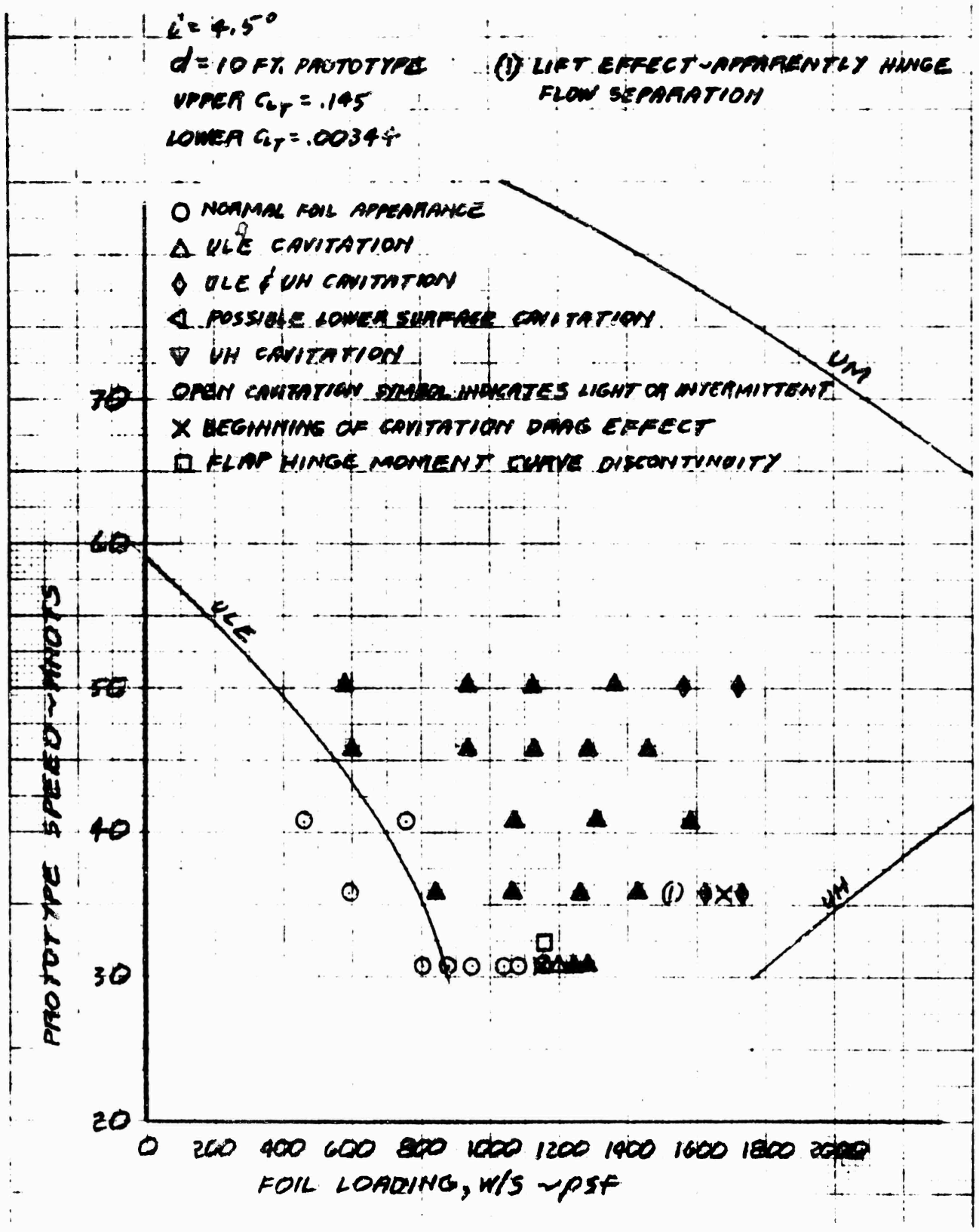


Figure E37. Cavitation Characteristics, $\alpha = 0$

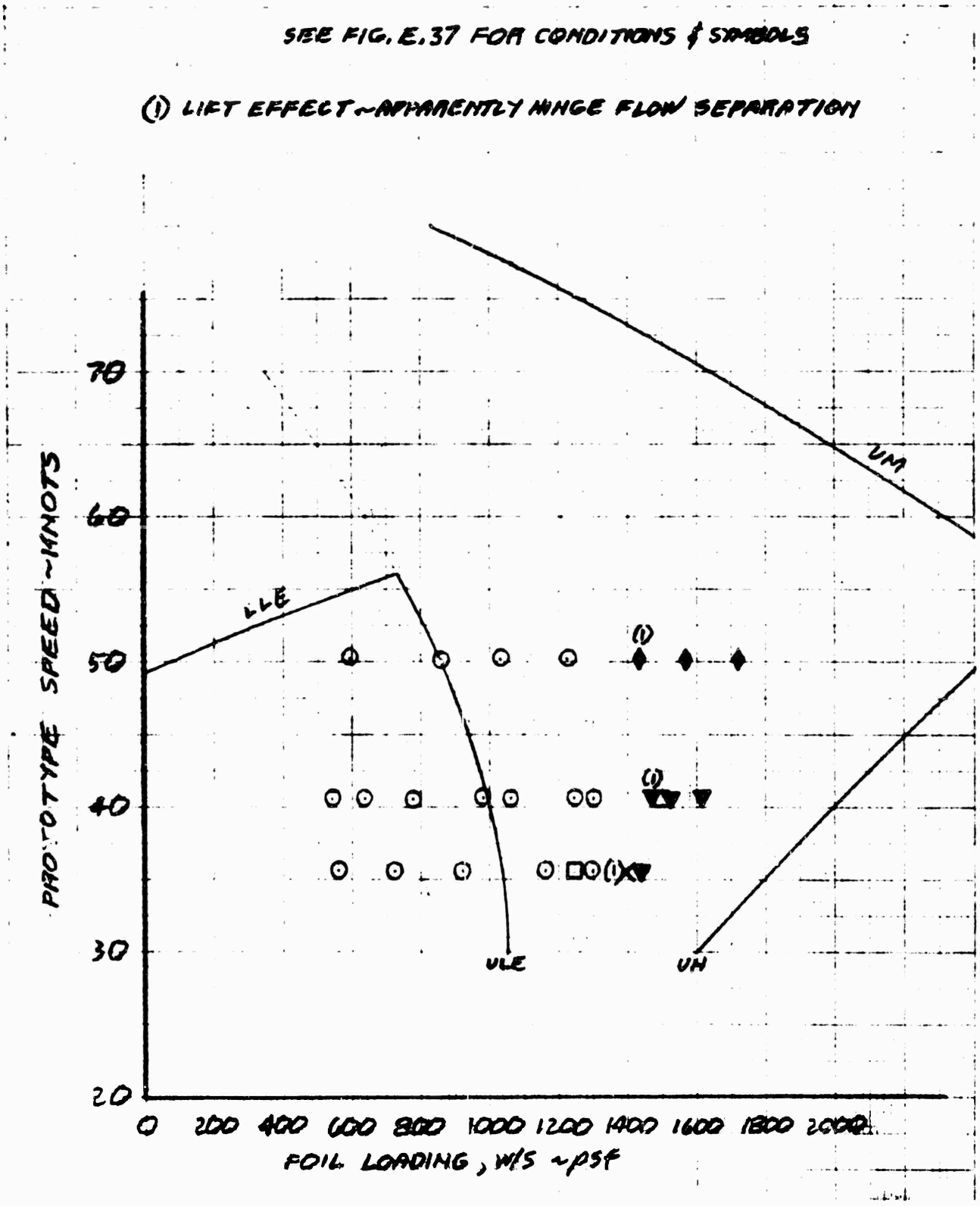


Figure E38. Cavitation Characteristics, $\alpha = -1.5^{o}$

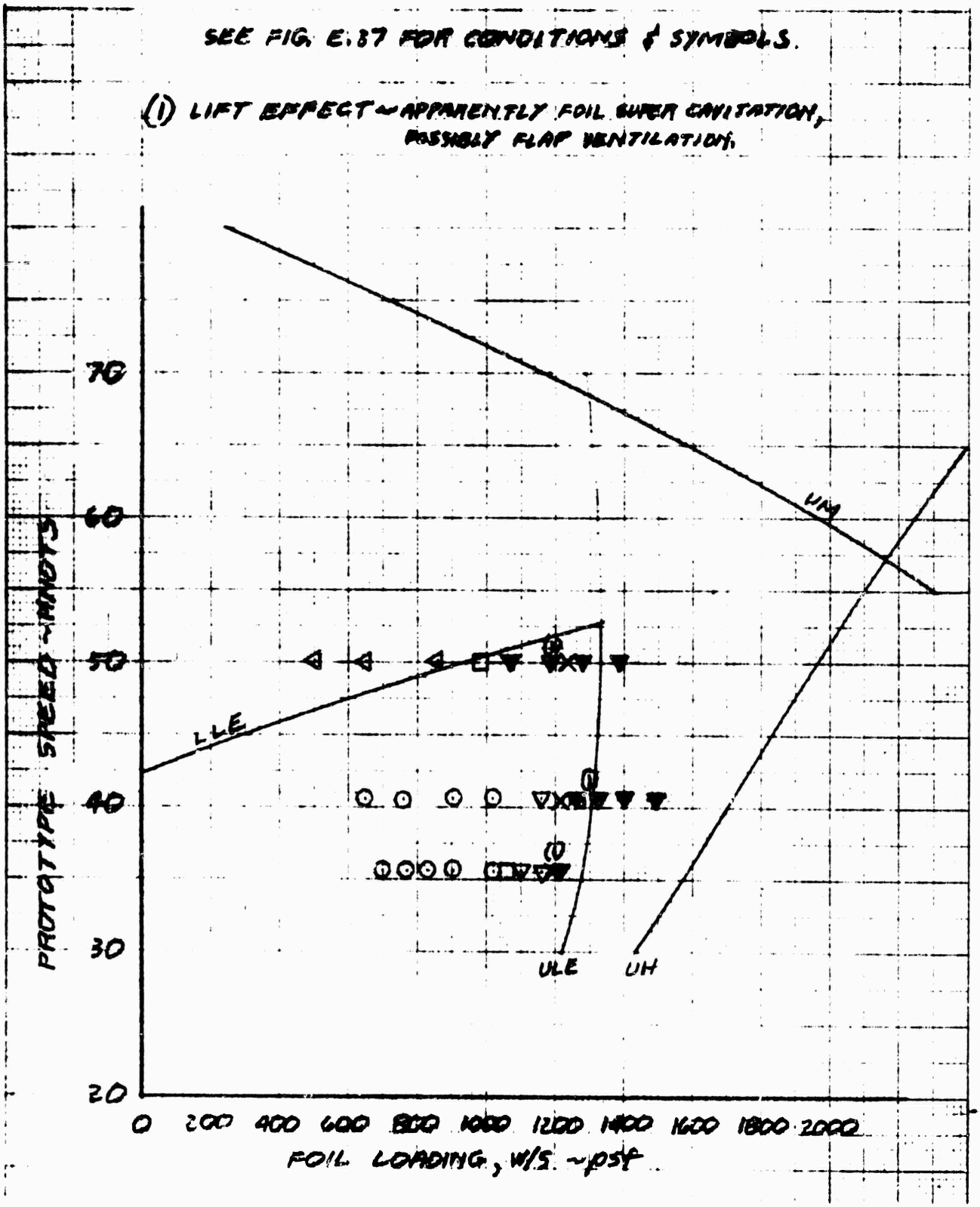


Figure E39. Cavitation Characteristics, $\alpha = -3^{o}$

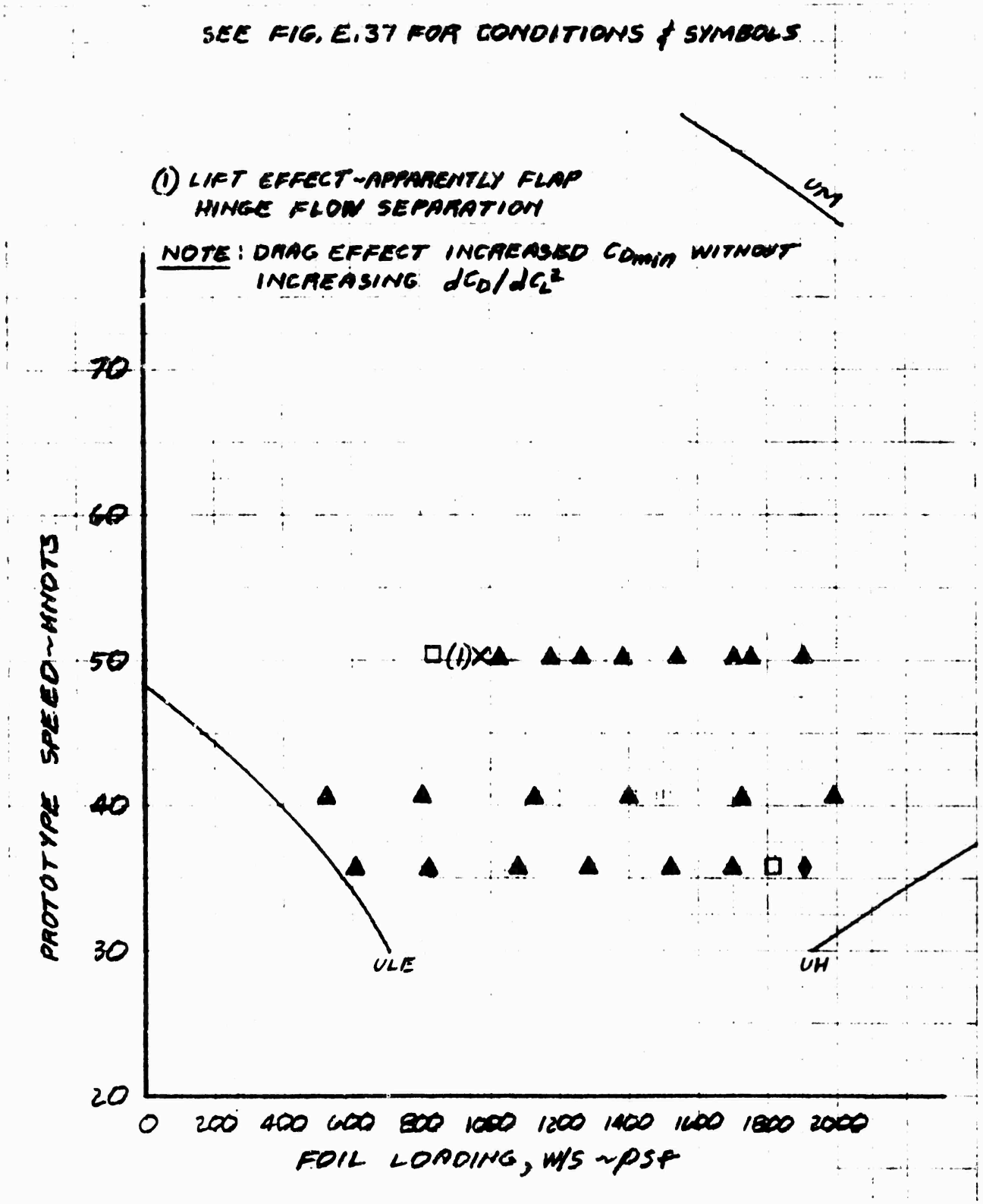


Figure E40. Cavitation Characteristics, $\alpha = 1.5^{o}$

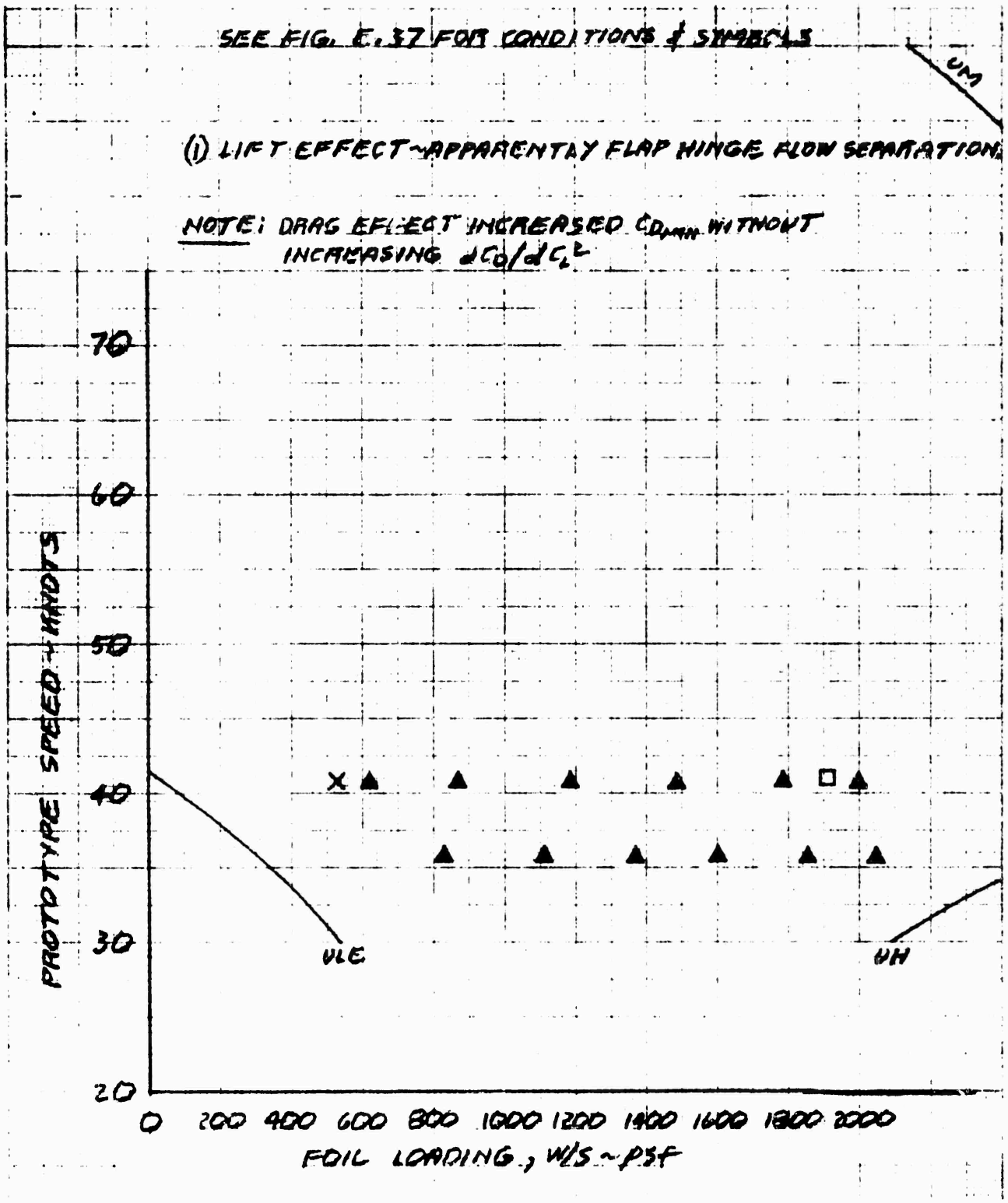
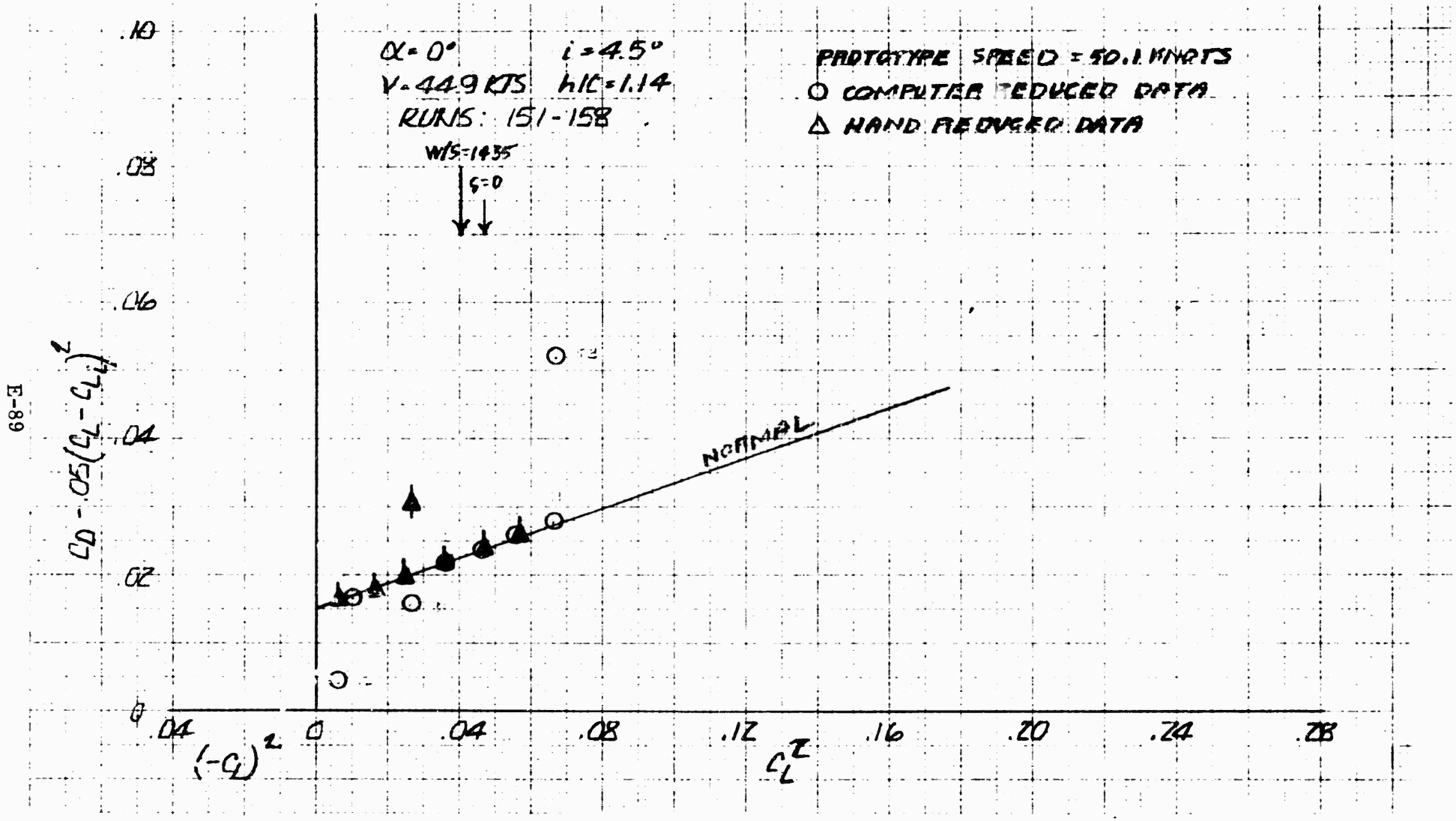


Figure E41. Cavitation Characteristics, $\alpha = 3^{o}$



E-89

Figure E42. Cavitation Drag Effect, 44.9 Knots, α = 0, AG(EH) Fwd. Foil

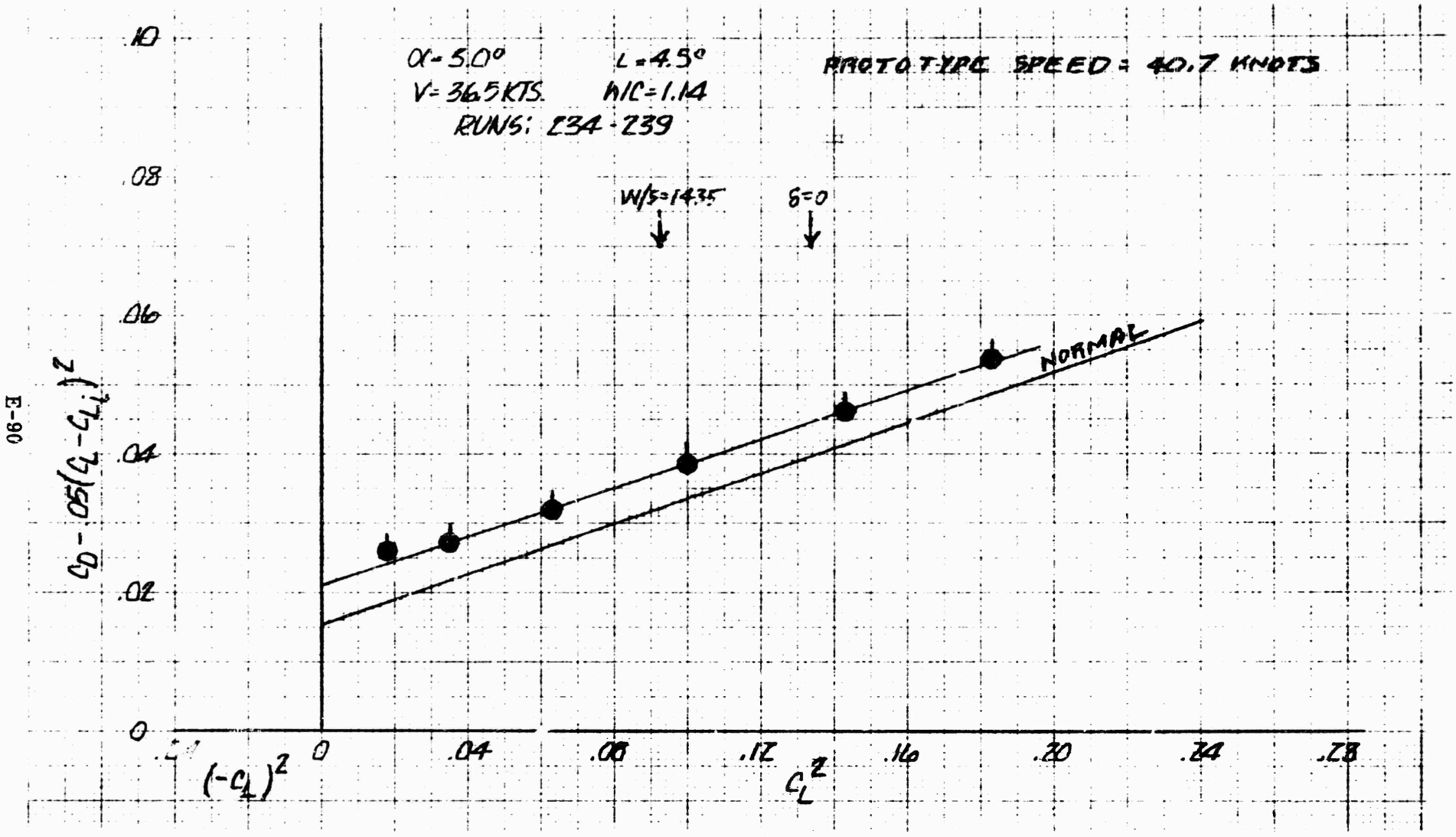


Figure E43. Cavitation Drag Effect, 36.5 Knots, $\alpha = 3^{\circ}$, AG(EH) Fwd. Foil

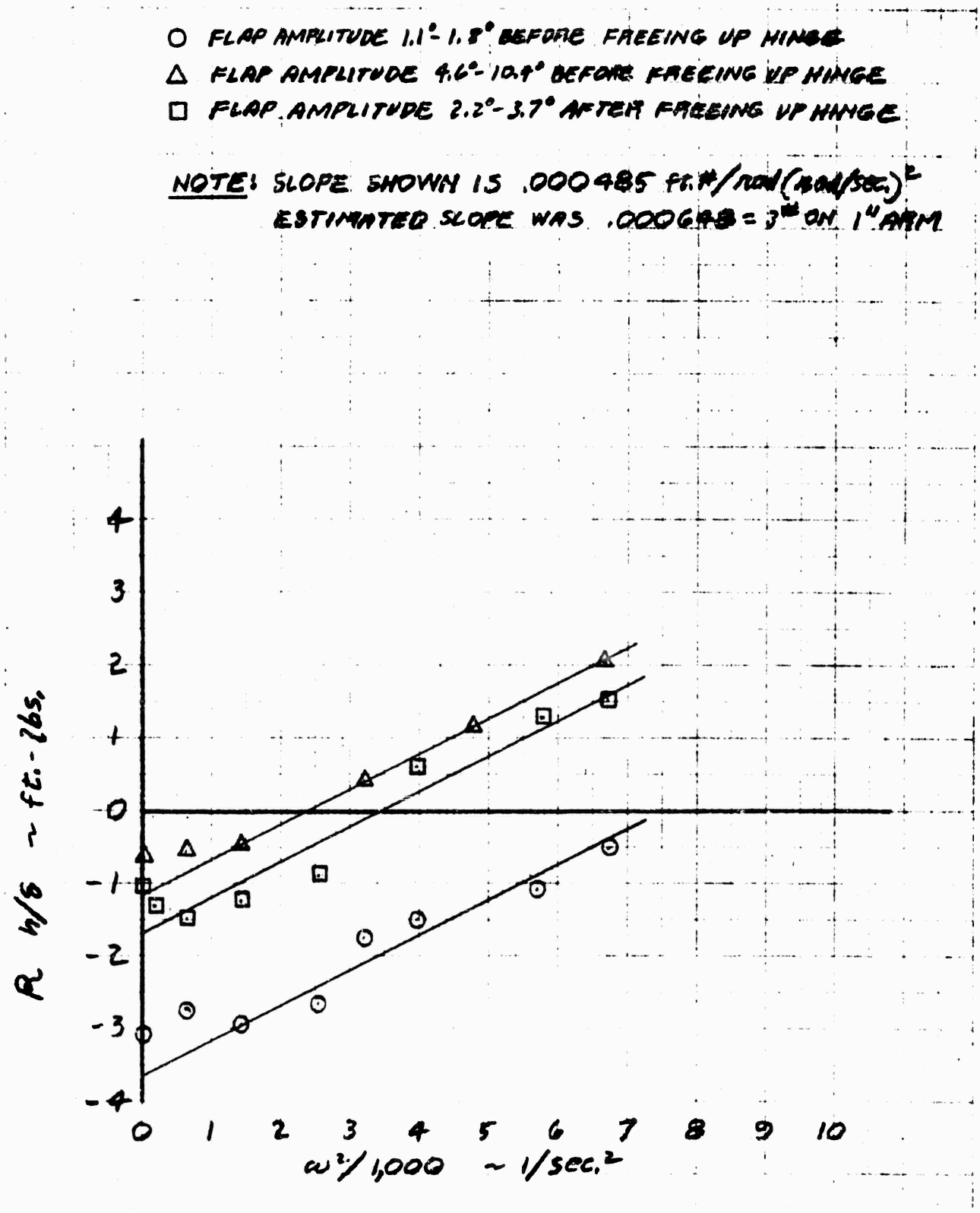


Figure E44. Flap System Inertia In Air

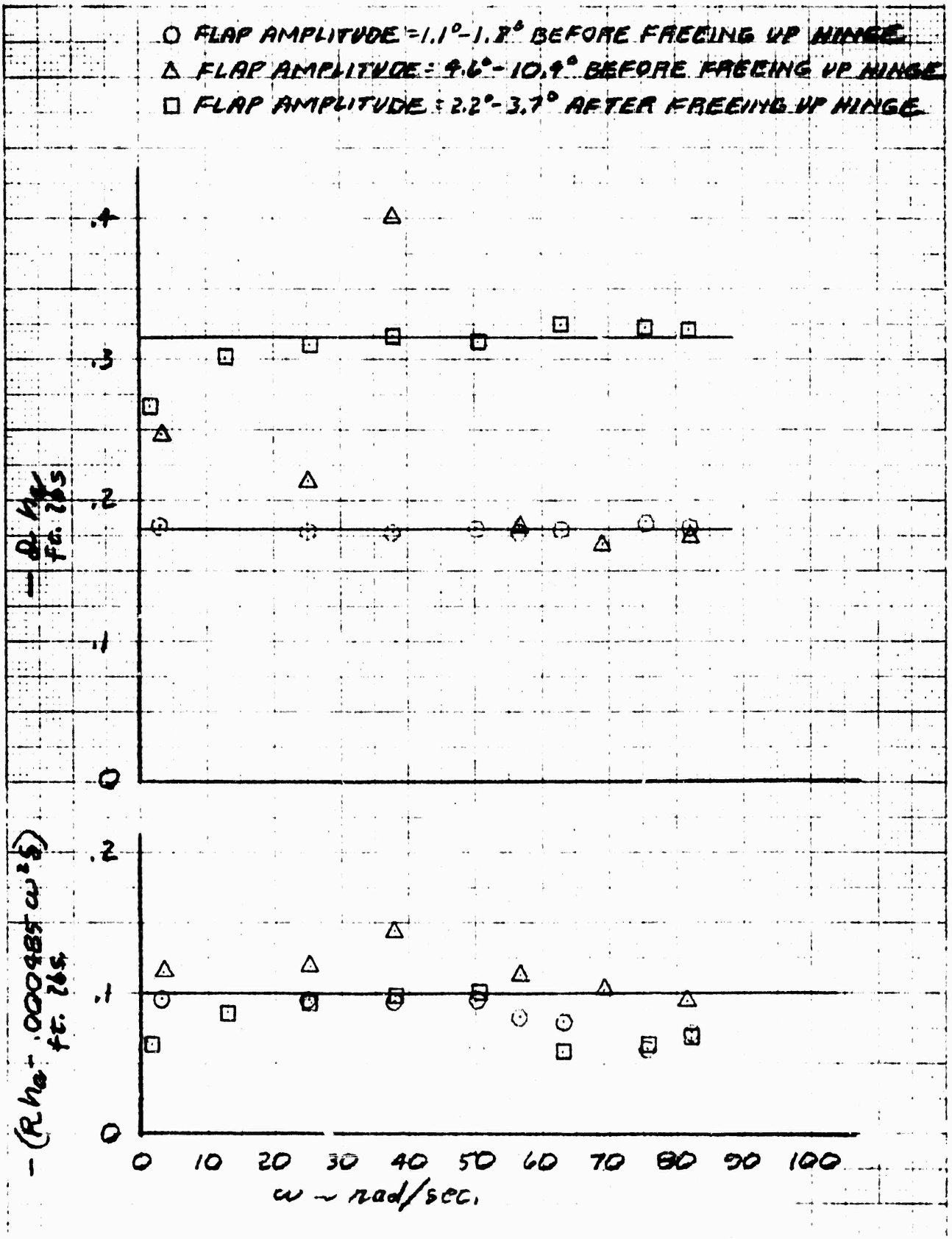


Figure E45. Flap Hinge Friction In Air

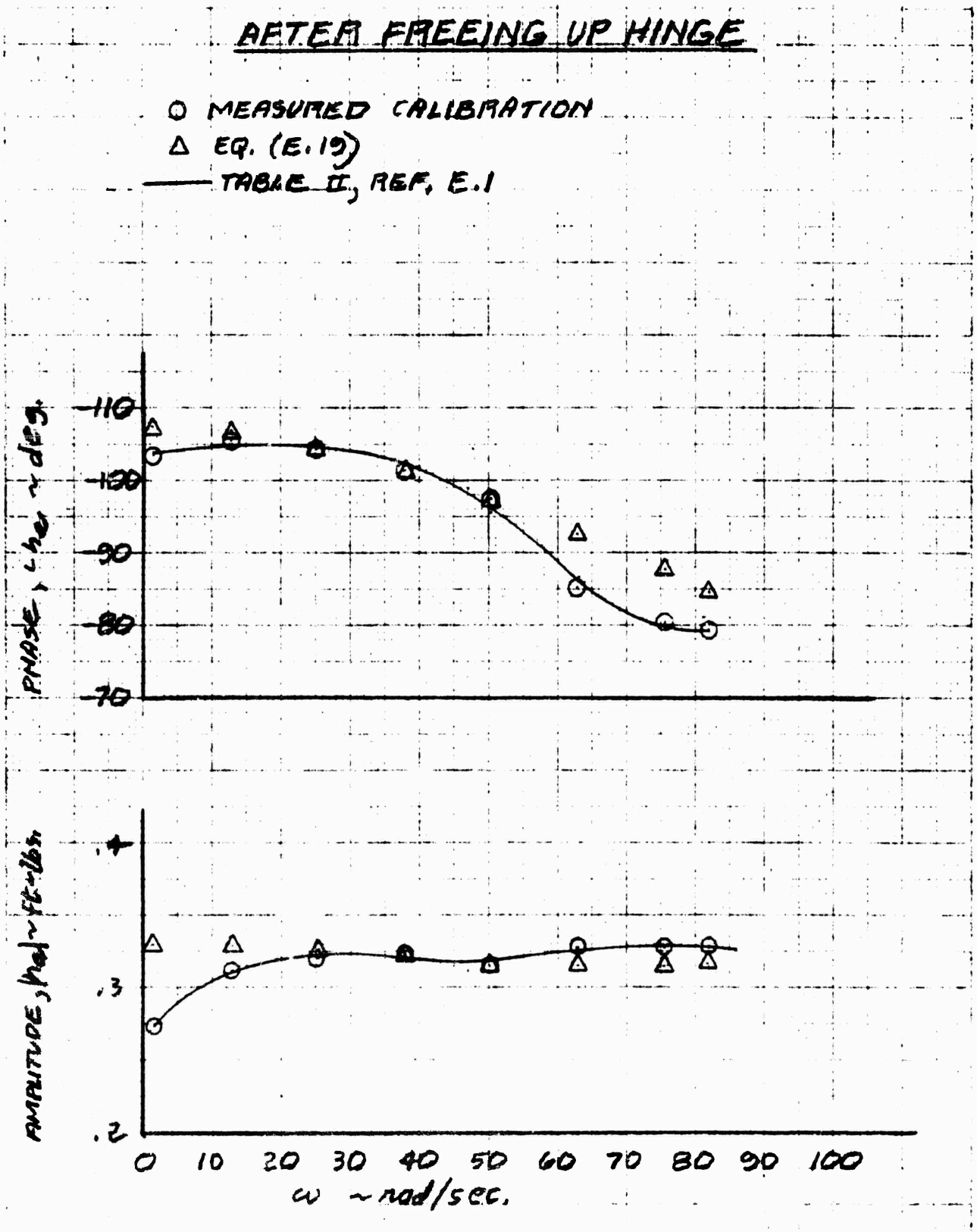


Figure E46. Flap Hinge Moment Air Calibration

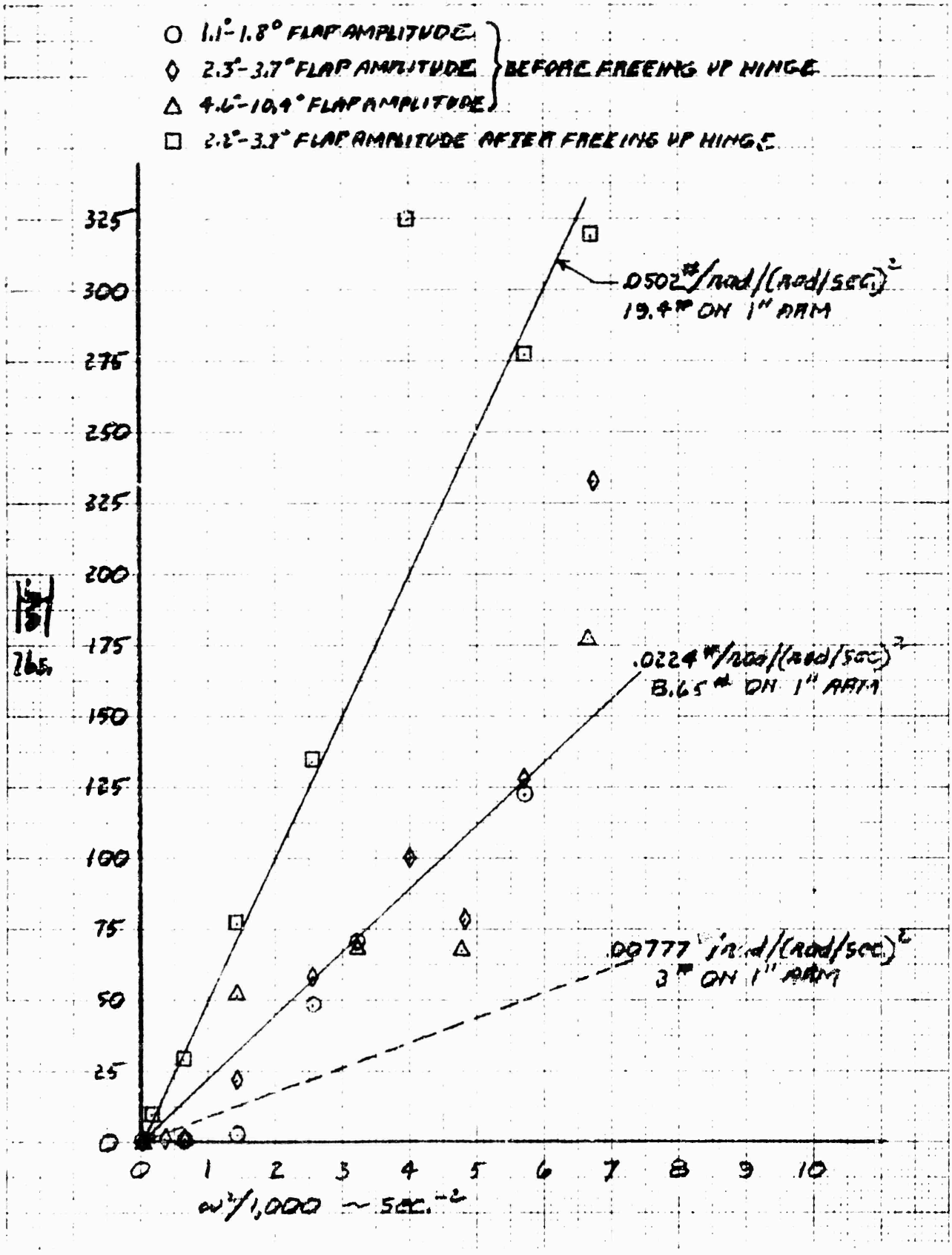


Figure E47. Lift Amplitude In Air

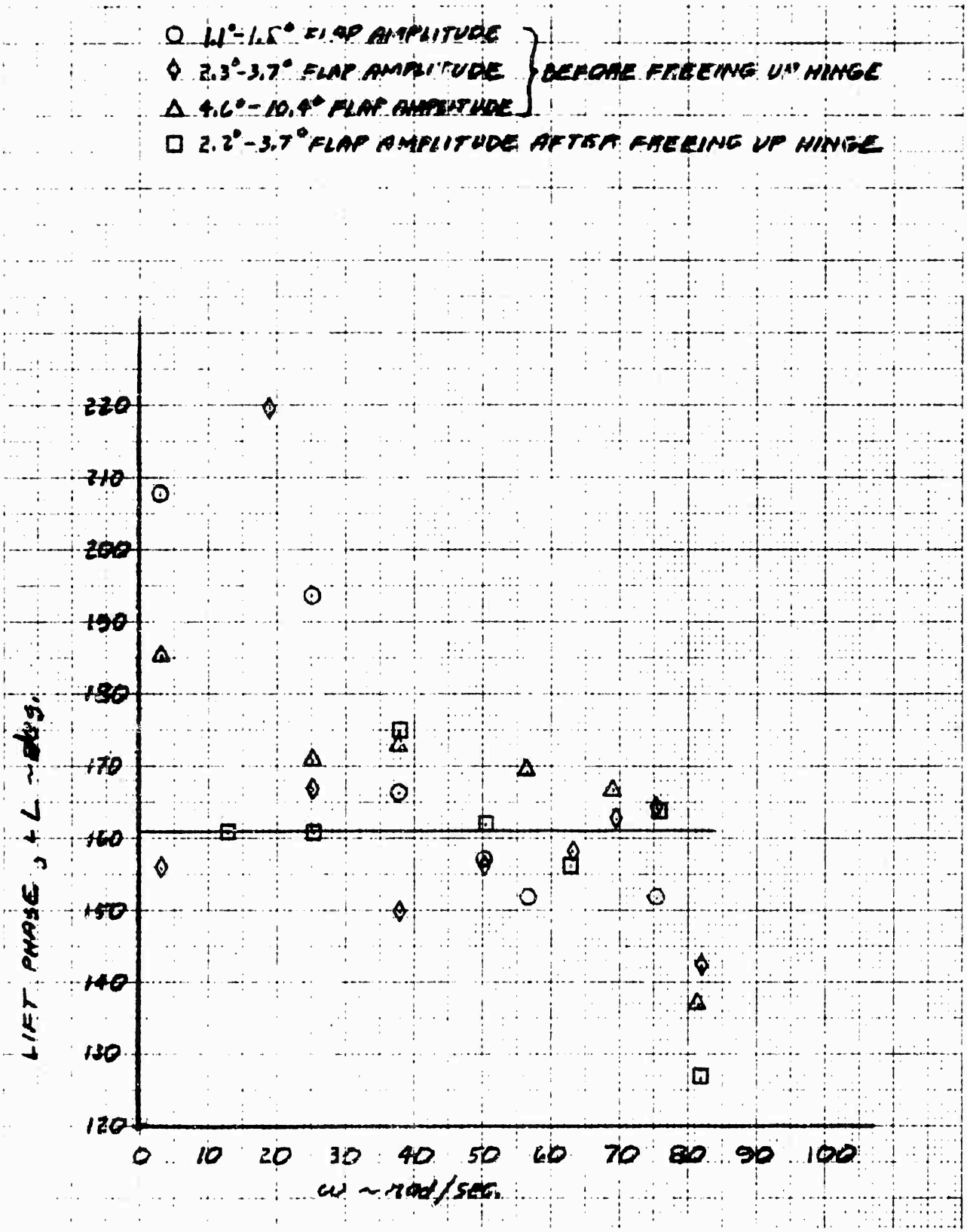


Figure E48. Lift Phase In Air

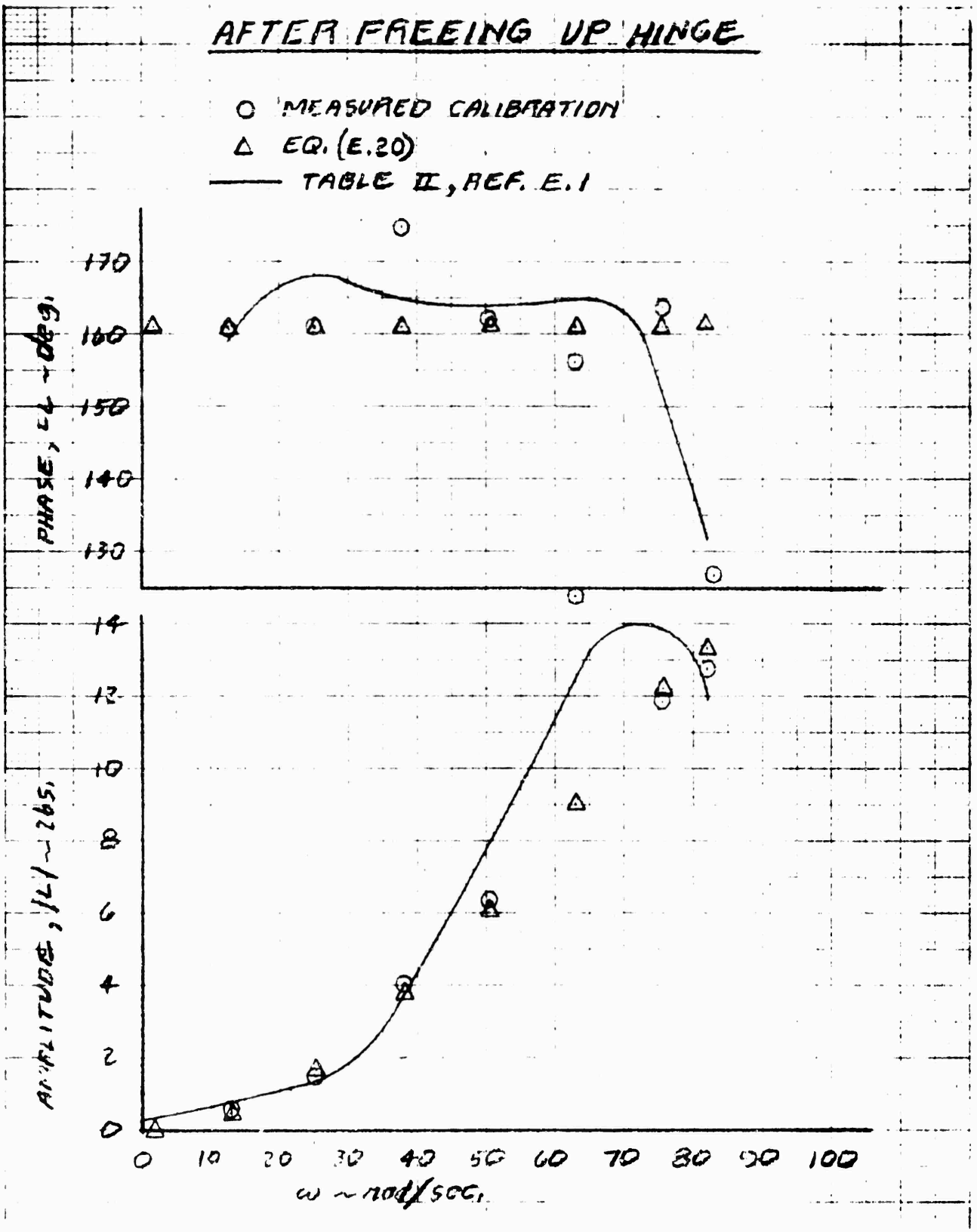


Figure E49. Foil Lift Air Calibration

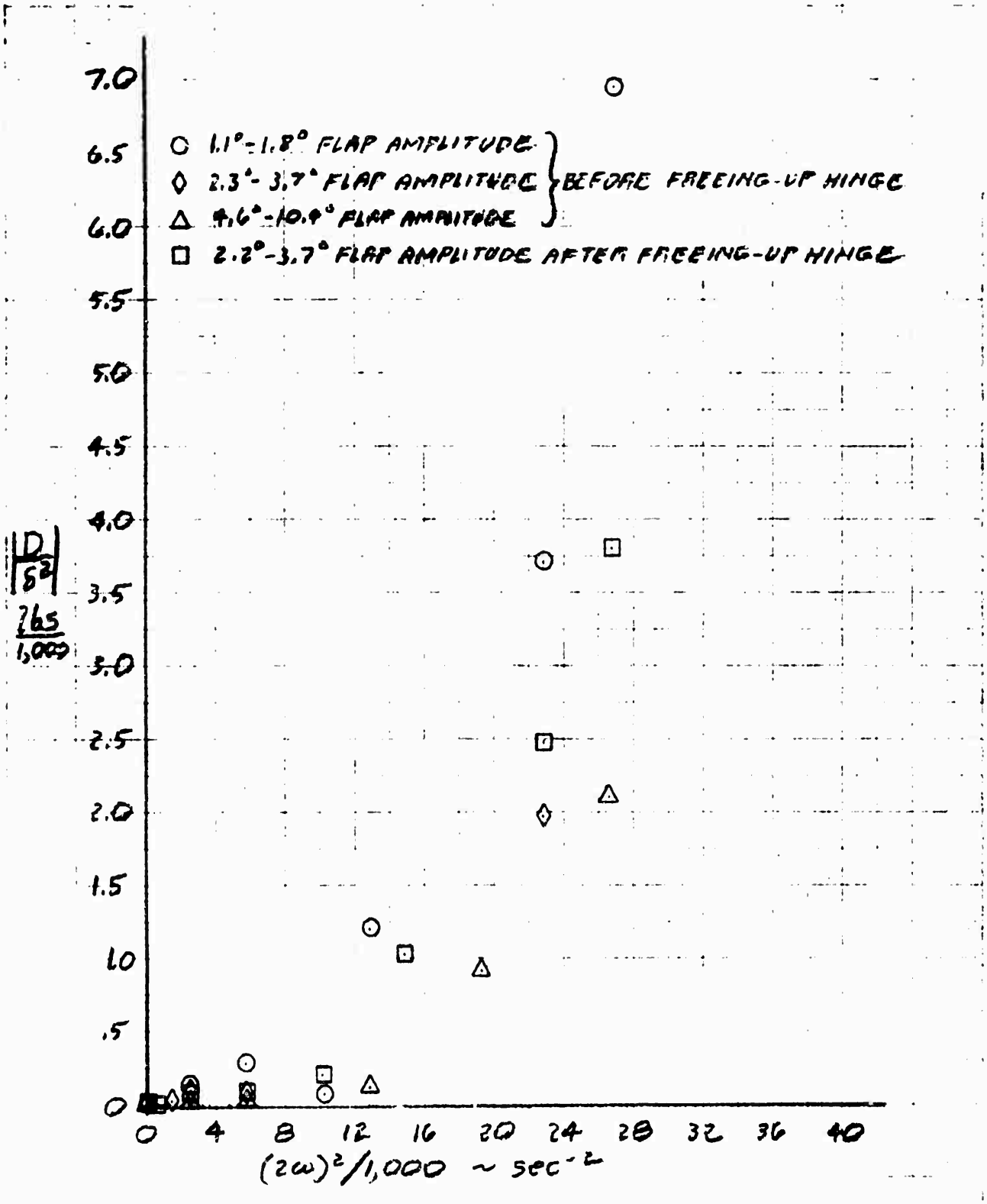


Figure E50. Drag Amplitude In Air, As Function of δ^2

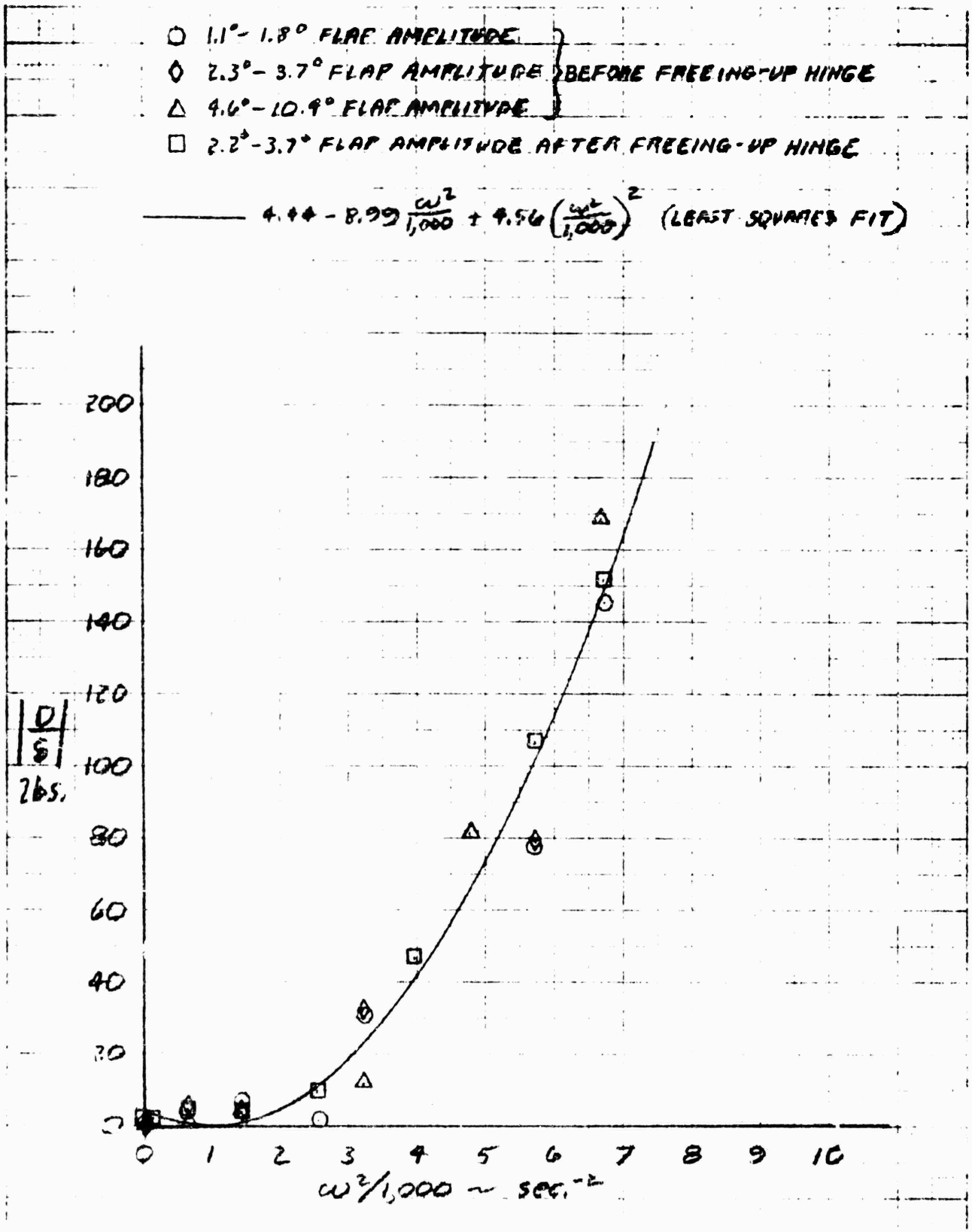


Figure E51. Drag Amplitude In Air

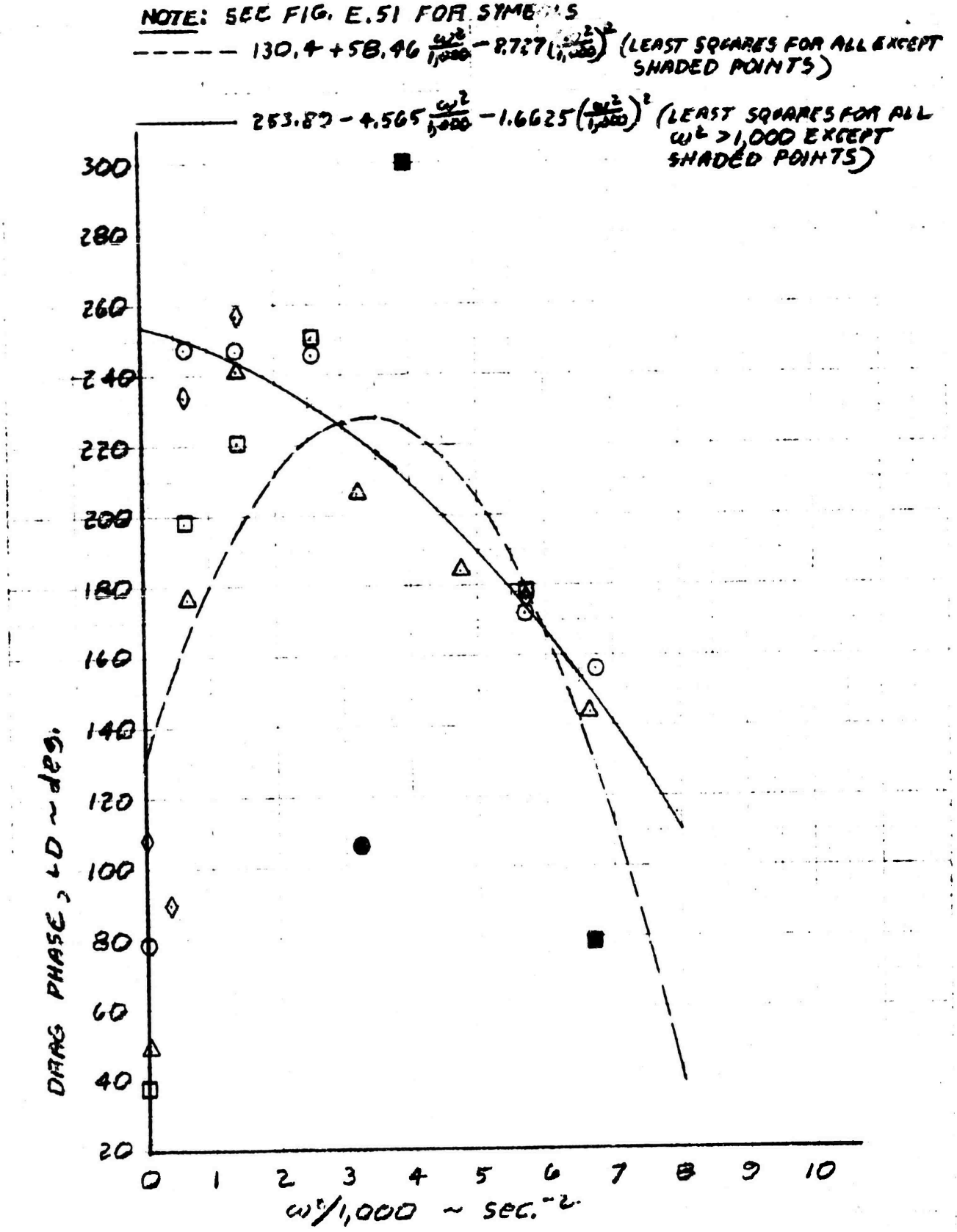


Figure E52. Drag Phase In Air

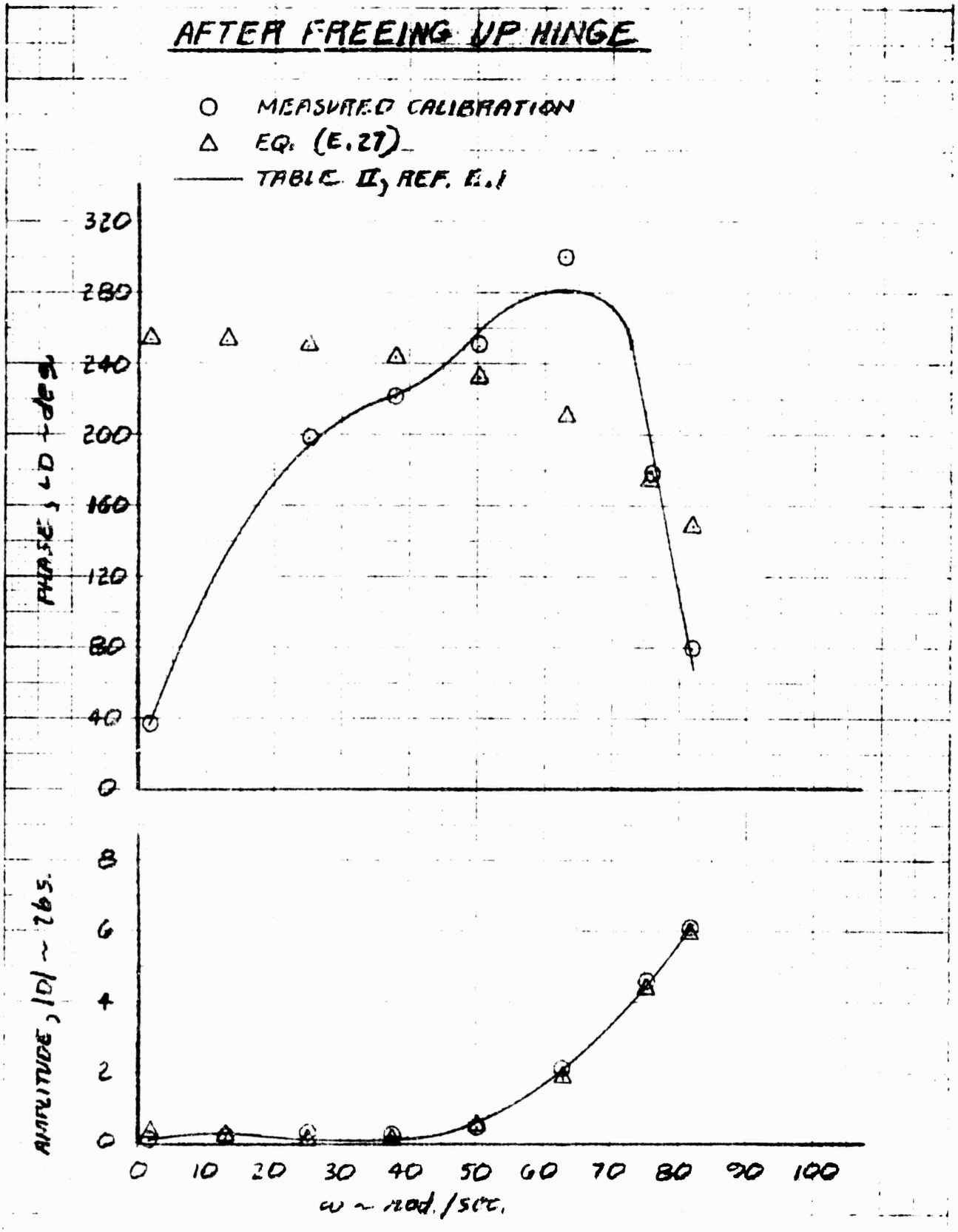


Figure E53. Foil Drag Air Calibration

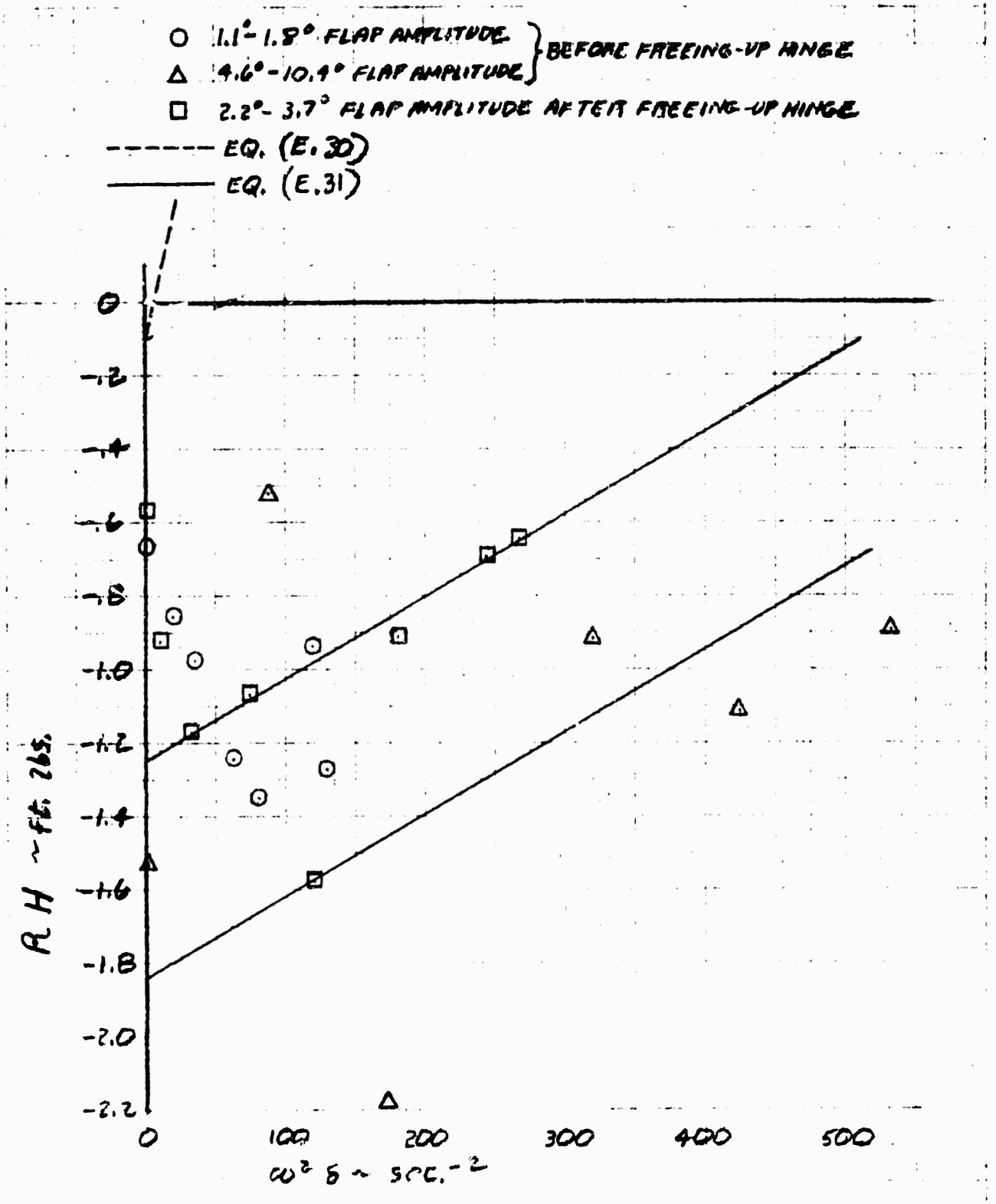


Figure E54. Foil Hinge Moment In Air, Real Part

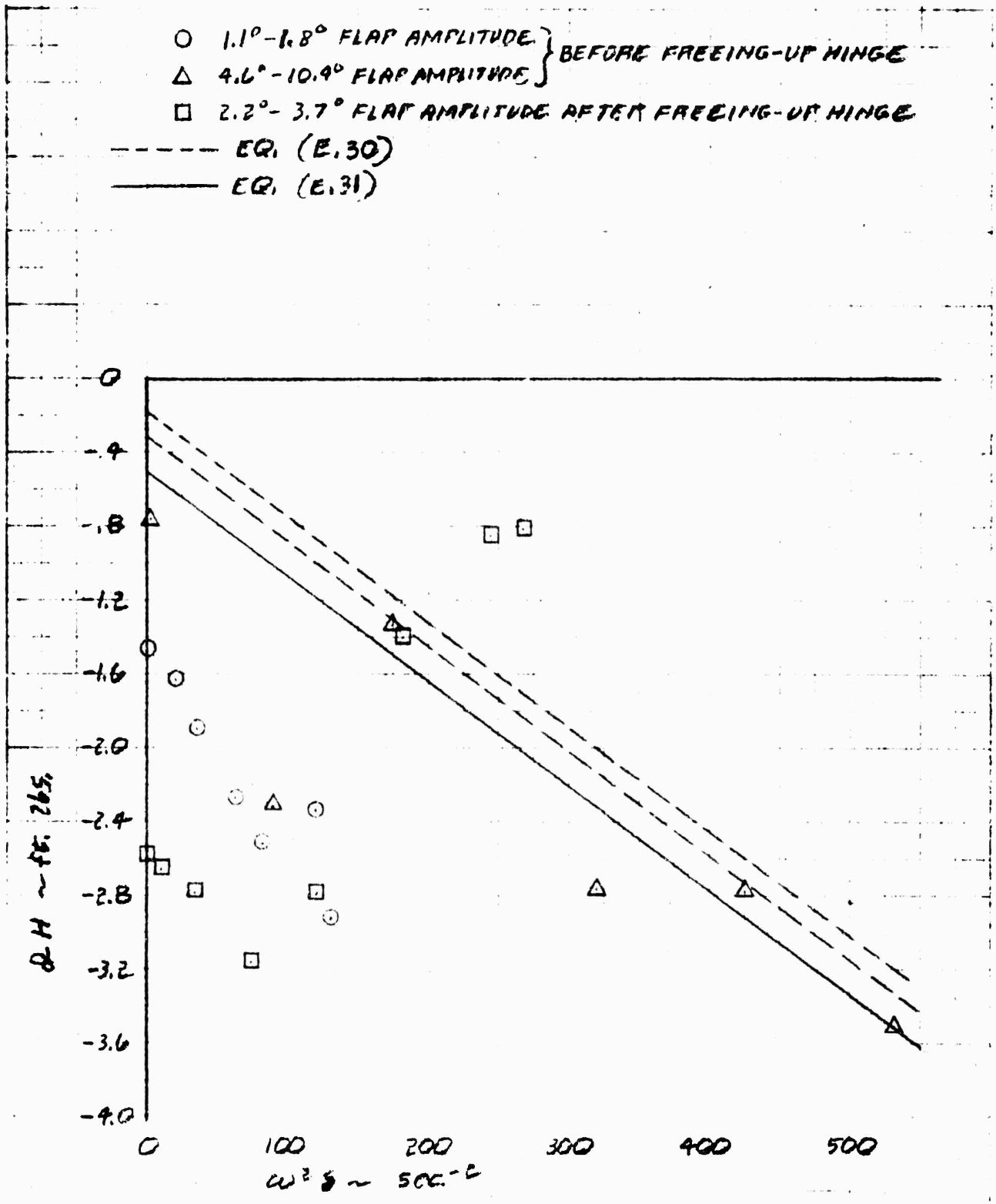


Figure E55. Foil Hinge Moment In Air, Imaginary Part

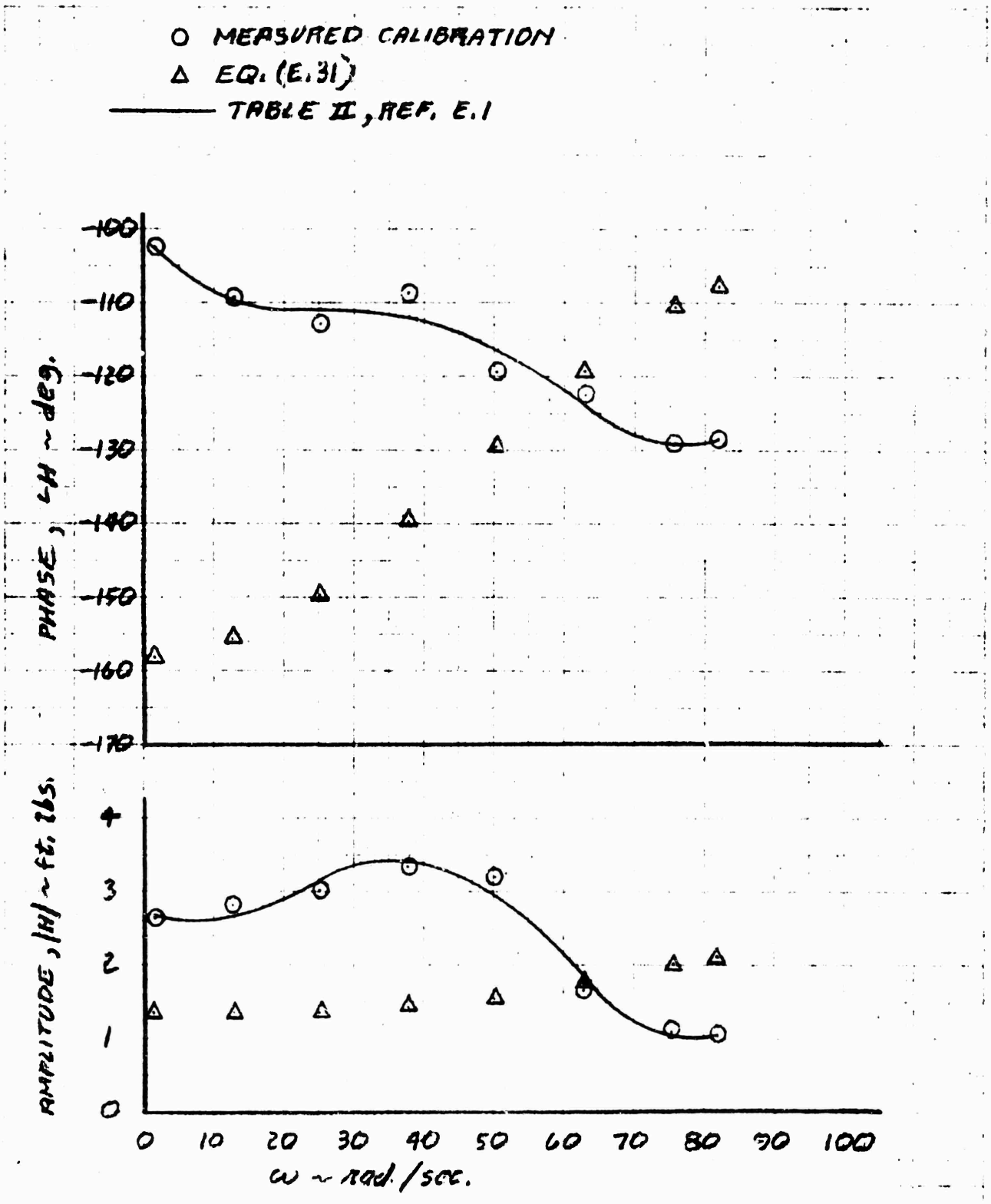


Figure E56. Foil Hinge Moment Air Calibration, After Freeing-Up Hinge

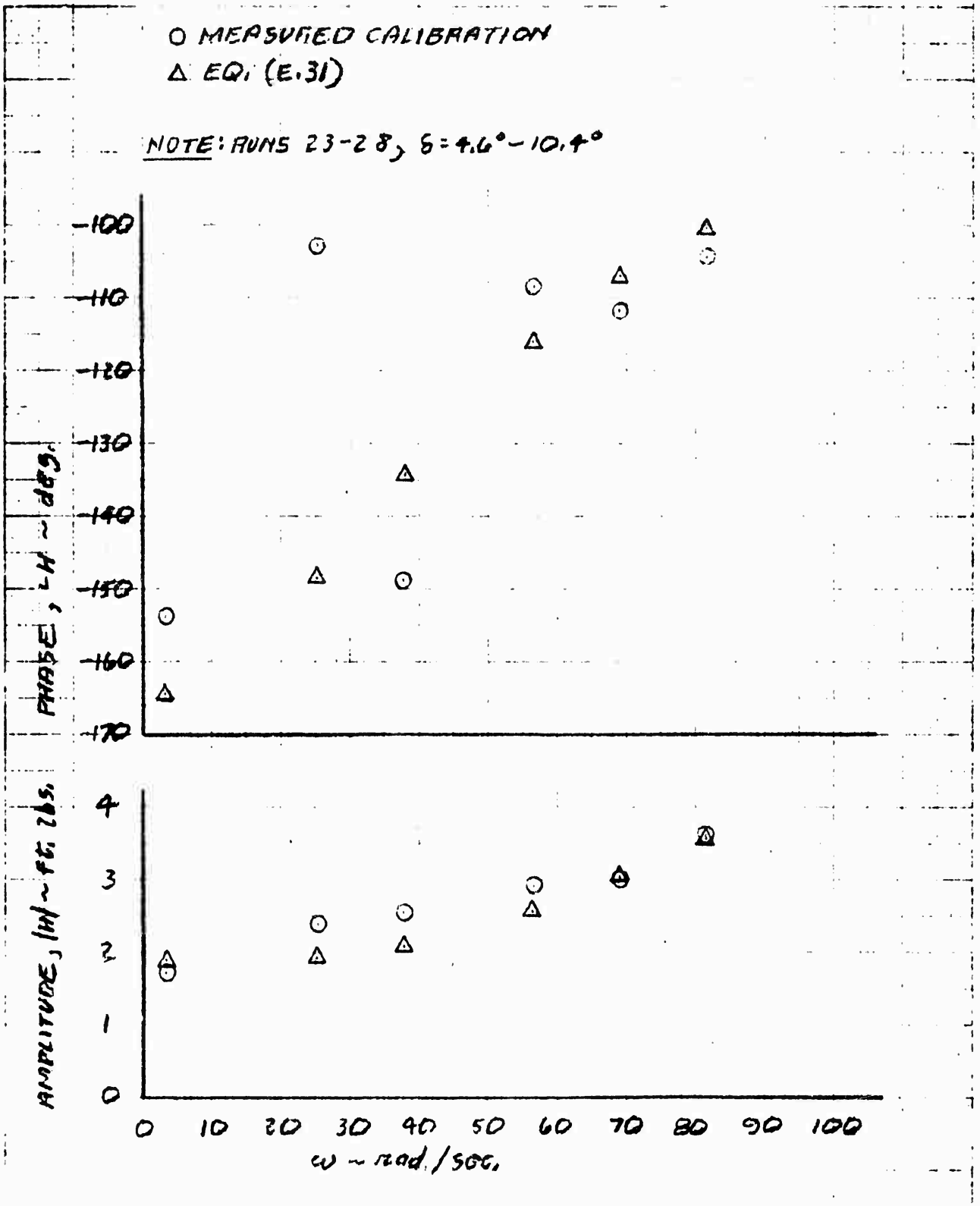


Figure E57. Foil Hinge Moment Air Calibration, Before Freeing-Up Hinge

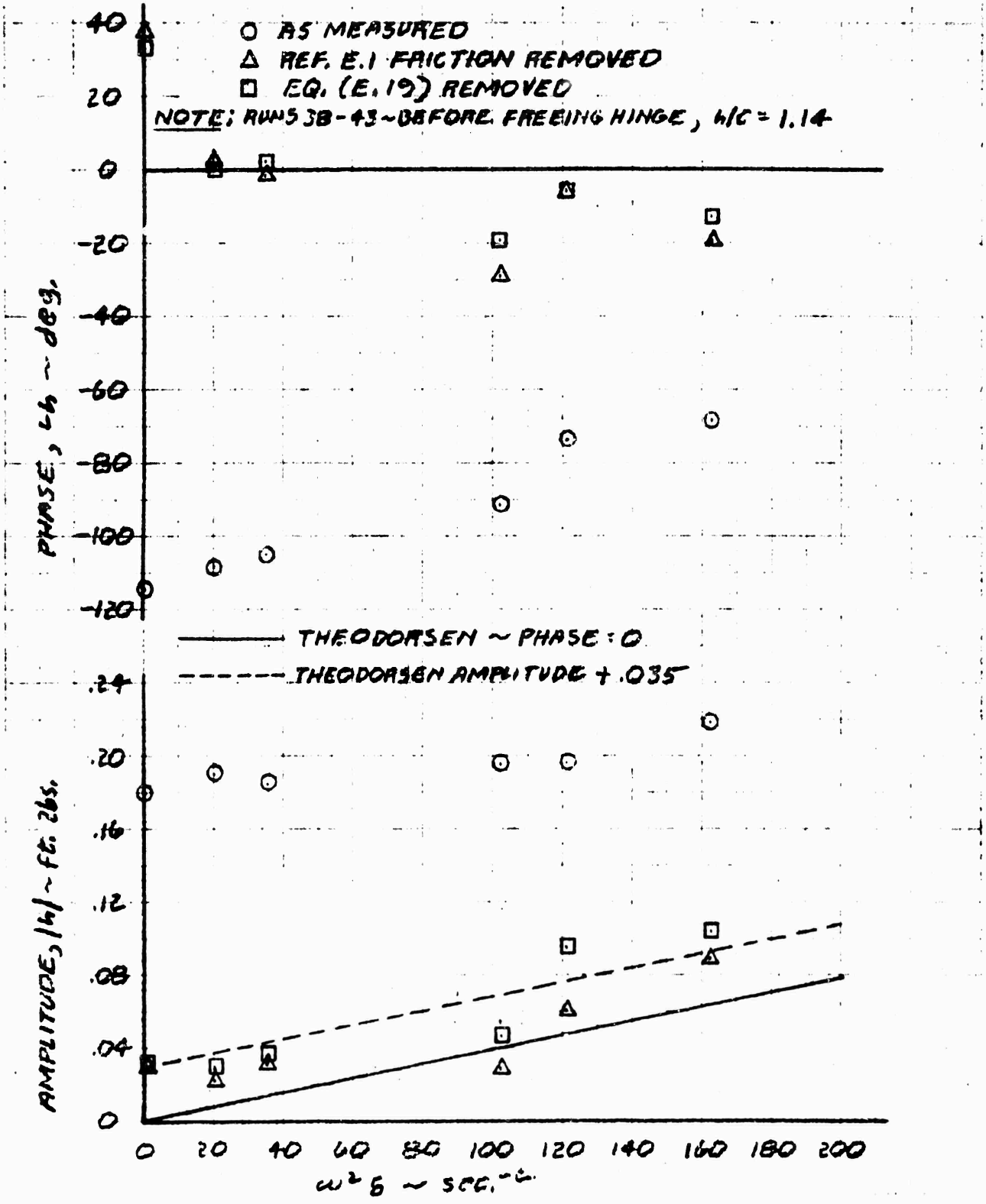


Figure E58. Static Calibration, Flap Hinge Moment

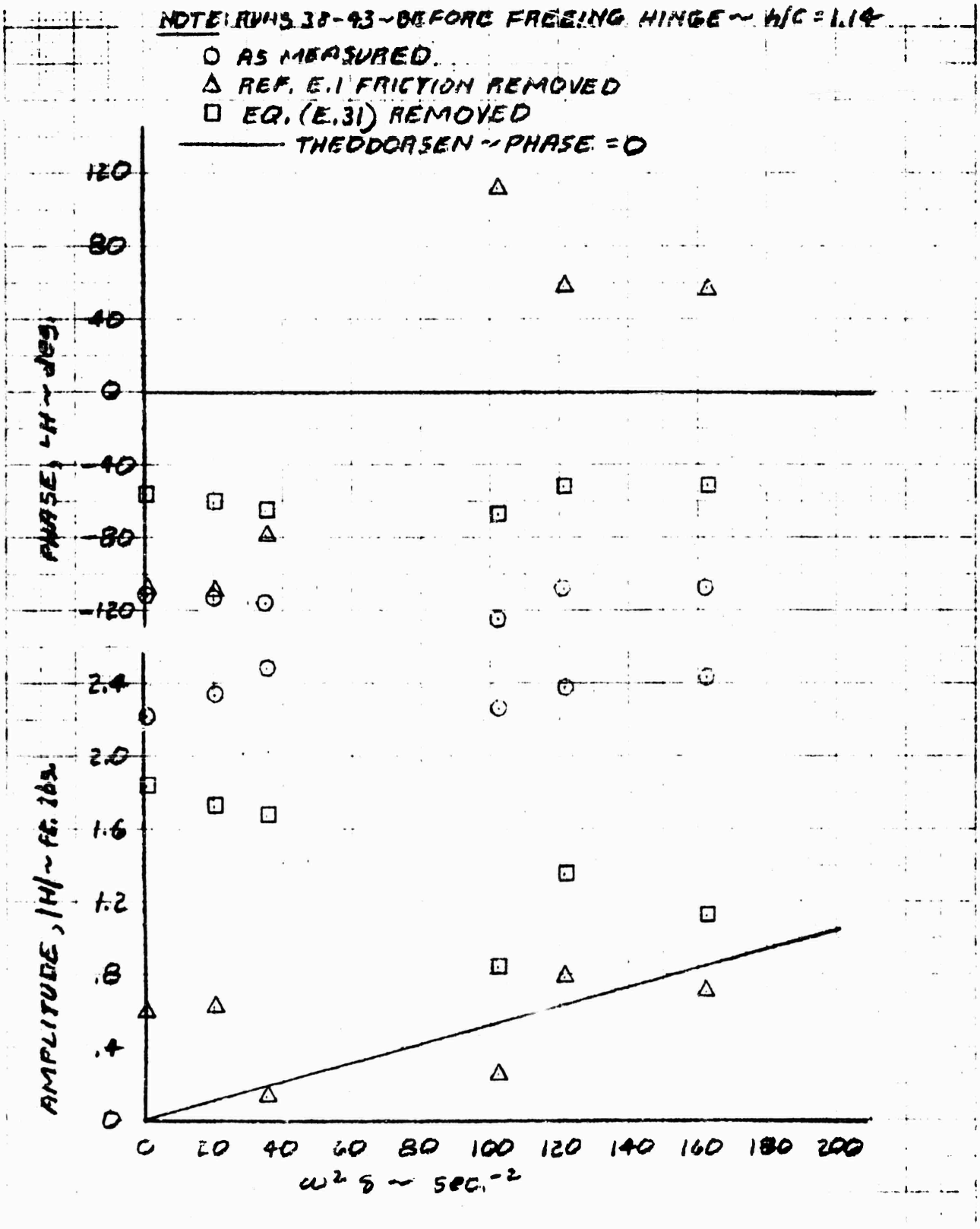


Figure E59. Static Calibration, Foil Hinge Moment

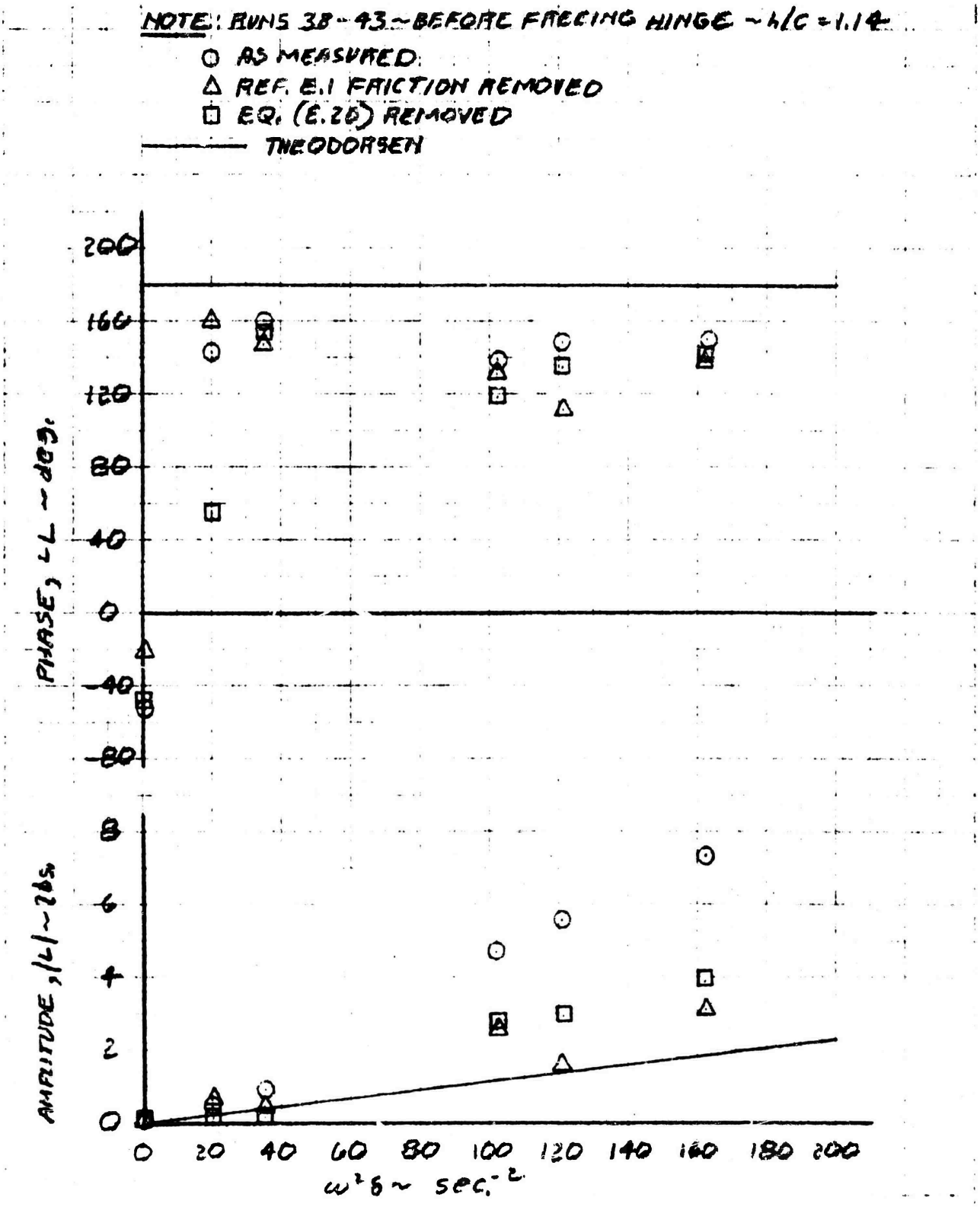


Figure E60. Static Calibration, Lift

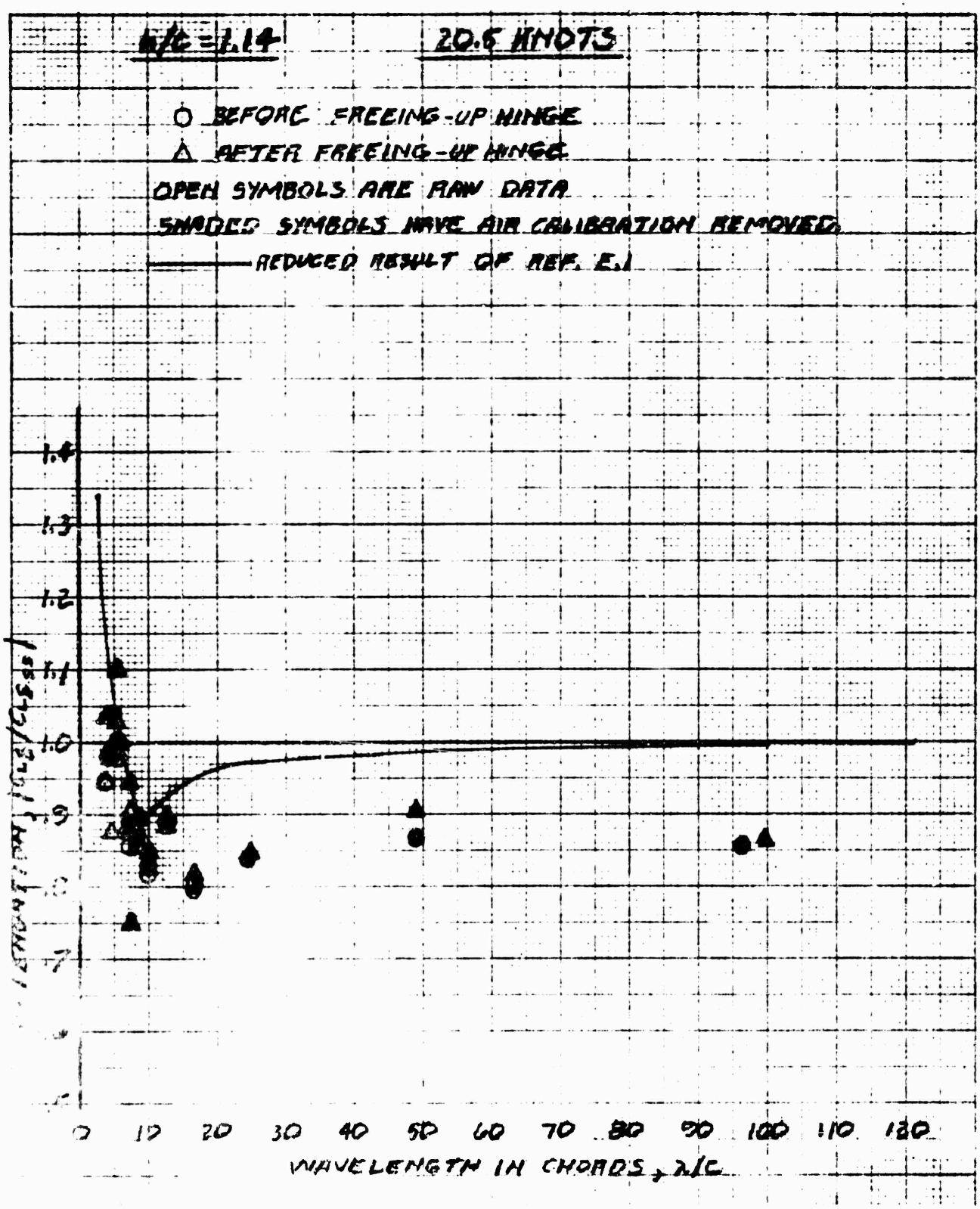


Figure E61. Calibration Effect, Flap Lift Amplitude

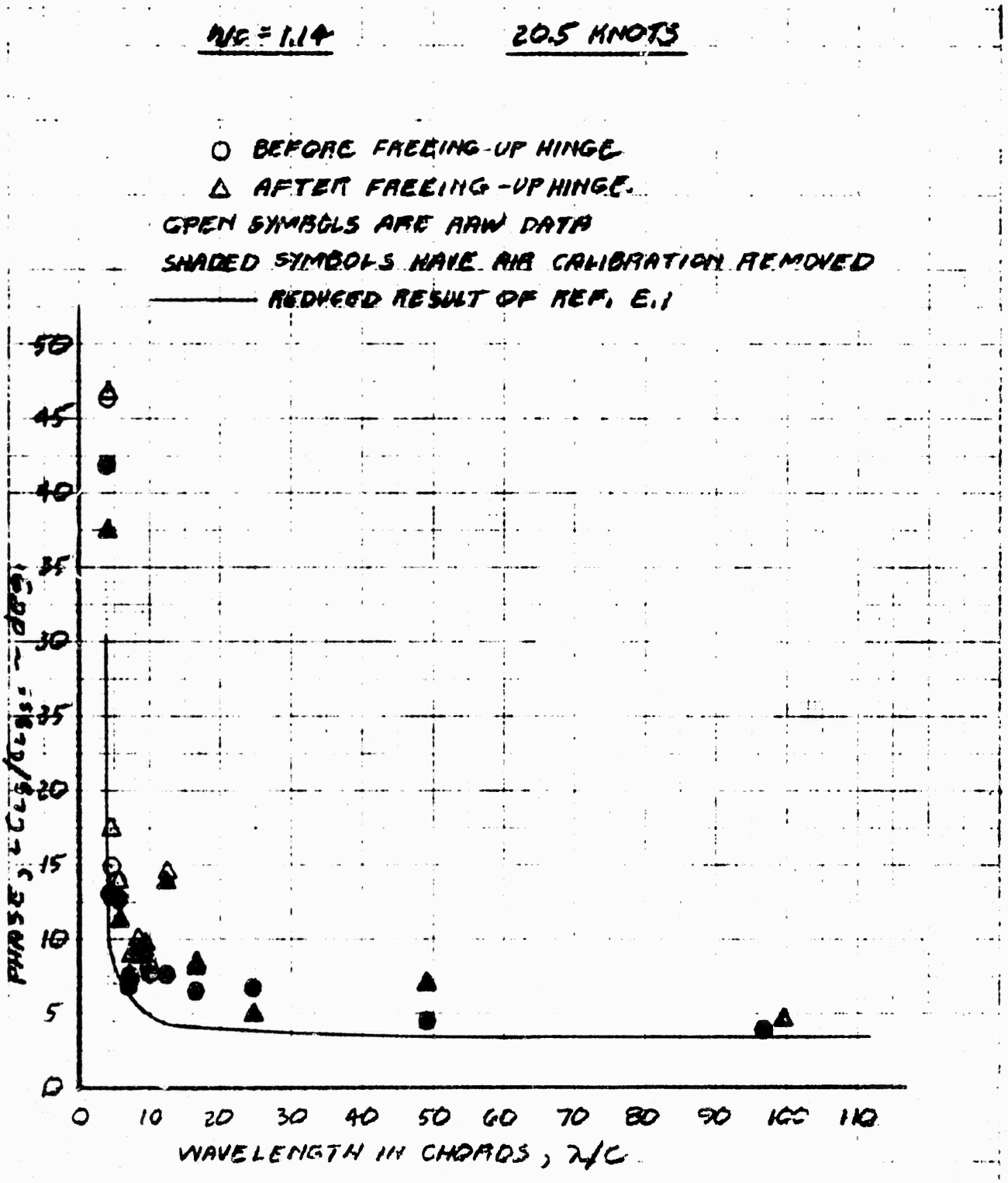


Figure E62. Calibration Effect, Flap Lift Phase

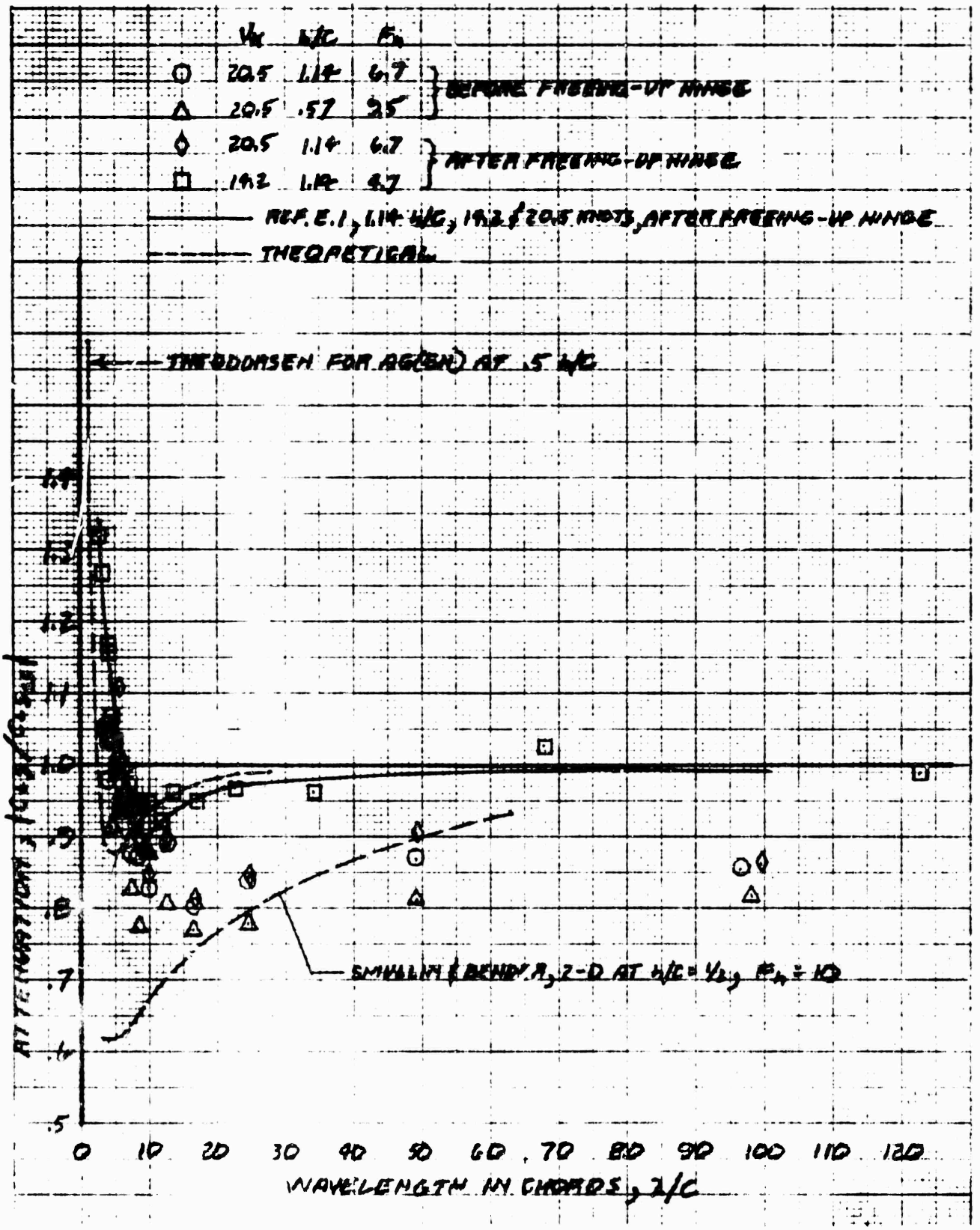


Figure E63. Flap Lift Amplitude

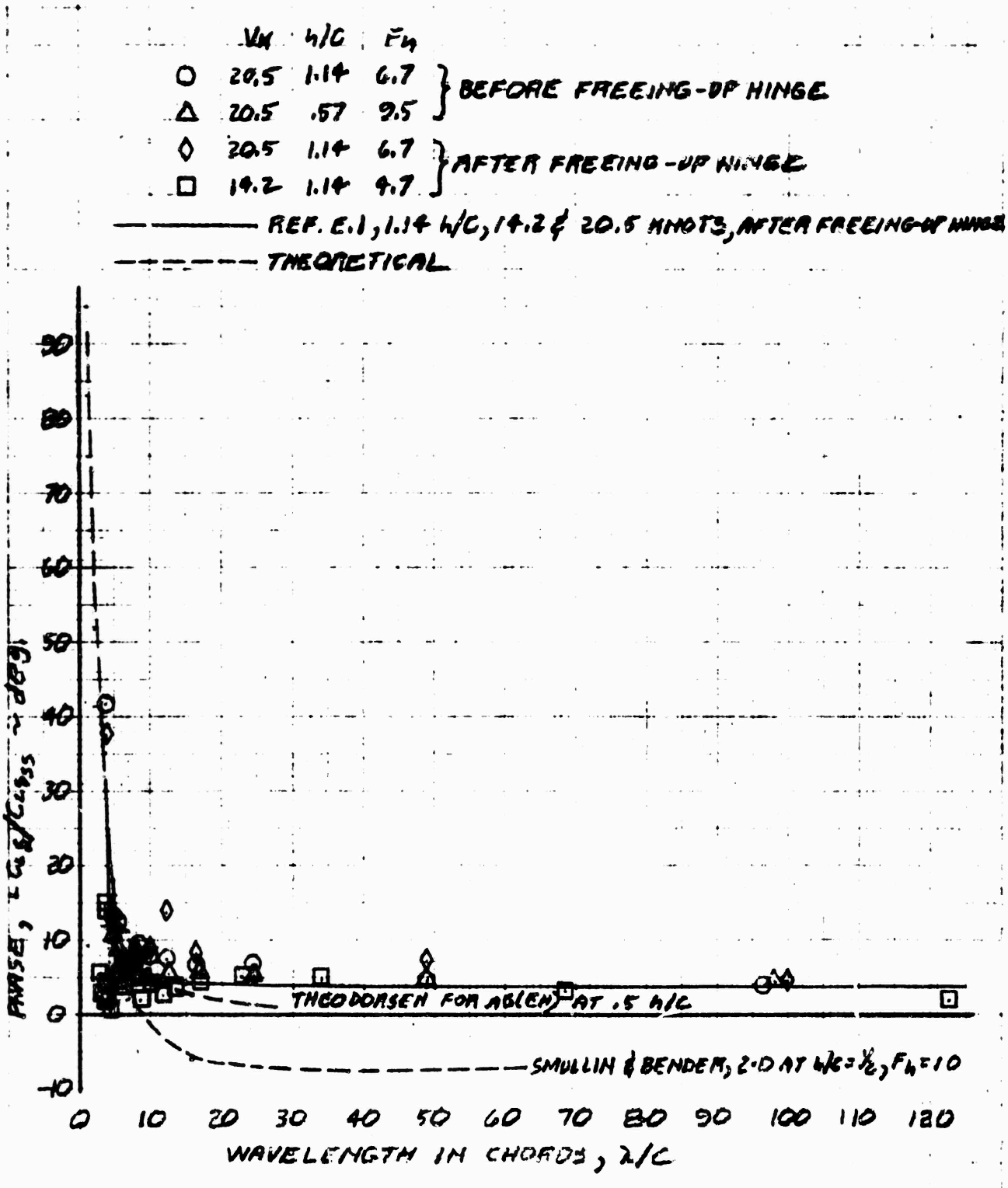


Figure E64. Flap Lift Phase

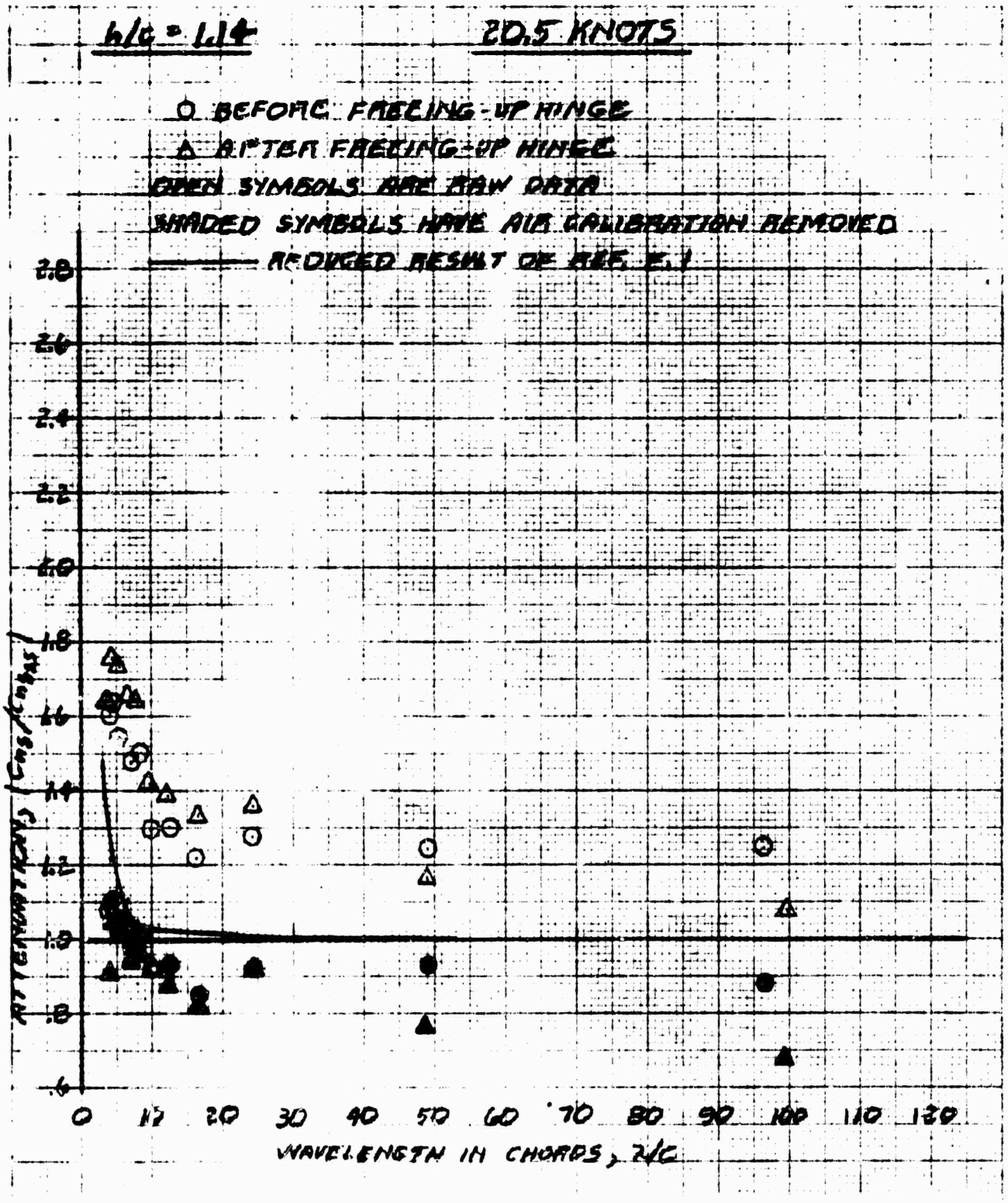


Figure E65. Calibration Effect, Flap Hinge Moment Amplitude

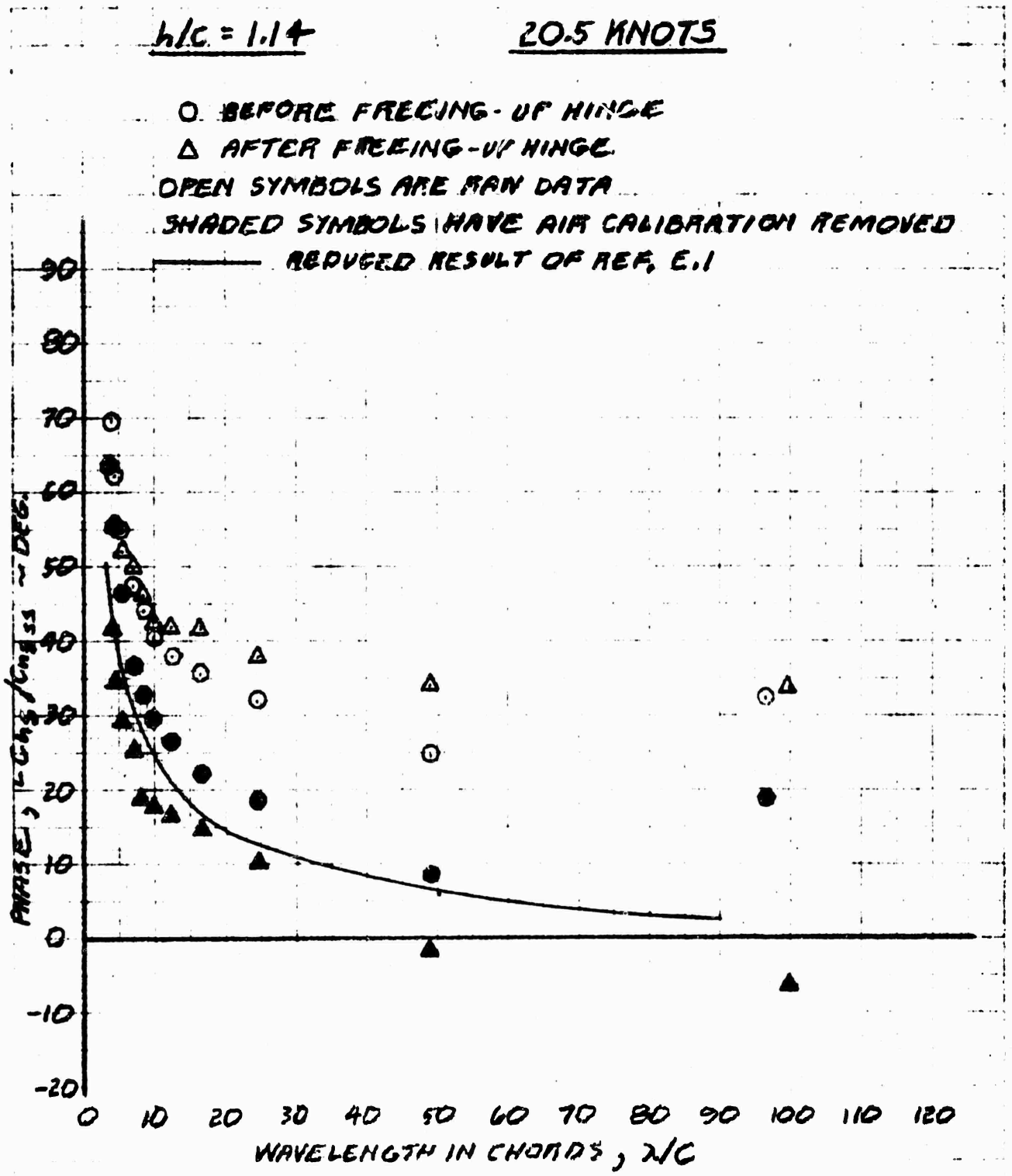


Figure E66. Calibration Effect, Flap Hinge Moment Phase

321

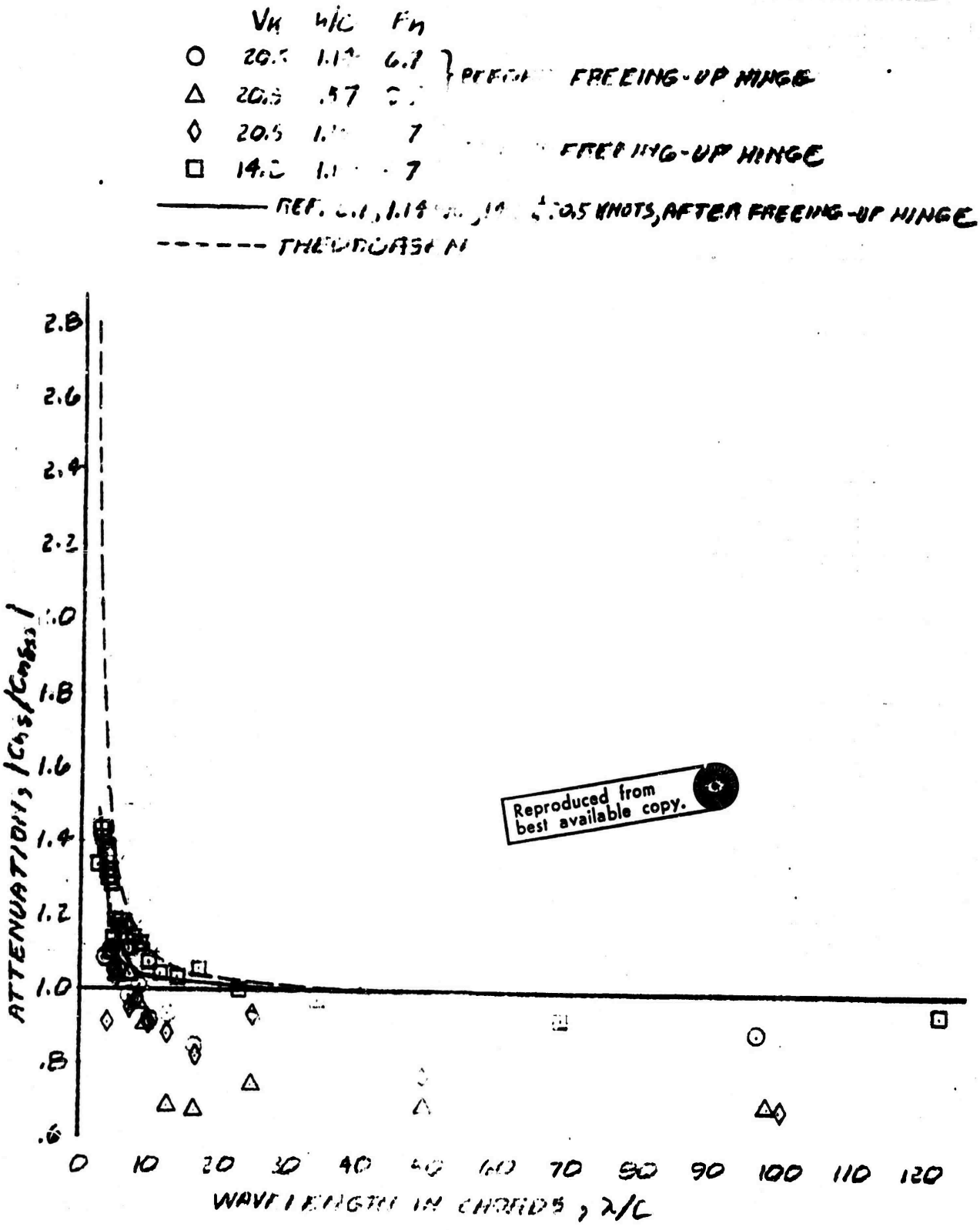


Figure E67. Flap Hinge Moment Amplitude

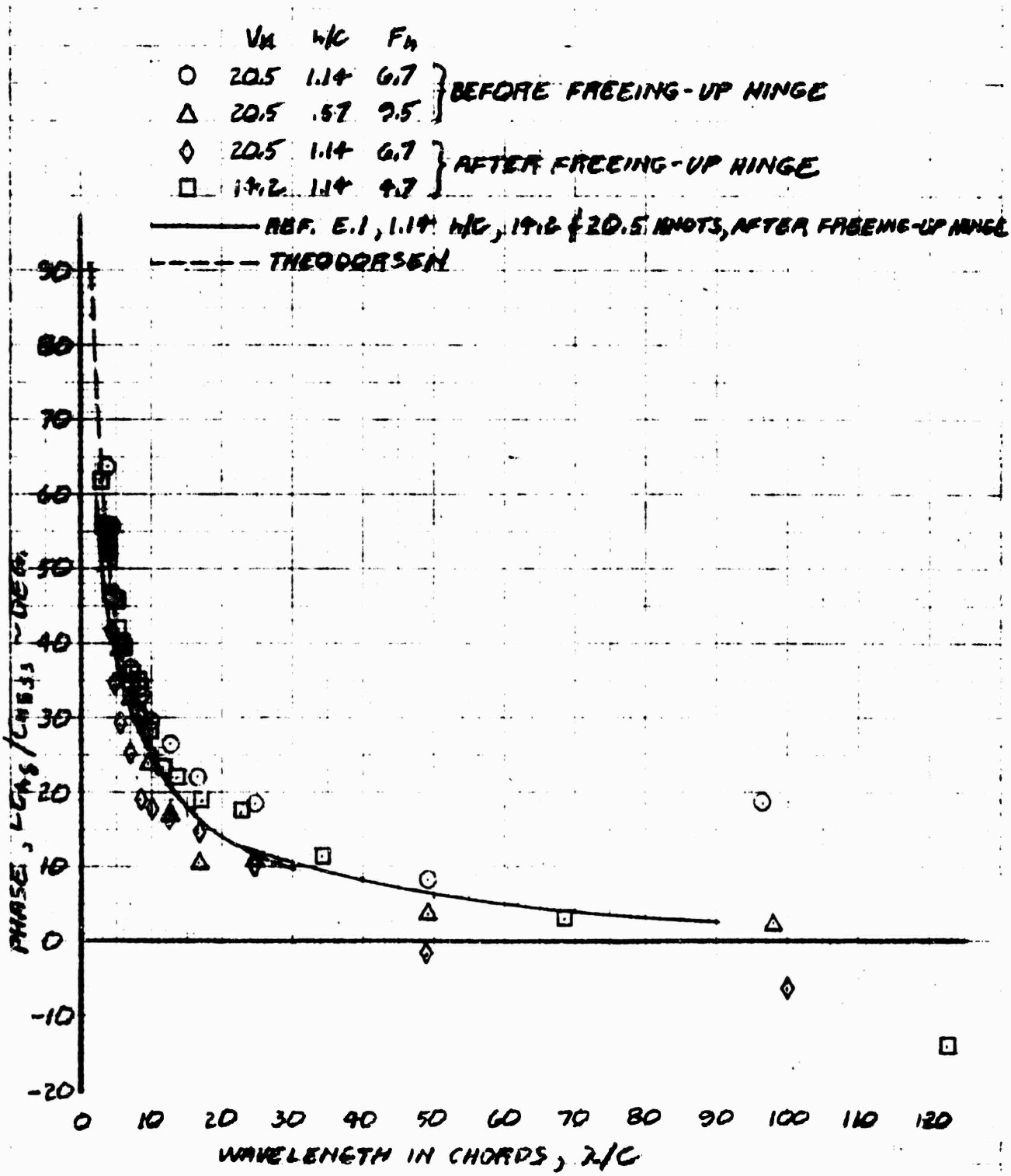


Figure E68. Flap Hinge Moment Phase

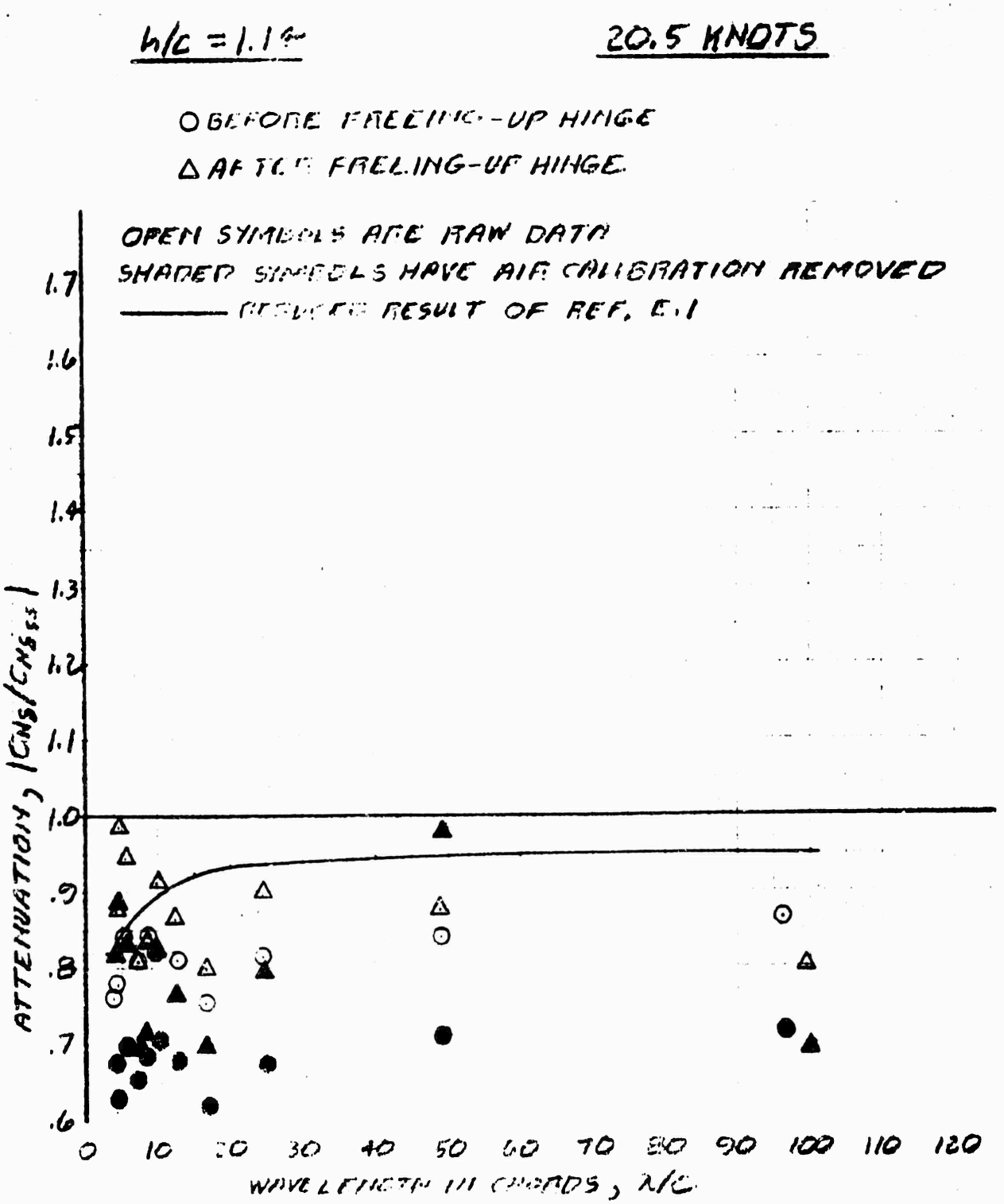


Figure E69. Calibration Effect, Foil Pitching Moment Amplitude

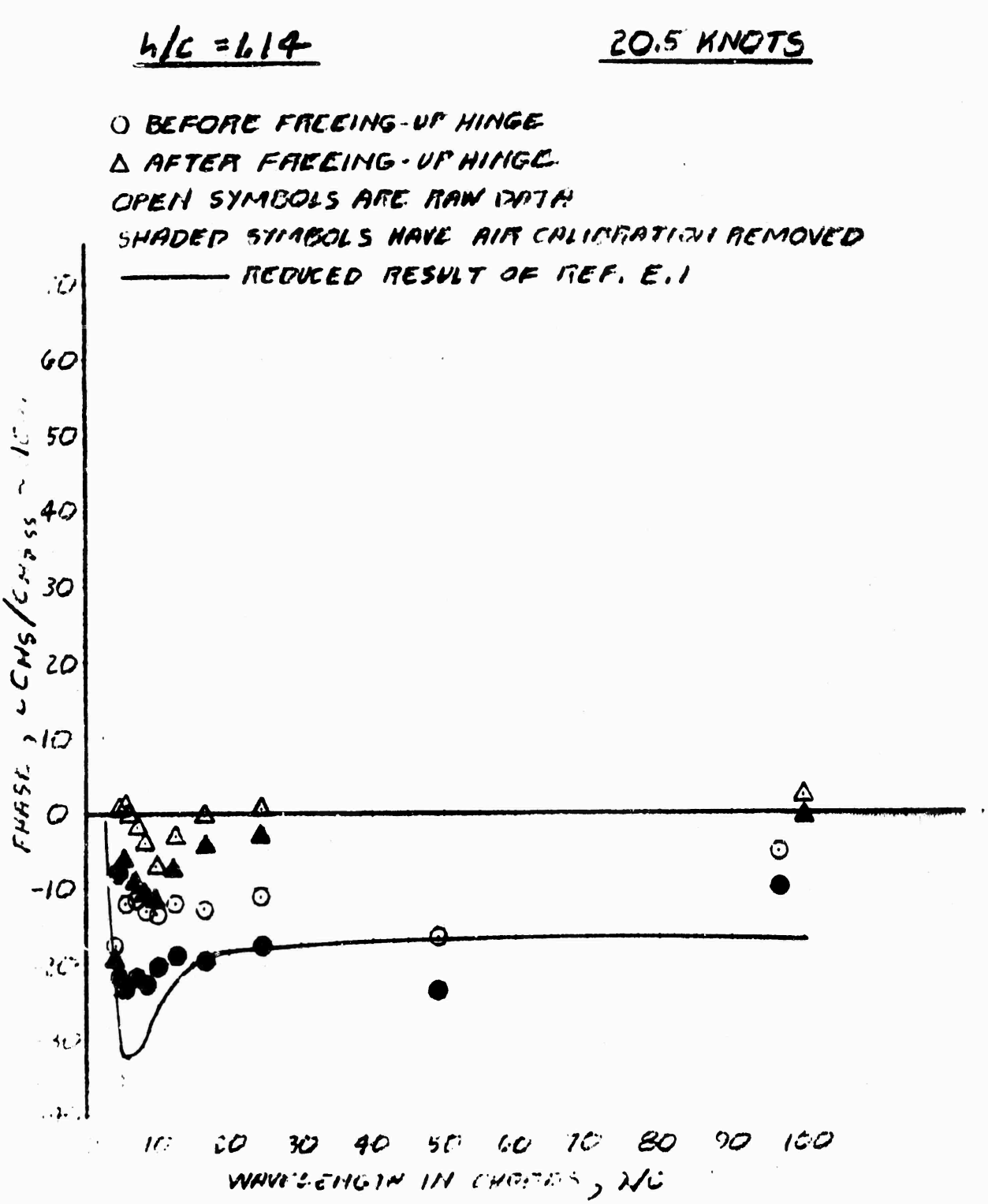


Figure E70. Calibration Effect, Foil Pitching Moment Phase

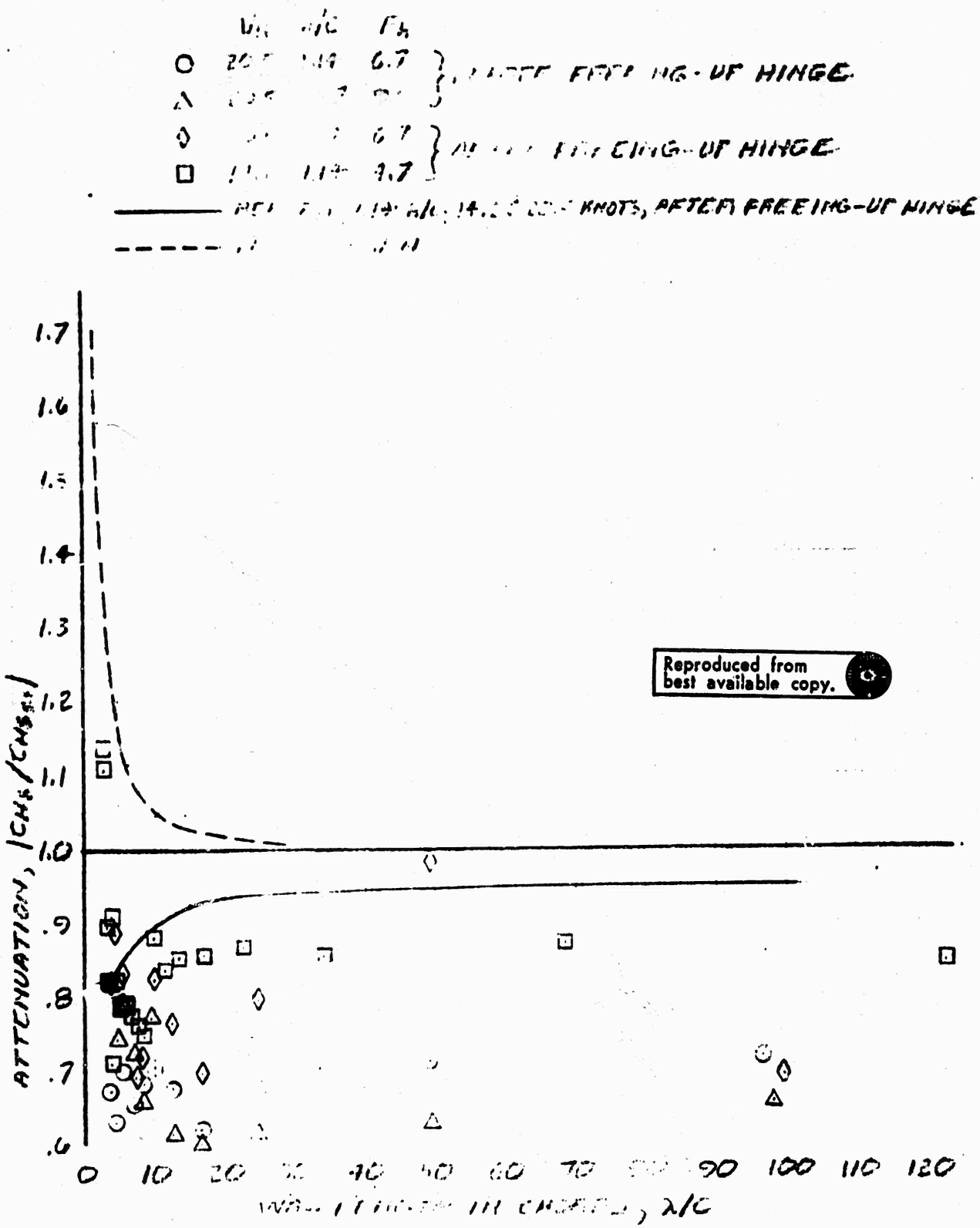


Figure E71. Foil Pitching Moment Amplitude

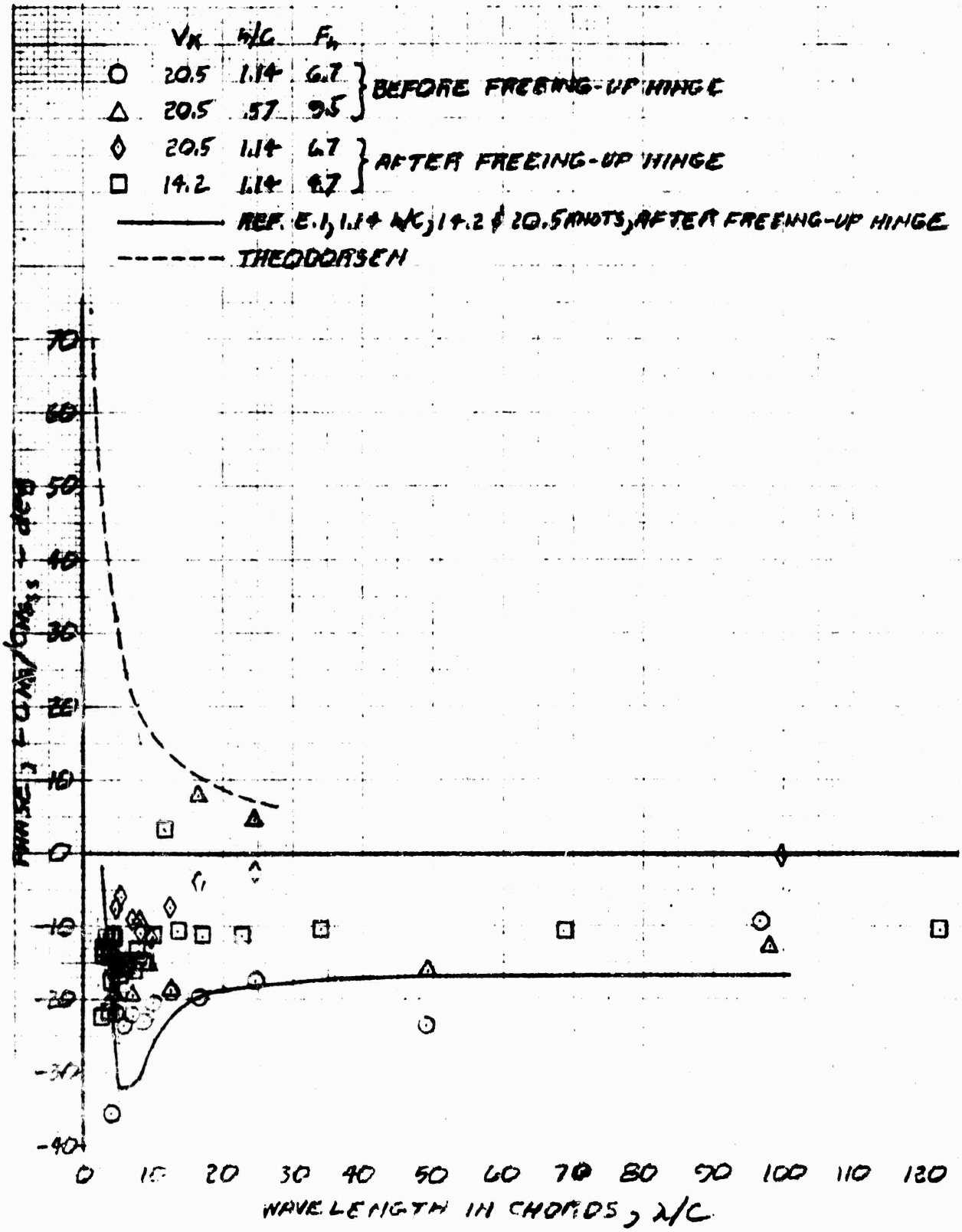


Figure E72. Foil Pitching Moment Phase